

## **General Disclaimer**

### **One or more of the Following Statements may affect this Document**

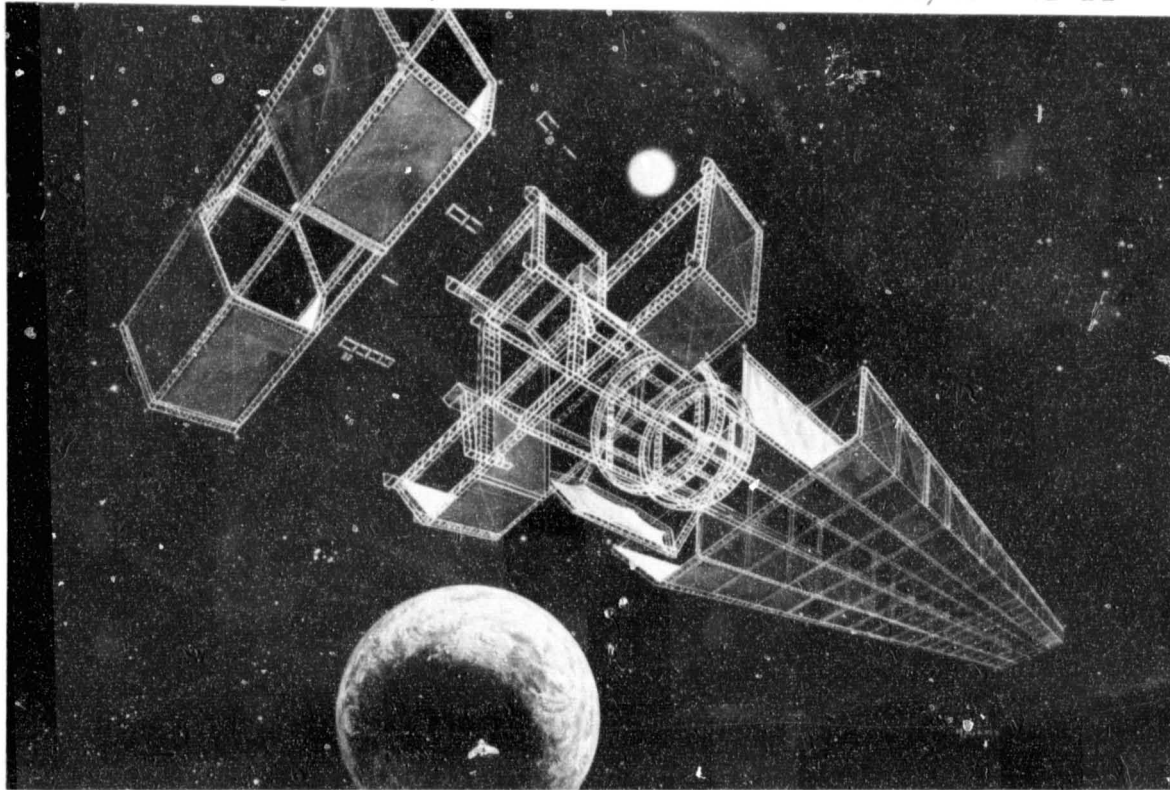
- This document has been reproduced from the best copy furnished by the organizational source. It is being released in the interest of making available as much information as possible.
- This document may contain data, which exceeds the sheet parameters. It was furnished in this condition by the organizational source and is the best copy available.
- This document may contain tone-on-tone or color graphs, charts and/or pictures, which have been reproduced in black and white.
- This document is paginated as submitted by the original source.
- Portions of this document are not fully legible due to the historical nature of some of the material. However, it is the best reproduction available from the original submission.

(NASA-CR-158066) SATELLITE POWER SYSTEMS  
(SPS) CONCEPT DEFINITION STUDY. VOLUME 3:  
SPS CONCEPT EVOLUTION Final Report  
(Rockwell International Corp., Downey,  
Calif.) 307 p HC A14/MF A01

N79-15138

Unclas  
42722

CSSL 22B G3/15



# Satellite Power Systems (SPS) Concept Definition Study

FINAL REPORT  
VOLUME III

## SPS CONCEPT EVOLUTION

April 1978



Rockwell International

Space Division  
12214 Lakewood Boulevard  
Downey, California 90241



SD 78-AP-0023-3

# Satellite Power Systems (SPS) Concept Definition Study

FINAL REPORT

VOLUME III

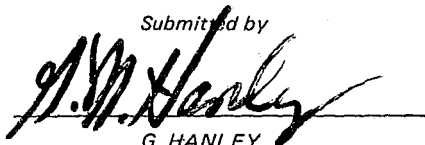
## SPS CONCEPT EVOLUTION

CONTRACT NAS8-32475

DPD 541 MA-04

April 1978

*Submitted by*



G. HANLEY  
*Program Manager*

*Approved*



C.H. GUTTMAN  
*SPS Study Team Manager, NASA/MSFC*

Prepared for:

National Aeronautics and Space Administration  
George C. Marshall Space Flight Center

Marshall Space Flight Center  
Alabama 35812



Rockwell International

Space Division  
12214 Lakewood Boulevard  
Downey, California 90241



## FOREWORD

This document, *SPS Concept Evolution*, is Volume III of the SPS Concept Definition Study (Contract NAS8-32475), Exhibits A and B, and also incorporates results of NASA/MSFC in-house effort. Other volumes of the final report that provide additional detail are listed below.

### Volume

I	Executive Summary
II	SPS System Requirements
IV	SPS Point Design Definition
V	Transportation and Operations Analysis
VI	SPS Technology Requirements and Verification
VII	SPS Program Plan and Economic Analysis



**REPLACING PAGE BLANK NOT FOR**  
**REPLACING PAGE BLANK NOT FOR**

CONTENTS

Section		Page
1.0	SPS CONCEPTS . . . . .	1-1
1.1	INTRODUCTION . . . . .	1-1
1.2	INITIAL CONCEPTS . . . . .	1-1
1.3	PREFERRED CONCEPTS . . . . .	1-4
	1.3.1 Solar Photovoltaic (CR = 2) . . . . .	1-4
	1.3.2 Solar Photovoltaic (CR = 5) . . . . .	1-5
	1.3.3 Solar Photovoltaic (CR = 1) . . . . .	1-5
	1.3.4 Solar Thermal (Boeing/Brayton) . . . . .	1-6
	1.3.5 Solar Thermal (Rankine) . . . . .	1-6
	1.3.6 Nuclear (Brayton) . . . . .	1-9
2.0	TRADE SUMMARY . . . . .	2-1
2.1	SOLAR PHOTOVOLTAIC . . . . .	2-1
	2.1.1 Concentration Ratio . . . . .	2-1
	2.1.2 Orbit Selection . . . . .	2-1
	2.1.3 Attitude Orientation . . . . .	2-2
	2.1.4 Array Geometry Determination . . . . .	2-2
	2.1.5 Silicon Versus GaAlAs Solar Cells . . . . .	2-3
	2.1.6 System Characteristics (GEO Orbit Construction). . . . .	2-4
2.2	SOLAR THERMAL . . . . .	2-7
	2.2.1 Concentrator Concept . . . . .	2-7
	2.2.2 Absorber . . . . .	2-7
	2.2.3 Power Conversion . . . . .	2-7
	2.2.4 Heat Rejection . . . . .	2-8
	2.2.5 System Characteristics . . . . .	2-9
2.3	NUCLEAR . . . . .	2-9
	2.3.1 Approach . . . . .	2-9
	2.3.2 Fuel Processing . . . . .	2-10
	2.3.3 Power Conversion Concept . . . . .	2-11
	2.3.4 System Characteristics . . . . .	2-11
2.4	CONCEPT SUMMARY . . . . .	2-13
	2.4.1 Criteria . . . . .	2-13
	2.4.2 System Specific Weight . . . . .	2-13
	2.4.3 Critical Developments . . . . .	2-14
	2.4.4 Material Availability Evaluation . . . . .	2-15
2.5	CONCLUSIONS . . . . .	2-16
2.6	POINT DESIGN . . . . .	2-19
	2.6.1 Photovoltaic . . . . .	2-19
	2.6.2 Solar Thermal . . . . .	2-21
3.0	TRADE STUDY ANALYSIS . . . . .	3-1
3.1	POWER CONVERSION . . . . .	3-1
	3.1.1 Photovoltaics . . . . .	3-1
	3.1.2 Thermal . . . . .	3-59
	3.1.3 Nuclear Power . . . . .	3-73
	3.1.4 DOE Program Support Requirements . . . . .	3-92



Section	Page
3.2 MICROWAVE SYSTEM . . . . .	3-93
3.2.1 Selected MPTS Candidate Design Concept . . . . .	3-93
3.2.2 MSFC MPTS Baseline Concept . . . . .	3-98
3.2.3 Interrupted Continuous-Wave Operation of MPTS . . . . .	3-114
3.2.4 Alternate Power Transmission Systems . . . . .	3-116
3.2.5 Conical Reflectors in Hexagonal Array . . . . .	3-117
3.2.6 Shaped Beam Alternates . . . . .	3-118
3.2.7 Power Amplifier Configurations . . . . .	3-122
3.2.8 Beam Retrodirection System . . . . .	3-131
3.2.9 DOE Program Support Requirements . . . . .	3-135
3.3 POWER DISTRIBUTION AND CONTROL SYSTEM . . . . .	3-139
3.3.1 POWER CONDITIONING . . . . .	3-140
3.3.2 Conductors . . . . .	3-151
3.3.3 Grounding . . . . .	3-154
3.3.4 Rotary Joint . . . . .	3-154
3.4 STRUCTURES . . . . .	3-162
3.4.1 Aspect Ratio . . . . .	3-162
3.4.2 Antenna Structure . . . . .	3-168
3.4.3 Materials . . . . .	3-171
3.4.4 Tribeam Subelement Study . . . . .	3-173
3.5 ATTITUDE CONTROL AND STATIONKEEPING SUBSYSTEM (ACSS) CONCEPT EVOLUTION . . . . .	3-179
3.5.1 Orbit Selection Trades . . . . .	3-179
3.5.2 Attitude Control Techniques Trades . . . . .	3-181
3.5.3 Stationkeeping Alternatives and RCS Propellant Requirements . . . . .	3-193
3.5.4 Control System/Structural Dynamic Interaction . . . . .	3-194
3.5.5 Stabilization and Control System Concept Evolution for an SPS Spacecraft Constructed in LEO . . . . .	3-200
3.5.6 Summary of Conclusions and Recommendations . . . . .	3-211
3.6 THERMAL CONTROL . . . . .	3-214
3.6.1 Concentration Ratio = 400 SPS . . . . .	3-214
3.6.2 BANDPASS FILTERS . . . . .	3-217
3.6.3 NaK/Heat Pipe Vs. Condensing Radiators . . . . .	3-219
3.6.4 Klystron Thermal Control Design . . . . .	3-224
3.6.5 Thermal Considerations at LEO Vs. GEO . . . . .	3-224
3.6.6 Relative Orientation of Electrical Conductors . . . . .	3-233
3.6.7 DOE Program Support Requirements . . . . .	3-233
3.7 INFORMATION MANAGEMENT AND CONTROL . . . . .	3-235
3.7.1 Central Vs. Distributed Processing . . . . .	3-236
3.7.2 Data Bus Trade . . . . .	3-244
3.7.3 Ground-Based Information Management and Control Subsystem (IMCS) . . . . .	3-253
3.7.4 DOE Program Support Requirements . . . . .	3-259



ILLUSTRATIONS

Figure		Page
1.2-1	Initial Concepts Matrix . . . . .	1-2
1.3-1	Solar Photovoltaic (5 GW), CR = 2 . . . . .	1-4
1.3-2	Solar Photovoltaic (5 GW), CR = 5 . . . . .	1-5
1.3-3	Solar Photovoltaic Non-Concentrated Concept (5 GW) . . . . .	1-6
1.3-4	Boeing/Brayton Reference Concept (10 GW) . . . . .	1-7
1.3-5	Rankine Solar Thermal Concept (5 GW) . . . . .	1-8
1.3-6	Nuclear-Powered Concept (5 GW) . . . . .	1-9
2.1-1	Selection of Flight Conditions . . . . .	2-2
2.1-2	Array Geometry Determination . . . . .	2-3
2.1-3	Silicon Vs. GaAlAs Solar Cells . . . . .	2-4
2.1-4	Solar Photovoltaic System Characteristics (Geosynchronous Orbit Construction) . . . . .	2-5
2.2-1	Dynamic Conversion Efficiencies . . . . .	2-7
2.3-1	Fuel Management Schematic . . . . .	2-10
2.3-2	Nuclear Power Generation Block Diagram . . . . .	2-11
2.4-1	Weight Comparisons . . . . .	2-14
2.4-2	Material Availability Evaluation . . . . .	2-15
2.5-1	Concepts Comparison . . . . .	2-17
2.6-1	Photovoltaic Point Design Evolution . . . . .	2-19
2.6-2	Solar Photovoltaic CR = 2 Point Design (2-5 GW) . . . . .	2-21
2.6-3	Thermal Design Concept . . . . .	2-21
3.1-1	Power Conversion Subsystem Options . . . . .	3-3
3.1-2	Projected Performance of Solar Cell Candidates . . . . .	3-5
3.1-3	MSFC Baseline Solar Cell . . . . .	3-6
3.1-4	Solar Cell Configurations . . . . .	3-7
3.1-5	Solar Cell Efficiency Projection and Parameter Comparison . . . . .	3-8
3.1-6	Solar Cell Damage Equivalent 1 MeV Electron Fluence Vs. Shield Density . . . . .	3-10
3.1-7	Normalized Maximum Power Vs. 1-MeV Electron Fluence . . . . .	3-11
3.1-8	Solar Proton Model Environment . . . . .	3-13
3.1-9	GaAlAs Solar Cell Radiation Test Data . . . . .	3-13
3.1-10	GaAlAs Solar Cell Annealing Effects . . . . .	3-14
3.1-11	GaAlAs Solar Cell Voltage and Current Characteristics . . . . .	3-15
3.1-12	GaAlAs Solar Cell Blanket Cross Section . . . . .	3-15
3.1-13	Efficiency Vs. Thickness (Optimum Conditions) . . . . .	3-16
3.1-14	Deployed Area, Relative Power to Mass Ratio, and Mass of GaAs for SPS as a Function of Cell Thickness . . . . .	3-17
3.1-15	Subsystem Mass and Mass of GaAs for a 5-GW SPS as a Function of Solar Cell Thickness . . . . .	3-18
3.1-16	SPS Mass as a Function of Concentrator Configuration and Concentration Ratio (No Misorientation Allowances Included) . . . . .	3-20
3.1-17	Concentration Ratio Sensitivity . . . . .	3-21
3.1-18	Concentration Ratio Sensitivity with Misorientation Angle. . . . .	3-21



Figure		Page
3.1-19	5 GW Photovoltaic - CR-5 - Concept No. 2C . . . . .	3-22
3.1-20	Solar Vector Interception with Misoriented Array . . . . .	3-23
3.1-21	Solar Cell Blanket Illumination Pattern . . . . .	3-23
3.1-22	Array Sensitivity to Tilt Misorientation . . . . .	3-24
3.1-23	Array Sensitivity to Roll Misorientation . . . . .	3-25
3.1-24	Solar Array Power Loss as a Function of Misorientation Angle and Configuration . . . . .	3-25
3.1-25	Concentrator Array Sensitivity to Misorientation . . . . .	3-26
3.1-26	Planforms of Photovoltaic Systems . . . . .	3-27
3.1-27	5-GW Photovoltaic CR = 2 Concept No. 2F-4 Balanced Inertias . . . . .	3-29
3.1-28	5-GW Photovoltaic CR-2 Concept (60° Reflector Angle) . . . . .	3-30
3.1-29	5-GW Photovoltaic CR-2 Trough . . . . .	3-31
3.1-30	SPS Configuration Planform and Area Summary Data . . . . .	3-32
3.1-31	Photovoltaic Parametric Cost and Mass Comparisons . . . . .	3-34
3.1-32	Solar Photovoltaic SPS Configuration . . . . .	3-36
3.1-33	SPS Trade Studies . . . . .	3-37
3.1-34	SPS Size and Power Distribution Trade . . . . .	3-39
3.1-35	SPS Concept Comparison . . . . .	3-39
3.1-36	Sensitivity to Planform Shape . . . . .	3-40
3.1-37	SPS Configuration . . . . .	3-43
3.1-38	MSFC 5 GW Photovoltaic SPS . . . . .	3-43
3.1-39	Photovoltaic SPS Efficiency Chain . . . . .	3-46
3.1-40	SPS Concentrator Key Approaches . . . . .	3-49
3.1-41	Rectangular Solar Array Equivalent Power Conductor Length. . . . .	3-51
3.1-42	Triangular Solar Array Equivalent Power Conductor Length . . . . .	3-52
3.1-43	Elliptical Solar Array (Two Load Configuration) Equivalent Power Conductor Length . . . . .	3-53
3.1-44	Elliptical Solar Array (Load Centralized at Center) Equivalent Power Conductor Length . . . . .	3-54
3.1-45	SPS Solar Array Module . . . . .	3-56
3.1-46	SPS Solar Array Blanket-Reflector Cross Section . . . . .	3-58
3.1-47	Candidate Designs . . . . .	3-60
3.1-48	Brayton Absorber Design . . . . .	3-63
3.1-49	Power Cycle Diagrams . . . . .	3-64
3.1-50	Dynamic Conversion Efficiencies . . . . .	3-64
3.1-51	Dynamic Conversion Schematics . . . . .	3-65
3.1-52	Cesium/Steam Rankine Cycle . . . . .	3-68
3.1-53	Nuclear Power System Trade Tree (Options) . . . . .	3-73
3.1-54	Nuclear-Powered SPS (5 GW) - Concept No. 1 . . . . .	3-74
3.1-55	Nuclear-Powered SPS (5 GW) - Concept No. 2 . . . . .	3-75
3.1-56	Nuclear-Powered SPS (5 GW) - Concept No. 3 . . . . .	3-75
3.1-57	Concepts Comparison . . . . .	3-76
3.1-58	Nuclear SPS Reactor—Shadow Shield Mass . . . . .	3-76
3.1-59	Nuclear Reactor . . . . .	3-78
3.1-60	Reactor Subdivision . . . . .	3-79
3.1-61	Fuel Management Schematic . . . . .	3-82
3.1-62	Fuel Processing Plant (One per Module) . . . . .	3-85
3.1-63	Brayton Cycle PCU Schematic . . . . .	3-86
3.1-64	System Mass Vs. Separation Distance (Configuration 1) . . . . .	3-89
3.1-65	System Mass Vs. Separation Distance (Configuration 2) . . . . .	3-90





Figure		Page
3.1-66	System Mass Vs. Separation Distance (Configuration 3)	3-90
3.2-1	MPTS Trade Tree	3-93
3.2-2	Microwave Antenna Module Sizes	3-94
3.2-3	Gaussian Beam MW Antenna	3-95
3.2-4	Shaped Beam MW Antenna	3-95
3.2-5	Rectenna Installation	3-96
3.2-6	MPTS Efficiency Chain	3-97
3.2-7	The $f_d$ -p Plane showing Limits of Breakdown Processes	3-100
3.2-8	SPS Microwave Power Transmission System	3-102
3.2-9	SPS Microwave Concept	3-104
3.2-10	SPS Microwave Power System Efficiency	3-105
3.2-11	Baseline Concepts Comparison	3-107
3.2-12	Microwave Antenna Elements	3-108
3.2-13	SPS Microwave Antenna 1-m $\times$ 2.4 Element Construction	3-108
3.2-14	Amplitron Modified Heat Sink	3-109
3.2-15	Solid-State Antenna with Rockwell Suspension Frame Structure	3-111
3.2-16	SPS Rectenna	3-113
3.2-17	Rectenna with Direct AC Conversion	3-115
3.2-18	AC Waveform Generated by Convolution and Delay	3-115
3.2-19	Phasing on the Elliptical Rectenna	3-116
3.2-20	Conical Reflector Geometry	3-118
3.2-21	Gaussian Beam Compared with Shaped Beam	3-118
3.2-22	Influence of Aperture Phase Errors on Antenna Pattern	3-119
3.2-23	Taylor Distribution for 40 dB Sidelobe Level	3-121
3.2-24	Beam Pattern From Taylor Weighting Pattern (40 dB)	3-122
3.2-25	87 kW Transistor Amplifier Power Module	3-127
3.2-26	Transistor Chip Schematic	3-128
3.2-27	Chip Collector Configuration	3-128
3.2-28	Transistor Chip Layout	3-129
3.2-29	Transistor MIC Module	3-130
3.2-30	Common Base Push-Pull Amplifier	3-130
3.2-31	Simple Heterodyning Phase Conjugating Circuit	3-133
3.2-32	MPTX Phase Conjugation and Reference Distribution	3-134
3.2-33	MPTX Injection Locked Magnetron Subarray	3-134
3.2-34	Phase Control Distribution System	3-136
3.2-35	Antenna Phasing System	3-137
3.3-1	Power Distribution Control Subsystem Options	3-139
3.3-2	Conductor Weight Comparisons	3-141
3.3-3	Solar Photovoltaic Conductor Mass	3-142
3.3-4	Solar Thermal (D.C. Configuration) Conductor Mass Vs. Efficiency ( $\eta$ )	3-143
3.3-5	Power Distribution of Photovoltaic CR-1 Configuration (Left Wing Solar Array Shown - Right Wing Symmetrical).	3-145
3.3-6	Power Distribution of Photovoltaic CR-2 Configuration (Left Wing Solar Array Shown - Right Wing Symmetrical).	3-145
3.3-7	Power Distribution of Photovoltaic CR-5 Configuration (Left Wing Solar Array)	3-146
3.3-8	PDC Ground Facility	3-150
3.3-9	SPS Rotating Hub Assembly Free-Standing Slip Ring Structure	3-155



Figure		Page
3.3-10	SPS Rotating Hub Structure LEO/GEO Assembly . . . . .	3-155
3.3-11	SPS Rotating Hub Structure Slip Ring Structure Buildup . . . . .	3-156
3.3-12	15-meter-Diameter Slip Ring . . . . .	3-158
3.3-13	SPS Slip Ring - Brush Assembly . . . . .	3-159
3.4-1	Structural Subsystem Trades . . . . .	3-162
3.4-2	Configurations Evaluated . . . . .	3-163
3.4-3	Solar Photovoltaic Aspect Ratio/Gravity-Gradient Torque Comparisons . . . . .	3-163
3.4-4	SPS Aspect Ratio Analysis Load Diagram . . . . .	3-164
3.4-5	Satellite Frequency as a Function of Configuration and Tribeam Girder Cross-Sectional Area . . . . .	3-167
3.4-6	Major Structural Configuration Considerations . . . . .	3-167
3.4-7	SPS Solar Array Configuration Evaluation . . . . .	3-168
3.4-8	Microwave Antenna Structure Selected Design Concept . . . . .	3-168
3.4-9	Antenna Structural Concepts . . . . .	3-169
3.4-10	Microwave Antenna Structure Design Condition . . . . .	3-170
3.4-11	Microwave Antenna Mass Summary . . . . .	3-171
3.4-12	Large Space Structures Material Considerations . . . . .	3-172
3.4-13	SPS Materials Comparison . . . . .	3-172
3.4-14	Photovoltaic Wing Structure Tiering . . . . .	3-174
3.4-15	Temperature Gradient as Function of Subelement Shape . . . . .	3-174
3.4-16	Allowable Stress Levels as Function of Subelement Shape . . . . .	3-175
3.4-17	Square Tube Shape Optimization . . . . .	3-176
3.4-18	Allowable Stress Levels as a Function of Size and Shape . . . . .	3-177
3.4-19	Basic Beam Element Cap Section . . . . .	3-178
3.5-1	Orbit Selection Trade . . . . .	3-180
3.5-2	Rectenna Parameters Vs. Latitude . . . . .	3-181
3.5-3	Attitude Control Techniques Trade Tree . . . . .	3-182
3.5-4	Influence of S/C Size on Control Parameters . . . . .	3-183
3.5-5	Some Alternative Configurations Considered . . . . .	3-184
3.5-6	Additional Alternative Configurations Considered . . . . .	3-184
3.5-7	Attitude Control Subsystem Approaches . . . . .	3-186
3.5-8	Momentum Wheel Sizing Data . . . . .	3-187
3.5-9	Attitude Orientation Description . . . . .	3-188
3.5-10	Solar Thermal Configurations to Minimize ACSS Requirements . . . . .	3-191
3.5-11	Attitude Control Propellant and Reaction Wheel Mass Photovoltaic Configuration (Y-POP, X-IOP) . . . . .	3-192
3.5-12	Simplified Control Bandwidth Analysis Model . . . . .	3-196
3.5-13	ACSS Control Bandwidth Requirement . . . . .	3-196
3.5-14	Preliminary Control and Structural Frequency Requirements . . . . .	3-197
3.5-15	Bending Modes for Free-Free Beam . . . . .	3-198
3.5-16	Model for Control System Analysis . . . . .	3-198
3.5-17	Control System Dynamics - Root Locus . . . . .	3-199
3.5-18	Multisensor and Actuator Location . . . . .	3-200
3.5-19	SPS Control Coordinates . . . . .	3-202
3.5-20	Stability and Control Flow Diagram . . . . .	3-203
3.5-21	LEO Sunlight Conditions (Typical) . . . . .	3-204
3.5-22	Baseline MPD Electric Thruster . . . . .	3-207
3.5-23	Baseline LOX/LH <sub>2</sub> Chemical Thruster . . . . .	3-209
3.5-24	Electric Thruster Module Locations . . . . .	3-209



Figure		Page
3.6-1	Thermal Control Subsystem . . . . .	3-215
3.6-2	Comparison of Predicted GaAlAs Cell Efficiencies . . . . .	3-216
3.6-3	High Concentration Ratio GaAlAs Mass Comparison CR=400 . . . . .	3-217
3.6-4	Spectral Filter Concepts . . . . .	3-218
3.6-5	Band Pass Filters . . . . .	3-220
3.6-6	Organic Fluid Degradation . . . . .	3-221
3.6-7	Radiator Concepts . . . . .	3-222
3.6-8	Meteoroid System Mass Penalty Heat Pipe Radiator . . . . .	3-223
3.6-9	Effect of Meteoroid Protection on Radiator System Mass Rankine Cycle SPS . . . . .	3-224
3.6-10	Heat Radiators on Array Face . . . . .	3-225
3.6-11	One Meter Beam Construction . . . . .	3-226
3.6-12	SPS Structural Temperature, LEO, Construction Phase . . . . .	3-226
3.6-13	SPS Structural Temperature GEO Construction Phase . . . . .	3-227
3.6-14	SPS Thermal Distortion . . . . .	3-227
3.6-15	SPS Thermal Distortion, GEO Construction Phase . . . . .	3-228
3.6-16	SPS Structural Temperature LEO - Operational Phase . . . . .	3-228
3.6-17	SPS Structural Temperature GEO - Operational Phase . . . . .	3-229
3.6-18	SPS Thermal Distortion, LEO Operational Phase . . . . .	3-229
3.6-19	SPS Thermal Distortion . . . . .	3-230
3.6-20	SPS Structural Temperature Gradients . . . . .	3-231
3.6-21	SPS Structural Distortion Due to Temperature Gradient LEO - Operational Phase . . . . .	3-232
3.6-22	SPS Structural Distortion Due to Temperature Gradient GEO - Operational Phase . . . . .	3-232
3.6-23	Electrical Conductor Thermal Response . . . . .	3-234
3.6-24	Electrical Conductor Thermal Analysis . . . . .	3-234
3.7-1	Trade Tree - Information Management and Control Subsystem. . . . .	3-235
3.7-2	Distributed Computer Concept . . . . .	3-237
3.7-3	Analysis Approach . . . . .	3-237
3.7-4	Data System Computer Net (Preliminary) . . . . .	3-245
3.7-5	Spatial Distribution of Computers . . . . .	3-246
3.7-6	RAC and SM Interconnections (Thermal) . . . . .	3-248
3.7-7	Trade Approach for Data Bus Study . . . . .	3-248
3.7-8	Evaluation and Selection . . . . .	3-249
3.7-9	Definition of Functional Levels . . . . .	3-254
3.7-10	Basic Energy Flow Diagram . . . . .	3-255
3.7-11	Model Rectenna System . . . . .	3-255



~~COPIED PAGE BLANK NOT FOR~~

TABLES

Table		Page
1.2-1	Basic SPS Design Concepts . . . . .	1-2
1.2-2	SPS Design Concept Variations . . . . .	1-3
2.1-1	Solar Array Sizing Models . . . . .	2-6
2.1-2	Solar Photovoltaic Mass Summary (GaAlAs Solar Cells) . . . . .	2-6
2.2-1	Power Conversion Concept Comparisons . . . . .	2-8
2.2-2	Solar Thermal System Characteristics . . . . .	2-9
2.3-1	Nuclear Reactor Concept Mass Summary . . . . .	2-12
2.4-1	Concepts Selection Criteria . . . . .	2-13
2.4-2	System Concept-Related Technology Issues . . . . .	2-14
2.6-1	Cost Differences for GEO and LEO/GEO Construction (GaAs Photovoltaic Satellite Point Design) . . . . .	2-20
3.0-1	Trade Studies Summary . . . . .	3-2
3.1-1	Solar Cell Relative Cost Comparisons . . . . .	3-9
3.1-2	Solar Cell Comparisons . . . . .	3-11
3.1-3	Solar Cell Configuration . . . . .	3-12
3.1-4	Reflector Degradation . . . . .	3-26
3.1-5	Photovoltaic System Comparisons . . . . .	3-28
3.1-6	Photovoltaic Mass and Cost Summary . . . . .	3-33
3.1-7	Comparison of Reflector Angles . . . . .	3-35
3.1-8	Subsystem Cost Comparison as a Function of Reflector Angles . . . . .	3-35
3.1-9	Summary Characteristics 10 GW Si Photovoltaic System . . . . .	3-36
3.1-10	Guidelines and Assumptions . . . . .	3-41
3.1-11	30-Year SPS Program Requirements Profile . . . . .	3-42
3.1-12	SPS Program Requirements Summary . . . . .	3-42
3.1-13	SPS Baseline System Characteristics . . . . .	3-45
3.1-14	Mass Summary of the 5-GW Photovoltaic SPS . . . . .	3-46
3.1-15	Solar Array Reference and Options Summary . . . . .	3-48
3.1-16	SPS Solar Array Baseline Module Characteristics (50 m x 250 m) . . . . .	3-57
3.1-17	Concentrator Concept Comparison . . . . .	3-61
3.1-18	Candidate Power Conversion Systems . . . . .	3-68
3.1-19	General Comparison of Brayton and Rankine Cycles . . . . .	3-70
3.1-20	Technology Advancement Requirements . . . . .	3-70
3.1-21	Production Costs . . . . .	3-72
3.1-22	Overall Power-Loop Cost Comparison . . . . .	3-72
3.1-23	Overall Power-Loop Point Ratings . . . . .	3-72
3.1-24	Nuclear Reactor Options . . . . .	3-77
3.1-25	Reactor Mass Breakdown . . . . .	3-81
3.1-26	Reactivity Changes . . . . .	3-81
3.1-27	Fuel Processing Plant Summary . . . . .	3-85
3.1-28	Brayton PCU Summary (336-MWe Module) . . . . .	3-86
3.1-29	Radiation Attenuation Characteristics . . . . .	3-87
3.1-30	Nuclear Reactor Concept Mass Summary . . . . .	3-91
3.1-31	DOE Program Support Requirements--Power Conversion . . . . .	3-92



Table		Page
3.2-1	Key MPTS Design Decisions . . . . .	3-97
3.2-2	Summary of MPTS Point Design Parameters . . . . .	3-98
3.2-3	LEO Vs. GEO Trade Guidelines and Requirements . . . . .	3-100
3.2-4	Assembly Location . . . . .	3-102
3.2-5	New System Elements . . . . .	3-104
3.2-6	SPS Microwave Antenna (1 km) Mass Properties Update . . . . .	3-110
3.2-7	Solid-State Antenna Mass Estimate . . . . .	3-112
3.2-8	Conversion Device Parametric Trade-Off . . . . .	3-123
3.2-9	Phase Control Trade-Offs . . . . .	3-132
3.2-10	Comparison of Four Phase-Conjugating Systems . . . . .	3-138
3.2-11	Data Needed from DOE . . . . .	3-138
3.3-1	Power Distribution Mass Comparisons . . . . .	3-146
3.3-2	Solar-Thermal AC Versus DC Comparison . . . . .	3-147
3.3-3	Comparison of Transformer Mass Vs. Frequency . . . . .	3-148
3.3-4	Klystron Voltage Converter Concept Comparisons . . . . .	3-149
3.3-5	Conducting Structure Comparison for 10-GW SPS . . . . .	3-152
3.3-6	Candidate Aluminum Alloys for Electrical Conductive Structures . . . . .	3-153
3.3-7	Conducting Structure Comparison for 5-GW SPS . . . . .	3-154
3.3-8	Rotary Joint Selection Considerations . . . . .	3-157
3.3-9	15-m-Diameter Slip Ring Design Parameters . . . . .	3-160
3.3-10	Major Subassembly Mass . . . . .	3-161
3.4-1	Rockwell Sensitivity Analysis . . . . .	3-165
3.4-2	Sizing Comparison . . . . .	3-166
3.4-3	SPS Microwave Antenna Structure . . . . .	3-169
3.5-1	Attitude Control System Concept Comparison for Photovoltaic Configurations . . . . .	3-190
3.5-2	Attitude Control Concepts Comparison for Solar Thermal Configurations . . . . .	3-191
3.5-3	Stationkeeping RCS Propellant Requirements . . . . .	3-193
3.5-4	Stability and Control Fuel Consumption During LEO to GEO Transfer . . . . .	3-205
3.5-5	Propulsion System Summary . . . . .	3-206
3.5-6	LEO Assembled SPS Propulsion System . . . . .	3-207
3.5-7	GEO Assembled SPS Propulsion System . . . . .	3-208
3.6-1	Passive Solar Array Performance Summary . . . . .	3-219
3.6-2	Meteoroid Study Ground Rules . . . . .	3-223
3.6-3	SPS Maximum Temperature Variations and Corresponding Dimensional Changes (Reference Temperature, 10°C) . . . . .	3-230
3.7-1	Assumed Equipment Characteristics . . . . .	3-241
3.7-2	Central Versus Distributed Computers . . . . .	3-242
3.7-3	Evaluation of Central Vs. Distributed Computers . . . . .	3-243
3.7-4	Data Bus Trade Characteristics . . . . .	3-250
3.7-5	Data Bus Evaluation Matrix . . . . .	3-253
3.7-6	Overall Functions for SPS Ground System . . . . .	3-256
3.7-7	Ground-Based IMCS Functions for Power Reception/Conversion and Distribution . . . . .	3-258



## 1.0 SPS CONCEPTS

### 1.1 INTRODUCTION

This volume presents the results of the various trades and analyses that were performed as a basis for the selection of the recommended SPS system point designs. The trades conducted included the evaluation of several candidate concepts identified during previous contract efforts (including NASA and other corporations) as well as several identified as likely approaches during the initial phases of this study.

The following sections describe the various candidate concepts considered and present the conclusions and recommendations considered in the derivation of the point design described in Volume IV.

The major emphasis during this study has been placed upon the definition of a solar photovoltaic satellite based upon the utilization of a GaAlAs solar cell. This emphasis is reflected in the depth to which the data have been evaluated in the following sections. However, to present the complete picture of the various areas investigated, all major subsystem trade results have been included in Section 3.0. The areas covered, in addition to the GaAlAs photovoltaics include silicon-based photovoltaics, solar thermal power conversion, microwave energy transmission, power distribution, structures, attitude control and stationkeeping, thermal, and information management and control.

### 1.2 INITIAL CONCEPTS

Previous SPS concepts were reviewed to obtain configuration, design, and performance characteristics and the data obtained were used to establish six candidate SPS design concepts. Existing concepts that had been previously investigated for SPS are illustrated in Figure 1.2-1, and include NASA/MSFC and NASA/JSC silicon systems, the Rockwell GaAlAs system, and the Boeing solar Brayton and thermionic systems. Other (new) concepts that were identified for further investigation are also shown in the figure, and include the solar Rankine system, the high concentration ( $>400$ ) GaAlAs photovoltaic system, and a nuclear Brayton reactor system. A general description of these basic concepts is shown in Table 1.2-1. Engineering drawings and/or sketches were generated for the six concepts along with overall SPS system characteristics such as performance, weight, size, efficiencies, and mission parameters.

Each concept was evaluated to determine the major design drivers that effect configuration, weight, cost, and performance. From this evaluation, a total of 20 additional variations were identified for detailed evaluation; these are shown in Table 1.2-2. The five major subsystems that effect SPS configuration are power conversion, microwave transmission, power distribution, structures, and attitude control. Major variables that impact design are listed in the *rationale* column.

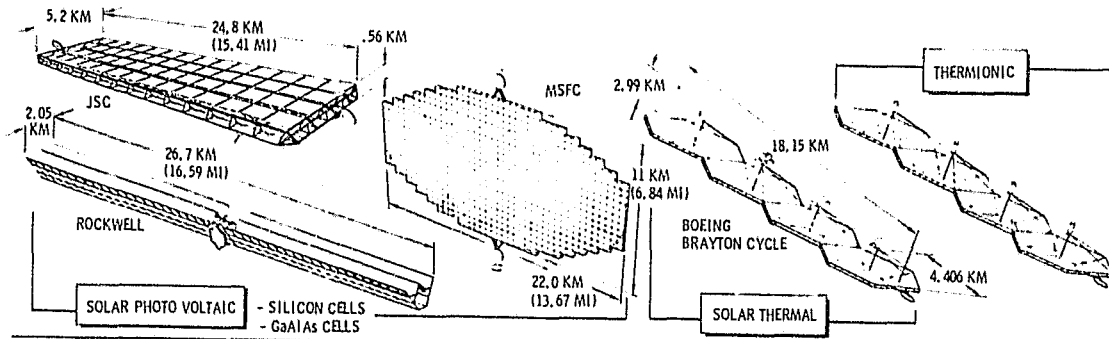
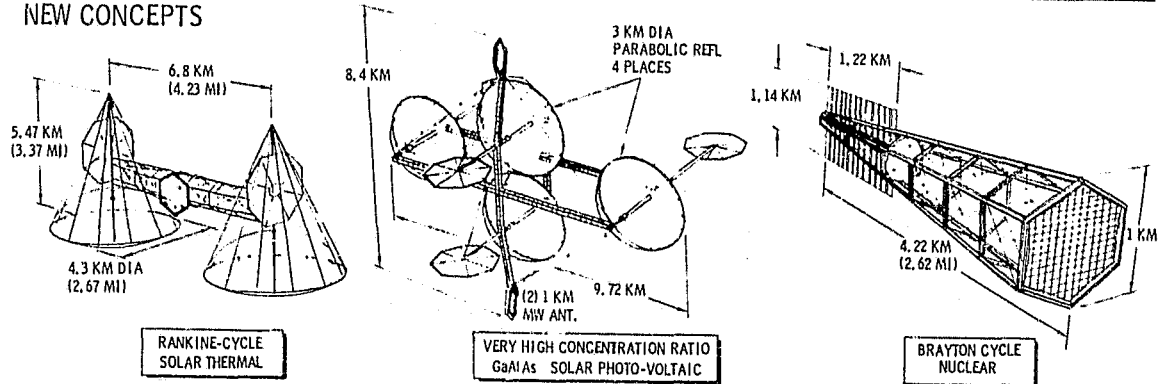
**EXISTING CONCEPTS**

**NEW CONCEPTS**


Figure 1.2-1. Initial Concepts Matrix

Table 1.2-1. Basic SPS Design Concepts

CONCEPT	POWER CONVERSION	MICROWAVE TRANSMISSION	POWER DISTRIBUTION	STRUCTURAL CONFIG.	ATTITUDE CONTROL FLT MODE	THERMAL CONTROL	RATIONALE
1. NASA MSFC SOLAR PHOTOVOLTAIC	10 GW SILICON CELLS CR = 2 NON-DISTRIBUTED	AMPLITRONS 2 ANTENNAS 2 RECTENNAS	20 KV PARTIALLY INTEGRATED WITH STRUCT.	ELLIPTICAL	PERPENDICULAR TO SUN	PASSIVE	SILICON OPTION - ADV TECHNOLOGY STATUS ELLIPTICAL SHAPE - AFFECTS OVERALL CONFIGURATION
2. ROCKWELL SOLAR PHOTOVOLTAIC	5 GW GaAs CELLS CR = 2 NON-DISTRIB.	AMPLITRONS 1 RECTENNA 1 ANTENNA	20 KV INDEPENDENT OF STRUCTURE	TRUSS HIGH-ASPECT RATIO	EARTH ORIENTED	PASSIVE	"BASELINE"
3. NASA JSC PHOTOVOLTAIC	10 GW SILICON CELLS CR = 2 NON-DISTRIB.	KLYSTRONS 2 ANTENNAS 2 RECTENNAS	40 KV	TRUSS LOW-ASPECT RATIO	EARTH ORIENTED	PASSIVE	KLYSTRON - HIGHER POWER & VOLTAGE DEVICE LOW ASPECT RATIO - AFFECTS OVERALL CONFIGURATION
4. BOEING SOLAR THERMAL	10 GW BRAYTON CR = 2000 T = 1389°C FACETED MIRROR	AMPLITRONS 2 ANTENNAS RECTENNA	400 KV AC		SUN ORIENTED	NaK/HEAT PIPE	"EXCELLENT REFERENCE DATA BASE FOR COMPARISON"
5. ROCKWELL SOLAR THERMAL	5 GW RANKINE CR = 1500 T = 1040°C INFLATABLE MIRROR	AMPLITRONS 1 ANTENNA 1 RECTENNA	400 KV AC		SUN ORIENTED	CONDENSING RADIATOR	"CONTAINS MAJOR OPTIONS FOR SOLAR THERMAL"
6. ROCKWELL NUCLEAR THERMAL	NUCLEAR 5 GW BRAYTON T = 1389°C	AMPLITRONS	400 KV AC		GRAVITY GRADIENT	CONDENSING RADIATOR	"PERMITS INSIGHT INTO NEW APPROACH"



ORIGINAL PAGE  
OF POOR QUALITY

Table 1.2-2. SPS Design Concept Variations

Config-uration No.	Concept Variation No.	Power Conversion	Microwave Transmission	Power Distribution	Structural Configuration	Attitude Control Flight Mode	Rationale
1	1A	5 GW Distributed			Truss, medium aspect ratio	Earth oriented	<u>Distributed</u> - Avoids problems (tensioning, non-uniformity of solar)
2	1B	5 GW Distributed	2 amplitrons in series	40 kV Independent of structure		Earth oriented	<u>Medium Aspect Ratio</u> - Affects overall configuration
3	2A		Klystrons	40 kV		Canted/momen-tum wheels	<u>CR = 5; CR = 1</u> - Major variables
4	2B						
5	2C	CR = 5		Integrated w/struc-ture and/or reflectors		Balanced mo-ments of inertia	<u>Canted; Balanced Moments of Inertia; Free Oscillation</u> - Offer lower resupply requirements
6	2D	CR = 400					
7	2E	CR = 1 Polycrystal GaAs					
8	2F	CR = 2 Polycrystal GaAs					
9	2G	10 GW CR = 2	2 antennas 2 antennas				
10	2H	10 GW CR = 2	2 antennas 1 rectenna				
11	2I					Free oscillation	
12	2J	5 GW	2 antennas 2 rectennas				
13	4A	T = 1040°C					T = 1040C, - Major Variable
14	4B	Inflatable reflector		40 kV		Balanced mo-ments of inertia	
15	5A	10 GW	2 antennas 2 rectennas			Balanced mo-ments of inertia	T = 1370C; T = 816C - Major variables
16	5B	T = 1370°C					
17	5C	T = 816°C					
18	7	0.5 GW	Reflector relays				
19	8	5 GW	Direct conver-sion (solid state)				<u>Solid State</u> - Major alternative
20	9	5 GW	Laser/relay satellite				





### 1.3 PREFERRED CONCEPTS

On the basis of the preliminary assessment, six preferred concepts were identified. Concepts 1, 2, and 3 being solar photovoltaic energy conversion with GaAlAs solar cells, provide a basis for selecting an optimum concentration ratio. The baseline Rockwell concept (CR = 2) was used to develop structural shapes and designs for CR = 1 and CR = 5 to provide a basis for commonality. The Boeing Brayton solar thermal concept was used as a reference. A solar thermal Rankine concept was also defined to permit the evaluation of major design options, e.g., inflatable collectors, open absorber, and condensing radiator. A nuclear concept definition was included to gain insight into this approach. The basic satellite system characteristics studied considered both common and unique features for each concept.

#### 1.3.1 SOLAR PHOTOVOLTAIC (CR = 2)

A photovoltaic system with a concentration ratio of 2 (CR = 2) was taken as the baseline (Figure 1.3-1). This concept utilized high-efficiency GaAlAs solar cells sized to deliver 5 GW at the utility interface on the ground. This SPS concept was 2.05 km wide, approximately 1.4 km deep, and 26.7 km long. Reflective mirrors were employed to enhance the solar energy impinging on the solar cells. The solar cells operate at a temperature of 125°C and have an efficiency of 17.6 percent. (NOTE: Efficiency of the cells at AMO and 28°C is 20%). Overall efficiency was calculated to be 7.5 percent and an on-orbit weight,  $24.15 \times 10^6$  kg. Major trade operations that were considered included aspect ratios, flight modes, and reflector configuration designs.

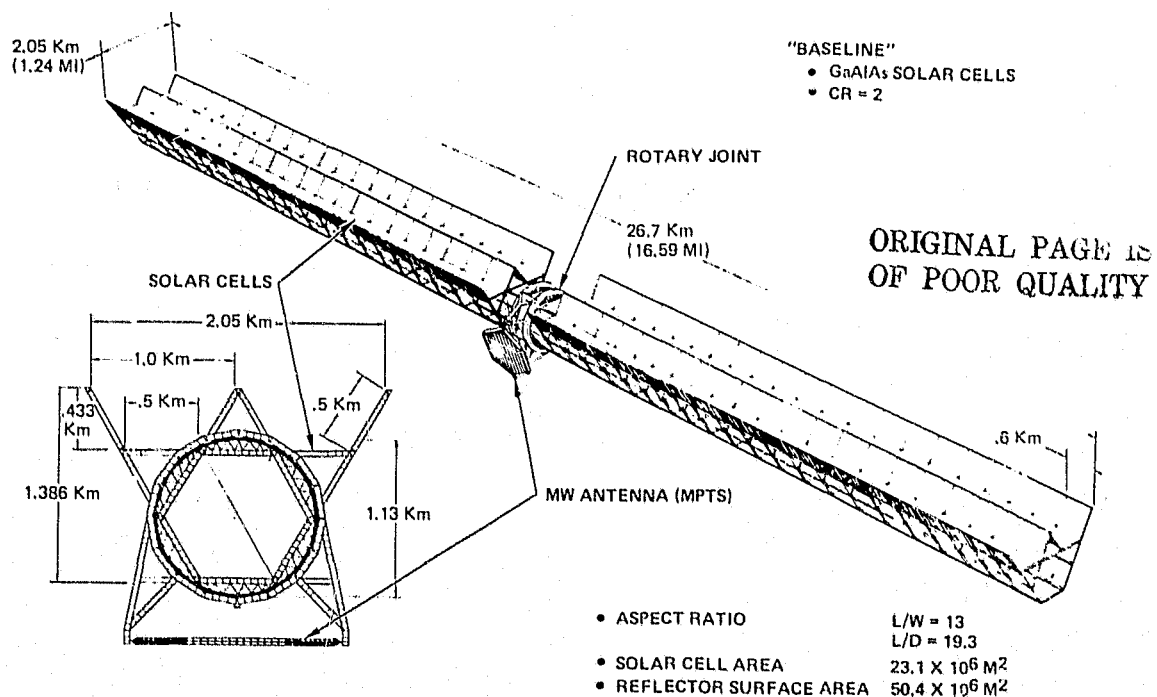


Figure 1.3-1. Solar Photovoltaic (5 GW), CR = 2



### 1.3.2 SOLAR PHOTOVOLTAIC (CR = 5)

This concept consisted of a trough configuration having a concentration ratio of 5, and again employed GaAlAs solar cells (Figure 1.3-2). The solar blankets were 35 m wide and mounted on triangular truss members. The reflectors consisted of two sides, each having a length of 305 m. This 305-m reflector was further broken down into five flat strips varying from approximately 56 to 65 m in width. The use of flat strips permits a simpler support structure and elimination of a three-dimensional figure control system. This system was sized to deliver rated power for misorientation angles of  $\pm 1$  degree. The concept consists of a total of six troughs, with the satellite 3.465 km wide and 25.7 km long. Trade options included selective bandpass filters, flight modes, and reflector configuration designs.

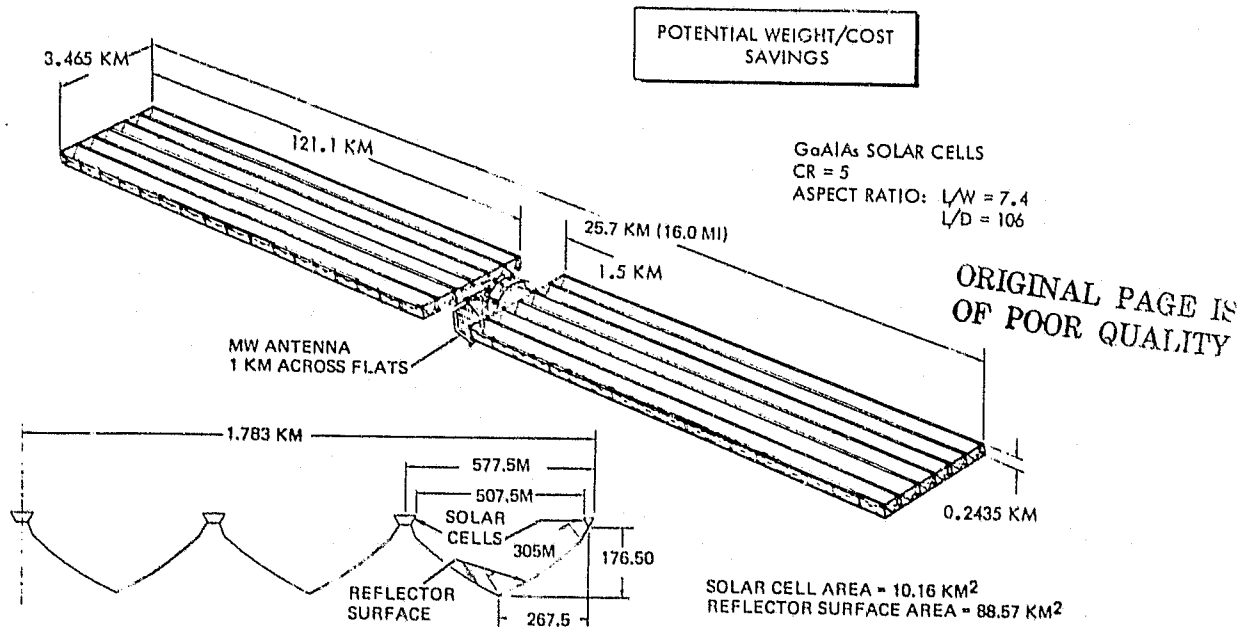


Figure 1.3-2. Solar Photovoltaic (5 GW), CR = 5

### 1.3.3 SOLAR PHOTOVOLTAIC (CR = 1)

The GaAlAs solar cell configuration for a concentration ratio of 1 had an overall length of 17.3 km and a width of 2.75 km (Figure 1.3-3). The weight was approximately  $29.3 \times 10^6$  kg. This configuration had the simplest design with the elimination of reflectors. A simpler design also resulted in simplified construction, transportation, operations, and maintenance requirements and support. System mass was competitive with concentrator configurations. Larger quantities of gallium were required than for the other systems and therefore high efficiency, thinner cell junction thickness, and cost and availability of gallium became more important. The trade options included aspect ratios, flight modes, use of silicon solar cells, varying solar cell efficiencies and thickness, choice of solar cell substrate materials, and solar array planforms.

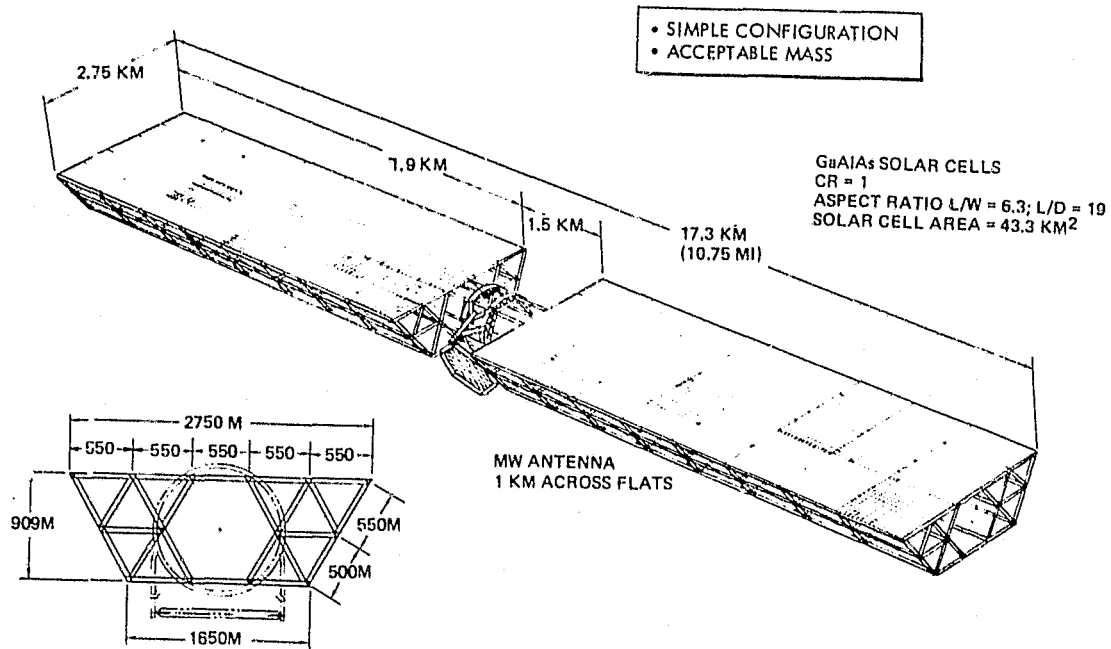


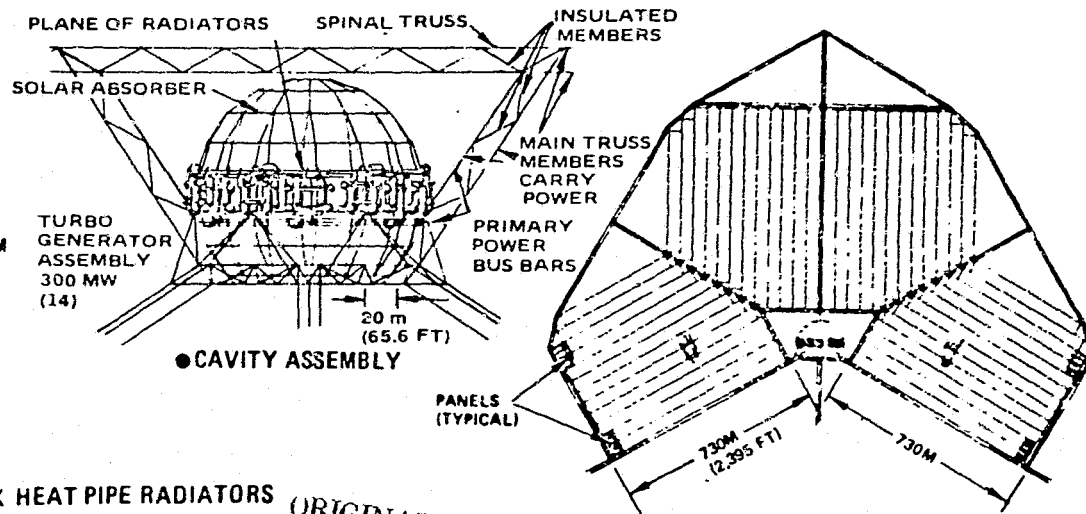
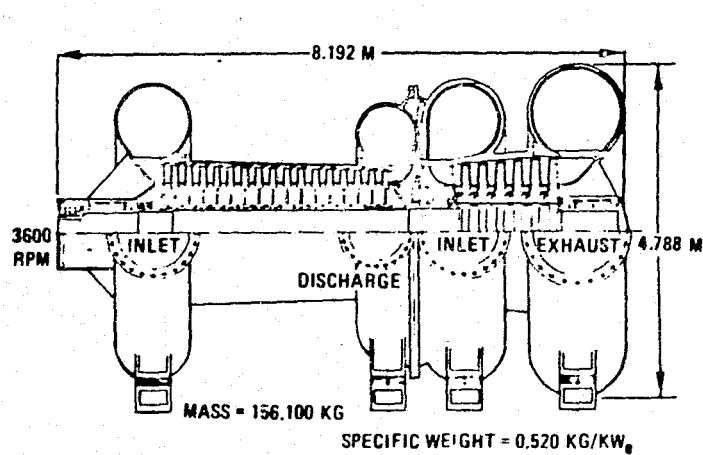
Figure 1.3-3. Solar Photovoltaic Non-Concentrated Concept (5 GW)

#### 1.3.4 SOLAR THERMAL (BOEING/BRAYTON)

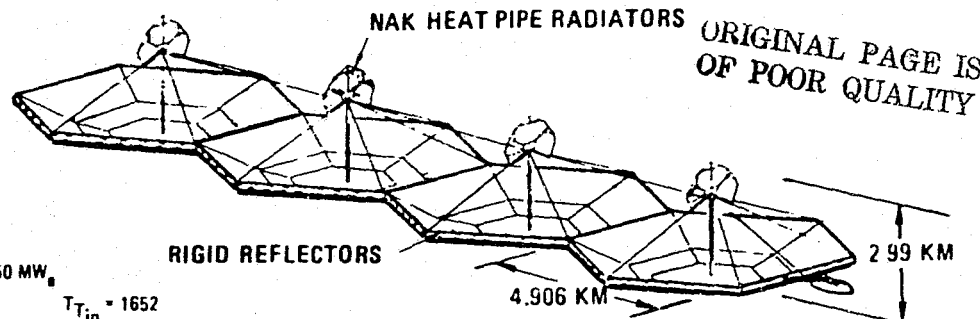
This design, shown in Figure 1.3-4, developed by Boeing under NASA/MSFC contract, was used as a reference concept for comparison with the Rockwell solar thermal approach. This concept was sized to deliver 10 GW at the utility interface and used a faceted concentrator, cavity absorber, and 300-MW Brayton turbo power modules. Ceramic heater tubes and turbine blades were provided to handle peak cycle temperatures of 1379°C (2500°F). Compressor inlet temperature was 128°C (261°F), and cycle efficiency was 45.4 percent. Trade options included lower turbine inlet temperatures.

#### 1.3.5 SOLAR THERMAL (RANKINE)

This design features two 2.5-GW modules, joined by a beam which located the transmitter at the center of gravity of the satellite (Figure 1.3-5). This permitted use of the rotary joint for mounting and orienting electrical thrusters for self-powered transfer from LEO to GEO. Inflatable concentrators with focusing control offered a 3:1 reduction in concentrator weight over a faceted design (including structure). A cesium Rankine system provided high cycle efficiency at modest turbine inlet temperatures (1038°C) without requiring ceramic components, and permitted use of lightweight open-disc absorber (i.e., lowered technology requirements). Trade options included layer power outputs, two antennas, cascaded bottoming cycle, higher and lower turbine inlet temperatures, different radiator fluids and heat pipe concepts, varying power conversion module sizes, momentum storage devices, and varying radiator temperatures.

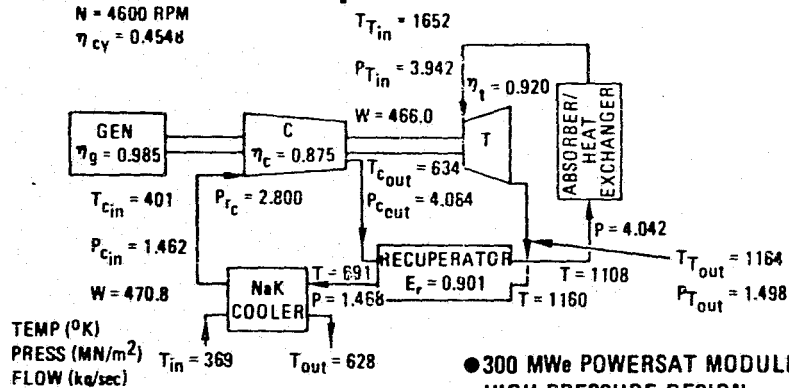


● SECOND GENERATION TURBOCOMPRESSOR L/O



● NaK HEAT PIPE RADIATOR

GENERATOR OUTPUT = 50 MW<sub>e</sub>  
 N = 4600 RPM  
 $\eta_{cy} = 0.4548$



● 300 MWe POWERSAT MODULE HIGH PRESSURE DESIGN

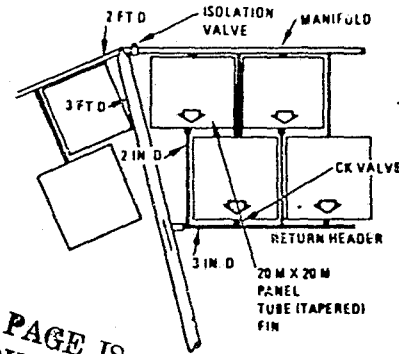
● FACETED CONCENTRATOR

Figure 1.3-4. Boeing/Brayton Reference Concept (10 GW)

SD 78-AP-0023-3

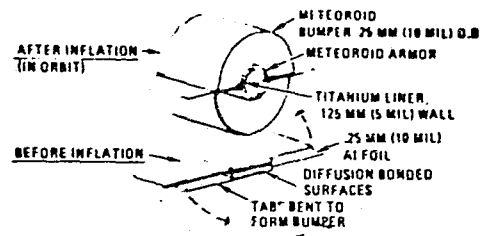
CONTAINS MAJOR DESIGN OPTIONS

RADIATOR PLUMBING DETAIL

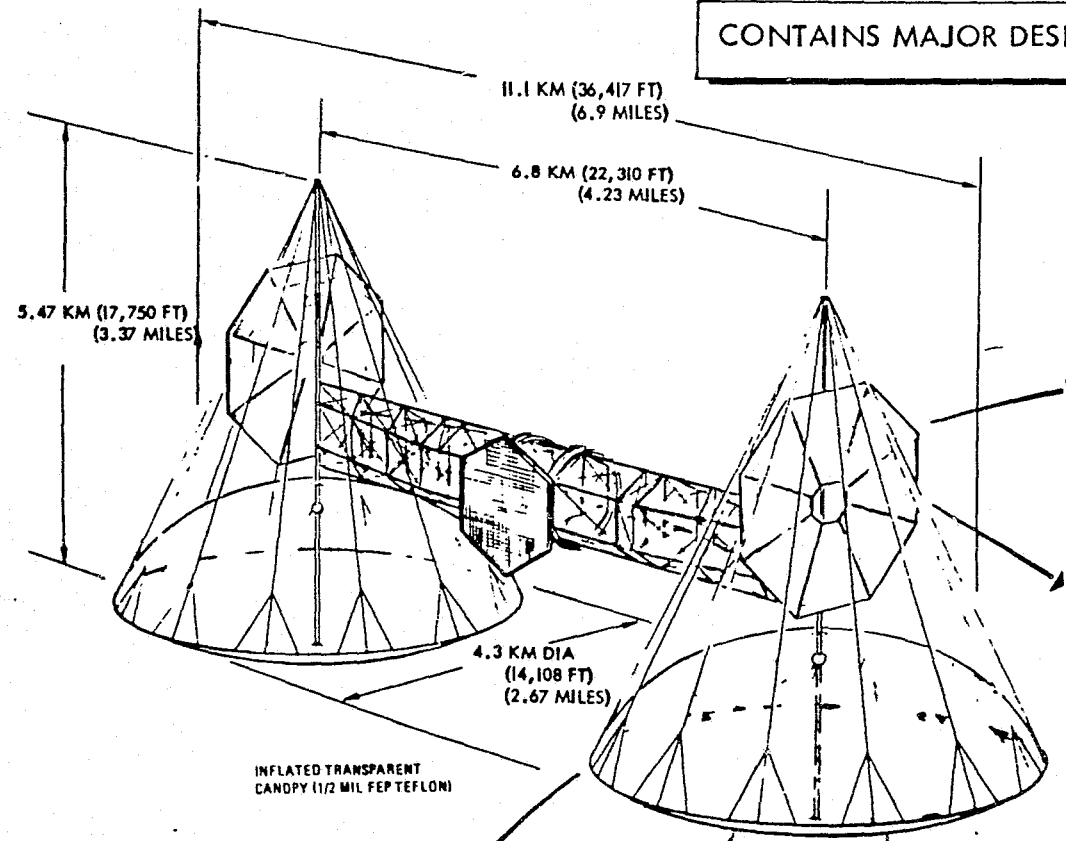


ORIGINAL PAGE IS OF POOR QUALITY

RADIATOR TUBE #1 IN DETAIL



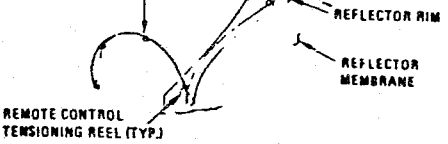
1-8



INFLATED TRANSPARENT CANOPY (1/2 MIL FEP TEFLON)

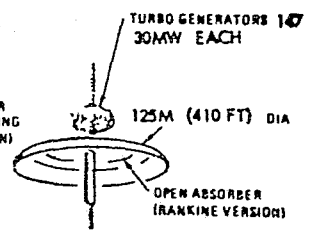
INFLATED PARABOLIC REFLECTOR (1/2 MIL METALLIZED KAPTON)

AUTOMATIC TENSIONING AND FOCUSING SYSTEM



REFLECTOR GORES ALIGNED IN "TEPEE" BEFORE SEALING (IN ORBIT)

GORE EDGES AFTER AUTOMATED SEALING (BEFORE INFLATION)



SD 78-AP-0023-3

Figure 1.3-5. Rankine Solar Thermal Concept (5 GW)



### 1.3.6 NUCLEAR (BRAYTON)

The nuclear concept was very compact compared to the solar thermal. This approach utilized a breeder pebble bed reactor and a Brayton thermal conversion cycle (Figure 1.3-6). The microwave antenna was separated from the reactor to avoid radiation damage and was located in front of the shadow shield. The concept was comprised of 26 reactor modules, each with its own radiator and power conversion unit. Trade options included Rankine power conversion and use of an intermediate coolant loop between reactor and power conversion.

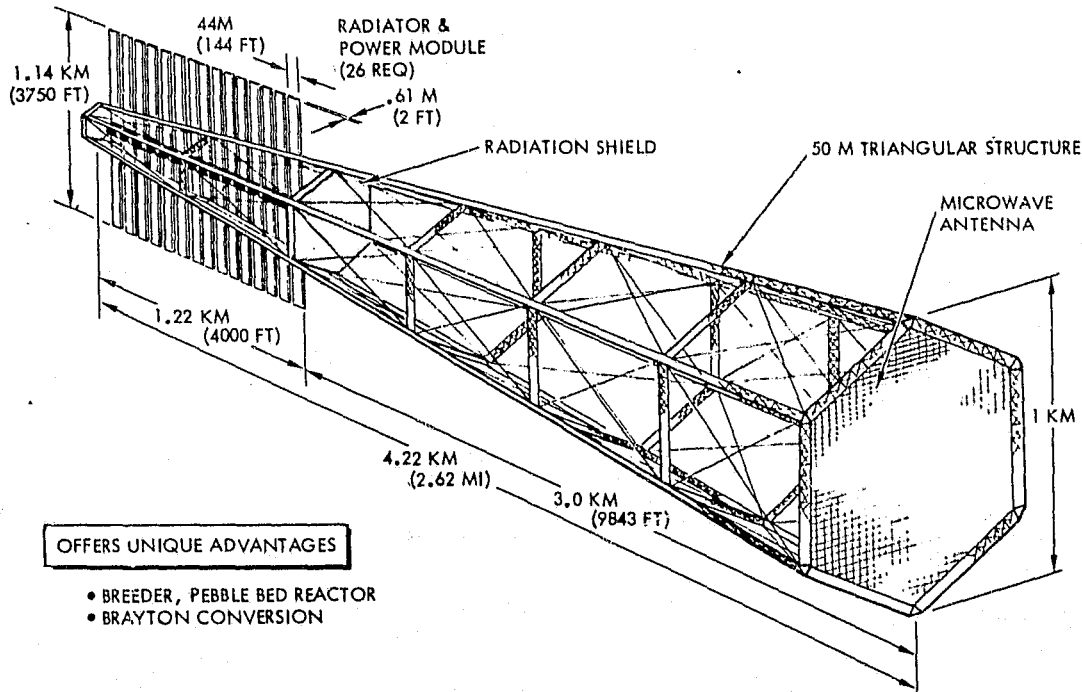


Figure 1.3-6. Nuclear-Powered Concept (5 GW)

These candidate concepts and trade studies, developed during the first 90 days of the study, formed the initial basis for concept evaluation and selection. Subsystem trade studies (described in Section 3.0) were conducted in parallel with LEO/GEO construction evaluation. The results of these efforts were iteratively integrated, resulting in the definition of candidate conceptual designs. Preliminary cost analyses of these concepts were conducted and preliminary evaluations made to determine which concepts should be selected for point design.



~~REPLACING PAGE BLANK NOT ENDS~~

## 2.0 TRADE SUMMARY

This section presents a summary of the results of the various trade studies and analyses conducted during the course of this study. Major emphasis was placed upon the overall factors leading to the selection of a power conversion system suitable for geosynchronous equatorial operation in the 1995-2025 time period. Other subsystem data (attitude control, structures, thermal, etc.) are introduced only when necessary to evaluate the power conversion approach being considered. Detailed summaries of the trades conducted within each subsystem discipline are presented in Section 3.0.

### 2.1 SOLAR PHOTOVOLTAICS

The major trade areas (other than the obvious selection of solar cell type) for the solar photovoltaic concepts included (1) determination of concentration ratios, (2) selection of flight mode, and (3) determination of geometry. All of these trades interact across several disciplines, and it is necessary to develop integrated data at the total system level (including both the satellite and rectenna for the flight mode trade).

#### 2.1.1 CONCENTRATION RATIO

The major parameters that influence the design of concentrator photovoltaic systems are identified: temperature, reflector shape, tensioning requirements, environmental degradation, and pointing requirements. Selective bandpass filters can reduce cell operating temperatures and increase performance. The effects of thermal self-annealing of the cells appear to occur at approximately 125°C (and higher) and may result in the preferred design operating temperature.

The configuration for CR = 5 results in cell operating temperatures of 182°C. The cell cover would have to be glass; however, the technology base for blanket temperature in excess of 182°C has been developed for the SPS array.

The use of concentrators and the design values for reflectivity, tensioning, degradation, and pointing accuracy of the membranes are needed for the on-orbit environment. Resolution of these issues is difficult because of conflicting data in the literature and lack of long-duration orbit data. This is identified as a critical area where experimental data are needed, because of the major impact on satellite configuration, weight, and cost.

#### 2.1.2 ORBIT SELECTION

The orbit planes considered for the SPS include the ecliptic, equatorial, and a 7.3-degree inclined orbit which eliminates the north-south stationkeeping  $\Delta V$  requirement. The ecliptic plane has the advantage that perfect collector pointing can be achieved in a "wings level" (Y-POP) attitude, which minimizes the gravity-gradient induced RCS propellant consumptions. This orbit results



in a daily earth eclipse period. The equatorial plane produces photovoltaic collector losses up to 8 percent for the wings-level attitude. The trade study results indicate the *equatorial orbit* to be preferred—primarily due to the dominant cost impact of the increased rectenna sizes for the ecliptic and 7.3-degree inclined orbits.

### 2.1.3 ATTITUDE ORIENTATION

The three attitude orientations illustrated in Figure 2.1-1 have been evaluated in the ACSS trade studies. The wings-level attitude (Y perpendicular to orbit plane, X in orbit plane) is preferred over the Z-sun, X-IOP attitude because of the large savings in RCS propellant resupply. The X-sun, X-IOP attitude places the long axis of the vehicle in the orbit plane. This orientation requires two microwave antennas in order to simultaneously prevent interference of the microwave beam with the spacecraft structure and obtain acceptable solar pressure torque balancing. The requirement for two antennas and the double sizing of the spacecraft results in additional complexity and power distribution mass penalties. On this basis, the Y-POP, X-IOP is the preferred orientation.

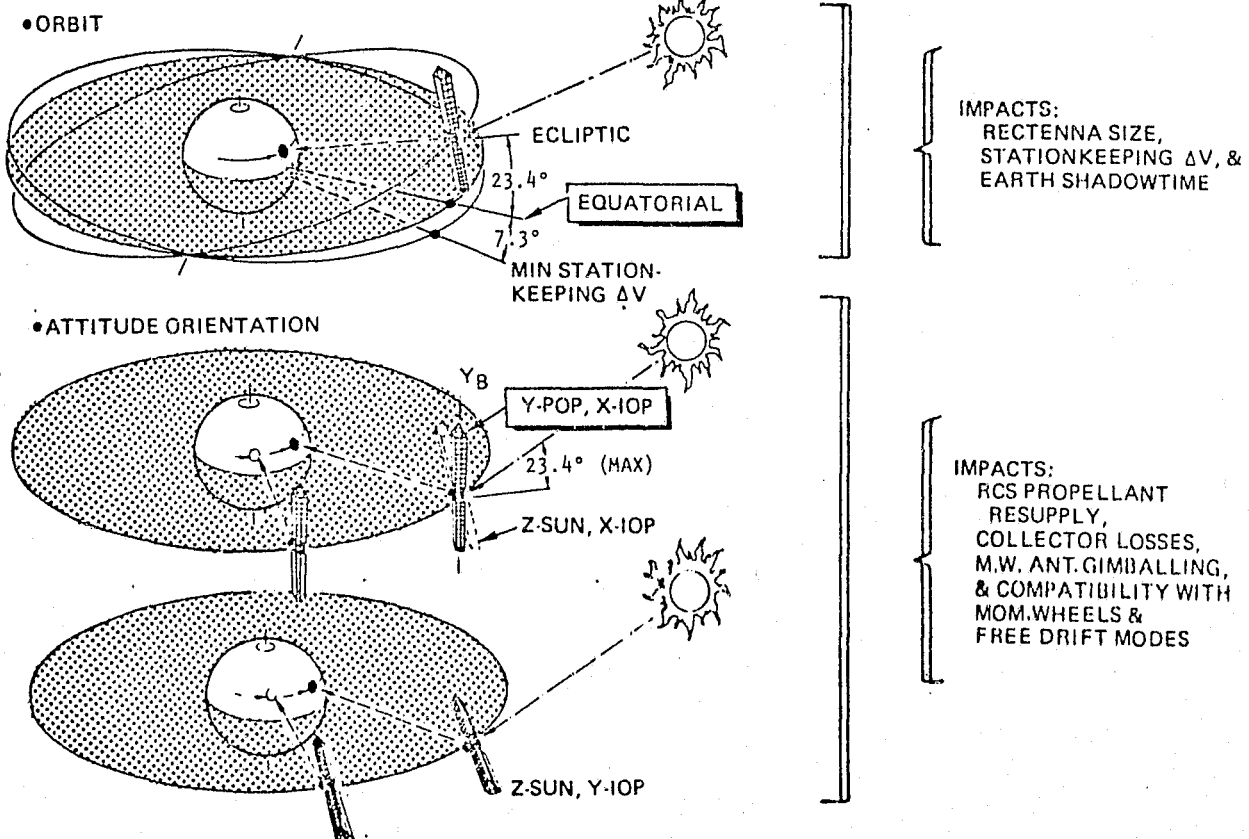


Figure 2.1-1. Selection of Flight Conditions

### 2.1.4 ARRAY GEOMETRY DETERMINATION

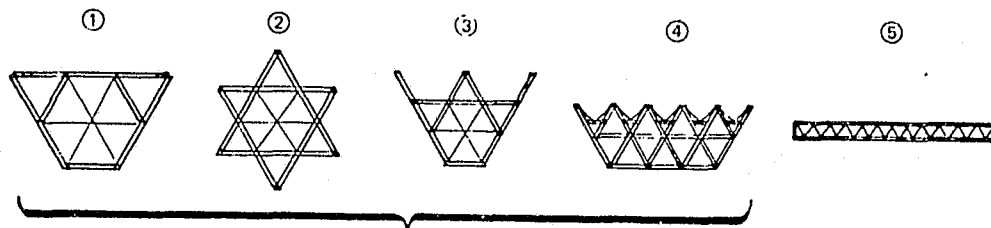
The selection of a photovoltaic array shape or geometry is dependent on a number of factors or considerations. Figure 2.1-2 lists these major considerations and the impact they have on the geometry. The figure also depicts





the configuration cross-sections which have received major emphasis during the course of the study. Each configuration is assigned a code number. For each consideration listed, those configurations which best resolve (or minimize) the associated impact are indicated by their code number. For example, Configurations 1, 2, and 3 will, by nature of their length-to-depth ratios, have relatively high natural frequencies—thus minimizing or eliminating problems associated with attitude control system/structure coupling.

• GEOMETRY CONSIDERATIONS		• IMPACTS	
①②③	STRUCTURE/ACS COUPLING _____	LENGTH/DEPTH RATIO- $MAX_f$	
①②	PROPELLANT CONSUMPTION _____	X SECTIONAL MASS DIST.	
⑤	PROJECTED AREA REOMTS _____	LENGTH/WIDTH RATIO	
①②③④	ENVIRONMENT _____	SIZE, SHAPE & MASS	
	• PHYSICAL	• SECTION PROPERTIES	
	• THERMAL	• MATLS & COATINGS	
③④	CONCENTRATION RATIO _____	X-SECTION SHAPE	
②	LEO CONSTRUCTION _____	LENGTH/DEPTH RATIO- $MAX_f$	
①	CONSTRUCTION COMPATIBILITY _____	X-SECTION COMPLEXITY	
⑤	WIRING _____	PLANAR AREA SHAPING	
①	STRUCTURE MASS	OVERALL SYSTEM MASS	



CONTENDERS DEPENDING ON:  
CONSTRUCTION SITE & CONCENTRATION RATIO

Figure 2.1-2. Array Geometry Determination

Since no configuration is an obvious winner, those indicated were considered contenders and were subjected to more rigorous analysis. The current configurations appear to satisfy most of the driving requirements.

### 2.1.5 SILICON VERSUS GaAlAs SOLAR CELLS

Silicon (Si) and GaAlAs solar cells are compared in Figure 2.1-3. Efficiency as a function of cell thickness shows that a GaAlAs cell requires only a 5- $\mu$ m thickness for optimum efficiency as compared to 100  $\mu$ m for Si cells. The GaAlAs is twice as dense as Si, but because of the thinner cell the basic material required for the cell junction has the potential of being one-fifth the weight of Si.

The amount of gallium required is shown as a function of the substrate material and concentration ratio. The preferred substrate is  $Al_2O_3$ , which is an existing, commercially available, semiconductor grade, sapphire material.

Based on the existing studies, and using the  $Al_2O_3$  substrate and an 80-percent recovery from bauxite, there is sufficient Ga for the SPS program. Recovery from flyash, seawater, or new deposits would increase the availability of gallium. There is no problem with availability of arsenic.

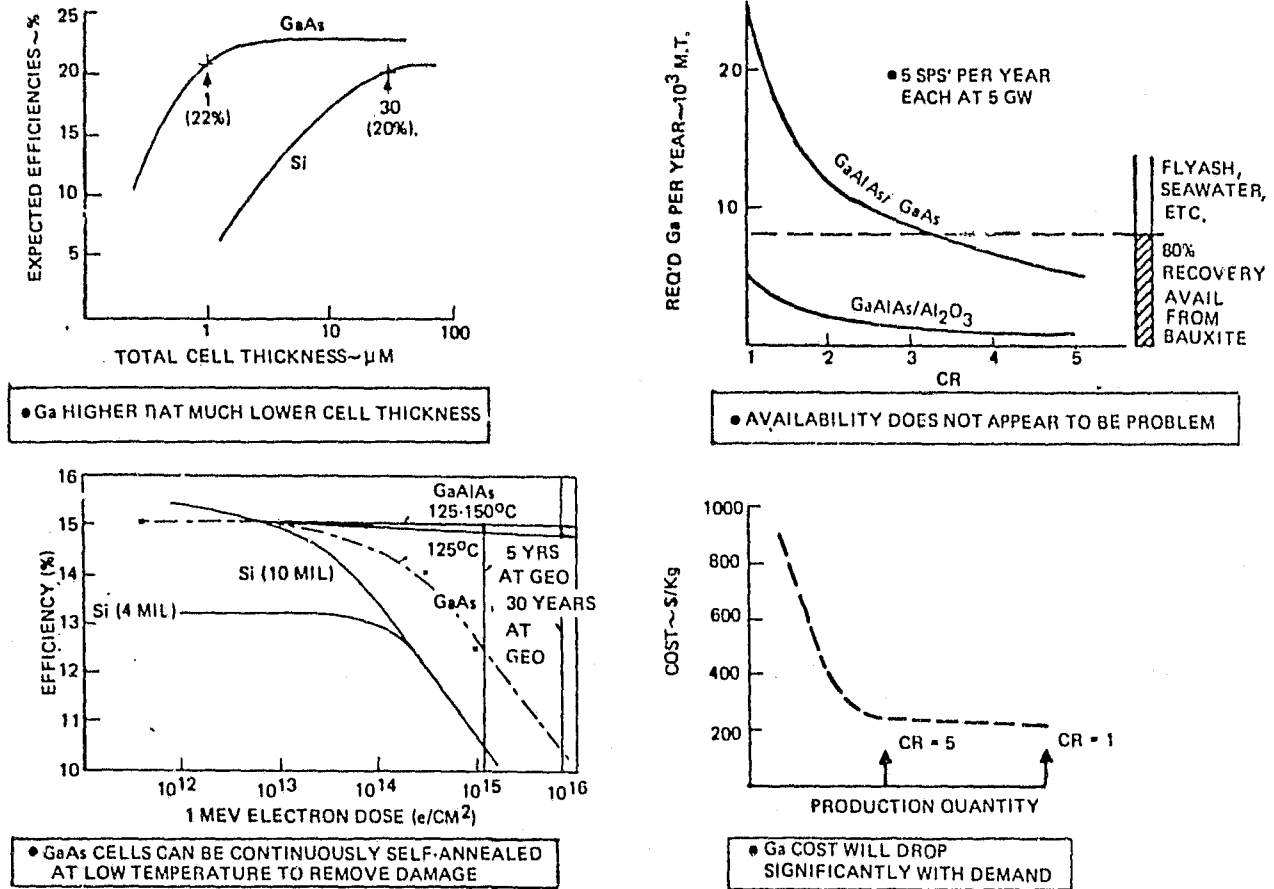


Figure 2.1-3. Silicon Vs. GaAlAs Solar Cells

The efficiency of solar cells as a function of radiation fluence is illustrated in Figure 2.1-3. The GaAlAs cell is approximately an order of magnitude more resistant to the radiation environment than Si cells. Also, preliminary testing of GaAlAs cells has shown that some of the cells tested recovered from radiation damage when the cells were heated at approximately 125°C or above. Additional work is being performed on the thermal annealing of GaAlAs cells to verify the data and to determine the major variables that influence thermal annealing.

The present cost of gallium is approximately \$500/kg. Figure 2.1-3 shows, based on a past history of cost and production curves, that as demand increases the cost decreases. In the study, the \$500/kg cost was used; however, the potential for a significant cost reduction exists and would reduce the overall cost of the GaAlAs photovoltaic systems.

#### 2.1.6 SYSTEM CHARACTERISTICS (GEO ORBIT CONSTRUCTION)

As a result of the trade studies and system integration, the major solar photovoltaic concepts characteristics, shown in Figure 2.1-4, were determined. The CR = 1 (non-concentrated) concept has GaAlAs solar cells (with silicon cells as an alternative). The concentrated CR = 2 and 5) concepts both have GaAlAs solar cells. All concepts use an equatorial geosynchronous orbit

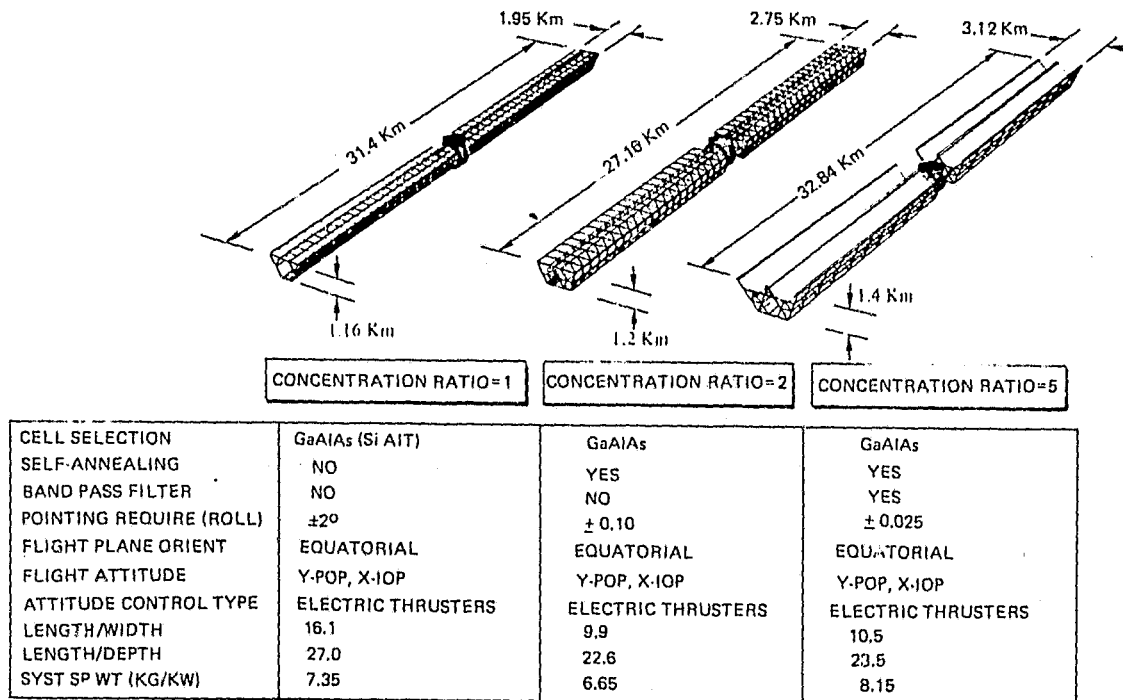


Figure 2.1-4. Solar Photovoltaic System Characteristics  
(Geosynchronous Orbit Construction)

plane. Because of the high temperatures on the CR = 5 cells, it is assumed that they can be continuously self-annealed to repair natural radiation damage.

Basic solar array sizing for CR = 1, CR = 2, and CR = 5 concepts are shown in Table 2.1-1 and were used in the overall evaluations. Projected area (intercepted solar energy) is obtained from total energy requirements and a solar constant, 1353 W/m<sup>2</sup>. Energy onto the cells is total intercepted area, reduced by actual reflectivity values. Solar cell area is calculated from performance analysis. For example, at CR = 5, the solar cell output is 918 W/m<sup>2</sup> after reducing initial outputs of 1470 W/m<sup>2</sup> by factoring array design losses, seasonal variation in solar output, temperature losses, and environmental degradation. Based on an array output requirement of 9.56 GW, the solar cell area requirement is 10.4 × 10<sup>6</sup> m<sup>2</sup>.

The SPS solar photovoltaic weight summary is presented in Table 2.1-2. Only slight weight difference is indicated between CR = 1 and CR = 5; however, a significant weight savings appears at CR = 2. These comparisons were used in overall evaluation at the mid-point of the study. Revised weight statements have resulted from detailed design analysis during the second half of study, as shown in subsequent sections of this report.



Table 2.1-1. Solar Array Sizing Models

	CR = 5 (M <sub>0A</sub> = 4.7%) CR <sub>g</sub> = 7.55	CR = 2 (M <sub>0A</sub> = 6.2%) CR <sub>g</sub> = 2.58	CR = 1 (M <sub>0A</sub> = 7.5%)
INTERCEPTED (PROJECTED) AREA	78.5 X 10 <sup>6</sup> M <sup>2</sup> (106.4 GW)	59.63 X 10 <sup>6</sup> M <sup>2</sup> (80.86 GW)	48.9 X 10 <sup>6</sup> M <sup>2</sup> (66.3 GW)
ENERGY BOL	95.9 GW (CR = 6.8)*	75.7 (CR = 2.41)**	66.3
ONTO CELLS EOL	76.5 GW (CR = 5.42)*	67.0 (CR = 2.22)**	66.3
CELL AREA	10.4 X 10 <sup>6</sup> M <sup>2</sup>	23.2 X 10 <sup>6</sup> M <sup>2</sup>	48.9 X 10 <sup>6</sup> M <sup>2</sup>
<u>EOL PERFORMANCE (FACTORS)</u>			
CELL η (T)	.163 (176C)	.19 (58C)	.188 (68C TOP) (83C BOTTOM)
ARRAY DESIGN ENVIRON.	.876 } .11 (76.5 GW) = 8.4 GW	.876 } .125 (67.0 GW) = 8.4 GW	.876 } .127 (66.3 GW) = 8.4 GW
PWR DISTR. ON ARRAY	.96	.92	.92
SEASONAL VARIATIONS	.88	.90	.92
	.91	.91	.91
	* (CR = 1) 14.1 GW		
	** (CR = 1) 31.4 GW		

Table 2.1-2. Solar Voltaic Mass Summary (GaAlAs Solar Cells)

CONCENTRATION RATIO	CR = 5 10 <sup>6</sup> KG	CR = 2 10 <sup>6</sup> KG	CR = 1 10 <sup>6</sup> KG	GROWTH %
COLLECTOR ARRAY (NON ROT.)	(18,363)	(15,465)		(38.3)
PRIM./SEC. STRUCT./MECH.	9,306	3,993	2,805	25.0
ATTITUDE CONTROL	.300	0.212	.375	30.0
SOLAR CELLS	3,297	5,990	12,343	24.7
REFLECTORS	2,182	2,052	N/A	15.0
POWER CONDIT.	.387	.387	.387	50.0
WIRE HARNESS/SLIP RING	2,891	2,891	2,469	97.0
ANTENNA (ROTATING)	(9,794)	9,794	9,794	(23.1)
PRIM./SEC. STRUCT./MECH.	.268			25.0
COOLING	.200			50.0
PWR CONVERTERS	5,690			20.0
WIRING/SLIP RING	.096	SAME	SAME	94.0
WAVEGUIDES	3,540			20.0
IMS EQMT/CABLING	.240	.240	.240	88.0
PROPELLANT/YEAR	.100	.100	.100	0
SUBTOTAL SATELLITE SYST.	28.497	25.599	28.513	
GROWTH ALLOWANCE	8.882	8.115	8.766	31.2
TOTAL SATELLITE SYST.	37.379	33.714	37.279	

COMPARABLE SILICON CR = 1  
 WEIGHT = 48,589 X 10<sup>6</sup> KG



## 2.2 SOLAR THERMAL

The major trade areas for the solar thermal concepts included (1) concentrator concept (multi-faceted vs. inflatable), (2) open vs. cavity absorber, (3) power conversion concept, and (4) heat rejection.

### 2.2.1 CONCENTRATOR CONCEPT

The inflatable design showed a 75 percent weight saving over a faceted, rigid design but requires a greater advance in the state of the art. Efficiency for the faceted design is less because of area lost between the facets. The inflatable FEP Teflon canopy will probably have to be replaced in service (no power interruption) after 15 years, due to UV degradation. Makeup gas requirements are small. Open questions are film-tensioning requirements for good reflectivity, and assembly tolerances for the inflatable design. Sheldahl, Inc., has supported this analysis and provided film samples for testing.

### 2.2.2 ABSORBER

The Brayton cycle requires more surface area in the absorber because of the low heat transfer coefficient of gas (versus boiling liquid). This necessitates a cavity-type absorber design for the Brayton concept. A Rankine cycle can utilize an open, disc-type absorber with reflecting skirts. This results in a significant weight savings for the Rankine concept. The turbine/generator modules can be mounted on the insulated backside of each absorber.

### 2.2.3 POWER CONVERSION

At comparable cycle temperatures, a non-superheated Rankine system is substantially more efficient than a Brayton, as shown in Figure 2.2-1. This is chiefly due to lower pumping power requirements, which are ~2% of turbine

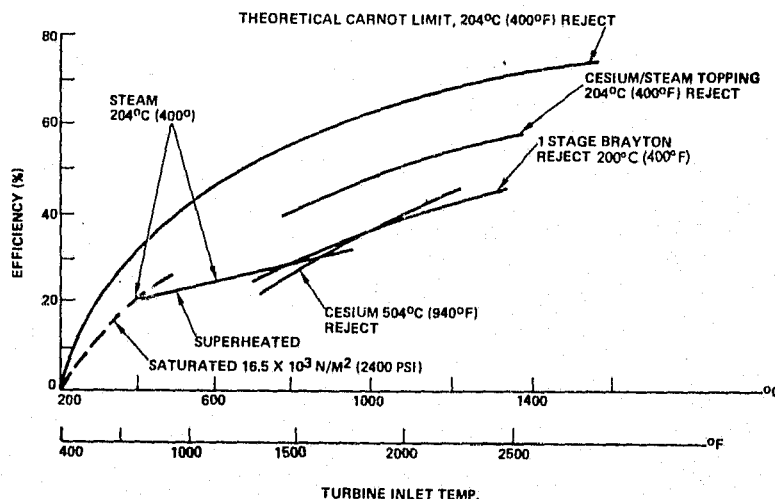


Figure 2.2-1. Dynamic Conversion Efficiencies



output for the Rankine cycle as compared to ~67% for the Brayton. This permits the Rankine cycle to compete in performance—with much lower inlet temperature and material requirements.

Three Rankine systems were compared (Table 2.2-1) at a common inlet temperature of 1038°C (1900°F) and a condensing temperature of 504°C (940°F), except for the cesium/steam binary cycle which condenses cesium at 593°C (1100°F) and steam at 204°C (400°F) in the radiator, thereby achieving the highest cycle efficiency and lowest specific mass. The Brayton system is heavier compared to the cesium/steam system despite its higher inlet temperature of 1379°C (2514°F) which requires ceramic absorbers, plumbing, and turbine blades. Drawbacks to the Rankine system are the problems of two-phase flow stability and turbine erosion. Standard, proven methods are available for handling these problems.

Table 2.2-1. Power Conversion Concept Comparisons

WORKING FLUID	BRAYTON HELIUM/XENON	POTASSIUM	RANKINE CESIUM	CESIUM/STEAM
TURBINE INLET TEMP (°C)	1379	1038	1038	1038
CYCLE EFFICIENCY (%)	45	36	36	47
TURBINE PRESSURE RATIO	2.35	40.6	85.5	29.97
COMPRESSOR/PUMP LEF %	87.5	60	60	60
COMPRESSOR INLET TEMP °C	127	-	-	-
CONDENSING TEMP	-	504	504	593/204
RADIATOR (CONDENSING, TUBE FIN)	COMPOUND STEAM	DIPHENYL	DIPHENYL	STEAM
EFFECTIVE TEMP C	204	343	343	204
TOTAL RADIATOR AREA KM <sup>2</sup>	2.35	1.35	1.35	2.2
POWER LOOP WT KG/KW	1.3	3.37	1.47	0.65
RADIATOR WEIGHT KG/KW	2.3	2.62	2.62	1.95
SOLAR COLLECT/ABSORBER WT KG/KW	0.895	.335	.335	0.256

#### 2.2.4 HEAT REJECTION

The majority of space experience related to active radiator systems has been devoted to tube/fin and heat pipe systems. In the late 1960's, a number of studies were devoted to zero-g application of space radiators using condensing fluids. Fluids evaluated included potassium, mercury, Dowtherm A, and Refrigerant 12 (R-12). Although testing has been restricted to simulated zero-g drop towers and aircraft flying Keplerian trajectories, the limited data available suggest that condensing systems are feasible for space operation. Consequently, in developing radiator concepts, both heat pipe and condensing fluid systems have been considered although, for purposes of simplicity, condensing liquid-metals have not been included.

Analysis was conducted to compare heat pipes and condensing tubes for the active thermal control steam radiator system. Major conclusions of this trade were (1) selection tends to reduce to a comparison of a highly complex and extensive valving system with a network requiring advanced technology heat pipes, and (2) the maintenance-free lifetime requirements that are a substantial factor in defining optimal heat rejection design. As a result of this investigation the heat pipe approach was selected because of its comparative simplicity, flexibility for varying lifetime operation, and demonstrated advanced technology development potential.



### 2.2.5 SYSTEM CHARACTERISTICS

The two-module, 5-GW SPS design features articulated inflatable collectors which track the seasonal excursions of the sun without incurring attitude control propellant penalties. The rotary joint is located at the satellite c.g. by means of an offset structure, to facilitate LEO/GEO transfer with electrical thrusters mounted on the rotary joint. The Boeing 10-GW, 16-module SPS uses faceted collectors aimed at a cavity absorber whose aperture is enlarged with a compound parabolic reflector skirt. Values shown in Table 2.2-2 are for the Rockwell two-module design. The Rankine cesium/steam system has the lowest specific mass of the four cases studied.

Table 2.2-2. Solar Thermal System Characteristics

	BRAYTON	RANKINE	RANKINE	RANKINE
WORKING FLUID	HELIUM/XENON	CESIUM	CESIUM/STEAM	POTASSIUM
AREA (REFLECTOR) KM <sup>2</sup>	24	30.32	23	30.32
η <sub>OA</sub> %	15	12	16	12
CYCLE η %	45	36	47	36
TURBINE INLET TEMP <sup>o</sup> C	1379	1038	1038	1038
GENERATOR SIZE MW	30	30	30	30
SAT. ORIENT	Y-POP, X-10P	Y POP, X 10P	Y POP, X 10P	Y POP, X 10P
RADIATOR AREA KM <sup>2</sup>	2.35	1.35	2.2	1.35
SYSTEM SP. WT. KG/KW	8.65	8.35	6.9	11.0

ORIGINAL PAGE IS  
OF POOR QUALITY

### 2.3 NUCLEAR

The major trade areas for the nuclear concept included (1) approach, (2) fuel processing, and (3) power conversion concept.

Previous study (Boeing, MSFC contract) had concluded that a nuclear-powered SPS was a viable option. The available material for breeder reactor fuel represents a large energy reserve which cannot be ignored. The objections to terrestrial siting of nuclear breeders encompass channeling bred Pu-238 into nuclear weapons, problems of radioactive waste disposal, and hazards from nuclear reactor operations. Operation of nuclear breeder reactors in geosynchronous orbit would eliminate these siting objections. Also, the nuclear SPS option offers unique operational advantages over the solar-powered SPS.

#### 2.3.1 APPROACH

Study results concluded that the nuclear-powered SPS must be a breeder due to the limited availability of the natural occurring U-235 fissile material. It is estimated that there will be  $615 \times 10^{18}$  Btu energy available from breeding Pu-239 from non-fissile Pu-238; this exceeds the U.S. known coal reserves by a factor of 30.



A high reactor core temperature, 1660 K (2500°F), is required to obtain good power conversion efficiencies with the Brayton cycle consistent with minimum radiator areas. These high temperatures are also compatible with advanced Rankine power conversion systems using liquid-metals as a working fluid.

Fuel processing must be integrated with the reactor power module to achieve modularity. The selected design was a pebble bed fast reactor, cooled by helium gas and fueled by plutonium with U-238 as the breeding material.

### 2.3.2 FUEL PROCESSING

The fuel elements are 1/4-inch spheres consisting of the mixed oxide of uranium and plutonium ( $UO_2/PuO_2$ ), carbon-coated to prevent the escape of fission products.

Spent fuel is recycled out of the reactor and reprocessed by either the Airox or the Modified Purex process, depending on the amount of fission product poisons to be removed from the fuel prior to refabrication (Figure 2.3-1). The Airox process used a series of oxidation-reduction heating cycles, causing the fuel to swell and crack, thereby releasing only the gaseous fission products. The final reduction reaction leaves the fuel in a powdered form, still containing remaining fission product solids and inerts. The mass proceeds to refabrication, where it is mixed with resupply  $UO_2$ , formed into carbon-coated pellets, and recycled back to the reactor.

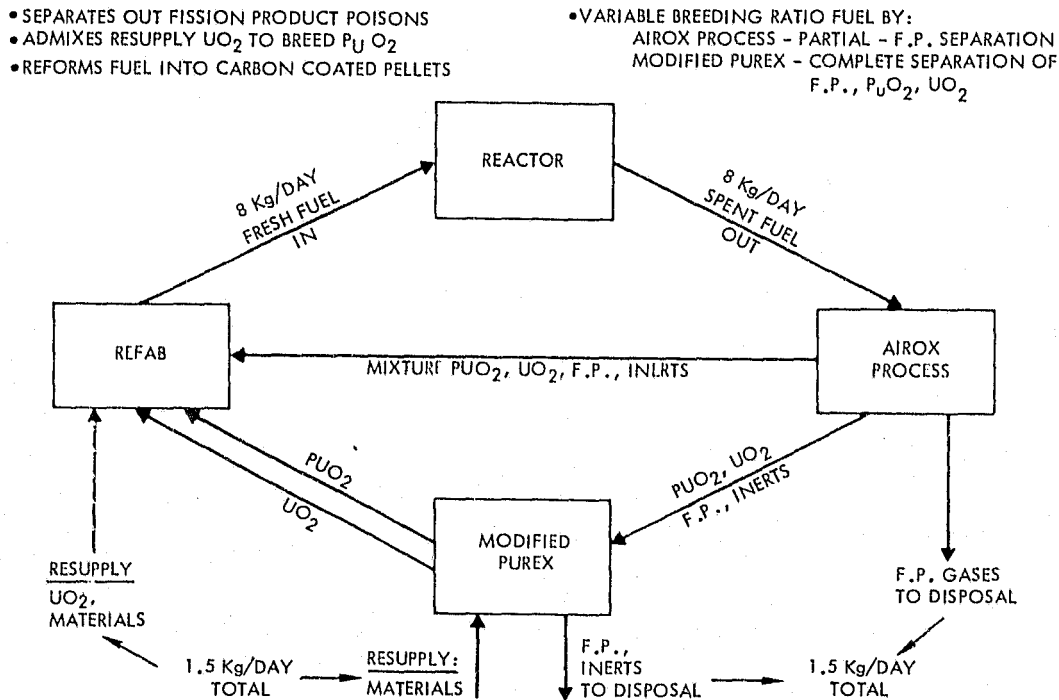


Figure 2.3-1. Fuel Management Schematic



Depending upon the buildup of fission product poisons and inerts in the reactor core, the fuel mixture leaving the Airox process may also be treated in the Modified Purex process. The latter consists of a series of counterflow solvent extraction columns. The fuel mixture is first dissolved in aqueous  $\text{HNO}_3$  and the fission products, inerts, and higher oxides of Pu and U are separated out successively with a counterflow organic stream of bri-butyle phosphates. The resultant separated  $\text{PuO}_2$  and  $\text{NO}_2$  are then sent to Refabrication. The Refabrication process mixes the processed fuel with resupply  $\text{UO}_2$ , and forms pellets which are sintered and then carbon-coated. The resulting pellets are then returned to the reactor.

### 2.3.3 POWER CONVERSION CONCEPT

Brayton power conversion was found best for a helium-cooled reactor concept. A direct closed cycle helium loop can be used, thus eliminating complex intermediate heat exchangers. Also by changing gas pressure and reactor power, electrical output can be modulated to compensate for nuclear power generating module failure or changing electrical power demand. Gas-cooled reactors have been operating in Europe since 1956, with the first U.S. electrical power generation with helium-cooled reactors taking place in 1967. The Brayton cycle is an advanced state of development. Millions of operating-hours experience are available on aircraft gas turbines. NASA/Lewis has extensive test experience of a closed Brayton cycle development program, and European fossil-fueled closed Brayton systems have thousands of hours of data back to the 1950's.

### 2.3.4 SYSTEM CHARACTERISTICS

A block diagram of the nuclear power generation system is shown in Figure 2.3-2. Heat is removed from the reactor by the helium working fluid of the closed Brayton cycle. High-temperature/high-pressure He exits the reactor to a cyclone separator for removal of entrained fuel particles, and

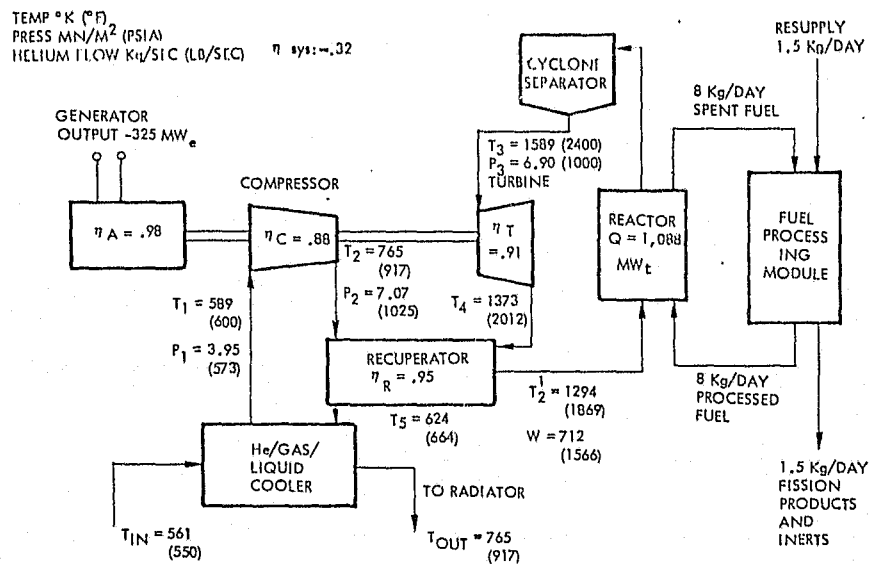


Figure 2.3-2. Nuclear Power Generation Block Diagram



then passes to the Brayton cycle turbine, where it undergoes an expansion with a subsequent drop in pressure and temperature. The mechanical working fluid extracted from the gas is used to operate both the compressor and generator which are mounted on the same shaft. The He passes to a recuperator for exchange of heat with the steam leaving the compressor. It then passes to the cooler where it is further cooled by the radiator coolant. Leaving the cooler, the He stream is fed to the compressor where it undergoes an increase in pressure and temperature, and then passes successively to the recuperator and reactor to start another cycle. The reactor outlet gas temperature is 1589 K at a pressure of 6.9 MN/m<sup>2</sup>, the entering temperature T<sub>1/2</sub> is 1294 K, and the compressor ratio is approximately 2.0. The system efficiency for the conditions shown was computed to be 32 percent.

Table 2.3-1 shows the nuclear reactor concept mass statement. A comparison is also shown between solar photovoltaic, solar thermal, and nuclear concepts. Considerable potential for mass reduction exists for the nuclear concept. It was felt that an optimization of the radiator design could potentially reduce this by 5.78x10<sup>6</sup> kg (i.e., 20.73x10<sup>6</sup> kg for reactor/power conversion/radiator reduces to 14.95x10<sup>6</sup> kg). Also, an approach utilizing a gaseous core reactor/MHD could potentially reduce the subtotal by 18.74x10<sup>6</sup> kg. Both of these differences would require major study.

Table 2.3-1. Nuclear Reactor Concept Mass Summary

	(10 <sup>6</sup> KG)	GROWTH %
PRIMARY STRUCTURE	0.361	25.0
SEC. STRUCT.	1.112	25.0
AITITUDE CONTROL	0.20	30.0
SHEILDING	0.54	30.0
REACTORS (26)	2.06	30.0
FUEL PROCESSING	1.01	30.0
TURBO-EQUIPMENT	3.34	30.0
GENERATORS	1.83	30.0
RADIATORS	11.94	30.0
POWER CONDIT.	1.839	50.0
WIRE HARDNESS	0.60	100
ANTENNA	9.88	23.1
IMS EQUIP.	0.061	50.0
IMS CABLING ITS	0.179	100
PROPELLANT/YEAR	0.10	0
SUBTOTAL	35.052	-
GROWTH ALLOWANCE	10.411	29.6
TOTAL SATELLITE SYST.	45.463	

CONCEPT WEIGHT COMPARISONS			
POWER CONVERSION CONCEPT	BASE WEIGHT (10 <sup>6</sup> KG)	GROWTH (%)	TOTAL WEIGHT (10 <sup>6</sup> KG)
CR = 1	28.513	30.7	37.279
2	25.599	30.0	33.714
5	28.497	31.2	37.379
RANKINE CS/STEAM	26.386	31.2	34.605
NUCLEAR	35.056	29.6	45.465

\*GASEOUS CORE REACTOR/MHD COULD POTENTIALLY REDUCE THIS TO 1.99 X 10<sup>6</sup> KG - REFERENCE: 8TH IECEC PAPER 739018, 1973

RADIATOR OPTIMIZATION COULD POTENTIALLY REDUCE THIS TO 14.95 X 10<sup>6</sup> KG - CONDENSING STEAM RADIATOR (LOWER TEMPERATURE)



## 2.4 CONCEPT SUMMARY

The following sections describe concept factors that led to point design selection.

### 2.4.1 CRITERIA

A set of criteria for eventual selection of SPS concepts has been developed to guide the study. Not all the the criteria shown in Table 2.4-1 are of equal importance as concept differentiators. Those that are the most significant differentiators are shown with an asterisk. Additionally, the key study issues are addressed in these criteria (items having a key next to them) if they serve as concept differentiators. For example, the issues related to the microwave power portion of the system are common to all systems and, therefore, are not evaluated at this overall system level. Not all of these criteria have been pursued in depth. A number of examples will be given to demonstrate implementation of the criteria to arrive at preferred concept selections.

Table 2.4-1. Concepts Selection Criteria

<p><u>COST</u></p> <ul style="list-style-type: none"> <li>● DDT&amp;E</li> <li>● INITIAL CAPITAL INVESTMENT*</li> <li>● REPLACEMENT CAPITAL INVESTMENT</li> <li>● OPERATIONS AND MAINTENANCE*</li> <li>● COST SENSITIVITY               <ul style="list-style-type: none"> <li>- TO SATELLITE BUILD-UP RATE</li> <li>- TO TRANSPORTATION COSTS</li> <li>- TO CRITICAL SUBSYSTEM COSTS*</li> </ul> </li> </ul> <p><u>TECHNOLOGY REQUIREMENTS</u></p> <ul style="list-style-type: none"> <li>● CRITICAL DEVELOPMENTS (NUMBER &amp; TYPE)*</li> <li>● VERIFICATION TESTING COMPLEXITY (ANALYTICAL, GROUND, SPACE &amp; RELATIVE COST/COMPLEXITY)</li> <li>● SCHEDULE IMPACTS (STATE-OF-THE-ART CUT-OFFS)</li> <li>● GROWTH POTENTIAL (<math>\Delta\eta</math>, <math>\Delta W</math>)</li> <li>● MODULARITY/SCALEABILITY</li> </ul> <p><u>MATERIAL AVAILABILITY</u></p> <ul style="list-style-type: none"> <li>● GALLIUM &amp; CESIUM*</li> </ul>	<p><u>ENVIRONMENTAL IMPACTS</u></p> <ul style="list-style-type: none"> <li>● SPACE IMPACT (SATELLITE SIZE, RFI &amp; NUCLEAR RADIATION)</li> <li>● TRANSPORTATION IMPACT (NO. OF LAUNCHES)</li> <li>● NUCLEAR - (DISPOSAL, PROCESSING, ETC.)*</li> </ul> <p><u>OPERATIONAL CONSIDERATIONS</u></p> <ul style="list-style-type: none"> <li>● RELIABILITY (FMEA DATA)</li> <li>● SUPPORT REQUIREMENTS (SUCH AS SPECIAL EQUIPMENT FOR NUCLEAR)</li> <li>● SAFETY CONSIDERATIONS (HAZARDS - TO THE SATELLITE &amp; CREW)</li> <li>● PERFORMANCE DEGRADATION (SOLAR CELLS, REFLECTORS, RADIATORS, &amp; MACHINERY)</li> <li>● MAINTAINABILITY (DOWN-TIME)</li> <li>● ECLIPSE FACTORS (SATELLITE OVERSIZE &amp; GROUND REQUIREMENTS)</li> </ul> <p><u>COMPLEXITY</u></p> <ul style="list-style-type: none"> <li>● DESIGN COMPLEXITY</li> <li>● MANUFACTURING AND ACCEPTANCE</li> <li>● CONSTRUCTION AND ASSEMBLY</li> <li>● SUBSYSTEM INTERFACES</li> </ul>
*PRIMARY CONCEPT DIFFERENTIATORS	

### 2.4.2 SYSTEM SPECIFIC WEIGHT

Cost sensitivity to transportation is a direct function of concept mass. The SPS specific weight as a function of power is the total weight of the satellite divided by the electrical power delivered to the utility user. It is postulated that specific weights of 8 to 10 kg/kW are an upper limit for the SPS to be competitive with other proposed concepts. Solar cell systems, solar dynamic, and nuclear dynamic concepts are shown in Figure 2.4-1. The satellite system variable uncertainty is a function of the design concept, operating temperatures and efficiencies, degradation, and technology development. A weight allowance of approximately 31 percent is also provided for growth.

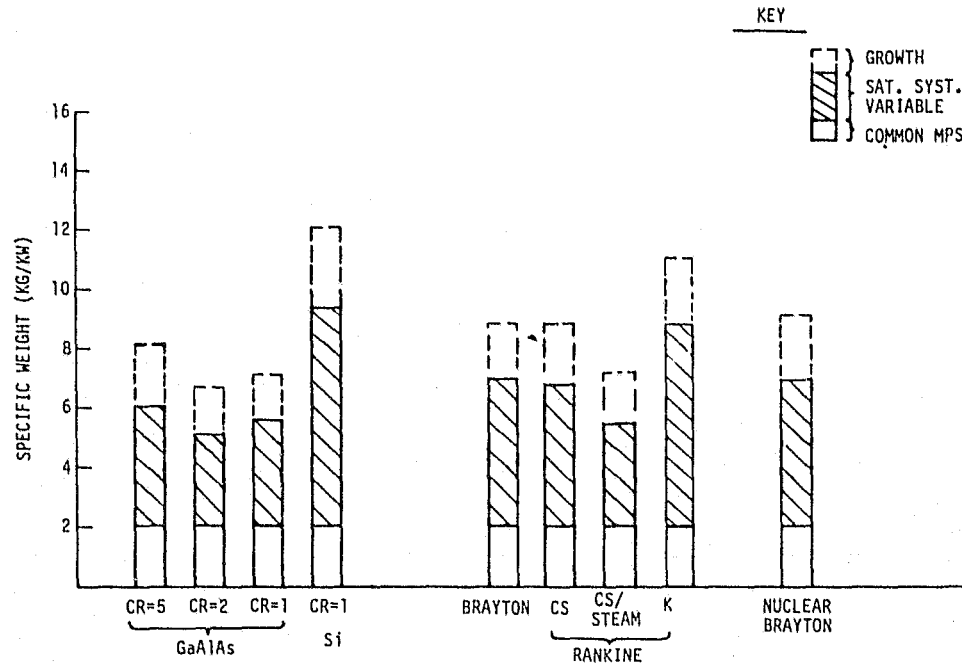


Figure 2.4-1. Weight Comparisons

### 2.4.3 CRITICAL DEVELOPMENTS

Critical driver technology issues unique to each of the system concepts under study are summarized in Table 2.4-2. Technology issues for photovoltaic system contenders center on solar cell and solar blanket requirements, while

Table 2.4-2. System Concept-Related Technology Issues

SYSTEM CONCEPT	CRITICAL TECHNOLOGY ISSUES
<ul style="list-style-type: none"> <li>● <u>SOLAR PHOTOVOLTAIC</u> <ul style="list-style-type: none"> <li>● SILICON SOLAR CELLS</li> <li>● GaAs SOLAR CELLS</li> <li>● COMMON REQTS</li> </ul> </li> <li>● <u>SOLAR THERMAL</u> <ul style="list-style-type: none"> <li>● BRAYTON CYCLE</li> <li>● RANKINE CYCLE</li> <li>● COMMON REQTS</li> </ul> </li> <li>● <u>NUCLEAR THERMAL</u></li> </ul>	<p>THIN FILM SILICON - HIGH TEMPERATURE ANNEALING, WEIGHTS, EFFICIENCY</p> <p>SELF-ANNEALING TEMP. CONTROL, <math>Al_2O_3</math> SUBSTRATE, MAT'L COSTS</p> <p>LOW COST SOLAR BLANKET PRODUCTION</p> <p>HIGH TEMP. HEAT EXCHANGER MATERIALS - LIQUID METAL COOLING - RIGID CONCENTRATOR MATERIALS - CAVITY ABSORBER</p> <p>INFLATABLE CONCENTRATOR MATERIALS/SURFACE DEGRADATION CONDENSING TUBE/FIN RADIATOR</p> <p>FABRICATION/ASSEMBLY TOLERANCES - SOLAR POINTING REQTS OPTICAL PROPERTIES - AC GENERATION/HIGH VOLTAGE TRANSMISSION</p> <p>HIGH TEMP BREEDER REACTOR TECHY (FUEL PROCESSING PLANT) RADIATION SHIELDING - MAINTENANCE</p>

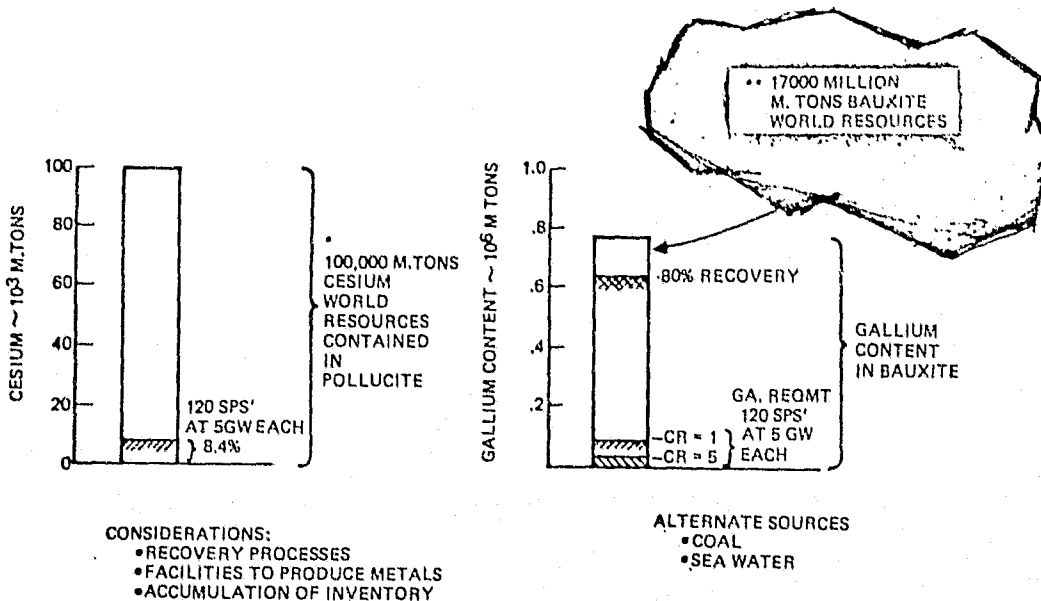


the solar thermal technology drivers relate to high-temperature materials development, concentrator materials degradation, and common problems of assembly tolerances, optical properties, and high-voltage power distribution. Common subsystem-critical technology elements, such as the MP'S, are not included.

#### 2.4.4 MATERIAL AVAILABILITY EVALUATION

Cesium is the preferred alkali metal for the solar thermal Rankine cycle system. Projected cesium requirements for the SPS program (120 satellites) are less than 10 percent of the known world reserves. The main areas where the cesium deposits are located are Canada and Africa. Cesium is relatively expensive at the present time, but a large reduction in price is expected as production quantities are increased. Present production of cesium is approximately eight tons per year.

The amount of gallium required for the photovoltaic system, compared to the known world resources contained in bauxite ores, is shown in Figure 2.4-2. Studies by Alcoa for Rockwell have indicated that with an 80-percent recovery process and a capital investment of \$600,000 to \$750,000 per annual ton of production capacity, that approximately  $6 \times 10^5$  M ton of gallium would be available. The quantities of gallium for CR = 1 and CR = 5 are shown on the figure, and are less than 12 percent of the known resource contained in bauxite ores. Gallium may also be recovered from coal and seawater and, thereby, increase the quantity of gallium beyond the  $6 \times 10^5$  M tons shown. The desulfurization of low-grade, high-sulfur Western United States coal may be a far greater source of gallium than bauxite.



\*KAWECKI BERYLCO INDUSTRIES, INC. (AUG 3, 1977)  
\*\*ALCOA (OCT., 1976)

Figure 2.4-2. Material Availability Evaluation



## 2.5 CONCLUSIONS

The trade studies conducted have resulted in the following conclusions:

### ✓ SOLAR PHOTOVOLTAIC

- Gallium-arsenide (GaAs) solar cells with concentrator offers "best bet" for SPS.
- Potential cost savings exist at higher concentration ratio (i.e., >2).
- Gallium-arsenide solar cells are cost competitive with silicon when normalized to include transportation.
- Silicon solar arrays (without cell annealing) are too heavy!

GaAs solar cells are preferred over silicon. Higher efficiency and lighter weight characteristics of GaAs lead to overall SPS savings. Silicon solar cell blankets are ~2.1 times heavier compared to GaAs (~ $14 \times 10^6$  kg weight penalty for a 5-GW SPS). Adding the delta cost of a silicon solar cell system to normalize the solar cell selection makes the GaAs solar cell cost competitive.

An equivalent 30-year 1-MeV (electron) fluence of  $4.9 \times 10^{15}$  e/cm<sup>2</sup> is estimated using silicon relative damage coefficients, 10 mg/cm<sup>2</sup> silica cover, and 15 mg/cm<sup>2</sup> back-shielding. At this fluence level, silicon cells will degrade to approximately 75% beginning-of-life (BOL) power. A comparable gallium-arsenide degradation would be 16%. It is obvious that large degradation values lead to unacceptable weight penalties and the self-annealing characteristics of GaAs become an essential feature of the SPS design concept.

### ✓ SOLAR THERMAL

- Cesium/steam Rankine best solar thermal option
- Open absorber best choice for Rankine
- Brayton concept reduced as strong option
- Potassium concept imposes heavy weight penalty

To be competitive with solar photovoltaics, this concept depends on light-weight reflectors and radiators. The technology issue of inflatable collectors and condensing radiators needs to be resolved. An open absorber design at the lower temperature of the Rankine cycle offers less technical risk compared to the cavity absorber. The Brayton cycle concept suffers by heavier weight and to be competitive requires greater technology advancement because of its higher operating temperature. Ceramic technology for 30-year life at >2500°F needs to be demonstrated.

The solar thermal cesium/steam Rankine concept proved to be the lightest solar thermal concept studied, but was heavier than the GaAs solar photovoltaic CR = 2 ( $\Delta$  mass =  $5.76 \times 10^6$  kg ~15% heavier).

✓ NUCLEAR

- Nuclear Brayton SPS heaviest weight of concepts studies
- Brayton conversion best for nuclear reactor concept
- Shielding penalties not excessive for reactor operation
- Gaseous core reactor technology potentially could lead to significant weight savings

Sizes of three nuclear-powered SPS concepts are compared in Figure 2.5-1 with solar-powered concepts based on the same scale. Note that the MSFC silicon solar cell and the Boeing Brayton are sized for 10 GW output. Therefore, one-half the area would be required for 5 GW when compared with the nuclear SPS. The preferred nuclear concept (No. 3) occupies a volume approximately 2 km in diameter at the large end, a 1-km-diameter antenna, and is 3 km in length. This compact size, when compared to solar concepts, should lend itself to in-orbit assembly.

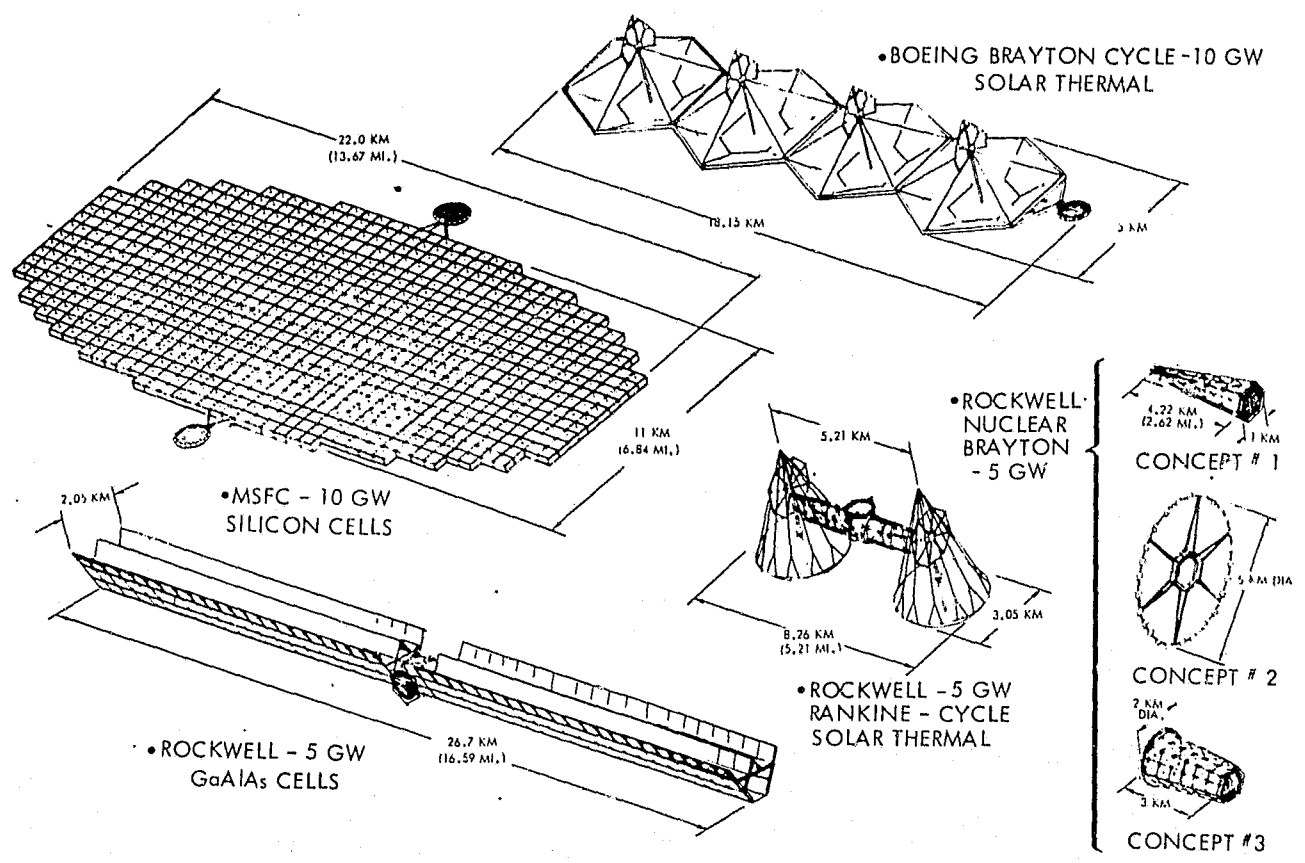


Figure 2.5-1. Concepts Comparison

The nuclear Brayton SPS shows the heaviest weight of concepts studied (31% heavier than solar thermal Rankine/Cs steam). This is primarily due to the radiator design. Optimization of the design should tend to show a more favorable nuclear SPS weight when compared to other concepts. The Brayton



power conversion is best for a helium-cooled reactor concept. A direct closed cycle helium loop can be used, thus eliminating complex intermediate heat exchangers. Also, by changing gas pressure and reactor power, electrical output can be modulated to compensate for nuclear power generating module failure or changing electrical power demand.

The baseline shadow shield weight is approximately three percent of the power module weight. An intermediate reactor technology was selected for this study. Gaseous core reactors potentially offer higher temperatures. This would allow use of radiators with higher operating temperatures and still achieve good cycle efficiency. Preliminary estimates indicate use of gaseous core reactors could result in a 50-percent weight reduction for the nuclear SPS power generation module.

It is obvious that if a nuclear SPS can be shown to be cost-competitive with solar-powered SPS's, then terrestrial siting would result in still lower electrical power generating costs. Objections to terrestrial siting are: (1) thermal pollution, (2) accidents, (3) fuel element shipping, (4) safeguards, and (5) disposal of radioactive wastes. The nuclear concept for SPS should eliminate the radioactive fuel element shipping and safeguards problems. Fuel elements (pebble) reprocessing would be done at the site. A breeding ratio of 1.0 would allow the reactor to consume all plutonium 239 produced. It is concluded that the space-based versus ground-based nuclear system is more a national policy and environmental issue than a technical issue.





## 2.6 POINT DESIGN

During the first quarter of the study, a matrix of concepts were developed. Trade studies were conducted during the second quarter to select concepts for point design definition. Two concepts were selected—a photovoltaic concept with GaAs solar cells, and a solar thermal concept with a cesium/steam Rankine cycle. Major point design emphasis was placed on the photovoltaic concept.

### 2.6.1 PHOTOVOLTAIC

The initial GaAs solar cell photovoltaic concept, having a concentration ratio of 2, had two troughs as shown in Figure 2.6-1. Studies of construction location indicated that a satellite partially constructed in low earth orbit (LEO) has to accommodate very large gravity-gradient torques during the time in LEO and during much of the transfer during self-propulsion from LEO to GEO. This results in attitude control penalties for concepts which are poorly balanced about the Y-axis (axis perpendicular to the orbit plane during operations). The concept shown for combined LEO/GEO construction has three troughs, arranged (end view) like an equilateral triangle, which gives the desired balance about the Y-axis. Because of the spreadout (about the Y-axis) nature of this configuration, it appears that construction would be difficult.

When construction is accomplished totally in GEO, large gravity gradients are no longer as significant a problem. As a result, the concept shown for GEO construction represents a compromise between Y-axis balancing and constructability. Although the concept still has three troughs, they are not arranged in an equilateral triangle and the resulting concept is more compact about the Y-axis. Although not perfectly balanced, the balance is adequate to reduce operational attitude control requirements due to gravity-gradient torque to a low level.

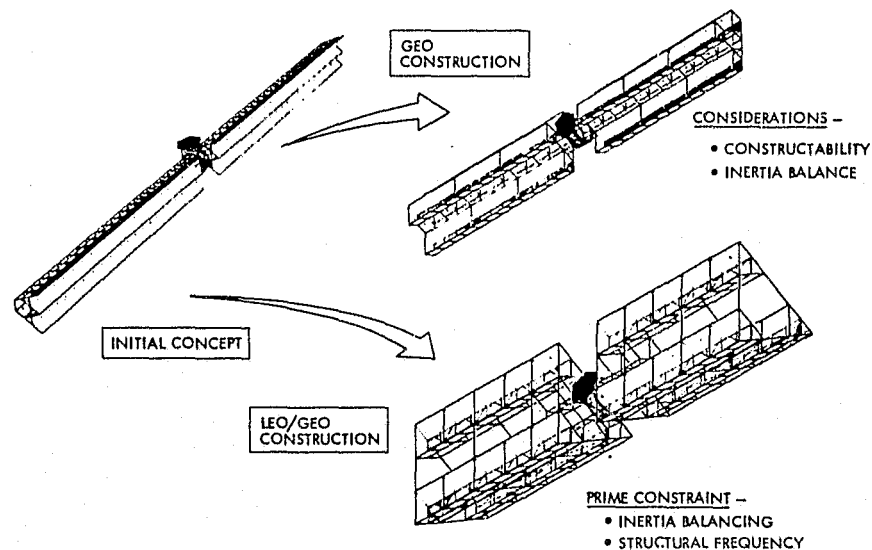


Figure 2.6-1. Photovoltaic Point Design Evolution



Full assembly at LEO was ruled out because of the significant penalties resulting from Van Allen belt radiation damage to the full complement of solar cells, the exposure of larger areas over longer durations to possible impact from space debris, and the significant increases in chemical attitude control propellants required during eclipse periods of the LEO-to-GEO transfer.

For the GaAs CR = 2 solar photovoltaic concept, a first-order cost comparison was made for three different construction/OTV approaches: (1) chemical OTV—GEO construction, (2) electric OTV—LEO/GEO construction, and (3) electric OTV—GEO construction. GEO construction using a chemical OTV for cargo transfer from LEO to GEO costs about \$600 million more than GEO construction using an electric OTV (no solar cell annealing). When electric propulsion is used, GEO construction is about \$320 million greater than combined LEO/GEO construction without solar cell annealing. As indicated in Table 2.6-1, solar cell self-annealing results in virtually the same cost for combined LEO/GEO construction and all GEO construction.

Table 2.6-1. Cost Differences for GEO and LEO/GEO Construction (GaAs Photovoltaic Satellite Point Design)

PHOTOVOLTAIC SATELLITE  
POINT DESIGN CONFIGURATION  
CONCENTRATION RATIO = 2

	CHEMICAL OTV	ELECTRIC OTV	
	GEO CONSTRUCTION	LEO/GEO CONSTRUCT.	GEO CONSTRUCTION
MASS LAUNCHED TO LEO	90.283 x 10 <sup>6</sup> KG (INCL. CHEM. OTV)	37.285 x 10 <sup>6</sup> KG (INIT. 38.047 x 10 <sup>6</sup> KG)	39.654 x 10 <sup>6</sup> KG (INIT. 46.573 x 10 <sup>6</sup> KG)
NO. OF HLLV LAUNCHES	1092	451	480
EARTH LAUNCH COSTS	\$2597 x 10 <sup>6</sup>	\$1,026 x 10 <sup>6</sup>	\$1092 x 10 <sup>6</sup>
ELEC. PROP. MODULE REPLACEMENT COSTS	-	128 x 10 <sup>6</sup>	156 x 10 <sup>6</sup>
SOLAR BLANKET REPLACEMENT COSTS	-	46 x 10 <sup>6</sup>	522 x 10 <sup>6</sup>
SATELLITE OVERSIZING COSTS	-	202 x 10 <sup>6</sup>	-
Δ INTEREST COSTS (7.5%)	-	272 x 10 <sup>6</sup>	225 x 10 <sup>6</sup>
TOTALS	\$2597 x 10 <sup>6</sup>	\$1,674 x 10 <sup>6</sup>	\$1995 x 10 <sup>6</sup>

Construction in GEO environment circumvents the penalties associated with gravity gradient, drag makeup, and the light-dark and thermal cycles encountered at LEO.

The photovoltaic concept shown in Figure 2.6-2 was selected for point design definition. The concept was designed for construction at GEO. This three-trough configuration delivers 5 GW to the utility interface on the ground. It has a single microwave antenna, located in the center of the configuration. GaAs solar cells are used to produce the power using concentrators that give a 2:1 concentration ratio. Detailed description of this concept is provided in Volume IV.



ORIGINAL PLAN  
OF POOR QUALITY

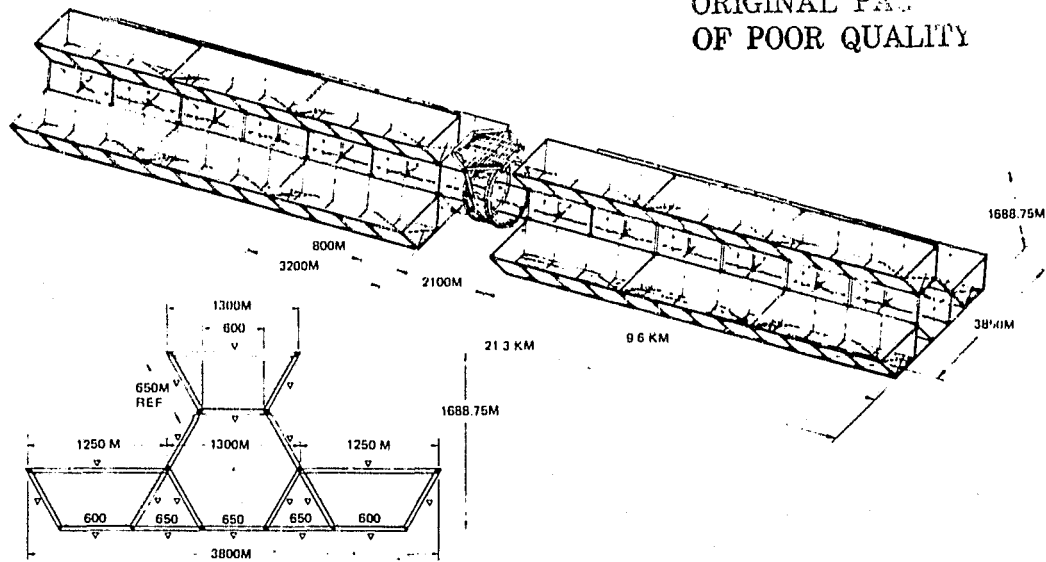


Figure 2.6-2. Solar Photovoltaic CR = 2 Point Design (2-5 GW)

### 2.6.2 SOLAR THERMAL

An alternate solar thermal concept, Figure 2.6-3, was selected for further definition. This concept consisted of two separate collector modules, each hinged to the structure to permit seasonal tracking of the sun without affecting gravity-gradient balance. Each collector module supported 158 independent power modules utilizing a cesium/steam Rankine cycle. Waste heat was rejected to a condensing steam radiator (heat pipes and fins). A detail description of this concept is provided in Volume IV.

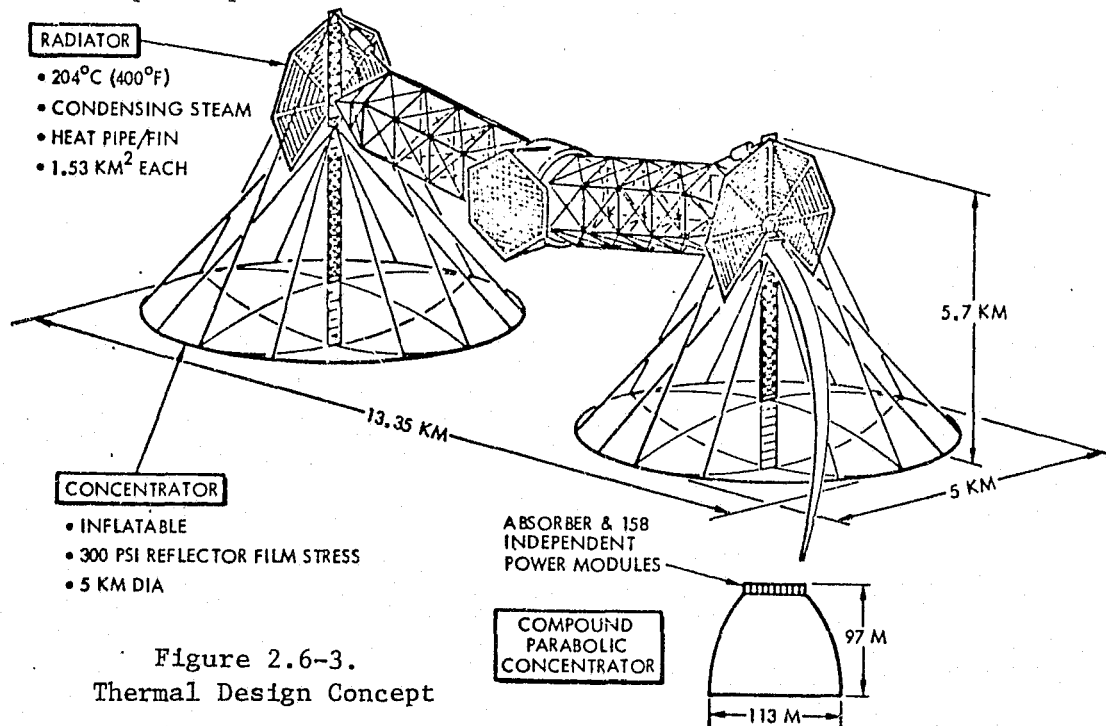


Figure 2.6-3.  
Thermal Design Concept



~~REPLACING PAGE BLANK NOT F~~

### 3.0 TRADE STUDY ANALYSIS

A major part of the second quarter activity was the completion of trade studies in support of conceptual designs and selection of point designs. A list of 28 trades were identified for completion as shown in Table 3.0-1. The mid-term review at MSFC addressed the details of these supporting trades. Out of this review NASA-MSFC selected the Solar Photovoltaic, GaAs, CR-2 and the Solar Thermal Cesium Rankine concepts for point design definitions. This section provides the results of these completed SPS trade studies.

#### 3.1 POWER CONVERSION

The power conversion trade tree is shown in Figure 3.1-1. The nuclear HTGR Brayton SPS was the heaviest weight of concepts studied ~ 35% heavier than the CR-2 solar photovoltaic. This is primarily due to the radiator design. A gaseous core reactor/MHD could potentially reduce the weight to be competitive. It was concluded that the major issues of nuclear reactor concepts are political and environmental and, therefore, this approach should be set aside for further ERDA evaluation of these issues. A low concentration ratio (CR-2) was selected for the detailed point design definition. Concentration ratios of 5 or more resulted in complex configuration control requirements but probably would result in lower overall cost. Non-concentrated solar arrays are the simpler configuration but result in the highest weight and cost.

Gallium arsenide solar cells are preferred over silicon. Greater efficiency and lighter weight combine to offer overall SPS savings in weight and cost. Radiation damage self-annealing characteristics of GaAs is a key consideration. To conserve on gallium requirements it is necessary to select a thin film design ~ 5  $\mu$ m of active region.

The cesium/steam Rankine appears to be the best selection for the solar thermal option. The Brayton concept is no longer as strong an option. It suffers by heavier weight and requires greater technology advancement because of its higher operating temperature. Ceramic technology for 30 year life at >2500°F needs to be demonstrated. The availability of cesium looks adequate for the SPS requirements. Cesium should not be ruled out because of availability.

##### 3.1.1 PHOTOVOLTAICS

###### GaAlAs vs Silicon Solar Cell Trades

Performance of Candidate Solar Cells. The projected IOC for the 1998 era requires that most photovoltaic system studies to be based on the technology readiness projected for about 1985. Two of the more difficult tasks are to reasonably predict the characteristics of advanced technology components and to develop adequate confidence in performance and cost projections. Several

Table 3.0-1. Trade Studies Summary

I.D. NO.	TRADE	RESPONSIBILITY	LEVEL OF TRADE (EMPHASIS)	MILESTONES		ERB REVIEWS
				COMP TRADES	PRELIM. RESULTS	
1	LEO VS. GEO*	BILL McRAE	SYSTEM	SEPT 15	AUG 26	SEPT 1
2	OPTIMUM SPS SIZE ✓	BILL McRAE	SYSTEM	SEPT 15	AUG 26	AUG 25
3	CONCENTRATION RATIO*✓	D. TONELLI	SUBSYSTEM	JULY 29		AUG 1
4	BRAYTON VS. RANKINE*	B. BRUX	SUBSYSTEM	AUG 15		AUG 16
5	GaAlAs VS. SILICON*	D. TONELLI	SUBSYSTEM	SEPT 15	AUG 26	AUG 1
6	NUCLEAR COMPARISONS*	W. SCHMILL	SYSTEM	AUG 15	JULY 22	AUG 18
7	ELECTRICAL VS. CHEMICAL OTV	R. BERGERON	SYSTEM	SEPT 15	AUG 26	SEPT 1
8	POINT DESIGN(S) SELECTION	B. McRAE	SYSTEM	SEPT 1	AUG 26	-
9	ALTERNATIVE TECH. VERIFICATION SCENARIOS	B. ROTH	SYSTEM	AFTER 9/15		NOV 1
10	ASPECT RATIO (PLANE FORM)*✓	LEE SMITH	SUBSYSTEM	JULY 29		AUG 2
11	MICROWAVE CONVERSION DEVICES ✓	C. TOMITA	SUBSYSTEM	SEPT 15	JULY 29	AUG 10
12	ANTENNA STRUCTURE ✓	L. SMITH	SUBSYSTEM	JULY 29		AUG 2
13	ANTENNA/RECTENNA SIZE/NUMBER ✓	C. TOMITA	SUBSYSTEM	JULY 29		AUG 8
14	FREE OSCILLATION VS. ACTIVE CONTROL*✓	R. OGLEVIE	SUBSYSTEM	JULY 29		AUG 8
15	SOLAR REFERENCE PLANE VS. 0-DEG INCLINATION✓	R. OGLEVIE	SUBSYSTEM	JULY 29		AUG 8
16	STRUCTURAL SUBELEMENTS✓	L. SMITH	SUBSYSTEM	JULY 29		AUG 11
17	NON-ALKALI VS. ALKALI METALS	L. SMITH	SUBSYSTEM	SEPT 15		AUG 18
18	FIG. CONTROL VS. POINTING ACCURACY*✓ (ACTIVE VS. PASSIVE)	R. OGLEVIE	SUBSYSTEM	JULY 29		AUG 17
19	INERTIA BALANCING*✓	R. OGLEVIE	SYSTEM	JULY 29		AUG 8
20	INFLATABLE VS. RIGID FACETS*✓	B. BRUX	SUBSYSTEM	JULY 29		AUG 16
21	OPEN RECEIVER VS. CAVITY*✓	B. BRUX	SUBSYSTEM	JULY 29		AUG 16
22	NaK/HEAT PIPE VS. CONDENSING RADIATORS*✓	M. MANOFF	SUBSYSTEM	JULY 29		AUG 16
23	PENCIL VS. SHAPED BEAM✓	C. TOMITA	SUBSYSTEM	SEPT 1	AUG 26	AUG 30
24	BANDPASS FILTERS VS. NON* ✓	M. MANOFF	SUBSYSTEM	JULY 29		AUG 1
25	WAVEGUIDE RCR DESIGN✓	C. TOMITA	SUBSYSTEM	JULY 29		AUG 10
26	PHASE CONTROL	C. TOMITA	SUBSYSTEM	SEPT 1		AUG 30
27	AC VS. DC	J. JANDRASI	SUBSYSTEM	JULY 29		SEPT 4
28	BEAM MACHINE VS. ERECTABLES	L. SMITH	SUBSYSTEM	SEPT 1		DELETED
29	IONOSPHERIC AFFECTS	J. HAFFNER				AUG 10
30	915 MHz VS. 2.45 GHz	C. WILEY				AUG 10
31	INFORMATION MANAGEMENT SUBSYSTEM	A. GORDON				AUG 17

\*TRADE COMPARISONS NEEDED TO SUPPORT POINT DESIGN SELECTION

✓TRADE COMPARISONS NEEDED TO DEVELOP PRELIMINARY CONCEPTUAL DESIGNS

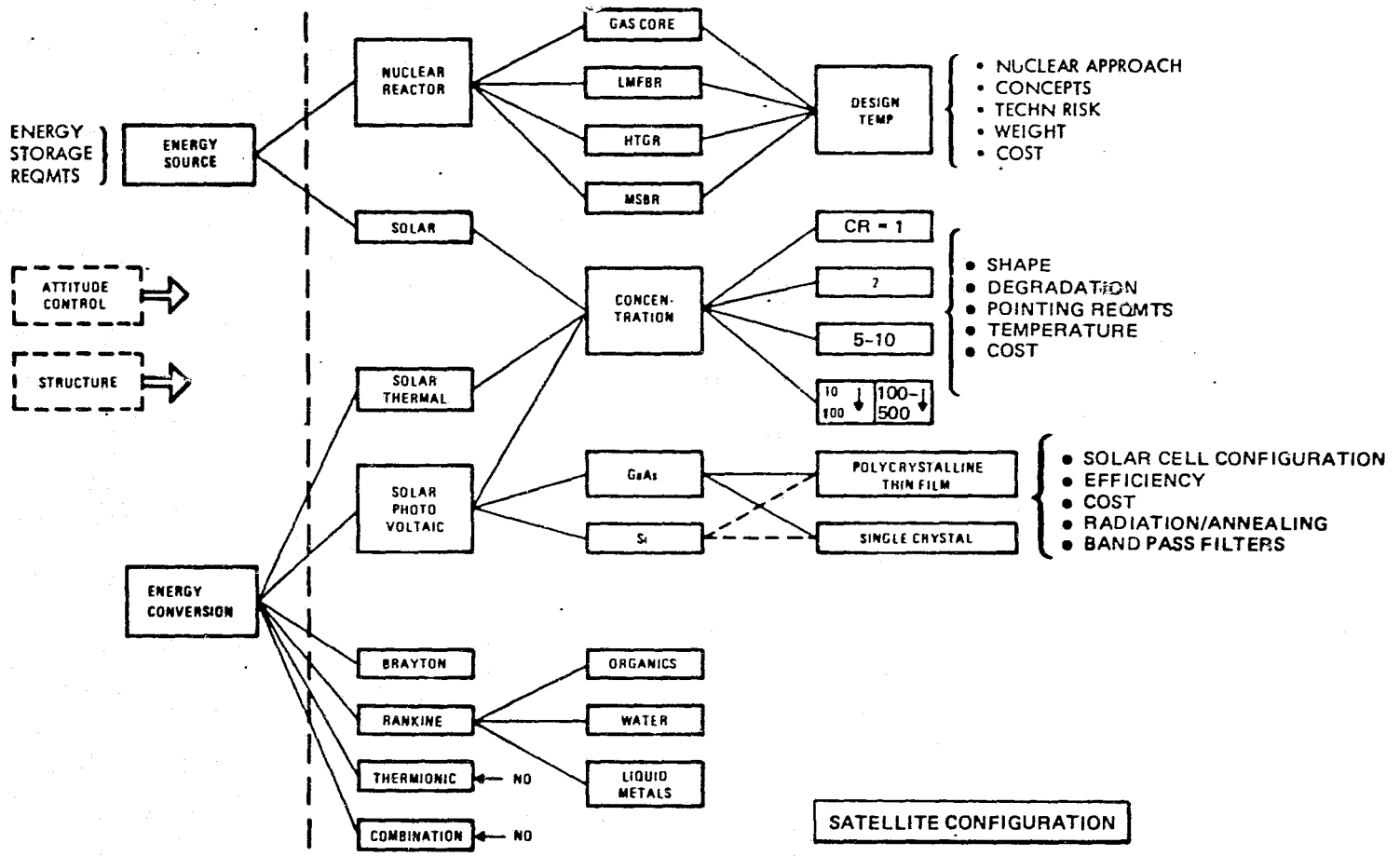


Figure 3.1-1. Power Conversion Subsystem Options





of the more promising candidates for each major component were considered. Ongoing and near future technology efforts and trends projected, provide information to select components.

Figure 3.1-2 shows typical performance projections for three solar cell candidates. The curves are based on recent published predictions by solar cell and array manufacturers; such information can vary widely depending on the source and the technology being promoted. The highest performance is projected for GaAlAs cells. Although significant improvements are projected for cadmium sulfide (CdS) cells, they remain the low performance option, and are not expected to surpass silicon cell performance.

The long-term solar array performance is primarily determined by the four solar cell characteristics indicated on this chart. The thickness of cells and covers (a principal contributor to weight and transportation cost) represents a major trade-off with other characteristics. All must be considered simultaneously to optimize performance and cost of the overall system. The large quantity requirements of the SPS and its sensitivity to photovoltaic performance dictate that an optimized cell design should be pursued at an early date. This can be done initially through computer simulation of solar array performance and cell design, but must eventually be supported by actual devices and test data.

MSFC Baseline Si Solar Cell. To establish a reference design for a solar array module, it was necessary to define both Si and GaAlAs solar cells. An investigation of various cells used in previous programs and of cells tested in recent R&D was made to note means of improving performance.

Silicon cell technology predictions for 1985 show AMO efficiencies between 17 and 20 percent at 28°C, open-circuit voltages between 0.65 V and 0.79 V, low resistance cells with low thermal coefficients, and cells responsive to a broader range of the solar spectrum. With a reasonable R&E effort, cells with the characteristics predicted in Figure 3.1-3 are considered feasible.

Most recent solar cell improvements result from increasing the short circuit current, the quantum yield, and the fill factors. Si cells with an efficiency up to 16% have been made, and 15% cells are available in some quantity. Typical high efficiency cells of today have an open-circuit voltage around 0.57 V to 0.59 V, and 0.63 V has been obtained in the laboratory. A cell with an efficiency of 18% is possible if an open circuit voltage of about 0.67 V is achieved. With improved doping and junction control, it appears reasonable to expect better diode characteristics and higher voltages. For the MSFC baseline Si cell, an open-circuit voltage of 0.70 V at 30°C was predicted. Thin, shallow junction cells with improved diode characteristics may be more resistant to radiation. With other possible means of reducing degradation, an improvement in radiation resistance, as shown, is predicted. Further work in the area of radiation damage annealing will help maintain the array output over the SPS life.

A comparison of a silicon solar cell with GaAlAs solar cells is presented in Figure 3.1-4. The Si cells for advance applications are projected to weigh from 0.53 to 0.338 kg/m<sup>2</sup>. Weight improvements for Si cells are from use of thinner cells (4 to 2 mils thick) and thinner covers.

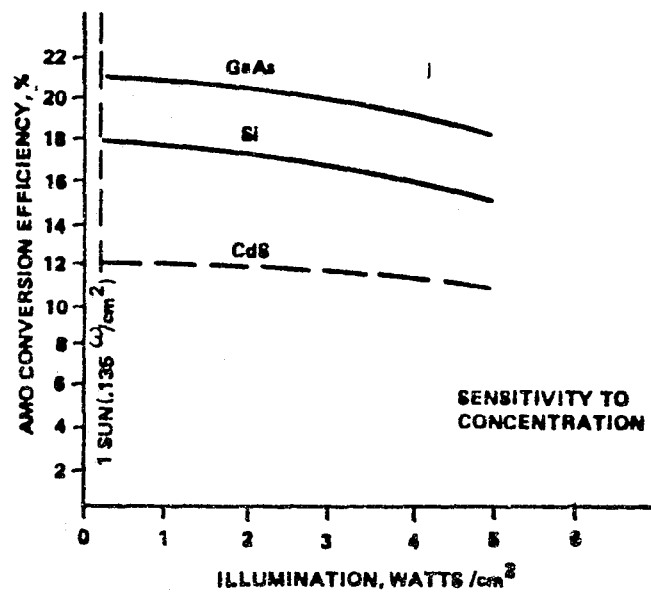
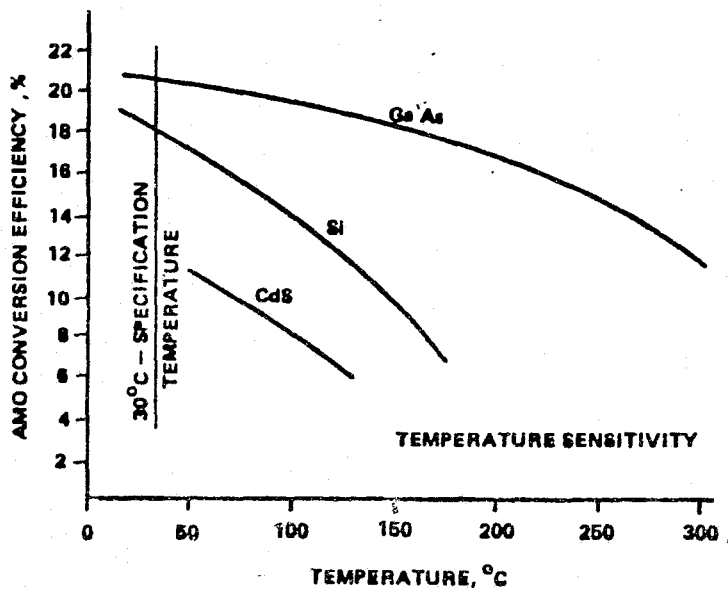
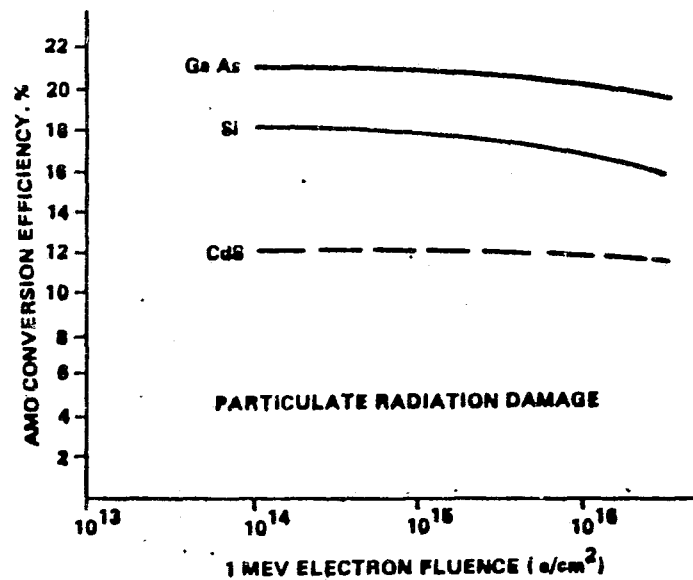
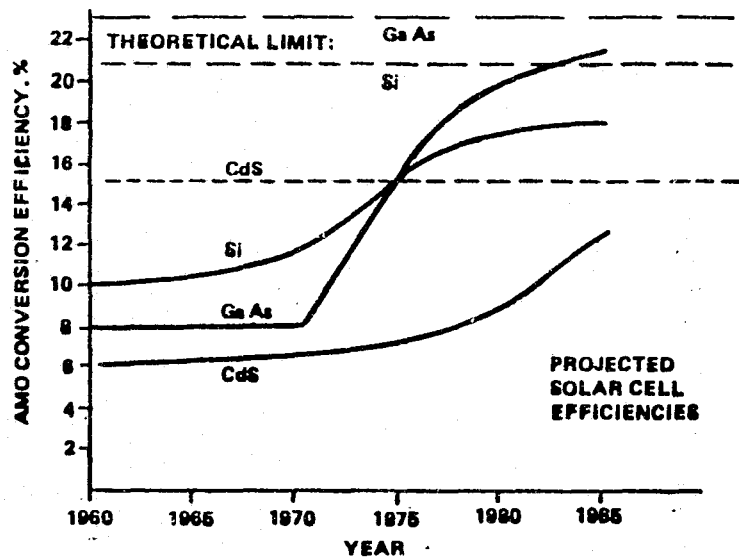


Figure 3.1-2. Projected Performance of Solar Cell Candidates

3-5

SD 78-AP-0023-3



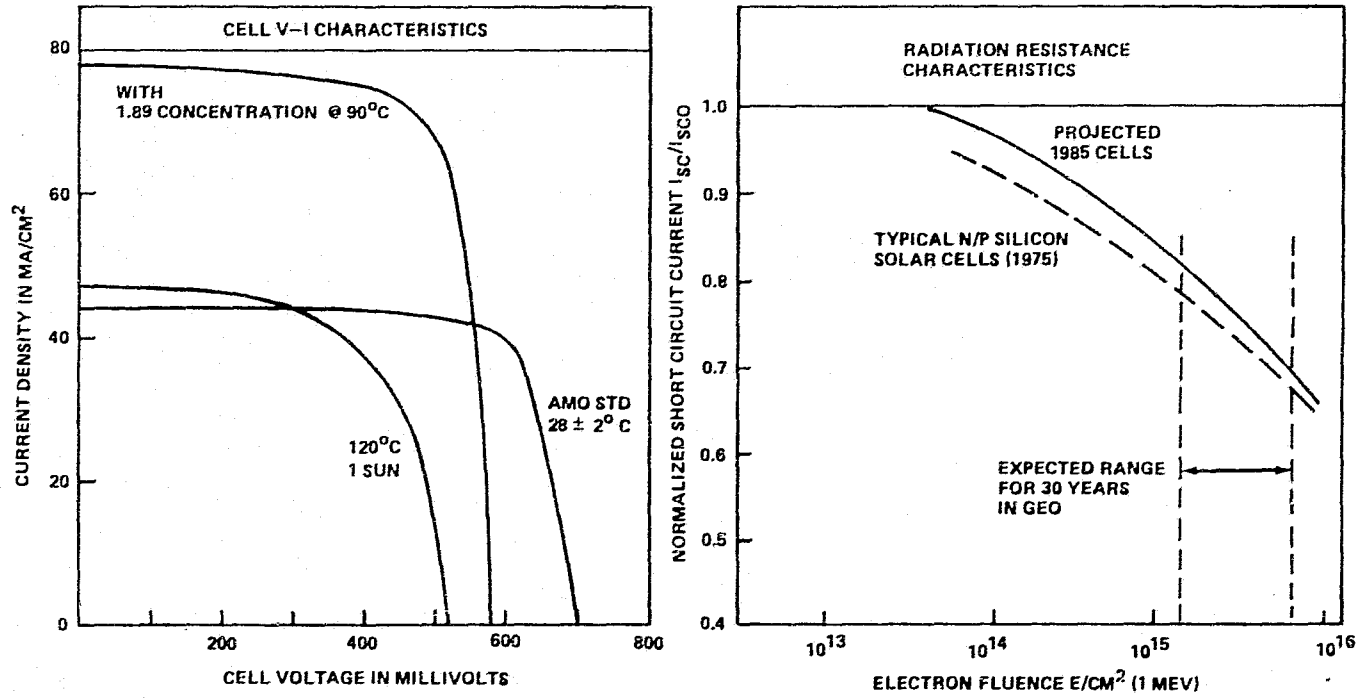
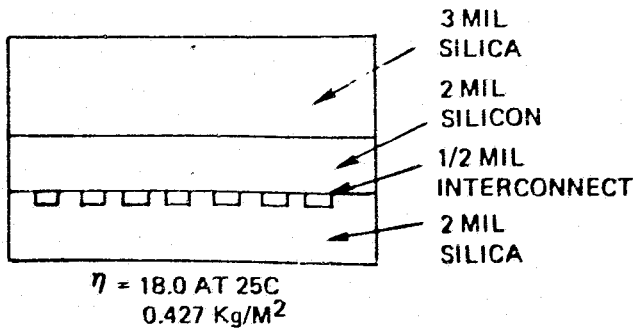


Figure 3.1-3. MSFC Baseline Solar Cell



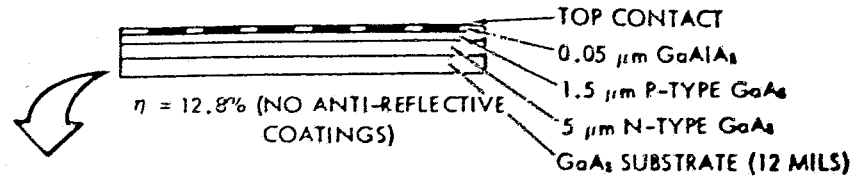
SILICON



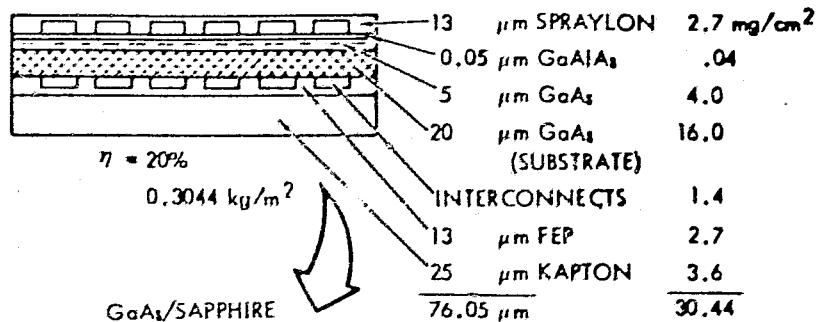
3 MIL SILICA	16.76 MG/CM <sup>2</sup>
2 MIL SILICON	11.58
1/2 MIL INTER	1.14
2 MIL SILICA	11.18
<hr/>	
5%	40.66
	2.03
<hr/>	
	42.69
	(0.427 Kg/M <sup>2</sup> )*

\*BOEING REF

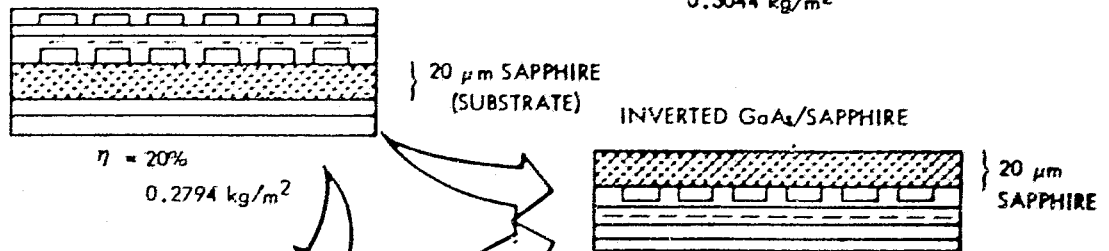
ERD - EXPERIMENTAL GaAlAs CELL



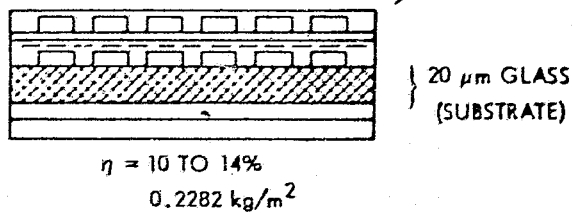
GaAs/GaAs ROCKWELL SPS BASELINE CELL



GaAs/SAPPHIRE



GaAs/GLASS



\*\*REPLACE FEP/KAPTON WITH 2 MILS SILICA ~ 0.317 Kg/M<sup>2</sup>

Figure 3.1-4. Solar Cell Configurations

3-7

SD 78-AP-0023-3



GaAlAs Solar Cells. GaAlAs solar cell weights are projected to range from 0.304 to 0.228 kg/m<sup>2</sup>. In the study, SPS mass statements were based on GaAlAs cell weights of 0.252 kg/m<sup>2</sup>. The GaAlAs cells are presently under development and appear to offer a high potential to achieve this low weight, with high efficiency and mass production capabilities. A particularly unique configuration is the inverted GaAs/Sapphire cell where the transparent Sapphire is utilized as the cover; thereby, removing a basic weight item. The point design solar array SPS utilizes the inverted GaAlAs/Sapphire cell concept.

A review of the literature was conducted, and discussions were held with experts on GaAlAs solar cells to determine the performance and efficiency trends. Efficiency projections based on these data are shown in Figure 3.1-5. The basic performance and projected technology for both Si and GaAlAs cells are shown; experimental data points by the Science Center (Rockwell), Hughes and IBM and projected development efforts of the USAF are shown. Based on the present rate of development, it is projected that the GaAlAs solar cell has the potential of attaining a 20% efficiency (AMO, 28°C) for the post 1982 period. A Rockwell proposal to the USAF calls for the development of a cascaded solar cell to deliver power at 25% (AMO, 28°C) within the next three years.

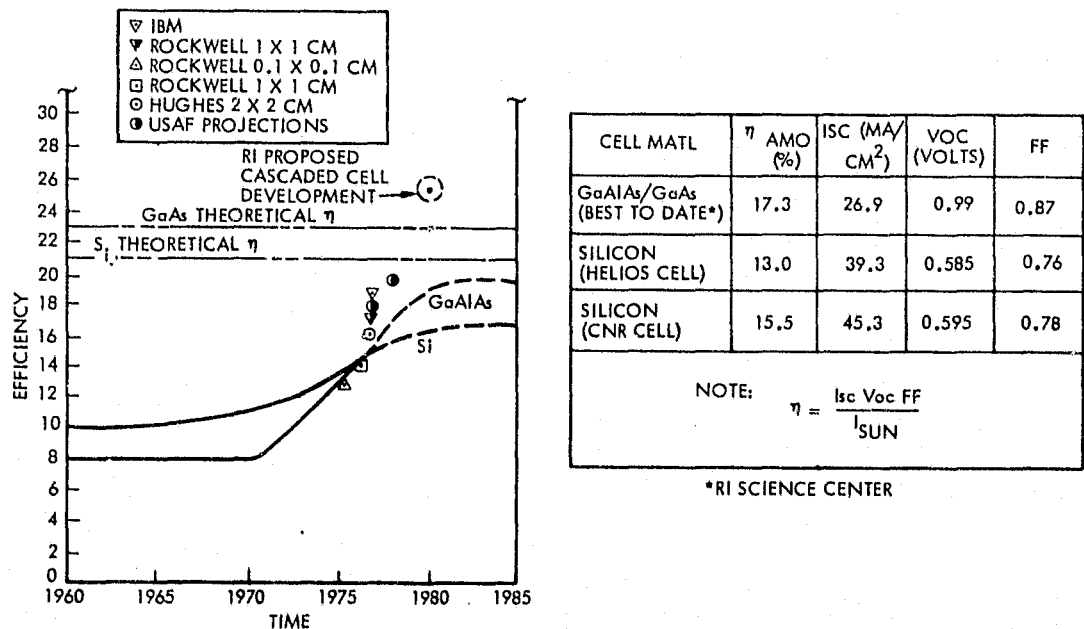


Figure 3.1-5. Solar Cell Efficiency Projection And Parameter Comparison

A cost analysis based on materials cost, cell manufacturing process costs and blanket manufacturing process costs was performed for the GaAs and Si cell configurations. The results are presented in Table 3.1-1. Based on today's material costs, the basic GaAs blanket solar cell cost is \$0.350/watt compared to silicon at \$0.194/watt. The solar cell costs shown are for the solar cell material and blanket production costs and does not include efficiency losses when integrated into a solar blanket and SPS integration or transportation costs.



Table 3.1-1. Solar Cell Relative Cost Comparisons

SOLAR CELL CONFIGURATION	CELL/BLANKET MAT'L \$/M <sup>2</sup>	CELL PROCESS \$/M <sup>2</sup>	BLANKET PROCESS \$/M <sup>2</sup>	TOTAL \$/M <sup>2</sup>	\$/WATT
GaAs/Al <sub>2</sub> O <sub>3</sub> η = 20%	37.60	17.00	17.00	71.60	0.264**
GaAs/GaAs η = 20%	62.05	17.00	17.00	96.05	0.35
GaAs/GLASS η = 12%	13.80	17.00	17.00	47.80	0.294
SILICON η = 18%	13.20	17.00	17.00	47.20*	0.194

MAT'L COSTS (\$/KG)

Ga	= \$500
As	= 150
Al <sub>2</sub> O <sub>3</sub>	= 325
Si	= 60
Transp.	= 60 (TO GEO)
Others	= 20

\*NORMALIZED = \$85.10/M<sup>2</sup>

NORMAL	=	47.20
EFFICIENCY Δ	=	+ 5.30
(18%) DEGRADATION Δ	=	+11.50
TEMP. Δ	=	+ 1.10
TRANSP. Δ	=	+20.00
		<u>\$85.10</u>

\*\*SCALE FACTORS:

CR-2	=	0.58
CR-5	=	0.30

The effects of design and integration penalties for the Si cells are also shown in the chart relative to the GaAs cells. The delta costs include transportation, efficiency losses, cell degradation, and temperature effects which results in a cost of \$85.10/m<sup>2</sup> for Si arrays. Using the basic Si solar cell blanket cost of \$0.194/watt and adding the delta cost penalties, the cost of a silicon solar cell system in GEO is \$0.350/watt. The cost of the GaAs solar cell system for a sapphire substrate (Al<sub>2</sub>O<sub>3</sub>) is projected to be \$0.264/watt or a cost reduction of approximately 24% compared to a silicon system. If a concentration ratio of 2 is used the scaling factor of 0.58 is used and the GaAlAs array cost is then 0.58 x \$0.264 = \$0.153/watt.

The solar array electrical output is affected by the on-orbit environment which includes trapped particle radiation, solar flare proton radiation, ultra-violet radiation, and the temperature cycling associated with the eclipse seasons. The natural trapped particle radiation environment was obtained from the "Solar Cell Radiation Handbook," TRW Report 21945-6001-RV-00. The trapped electrons are based on the AE-4 model of the outer radiation zone electron environment. For solar cells with minimal shielding, trapped protons may be neglected at geosynchronous orbit. The solar flare proton model was obtained by averaging the integral flux values for the five worst years of the 19th and 20th solar cycles. The values for damage equivalent 1 MeV electrons are taken from "A Proposal for Global Positioning Satellite Electrical Power Subsystem," General Electric, Space Division Proposal No. N-30065, 28 February 1974.

The values of solar flare protons equivalent 1 MeV e<sup>-</sup> flux shown in the above report are multiplied by 1.35 to allow for the six quiet years of the solar cycle. The values for a 11 year cycle are then multiplied by a factor of 3 to obtain a 30 year model. The data is presented in Figure 3.1-6.

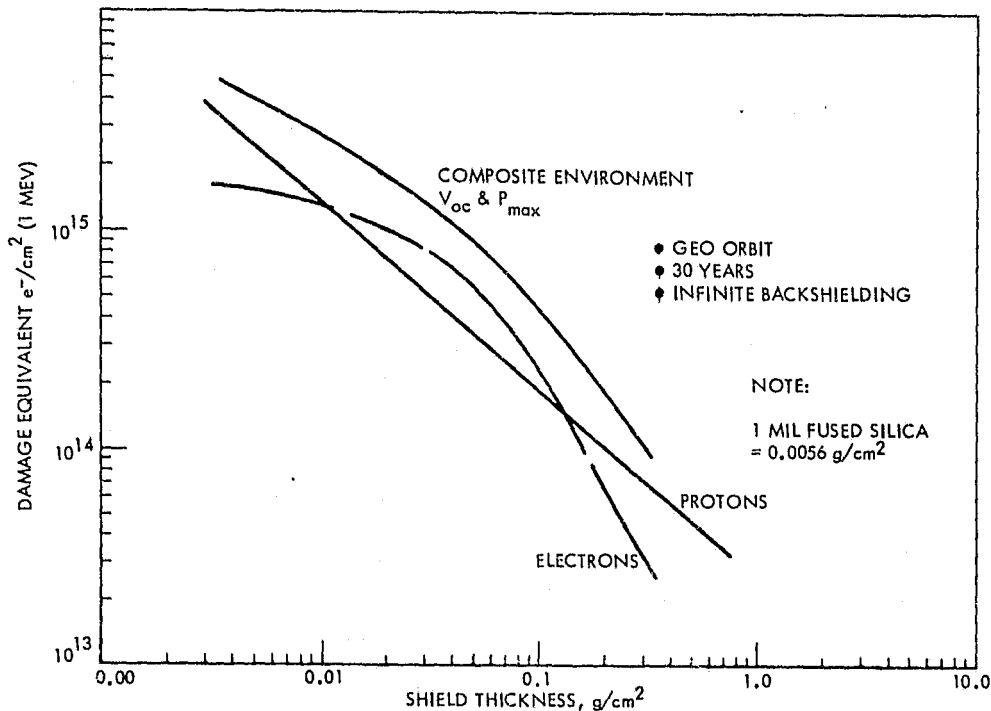


Figure 3.1-6. Solar Cell Damage Equivalent 1 MeV Electron Fluence Vs. Shield Density

Figure 3.1-7 shows the effect of 1 MeV electron radiation on solar cell power for 1-3 ohm-cm N/P silicon solar cells of varying thickness. These data are from the "Solar Cell Radiation Handbook," TRW Report 21945-6001-RV-00. The data shown are a composite of data from several sources and represents the mean behavior of n-p conventional Si solar cell production in the United States. Solar cells produced with significant changes in composition may not show the same radiation loss factors. The significance of the data shown is that thinner solar cells, percentagewise, show less radiation degradation than thicker cells. The data shown is obtained by dividing solar cell maximum power at each radiation fluence by the cell output (different for each cell thickness) before irradiation. The referenced TRW data also shows that absolute solar cell output is independent of cell thickness at radiation fluence of  $10^{15} e^-$  (1 MeV)/ $cm^2$ .

A comparison of silicon cell configurations and GaAlAs cell configurations and performance are shown in Table 3.1-2. The basic silicon cell design weights vary from 0.427 to 0.53  $kg/m^2$ . The power density of the silicon cells are shown for concentration ratios of 1 and 2. For a passive heat rejection system the silicon cell operates at too high a temperature for CR-5 and is not a practical design concept. The weights of the GaAlAs cells varies from 0.252 to 0.317  $kg/m^2$  depending on the design parameters. The GaAlAs efficiency is 20% at AMO and 28°C.

The power rating of the GaAlAs cell configurations are seen to vary from 187  $W/m^2$  to 918  $W/m^2$  for concentration ratios of 1 to 5 respectively. The

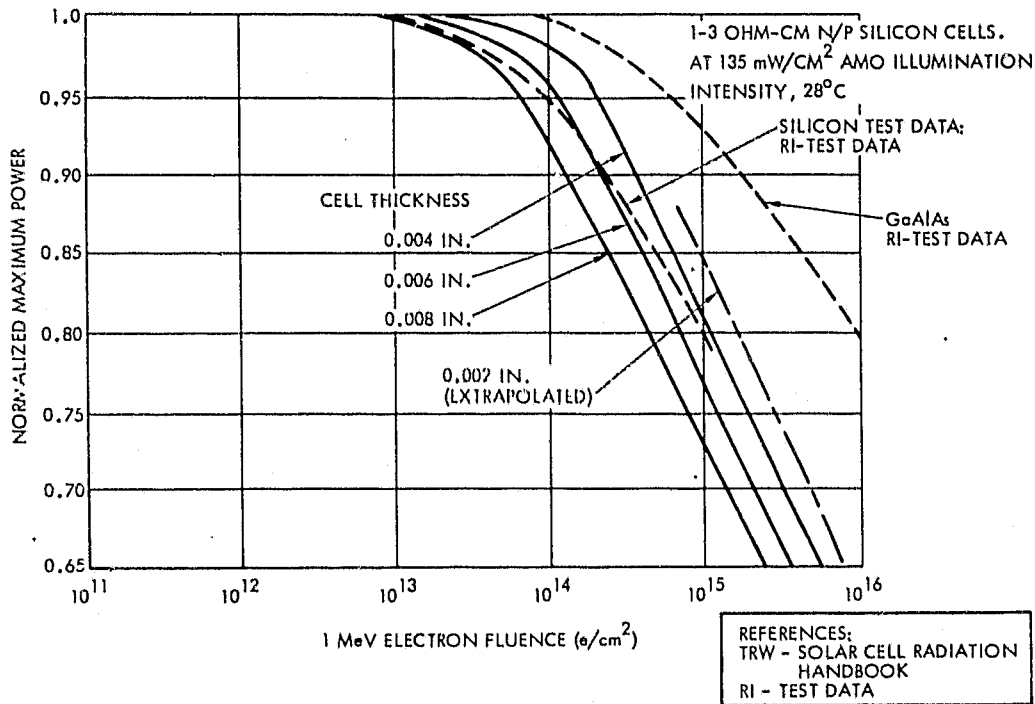


Figure 3.1-7. Normalized Maximum Power Vs. 1-MeV Electron Fluence

Table 3.1-2. Solar Cell Comparisons

CONCENTRATION RATIO (E.O.L.)		CR = 1	CR = 2.13	CR = 5.42
<b>SILICON</b> INTENSITY ONTO CELLS		1353 W/M <sup>2</sup>	2880 W/M <sup>2</sup>	7350 W/M <sup>2</sup>
	3 MILS SILICA 2 MILS SILICON 2 MILS SILICA (18%) <b>(BOEING)</b>	183 W/M <sup>2</sup> (ANNEALING)	272 W/M <sup>2</sup> 223 W/M <sup>2</sup>	N/A N/A
	3 MILS SILICA 4 MILS SILICON 2 MILS FEP/KAPTON (16.5%) <b>(MSFC)</b>	150 W/M <sup>2</sup> (18% DEGRADATION) 138 W/M <sup>2</sup> (18% DEGRADATION)	175 W/M <sup>2</sup>	N/A
<b>GaAlAs</b>				
	.5 MIL SPRAYLON 1 MIL GaAlAs/Al <sub>2</sub> O <sub>3</sub> 2.5 MILS FEP/KAPTON (20%)	203 W/M <sup>2</sup>	437 W/M <sup>2</sup>	N/A
	1 MIL GaAlAs/Al <sub>2</sub> O <sub>3</sub> 2.5 MILS FEP/KAPTON (20%)	187 W/M <sup>2</sup> (8% DEGRAD)	403 W/M <sup>2</sup> 8% DEGRAD	N/A
	1 MIL GaAl/Al <sub>2</sub> O <sub>3</sub> 2 MILS SILICA (20%)		420 W/M <sup>2</sup> (SELF ANNEALING)	918 W/M <sup>2</sup> (SELF ANNEALING)

power output of the GaAlAs arrays are greater than for the silicon blankets and they are also lighter and require less planform area for the same power rating.

Table 3.1-3 summarizes what has been learned about the solar cell configurations. Gallium availability is not a key issue provided that very thin active regions in the order of 5  $\mu\text{m}$  can be utilized. Rockwell Autonetics Group has demonstrated high performance on a sample gallium arsenide cell with an active region thickness of 6.5  $\mu\text{m}$  grown by the CVD process on a gallium arsenide substrate. It is yet to be demonstrated that this same performance can be achieved on an alternate single crystal substrate such as sapphire.

Table 3.1-3. Solar Cell Configuration

<ul style="list-style-type: none"> <li>● GaAs SOLAR CELL CRITICAL ISSUE IS TECHNOLOGY 5 <math>\mu\text{m}</math> THICK ACTIVE REGION ALTERNATE SUBSTRATE (i.e., SAPPHIRE)</li> </ul>				
<div style="border: 1px solid black; padding: 2px;">NOTE: TECHNOLOGY ADVANCEMENT REMOVES GALLIUM AVAILABILITY AS ISSUE</div>				
<ul style="list-style-type: none"> <li>● GALLIUM ARSENIDE SOLAR CELLS COST COMPETITIVE WITH SILICON WHEN NORMALIZED TO INCLUDE TRANSPORTATION</li> <li>● SILICON SOLAR CELL BLANKETS ~ 2.1 TIMES HEAVIER COMPARED TO GaAs</li> </ul>				
SOLAR ARRAY (CR = 1)				
MAT'L	CELL MASS	POWER OUTPUT	AREA	MASS
SILICON	0.427 kg/m <sup>2</sup>	150 W/m <sup>2</sup>	61x10 <sup>6</sup> m <sup>2</sup>	26x10 <sup>6</sup> kg
GaAs	0.252 kg/m <sup>2</sup>	187 W/m <sup>2</sup>	48.9x10 <sup>6</sup> m <sup>2</sup>	12.3x10 <sup>6</sup> kg
NOTE: SIZED FOR 9.15 GW TOTAL OUTPUT				
<ul style="list-style-type: none"> <li>● CONCENTRATOR REPLACEMENT OF SOLAR CELLS SHOULD BE COST AND WEIGHT EFFECTIVE</li> </ul>				

The trapped proton radiation fluence as shown in Figure 3.1-8 is small at geosynchronous orbit. Proton damage from solar flares is order(s) of magnitude higher than the trapped proton fluence. Different solar proton modules are also presented in the figure, compared to the August 1972 event (the largest ever recorded). Utilizing the inverted GaAlAs on sapphire solar cell design trapped protons are shielded out. The 20  $\mu\text{m}$  sapphire is the cell substrate that the junction is grown on and in the inverted configuration acts as the radiation shielding cover. The cells operate at 125°C, and thermal annealing will also occur.

Degradation (in maximum power) versus fluence curves for 1, 3, and 10-MeV protons and 0.7 and 1-MeV electrons on GaAlAs cells are presented in Figure 3.1-9. The GaAlAs cells show higher radiation resistance than silicon cells (except for 1 MeV proton radiation), but all low proton damage (less than 1 MeV) can be completely shielded out with 5  $\mu\text{m}$  (0.2 mils) Al<sub>2</sub>O<sub>3</sub> (sapphire) cover. Total 1 MeV electron equivalent fluence with respect to silicon cells for 30 years at GEO are also presented as a function of cover thickness.

A comparison of GaAlAs solar cell annealing effects as a function of annealing temperatures and times are presented in Figure 3.1-10. Over 400 small area (1/16-inch square) solar cells have been tested. The typical and best cells annealing results are also shown in the figure. It appears that

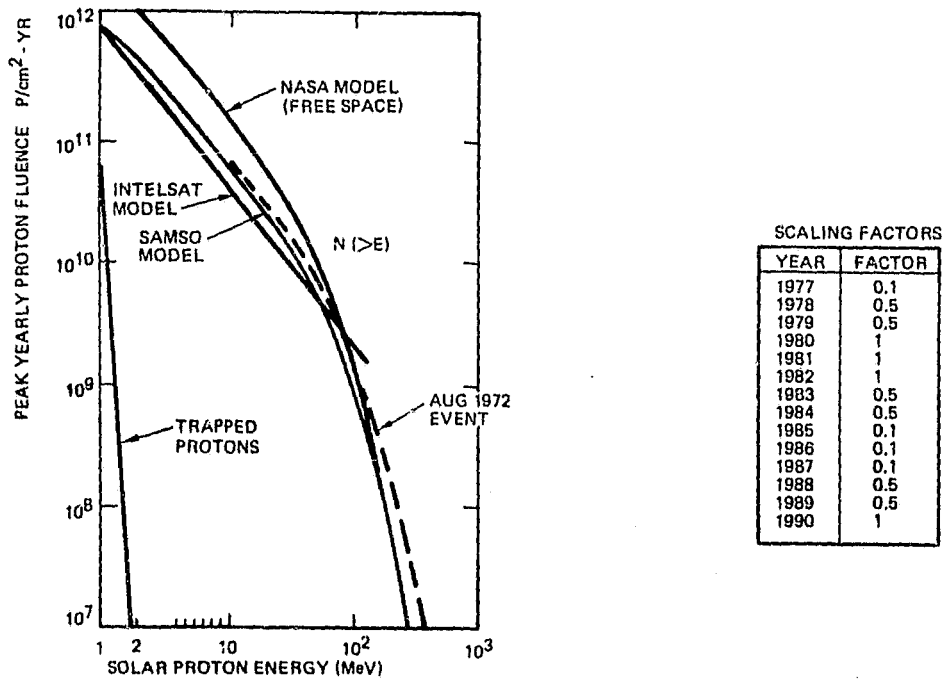


Figure 3.1-8. Solar Proton Model Environment

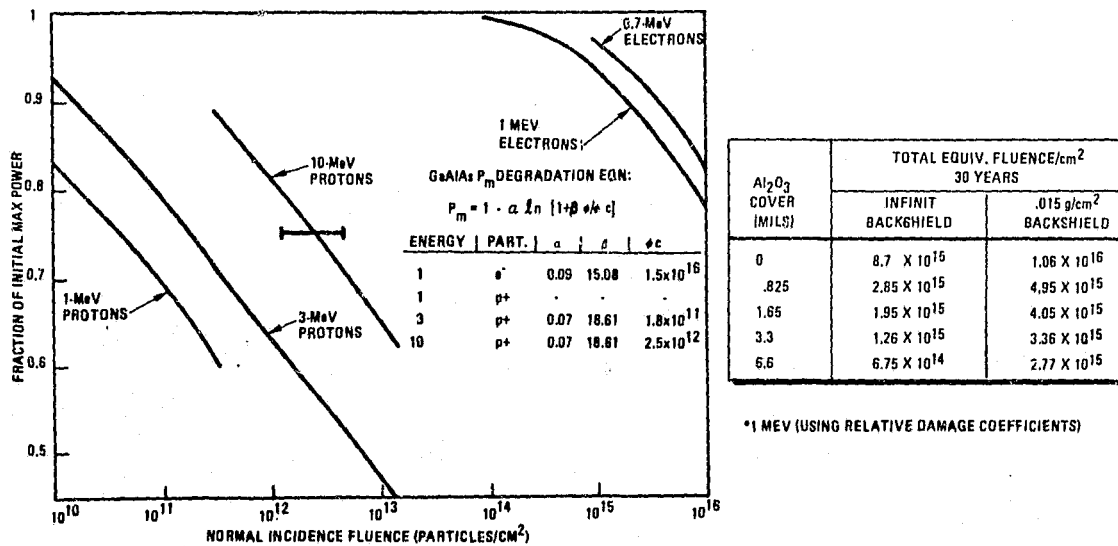
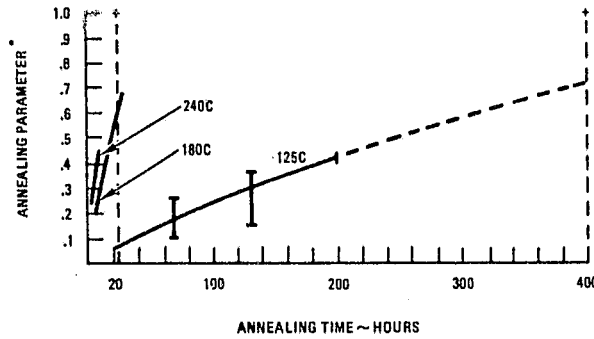


Figure 3.1-9. GaAlAs Solar Cell Radiation Test Data





\* ANNEALING PARAMETER

$$\frac{P_A - P_R}{P_I - P_R} = f(1 - e^{-\frac{t}{\tau}})$$

- P<sub>A</sub> = POWER AFTER ANNEAL
- P<sub>R</sub> = POWER AFTER IRRADIATION
- P<sub>I</sub> = POWER INITIAL
- t = ANNEALING TIME
- τ = RECOVERY TIME
- f = RECOVERY FACTOR

PHOTON TEST DATA (ROCKWELL)

RADIATION** ANNEALING TEMP ANNEALING TIME	10 MEV (6.6 X 10 <sup>10</sup> ) 130C 65 HRS		3 MEV (3.3 X 10 <sup>10</sup> ) 130C 65 HRS		1 MEV (1 X 10 <sup>12</sup> ) 180C 17 HRS	
	BEST	TYPICAL	BEST	TYPICAL	BEST	TYPICAL
INITIAL						
V <sub>oc</sub>	0.987 V	0.87 V	0.90 V	0.85 V	0.889 V	0.85V
I <sub>sc</sub>	0.62 MA	0.61 MA	0.66 MA	0.63 MA	0.34 MA	0.44 MA
AFTER IRRADIATION						
V <sub>oc</sub>	98.6%	93.7%	98.5%	96%	68.1%	64%
I <sub>sc</sub>	90.1%	76.4%	91.3%	85.3%	54.1%	45.8%
RECOVERY						
V <sub>oc</sub>	99.3%	97.2%	99.2%	97.8%	83.6%	73.1%
I <sub>sc</sub>	95.1%	88.3%	94.2%	93.1%	80%	75.2%

\*\*PROTONS/CM<sup>2</sup>

Figure 3.1-10. GaAlAs Solar Cell Annealing Effects

all of the radiation damage can be annealed out with sufficient time and proper temperature.

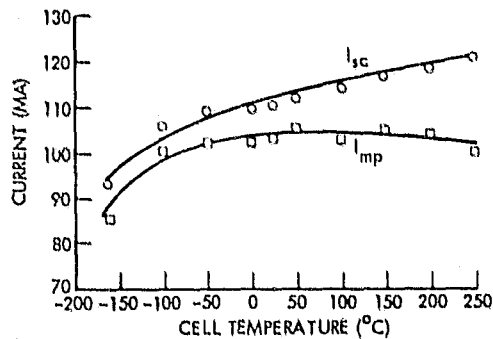
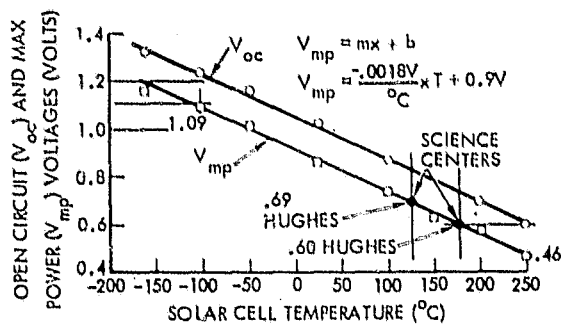
The open circuit voltage, maximum power voltage, short circuit current, and maximum power current curves of the GaAlAs cells are shown in Figure 3.1-11. The curves are the experimental results of the Rockwell Science Center and the Hughes Research Center GaAlAs solar cell development programs. The relationship for the maximum power voltage is

$$V_{mp} = -0.0018 \frac{V}{^{\circ}C} \times T + 0.9 V.$$

At the solar array operating temperature of 125°C, the maximum power voltage of the cell is 0.69 V.

Figure 3.1-12 shows the point design GaAlAs solar cell cross-sectional thickness and mass. Assembly of cells is automated in strips approximately 11.1 cm wide. Each individual cell is 2.04 cm x 3.59 cm with three parallel cells assembled onto the 11.1 cm strip. The active GaAs region is grown onto the edge field growth (EFG) sapphire ribbon by MO-CVD process. Total mass of the solar array blanket is 0.252 kg/m<sup>2</sup>. The EOL blanket output is 324 watts/m<sup>2</sup>, resulting in a specific power output of 1285 watts/kg (585 watts/lb).

GaAs Junction Thickness On Power Conversion Design. The effect of the GaAs junction thickness on cell efficiency, array weight, deployed area, power to weight ratio and gallium requirement was investigated in the study. The basic efficiency of the GaAs and Si type solar cells as a function of cell thickness are shown in Figure 3.1-13. The theoretical efficiencies of GaAs



TODAYS XPMT CELLS (HUGHES)  
(2 x 2 CM)  
CR=1; 125C  
 $\eta$ =13.1% (AMO)  
 $V_{MP}$ =0.69 VOLTS/CELL  
 $I_{MP}$ =107 MA ~ 53.5 MA/CM (WIDTH)

SPS DESIGN B.O.L.  
(2.04 x 3.59 CM)  
CR=1.72; 125C  
 $\eta$ =17.6%  
 $V_{MP}$ =0.69 V/CELL (0.642 V/CM)  
 $I_{MP}$ =123 MA/CM (WIDTH) (105.4 MA/CM)

( ) = EOL

Figure 3.1-11. GaAlAs Solar Cell Voltage And Current Characteristics

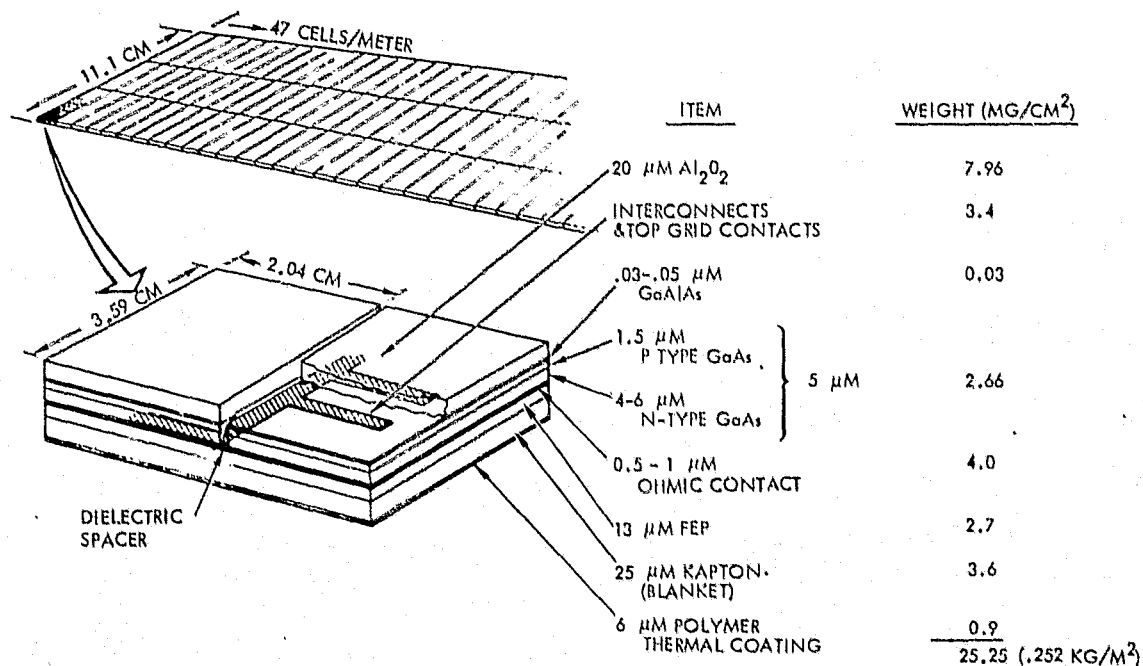


Figure 3.1-12. GaAlAs Solar Cell Blanket Cross Section

and Si cells are 22% and 20% respectively. The GaAs cell is seen to reach optimum efficiency at a thickness of approximately 5  $\mu\text{m}$  and the Si cell at 75 to 100  $\mu\text{m}$  (25  $\mu\text{m}$  = 1 mil) thickness. An analysis was conducted on the GaAs cell utilizing the efficiency versus thickness values to determine the power to weight ratio. The power to weight ratio is plotted in Figure 3.1-14. Normalizing the power to cell weight ratio based on a 5  $\mu\text{m}$  junction thickness, the curve indicates that the maximum power to weight ratio for GaAs cells is for a junction thickness of approximately 1 to 2  $\mu\text{m}$  and results in a 15% power to weight increase compared to the 5  $\mu\text{m}$  cell.

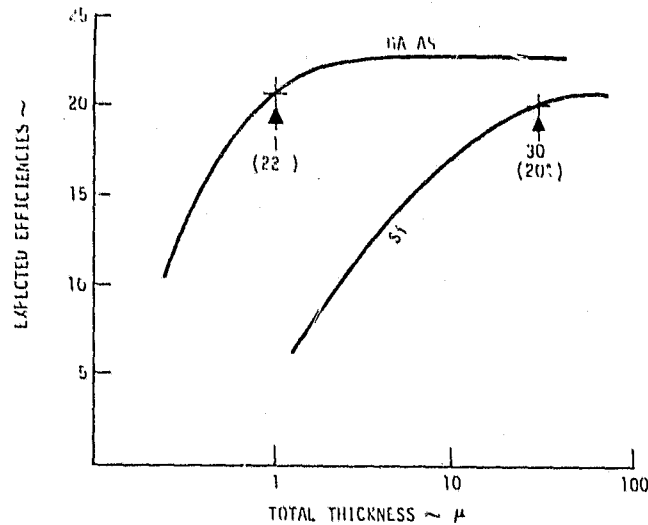


Figure 3.1-13. Efficiency Vs. Thickness  
(Optimum Conditions)

Figure 3.1-14 also shows the deployed solar cell area requirement and the weight of GaAs required for a 5 GW SPS having a concentration ratio of 2. The 5  $\mu\text{m}$  cell junction was selected for the point design concept. However, if junction thicknesses of 1 to 2  $\mu\text{m}$  are used, there is only a slight penalty in the deployed solar cell area required but a potential of reducing the GaAs requirement by over 50%.

The GaAs weight, Ga weight and combined weights of the solar cell blankets, reflectors, structure, wiring and attitude control subsystems are presented in Figure 3.1-15 as a function of the GaAs junction thickness. The combined subsystem weight is almost constant for cell junction thicknesses of 2 to 10  $\mu\text{m}$  and the combined weight is not a real discriminator in choosing the cell thickness. The main variables for choosing the cell thickness are the cost of Ga, quantity of Ga required, and fabrication/manufacturing complexity as thickness decreases below 5  $\mu\text{m}$ . In the study, a 5  $\mu\text{m}$  cell thickness was used in the point design concept. However, there is a potential reduction of 50% or more in the quantity of Ga required for the SPS with very little penalty in the combined subsystem weight and deployed solar cell area if the cell can be made with junction thicknesses of 1 to 2  $\mu\text{m}$ .

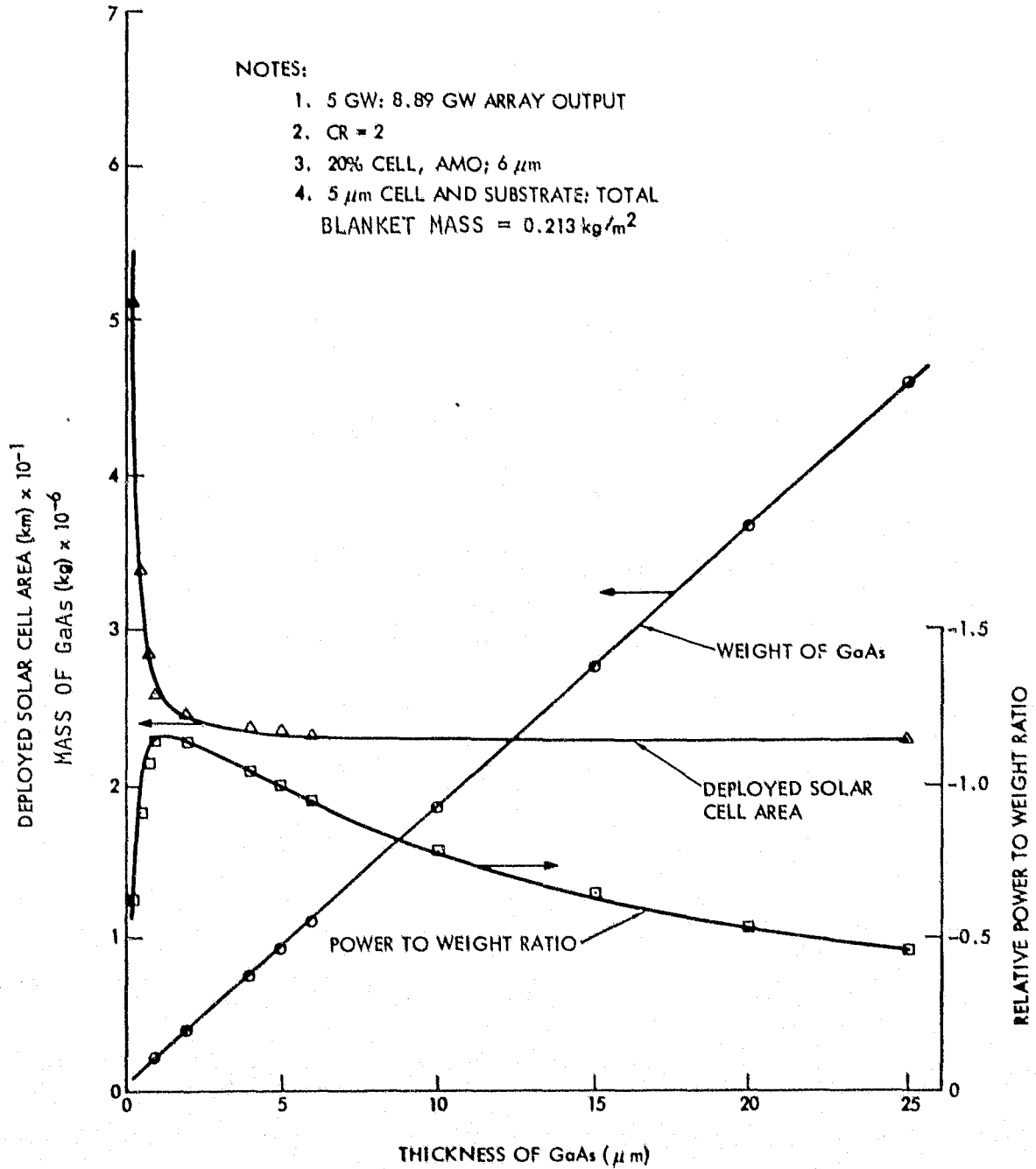


Figure 3.1-14. Deployed Area, Relative Power to Mass Ratio, and Mass of GaAs for SPS As A Function Of Cell Thickness

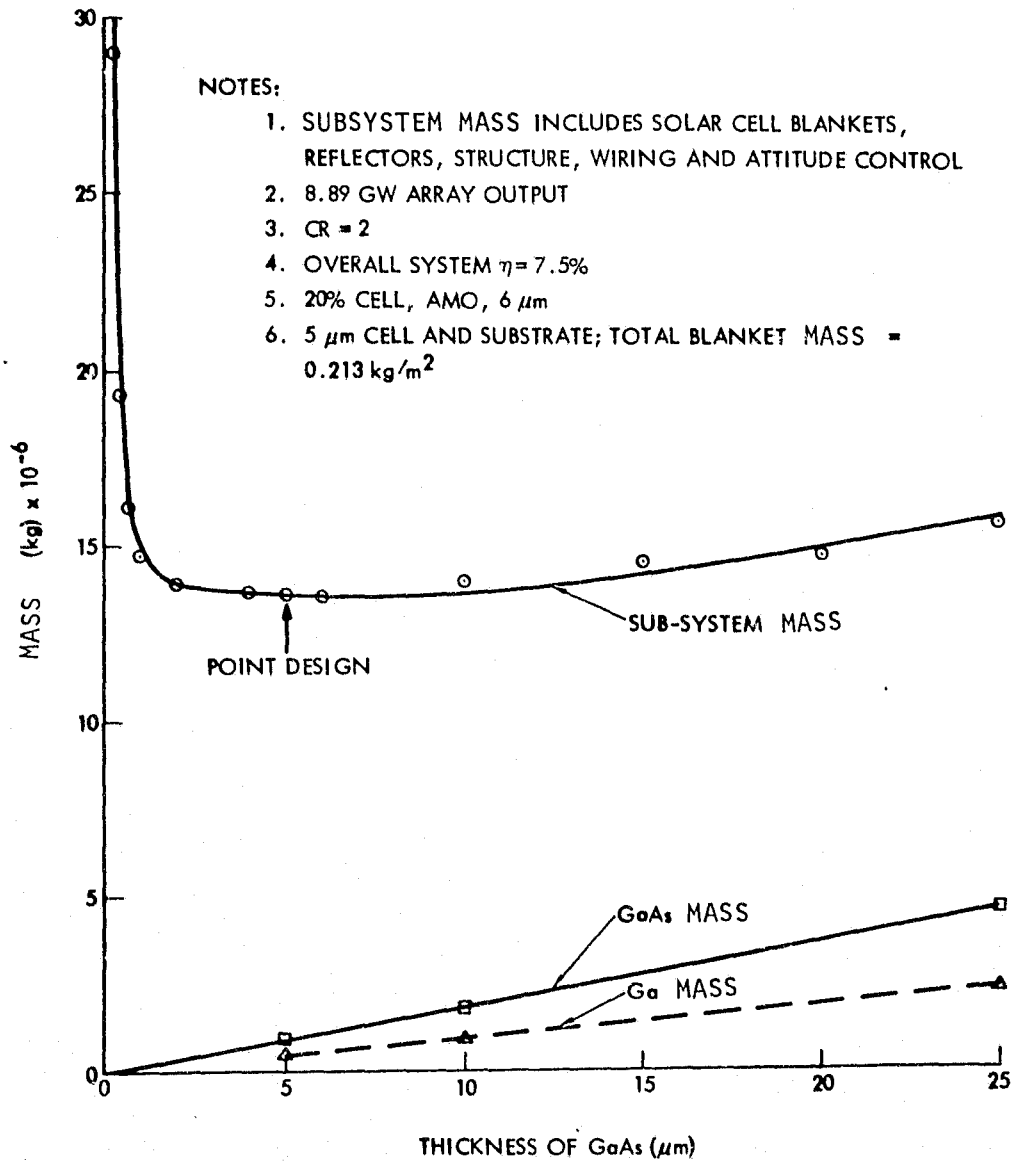


Figure 3.1-15. Subsystem Mass and Mass of GaAs For A 5 GW SPS As A Function Of Solar Cell Thickness



## Configuration Trades

### Concentration Ratio Vs. Orientation Sensitivity.

The weights of several SPS configurations were calculated as a function of the design concept and the concentration ratio and are shown in Figure 3.1-16. The flat plate 4 sided reflector configuration, compound parabolic, Vee trough and a GaAlAs planer arrays for a 5 GW system were evaluated. Preliminary data indicates that the two sided Vee trough configuration is the lightest weight system of those investigated. At concentration ratios greater than 2, the design is more complex and the requirement for primary and secondary structure and orientation accuracy increases and adds additional mass penalty to the system. The free standing 4 sided flat plate and compound parabolic configuration using 3 mil Al foil for the reflector is seen to be approximately 23% heavier than the trough configuration at CR-2.

Analyses were performed and engineering drawings were generated to determine the impact of misorientation of the solar array and reflectors on the sizing of the SPS. Concentration ratios of 1, 2, 5 and 8 were investigated. The major emphasis was placed on the sizing and design of the arrays and reflectors.

The ray trace for a  $\pm 1$  deg misorientation for the open trough configuration is shown in Figure 3.1-17. A misorientation of  $-1$  deg results in the reflected beam hitting partially above the solar blanket and, at the same time, is illuminating a smaller area; therefore, the concentration ratio will be slightly higher than the nominal value. For a  $+1$  deg misorientation, the reflected beam hits partially below the solar blanket and at the same time is illuminating a larger area; therefore, the concentration ratio will be slightly lower than the nominal value. In order to still provide full power out of the array for misorientation angles, the solar cells will have to be placed only where there is continuous illumination, as defined as the effective solar cell area in the diagram. In order to still provide the full power rating, the number of troughs must increase and/or the length of the wings must increase because the active solar cell area has to be constant.

The reflector surface area penalty required to "desensitize the system to misorientation angles is shown in the table (Figure 3.1-17). The area penalty is shown as a function of concentration ratio and misorientation angle. The table shows that as the concentration ratio exceeds 5, or  $\pm 2$  degrees misorientation at CR=5, the reflector surface area penalty exceeds 200 percent which adds excessive structure, power distribution, attitude control and reflector weight to the system.

The sensitivity of the reflector size as a function of concentration ratio and misorientation angles is shown in Figure 3.1-18. The curves show the variation of the concentration ratio across the plane of the solar cells. The curves indicate that as the misorientation angle increases, less of the reflected energy is reflected onto the plane of the solar cell and therefore power is lost because less energy is falling on the solar cells. At concentration ratios of 5 or greater, the intensity is starting to vary sufficiently to cause design problems with the output of the solar cells, then the attitude

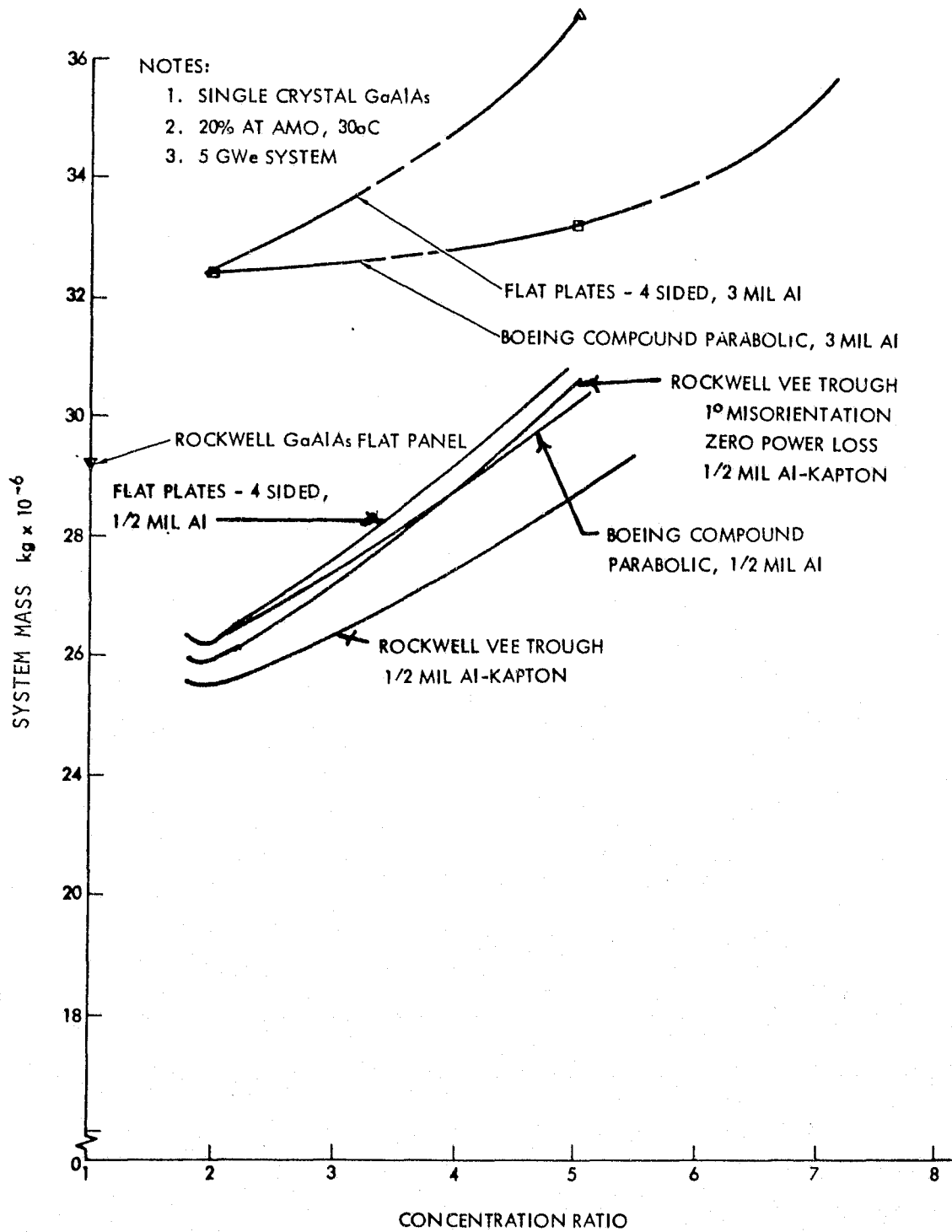


Figure 3.1-16. SPS Mass As A Function of Concentrator Configuration And Concentration Ratio (No Misorientation Allowances Included)

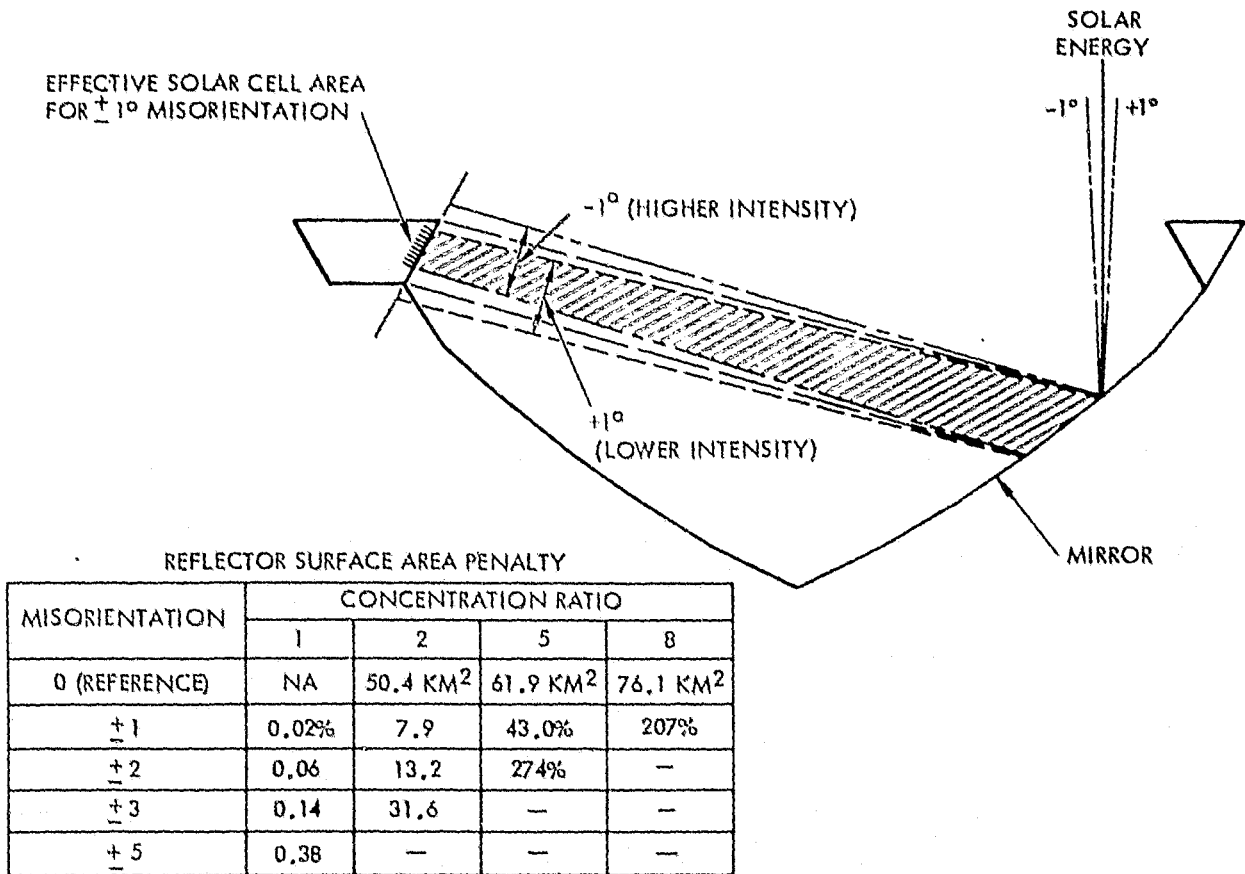


Figure 3.1-17. Concentration Ratio Sensitivity

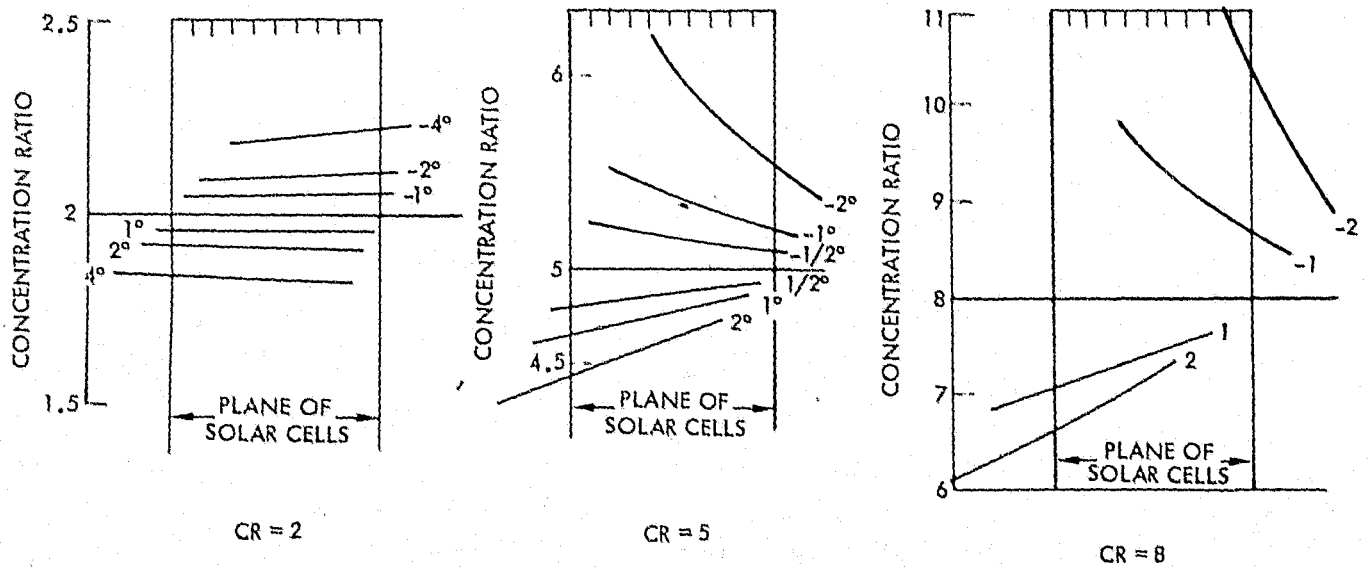


Figure 3.1-18. Concentration Ratio Sensitivity With Misorientation Angle





control system will have to control the reflectors to  $\pm 0.1$  deg misorientation or less, depending on the concentration ratio.

A conceptual drawing of the 5 GW GaAlAs photovoltaic system with a concentration ratio of 5.0 is shown in Figure 3.1-19. The satellite is 30.54 km long and 3.35 km wide. The standard size bay is 650 m by 660 m and the active cell area is 10.16 km<sup>2</sup>. The reflector area and satellite were sized from this analysis to generate 5 GW of power with a total misorientation and figure control error of  $\pm 1^\circ$ . The reflector surfaces shown in Figure 3.1-19 are stretched aluminized kapton on a frame which is approximately 60 m wide and 660 m long. A minimum of 10 reflector surfaces are required for each bay.

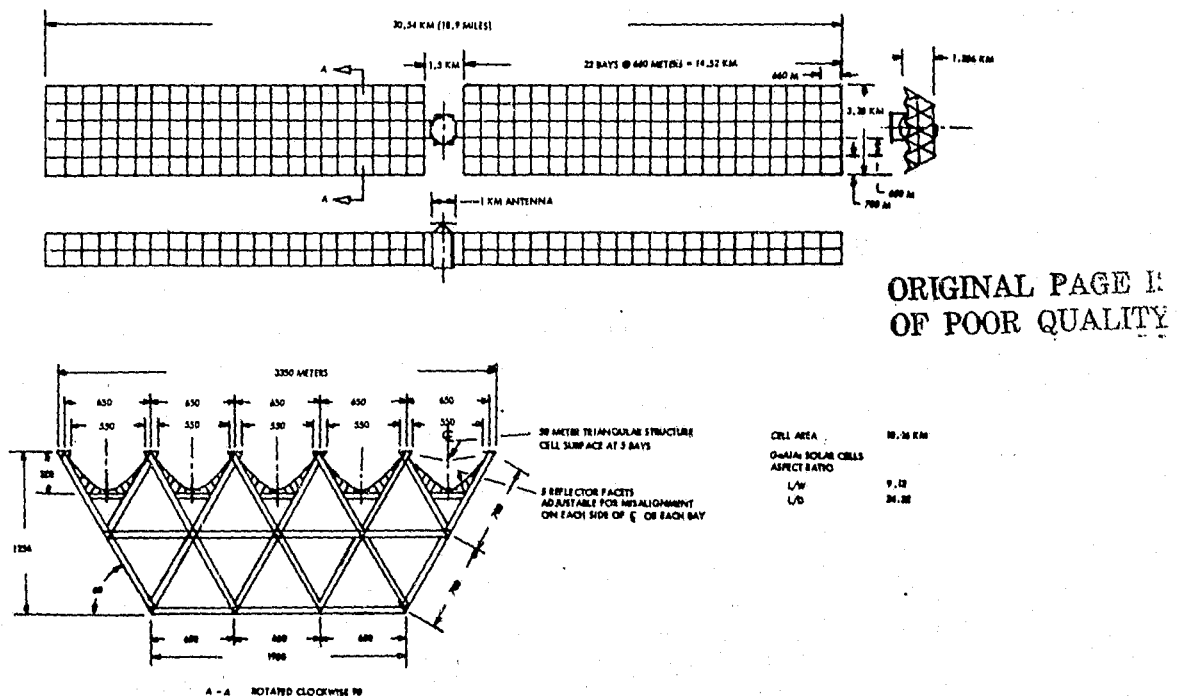
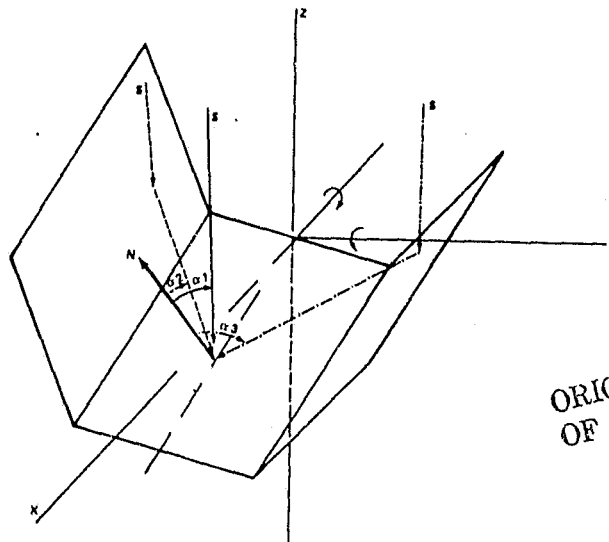


Figure 3.1-19. 5 GW Photovoltaic - CR-5  
- Concept No. 2C

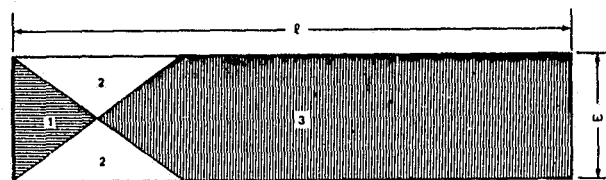
Misalignment of the array effects the performance by varying the effective concentration ratio and temperature. Change in effective concentration ratio results from (1) change in angle of incidence, (2) loss in area illuminated by reflectors, and (3) reflector shadowing and/or loss of solar interception. The factor influencing the performance of a concentrating array include effective concentration ratio ( $N_e$ ), temperature, and cell efficiency most of which are interdependent and are either directly or indirectly influenced by pointing. Under sun oriented conditions the effective concentration ratio is described by  $N_e = 1 + 2\eta_1 \eta_2 \cos\alpha$ . The reflected energy angle of incidence ( $\alpha$ ) being a function of the reflector angle. As the array is maneuvered such that misalignment with the solar vector is encountered,  $N_e = \cos\alpha_1 + \eta_1\eta_2 (\cos\alpha_2 + \cos\alpha_3)$ . See Figure 3.1-20 for angle definition.



ORIGINAL PAGE IS  
OF POOR QUALITY

Figure 3.1-20. Solar Vector Interception  
With Misoriented Array

Misorientation about the y axis causes an illumination pattern on the solar blanket similar to Figure 3.1-21 to occur. Area 1, Figure 3.1-21 is illuminated only by direct sun, area 2, by direct plus 1 reflection and area 3, by direct plus 2 reflections. The size of these areas are influenced by the reflector angle, angle off the sun line, and the L/W ratio of the solar cell area. The L/W ratio has the greatest influence on size of the area. In the MSFC proposed design, the losses from this area becomes negligible because of the high L/W ratio. On other concepts where L/W is not as high, this loss should be taken into consideration.



AREA	ILLUMINATION
1	D
2	D+1R
3	D+2R

ILLUMINATION LEVEL INCLUDES  
ENERGY FROM DIRECT SUN  
AND FROM REFLECTORS

AREAS AND AVERAGE VARY WITH L/W RATIO, ANGLE OF REFLECTOR  
AND ANGLE OF MISORIENTATION WITH SUN VECTOR

Figure 3.1-21. Solar Cell Blanket Illumination Pattern



Misorientation about the x-axis causes area 2, Figure 3.1-21 to extend along the edge of cell area decreasing the effectivity of the concentrator. Large angle of incidence and loss of illumination area become a problem when large misalignment errors are encountered about this axis.

The impact of misalignment about the y-axis only is shown in Figure 3.1-22. Figure 3.1-23 shows effect of pointing error about the x-axis. Data are presented as a percent of maximum array capability at BOL with array normal to the sunline. A comparison of the sensitivity of a planer array and concentrator arrays for CR-2 and CR-5 to the misorientation angle are shown in Figure 3.1-24. Off sun pointing errors in both axes for the Vee trough MSFC design are shown in Figure 3.1-25. The results show that only a small percentage loss ( $\approx 3\%$ ) would be incurred if misalignment is restricted to  $< + 5^\circ$  about both axes. Concepts having a lower L/W ratio would experience higher losses.

The low concentration systems result in a simpler design and higher tolerance to solar pointing requirements. The higher concentration systems offer the advantage of reduced number of solar cells and thereby lower potential system costs and reduced quantities of Ga required per satellite. A major consideration in the design of the concentrator systems is the performance and reflectivity of the aluminized thin film reflectors. A list of the reflector parameters is shown in Table 3.1-4. Resolution of these issues is difficult because of conflicting data in the literature and lack of long duration on orbit test data. This is identified as a critical area where experimental data is needed, because of the major impact on satellite configuration, weight and cost.

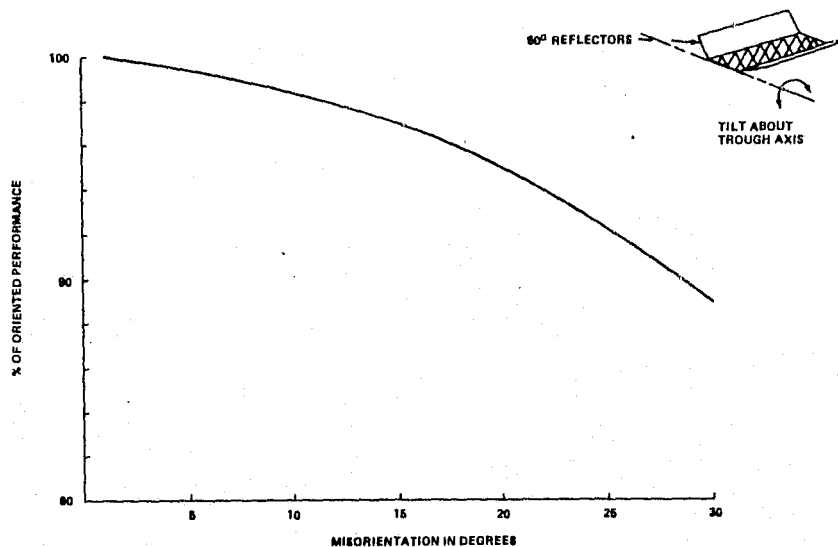


Figure 3.1-22. Array Sensitivity To Tilt Misorientation

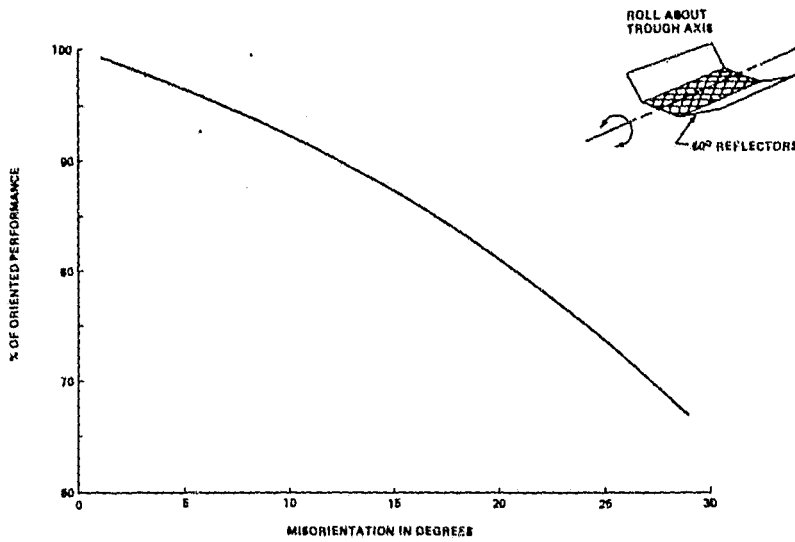


Figure 3.1-23. Array Sensitivity To Roll Misorientation

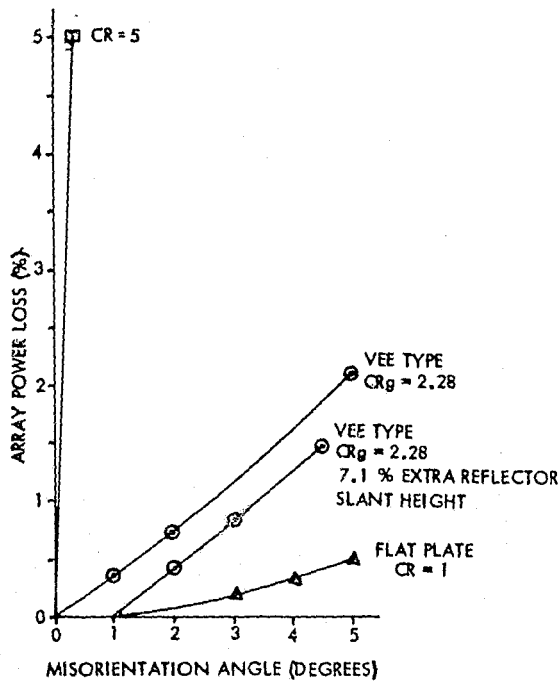


Figure 3.1-24. Solar Array Power Loss As A Function Of Misorientation Angle And Configuration

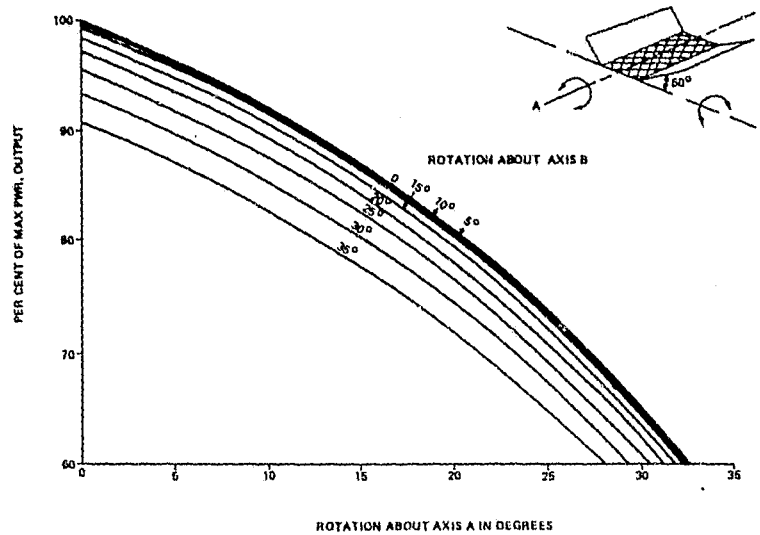


Figure 3.1-25. Concentrator Array Sensitivity To Misorientation

Table 3.1-4. Reflector Degradation

1. OXIDATION OF FILM DURING MANUFACTURE, STOWAGE, STORAGE, AND LAUNCH
2. MECHANICAL WEAR OF FILM DUE TO WINDING AND UNWINDING, AIR CURRENTS, AND PARTICULATE CONTAMINANTS
3. SPACE ENVIRONMENT
• IONIZED RADIATION EFFECTS
• DEPOSITS ON FILM FROM SPACE PARTICLES AND EXHAUST PRODUCTS OF SATELLITE
• CHEMICAL REACTION OF DEPOSITS ON FILM
• METEOROIDS
4. SELECTED DESIGN VALUES
$R_{BOL} = 0.9$
$R_{EOL} = 0.72$
NOTE: ECHO SATELLITES (12.5 $\mu$ m MYLAR WITH 0.22 $\mu$ m Al COATING) FLEW IN INTENSE REGIONS OF THE VAN ALLEN RADIATION BELTS WITH APPARENTLY LITTLE DEGRADATION.

The photovoltaic system utilizing GaAlAs cells have been configured for CR-1, 2 and 5. A Si photovoltaic system for CR-1 has also been investigated for comparison purposes. The planform areas of the systems are shown in Figure 3.1-26. The first configuration is for Si cells and the remaining five configurations are based on GaAlAs solar cells. Two of the major design drivers for the concentrator photovoltaic systems are the on orbit reflector degradation and the allowable misorientation angle of the reflectors. The designs investigated employ an active reflector control system or a passive system to accommodate a  $\pm 1^\circ$  misorientation. Analysis to date tend to

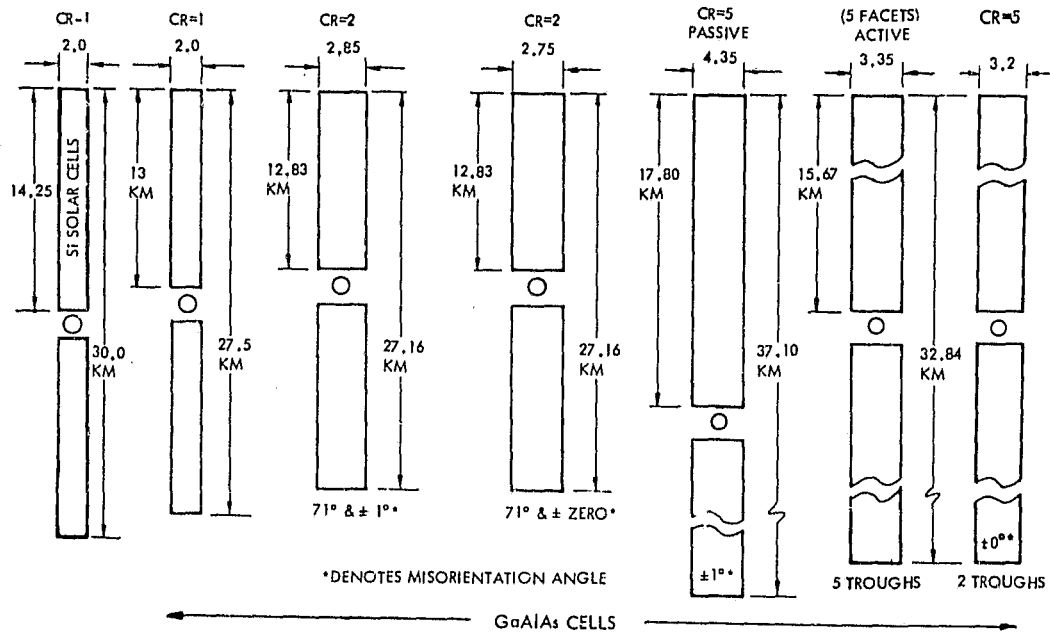


Figure 3.1-26. Planforms Of Photovoltaic Systems

indicate that a misorientation of  $\pm 0.1^\circ$  may be attained. The systems as shown in the planform figure were investigated for misorientations of  $0^\circ$  and  $\pm 1^\circ$ .

The reflector degradation from ionized radiation was taken as a 20% loss and reflector membrane tensioning of 100 psi or below compared to 1000 psi. Membrane tensioning below 100 psi appears to be adequate for obtaining good performance. Lockheed has conducted tests on the SEPS test array with concentrators (2:1) with membrane tensioning below 100 psi and have obtained excellent performance results in agreement with predicted values for perfect tensioning. Based on these results and other vendor inputs, 1000 psi membrane tensioning is deemed too high.

A system comparison is shown in Table 3.1-5. Weight penalties for each of the GaAlAs configurations for reflector degradation,  $\pm 1^\circ$  misorientation, and tensioning load on the reflector are shown.

#### GaAlAs Solar Cell Configuration Trades.

*Configuration Analysis CR-2.* The CR-2 configuration for GEO assembly was investigated in further detail to aid in determining configuration advantages and disadvantages. Three basic concepts were sized and listed below:

1. "Vee" trough  $71^\circ$  reflector slant angle
2. "Vee" trough  $60^\circ$  reflector slant angle
3. Flat-open trough

Table 3.1-5. Photovoltaic System Comparisons

CR	MIS-ORIENTATION ANGLE (DEGREES)	OVERALL SYSTEM <sup>7</sup> (%)	SOLAR CELL AREA (km <sup>2</sup> )	TOTAL CELL/REFLECTOR PLANE FORM AREA (km <sup>2</sup> )	REFLECTOR SURFACE AREA (km <sup>2</sup> )	MASS <sup>*</sup> (kgX10 <sup>-6</sup> )		
1	+1	7.53	48.99	48.99	0	37.279		
2	(71°)	+0	6.18	23.76	61.78	116.8	33.714	
	(71°)	+1	6.18	23.76	64.24	124.4	33.964	
5	5 TROUGHS	PASSIVE	+0	4.69	10.4	79.9	88.6	39.250
			+1	4.69	10.4	140.3	140.9	44.137
	2 TROUGHS	ACTIVE	-	4.69	10.4	79.9	88.6	39.436
			PASSIVE	+0	4.69	10.4	80.4	89.2

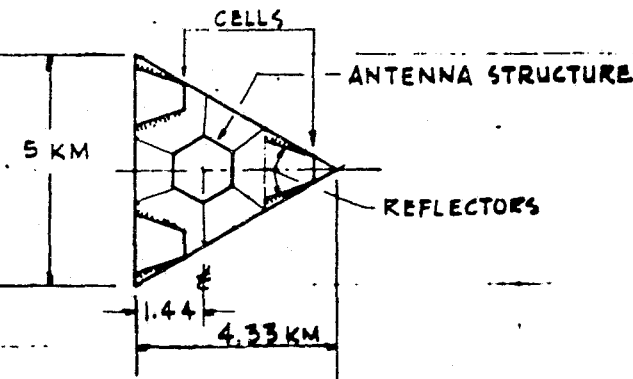
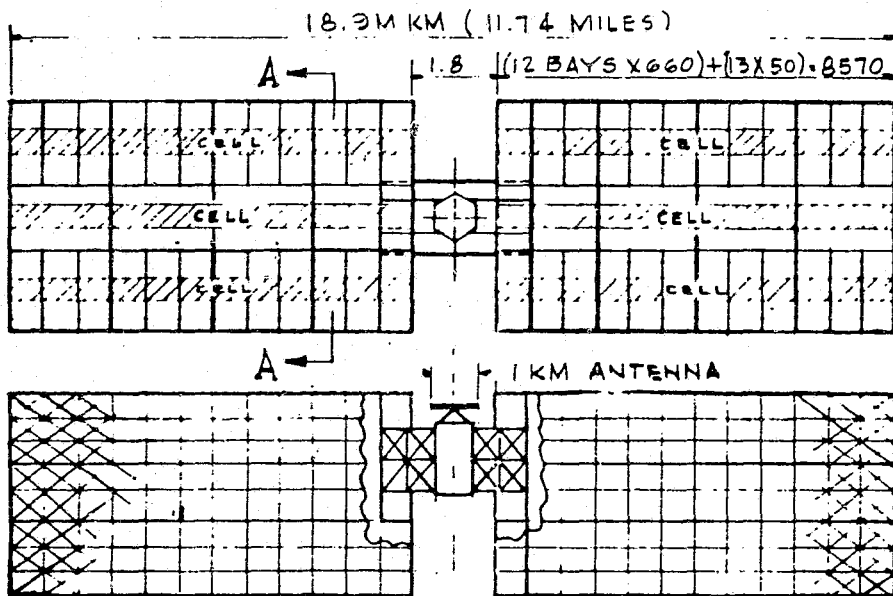
\*Includes average of 31.2 percent growth.

ORIGINAL PAGE IS  
OF POOR QUALITY

The drawings for the three configurations are shown in Figures 3.1-27, 3.1-28, and 3.1-29 and are based on the "wedge" cross sectional structural configuration. The 71° reflector configuration (shown in Figure 3.1-27 is designed to minimize the deployed solar cell area and compensate for a 20% reflector degradation by deploying additional reflector area. The 71° reflector design has a BOL concentration ratio of 2.44 and an EOL concentration ratio of 2:15. The overall SPS dimensions are 5 km x 18.9 km.

The 60° Vee trough configuration is shown in Figure 3.1-28. Because of the 60° angle constraint, and the optics, additional solar cells must be deployed to compensate for the decrease in performance of the reflectors. Utilizing the 60° reflector angle, the geometric concentration ratio is 2.0. The BOL concentration ratio is 1.9 and the EOL concentration ratio is 1.72. The SPS size of the configuration is 3.15 km x 23.2 km. The 60° Vee trough configuration requires 29.5 km<sup>2</sup> of solar cells compared to 23.76 km<sup>2</sup> of cells for 71° Vee trough configuration.

The flat open trough configuration is shown in Figure 3.1-29. The solar cells do not receive direct sunlight as in the 71° "Vee" configuration and the 60° configuration. The open trough configuration has the overall dimensions of 4.16 x 22.9 km. The open trough configuration also requires the minimum size solar array. Comparing the open trough to the 71° Vee trough, both configurations require the minimum solar cell area but the open trough requires the minimum reflective surface area. The lower reflective surface (approximately 36 km<sup>2</sup>) is the result of the improved utilization of shape and area of the reflector for the open trough compared to the 71° configuration. A summary of the overall configuration parameters for the three configurations is presented in Figure 3.1-30.

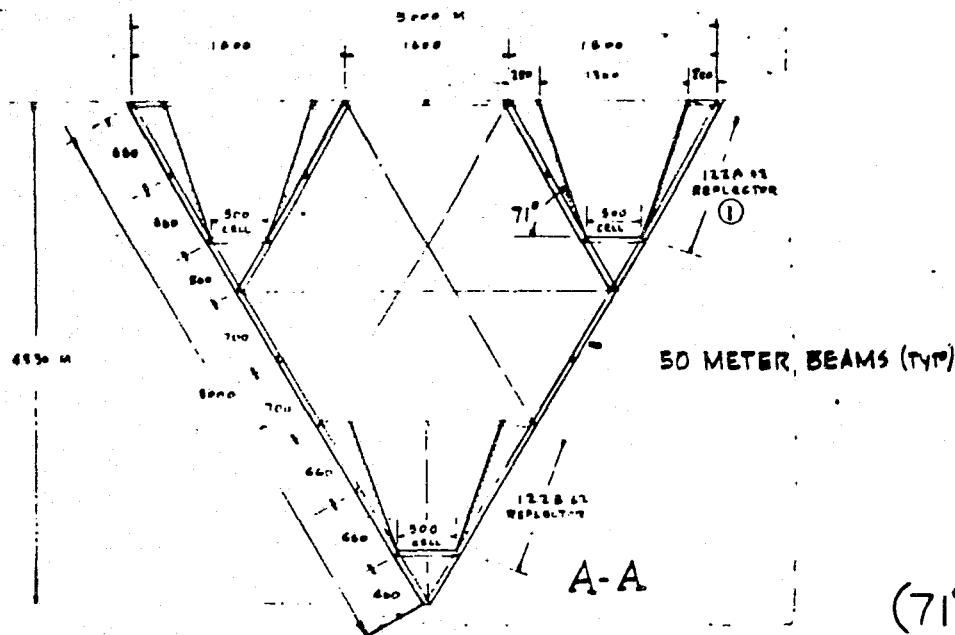


ORIGINAL PAGE IS  
OF POOR QUALITY

ORIGINAL PAGE IS  
OF POOR QUALITY

3-29

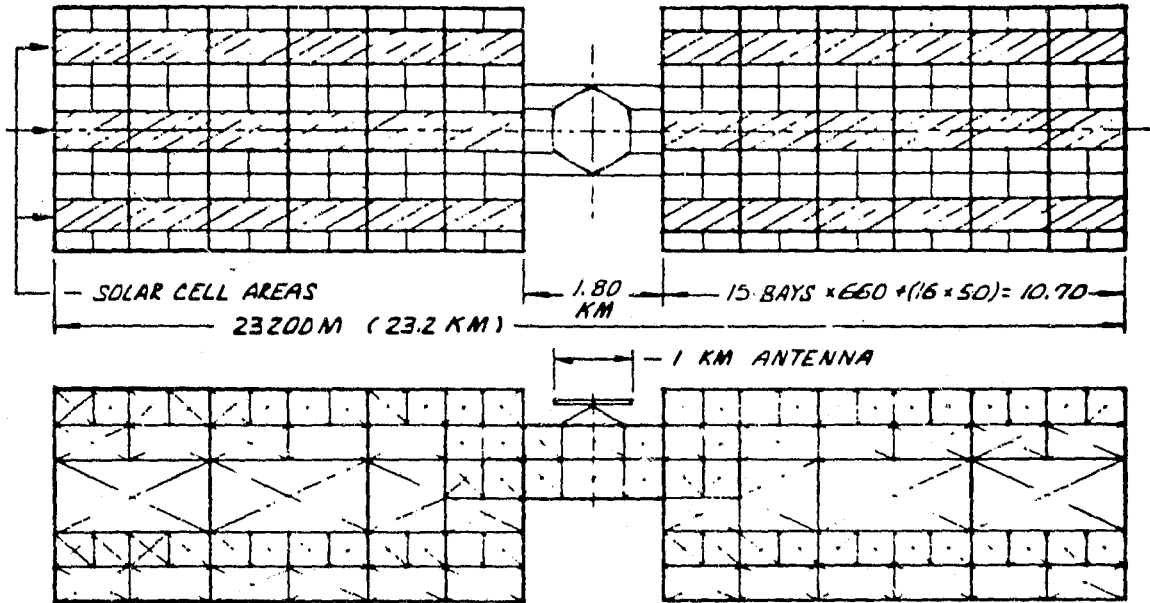
SD 78-AP-0023-3



- REFLECTOR SURFACE AREA 116.77 KM<sup>2</sup>
- REFLECTOR INTERCEPT AREA 61.78 KM<sup>2</sup>
- CELL AREA (GaAlAs) 23.76 KM<sup>2</sup>
- ASPECT RATIO
- L/W 3.78
- L/D 4.36
- CR (NOM) 2.0
- CR (GEO) 2.6
- ① ● LENGTH OF REFLECTOR DETERMINED BY OPTICS LAYOUT TO ACCOMMODATE ZERO DEGREE MISALIGNMENT

Figure 3.1-27. 5-GW Photovoltaic CR = 2 Concept No. 2F-4 Balanced Inertias





- REFLECTOR SURFACE AREA 59.4 KM<sup>2</sup>
- REFLECTOR INTERCEPT AREA 59.4 KM<sup>2</sup>
- CELL AREA (GaAs) 29.5 KM<sup>2</sup>
- ASPECT RATIO
  - L/W 7.73
  - L/D 8.37
- CR (NOM) 2.0
- CR (GED) 2.0

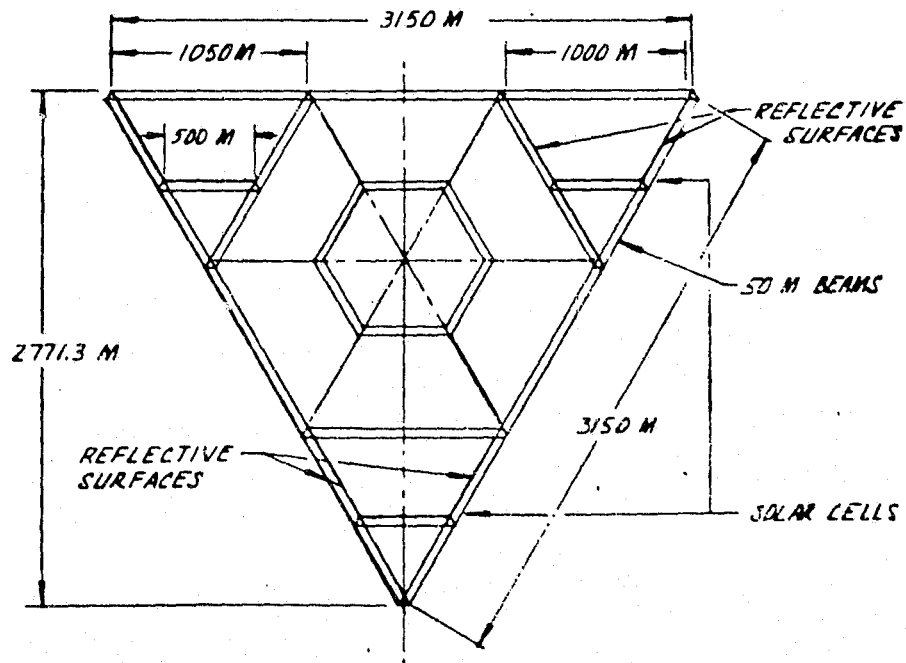
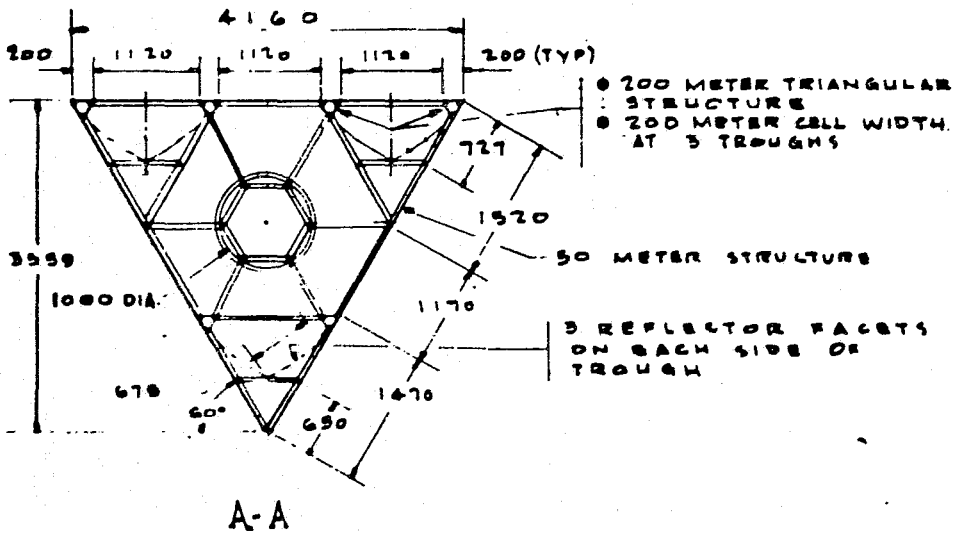
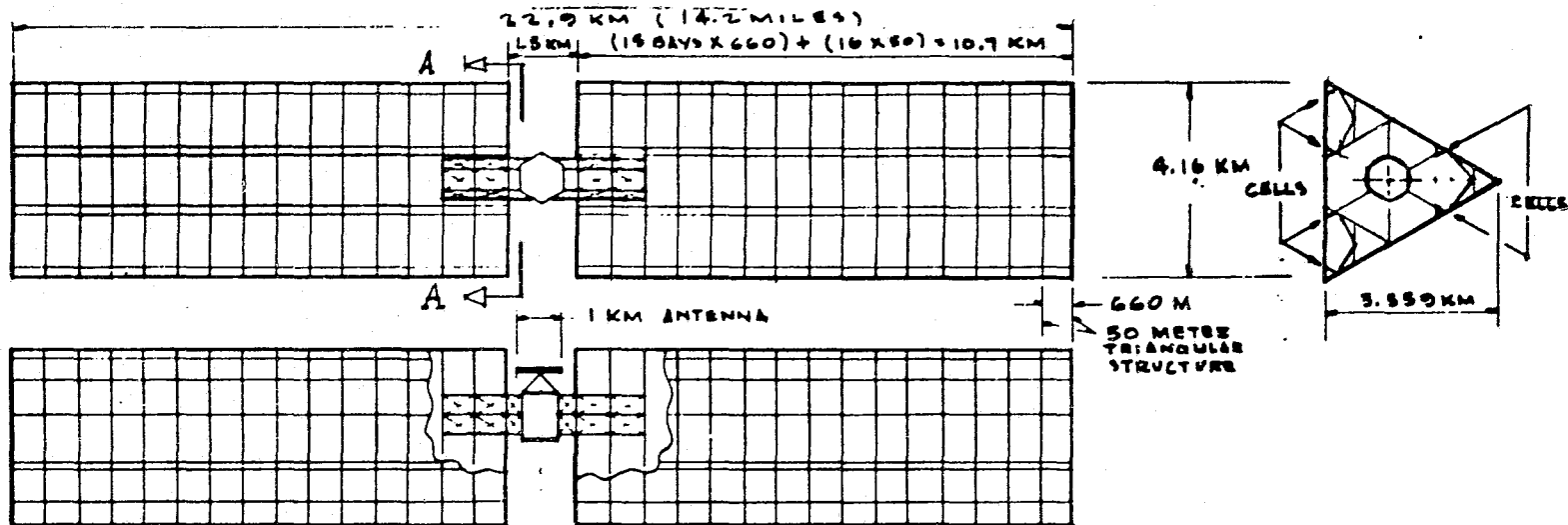


Figure 3.1-28. 5-GW Photovoltaic CR-2 Concept  
(60° Reflector Angle)

3-31

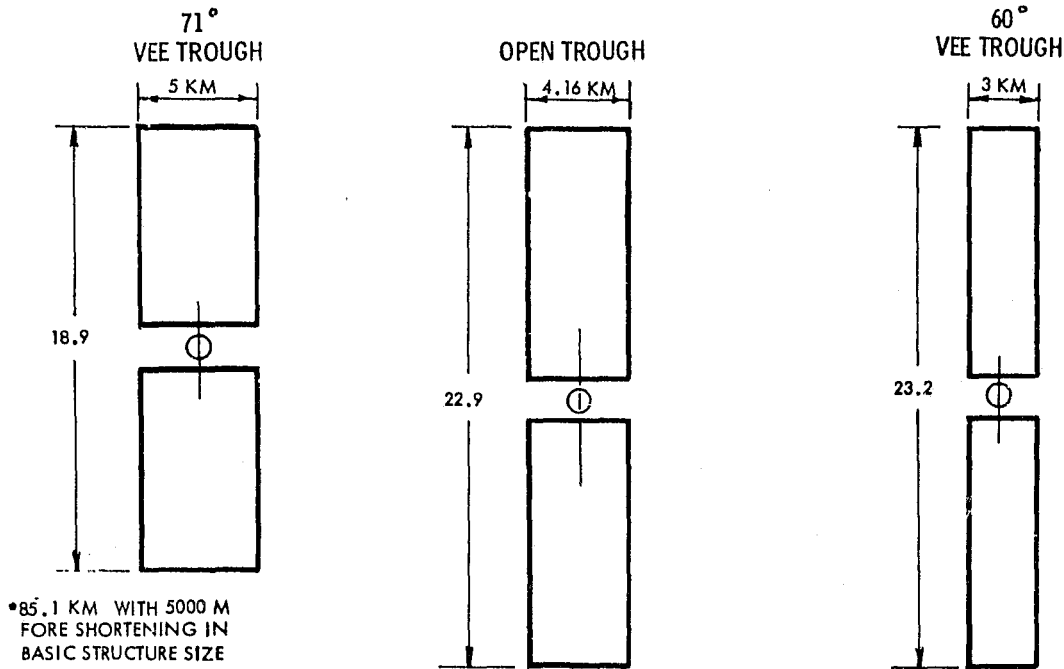


- REFLECTOR SURFACE AREA 80.19 KM<sup>2</sup>
- REFLECTOR INTERCEPT AREA 66.53
- CELL AREA (GA AL AG) 23.76 KM<sup>2</sup>
- ASPECT RATIO L/W
- CR (NOM) 5.8
- CR (660) 5.403

ORIGINAL PAGE IS  
OF POOR QUALITY

Figure 3.1-29. 5-GW Photovoltaic CR-2 Open Trough

SD 78-AP-0023-3



CONFIGURATION	71° VEE (KM <sup>2</sup> )	OPEN TROUGH (KM <sup>2</sup> )	60° VEE (KM <sup>2</sup> )
SOLAR CELLS	23.76	23.76	29.5
REFLECTORS	116.8	80.2	59.2
PLANFORM	94.5 *	95.3	69.6

Figure 3.1-30. SPS Configuration Planform and Area Summary Data

Trade off studies to determine the mass and cost were also performed to define in more detail the baseline design point for the "wedge" type structural configuration having a CR-2. Table 3.1-6 shows the areas, mass and costs of the solar cell, reflector, array conductor and structure as a function of efficiency and launch costs of \$10 to \$60/kg to GEO. The data from Table 3.1-6 is plotted in Figure 3.1-31. This data was utilized in determining optimum power distribution efficiency based on minimum cost. The SPS configuration has a deployed solar cell array of 30.376 km<sup>2</sup> for a power distribution efficiency of 94%.

Point Design GaAlAs Solar Cell Configuration. The point design solar array was further analyzed to show parametric impact of the reflect slant angle on the weight and cost of the system. Reflector slant angles were parameterized at 60°, 65° and 71° for the GaAlAs "Vee" trough configuration. The subsystems affected by the reflector slant angle and included in the analysis consists of the following:

1. Reflectors
2. Solar cell array
3. Primary/secondary structure
4. Power distribution

ORIGINAL PAGE 13  
OF POOR QUALITY

Table 3.1-6. Photovoltaic Mass and Cost Summary

DIST. η (%)	OVERALL SYSTEM (%)	SOLAR ARRAY AREA (KM <sup>2</sup> )	REFLECTOR AREA (KM <sup>2</sup> )	BLANKET		WEIGHTS (KG×10 <sup>-6</sup> )					COSTS IN MILLIONS OF DOLLARS				
				LENGTH (M)	WIDTH (M)	SOLAR CELL 0.2 KG/M <sup>2</sup>	REFLECTOR 0.018 KG/M <sup>2</sup>	DIST. WIRES INS. SEC STRUCT.	STRUCTURE	TOTAL WEIGHT	STRUCTURE NASA CER ***	SOLAR CELLS (\$65/M <sup>2</sup> )	REFLECTORS 2.47*	POWER DIST. NASA CER ***	SUBTOTAL
90	5.485	33.684	67.34	747	835	6.737	1.213	1.288	3.176	12.414	15.944	2189.5	166.4	5.2	2377.04
92	5.616	32.908	65.82	730	835	6.582	1.185	1.590	3.141	12.498	15.768	2139.0	162.6	4.8	2322.17
94	5.737	32.208	64.42	714	835	6.442	1.159	2.153	3.110	12.864	15.612	2093.5	159.1	4.7	2272.91
96	5.859	31.538	63.08	699.4	835	6.308	1.135	3.861	3.044	14.384	15.281	2050.0	155.8	4.6	2225.68

VEHICLE LENGTH, 19.9 KM  
54 ACTIVE BAYS  
2 BAYS IN SERIES, 50.1 KW  
CELL TEMP, 160°C EOL AVERAGE  
BAY LENGTH OF CELLS = 835 M

η (%)	TOTAL WEIGHT × 10 <sup>-6</sup> KG	COSTS IN MILLIONS OF DOLLARS						
		LAUNCH			SUBSYS. TOTAL	TOTAL COSTS		
		\$10/KG	\$30/KG	\$60/KG		\$10/KG	\$30/KG	\$60/KG
90	12.414	124.14	372.42	744.84	2377.04	2501.18	2749.46	3121.88
92	12.498	124.98	374.94	749.88	2322.17	2447.15	2697.11	3072.05
94	12.864	128.64	385.92	771.84	2272.91	2401.55	2658.83	3044.75
96	14.384	143.84	431.52	863.04	2225.68	2369.52	2657.83	3088.72

\*22¢/FT<sup>2</sup> 1/2-MIL KAPTON + 1¢/FT FOR AL. COATING = \$2.47/M<sup>2</sup>  
 \*\*C = 4.02 T (CF) × 10<sup>-6</sup>  
 \*\*\*C = 5.02 10<sup>-6</sup> T(CF)

3-33

SD 78-AP-0023-3



1. 5 GW, CR=2, 60° REFLECTOR ANGLE
2.  $\eta_{th} = 61.3\%$
3. WEIGHT INCLUDES SOLAR ARRAY, REFLECTORS, STRUCTURE & POWER DISTRIBUTION
4. COST INCLUDES SUBSYSTEM COSTS OF ITEM PLUS LAUNCH COSTS
5. SOLAR ARRAY COST =  $\$65/M^2$ ; REFLECTOR COSTS  $\$2.47/M^2$ ; OTHER COSTS BASED ON NASA CER

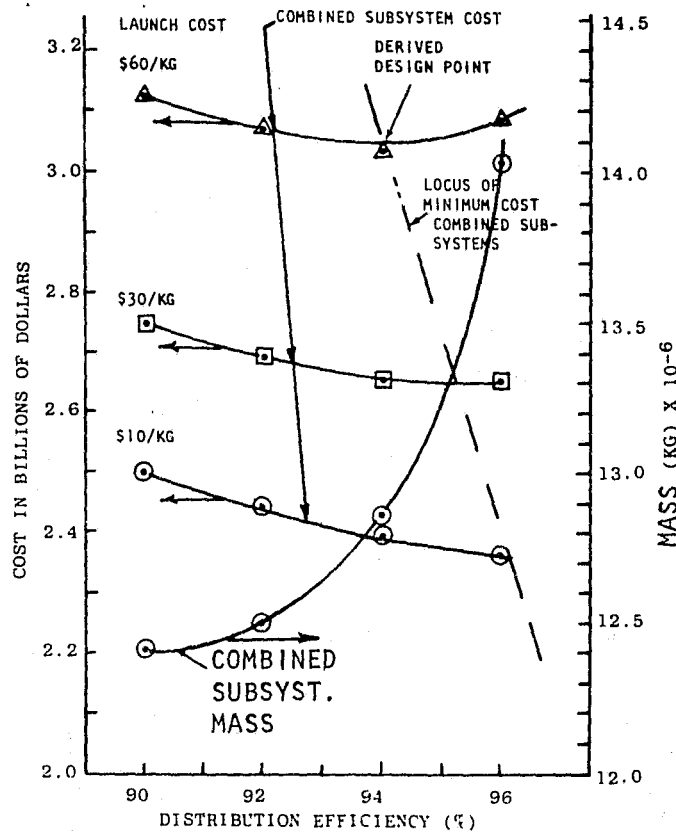


Figure 3.1-31. Photovoltaic Parametric Cost And Mass Comparisons

A comparison of various configurations showing concentration ratios, areas, lengths, widths, and weights are presented in Table 3.1-7. The weight has increased from the mid-term configuration due to refinement in the design and the decision to go to the trough type configuration compared to the triangular wedge configuration that was proposed for the mid-term. The minimum weight system is obtained when the reflector slant angle is approximately 65°. As the reflector angle increases, the concentration ratio increases and the solar cell area decreases which results in lower weights. However, after a certain range (approximately 65°) the structure and reflector weights are increasing at a faster rate than the savings in solar cell weight because of the increase complexity in the design.

A computer cost analysis was performed to determine the cost difference in the costs of the four subsystems that are affected by changing the reflector angle. The cost data is presented in Table 3.1-8 showing the subsystem and subtotal costs for the configurations.



Table 3.1-7. Comparison of Reflector Angles

	MID-TERM 71° "Vee"	3RD QUARTER		
		60° "Vee"	65° "Vee"	71° "Vee"
Concentration Ratio				
GEO	2.7	2.0	2.285	2.58
BOL		1.9	2.16	2.42
EOL	2.15	1.72	1.93	2.14
Reflector Angle (Deg)	71	60	65	71
Reflector Ratio (Ref/Cells)	5.27	2	3.042	4.841
Reflector Surface Area (km <sup>2</sup> )	124.4	60.8	80.9	114.2
Solar Cell Area (km <sup>2</sup> )	23.6	30.4	26.6	23.6
Cell Blanket Width at Base of Troughs (m)		Top 600m Bottom 550m	Top 600m Bottom 550m	Top & Bottom 500m
Length of Each Wing (km)		9.6	8.47	8.6
Overall SPS Length (km)		21.3	19.04	9.3
SPS Width (km)		3.850	3.936	4.384
Weights (Millions of kg)				
Collector Array (Non-Rotating)				
Prim/Sec Struct/Mech	3.993	3.857	3.692	4.416
Attitude Control	0.312	0.135	0.135	0.135
Solar Cells	5.99	7.661	6.703	5.947
Reflectors	2.052	1.094	1.456	2.056
Power Conditioning	0.387	0.673	0.673	0.673
Wire Harness/Slip-Ring/Avionics	2.83	1.399	1.298	1.314
Antenna (Rotating)	10.034	13.390	13.390	13.390
Subtotal	25.599	28.209	27.347	27.931
Growth	8.115	8.463	8.204	9.379
Total SPS Satellite	33.714	36.672	35.551	36.310

Table 3.1-8. Subsystem Cost Comparison As A Function Of Reflector Angles

SUBSYSTEM	COST IN MILLIONS OF DOLLARS		
	3RD AND 4TH QUARTER 60° "Vee"	4TH QUARTER 65° "Vee"	4TH QUARTER 71° "Vee"
Power Source Structure	\$ 19.36	\$ 18.53	\$ 22.17
Solar Blankets	2135.46	1815.80	1670.04
Reflectors	151.94	200.50	279.73
Power Distribution & Conditioning	1655.31	1655.16	1655.18
SUBTOTAL COST	\$3962.07	\$3749.99	\$3627.12

MSFC Si Solar Cell Configuration Trades.

Satellite Systems. This section is devoted to summarizing the evolution of the MSFC 10 GW baseline SPS as documented in NASA TMX-73344 to a 5 GW Baseline that was used as a study reference.

ORIGINAL PAGE IS  
OF POOR QUALITY

*Evolution of Baseline.* After the 10 GW Baseline SPS, as shown in Figure 3.1-32 and summarized in Table 3.1-9, was established many trades studies were performed by MSFC. Some of these trades indicates that significant improvements could be achieved by changes in the design. Three typical trades are shown in Figure 3.1-33 to represent some of the areas where improvements were made.

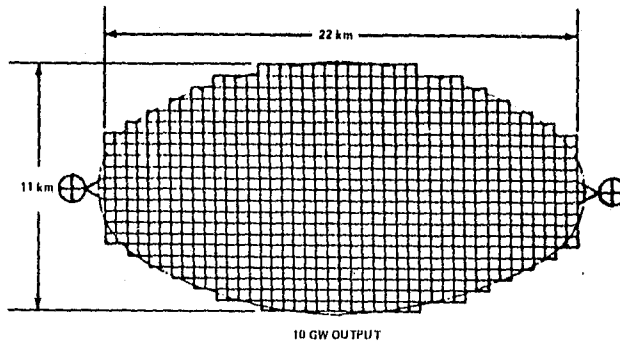

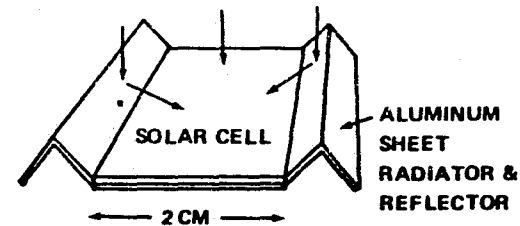
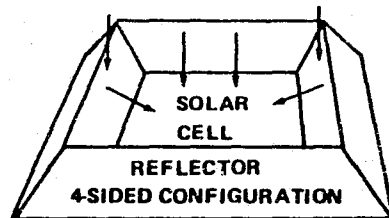
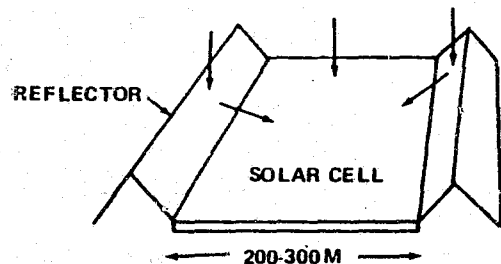


Figure 3.1-32. Solar Photovoltaic SPS Configuration

Table 3.1-9. Summary Characteristics 10 GW Si Photovoltaic System

BASIC CHARACTERISTICS		SUBSYSTEM WEIGHTS	
SUBSYSTEM	CURRENT CONCEPT CHARACTERISTICS	SUBSYSTEM/COMPONENT	WEIGHT (kg x 10 <sup>6</sup> )
SOLAR ARRAY		SOLAR ARRAY	(73.01)
CONCENTRATION RATIO	2 	BLANKETS	46.48
TOTAL ARRAY AREA (PLANFORM)	191.53 km <sup>2</sup>	CONCENTRATORS	4.17
SOLAR BLANKET AREA	88.04 km <sup>2</sup>	TENSION MECH & HARD	1.01
CELL WEIGHT/AREA	0.513 kg/m <sup>2</sup>	NON CONDUCTING STRUCT	7.34
WATTS OUTPUT/MODULE AREA	237 WATTS/M <sup>2</sup>	BUSSES, SWITCHES	9.54
		MAST	4.46
MICROWAVE ANTENNA (2 EA)		MICROWAVE ANTENNAS (2)	(14.48)
DIAMETER	1 km	AMPLITRONS	4.76
DC-RF CONVERSION	AMPLITRON	WAVEGUIDES	6.84
POWER DISTRIBUTION		IRF AMPLIFIER	1.36
CONCEPT	USE STRUCTURE	PHASE CONT. ELECT.	0.08
VOLTAGE	20 KV DC	POWER DISTRIBUTION	0.08
CONFIGURATION		CONTOUR CONTROL	0.24
SHAPE	ELLIPTICAL	STRUCTURE	0.40
STRUCTURE		ROTARY JOINTS (2)	(0.40)
ARRAY	TRIANGULAR	MECHANISM	0.18
ANTENNA	HEXAGONAL	STRUCTURE	0.22
ASSEMBLY ORBIT	LEO	CONTROL SYSTEMS	(1.73)
ATTITUDE ORIENTATION	PERPENDICULAR TO SUN	ACTUATORS	0.87
		PROPELLANT/YR	0.86
		SUB-TOTAL	(89.91)
		CONTINGENCY (30%)	(26.97)
		TOTAL SYSTEM	117.09

**SOLAR ARRAY CONCEPTS**



3-37

SD 78-AP-0023-3

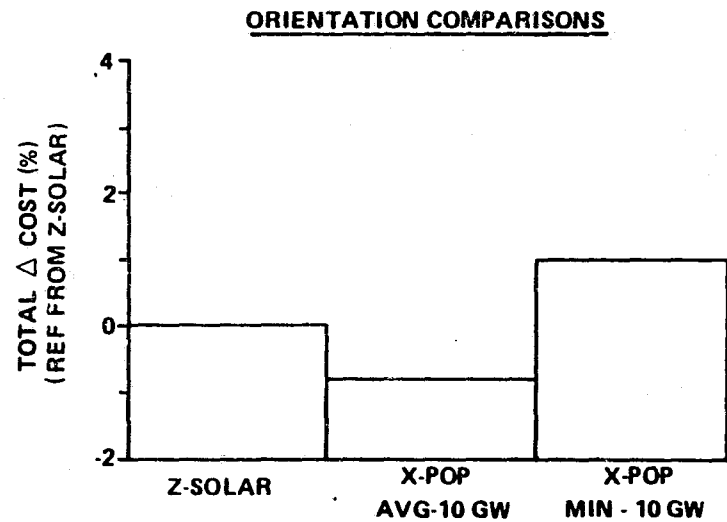
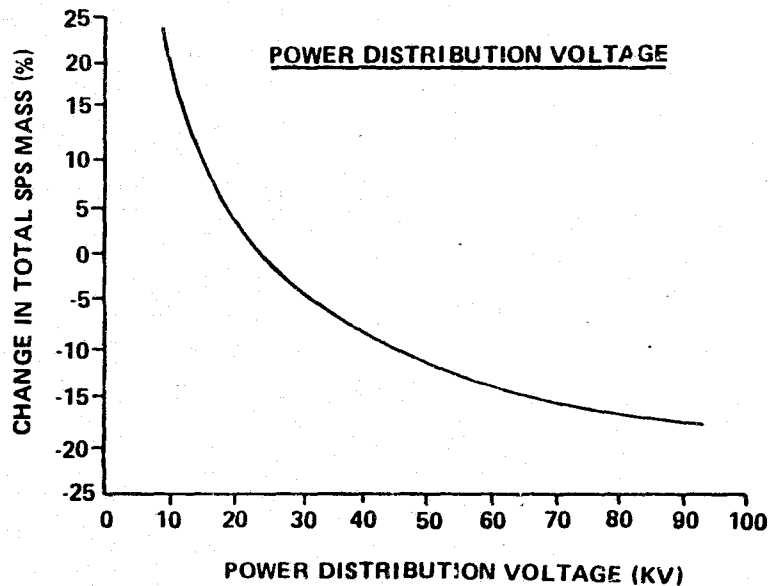


Figure 3.1-33. SPS Trade Studies





Many solar cell options were studied (MSFC Internal Note IN-DO-77-1) as potential improvements to the baseline. The concepts include parabolic, and two-sided and four-sided reflectors. One option which was studied and later incorporated into the next baseline was the use of small width cells that utilized the reflectors as a heat radiating surface. This resulted in a higher operating cell efficiency thus reducing the SPS solar cell and plan-form area requirements.

In some of the other trades, it was shown that the complexity of the system could be reduced. If the SPS was oriented X-POP (longitudinal axis of the spacecraft maintained perpendicular to the orbital plane) rather than Z-SOLAR (solar arrays maintained perpendicular to solar illumination), the complexity of the rotary joint could be significantly reduced. A two-axis rather than a three-axis gimbal could be used for microwave antenna pointing. Also the total cost would be somewhat less, primarily due to the smaller propellant requirements.

An analysis was performed to determine the effect of increased power distribution voltage on SPS. As the voltage increases the power distribution efficiency also increases. This also results in less mass for the power conductors.

It was also shown (Figure 3.1-34) that two 5 GW SPS's result in less mass than one 10 GW SPS. The average distance that the current must travel is greater for the 10 GW system than for the 5 GW system. Since the distance is greater, a more massive power distribution system is required. Also the greater distances result in a less efficient power distribution system which in turn requires a larger solar array area to provide the necessary power output.

An analysis was performed to determine the impact of the various antenna locations on the SPS mass for the 5 GW system (Figure 3.1-35). The elliptical configuration with a center-mounted antenna was chosen for the baseline since it is lighter and more rigid than the other configurations. The end mounted configurations require further distances for power conduction and thus have greater distribution losses.

As part of the study activity the diamond configuration was compared to the ellipse (Figure 3.1-36). The power distribution system requirements are essentially identical for both concepts. The diamond shape is somewhat better from a control system standpoint. A comparative structural analysis of the two concepts was not made but it is believed that they would be very similar. However, for the baseline update it was decided to remain with the ellipse based on assembly considerations.

Many of the guidelines and assumptions which were used to establish the baseline were derived from observations and trade results of previous studies. However, some guidelines and assumptions were based on arbitrary selections in order to become more knowledgeable in selected areas. The guidelines and assumptions which were used are shown in Table 3.1-10.



OPTION	CONFIGURATION	ITEM	MASS- kg <sup>6</sup>	
			20 kV POWER DISTRIBUTION	40 kV POWER DISTRIBUTION
TWO 5 GW SPS WITH ONE 5 GW ANTENNA EACH		SOLAR ARRAY	53.90	52.02
		POWER DISTRIBUTION	4.52	2.24
		MICROWAVE ANTENNA	12.78	12.78
		ROTARY JOINT	0.78	0.78
		CONTROL SYSTEM	1.34	1.22
		CONTINGENCY (30%)	22.00	20.72
		TOTAL	95.30	89.76
ONE 10 GW SPS WITH TWO 5 GW ANTENNA EACH		SOLAR ARRAY	55.40	52.77
		POWER DISTRIBUTION	6.52	3.18
		MICROWAVE ANTENNA	12.78	12.78
		ROTARY JOINT	0.78	0.78
		CONTROL SYSTEM	2.46	2.15
		CONTINGENCY (30%)	23.38	21.50
		TOTAL	101.32	93.17

Figure 3.1-34. SPS Size And Power Distribution Trade

ITEM	CONFIGURATION		
SPS 5 GW CONCEPTS			
POWER DISTRIBUTION EFFICIENCY	96.6%	93.8%	94.9%
PLANFORM AREA	54.7 km <sup>2</sup>	56.3 km <sup>2</sup>	55.7 km <sup>2</sup>
BLANKET AREA	25.2 km <sup>2</sup>	25.9 km <sup>2</sup>	25.6 km <sup>2</sup>
MASS - kg X 10 <sup>6</sup>			
SOLAR ARRAY	26.01	26.79	26.49
POWER DISTRIBUTION	1.12	2.07	1.69
MICROWAVE ANTENNA	6.39	6.39	6.39
ROTARY JOINT	0.39	0.39	0.39
CONTROL SYSTEM	0.61	0.66	0.75
CONTINGENCY (30%)	10.36	10.89	10.71
TOTAL MASS	44.88	47.19	46.42
	✓		

Figure 3.1-35. SPS Concept Comparison

3-40

SD 78-AP-0023-3

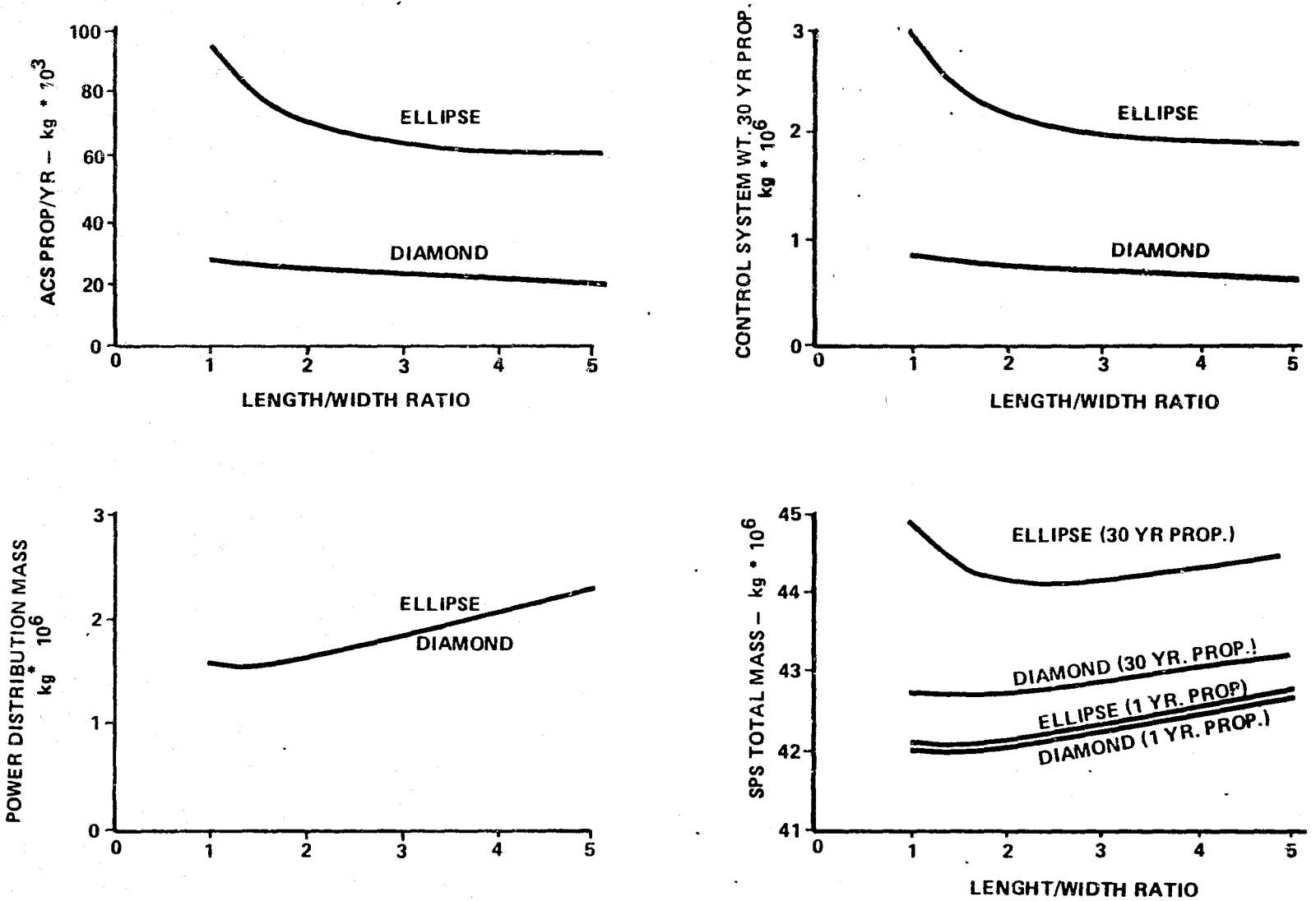


Figure 3.1-36. Sensitivity To Planform Shape



Table 3.1-10. Guidelines And Assumptions

THE MICROWAVE SYSTEM SHALL BE SIZED SUCH THAT EACH MICROWAVE ANTENNA SHALL PRODUCE 5 GW OUT TO THE POWER INTERFACE ON THE GROUND.

THE MICROWAVE SYSTEM DESIGN SHALL PRODUCE NO MORE THAN 23 mW/cm<sup>2</sup> POWER DENSITY AT THE RECTENNA CENTER.

THE PHOTOVOLTAIC SPS WILL UTILIZE SMALL WIDTH SILICON CELLS WITH RADIATING REFLECTORS AT A NOMINAL CONCENTRATION OF TWO.

THE BASELINE ATTITUDE ORIENTATION SHALL BE X-POP FOR THE PHOTOVOLTAIC CONCEPT.

THE POWER DISTRIBUTION SYSTEM SHALL BE AN INDEPENDENT CONDUCTING SYSTEM (NOT PART OF BASIC STRUCTURE).

THE PHOTOVOLTAIC SYSTEM WILL DISTRIBUTE DC AT 40,000 VOLTS TO THE ROTARY JOINT.

THE SPS WILL BE TRANSPORTED AND ASSEMBLED AT GEOSYNCHRONOUS ALTITUDE. A LEO STAGING DEPOT IS ASSUMED.

THE INITIAL OPERATIONAL SPS IS ASSUMED TO BE OPERATIONAL IN 1995.

THE SATELLITE AND GROUND RECEIVING SITE SHALL BE ASSUMED TO HAVE A 30 YEAR LIFE WITH APPROPRIATE MAINTENANCE.

THE SPS IS CONSIDERED AS A BASE LOAD POWER PLANT WITH AN 85 PERCENT LOAD FACTOR.

TOTAL SATELLITE MASS WILL BE SHOWN AS THE ESTIMATED MASS WITH AN ADDITIONAL 30 PERCENT CONTINGENCY TO ARRIVE AT THE TOTAL.

EACH SPS WILL HAVE ATTACHED A MINIMUM SIZE CREW SUPPORT, LOGISTICS, AND MAINTENANCE FACILITY.

The 30 year SPS program requirements profile which was defined as part of the guidelines and assumptions is shown in Tables 3.1-11 and 3.1-12. The SPS configuration which was defined, as shown in Figure 3.1-37 has an elliptical planform with a major axis of 13,900 m and a minor axis of 6000 m. A 1 km microwave antenna is attached to the center of the satellite. The antenna rotates 360 degrees per day with respect to the solar array. This rotation is accomplished with a rotary joint.

The structure is made of 220 segments. Each segment is 500 m by 500 m with a depth of 200 m. The solar blanket concept, as shown in Figure 3.1-38, is attached to the upper surface of the structure. There are 20 solar blanket modules in each of the 220 structural segments. These modules are 50 by 250 m. Each module consists of the silicon solar blanket, supporting wires, and packaging container. The solar blanket is a multi-trough concept with each trough being 2.2 cm in width with a concentration ratio of two. The blanket is designed so that the concentrators serve as a reflector, radiator, and power conductor. The concept allows the cells to operate at a high efficiency since the radiator serves to lower the cell operating temperature.

Table 3.1-11. 30-Year SPS Program Requirements Profile

YEAR SYSTEM	1995				2000				2005				2010				2015				2020				2025						
	6	7	8	9	1	2	3	4	6	7	8	9	11	12	13	14	16	17	18	19	21	22	23	24							
10-GW SYS/YR	1		1	1	2	2	2	2	2	2	2	2	2	2	2	2	2	2	2	2	2	2	2	2	2	2	3	3	3		
TOTAL SYS.	1		2	3	5	7	9	11	13	15	17	19	21	23	25	27	29	31	33	35	37	39	41	43	45	47	49	51	54	57	60
5-GW SYS/YR	1	1	2	3	3	4	4	4	4	4	4	4	4	4	4	4	4	4	4	4	4	4	4	4	5	5	5	5	5	5	
TOTAL SYS.	1	2	4	7	10	14	18	22	26	30	34	38	42	46	50	54	58	62	66	70	74	78	82	86	90	95	100	105	110	115	120

3-42

Table 3.1-12. SPS Program Requirements Summary

GUIDELINES	YEAR	
	2005	2025
REQ'D SYS OUTPUT (GW)	170	600
NO. SYSTEMS @ 5 GW	34	120
NO. SYSTEMS @ 10 GW	17	60

SD 78-AP-0023-3

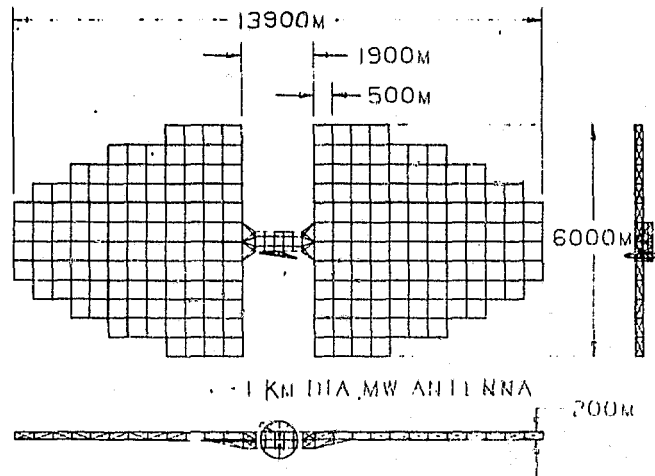
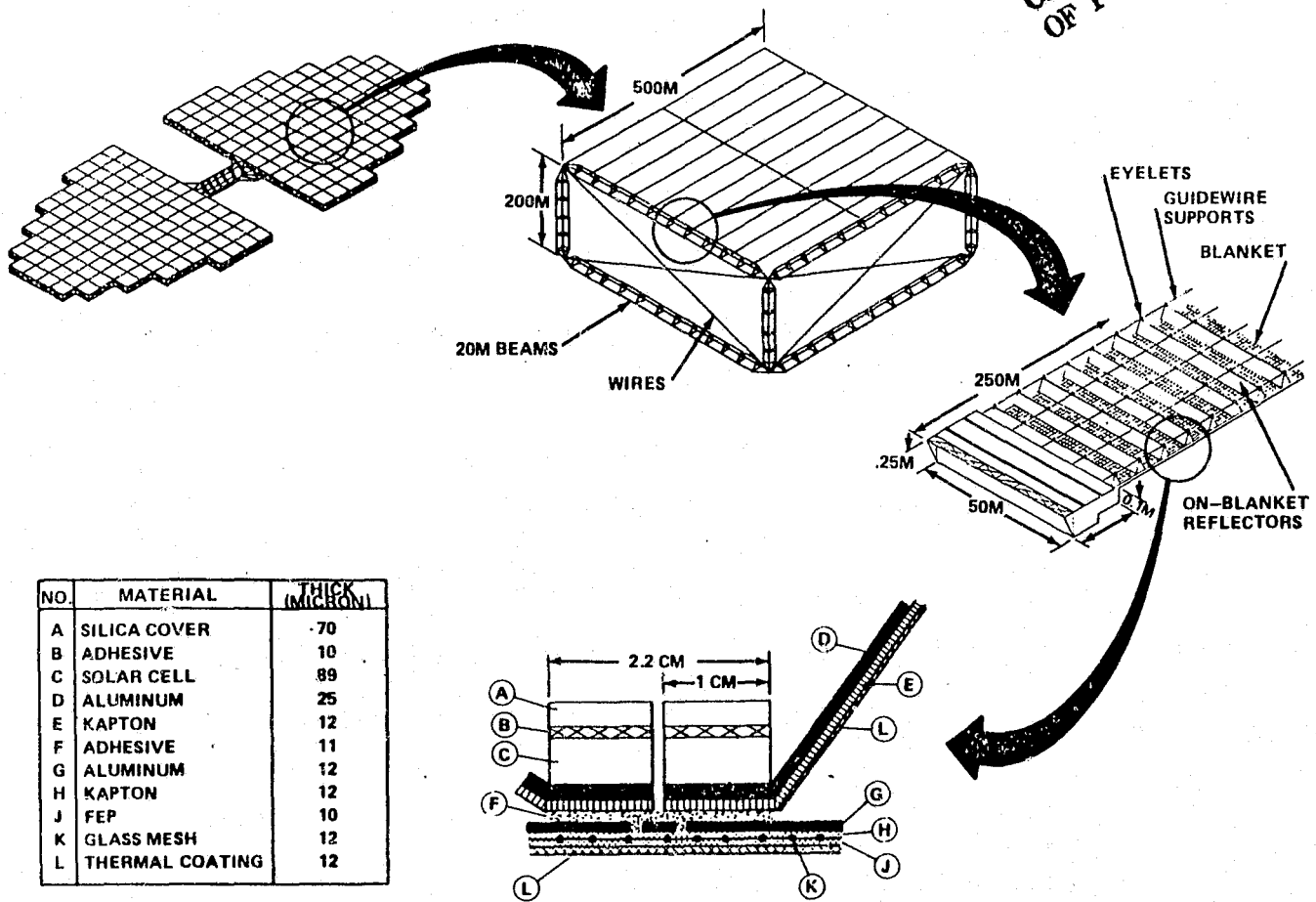


Figure 3.1-37. SPS Configuration

ORIGINAL PAGE IS  
OF POOR QUALITY



NO.	MATERIAL	THICK (MICRON)
A	SILICA COVER	70
B	ADHESIVE	10
C	SOLAR CELL	89
D	ALUMINUM	25
E	KAPTON	12
F	ADHESIVE	11
G	ALUMINUM	12
H	KAPTON	12
J	FEP	10
K	GLASS MESH	12
L	THERMAL COATING	12

Figure 3.1-38. MSFC 5 GW Photovoltaic SPS



The summary characteristics of this SPS are given in Table 3.1-13 and the weight summary in Table 3.1-14. This baseline has a significantly higher efficiency, as shown in Figure 3.1-39, than the previous Si design. The array power distribution efficiency increased from 90.2% to 96.5%. This was a result of the smaller size SPS (5 GW rather than 10 GW) and utilization of a 40 kV distribution system rather than 20 kV. Also the dc-RF conversion efficiency increased from 82% to 87%.

*Silicon Solar Cell Baseline Configuration.* The initial baseline configuration established by MSFC was for a silicon cell photovoltaic SPS rated to deliver 10 GW from its ground-based rectenna. Considering subsystem efficiencies, system losses, and degradation factors for space operations and for LEO to GEO transit, the power conversion system was sized to deliver 19.4 GW (BOL). The MSFC baseline photovoltaic power conversion system consisted of large, silicon solar cell blankets and large, flat, thin film concentrator blankets which were supported by a lightweight, space fabricated, aluminum structure. A solar cell blanket area of 88 km<sup>2</sup>, and a total plan form area of 191.5 km<sup>2</sup>, was required. The weight of the power conversion system (excluding structure) was 73x10<sup>6</sup> kg.

Originally, nominal system voltage rating of 20 kV was used to define the initial baseline system. This voltage was chosen since it satisfied the major power users (the microwave subsystem amplitrons) and because it avoided the high weight and cost penalties of power conditioning elements capable of handling unprecedented power levels. Subsequent concept studies and sensitivity analyses exposed major design, technology, and operational constraints on the performance and economic feasibility of the SPS. As the need was indicated, system requirements and guidelines were revised early in 1977 to reflect improvements in subsystem concepts and to investigate alternate operational concepts and/or compromises between subsystems that could enhance the overall system performance. The higher efficiency and higher voltage concepts (i.e., klystrons or amplitrons in series) developed for the microwave subsystem permitted significant improvements in the design and performance characteristics of the power conversion system.

An updated silicon solar array was designed and established as the new power conversion system baseline for subsequent Si cell SPS studies. The characteristics of the updated solar array are compared with those of the initial baseline, described above, to indicate design and performance improvements and to show penalties incurred by considering practical aspects not covered in the initial system study.

Although parametric/sensitivity analyses were continued to investigate the effects of variations in design and performance factors on the system, the centerline requirements and guidelines for the revised power conversion system baseline are summarized below:

- A single SPS will be rated to deliver 5 GW of power from its ground-based rectenna.
- Provide for  $\pm 23.5^\circ$  off-sun pointing to minimize attitude control and stabilization requirements and to enhance rotary joint concepts.



Table 3.1-13. SPS Baseline System Characteristics

<u>SUBSYSTEM</u>	<u>BASELINE</u>	<u>SUBSYSTEM</u>	<u>BASELINE</u>
CONCEPT		SOLAR ARRAY CONT'D	
POWER CONVERSION	PHOTOVOLTAIC	REFLECTOR LOCATION	ON-BLANKET
POWER OUTPUT	5 GW, GROUND	REFLECTOR THICKNESS	25 $\mu$
ARRAY SHAPE	ELLIPTICAL	CELL TEMPERATURE	90°C
MW ANTENNA LOCATION	C.G. OF ARRAY	SUBSTRATE	37 $\mu$ KAPTON LAMINATED GLASS FIBER REINFORCED
OVERALL DIMENSIONS	13.9 X 6 km	BLANKET SPECIFIC POWER	157 W/M <sup>2</sup>
SYSTEM MASS (30% CONT.)	45 X 10 <sup>6</sup> kg	CELL SPECIFIC POWER	341 W/M <sup>2</sup>
SOLAR ARRAY		BLANKET SPECIFIC WT	0.405 kg/m <sup>2</sup>
CELL TYPE	N/P S:	BLANKET MASS	22.2X10 <sup>6</sup> kg
CELL SIZE	1X101.5X .0089 cm	POWER DISTRIBUTION	
CELL EFFICIENCY	18% AMO, 30°C	TYPE	INDEP OF STRUCTURE
EFFECTIVE CELL AREA	98.5%	BUSS MATERIAL	ALUMINUM
CELL COVER	COATED SILICA	VOLTAGE	40 kVDC
CELL COVER COATING	BANDPASS FILTER	POWER LOSS	3.5 %
CONCENTRATOR CONCEPT	USES REFLECTOR FOR RADIATOR & CONDUCTOR	MASS	1.1 X 10 <sup>6</sup> kg
CONCENTRATION RATIO	1.89	ARRAY STRUCTURE	20 m TRIANGULAR
RECTENNA		TYPE BEAMS	220
TYPE	DIODE	NO. OF SEGMENTS	500X500X200 m
DIMENSIONS	8.5X11 km	SIZE OF SEGMENTS	
PEAK POWER DENSITY	23 mW/cm <sup>2</sup>	ANTENNA STRUCTURE	HEXAGONAL
EDGE POWER DENSITY	2 mW/cm <sup>2</sup>	TYPE	
MICROWAVE ANTENNA		ATTITUDE CONTROL	X-POP
TYPE	PLANAR PHASED ARRAY	ORIENTATION	$\pm$ 1 DEG
DIAMETER	1 km	MAIN BODY ACCURACY	$\pm$ 1 ARC MIN
DC-RF CONVERSION	AMPLITRON	ANTENNA COARSE ACC	$\pm$ 3 ARC SEC
FREQUENCY	2.45 GH <sub>2</sub>	ANTENNA FINE ACC	MPD
TAPER	9 db	THRUSTER TYPE	1000 SEC
MASS	6.4 X 10 <sup>6</sup> kg	THRUSTER ISP	
ROTARY JOINT		ASSEMBLY	HIGH AUTOMATION
TYPE	SLIP RING	TYPE	GEO
SLIP RING DIAMETER	15 m	LOCATION	
ROTARY JOINT DIA	500 m		
WEIGHT	0.4X10 <sup>6</sup> kg		





Table 3.1-14. Weight Summary of the 5 GW Photovoltaic SPS

SUBSYSTEM/COMPONENT	WEIGHT - KG X 10 <sup>6</sup>	
SOLAR ARRAY		27.13
BLANKETS	22.16	
TENSION & ASSEMBLY MECH.	0.74	
STRUCTURE	3.12	
POWER DISTRIBUTION MAST	0.80	
LATERAL DISTRIBUTION FEEDERS	0.31	
MICROWAVE ANTENNA		6.39
AMPLITRONS	1.98	
WAVEGUIDES	1.95	
IRF AMPLIFIERS	1.98	
PHASE CONTROL ELECTRONICS	0.11	
POWER DISTRIBUTION	0.05	
CONTOUR CONTROL	0.12	
STRUCTURE	0.20	
ROTARY JOINT		0.39
SLIP RINGS	0.12	
STRUCTURE	0.27	
CONTROL SYSTEM		0.61
PROP. SYSTEM & TANKAGE	0.51	
PROPELLANT/YEAR	0.10	
CONTINGENCY (30%)		10.36
TOTAL		44.88

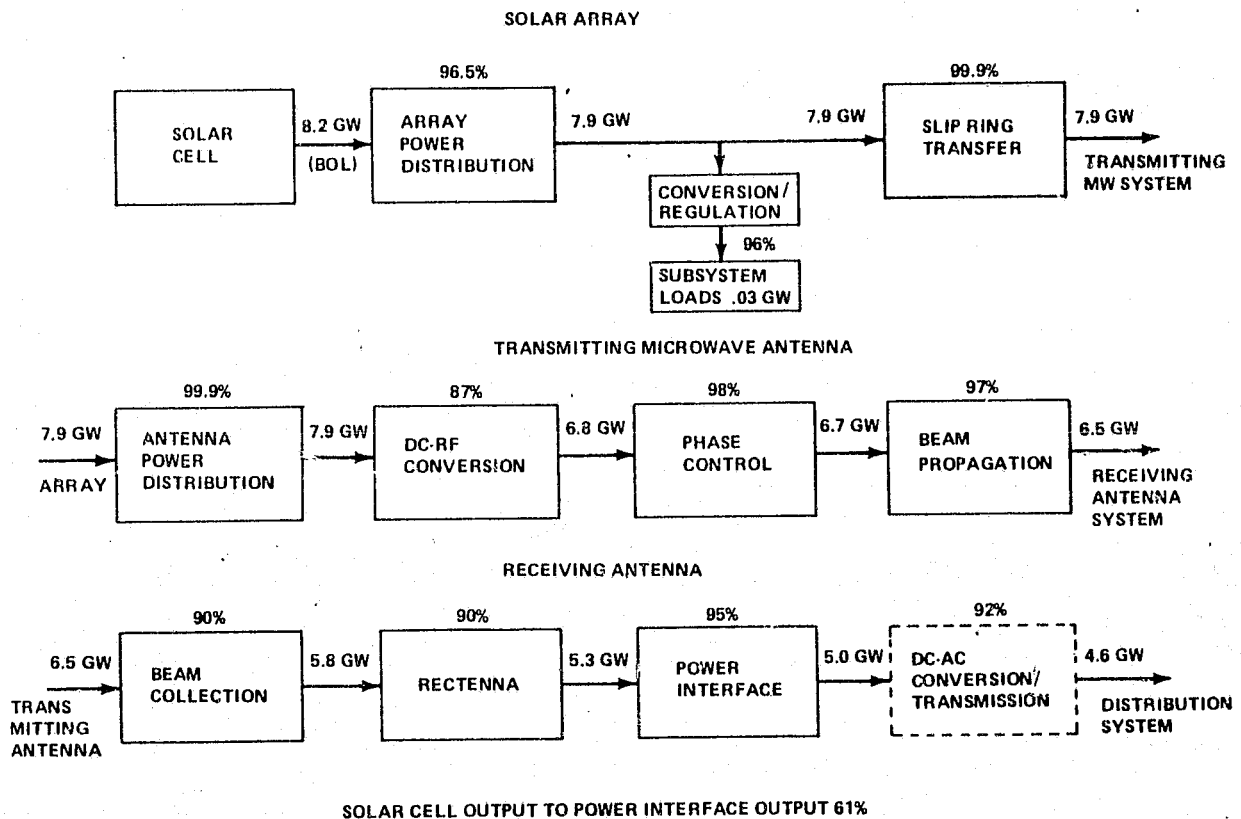


Figure 3.1-39. Photovoltaic SPS Efficiency Chain



- The nominal system voltage will be 40 kV. Power conditioning, as required, will be defined for low power, low voltage subsystems.
- The array will be deployed after arrival in geosynchronous Earth orbit (GEO). Other studies will consider the effect of assembly in low Earth orbit (LEO) and transit between LEO and GEO.
- The size and weight of the largest module or assembly to be transported will be within payload capabilities defined for the HLLV.
- Consider recent characteristics projected for advanced solar cell candidates such as GaAlAs, but continue to use silicon solar cells for the MSFC baseline.
- Use updated subsystem efficiencies defined for the new baseline SPS.

The revised solar array baseline was sized in accordance with the photovoltaic SPS efficiency chain shown in Figure 3.1-39. Compared to earlier efficiency chains, the dc-RF efficiency of the microwave subsystem increased from 82% to 87%. The distribution efficiency increased from 90.2% to 96.5% because the system voltage increased from 20 kV to 40 kV and the size of the SPS decreased when the output requirement decreased from 10 GW to 5 GW.

*Solar Array Components Summary.* The reference components and characteristics for the present 5 GW system study are listed in Table 3.1-15, and are compared with those of the previous 10 GW system study. The feasibility of a large solar array would not be questioned if unconstrained support and resources were provided. The major concerns are: (1) to assure that the design is practical and cost-effective for the concepts, (2) to assure that elements survive space exposure with acceptable degradation and maintenance, (3) to assure that components, materials, and characteristics are properly traded to optimize the system, (4) to assure that cost projections are realistic and consistent with performance projections, and (5) to assure the overall system is cost-effective and economically practical.

Silicon cells were retained by MSFC as their baseline because Si cells represent a known technology and industry, and improved performance and low cost can be projected at low risk. GaAlAs cells offer the potential for higher efficiency and radiation resistance. It is possible that significant cost reductions can be obtained as GaAlAs technology matures. Long ribbon silicon cells were chosen to reduce part count and assembly cost. R&D work may result in cells much thinner than the baseline design with the potential for large mass reductions. Although they represent a sizeable part of the solar array mass and cost, 70-micron, coated cell covers were retained for optical-thermal performance and radiation protection. Hopefully, a lighter, cheaper approach can be developed without sacrificing solar array performance.

*Solar Array - Concentrator Configurations.* A number of solar array concepts have been examined in previous studies for both 5 GW and 10 GW SPS systems. The four approaches in Figure 3.1-40 show the range of array configurations studied. All used reflectors to concentrate the solar energy on the solar cells in order to reduce size, weight, and cost. In general,

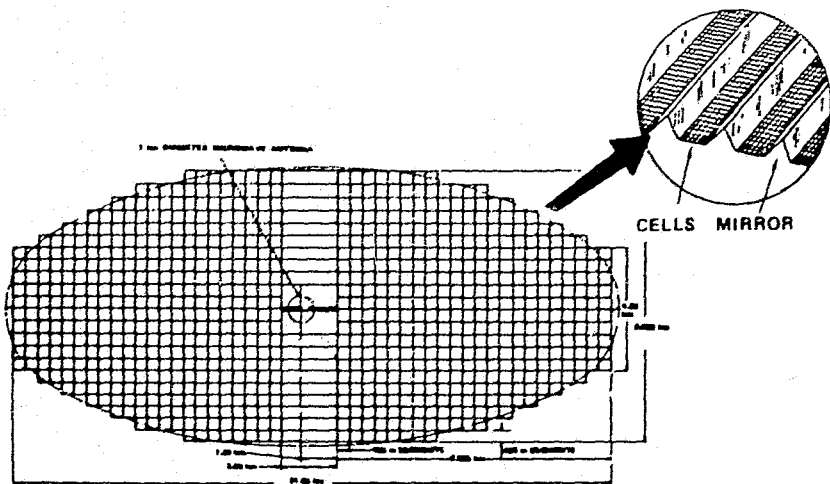
Table 3.1-15. Solar Array  
Reference and Options Summary

ARRAY COMPONENT CHARACTERISTIC	PREVIOUS BASELINE	PRESENT REFERENCE	OPTIONS/TRADES
SOLAR CELL	N/P SILICON 2-3 OHM-CM	N/P SILICON 1 OHM-CM	<ul style="list-style-type: none"> <li>● GaAlAs (18-20%)</li> <li>● CdS - (6-10%)</li> <li>● PERFORMANCE, WT., COST</li> <li>● DEGRADATION STUDIES</li> </ul>
- SIZE (CM)	4 x 12 x 0.0102	1 x 101.5 x 0.0089	
- EFFICIENCY	18% AMO, 28°C	18% AMO, 30°C	
CELL COVER	COATED SILICA	COATED SILICA	<ul style="list-style-type: none"> <li>● GLASS</li> <li>● SPRAYLON</li> <li>● VARIOUS COATINGS</li> <li>● OPTICAL-THERMAL-RADIATION TRADES WITH WEIGHT/COST</li> </ul>
- SIZE (CM)	4 x 12 x 0.0076	1 x 101.5 x 0.0071	
- COATINGS	UV FILTER	BANDPASS FILTER	
- TRANSMISSIVITY	0.96	0.97	
REFLECTOR (ALUMINIZED)	FLAT, CR = 2	FLAT, CR = 1.89	<ul style="list-style-type: none"> <li>● OPTIMIZE (CR UP TO 4:1)</li> <li>● THICKNESS, AREA</li> <li>● MATERIALS, FILTERS, COATINGS TO IMPROVE THERMAL OPTICAL PERFORMANCE</li> </ul>
- LOCATION	SEPARATE	ON-BLANKET	
- SIZE	216 x 433 M (EA)	0.02 x 50 M	
- THICKNESS	13 μ	25 μ	
- REFLECTIVITY	0.85	0.90	
TEMPERATURE (CELLS)	117°C	99°C	<ul style="list-style-type: none"> <li>● OPTIMIZE (~ 80°C)</li> </ul>
INTERCONNECTS	25 μ COPPER	INTEGRAL W/ REFLECTORS (25 μ ALUMINUM)	<ul style="list-style-type: none"> <li>● ELECTRICAL-THERMAL TRADES</li> <li>● MECHANICAL PROPERTIES</li> </ul>
SUBSTRATES	25 μ KAPTON/FEP (LAMINATED)	37 μ KAPTON LAM- INATED (GLASS FIBER REINFORCED)	<ul style="list-style-type: none"> <li>● MATERIALS TO IMPROVE</li> <li>● STRENGTH, CREEPAGE</li> <li>● RADIATION RESISTANCE</li> <li>● THERMAL PROPERTIES</li> </ul>
ASSEMBLIES	LARGE FLAT BLANKET NO STOWAGE/HANDLING CONCEPT	250 x 50 x 0.018 M MODULE W/DEPLOY/ SUPPORT MECH.	<ul style="list-style-type: none"> <li>● CONFIGURATION VS CR/LOSSES</li> <li>● PRACTICAL HANDLING/DEPLOY</li> <li>● TENSION, STRENGTH, SUPPORT CONCEPTS</li> </ul>

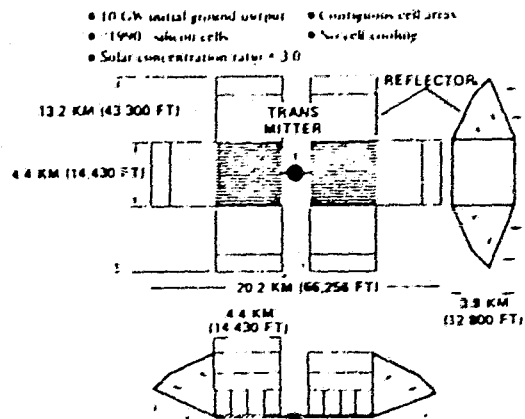
3-48

SD 78-AP-0023-3

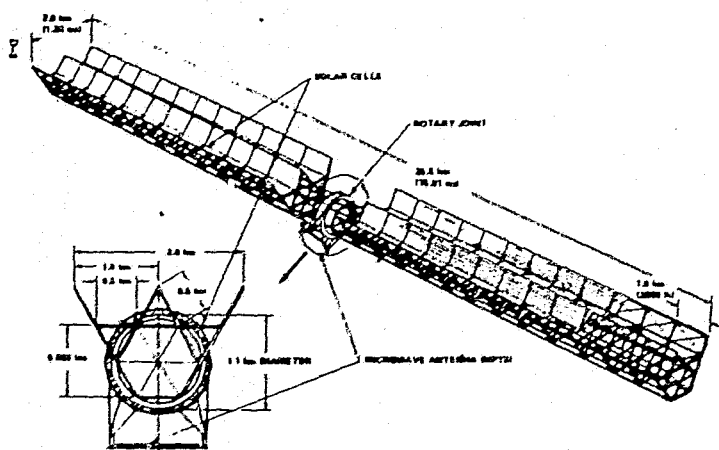
ORIGINAL PAGE IS  
OF POOR QUALITY



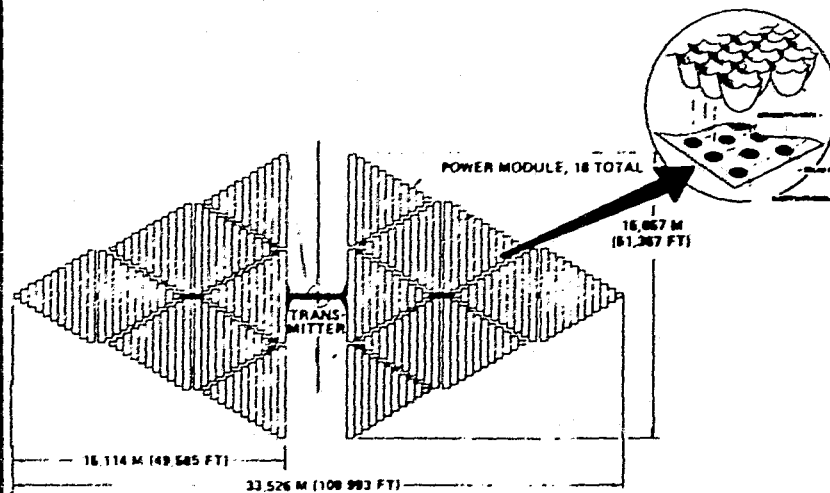
MSFC  
CONCENTRATION RATIO 2:1 SILICON SOLAR CELLS



BOEING  
CONCENTRATION RATIO 3:1 SILICON SOLAR CELL



ROCKWELL  
CONCENTRATION RATIO 2:1 SILICON SOLAR CELLS



BOEING  
CONCENTRATION RATIO > 4 GaAs SOLAR CELLS

Figure 3.1-40. SPS Concentrator Key Approaches

3-49

SD 78-AP-0023-3



passively cooled arrays with concentration ratios below 4:1 have been baselined. High concentrations result in high cell temperatures which can drastically reduce the output of the Si solar cells. Because of their cost, higher concentrations are preferred for GaAlAs cells.

Rectangular, elliptical, and triangular shaped solar arrays have been considered. These configurations evolved from system trade studies made to enhance attitude control system (ACS) requirements, rotary joint concepts, and microwave antenna pointing. The ACS prefers a system with a length to width ratio of 2:1 or more. The very long, thin configurations represent an attempt to optimize the rotary joint design and to avoid having the antenna look through a "transparent" structure. Long, narrow configurations, on the other hand, impose penalties on the structure, the power distribution system, and the solar array. The optimum configuration has yet to be determined and will depend on numerous system/subsystem factors.

The various shapes were analyzed from an electrical standpoint, considering the output power, the system voltage, the solar array performance, and the orientation/operating conditions. The power losses, the distribution weight, the array size, and the array weight were minimum for all shapes when the length to width (L/W) ratio is near 1:1 (see Figures 3.1-41 through 3.1-44). Theoretically the triangular array offers the lowest loss, size, and weight. At an L/W ratio of 2, the ellipse theoretically increases losses, sizes, and weight by about 1.6% (see Figure 3.1-44). The rectangular shape is about 6% worse than the triangular shape. At 20 kV, the absolute differences are great. For the 40 kV baseline system the differences to the overall system are not as significant.

Considering structural requirements and concepts and the fact that the reflector must be parallel with the X-axis, the array structure is to be assembled from large, square blocks. Therefore, the actual array must be quasi-ellipse or a quasi-triangle. The ellipse is superior to the triangle in this respect since the needed area and L/W ratio can be more easily approached. For example, suppose  $54.7 \text{ km}^2$  is required with an L/W of 2:1 and that the structural blocks are 500 m x 500 m. A quasi-ellipse can be within 3% of the area of a true ellipse for such conditions. The closest quasi-triangle would have an area about 10% smaller than needed for the same conditions. For this reason, the quasi-ellipse was preferred to the quasi-triangle from an electrical viewpoint.

*Baseline Solar Array Module.* The module buildup concept of the SPS Si solar array is depicted in Figure 3.1-38. The solar array consists of two semi-elliptical shaped wings separated/joined together by a narrow hexagonal structure at the center. The central structure accommodates the rotary joints and the microwave antenna subsystem which receive most of the power generated by the solar array. The array buildup consists of systematic attachment and deployment of array modules to make up the array block leading to the construction of a wing and finally the entire array. The solar blanket is a multi-trough concept with each trough being 2.1 cm in width with a concentration ratio of two. The blanket is designed so that the concentrators serve as a reflector, radiator, and power conductor. This concept allows the cells to operate at a higher efficiency since the radiator serves to lower the cell operating temperature.

3-51

SD 78-AP-0023-3

2-2

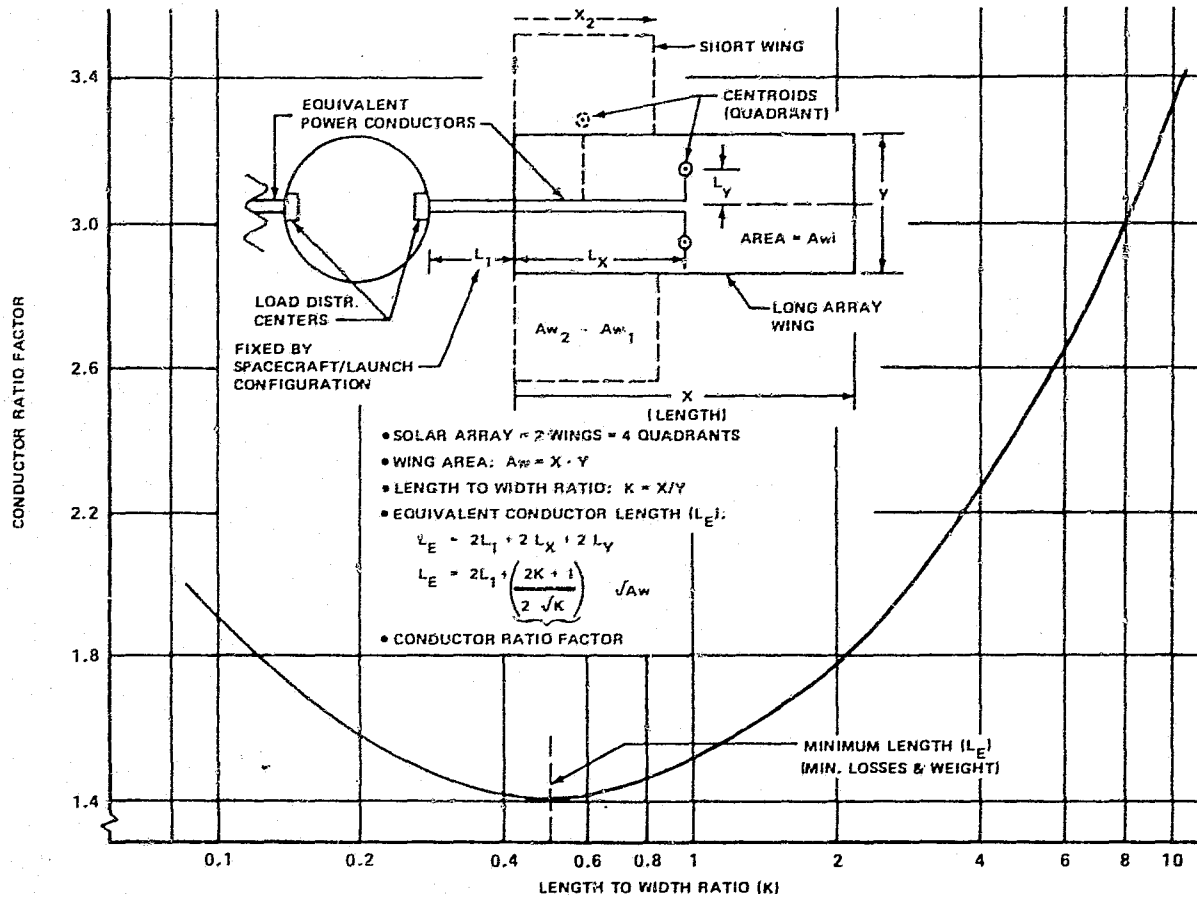


Figure 3.1-41. Rectangular Solar Array  
Equivalent Power Conductor Length

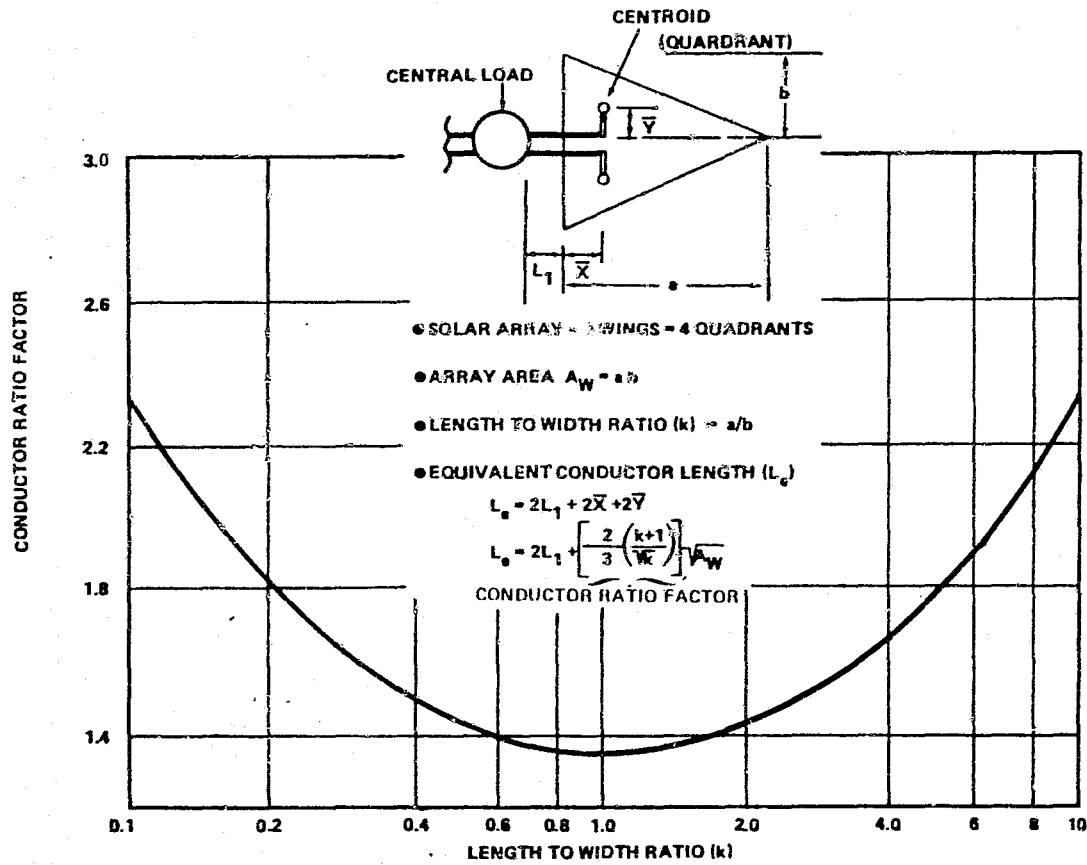


Figure 3.1-42. Triangular Solar Array  
Equivalent Power Conductor Length

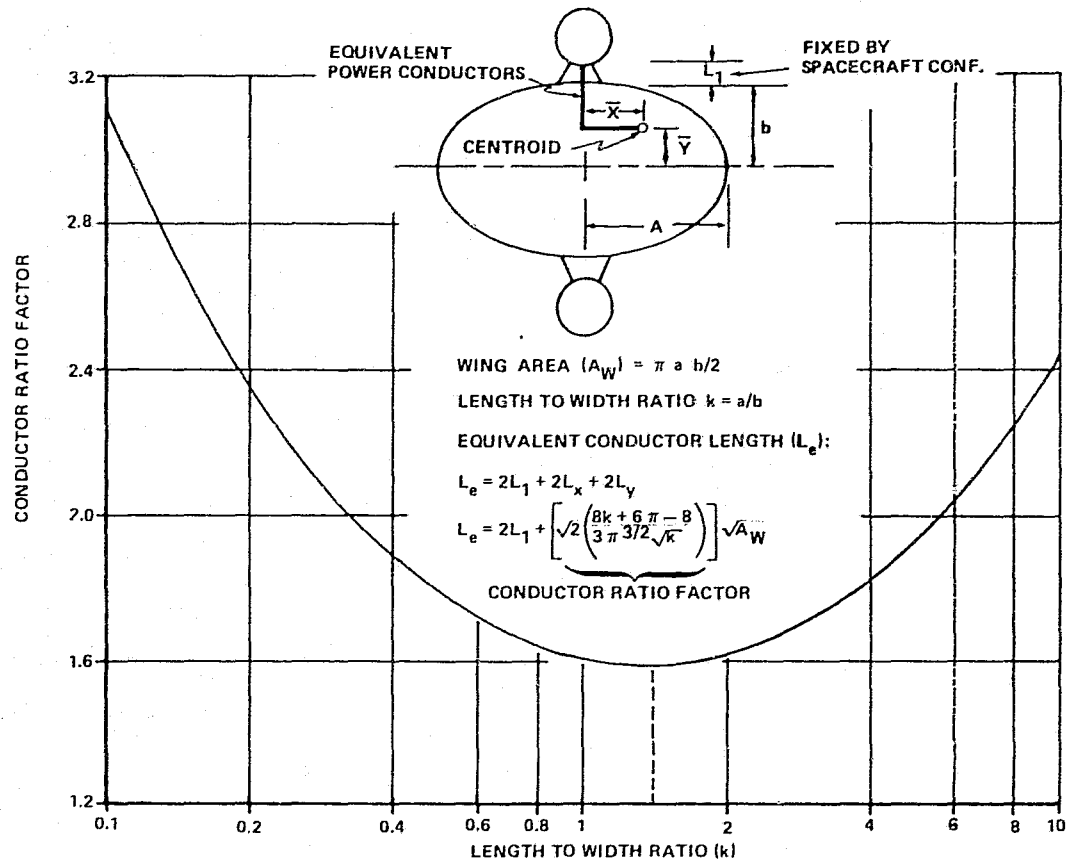


Figure 3.1-43. Elliptical Solar Array  
 (Two Load Configuration)  
 Equivalent Power Conductor Length



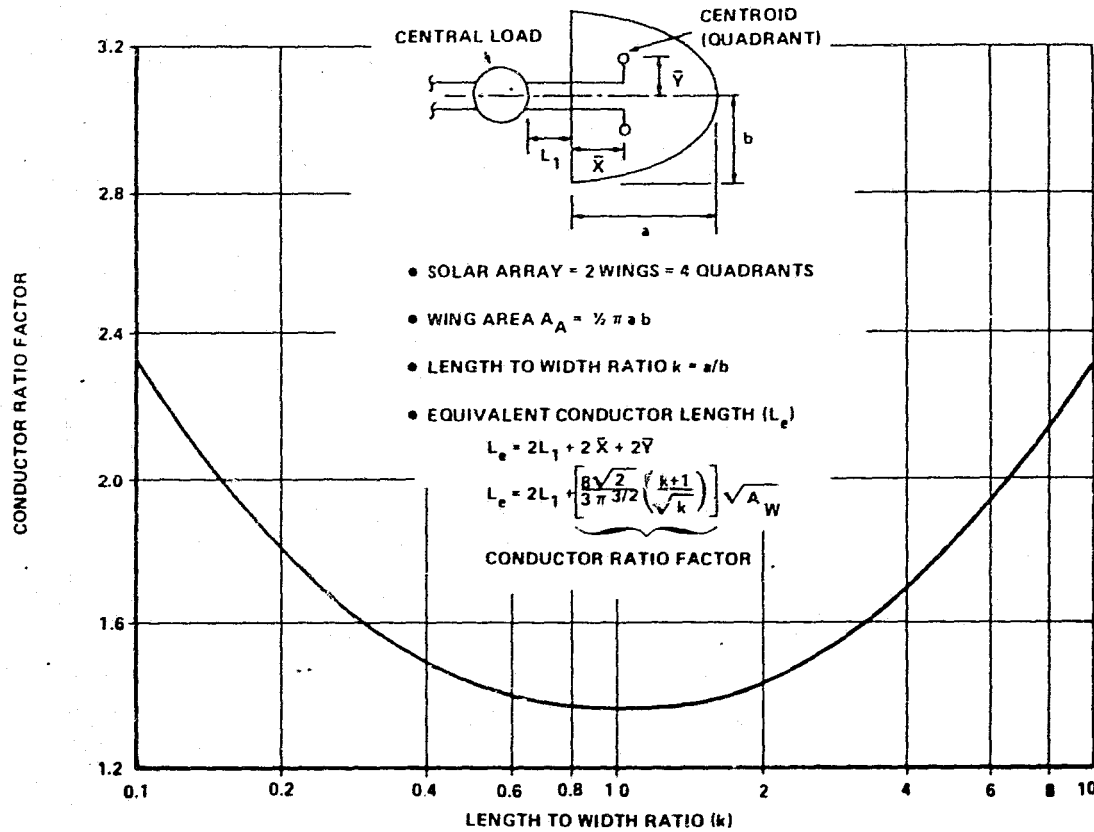


Figure 3.1-44. Elliptical Solar Array  
(Load Centralized At Center)  
Equivalent Power Conductor Length



The revised baseline SPS, shown in Figure 3.1-38 was sized to deliver 5 GW to the ground. Based on the system efficiency, the solar array must deliver 8.2 GW. The array area required, excluding degradation is 54.7 km<sup>2</sup>. The baseline configuration provides 55 km<sup>2</sup> of area for the array. Each wing consists of 110 structural blocks, 500 m x 500 m, defined by the primary structural beam pattern. An intermediate structural element is located in the middle of each block, along the X-axis, to avoid length stress problems in the solar cell blankets.

It is noted that, based on configuration trade studies, the structural blocks of each wing are arranged to simulate a semi-ellipse. The length of the semi-major axis and the semi-minor axis was 6 km and 3 km, respectively. Thus the length to width ratio of the array only was 2 to 1. When the length of the central structure is included, the overall length to width ratio of the SPS becomes 2.3.

A basic solar array module sized to provide practical storage handling, transportation, and assembly concepts was established to make up the structural blocks. The module consisting of a solar cell blanket with on-blanket reflectors; a housing; and deployment, support, and tensioning mechanisms has the dimensions of 50 m x 250 m when deployed. Twenty modules can be supported in each structural block; thus the baseline array has the capacity for 4400 solar array modules.

The concept seeks to maximize the size (area) of the module consistent with minimum overall weight, practical handling and assembly facilities, and minimum in-space assembly time. Considering the characteristics of present materials and substrates and tensioning and stress requirements, the length of the module was limited to 250 m. The 50 m width (which becomes the longest stowed dimension) was selected to be compatible with the longest nose cone considered for the HLLV. A full complement (4400) of the solar array modules will produce 8.6 GW at 43.8 kV and the weight of the solar array, excluding structure, will be  $23.03 \times 10^6$  kg.

The module is the smallest building block of the array structure. Figure 3.1-45 shows the general construction of the module. The integrated cell/concentrator solar blanket is accordian folded as shown in Figure 3.1-45. This design is adopted from the Lockheed folded solar array and designs investigated during the SEPS and Halley Comet Rendezvous Mission studies.

The module blanket is stored in a housing assembly approximately 5.33 m x 25 m x 50 m for transportation. A somewhat rigid housing assembly is required for stowage and protection of the array blankets during transportation and assembly operations. The housing also serves to distribute the solar array mechanical loads along the large, lightweight structural beams. The principal design and performance characteristics of the baseline solar array module are given in Table 3.1-16. A total of 4380 modules, rated at 1959 kW each, are required to meet the system power requirements presently defined, allowing a 4.8% increase in area to compensate for X-POP orientation. The structure provides space for 4400 modules.

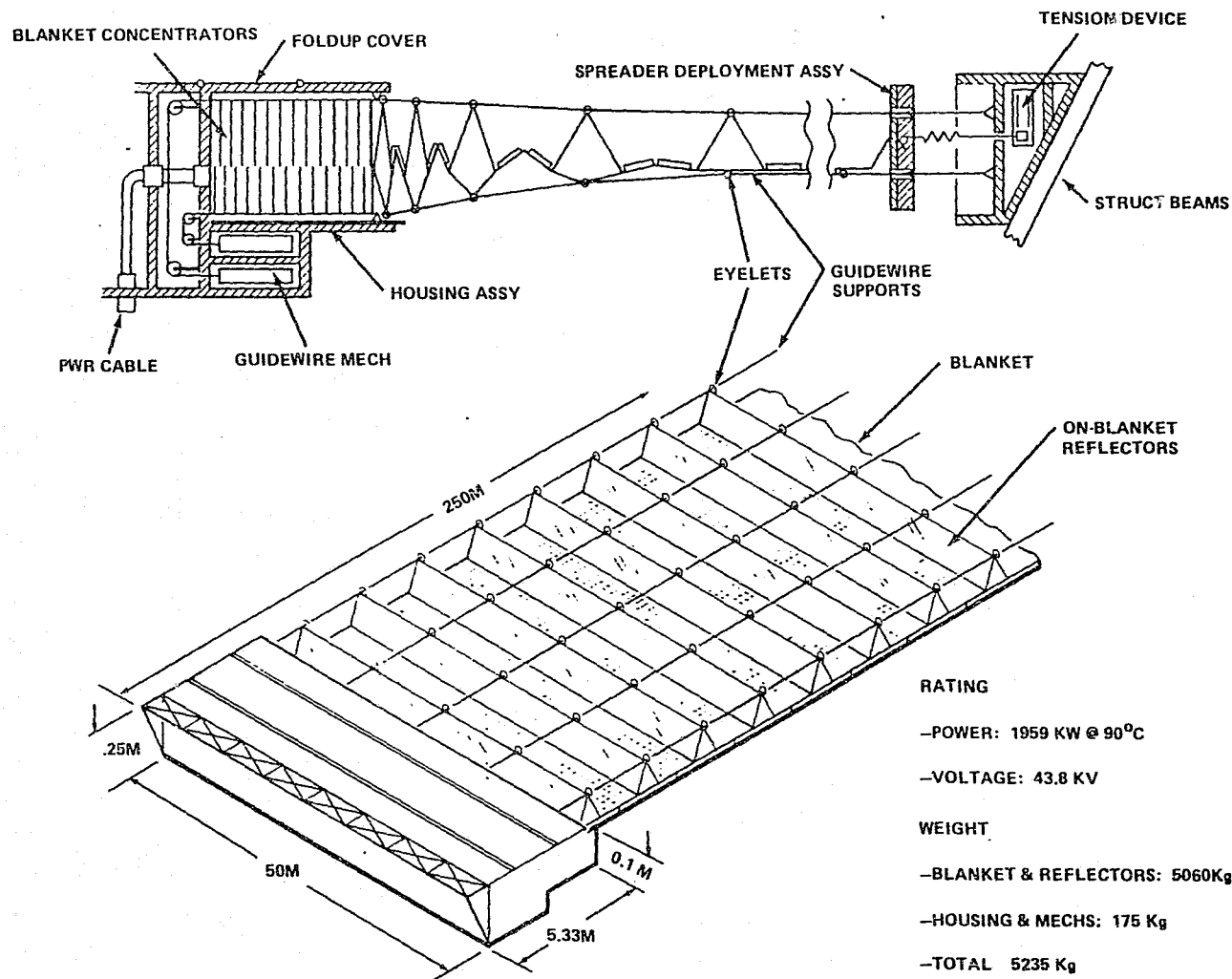


Figure 3.1-45. SPS Solar Array Module

3-56

SD 78-AP-0023-3

C-2



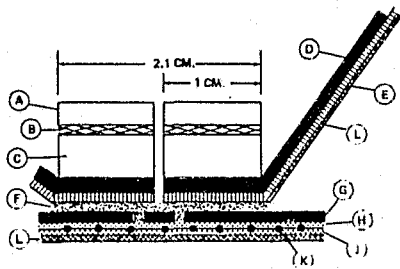
Table 3.1-16. SPS Solar Array  
Baseline Module Characteristics  
(50 m x 250 m)

ELECTRICAL RATING AT 90°C		1 959 KW
-	OUTPUT POWER (ORIENTED)	1 959 KW
-	BUS VOLTAGE	43.81 KV
-	CURRENT	44.73 AMP
WEIGHT - TOTAL MODULE		5 235 KG
-	BLANKET-REFLECTOR ASSEMBLY	5 060 KG
-	HOUSING AND ATTACHMENTS	85 KG
-	GUIDEWIRE AND TENSION ASSEMBLIES	90 KG
AREA - TOTAL MODULE		12 500 M <sup>2</sup>
-	BLANKET-REFLECTOR PLANFORM	12 395 M <sup>2</sup>
-	BLANKET TROUGHS	6 493 M <sup>2</sup>
-	CELL SPACING FACTOR	0.886
-	HOUSING AND SPACER LOSS	105 M <sup>2</sup>
CONCENTRATION RATIO		1.89
CELLS - TOTAL NUMBER		566 688
-	SERIES CONNECTED	94 448
-	PARALLEL	6
STOWAGE VOLUME		37 M <sup>3</sup>

The module performance is based on the characteristics projected for silicon solar cells in the 1983-85 time period. The reference cell is an N/P, 1-ohm-cm cell with an AMO efficiency of 18% at 30°C. Fused silica covers with antireflection and UV rejection filters were used to enhance the optical-thermal-performance and to protect cells against radiation.

The on-blanket reflector concept increases the specific weight of the blankets but promises to improve the thermal-electrical characteristics significantly. A concentration ratio of 2.0 was used for the initial baseline. Thermal properties of the reflector/radiator confirmed in thermal vacuum tests on the Halley's Comet Rendezvous Mission indicate that lower temperatures than predicted will occur. These lower temperatures should change the optimum concentration ratio (weight optimized) to a geometric concentration ratio greater than 2:1.

*SPS Solar Array Cross Section.* A cross sectional diagram of the solar cell reflector blanket, as baselined, is shown in Figure 3.1-46. The table identifies the materials used, their specific gravity, and density per unit area. Since the spacing allowed for the several layers of materials differs (e.g., the top layer of aluminum covers only about 88% of the top surface) the last column of the table is included to give the total weight of each material on one solar array module blanket. The sum of the material weights



NO	MATERIAL	SP. GRAV.	THICK (MICRON)	DENSITY (GM/CM <sup>3</sup> )	WEIGHT PER BLANKET (KG)
A	SILICA COVER	2.33	70	0.1631	938.1
B	ADHESIVE	1.00	10	.00100	57.5
C	SOLAR CELL	2.85	89	.02359	1356.9
D	ALUMINUM	2.70	25	.00675	1182.2
E	KAPTON	1.42	12	.00188	105.3
F	ADHESIVE	1.57	11	.00324	195.7
G	ALUMINUM	2.70	12	.00188	204.6
H	KAPTON	1.42	10	.00215	257.6
J	FEP	2.15	10	.00003	1.5
K	GLASS MESH	2.30	12	.00126	448.1
L	THERMAL COATING	1.80	12		
TOTAL MODULE BLANKET				.04049 <sup>(1)</sup>	5061
(1) BASED ON TOTAL PLANFORM AREA OF 12,500 M <sup>2</sup>					

Figure 3.1-46. SPS Solar Array Blanket-Reflector Cross Section

gives a total of 5061 kg for the entire blanket assembly. Allowing space at each end of the blanket for tensioning mechanisms and housing, the blanket planform area was 12,393 m<sup>2</sup>. The total blanket weight divided by the planform area gives a specific weight of 0.4083 kg/m<sup>2</sup>.

Compared to the earlier large reflector approach, the on-blanket small reflector concept offers a significant improvement in array performance because solar cell temperatures are lower by the small reflectors which provide heat rejection for the cells as well as a means of concentrating sunlight on the cells. The top layer of aluminum also serves to electrically interconnect parallel groups of cells while the lower layer provides series connections. The width of the cells must be kept small to obtain good thermal performance. A width of 1 cm was arbitrarily chosen for the baseline. Trade analysis show that the effectiveness of the radiators begin to decline after the total width of the trough approaches 2 cm.

A glass fiber mesh was included to increase the strength and to decrease the mechanical creepage of the substrate that may be expected at elevated temperatures or with age. The integrity and endurance of the substrate and its ability to maintain its concentrator shape are important characteristics requiring further investigation. Considering high voltage plasma conditions, electrical insulation properties and the spacings/configurations needed to avoid electrical creepage are considered highly important and deserving more investigation. Alternate materials, thermal coatings, and possible band-pass filters are candidates for further improving the performance and cost of the solar array.



### 3.1.2 THERMAL

A solar thermal system generates power by concentrating sunlight (solar energy) upon a thermal absorber. The absorber consists of a series of tubular passages containing a pressurized fluid that is heated to an elevated temperature which, in turn, is used to drive a turbine/generator set. Cycle efficiency for this form of power generation is typically in the range of 30 to 50 percent. Waste heat from the turbine exhaust is dissipated to space by means of a radiator subsystem (part of the thermal subsystem network), after which the working fluid is returned to absorber pressure by means of a pump/compressor.

The following sections present a summary of the various trades and/or analyses that were made in support of the final point design selection.

#### Objective

The objective of the various trades was to select the basic subsystem configuration for optimization and elaboration in a point design. Selection of the subsystem configuration was based on the following criteria:

1. Environmental capability
2. Material availability
3. Development risk
4. Overall power cost (cents per kW-hr)
  - a. Development costs
  - b. Production costs
  - c. Construction costs
  - d. Transportation costs (satellite mass and density)
  - e. Maintenance costs (including reliability)
  - f. Operational costs

#### Solar Concentrator Trades

The basic requirements for the SPS solar concentrator are: (1) high concentration ratio, ~2000:1; and (2) emergency defocusing, 10 seconds. Special problems associated with large SPS concentrators are:

1. Structural distortions
2. High pointing accuracy
3. Performance degradation
4. Static electric charge buildup during eclipse
5. Meteorite damage

The candidate designs considered were:

1. Rigid (steerable facets and fixed facets)
2. Inflated
3. Tensioned net

Common to all these candidates is the use of lightweight, metallized plastic film as the reflective surface. Refractive-type (lens) concentrators were ruled out on the basis of mass.

Rigid Faceted Design. The structural configuration of this candidate design is shown in Figure 3.1-47. A large number of facets (~16,000) are mounted on the dish-shaped structure and individually steered by means of closed-loop servos to focus on the absorber aperture at the concentrator focal point; this releases the rigidity and precision requirements of the structure at the expense of complexity. Each facet consists of a hexagonal panel of film tensioned at three opposite sides to provide a precision flat reflective surface<sup>1</sup> with a film stress of ~1000 psi. The film material is aluminized Kapton 0.0012 cm (0.0005 in.) thick.

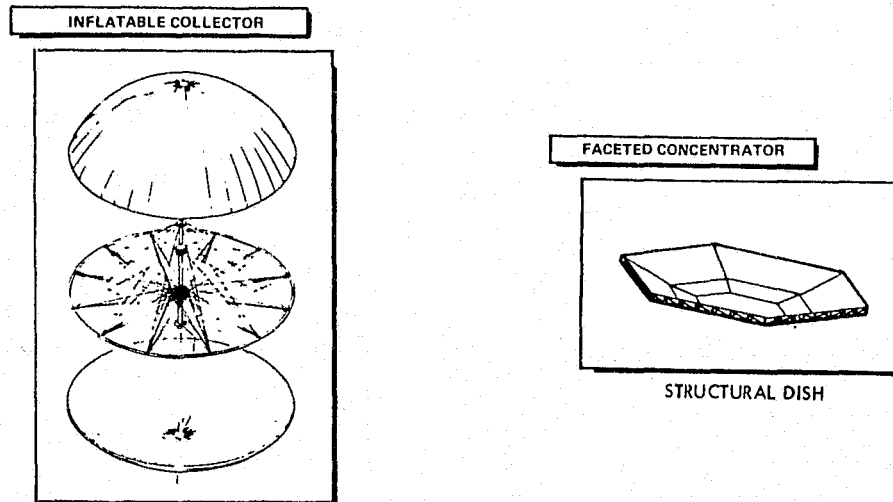


Figure 3.1-47. Candidate Designs

Inflated Design. Figure 3.1-47 shows a structural rim (tension spoke design) to which is attached a parabolically shaped reflector film and a convex, transparent canopy film to contain the inflation gas and pass sunlight in both directions. An inflated rim was considered but rejected because of potential problems in holding an accurate geometric shape. The reflector dish is composed of tapered gores of aluminized Kapton film 0.0012 cm (0.0005 in.) thick and pressurized to a film stress of ~300 psi. The transparent canopy is similarly formed from gores of FEP Teflon; however, geometric tolerances are non-critical. The edge of the reflector membrane is attached to flat spring elements or "fish poles" mounted on the rim, to maintain film tension and permit rapid defocusing in emergencies. Static-charge buildup can be controlled by metallizing both sides of the reflector film and use of conductive transparent coatings on the canopy.

<sup>1</sup>Boeing Aerospace Company, *Space-Based Power Conversion and Power Relay Systems, Preliminary Analysis of Alternate Systems*, Briefing to MSFC (Contract NAS8-31628), 14 April 1976.



Reflective area loss due to meteorite damage is less than one percent in 30 years. Due to the extremely low inflation pressure of 2.4 microns ( $10^{-4}$  psf), makeup gas requirements are less than one percent of total satellite mass over its 30-year life. This includes leakage caused by meteorite punctures of the film.

Tensioned Net Design. The tensioned net concept uses either a structural mast or a drum to which is strung a large number of cables in order to form a paraboloidal net or spinder web. Panels of reflector film are stretched between the cables, thereby forming individual facets. Focusing control is accomplished by adjusting the relative tension of the cables and their attached rigging lines. Because a large expenditure of effort would be required for adjusting the many cables to achieve an accurate shape and a high concentration ratio, the tensioned net concept was considered only as a backup to the rigid or inflatable design.

Results. Table 3.1-17 compares the characteristics of representative baseline designs for the faceted and inflated concepts. While the inflated design has lower collection efficiency (65% vs. 69%) because of transmission losses through the transparent canopy, its total mass is 58 percent less due to elimination of the rigid dish structure. Maintenance required on the inflated design consists chiefly of replacing the canopy after 15 years of service, when its transmission properties are degraded. This can be done without interruption of service by overlaying and joining the new gores in place and peeling off the old film from within the pressurized space. Maintenance of the faceted concept would consist mostly of repairing or replacing failed pointing servos.

Table 3.1-17. Concentrator Concept Comparison

	RIGID, FACETED	INFLATED
CONCENTRATION RATIO (ACTUAL)	2000	2000
COLLECTOR DIA. (KM)	5.3 (HEX)	5.0
NUMBER OF FACETS	~18,000	N/A
REFLECTOR MATERIAL	AL KAPTON	AL KAPTON
FILM STRESS - KN/M <sup>2</sup> (PSI)	6900 (1000)	2070 (300)
FILM THICKNESS - CM (MIL)	0.0012 (0.5)	0.0012 (0.5)
FILM LIFE - REFLECTIVITY (YR)	30	30
SPECULAR REFLECTANCE (1.8°), EOL (%)	90	90
CANOPY LIFE (YR)	N/A	15
INFLATION PRESSURE - KN/M <sup>2</sup> (PSF)	N/A	$4.79 \times 10^{-3}$ ( $10^{-4}$ )
EMERGENCY DEFOCUS (SEC)	2	5
CANOPY TRANSMISSION, 2-WAY, EOL (%)	N/A	80
APERTURE VIEW ANGLE (DEG)	1.8	1.8
COLLECTION EFFICIENCY (%)	69	65
FILM MASS (KG)	$0.25 \times 10^6$	$0.6 \times 10^6$
STRUCTURE MASS (KG)	$3.0 \times 10^6$	$0.4 \times 10^6$
SERVOACTUATOR MASS (KG)	$0.1 \times 10^6$	N/A
MAKEUP GAS - H <sub>2</sub> , 30 YR (KG)	N/A	$0.4 \times 10^6$
TOTAL MASS (KG)	$3.35 \times 10^6$	$1.4 \times 10^6$
MAINTENANCE	MODERATE	MODERATE
DEVELOPMENT RISK	MODERATE	MODERATE
TOTAL COST (RELATIVE)	~3.0	1.0

Development risk of the inflated concept lies chiefly in the fact that large inflated structures have never been built previously to the close





tolerances required by SPS. The closest achievement to date is the Echo satellite which was a sphere, 100 feet in diameter, built to a diametral tolerance of  $\pm 1$  percent. Sheldahl, Inc., manufacturer of the Echo satellites, has performed a design feasibility and producibility study of the SPS inflatable design and foresees no fundamental problems, including achievement of the final accuracy. Development risk of the rigid, faceted concept lies chiefly in the pointing error detectors (charge-coupled devices) and servo actuator systems.

Based on a mass and complexity comparison, the total overall cost of the faceted concept is considered to be at least three times that of the inflatable concept. It is recommended that no further design or development effort be expended on the faceted concept unless it is later determined that the inflatable concept is not feasible. The inflatable concept was selected for use in the point design, and the faceted and tensioned net concepts will be retained as backup designs.

#### Solar Absorber Trades

The basic function of the absorber is to transfer heat from the concentrated solar radiation to the working fluid of the thermal power cycle. As such, it is essentially a tubular heat exchanger with solar radiation impinging on the outside and the working fluid flowing inside. The basic requirements are (1) high solar capture and absorption efficiency, (2) low pressure drop, and (3) low mass. The special problems associated with SPS application are:

- High-temperature environment
- Re-radiation losses
- Meteorite environment
- Thermal cycling during eclipse
- Freezing of Rankine fluids

Candidate designs considered were:

1. Internal (spherical or cylindrical cavity)
2. External (disc or cylinder)

Brayton Cycle Applications. This cycle, which uses a single-phase gas as its working fluid, imposes the problems of relatively low film heat transfer coefficients inside the absorber tubes, and the extreme criticality of pressure drop for cycle efficiency. This drives the design toward a large absorber surface area and, consequently, to a cavity design as shown in Figure 3.1-48. This is because the required surface area is several times that of the minimum aperture size (61 m or 200 ft) which is used to minimize re-radiation losses and exposure to meteorite flux. This minimum size is determined by the smallest subtended view angle of the aperture which the solar concentrator can use without excessive "spill over" losses. It assumes use of a 45-degree compound parabolic reflector skirt which decreases the allowable aperture diameter by 29 percent, and also shields against most of the incident meteorite flux. Use of either an external absorber or a larger aperture would result in higher losses and require a larger, heavier concentrator. A spherical (geodesic) cavity was not used because it excludes use of rectangular panels of tubing, which are considerably less expensive than other panel shapes.

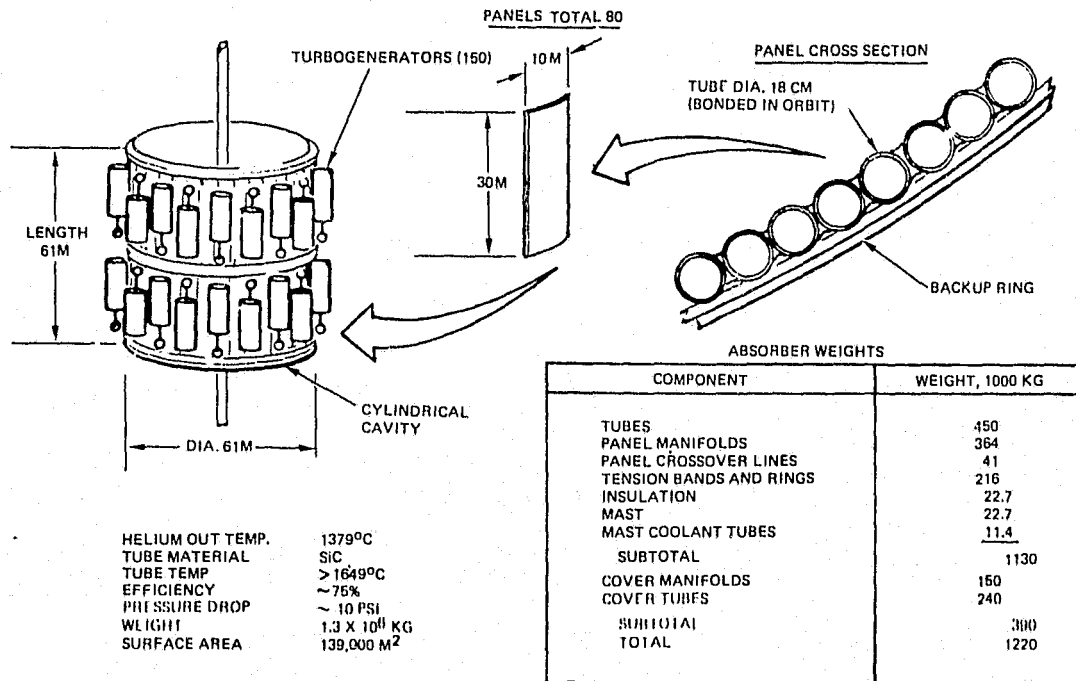


Figure 3.1-48. Brayton Absorber Design

Rankine Cycle Applications. Since two-phase flow occurs inside the Rankine cycle absorber, the inside film heat transfer coefficients are an order of magnitude better than for the Brayton cycle (boiling film vs. gas film). This allows the absorber surface area to be as small as that of the minimum aperture—resulting in a disc-shaped absorber which takes the place of the aperture opening. Use of a cavity to increase the absorber surface area (with the same size aperture) would reduce re-radiation losses somewhat due to a slightly lower wall temperature, but would increase the area and mass of the absorber surface and the overall mass of the SPS. (Re-radiation losses at a given temperature depend on the size of the aperture opening, not the inside cavity area.)

Results. It is concluded that the optimum absorber configuration for the Brayton cycle application is a cylindrical cavity; whereas for the Rankine cycle, it is a flat disc. Both configurations can benefit from use of a compound parabolic reflector skirt to reduce minimum aperture size, which reduces re-radiation losses and exposure to meteorite flux. The skirt also shields the vulnerable (uninsulated) side of the absorber from most of the incident meteorite flux. The absorber configuration used for the point design will depend on which thermal power cycle is used.

### Thermal Power Cycle

Among the various thermodynamic cycles applicable to SPS, only the Brayton and Rankine were considered well enough developed for 1995 IOC. Thermionic devices, however, show promise for later use in a topping cycle on either a Brayton or Rankine system. The following candidate cycles were evaluated in this trade study: (1) Helium/Xenon Brayton, (2) Potassium Rankine, (3) Cesium Rankine, and (4) Cesium/Steam Rankine.

Brayton Cycle. As shown in Figure 3.1-49, this cycle operates entirely within the gas phase region and, as such, requires a gas compressor to raise the pressure of the working fluid. This requires approximately 65% of the total expander (turbine) power, as compared to approximately 2% for the liquid pump of a Rankine cycle. The compressor working fluid is delivered back to

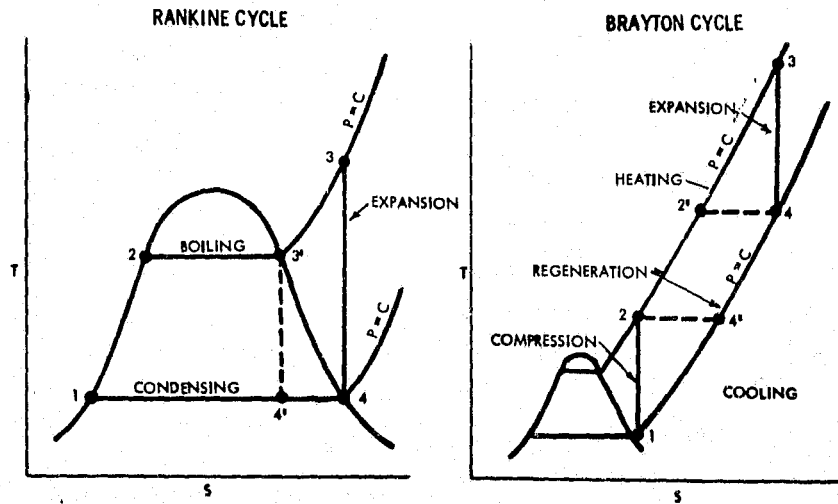


Figure 3.1-49. Power Cycle Diagrams

the turbine as fluid energy; however, system pressure losses and inefficiency in the compressor and turbine impose a much stronger penalty on cycle efficiency than for the Rankine cycle since they are a much larger part of the net turbine output. For this reason, the efficiency of a Brayton cycle is usually about three-fourths that of an equivalent Rankine cycle, as shown in Figure 3.1-50. The relatively low film heat transfer coefficient of a gas (compared to boiling and condensing coefficients) requires larger, heavier heat exchangers

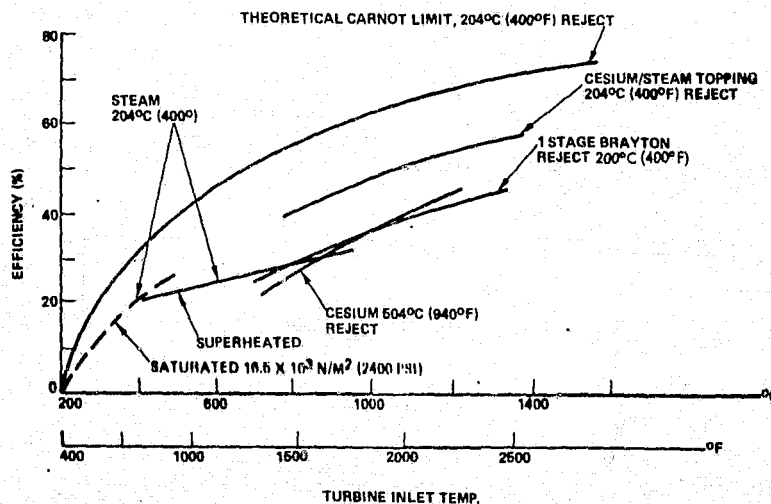


Figure 3.1-50. Dynamic Conversion Efficiencies

(heaters, regenerators, coolers) than for the Rankine cycle. The Brayton cycle, however, avoids some of the system complexity of the Rankine, including problems such as two-phase flow stability, turbine erosion, and freezing of the working fluid during an eclipse.

The major problems to be considered in an SPS Brayton system are listed below.

- Component efficiencies and pressure losses
- High-temperature corrosion due to trace impurities (oxygen, CO<sub>2</sub>)
- Thermal cycling of heat exchangers
- Heat exchanger mass
- Relatively low cycle efficiency
- Bearings and shaft seals
- Rotating machine life
- Fluid leakage
- High-temperature material requirements
- Development risk
- Startup and shutdown procedures
- Control complexity
- System reliability
- Maintenance

The reference design chosen for evaluation is shown in Figure 3.1-51. To be competitive with the Rankine cycle efficiency, a very high turbine inlet temperature [1371°C (2500°F)] was used, which requires development of ceramic

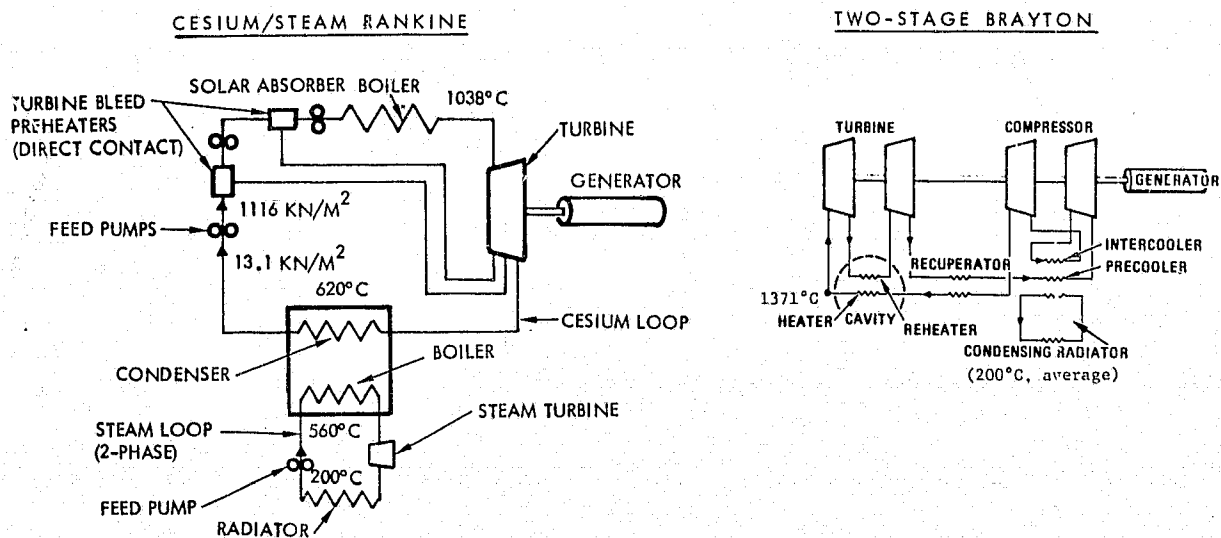


Figure 3.1-51. Dynamic Conversion Schematics

turbine blades and absorber tubes. One stage of turbine reheat and compressor intercooling was included to increase efficiency. The recuperator heat exchanger (which is the heaviest part of the system) is also required for efficiency



reasons. The working fluid chosen was a helium-xenon mixture having a molecular weight of 8, which gives an optimum combination of high heat transfer (helium) and small turbine/compressor size (xenon). A pressure ratio of 2.45 was selected, giving a cycle efficiency of 0.45 based on an overall system pressure drop of 9 percent. A turbine/generator size of 30 MW at 7000 rpm was selected for minimum specific system mass.

The cavity solar absorber design (shown in Figure 3.1-48) was assumed for the helium heater. The sensible waste heat from the cycle is rejected in the cooler (Figure 3.1-49) over a considerable range of temperature from point 4' to point 1. This corresponds to a temperature of  $\sim 730^{\circ}\text{C}$  ( $698^{\circ}\text{F}$ ) at the cooler inlet, and  $\sim 125^{\circ}\text{C}$  ( $257^{\circ}\text{F}$ ) at the cooler outlet in the reference design. To minimize radiator weight, it is desirable to keep the average radiator temperature as high as possible. This can be accomplished easily with a single-phase radiator fluid such as NaK or diphenyl by matching its sensible heat and temperature change to that of the helium in the cooler. The inlet temperature at the radiator would then be  $\sim 340^{\circ}\text{C}$  ( $644^{\circ}\text{F}$ ) and the outlet  $\sim 100^{\circ}\text{C}$  ( $212^{\circ}\text{F}$ ), allowing for a reasonable heat transfer  $\Delta T$  in the cooler. The mass of fluid inventory required, however, is quite high, and it was found that a lighter total radiator mass would result from a two-phase condensing radiator using a fractionating fluid mixture such as diphenyl/toluene. The diphenyl would boil and condense mostly at the high end of the temperature range while the toluene would do so mostly at the lower end. Consequently, most of the radiator plumbing volume would be occupied by vapor instead of liquid, at a considerable savings of fluid mass and pumping power. The radiator mass flow rate would also be less due to the high value of latent heat, relative to the sensible heat of the fluid. A water/glycol mixture would allow an even smaller fluid inventory; however, glycol is not chemically stable at the high radiator temperatures desired.

If a single condensing fluid were used, a constant, much lower radiator temperature and higher mass would result. The radiator design finally chosen for the reference Brayton system was a compound-condensing steam design, using three parallel independent loops of steam at conditions of  $300^{\circ}\text{C}$  ( $572^{\circ}\text{F}$ ),  $200^{\circ}\text{C}$  ( $392^{\circ}\text{F}$ ), and  $100^{\circ}\text{C}$  ( $212^{\circ}\text{F}$ ). This gave a somewhat lower average radiator temperature and a higher fin mass than a dual-fluid, but this was more than offset by the extremely high latent heat of steam and the resulting reduction in mass flow rate, plumbing size, fluid inventory, and pumping power.

Rankine Cycle. This cycle operates in both the liquid and gaseous phase (Figures 3.1-49 and 3.1-51) with a liquid pump and boiler replacing the compressor and heater of the Brayton cycle, and a condenser replacing the cooler. In contrast to the Brayton cycle, heat addition and rejection occur at a practically constant temperature. As discussed previously, the Rankine cycle efficiency is substantially higher than the Brayton (at same temperature ratio) because of lower pumping power requirements.

The major problems to be considered in a liquid-metal Rankine system are:

- Two-phase flow stability
- High-temperature corrosion from trace impurities (oxygen,  $\text{CO}_2$ )
- Thermal cycling of heat exchangers



- Turbine erosion
- Freezing of working fluid
- Bearings and shaft seal life
- Rotating machine life
- Fluid leakage
- High-temperature material requirements
- Development risk
- Startup and shutdown procedures
- Control complexity
- System reliability
- Maintenance

The three reference Rankine cycles chosen for detail evaluation were (1) potassium, (2) cesium, and (3) cesium/steam). These were all compared at a turbine inlet temperature of 1038°C (1900°F) to utilize the highest inherent efficiency of the Rankine cycle for relaxing the temperature and material requirements in the absorber and turbine inlet. This allowed use of state-of-the-art refractory metals rather than undeveloped ceramics. Potassium was evaluated because of its relative abundance and extensive test experience. Cesium has less test experience but has higher vapor pressure and density characteristics, which reduce turbine mass by a factor of 3.5 over potassium. A steam bottoming cycle was also studied to evaluate the benefits of raising the cesium condensing temperature and vapor density (cesium turbine size), and the benefit of higher cycle efficiency permitted by a lower cycle heat rejection temperature. A straight steam cycle was not evaluated in detail because it would require ceramic components (at 1038°C) to overcome problems of steam dissociation and resulting oxidation. Competitive cycle efficiencies would also require use of a massive surface-type regenerative heat exchanger, such as required for the reference Brayton cycle, because steam at 1038°C is so deeply into the superheat region. Such a system would be justified only if problems with liquid metals proved to be insoluble. To date, workable solutions have been found for all of the problems encountered with potassium or cesium. Organic working fluids were not considered, even for bottoming, because of chemical degradation at the temperatures involved.

The schematic of Figure 3.1-52 outlines the cesium/steam system, but is also applicable to the cesium and potassium systems if the steam turbine is removed from the radiator steam loop. This shows that the added complexity of a bottoming cycle is fairly minor, since a second fluid is needed for the radiator anyway. Thermal regeneration is accomplished by directly mixing turbine interstage bleed flow with feed-liquid entering the boiler—thereby avoiding heavy surface-type heat exchangers.

Results. Table 3.1-18 compares the characteristics of the four candidate systems and their corresponding SPS satellite designs. The satellite configuration of Figure 3.1-51 was assumed for each case, differing only in the size of the solar concentrators required.

The Brayton and cesium/steam Rankine systems both use an average radiator temperature of 204°C (400°F) and exhibit cycle efficiencies of 45% and 47%, respectively. The potassium and cesium Rankine systems use a higher radiator temperature of 343°C (650°F) to avoid excessively low vapor densities at the turbine exhaust which would result in a very high turbine mass. Their cycle efficiencies are both 36 percent.

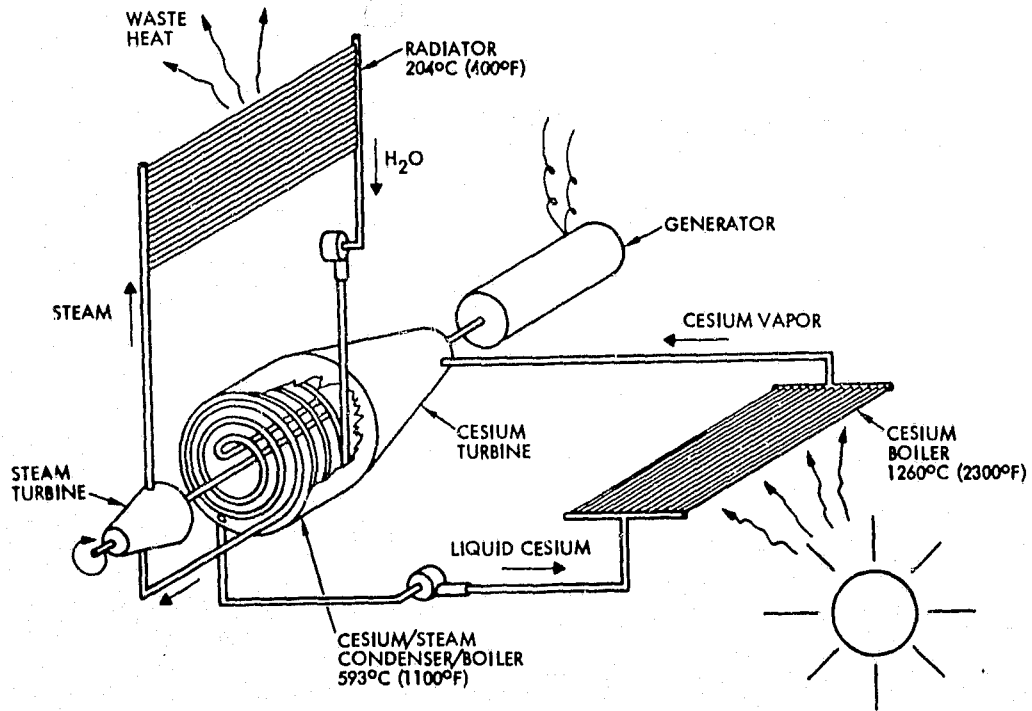


Figure 3.1-52. Cesium/Steam Rankine Cycle

Table 3.1-18. Candidate Power Conversion Systems

	BRAYTON HELIUM/XENON	RANKINE POTASSIUM	RANKINE CESIUM	RANKINE CESIUM/STEAM
TURBINE INLET TEMP, °C (°F)	1379 (2514)	1038 (1900)	1038 (1900)	1038 (1900)
CONDENSING TEMP, °C (°F)	-	504 (940)	504 (940)	593 (1100)
RADIATOR TEMP, °C (°F)	204 (400)	343 (650)	343 (650)	204 (400)
CYCLE EFFICIENCY, %	45	36	36	47
TURBINE/GENERATOR SIZE, MW	30	30	30	30
RADIATOR FLUID (CONDENSING)	COMPOUND STEAM	DIPHENYL	DIPHENYL	STEAM
SOLAR CONCENTRATOR MASS, 10 <sup>6</sup> KG	1.092	1.380	1.380	1.057
SOLAR ABSORBER MASS, 10 <sup>6</sup> KG	3.380	0.299	0.299	0.221
TURBOMACHINE MASS, 10 <sup>6</sup> KG	0.780	16.900	4.55	1.040
RECUPERATOR/COOLER MASS, 10 <sup>6</sup> KG	4.134	0.104	0.104	0.104
CONDENSER, 10 <sup>6</sup> KG	-	1.170	1.170	0.585
POWER LOOP FLUID MASS, 10 <sup>6</sup> KG	0.143	0.091	0.091	0.091
GENERATOR MASS, 10 <sup>6</sup> KG	1.430	1.430	1.430	1.430
RADIATOR MASS, 10 <sup>6</sup> KG	11.52	13.169	13.169	9.75
POWER COND, DIST MASS, 10 <sup>6</sup> KG	5.203	5.203	5.203	5.203
STRUCT, MECH, ATT CONTR MASS, 10 <sup>6</sup> KG	2.932	3.034	3.034	2.774
ANTENNA MASS, 10 <sup>6</sup> KG	12.350	12.350	12.350	12.350
TOTAL MASS, 10 <sup>6</sup> KG *	43.154	55.131	42.781	34.605
*INCLUDES APPROX 30% GROWTH ALLOWANCES				



Table 3.1-18 also compares the mass characteristics of the four candidate systems, including a 30-percent growth allowance. Concentrator mass varies simply as the inverse of cycle efficiency, as does the mass of the open-disc absorber used for the three Rankine candidates. The Brayton cavity absorber is considerably heavier due to the lower heat transfer properties of helium and the larger required surface area. Heat losses are also higher for this absorber because of its higher re-radiation temperature (1650°C vs. 1315°C) and the larger external insulation area. Despite the need for a gas compressor, the Brayton turbomachine mass is the lightest of the four candidates because of its relatively high turbine exit pressure and low required exit flow area.

Due to the use of a bottoming cycle, the cesium condensing temperature and cesium turbine exit vapor density are much higher for the cesium/steam cycle than for the straight cesium system. Consequently, the cesium/steam turbine is approximately four times lighter than the straight cesium turbine. For similar reasons, the potassium turbine mass is approximately 3.5 times that of the straight cesium turbine, becoming the heaviest single component item of any of the four candidates.

The Brayton system takes a large mass penalty in its surface-type regenerator/cooler, as compared to the Rankine direct contact preheaters and surface condensers. Both the Brayton and cesium/steam systems were able to use condensing steam as a radiator fluid by virtue of their relatively low heat rejection temperature. The potassium and cesium systems required the use of a high-temperature organic fluid (diphenyl). Despite a higher operating temperature, these radiators were heavier than the steam versions because of lower fluid latent heat and higher mass flow rate, which requires a larger fluid inventory. Also, their lower cycle efficiency increased the rejected heat load. Direct condensing of the potassium and cesium turbine exhaust vapor in the radiator was not considered because of the low vapor density and a resulting large duct size and mass.

On the basis of overall SPS mass, the cesium/steam system is easily the lightest of the four candidate systems. Because the three Rankine candidates are roughly equivalent in terms of evaluation criteria other than mass, the overall choice is narrowed down to the cesium/steam Rankine system vs. the helium/xenon Brayton system. It is possible to have a hybrid system with a Brayton cycle topping a Rankine cycle; however, no significant advantages are apparent. Performance would be halfway between the two, and development costs would be higher than for either cycle alone.

Table 3.1-19 summarizes the basic physical comparisons between the Brayton and Rankine candidates. Table 3.1-20 compares their technology advancement requirements for 11 significant categories. Material and fabrication problems are rated greater for Brayton because of the undeveloped status of ceramics vs. refractory metals. It remains to be demonstrated that reliable ceramic joining methods can be achieved. Corrosion problems are moderate for both cycles if proper attention is given to excluding trace amounts of oxygen-bearing contaminants from the working fluid. Standard, proven methods such as the use of oxygen-getter materials in the flow loop are available. Turbine advancement requirements are greater for Brayton because of its higher temperatures and the need for ceramic blading. Although erosion is a problem in





Table 3.1-19. General Comparison of Brayton and Rankine Cycles

	BRAYTON	RANKINE
WORKING FLUID	SINGLE PHASE (GAS)	TWO PHASE (LIQUID, VAPOR)
COMPRESSOR/PUMP WORK	LARGE (2 X NET OUTPUT)	SMALL
COMPRESSION/PUMP LOSSES	LARGE	SMALL
ROTATING MACHINE SIZE	LARGE	SMALL
CYCLE EFFICIENCY	MODERATE	HIGH
HEAT TRANSFER COEFFICIENTS	LOW	HIGH
HEAT EXCHANGER SIZE	LARGE	SMALL
MACHINE LIFE	30 YR	30 YR
CORROSION (HIGH-TEMPERATURE)	MODERATE	MODERATE
SYSTEM SPECIFIC WEIGHT, KG/KW	MODERATE	LOW

Table 3.1-20. Technology Advancement Requirements

CRITERIA	BRAYTON	RANKINE
MATERIALS	VERY HIGH	HIGH
FABRICATION	HIGH	MODERATE
CORROSION	MODERATE	MODERATE
TURBINES	HIGH	MODERATE
PUMPS	NO	MODERATE
EROSION	NO	MODERATE
BEARINGS	HIGH	HIGH
SEALS	HIGH	HIGH
2-PHASE FLOW	NO	MODERATE
FREEZING PROVISIONS	RADIATOR ONLY	POWER LOOP ALSO
OVERALL EFFORT	HIGH	HIGH



the Rankine turbine, standard methods capable of providing 30-year life are available:

- Suction grooves in stator blade trailing-edges and rotor housing to remove impinged droplets
- Interstage moisture removal (external to turbine)

Due to a tendency to form exceedingly fine liquid droplets, the erosion problem with cesium is estimated to be ~20 times less than for potassium<sup>1</sup>. New developments will be required in fluid dynamic bearings and dynamic seals for both Brayton and Rankine turbines. New high-temperature pumps are required for the Rankine system, but would not be much beyond the present state of the art. Standard methods are also available for stabilizing two-phase flow, as found in the Rankine system boiler and condenser:

- Adequate flow velocity
- Large pressure drop (negligible power penalty for Rankine)

Provisions for draining water from the radiator must be made for both Brayton and Rankine radiators, in addition to draining cesium from the Rankine boiler. Other parts of the flow loops are sufficiently insulated to prevent freezing during eclipse.

All in all, development risk and cost are seen to be approximately equal for the two systems. Table 3.1-21 compares the other major cost items of the Brayton and Rankine power loops. Table 3.1-22 summarizes the items and presents an estimated overall relative cost, taking appropriate weighting factors into account. Table 3.1-23 provides an overall point rating comparison between the two systems. Material availability is rated fair for both systems, based on estimated reserves of cesium and helium. Cesium requirements for a 120-satellite program are approximately 2% of estimated actual reserves<sup>2</sup>. Availability of xenon is poor, but krypton or argon can be substituted without serious increase in the Brayton system hardware sizes. The only environmental impact anticipated is possible contamination of the earth's upper atmosphere with combustion products from a chemical propulsion transport system. The impact is assumed to be proportional to total satellite mass. The safety hazard of the cesium/steam Rankine cycle is rated worse because cesium reacts hypergolically with air and special precautions must be taken during ground testing. Leakage of steam from a boiler tube into the cesium loop also causes an exothermal reaction which can be controlled with pressure-relief devices and automated shutdown provisions. This is considered to be relatively remote failure mode and can be isolated by shutting down an entire power module (out of a total of 318 modules).

<sup>1</sup>W. D. Pouchot, et al, *Basic Investigation of Turbine Erosion Phenomena*, Westinghouse Electric Corporation, November 1971, NASA CR-1830.

<sup>2</sup>U.S. Bureau of Mines, *Mineral Facts and Problems*, 1975 Edition, Bulletin 667, Superintendent of Documents, Washington, D.C.

Table 3.1-21. Production Costs

	BRAYTON	RANKINE	DISCRIMINATOR
<u>PRODUCTION COSTS</u>			
WEIGHT FACTOR	1 (BASE)	0.6	HEAT EXCHANGERS, RADIATOR PLUMBING, CONTROLS
COMPLEXITY FACTOR	1	1.5	
MATERIAL FACTOR (\$/LB)	1	1.0	CERAMICS
FABRICATION FACTOR	1	0.7	
OVERALL PROD. COST FACTOR	1	0.63	
<u>CONSTRUCTION COSTS</u>			
COMPLEXITY FACTOR	1 (BASE)	0.8	ABSORBER CERAMIC JOINTS
FABRICATION AND ASSEMBLY	1	0.8	
OVERALL CONSTR COST FACTOR	1	0.8	
<u>MAINTENANCE AND OPERATIONS</u>			
COMPLEXITY FACTOR	1 (BASE)	1.5	AUXILIARIES
LEAKAGE FACTOR	1	1.0	
OVERALL MAINT & OPS COSTS	1	1.5	

Table 3.1-22. Overall Power-Loop Cost Comparison

	BRAYTON	RANKINE
DEVELOPMENT COST	1 (BASE)	1.0
PRODUCTION COST	1	0.63
TRANSP COST (WEIGHT, DENSITY)	1	0.6
CONSTRUCTION COST	1	0.8
MAINT & OPNS COST	1	1.5
OVERALL COST/KW-HR (30 YEARS)	1	0.75

Table 3.1-23. Overall Power-Loop Point Ratings

	MAXIMUM POINTS	POINTS	
		BRAYTON	RANKINE
COST (PER KW-HR)	100	75	100
DEVELOPMENT RISK	20	5	5
MATERIAL AVAILABILITY	5	3	3
ENVIRON. IMPACT (MASS)	5	2	3
SAFETY HAZARD	5	3	2
TOTAL	135	88	113

### Conclusions

The cesium/steam Rankine cycle with a rating of 113 points out of a total 135 seems to be significantly better than the Brayton cycle with a total of 88 (Table 3.1-23). On this basis, the Rankine cycle was selected for subsequent elaboration into a point design for the solar thermal SPS, with the Brayton system considered as a backup option.

### 3.1.3 NUCLEAR POWER

Previous study by Boeing had concluded that nuclear power was a viable option for SPS. Rockwell studied nuclear power in order to gain an insight into the nuclear system implications. To do this, it was necessary to re-evaluate and develop new design concepts for evaluation.

The available energy from breeder reactor fuels,  $\sim 615 \times 10^{18}$  Btu breeding Pu-239 from non-fissile Pu-238 (exceeds U.S. known coal reserves by a factor of 30), represents a large energy reserve which cannot be ignored. There is a limited availability of the natural occurring U-235 fissile material. For these reasons, the nuclear powered SPS must be a breeder. If terrestrial siting objections to nuclear breeders are strong enough, then space siting is the only alternative. The nuclear SPS option does offer some unique operational advantages over solar-powered SPS's. For example, nuclear power is "hardened" to the space environment, operates through solar eclipses, results in a small planar area, and minimizes the requirement for a rotary joint.

#### Trades

The major nuclear trade study areas are shown in Figure 3.1-53. The areas are configuration, reactor approach, and fuel processing. These considerations are described in detail in the following paragraphs.

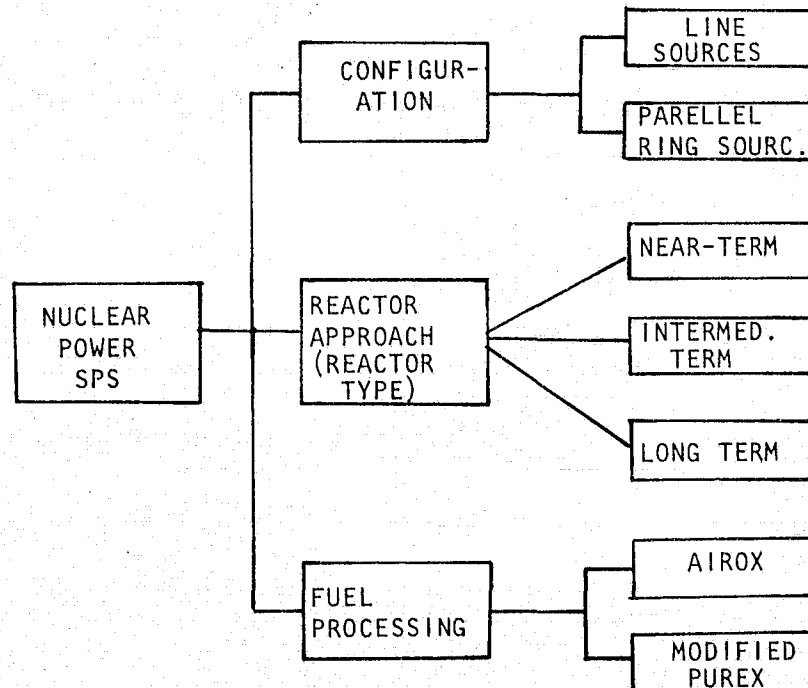


Figure 3.1-53. Nuclear Power System Trade Tree (Options)

Configuration. The nuclear reactor power system was sized to produce 7.85 GWe at its bus (5 GW on the ground). A modular design was selected consisting of 26 self-contained modules, each capable of generating 336 MWe of power. Each module consists of reactor heat source, fuel processing plant, Brayton power conversion equipment, and a heat-rejection radiator. The reactor, fuel processing plant, and Brayton PCS are enclosed in a cylindrical containment structure. The space radiator consists of a flat-tube fin structure fed by a manifold system which conveys the waste heat from the Brayton PCS.

Three satellite configurations were evaluated. The modules may be arranged either in line perpendicular to the plane of the antenna (as shown in Figure 3.1-54) or in a ring parallel to the antenna plane, as illustrated in Figures 3.1-55 and 3.1-56. Figure 3.1-57 compares the size of these three nuclear powered SPS concepts with solar powered ones based on the same scale. Note that the MSFC silicon solar cell and the Boeing Brayton are 10-GW outputs; therefore, one-half the space would be required for 5 GW when compared with the nuclear SPS. The preferred nuclear concept (Concept No. 3) occupies a volume approximately 2 km in diameter at the large end, has a 1-km-diameter antenna, and is 3 km in length. This concept size, when compared to solar concepts, should lend itself to in-orbit assembly.

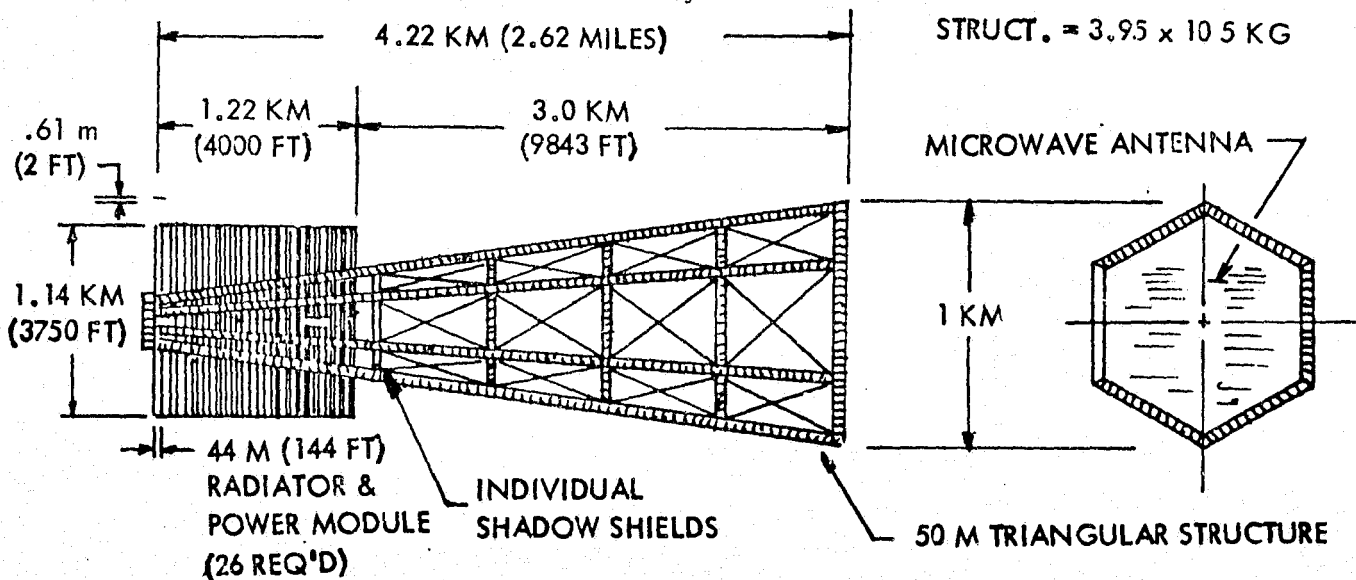


Figure 3.1-54. Nuclear-Powered SPS (5 GW) - Concept No. 1

Separation distance between modules and antenna was chosen to meet a requirement of 25 mrem per year at minimum weight for structure and radiator shield. Figure 3.1-58 shows the effect of varying reactor-antenna separation distance on shield and required structural weights to maintain a fixed 25 mrem/hr radiation dose at the antenna. At a distance of approximately 2 to 3 km, the total shield and structure weight becomes a minimum. The parametric shield weights shown (Figure 3.1-58) are for the 26 reactors and are based on a 10-ft shadow shield diameter.

3-75

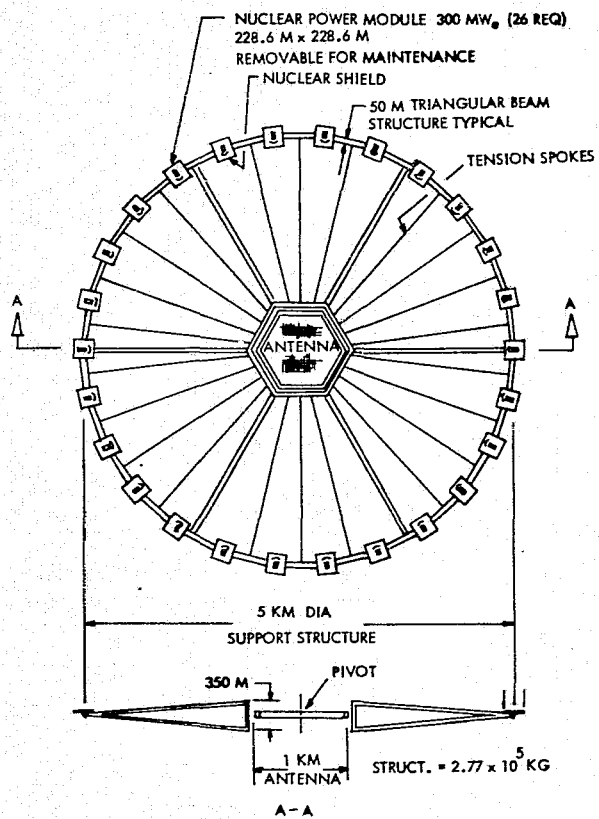


Figure 3.1-55. Nuclear-Powered SPS (5 GW) - Concept No. 2

SD 78-AP-0023-3

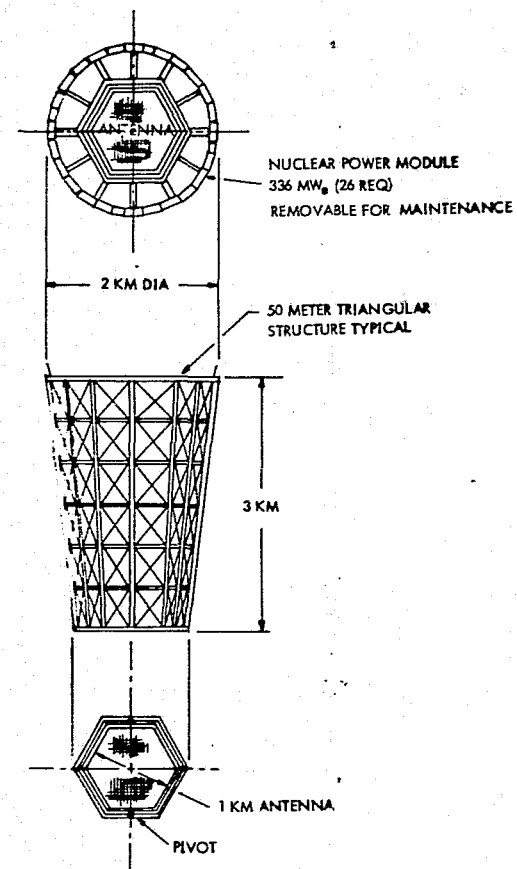


Figure 3.1-56. Nuclear-Powered SPS (5 GW) - Concept No. 3

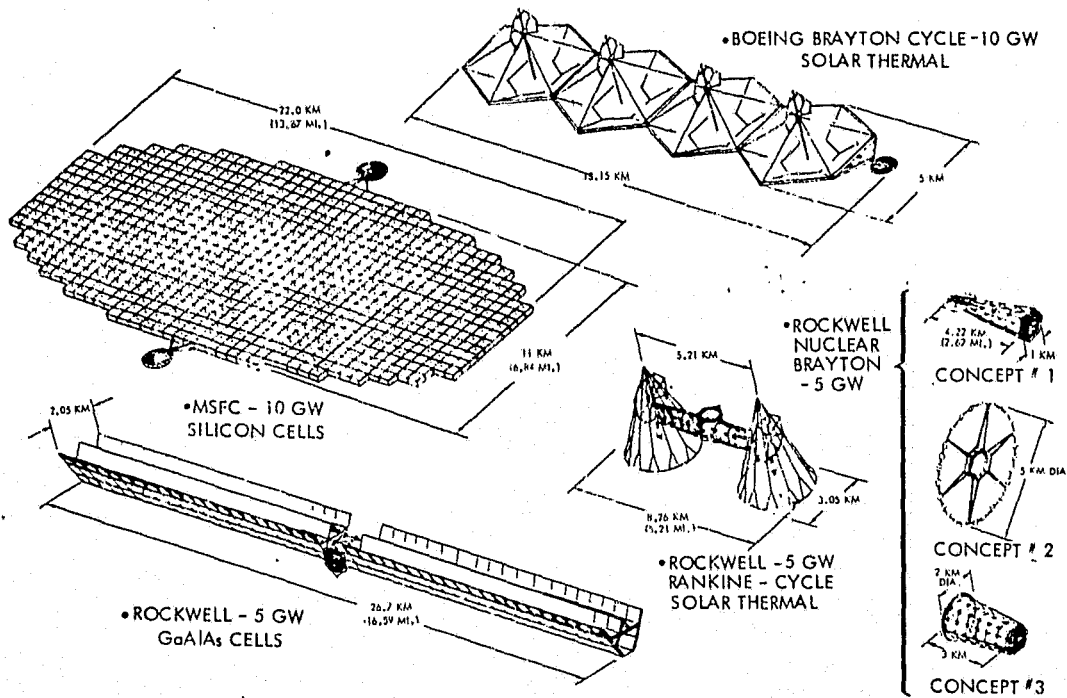


Figure 3.1-57. Concepts Comparison

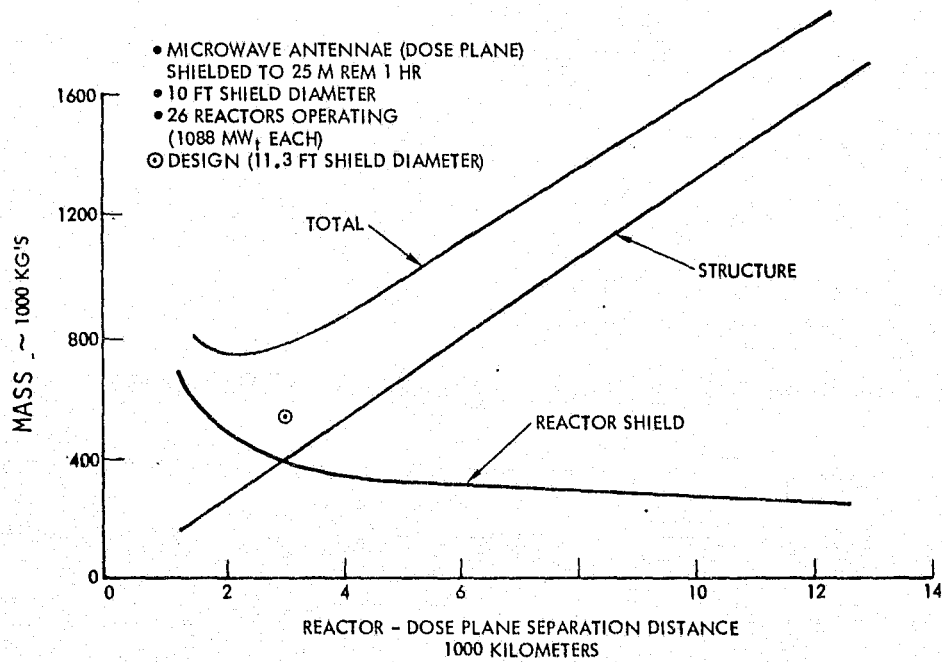


Figure 3.1-58. Nuclear SPS Reactor—Shadow Shield Mass

Reactor Approach. The nuclear-powered SPS must be a breeder due to the limited availability of the natural occurring fissionable material (U-235). A breeder reactor also reduces the logistic and hazards associated with transportation of fissionable materials. A high reactor core temperature, 1660 K (2500°F) is required to obtain good power conversion efficiencies with the Brayton cycle consistent with minimum radiator areas. These high temperatures are also compatible with advanced Rankine power conversion systems using liquid-metals as working fluids.

Reactor types and likely energy conversion schemes considered for this study are listed in Table 3.1-24. The criteria used for rejection are listed at the bottom of the table. Due to the 1991 availability requirement, a selection was required from reactors listed under "intermediate term."

Table 3.1-24. Nuclear Reactor Options

REACTOR TYPE	COSED BRAYTON CYCLE	POTASSIUM RANKINE	LIQUID- METAL MHD	PLASMA MHD	THERMIONIC
<u>NEAR TERM</u>					
FP LIQUID-METAL FAST BREEDER		X	X		
FP GAS-COOLED FAST REACTOR	X	X	X		
R MOLTEN SALT BREEDER REACTOR		X	X		X
<u>INTERMEDIATE TERM</u>					
NB CERAMIC THERMIONIC REACTOR					X
NB NERVA-TYPE REACTOR	X			X	
C ROTATING FLUIDIZED BED	X			X	
T COLLOID CORE REACTOR	X			X	
C UF <sub>6</sub> FUELED REACTOR	X			X	
✓ CERAMIC PEBBLE-BED REACTOR	X			X	X
<u>LONG TERM</u>					
T "LIGHT BULB" PLASMA CORE				X	
T "COAXIAL FLOW" PLASMA CORE				X	
T MULTI-PHASE REACTOR		X	X		X
T FUSION REACTOR				X	
NOTES: NB = NON BREEDER		R = PAST STUDY REJECTION			
T = LOW TECH STATUS		✓ = SELECTED			
FP = COMPLEX FUEL PROCESSING		C = ADDED COMPLEXITY			

A ceramic pebble bed reactor was selected to provide a high-temperature heat source for the Brayton cycle power conversion system. A large technology base exists for both this type of gas-cooled reactor and Brayton cycle power conversion loops. The 15-MWe AGV pebble bed reactor has been in operation in Germany for ten years at a 90-percent load factor. Some fossil-fueled closed Brayton cycle power generating systems have operated for over 100,000 hours. A Brayton power conversion is best for a helium-cooled reactor concept. A direct closed cycle helium loop can be used—thus eliminating complex intermediate heat exchangers. Also, by changing gas pressure and reactor power, electrical output can be modulated to compensate for nuclear power generating module failure or changing electrical power demand.





Nuclear Reactor Concept. The selected reactor concept is a fast breeder reactor and, as shown in Figure 3.1-59, is cylindrical in shape—having a diameter and a length of 8 feet. The ceramic pebble-type fuel receives helium coolant from the Brayton power unit at 1870°F and heats it to 2400°F at a thermal power of 1088 MWt.

Its nuclear materials are uranium-235 which is fissionable and uranium-238 which is a so-called fertile material. When the reactor achieves criticality and is brought up to power, the U-235 fissions and liberates neutrons which support the chain reaction. Some of the neutrons are absorbed by the U-238, which undergoes a series of transmutations and forms plutonium-239. Since PU-239 is also a fissionable material, the reactor is said to breed fissionable material. The reactor has a breeding ratio greater than one. With reactor operation, the amount of fissionable material increases while the quantity of fertile U-238 decreases. Eventually, the fission product inventory becomes large and begins to poison the reactor neutronically and also changes the fuel element materials properties. Therefore, periodically, some old fuel is removed from the reactor and new fuel is added. The old fuel is transferred to the fuel processing plant where the fission products are removed, new U-238 is added, and the fuel elements are reformed.

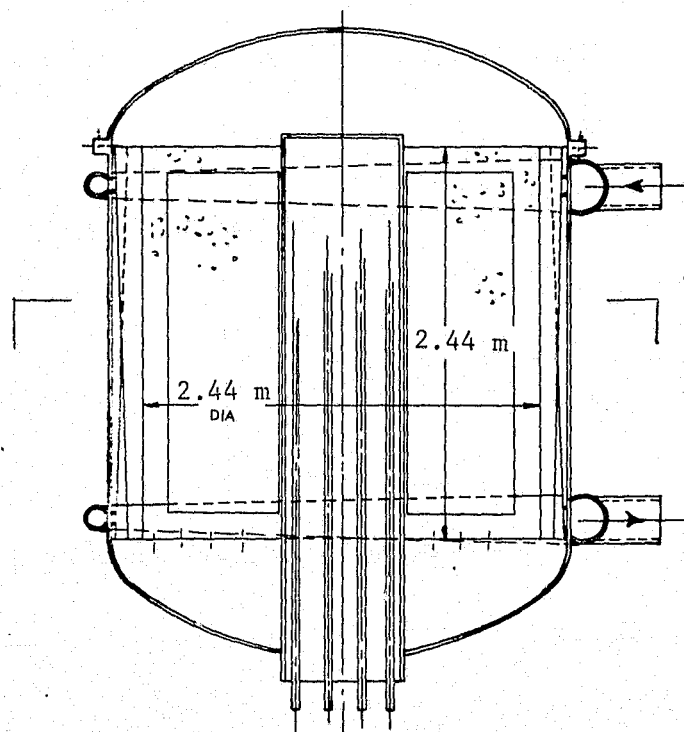


Figure 3.1-59. Nuclear Reactor

The fuel elements selected for the reactor are small spheres made of a mixture of  $\text{PuO}_2$  and  $\text{UO}_2$ . These spheres are about 1/4 inch in diameter and have a thin coating of carbon, plutonium carbide, and uranium carbide. There are several reasons why a pebble bed reactor was used: (1) it utilizes small spheres or pebbles of small size, thereby developing only small stresses;



(2) such pebbles can be used in layers where the stresses developed between adjacent spheres are readily relieved; (3) fuel in the form of small spheres possesses a large heat transfer area; (4) gas flow over spheres develops a relatively large heat transfer coefficient; and (5) a small spherical shape is relatively easy to manufacture, particularly since the dimensional tolerances can be relaxed.

Another feature of this reactor is that it uses an inert gas (helium) as the coolant. There are several disadvantages possessed by helium-cooled reactors. One, of course, is that the gas is noncorrosive—which alleviates problems in the fuel and reactor structure. Second, there are no problems of freeze-up, change of phase, or disassociation in this type of coolant. Third, helium can also function as the Brayton cycle working fluid—thus simplifying the power plant. Fourth, helium has no significant effect upon the reactor nuclear performance.

The use of a pebble bed reactor, in conjunction with helium as the coolant, forces the reactor to be constructed in layers such that the gas flow has an effectively large flow area and a relatively short heating path length. Such a flow keeps the pressure drop in the pebble bed at reasonable levels while the heat transfer remains acceptable. The best way to subdivide the reactor is shown schematically in Figure 3.1-60. In this arrangement, the fuel is packed in 36 layers which are spaced around a central island like the spokes in a wheel. The resulting active core is 2.13 meters in length and 2.13 meters in diameter, with a central island diameter of 0.76 m. Each pebble bed is 2.13 m long and 0.69 m in the radial direction. The layers have a thickness of 0.16 meter at the outer edge, and 0.06 meter at the central island. The pebble bed fuel layers are separated by gas gaps in which the helium gas flows radially inward or outward. The fueled layers are about one inch apart at the core outer radius and about 1.02 cm at the central island.

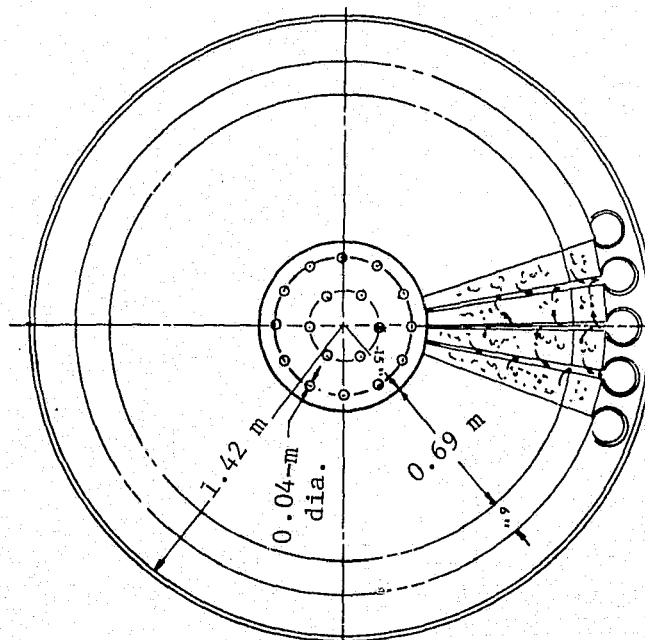


Figure 3.1-60. Reactor Subdivision



The reactor has a reflector on the cylindrical sides and both ends, which forms part of the wedge-shape fuel assembly. The reflector contains pebbles made of U-238, but has no fissionable materials except which is bred. The purposes of the reflector are to (1) return neutrons to the core, and (2) breed Pu-239 and improve the thermal power distribution. Helium flows through the reflector pebbles just as it does through the core pebbles, except that the flow rate per unit area is lower.

The helium enters the reactor at a pressure of about 6895 KN/m<sup>2</sup> and a temperature of 1021°C and at a flow rate of 712 kg/s. It departs at a temperature of 1316°C and at a pressure of about 6550 KN/m<sup>2</sup>. It enters alternate gas gaps between fuel layers and then divides and enters the fueled pebbles passing through the perforated structure. In the space of a few inches, the helium is heated to its peak temperature of 1316°C and then travels radially outward, leaving the core. The flow through the bed is controlled both by the bed resistance and the gas gap geometry. It is desired to have the gas temperature leaving the fuel to be at about the same temperature (1316°C) at all points. This is done by matching the local gas flows with the local power generated.

The reactor is controlled by 18 boron carbide control rods that are located in the central islands; these rods are about 2.54 cm in diameter and extend the length (2.13 m) of the reactor core. The outer 12 rods are for primary control, while the inner 6 rods are safety rods to be inserted only during unusual or hazardous situations. The rods are clad by a tantalum-tungsten alloy.

The fuel pebbles are contained in fuel assemblies of tantalum-tungsten alloy. Each assembly is 2.44 meters long and 0.84 meter high, while the width tapers from 0.18 meter to 0.06 meter. The reactor has 36 of these fuel assemblies.

The reactor is shut down every 12 months and one of the reactor end covers is removed. Twelve of the 36 fuel assemblies are removed and transported to the fuel reprocessing plant. Twelve refurbished fuel assemblies from the reprocessing plant are then inserted into the reactor. The old fuel assemblies contain a large amount of fission products which tend to poison the reactor. The fission products also tend to occupy a large volume in each fuel pebble so that the mechanical and physical properties are altered. The old fuel will have the fission products removed and fresh fertile material added in the reprocessing plant.

While the reactor is shut down, personnel can approach in a shielded vehicle to participate in the fuel replacement operations. This shielded vehicle would provide protection for the crew from radiation from the nearby shutdown reactors as well as from more distant operating reactors.

A detailed nuclear analysis of the selected reactor was beyond the scope of this effort. However, fast breeder reactors, similar to the present one, have been studied in the past, thus permitting the range of nuclear data expected in a reactor of this type to be established. More critical problems in the reactor are the achievement of high-cycle temperatures and satisfactory reactor life.



The core fuel pebbles occupy 4.04 m<sup>3</sup> of the reactor region which, at a solidity of 65 percent, leads to an actual fuel volume of 2.63 m<sup>3</sup>. At an effective density of 14,898 kg/m<sup>3</sup>, the fuel mass is 39,182 kg of mixed oxides of uranium. On the average, about 4.5 percent of this mass, or 1773 kg, is fissionable material. Most of the remaining material is fertile U-238. As the breeding ratio is greater than unity, there is a gradual increase in the amount of fissionable material during the core life to about 1864 kg. A reactor mass breakdown is given in Table 3.1-25.

Table 3.1-25. Reactor Mass Breakdown

<u>Component</u>	<u>Material</u>	<u>Mass (kg)</u>
Fueled pebbles	UO <sub>2</sub> - PuO <sub>2</sub>	39,591
End reflector	UO <sub>2</sub>	5,636
Side reflector	UO <sub>2</sub>	13,954
Side vessel	SS	2,091
Side manifolds	A-286	2,182
End vessels	SS	4,818
Control region	SS + B <sub>4</sub> C	2,045
Reactor structure	Tantalum	3,727
	Tungsten	955
	A-286	864
		<u>73,863</u>

The median energy of fission of this reactor is 0.14 MeV. Half of the fissions that occur are caused by neutrons above this energy and half are caused by those below. The fast neutron flux of this reactor is roughly  $2 \times 10^{15}$  neut/cm<sup>2</sup>-sec.

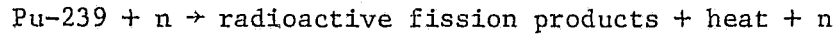
The reactivity of a reactor varies during its lifetime and must be accommodated by the control system. The primary control system consists of 12 boron carbide rods in the central island. Additional control in emergencies is performed by six additional rods in the island. The primary control will be capable of handling the reactivity changes shown in Table 3.1-26.

Table 3.1-26. Reactivity Changes

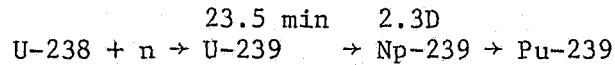
	<u>Reactivity (\$)</u>
Burnup decrement	0.60
Temperature decrement	4.50
One stuck rod	0.70
Operating margin	0.30
Shutdown margin	0.50
Uncertainty	<u>0.60</u>
Total	7.20

Fuel Processing. In the reactor, simultaneous fissioning and breeding of plutonium takes place due to the presence of a mixture of Pu-239 fuel and the U-238 breeding material in the pellet; the process is described by the following equations:

Fissioning



Breeding



The longer the fuel pellet resides in the reactor, the greater the build-up of the fission product poisons. Therefore, to maintain an adequate reactivity, the fuel must be purified in a fuel processing plant and the radioactive poisons removed. The spent fuel assemblies which are cycled from the reactor are transported to the fuel processing plant. Here, the fuel pellets are removed, undergo reprocessing for separation of fission poisons, reconstituted with fertile  $\text{UO}_2$ , refabricated, and loaded back into the fuel assemblies for return to the reactor.

Figure 3.1-61 shows the mass flow rates associated with the process. These numbers are based on a 1.2 GWT core heat source and an estimated core burnup of 150 MWd/kg. The recycle fuel rate of flow is given by:

$$\dot{W}_F = \frac{\text{Thermal power}}{\text{Burnup}} = \frac{1.2 \times 10^3 \text{ MW}}{150 \text{ MWd/kg}} = 8.0 \text{ kg/day (17.6 lb/day)} \quad (1)$$

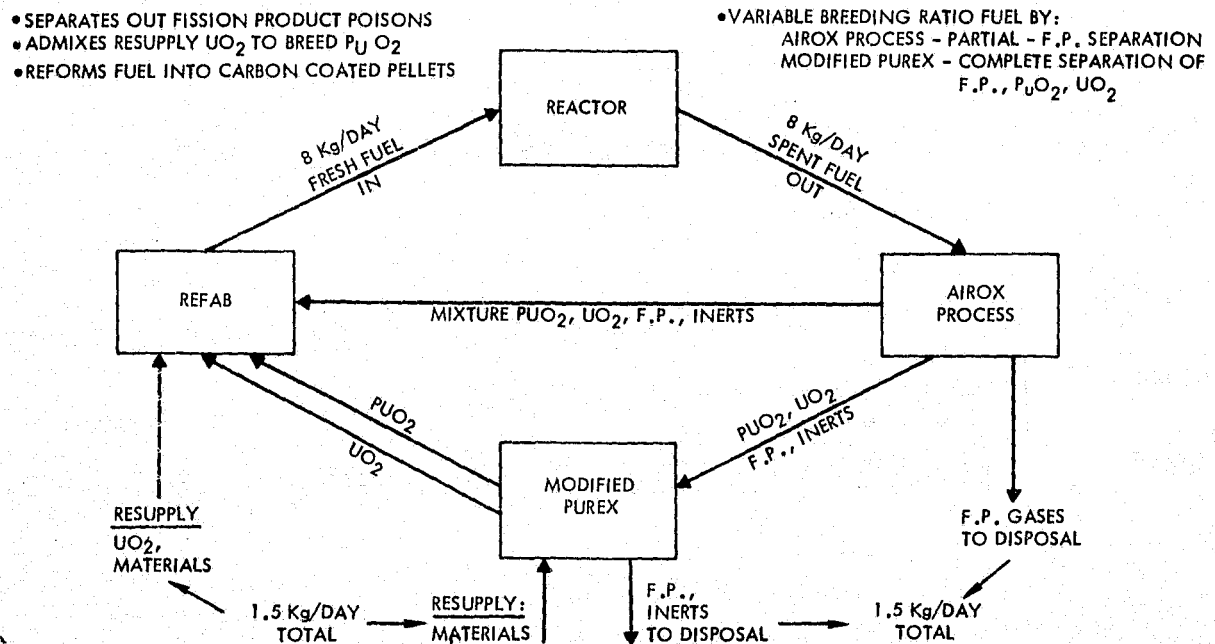


Figure 3.1-61. Fuel Management Schematic



This average daily total mass flow includes the fuel which has fissioned. Based on 1 MWd/gm, the fuel which has fissioned to produce 1.2 GWd is therefore 1.2 kg, which is converted to 1.2 kg/day of fission products in the form of gases and solids. The system must be supplied with 1.2 kg/day of fertile  $UO_2$  or 1.5 kg/day total, including chemicals. An average of 1.5 kg/day of fission products and inert wastes are removed from the fuel cycle and stored for periodic deep space disposal. The fuel has a maximum schedule residence time of three years in the reactor.

Fuel Processing Techniques. The spent fuel recycled out of the reactor is reprocessed by either the Airox process and/or a Modified Purex process, depending on the amount of fission poisons which must be removed from the fuel prior to refabrication. A fuel management schematic is shown in Figure 3.1-61.

The Airox process uses a series of oxidation-reduction heating cycles which cause the fuel to swell and crack, thereby releasing only the gaseous fission products. The final reduction reaction leaves the fuel in a powdered form which still contains the remaining fission product solids and inerts as shown in the figure. The mass proceeds to refabrication where it is mixed with resupply  $UO_2$ , formed into carbon-coated pellets, and recycled back to the reactor.

To reduce the buildup of fission product poisons and inerts in the reactor core, which would lower the reactivity and power density, the fuel mixture leaving the Airox process is treated in the Modified Purex process. The latter consists of a series of counterflow solvent extraction columns. The fuel mixture is first dissolved in aqueous  $HNO_3$  and the fission products, inerts, and higher oxides of Pu and U are separated out successively with a counterflow organic stream of bri-butyl phosphate. The resultant separated  $PuO_2$  and  $UO_2$  are then sent to Refabrication.

The Refabrication process mixes the processed fuel from either pretreatment process with resupply  $UO_2$ , and forms pellets which are sintered and then carbon coated. The resulting pellets are then returned to the reactor.

The Purex process was selected as typical of the more complete purification techniques. Should the process prove too unwieldy for a space mission, other alternatives such as the Molten Salt Pyrochemical process would be substituted.

Refabrication. The powdered fuel from the Airox process is ground if necessary to the desired average particle size. The resupply  $UO_2$  is added and blended and the mixture dried, pressed into pellets, and sintered with  $H_2$  to produce a dense oxide pellet. The pellets pass to a carbon coater where methane is introduced and leaves a thin carbon shell on the surface. The reprocessed fuel is then recycled back to the reactor.

Zero-G Processing. A significant problem arises in space processing operations that depend on a g-force; for example, phase separation of liquids and gases formed in a chemical reaction. This problem can be circumvented by either creating an artificial-g force by rotating the process plant about its axis or by rotation of individual hardware components. The disadvantage of



rotation of a large structure arises from the requirement of non-leaking rotating joints between the stationary and rotating structure. On the other hand, the use of centrifuges, cyclone separators, or permeable membranes in the individual processing steps, as required for phase separation, would avoid the problem of rotating intrastructure joints. Since the amounts of fuel processed at any one time are relatively small, the rotating processing equipment should not produce unusual dynamic disturbance to the satellite.

Automatic Processing, Repair and Control. The processing of spent nuclear fuels by definition, has required the development of remote handling and automatic control equipment. A further extension of the space system sophistication will be to incorporate automatic servicing, repair, and/or replacement of small hardware items such as valves, line segments, motors, sensors, etc. This may be accomplished by the use of a TV camera, circuits, robot manipulator machines, and a remotely located manned operations control room in which the master computer, control, and monitoring system are located.

In the event of a major malfunction, the module can be decoupled from the radiator, replaced by a substitute module, and the defective unit hauled to a space repair station by a man-operated radiation-shielded space tug.

Process Plant Sizing. The fuel processing plan is a subsystem of each power spacer module and contains four specific areas: Airox process, Purex process, fuel-forming, and storage.

The storage area serves the following functions:

- Holds up fuel being cycled from the reactor to permit radioactive decay between chemical processing steps
- Stores radioactive wastes for eventual deep space disposal
- Stores processed fuel pellets prior to return to reactor
- Stores resupply  $UO_2$  fertile fuel and process chemicals and materials

It must accommodate solids, liquids, and gases and store the radioactive fuel and wastes in a safe manner. Its geometry is a cylinder of diameter = 15.3 m (50 ft) and height = 3.05 m (10 ft), as shown in Figure 3.1-62. The resultant volume of  $556 \text{ m}^3$  ( $19,635 \text{ ft}^3$ ) is sufficient to process 8 kg/day recycle fuel and satisfy the storage requirements.

A summary of the sizing is presented in Table 3.1-27.

Brayton Cycle Power Conversion Unit (PCU). The Brayton PCU converts the reactor heat into electrical power. Figure 3.1-63 shows the system schematic. The working fluid is the helium gas which has been heated in the reactor. The component efficiencies selected were those expected to be reasonably achievable in the operational time frame. An in-house computer program at Atomic International Division of Rockwell was used to find the Brayton cycle operating parameters. The Brayton sizing for one module (336 MWe) was based on using

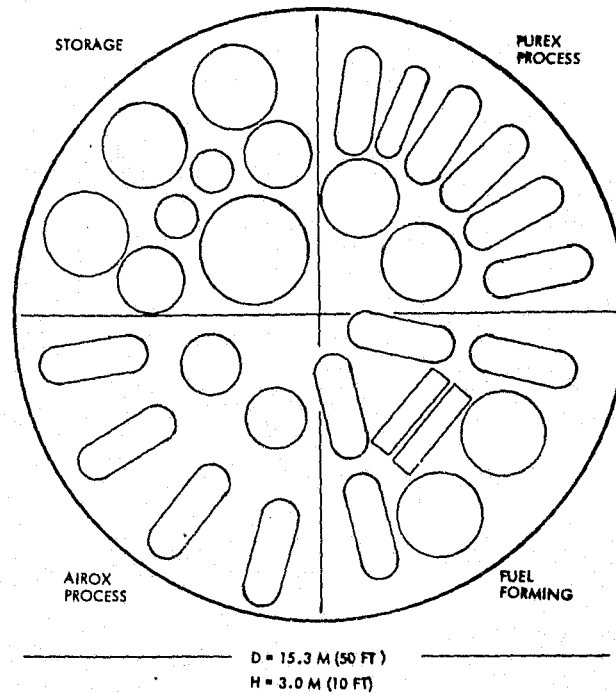


Figure 3.1-62. Fuel Processing Plant (One per Module)

Table 3.1-27. Fuel Processing Plant Summary

Cylinder shell diameter, 15.3 m; height, 3.05 m	
<u>Mass</u>	<u>kg</u>
Cylindrical shell and structure	6,900
Processing vessels	15,300
Processing materials/chemicals	16,000
Controls, motors, pumps, piping	450
Shielding	450
Total	39,100
30-year resupply @ 1.5 kg/day	16,400



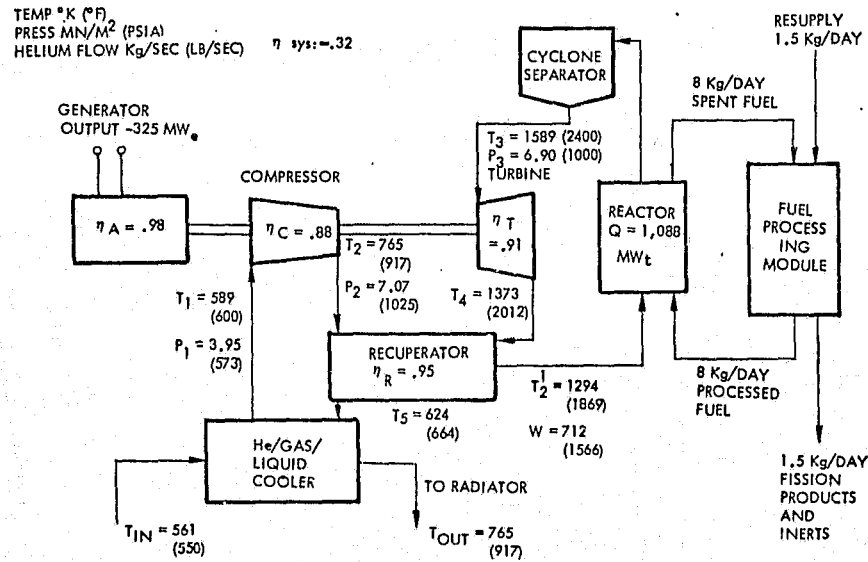


Figure 3.1-63. Brayton Cycle PCU Schematic

a maximum turbo compressor generator size of 168 MWe. Individual components were scaled from the Boeing study.<sup>1</sup> The PCU sizing and mass are given in Table 3.1-28.

Table 3.1-28. Brayton PCU Summary (336-MWe Module)

Item	No.	Size		Specific Mass (kg)	Mass (kg)
		Diameter (m)	Length (m)		
Turbo generators	2	2.8	13.9	0.113	$0.379 \times 10^5$
Recuperators	2	5.3	14.7	0.204	0.695
Coolers	2	4.3	10.3	0.074	0.249
Tank				0.056	0.188
Total	-	-	-	0.447	$1.5 \times 10^5$

Heat Rejection. The heat rejection radiator is required to radiate  $740 \text{ MW}_T$  to space. The radiator is the heaviest component in the nuclear SPS power plant.

Heat is rejected from the Brayton cycle by transferring heat from the gas working fluid to the radiator liquid coolant. The radiator coolant is

<sup>1</sup>Systems Definition Space-Based Power Conversion Systems, Boeing Aerospace Company, NAS8-31628, December 2, 1976



the organic compound, toluene, which is thermally stable at the operating temperatures but has a low freezing point. The toluene enters the radiator at 473°C and leaves at 269°C at a flow rate of 1202 kg/s.

The radiator is flat and radiates from both sides. It has a projected area (one side only) of 52,256 m<sup>2</sup>; and is made up of smaller squares, each 19 m on a side. Each square is essentially a sheet of copper with 1/4-in. O.D. stainless-steel coolant tubes bonded to the sheet parallel to each other and space 5.08 cm apart.

Aluminum cannot be used because of the high temperatures required. Steel is a low-cost material, but its low conductivity leads to a heavy radiator. The selected radiator material is copper; copper has a high thermal conductivity, can take the temperatures required, and its cost is far outweighed by the reduction in launch costs. Another design decision is that of the fin root thickness. A thin root leads to low mass, but the structural feasibility becomes doubtful; therefore, root fin thicknesses of 0.76 mm or greater are recommended.

The copper fins are 0.76 mm thick at the root, and 0.38 mm thick midway between the tubes. The mass of the fins is 268,636 kg. The tube mass, including the toluene coolant and a nominal thickness of armor for the tubes, is 68,182 kg. The total radiator weight is 336,818 kg. The mass of the manifolds, manifold coolant, and coolant pumps is 120,909 kg. Therefore, the heat rejection system mass is 457,727 kg.

Nuclear Shielding. Nuclear shielding studies were conducted to determine the size and mass requirements of a composite LiH-Pb shadow shield capable of reducing the neutron and gamma radiation emanating from the radiator to an acceptable biological level at specified distances from the source. Two shielding materials were selected: LiH for neutron attenuation, and Pb for gamma attention; these materials are shown in Table 3.1-29.

Table 3.1-29. Radiation Attenuation Characteristics

Material	Density (gm/cc)	Removal Length (cm)	
		L <sub>neutrons</sub>	L <sub>gammas</sub> (2.5 MeV)
Lithium hydride	0.75	6.7	34.2
Water	1.00	9.71	23.0
Polyethylene	0.93	8.9	23.3
Lead	11.4	8.55	2.06
Tungsten	18.9	6.44	1.24
Uranium-238	18.7	5.87	1.19

Three satellite configurations (see Figures 3.1-54, 3.1-55, and 3.1-56) were studied to determine the mass sensitivity of nuclear radiation shield and vehicle structure to separation distance between the reactors and the microwave antenna.



The single radiation shield of Configuration 1 was changed to individual reactor shadow shields as used with the other configurations. [The shadow shield was assumed to be a 3.05-m (10-ft) diameter disc located adjacent to each of the 26 reactors.]

The requirements were to reduce the neutron and gamma radiation at the antenna to a total of 25 mrem/hr from the 26 reactors.

The magnitudes of point source radiation from each reactor was estimated to be:

$$\begin{aligned} \text{Neutrons} &= 2.18 \times 10^{26} \text{ n/year} \\ \text{Gammas} &= 0.5 \times 10^{27} \text{ MeV/year} \end{aligned}$$

Analysis. Using the above sources and their energy levels, the unshielded dose rate at a distance R km from the point source was found to be

Neutrons:

$$D_n = \frac{6.48 \times 10^3}{R^2}, \text{ rem/hr} \quad (1)$$

Gammas:

$$D_\gamma = \frac{244}{R^2}, \text{ rem/hr} \quad (2)$$

The shielded dose rate at the antenna is related to the thickness of the shield by the following relationships:

Neutrons:

$$D_{ns} = \frac{6.48 \times 10^3}{R^2} e^{-t_1/6.7}, \text{ rem/hr} \quad (3)$$

Gammas:

$$D_{\gamma s} = \frac{244}{R^2} e^{-t_2/2.03}, \text{ rem/hr} \quad (4)$$

Subject to

$$\begin{aligned} D_{ns} + D_{\gamma s} &= 0.025 \text{ rem/hr (26 reactors)} \\ &\sim .001 \text{ rem/hr (1 reactor)} \end{aligned} \quad (5)$$

where

$t_1$  = LiH thickness, cm

$t_2$  = Pb thickness, cm

The composite shield specific mass is given by:

$$W'_s = 0.777 t_1 + 11.3 t_2, \text{ gm/cm}^2 \quad (6)$$

The total shield mass is the product of the specific mass  $W'_S$  and  $S$  the shield projected surface area ( $S = 7.31 \times 10^4 \text{ cm}^2$ ).

$$W_S = 73.1 W'_S, \text{ kg} \quad (7)$$

Method of Solution. Equations (3) through (7) were used to determine the shadow shield mass. Working curves were established from Equations (3) and (4) for dose rates of 0 to  $10^{-3}$  rem/hr, and different shield thicknesses were combined to satisfy Equation (5). The combination which produced a minimum shield specific mass, Equation (6), was then selected.

In the case of Configuration 1, where the reactor modules are in a linear arrangement and the antenna was 1 km from the closest reactor, the following single shield data resulted:

LiH:  $t_1 = 114.1 \text{ cm}$

Pb:  $t_2 = 23.6 \text{ cm}$

Shield specific mass:  $W'_S = 356 \text{ gm/cm}^2$

Shield mass ( $S = .7.31 \text{ m}^2$ ):  $W_S = 2.6 \times 10^4 \text{ kg}$

Shield mass, structure mass, and their sum were then plotted for varying separation distances, Figures 3.1-64, 3.1-65, and 3.1-66. The curves showed that with increasing separation distance,  $l_2$ , the increase in structure mass is much larger than the corresponding decrease in shield mass.

Other configurations at separation distances between reactor and shield (smaller than 1 km), for which mass crossovers and minimum totals could exist, were not investigated during this phase.

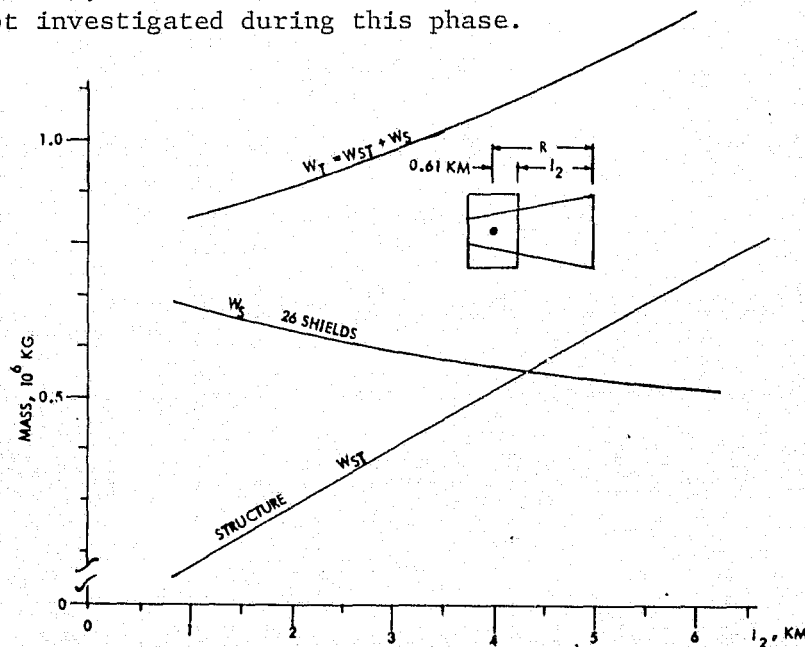


Figure 3.1-64. System Mass Vs. Separation Distance (Configuration 1)

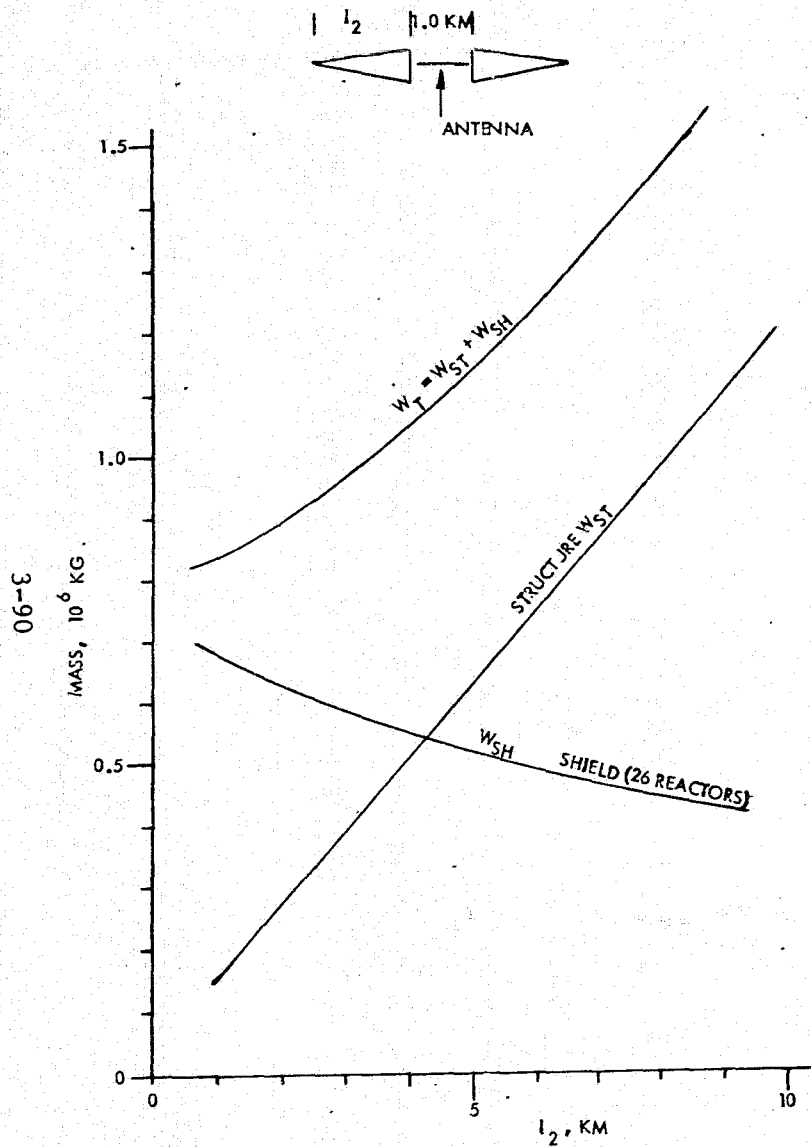


Figure 3.1-65. System Mass Vs. Separation Distance (Configuration 2)

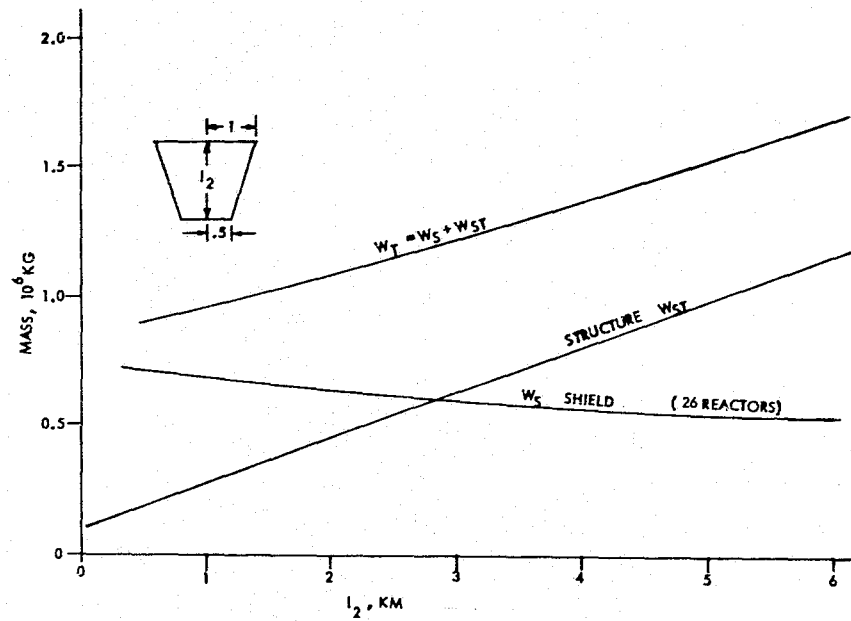


Figure 3.1-66. System Mass Vs. Separation Distance (Configuration 3)



Mass Summary. Mass comparisons are shown in Table 3.1-30; they are made between solar photovoltaic, solar thermal, and nuclear. Considerable potential for mass reduction exists in the nuclear concept. The primary structure mass is based on 10-mil aluminum beam machine material. The secondary structure is principally equipment supports. Power conditioning, distribution, and control mass were estimated—based on power characteristics, conductor runs, and conversion and temperature requirements. The mass growth was assigned to each element of the satellite, utilizing historical data developed by SAMSO/Aerospace Corporation. This growth was normalized to approach the desired 30 percent on the total satellite.

Table 3.1-30. Nuclear Reactor Concept Mass Summary

	(10 <sup>6</sup> KG)	GROWTH %
PRIMARY STRUCTURE	0.361	25.0
SEC. STRUCT.	1.112	25.0
ALTITUDE CONTROL	0.20	30.0
SHIELDING	0.54	30.0
REACTORS (26)	2.06	30.0
FUEL PROCESSING	1.01	30.0
TURBO-EQUIPMENT	3.34	30.0
GENERATORS	1.83	30.0
RADIATORS	11.94	30.0
POWER CONDIT.	1.839	50.0
WIRE HARDNESS	0.60	100
ANTENNA	9.88	23.1
IMS EQUIP.	0.061	50.0
IMS CABLING ITS	0.179	100
PROPELLANT/YEAR	0.10	0
SUBTOTAL	35.052	-
GROWTH ALLOWANCE	10.411	29.6
TOTAL SATELLITE SYST.	45.463	

20.73\*

POWER CONVERSION CONCEPT	Base Mass (10 <sup>6</sup> KG)	GROWTH (%)	Total Mass (10 <sup>6</sup> KG)
CR = 1	28.513	30.7	37.279
2	25.599	30.0	33.714
5	28.497	31.2	37.379
RANKINE CS/STEAM	26.386	31.2	34.605
NUCLEAR	35.056	29.6	45.465

\*GASEOUS CORE REACTOR/MHD COULD POTENTIALLY REDUCE THIS TO 1.99 X 10<sup>6</sup> KG - REFERENCE: 8TH IECEC PAPER 739018, 1973

RADIATOR OPTIMIZATION COULD POTENTIALLY REDUCE THIS TO 14.95 X 10<sup>6</sup> KG - CONDENSING STEAM RADIATOR (LOWER TEMPERATURE)

ORIGINAL PAGE  
OF POOR QUALITY



### 3.1.4 DOE PROGRAM SUPPORT REQUIREMENTS

Table 3.1-31 summarizes DOE areas of support for the SPS power conversion. A major requirement is to remove the speculativeness for gallium-arsenide solar cells. Present technology status constrains its performance and cost projections. The SPS concept depends upon utilizing thin-film gallium-arsenide substrate, such as sapphire. Gallium material and sapphire substrate development is needed to verify performance and cost expectations. The SPS program will impose increased production requirements on the solar cell industry to produce >9750 MW/year and cells with higher efficiency and produced with tighter quality control. Commercial viability of gallium arsenide solar cells must be demonstrated on an SPS scale.

Table 3.1-31. DOE Program Support Requirements  
—Power Conversion

- Material development—gallium arsenide
- Sapphire substrate development
- Commercial viability demonstration on SPS scale

Year 2000 Goals		Comments
Present DOE	SPS	
5000 MW/yr >10% eff. >20-yr life	9750 MW/yr >20% eff. >30-yr life	Increased production rates Higher efficiency Tight production and quality control
\$0.10 - \$0.30 peak watt	—————→	Firm costs

- SPS needs DOE to reduce uncertainties for GaAs solar cells
  - Performance
  - Cost

### 3.2 MICROWAVE SYSTEM

The MPTS trade tree is shown in Figure 3.2-1. Inputs are the required power into the power grid as well as the waveform characteristics such as beam frequency, beam type, beam power densities at the ionosphere, and side-lobe power densities over the earth's surface outside the rectenna installation. In addition, orbit mechanics would be a design driver.

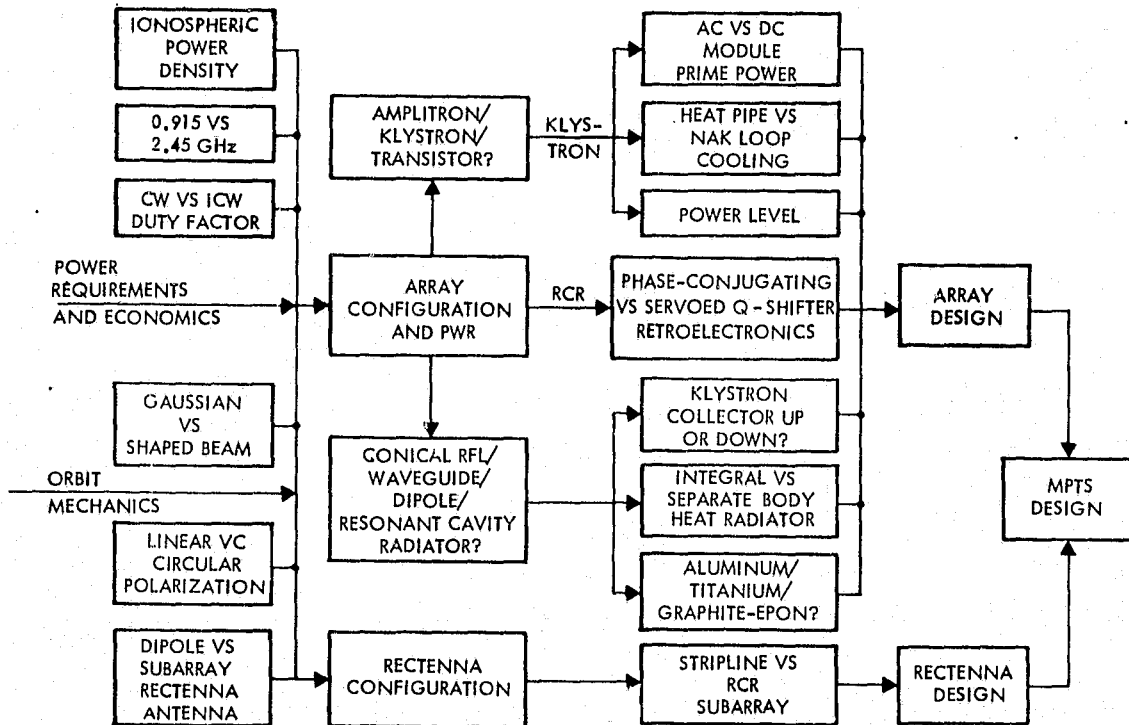


Figure 3.2-1. MPTS Trade Tree

The major design inputs are shown on the left side of the figure. The trades consist of RF device type, array configuration, waveguide type and configuration, and rectenna concept. Additional trades are shown on the right, and the array and rectenna designs are selected; these designs result in the point design concept for the microwave power transmission system (MPTS).

#### 3.2.1 SELECTED MPTS CANDIDATE DESIGN CONCEPT

The MPTS satellite array is mounted on trunnions between the two solar panels, as shown in the sections describing structural design. Power is fed through slip rings and distributed to the dc-to-microwave power converters mounted on the back of the radiating face of the array. The electronics required to excite the converters with proper phase to form a beam directed at the rectenna are mounted adjacent to the converters. An information management system is also distributed over the back of the array; it monitors array performance and controls the operation of the MPTS.



This entire complex of radiators, converters, electronics, and power distribution is supported by a tension-web structure consisting of catenary cables attached to a peripheral frame as illustrated in Figure 3.2-2. The array is broken up into subassemblies, about 30x35 m, which are attached to the catenaries by means of risers. These subassemblies will be called *mechanical modules*.

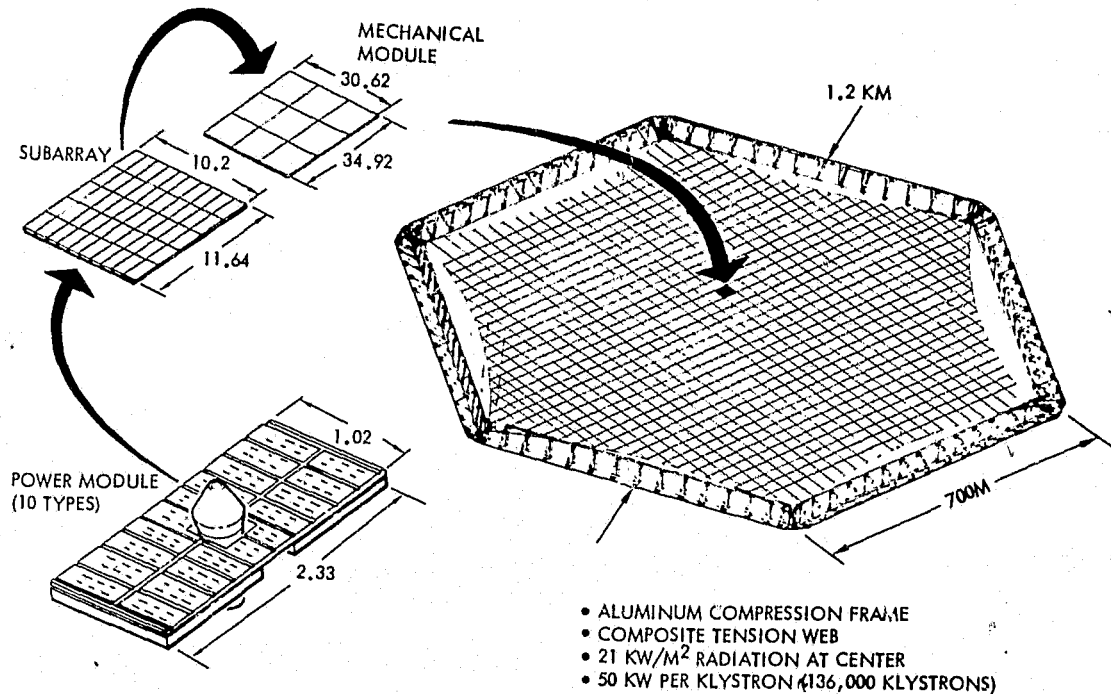


Figure 3.2-2. Microwave Antenna Module Sizes

The mechanical modules are in turn composed of nine planar arrays, each approximately 10 meters on a side. Each of these arrays are phased by a circuit which receives a pilot beam from the rectenna and generates excitation with a phase which is the conjugate of the pilot beam phase. Excitation of all the 10-meter planar array radiators in the total array in this manner produces a power beam directed at the rectenna even if the total array tilts or changes shape. The phase-conjugating circuits will be called the *retroelectronics*. The planar arrays, in conformance with standard array theory nomenclature, will be called *subarrays*. The decomposition of the array into these various module types is shown in Figures 3.2-3 and 3.2-4 for truncated Gaussian and shaped beam weighting functions. The subarrays are in turn composed of smaller planar radiators, each excited by a single power converter. In the case of the point design, these converters are klystrons. A power converter/radiator assembly will be called a *power module*. The power modules will vary in size in ten annular zones at increasing distances from the array center as shown in Figure 3.2.3. This change in size varies the number of converters per subarray and produces a variation in the power radiated per unit area of the array in each zone. Power density is highest in the array center and lowest at the area edge. This density taper is needed to control the power beam sidelobe level. The power modules are individually supported from the mechanical modules. There is a small space (crack) between the power



MECHANICAL MODULE PANEL  
 34.92 M X 30.80 M X 20 CM  
 (OPERATIONAL SIZE)  
 1088.84 M<sup>2</sup>/ELEMENT  
 TOTAL NO. OF  
 MECHANICAL  
 MODULES = 777

TYPE	NO OF MECH MOD	Kw/M <sup>2</sup> PWR DENSITY	WT (KG) PER MECH. MOD
1	17	21.05	756
2	32	18.94	726.7
3	44	16.84	674.6
4	44	15.16	651.6
5	63	12.63	610.3
6	68	10.52	573.8
7	87	8.42	526.1
8	110	6.31	501.1
9	170	4.21	476.2
10	142	2.52	408.8

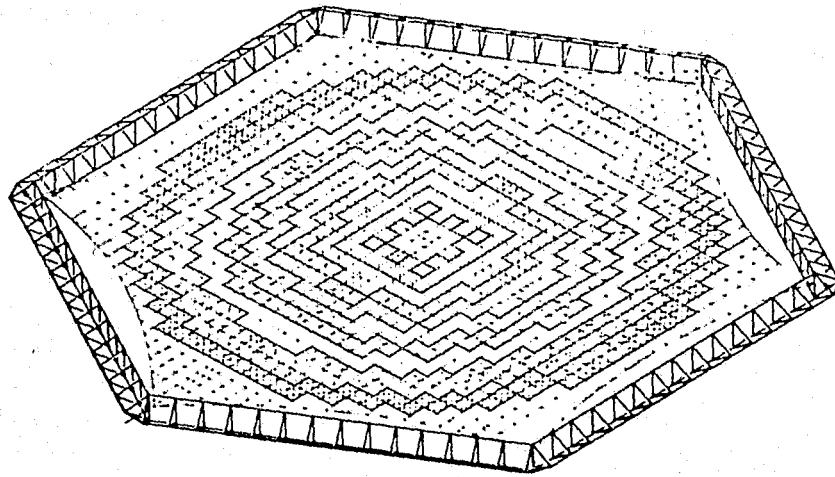
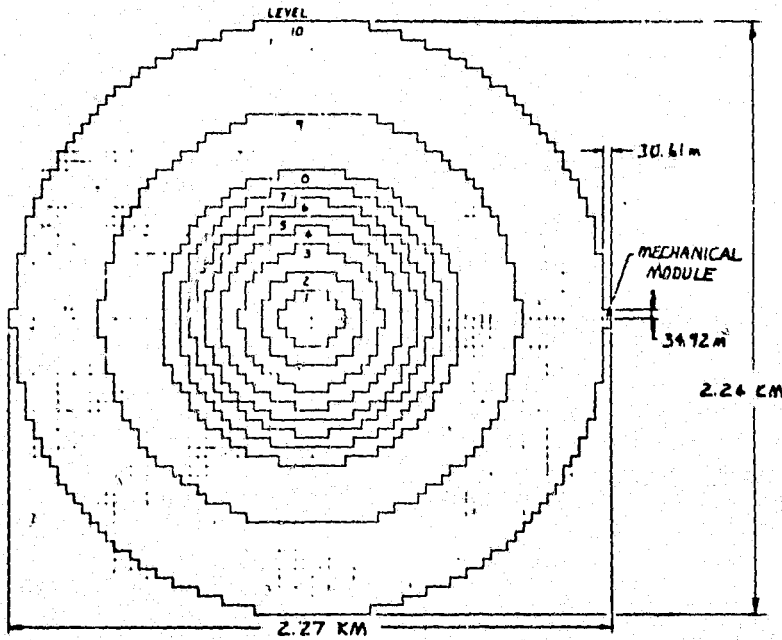


Figure 3.2-3. Gaussian Beam MW Antenna

ORIGINAL PAGE IS OF POOR QUALITY



LEVEL	PWR DENSITY KW/M <sup>2</sup>	NO. OF MECH MOD
1	19.76	36
2	16.84	64
3	12.63	108
4	8.42	128
5	5.02	128
6	3.37	116
7	2.02	150
8	1.01	192
9	.505	284
10	.674	1880

Figure 3.2-4. Shaped Beam MW Antenna



modules to allow for thermal dimension changes of the metal radiators. However, the mechanical module structures will be graphite-epon and, hence, will have an almost zero thermal coefficient of expansion. This permits them to be arranged side by side with cracks between power modules at mechanical module edges which are no wider than between interior power modules. Thus, excessive gap widths between modules (which would harm array performance) are avoided. The rectenna is shown in Figure 3.2-5. It consists of a series of panels (billboards), tilted so as to be normal to the power beam from the satellite. Since the satellite is in synchronous orbit, it has nearly a fixed location in the sky.

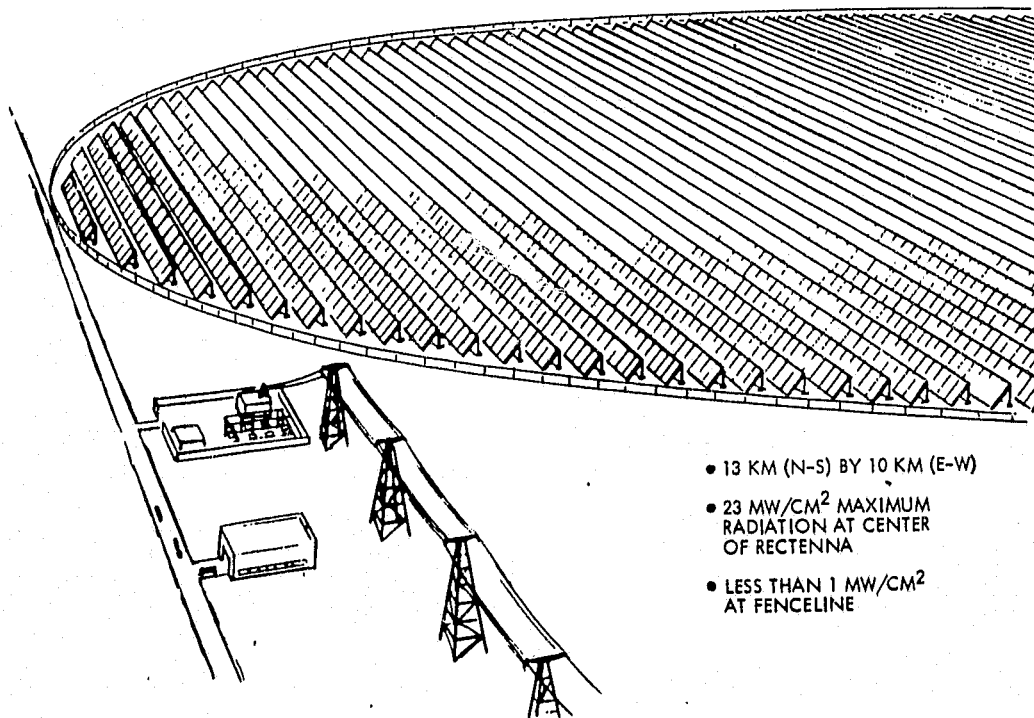


Figure 3.2-5. Rectenna Installation

The panels consist of a set of receiving antennas; each antenna output is rectified in a microwave-to-dc converter. The rectifier outputs are added in a bus network to form the power output from the panel. A larger power collection bus system then gathers the power from all the panels and delivers it to a central power station. The central station then converts the power to the correct form to be sent to the consumer by means of a power grid.

In the center of the rectenna there is a 30-ft dish which emits the pilot beam required by the satellite array retroelectronics system.

In arriving at a design for the MPTS, which has just been described in broad outline, a series of key design decisions must be made. These decisions will be discussed in detail in sections following this overview. At this point they will only be listed in Table 3.2-1.

Table 3.2-1. Key MPTS Design Decisions

DECISION ITEM	CHOICES	SELECTION
DUTY FACTOR	CW (100%) VS. INTERRUPTED CW (25%)	CW
POWER FREQUENCY	0.915 VS. 2.45 GHz	2.45 GHz
OUTPUT POWER TO GRID	2 TO 20 GW	5 GW
POLARIZATION	LINEAR VS. CIRCULAR	LINEAR
POWER CONVERTER	KLYSTRON/AMPLITRON/TRANSISTOR	KLYSTRON
RADIATOR STRUCTURE	DIPOLE/GUIDE/RCR/CONICAL RFL	RESONANT CAVITY RADIATOR
KLYSTRON BODY COOLING	NAK LOOP VS. HEAT PIPE	HEAT PIPE
KLYSTRON COLLECTOR COOLING	DIRECT HEAT RADIATION VS. HEAT PIPE	DIRECT RADIATION
PRIME POWER TO PWR MODULES	DC VS. AC	DC
COLLECTOR HEAT DISPOSAL	TOWARD EARTH VS. TOWARD SATELLITE	TOWARD EARTH
BODY HEAT DISPOSAL	TOWARD EARTH VS. TOWARD SATELLITE	TOWARD EARTH
KLYSTRON POWER LEVEL	5 KW TO 500 KW	50 KW
MIN. ARRAY POWER DENSITY	10 KW/M <sup>2</sup> TO 100 KW/M <sup>2</sup>	21 KW/M <sup>2</sup>
RETROELECTRONIC TYPE	PHASE CONJUGATION VS. SERVOED PHASE SHIFTER	PHASE CONJUGATING
ARRAY EXCITATION	GAUSSIAN WEIGHTING VS. SHAPED BEAM	GAUSSIAN
TEMP OF ARRAY ELECTRONICS ON ARRAY BACK	50°C TO 100°C	60°C
RADIATOR MATERIAL SELECTION	ALUMINUM VS. TITANIUM	ALUMINUM
IONOSPHERIC PWR DENSITY	1-25 MW/CM <sup>2</sup> AT BEAM PEAK	23 MW/CM <sup>2</sup>
RECTENNA ANTENNAS	DIPOLE VS. SUBARRAY	SUBARRAY
SUBARRAY TYPE	RCR WITH STRIPLINE FEED VS. STRIPLINE	STRIPLINE
RECTENNA PWR DENSITY COMPENSATION	VARIABLE SUBARRAY AREA OR DIODE SIZE	VARIABLE DIODE SIZE
RECTENNA DIODE TYPE	Si VS. GaAs AND SCHOTTKY/PN JUNCTION/PIN	GaAs SCHOTTKY
RECTIFIER CONFIGURATION	PUSH-PULL VS. SINGLE-ENDED	PUSH-PULL NEAR BEAM CENTER, SINGLE-ENDED ELSEWHERE

One of the most important properties of the MPTS is the efficiency it achieves in transmitting power from the output of the satellite power generation system to the output of the rectenna. These data are best given in the form of an efficiency chain showing the losses at each transmission stage, and are presented in Figure 3.2-6.

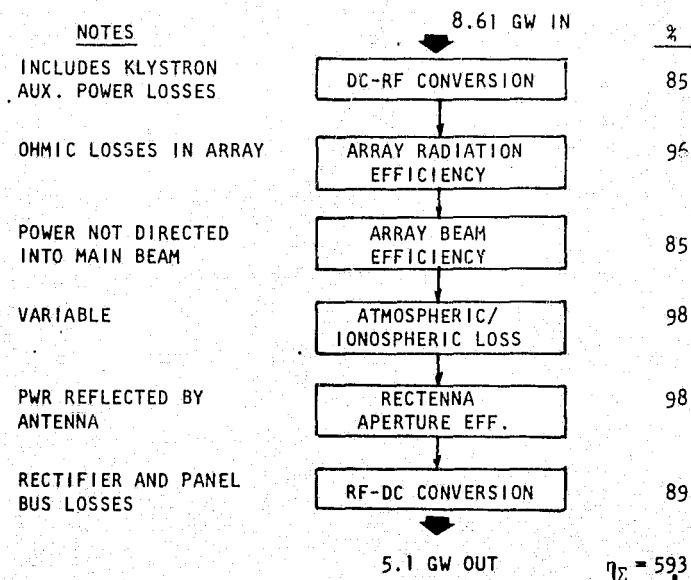


Figure 3.2-6. MPTS Efficiency Chain



It is now possible to summarize the major parameters characterizing the MPTS; this summary is presented in Table 3.2-2.

Table 3.2-2. Summary of MPTS Point Design Parameters

Parameter	Value
Input power	8.61 GW
MPTS efficiency	0.593
Output power to power grid	5 GW
Array diameter	1 km
All-up array mass	9000 metric tons
Maximum array power density	21 kW/m <sup>2</sup>
Number of subarrays	6993
Number of power modules (klystrons)	135,864
RMS array phase error	10 deg
Operating wavelength	12.24 cm
Maximum ionospheric power density	0.23 kW/m <sup>2</sup>
Rectenna dimensions for normal beam incidence	10×10 km
Rectenna dimensions (34° lat.)	10×13 km
Rectenna area	102.6 km
Number of panels (billboards)	395,296
Panel dimensions	14.69×12.24 m
Panel-to-panel spacing (34° lat.)	17.25 m

### 3.2.2 MSFC MPTS BASELINE CONCEPT

This section provides a review of MSFC's MPTS system design concept. It gives an overview of the MPTS using the 1976 NASA baseline concept.

#### Microwave Subsystem

The purpose of this section is to status the MSFC microwave study effort. There has been much effort in coordinating and analyzing new and different concepts in the microwave area during the course of the Rockwell SPS system study. The section will not elaborate on concepts that Rockwell has been specifically requested to study, but will consist mainly of a baseline update and a LEO-GEO trade study. The referenced baseline is NASA TM X-73344, Satellite Power System, dated November 1976.

Various components and methods have been use to describe the microwave power transmission system. Subarray size has varied from 10×10 m to 54×54 m, with the current MSFC size being 20×24 m. Subarray size has been correlated with the degree of error in electronic beam steering. The smaller the size, the more tolerance or less error for a given pointing requirement. The 20×24-m design is a physical dimension with phase control being accomplished to the device level. The system will have the minimum error for a given pointing requirement if the phase is controlled to the device or tube level. Several comparisons have been made between the klystron and amplitron, with the klystron appearing to have the most good points. However, there is still too much unknown for a clear choice to be made. There appears to be



significant justification to opening investigations of a solid-state antenna for power transmission. Rockwell has been asked to study this subject and their results are documented in another section of this report. The analysis of solid state is behind that of the klystron and amplatron, but will take a significant step forward in this study. Phase control remains a key technology issue and probably will not be resolved in the near future. Three methods—adaptive, command, and laser—have been studied with a combination of the command and adaptive systems providing a retro-directive method as the prohibitive favorite. The type of structure used on the antenna is very configuration oriented, but will have to be very stiff to meet the antenna flatness tolerances. The MSFC concept is the TRI/HEX module. Power distribution is generally better (less weight and loss) for the higher voltages required by the klystron and amplatron. The solid-state antenna will require low voltage to the power device, but may make ac transmission feasible from the solar wings. There is a big weight penalty for the power conditioning equipment required, but the MSFC preliminary analysis indicates the solid-state antenna is 1 to  $2 \times 10^6$  kg lighter than the klystron or amplatron design. The MSFC rectenna concept is an  $8.5 \times 11$ -km ellipse with about  $11 \times 10^9$  dipoles and diodes. Dipoles were selected because of their broad receiving pattern and ease of construction. Printed circuit spirals are an alternate but have not been investigated thoroughly. Spirals appear to be easy to automate but are more expensive than dipoles. Protecting the receiving circuit elements from the environment is a key concern. Test results from JPL indicate inter-electrode capacitances in the receive circuit can vary and affect efficiency if not protected. Many antenna radiating elements were considered. The slotted waveguide was the best choice for klystrons and amplitrons, and some type of printed circuit element appears best for the solid-state system. Thermal design of the antenna is critical. Presently, the klystron needs an active system and the amplatron a passive system. The solid-state system is TBD.

#### LEO-GEO Trade Analysis

The approach to this trade was to investigate the differences between the microwave antenna subsystems for a LEO and GEO construction location and to quantify these differences. Table 3.2-3 represents the specific guidelines and assumptions applicable to the microwave subsystem.

The trade identified three potential problem areas or differences. The first is ionization and multipaction. Usually, these are separate and distinct problems. However, the frequency and power level that SPS requires makes these problems mutually supportive. Figure 3.2-7 was taken from the IEEE Proceedings dated February 1969, and represents the RF voltage breakdown in coaxial transmission lines. Although these data are on coaxial cables, the data are equally applicable to slotted waveguide. The "d" in the figure for slotted waveguide would represent the width of the slot instead of the inner-to-outer conductor separation for a coaxial cable. The " $f_d$ " for SPS would be 2450 MHz-cm for a slot width of one centimeter. This is in the region of multipaction breakdown. The atmospheric pressure varies from  $10^{-4}$  to  $10^{-6}$  torr at 500 km altitude. If multipaction were to occur, the pressure in that localized area could increase sufficiently to cause ionization by electron collision. Multipaction is similar to secondary emission. Free electrons striking the metal surface create



Table 3.2-3. LEO Vs. GEO Trade Guidelines and Requirements

- The antenna is a 1-km-diameter, 5-GW, power-tapered design using amplitrans as the dc-RF converter.
- Maximum power density allowable on the ground in the main beam is 23 mw/cm<sup>2</sup>.
- Subarray testing is required at the assembly location.
- Antenna construction—1x2.4 m elements will be manufactured on the ground. The antenna subarrays will be assembled and installed on the substructure in orbit.

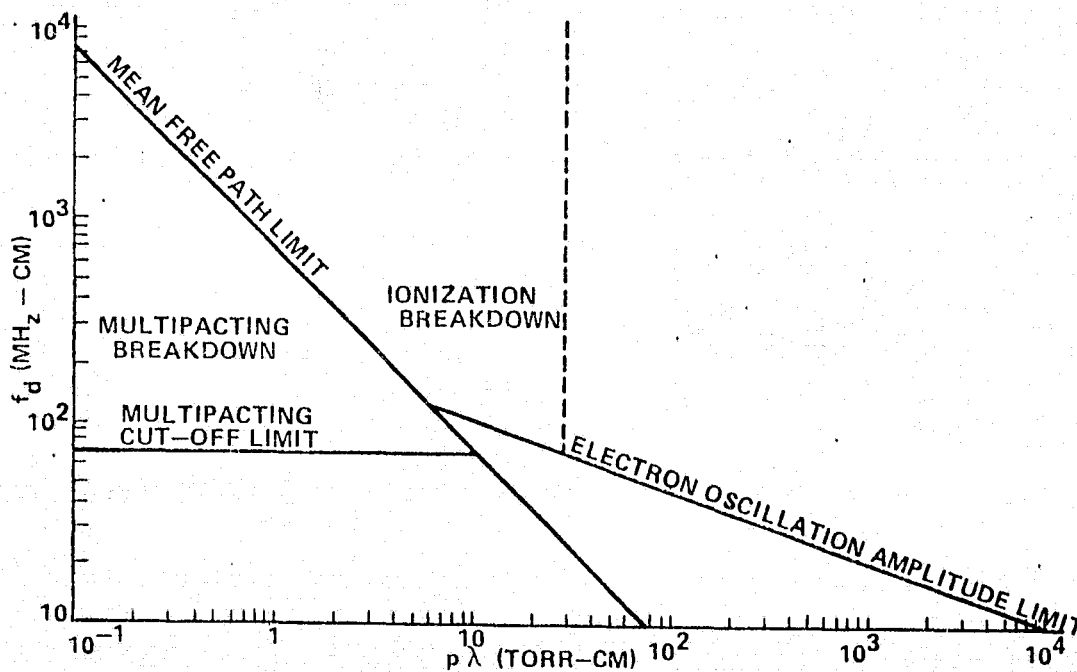


Figure 3.2-7. The  $f_d$ - $p$  Plane showing Limits of Breakdown Processes



more free electrons. This phenomenon by itself is not a problem in either GEO or LEO; however, it aids the ionization process and tends to sustain ionization. If this process is sustained and occurs across a waveguide slot, the result is a short and damage to the waveguide. Analysis indicates that sustained ionization is likely to occur in LEO but not in GEO because of the particle density difference. There are practically no neutral particles at GEO and about  $10^2$  ions/cm<sup>3</sup> at 36,000 km altitude. The solution to this problem for LEO operation and test is proper slot design and wall thickness of the waveguide. However, proper slot design to work around this problem will result in a 2 to 5% reduction in microwave transmission efficiency. This penalty will be necessary if the construction facility is in LEO, but not if it is in GEO. Further quantification of this problem will be dependent upon actual test data at the operational frequency, power level, and altitude to be investigated.

The second problem is the open envelope tube. Ion bombardment of the cathode results in degradation of the cathode and lowering of the MTBF. This degradation occurs whether the tubes are operating or not. Since there are many more ions in LEO and many neutral particles that can become ionized, the problem is much more pronounced in LEO than GEO. The actual effect on MTBF at GEO is negligible. Further quantification of this problem would be dependent on actual tube design and test at the altitudes desired. The solution to this problem for LEO assembly is a closed envelope tube. This would add another  $2 \times 10^6$  kg to the weight of the antenna. Analysis indicates the open envelope tube is practical for GEO assembly.

The third problem is a two-part problem involving the phase control system. The command phase control subsystem interprets the power beam on the ground and sends commands back to the SPS. It requires that the antenna be powered up for this test. From LEO, this would be approximately 2300 mw/cm<sup>2</sup> and would be 100 times greater than the proposed system. This test would have to be deferred until the SPS was in GEO. If the construction site were located in LEO, then the final checkout of this system would be completed in GEO. Should some problem arise that required some degree of disassembly of the microwave antenna, then the assembly facility would be some 36,000 km away.

The adaptive or retrodirective phase control subsystem is dependent upon a feedback loop from the dc-RF converters. It is not possible to test this system without the antenna being powered. The problem then becomes the same as above. In past space programs, complete checkout and verification has been performed at the launch site. Skylab is a precedence where the complete checkout was performed before launch and after insertion in orbit. The trend is always to complete verification as near to the operational altitude as possible. If the SPS is assembled in LEO, then it will be launched effectively with its most critical subsystem not tested and verified. With a GEO assembly the subsystem can be verified and then inserted into its proper location.

Table 3.2-4 is a summary of the LEO-GEO trade analysis. These data represent a preliminary analysis, but strongly indicate that the microwave subsystems prefer a GEO construction site for SPS.





Table 3.2-4. Assembly Location

SUBJECT	PROBLEM	SOLUTION	LEO	GEO
IONIZATION AND MULTIFACTON	WAVEGUIDE DETERIORATION.	WAVEGUIDE SLOT DESIGN	2-5% EFFICIENCY LOSS	NEGLIGIBLE PROBLEM
OPEN ENVELOPE TUBE	ION BOMBARDMENT OF CATHODE. LOWER MTBF	CLOSED ENVELOPE TUBE	2 X 10 <sup>6</sup> Kg WEIGHT PENALTY	NEGLIGIBLE EFFECT ON MTBF
COMMAND AND RETRODIRECTIVE PHASE CONTROL SUBSYSTEM TEST	ALL UP TEST REQUIRES ANTENNA TO BE POWERED	VERIFICATION TEST PERFORMED FROM GEO. PARTIAL TESTS FROM LEO WILL NOT ELIMINATE THE NEED FOR AN ALL UP SYSTEM TEST.	CAN NOT BE VERIFIED BEFORE LEAVING ASSEMBLY FACILITY. DENSITY (2300 Mw/cm <sup>2</sup> ) IMPINGING ON THE EARTH WOULD BE 100 TIMES OPERATIONAL DENSITY	CAN BE VERIFIED BEFORE LEAVING ASSEMBLY FACILITY

Microwave Power Transmission System

A variety of microwave transmission systems have been proposed. The basic components and functional concept of a microwave power transmission system are illustrated in Figure 3.2-8.

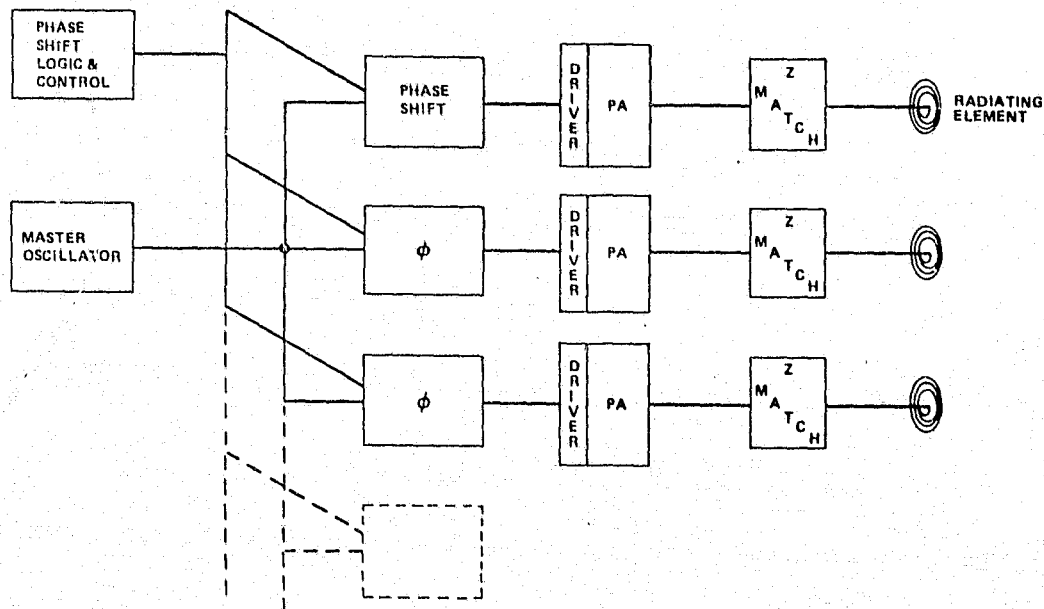


Figure 3.2-8. SPS Microwave Power Transmission System

The representative elements of the phased array antenna are shown as spirals. Several types of radiating elements have been studied and could possibly be used. The spiral element has the advantage of being circularly polarized and lends itself to sheet or roll fabrication—an attractive concept if a solid-state design becomes desirable. Dipoles could, of course, also be fabricated in the same manner. Currently, the favored or baseline system utilizes slotted waveguides as radiating elements (and to distribute the RF from the tube-type power amplifier).



The "power amplifier"—actually, more appropriately termed the dc-to-microwave power converter—is indicated in more current concepts as being a high-power tube-type device on the order of 5 kW RF output for an amplitron and 50 kW for a klystron. The use of much greater numbers of solid-state devices, but at a 50- to 100-W power level, is a concept that is surfacing as a candidate for detailed study and possible potential for a lighter weight system.

All dc-to-RF conversion devices (power amplifiers) require a driver amplifier. The drive level depends on the overall system selected but is postulated to be a solid-state unit whether klystron, solid state or amplitron. The amplitron does require considerably higher drive levels—in the range of 500 W or greater.

Maintaining proper phase relationships across the face of the transmit array is one of the key concerns for microwave power transmission. Therefore, a means of sensing and controlling phase must be included. In the system shown (Figure 3.2-8), each power conversion unit has an associated phase shifter. Groups of these phase shifters receive their reference and control signals from units which are part of the computer-controlled adaptive and command phase control systems.

Each "master" oscillator feeds several driver units and is a highly stable source which is locked to all other master oscillators in the system.

The current MSFC microwave system consists of a 1-km-diameter transmit antenna with amplitrons ( $1.1 \times 10^6$ ) as the power device and an  $8.5 \times 11$ -km rectenna with  $1.13 \times 10^6$  dipole elements. The transmit antenna has 1636 sub-arrays which are  $20 \times 24$  m. These subarrays are further broken down into two hundred  $1 \times 2.4$  m elements. These  $1 \times 2.4$  m elements are considered the lowest replaceable unit (LRU). The subarrays are arranged in six power quantization steps to form a 9-dB power taper. This system will form a spot on the earth,  $8.5 \times 11$  km, with the peak power density at the center being  $23 \text{ mw/cm}^2$  and  $2 \text{ mw/cm}^2$  at the edge. The third sidelobe has a peak power density of  $0.01 \text{ mw/cm}^2$  and occurs 17 km from the center of the rectenna. Approximately 6.5 GW is transmitted to give about 5 GW on the ground. Pointing requirements of 3 arc-seconds are accomplished through two control systems—the adaptive phase control system that sends a pilot beam back to the antenna to be used as a control signal, and a command control system that interprets the condition of the power beam on the ground and sends commands through the normal communication system to the antenna systems. The dc-to-dc system efficiency is 67 percent. Figure 3.2-9 is a representation of this system, and Table 3.2-5 is a summary of the updated system elements.

#### MSFC Baseline Update

Descriptions of the MSFC baseline update are presented below. They represent key changes that have been made in the MSFC microwave subsystems. Figure 3.2-10 reflects the early 1977 upgrading of efficiency estimates for certain microwave subsystems. The changes involved (increases) are all in the space system (transmit). There are no changes in efficiencies of the ground or "rectenna" system. However, note the overall efficiency figure is

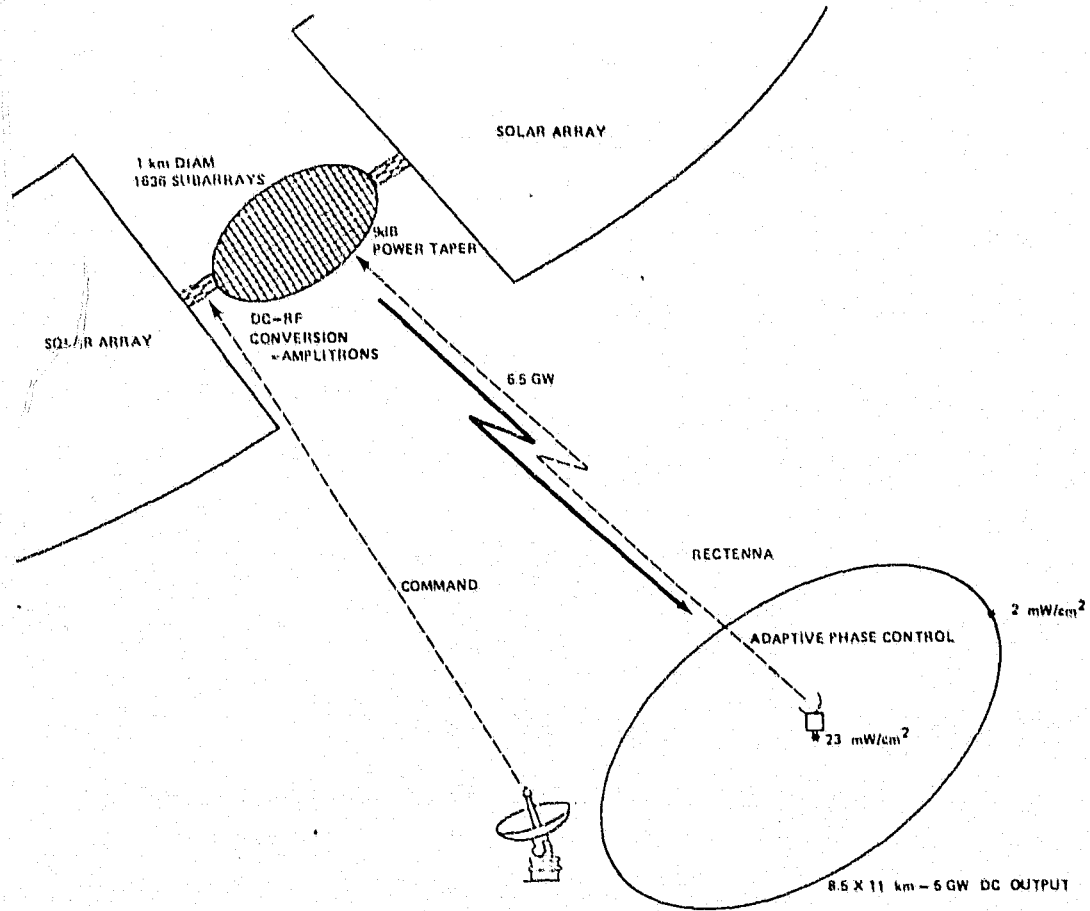


Figure 3.2-9. SPS Microwave Concept

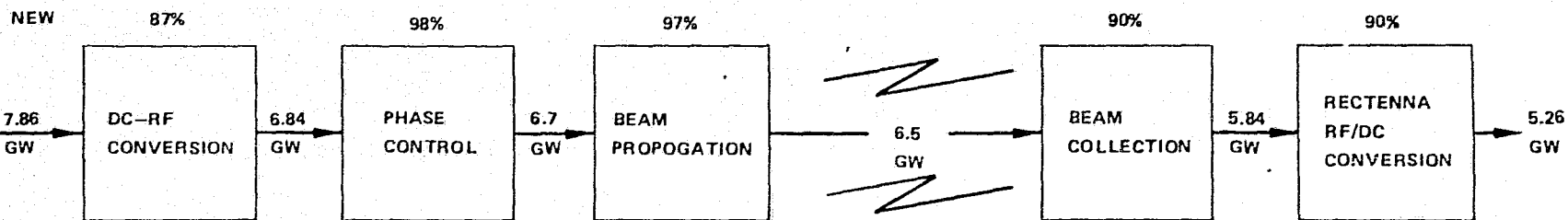
Table 3.2-5. New System Elements

Basic element (m)	1x2.4
Subarray (m)	20x24
Elements/subarray	200
Subarrays (total)	1636
Output power of amplitrans (W)	5800 (5780)
Output power of IRF amp (W)	500
Amplitrans efficiency (%)	89
IRF amp efficiency (%)	70
Number of amplitrans	$1.09 \times 10^6$
Number of IRF amps	$1.09 \times 10^6$

67% (UPDATE MAY ' 77)

XMIT ANTENNA  
OVERALL EFF.  
83%

RECEIVE ANTENNA  
OVERALL EFF. : 81%



76%  
OLD BASELINE

81%  
OLD BASELINE

62%

	OLD BASELINE	NEW BASELINE
POWER INTO DC/RF CONVERTER	8.55 GW	7.86 GW
MW XMIT EFF.	76%	83%
MW RCVE EFF.	81%	81%
OVERALL EFF.		
POWER OUT OF RF./DC DEVICES	5.26 GW	5.26 GW

Figure 3.2-10. SPS Microwave Power System Efficiency

3-105

SD 78-AP-0023-3



now the efficiency from dc-RF converter input to RF-dc rectenna output and does not include dc power distribution at the rectenna or on the transmit array. This overall efficiency baseline is now 67%—an improvement of 5% over the old baseline. The transmit system efficiency is now considered to be 83%. This is a 7% increase over the previous baseline figure of 76%. The elements of this system that have been assigned new efficiency projections are: dc-RF conversion, 82% to 87%; phase control, 97% to 98%; and beam propagation, 95.5% to 97%. These increases resulted in a lower dc input power requirement for the same output (as previous baseline). In order to maintain as much similarity as possible between new and old baseline systems, the only design parameters that were changed were the efficiencies, the dc input power, and the power of the converter device from 5300 to 5800 W. This change was preferable over completely reworking the theoretical design configurations. Most of the changes made were the results of study inputs from outside sources (Raytheon, Grumman, Rice University, Rockwell, etc.) that were evaluated and analyzed by the MSFC study team. Comparing these study results, it was concluded that the projected efficiency estimates in some areas were too low; these increases represent a compromise position.

A key change which impacted the weight and complexity of the systems was from a non-resonant to a resonant array concept. The original baseline design of the waveguide feed method was tailored to use a basic building block (waveguide) of 1 by 2 meters. Maximum power density and maximum packing of amplitrons was eight for that building block area. The theory of operation was that an intermediate amplifier drives the first amplitron in series chain; this amplitron provides output power for a proportionate number of radiating elements (slots) plus the approximate 500 W required to drive the next amplitron in the chain. This continues across the entire 1- by 2-meter basic unit until the last amplitron in the chain must dissipate the residual drive power in some sort of non-radiating load—thus, the name non-resonant array. This concept has at least one severe disadvantage—the beam generated from this configuration is not a broadside array (that is, the beam is displaced by some angle to the perpendicular). This presents control problems and potential power losses; therefore, a new baseline system is illustrated in Figure 3.2-11. This new system will generate a broadside beam and radiates 100% of converter output power (ideally).

Operationally, the difference in the two concepts is that the new baseline requires a driver amp for each dc/RF converter. There is no "residual power" involved in any section of waveguide; i.e., power is totally radiated from the slots or consumed in losses as it travels down the waveguide.

Obviously, the new baseline system requires the same number of IRF amps (drivers) as it does dc/RF converters (PA's). There is an attendant system weight increase, but the design is a far more realistic concept of a workable system.

The size of the new baseline "smallest replaceable unit" is also changed to 1x2.4 m to better accommodate the real dimensions involved and the power taper steps to be physically accomplished.

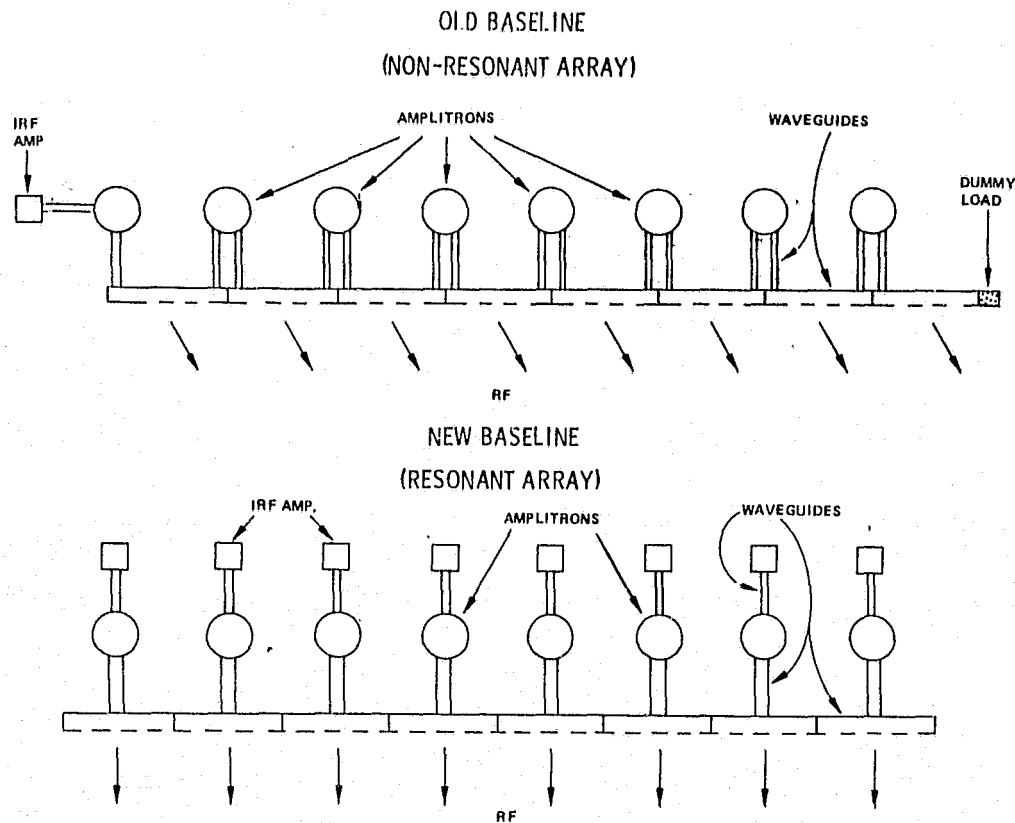


Figure 3.2-11. Baseline Concepts Comparison

The transmit antenna has three basic parts—the main structure, the substructure, and the waveguide subarray. The main structure is about 22 m deep and is a contiguous design over the 785,000 m<sup>2</sup> of antenna. This structure has to be very stiff and respond minimally to thermal loads across its surface. The substructure is about 1 m in depth and made in 20×24-m sections to match the subarray. It actually becomes a part of the subarray. It is attached to the waveguide and helps support the amplitrons and intermediate radio frequency (IRF) amplifiers. The last section is the waveguide with the amplitrons and IRF amplifiers mounted on the back. The mounting is for heat sink purposes and will require additional support from the substructure. The mechanical subarray leveling device (screwjack) is attached to the main structure and substructure. When a subarray is removed, the substructure is removed with it. Figure 3.2-12 is a sketch representing these three basic antenna elements.

The basic building block of the antenna is the lowest replaceable unit (LRU). The old baseline had a 1×2-m LRU and eight different elements (LRU's) corresponding to eight power quantization steps. The changes made were the result of errors in the old baseline and design changes to better accommodate the real dimensions involved and the power taper steps to be physically accomplished. Figure 3.2-13 shows a basic element taken from a subarray in the center portion of the antenna. There are eight amplitrons on this 1×24-m element that are arranged to maximize heat transfer. The back side of the

3-108

SD 78-AF-0023-3

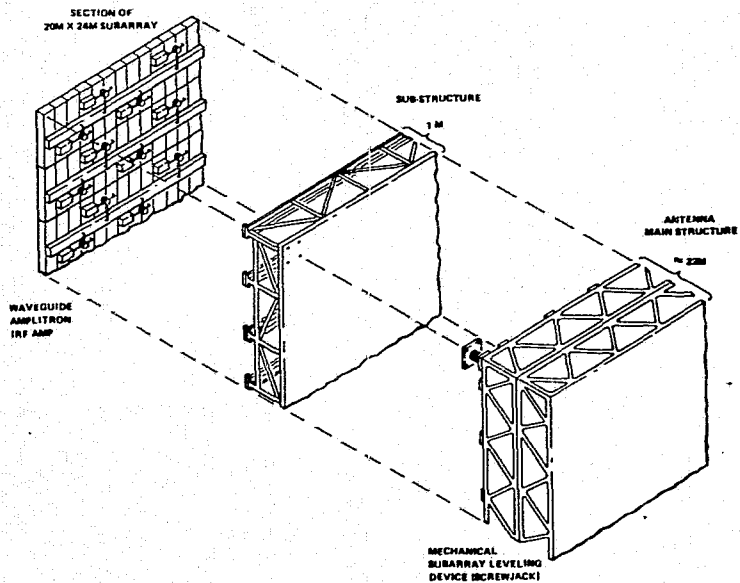


Figure 3.2-12. Microwave Antenna Elements

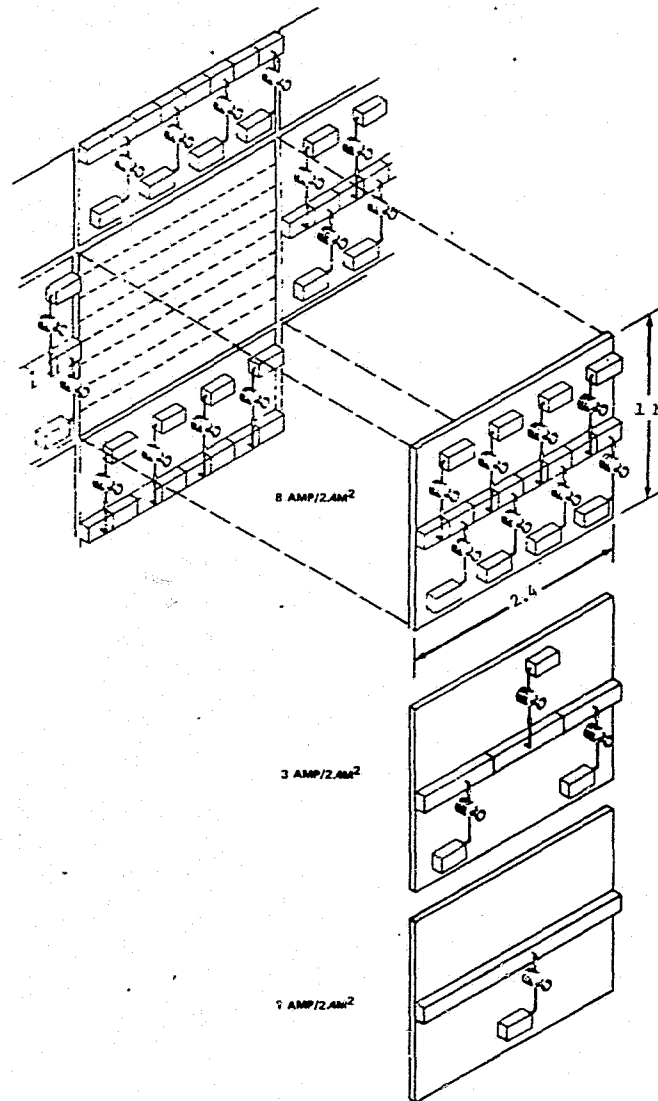


Figure 3.2-13. SPS Microwave Antenna 1-m x 2.4 Element Construction

waveguide has a coating of pyrolytic graphite on it to enhance radiation. The amplitrons and IRF amplifiers are mounted to this coating and are supported by the substructure. The 9-dB power taper is accomplished by making subarrays with elements of different power levels. Figure 3.2-13 shows three of the elements used to accomplish the power taper. There are six different elements corresponding to six power quantization steps. The power in the center of the antenna is about  $23 \text{ kW/m}^2$  and about  $2.4 \text{ kW/m}^2$  on the edge of the antenna.

A new idea which surfaced during 1977 and represented a better method of thermal control for the amplitron design was the distributed passive cooling concept. Figure 3.2-14 illustrates this concept which eliminates the very large cooling fin previously required for passive cooling of the amplitrons. Previous details of amplitron cooling systems indicate a large fin, approximately 50 cm in diameter, in addition to the relatively small 10-cm fin shown on the figure. Large savings in volume result from use of this concept, which would require graphite polyimide as the waveguide material with a pyrolytic graphite coating on one side as the thermal radiator. The concept also uses pyrolytic graphite in the construction of a relatively small cooling mass on the amplitron structure itself.

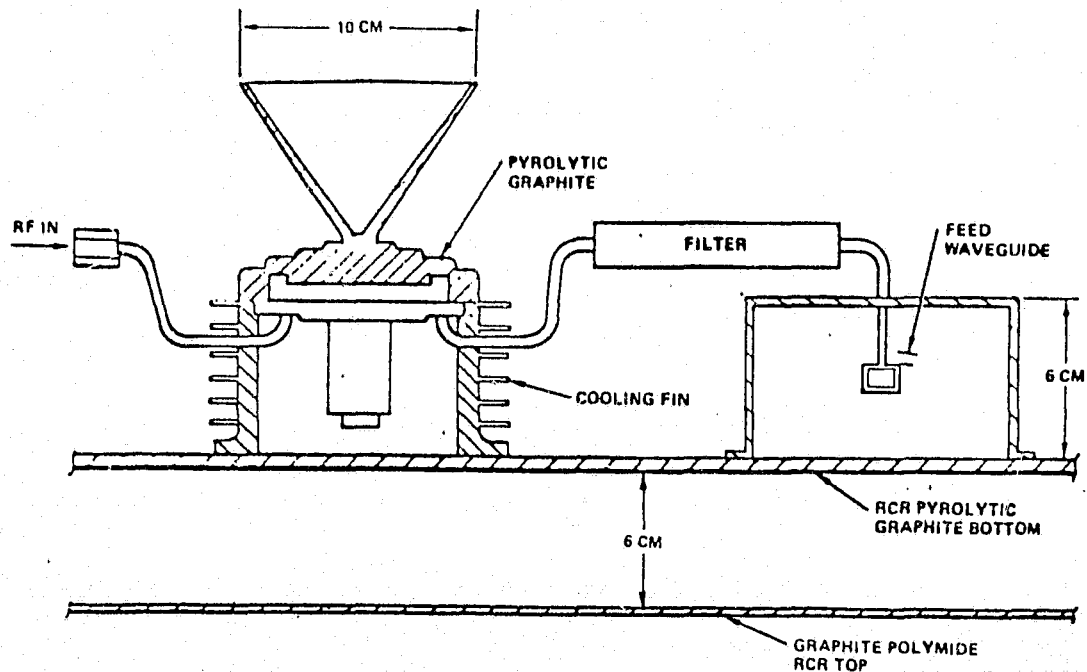


Figure 3.2-14. Amplitron Modified Heat Sink

This concept involves a more distributed area of radiating material than individual unit fins, but the use of a lightweight material such as graphite composite and utilization of the entire waveguide back surface as a radiator makes it an attractive concept. Present weight estimates predict total weight figures for both designs to be roughly equivalent. An in-depth analysis of this concept has not been performed. The complexity of constructing waveguide with these characteristics is questionable; however, it does represent a new idea with positive results at this time.





The system update would not be complete without a mass properties update. Table 3.2-6 describes the differences between the old baseline and the updated information as of October 1977. The main difference is in the mass of the waveguide. The lower mass was because materials were changed from aluminum to graphite. Graphite has better thermal characteristics. A non-resonant cascaded amplatron system was changed to a resonant approach with no cascading. This meant that there was an IRF amplifier and phase control box for each amplatron. The number difference occurs because of a basic flaw in the original design; this design flaw changed the number of amplatrons required to  $1.1 \times 10^6$ . Therefore, to maintain the same power density levels on the ground, the amplatron power out was changed from 5300 W to 5800 W.

Table 3.2-6. SPS Microwave Antenna (1 km) Mass Properties Update

OLD BASELINE			
	UNIT MASS	(X 10 <sup>6</sup> ) NUMBER	TOTAL (kg X 10 <sup>6</sup> )
	(AL)		
WAVEGUIDE	4.5 kg/m <sup>2</sup>	.76 m <sup>2</sup>	3.42
AMPLITRONS	1.8 kg	1.321	2.38
IRF AMP	1.8 kg	.38	.68
PHASE CONTROL	.1 kg	.38	.038
POWER DISTRIBUTION			.4
CONTOUR CONTROL			.122
STRUCTURE			.2
TOTAL			7.24
UPDATE			
	UNIT MASS	(X 10 <sup>6</sup> ) NUMBER	TOTAL (kg X 10 <sup>6</sup> )
	(GRAPHITE)		
WAVEGUIDE	2.56 kg/m <sup>2</sup>	.76 m <sup>2</sup>	1.95
AMPLITRONS	1.8 kg	1.1	1.98
IRF AMP	1.8 kg	1.1	1.98
PHASE CONTROL	.1 kg	1.1	.11
POWER DISTRIBUTION			.05
CONTOUR CONTROL			.12
STRUCTURE			.2
TOTAL			6.39

Solid-State Microwave Antenna

The klystron and amplitron have been the key power devices under consideration for the microwave antenna by nearly all studies. Aerospace Corporation introduced the concept of solid-state power conversion. MSFC investigated the reasons for solid state not being a contender in early studies and found it was rejected because solid-state technology could not be projected to produce a 1-kW to 5-kW transistor. A preliminary design by MSFC indicated an antenna might be possible with a 50-W to 100-W transistor. A survey was conducted of current transistor manufacturers for the state of the art of S-band transistors and projections of capabilities for the 1980's. Current technology is in the 40-W to 60-W range with efficiencies of about 60 percent. Most manufacturers indicated the development of a 100-W/90% efficient transistor was a matter of the demand for the product rather than a limitation on technology. Information on the transistor was encouraging enough for MSFC to add a special task to the Rockwell contract to investigate the feasibility of a solid-state antenna for SPS and produce a point design of a solid-state antenna. The parts count for the solid-state concepts is high; however, its light weight, automated producibility, low cost, and inherent high reliability make it an attractive concept. Rockwell has much more information on the solid-state design concept elsewhere in this report.

A brief description of the preliminary concept proposed by MSFC follows. Figure 3.2-15 is an example of an alternate concept for the antenna structure and main antenna elements. This structure gives the impression of a trampoline

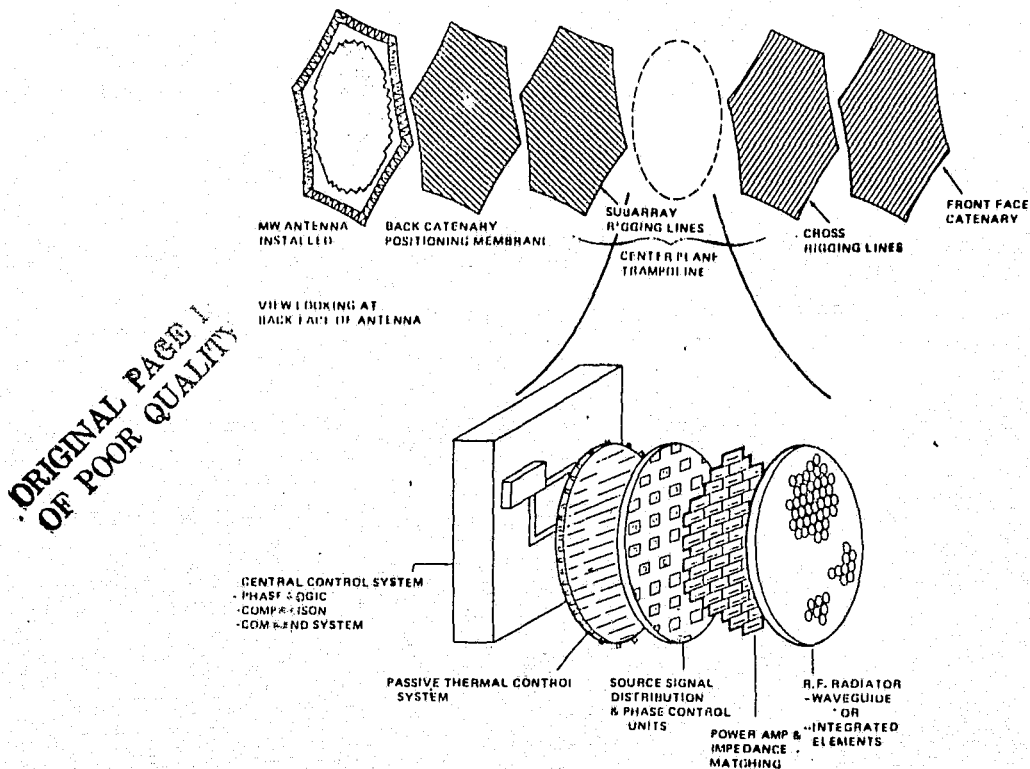


Figure 3.2-15. Solid-State Antenna with Rockwell Suspension Frame Structure



and actually would work well with some solid-state concepts. The solid-state antenna also could be supported with a more conventional structure. The elements of the solid-state antenna are the RF radiator which could be an integrated microstrip or printed circuit spiral on a thin sheet of Mylar with a conductive base, the power amplifier or transistor ( $152 \times 10^6$  required) which only needs to be 44 W for a 0-dB tapered antenna or 100 W maximum for a 9-dB power tapered antenna for 5 GW output on the ground, the reference phase signal distribution system and phase control units (it is estimated there would be one phase control unit for each 100 transistors), a passive thermal control system (hopefully), and a central command/control and phase logic comparison system. Table 3.2-7 is a preliminary estimate of the mass properties of the solid-state antenna. There is an extreme penalty for power distribution because of the low voltage (50 V) required by the transistors. If this penalty could be reduced, the mass of the solid-state antenna would be much less than the amplatron design. This design assumes passive cooling as no thermal analysis was conducted.

Table 3.2-7. Solid-State Antenna Mass Estimate

TRANSISTOR = 3 gr. X 152 X $10^6$ =	.456 X $10^6$ kg
PRINTED CIRCUIT SPIRAL = 1 kg/m <sup>2</sup> X .785 X $10^6$ =	.785 X $10^6$ kg
PHASE CONTROL = 280 gr., 1 PER 100 TRANSISTORS =	.426 X $10^6$ kg
POWER DISTRIBUTION =	3.1 X $10^6$ kg
CONTOUR CONTROL =	.122 X $10^6$ kg
STRUCTURE =	<u>.2 X <math>10^6</math> kg</u>
	5.1 X $10^6$ kg

### SP3 Rectenna

The total area encompassed by the rectenna is about 73 km<sup>2</sup>. To minimize the receiving element area, the rectenna is built in rows on an angle in order that the elements (dipoles) are perpendicular to the incident power beam; this also helps to reduce polarization losses. The total element area is about 57 km<sup>2</sup> and requires about  $11.3 \times 10^9$  dipoles and diodes. Figure 3.2-16 shows the parts of the rectenna. There is a base support structure with a screen on top for a ground plane and the dipole/diode elements are connected on top of the ground plane. The network is then series-parallel connected to give the distribution voltage desired. The diode required will be a 1-W device with a high (90%) conversion efficiency in the 2- to 20-mw/cm<sup>2</sup> range. Hewlett Packard currently has a silicon Schottky diode in the 1-W range that costs 3 to 5 cents apiece for orders over one million. Rockwell has an alternate

concept that uses subarrays on the rectenna to reduce parts count. Additional details on this concept can be found elsewhere in this report.

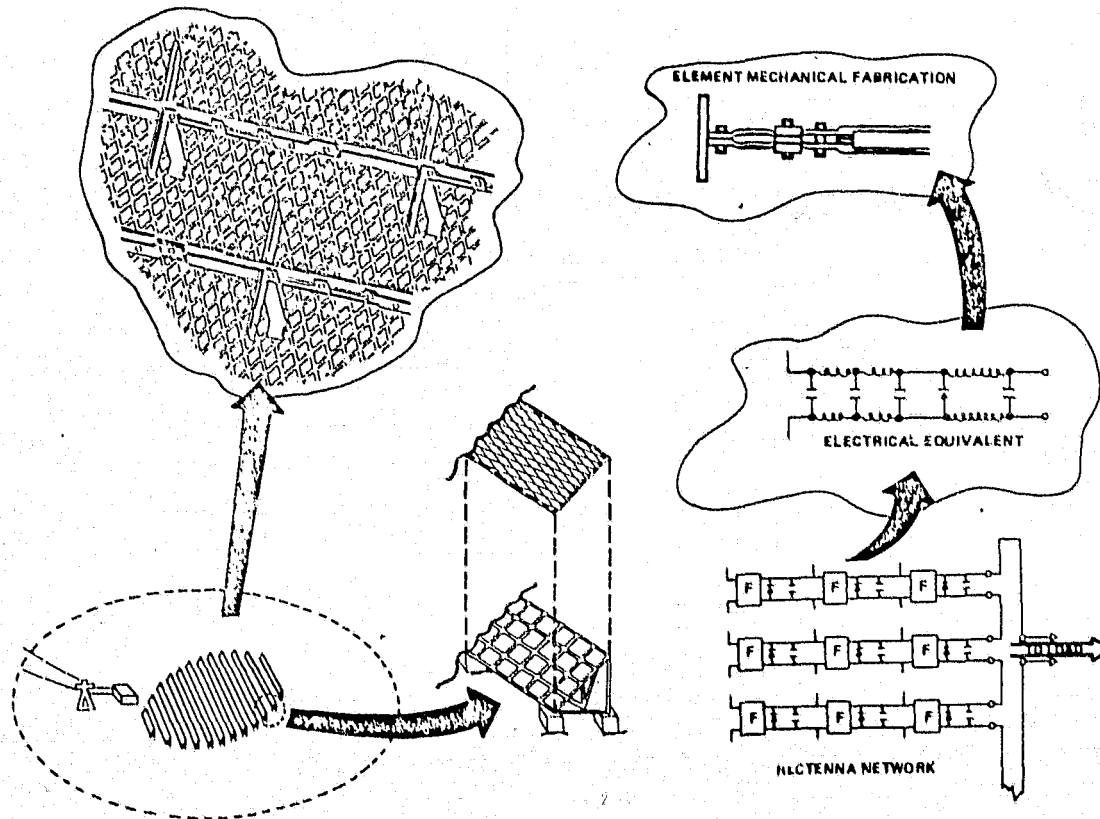


Figure 3.2-16. SPS Rectenna

### Observations

Continuous trades are being made on the power device for SPS. Nearly every device considered has some good points, but the task becomes one of picking the device with the best characteristics for SPS and developing engineering solutions for its weaknesses. The klystron's high gain, stability, and low noise figure make it very attractive; however, it is heavy, requires active cooling, and is not nearly reliable enough. However, the klystron appears to stack up more good points to its credit at this time than the amplatron. The MSFC baseline continues to carry the amplatron because of low weight, passive cooling, and long life. There is no doubt that the overall phase control of the antenna definitely is the key technology item in the microwave system.

All of the environmental questions are still unanswered and will remain so for some time to come. However, there is some positive work being done to devise ways to minimize sidelobe densities of the microwave beam. An example is the Rockwell shaped beam concept described elsewhere in this report. The solid-state antenna is at least as competitive at this time as the klystron/amplatron designs. Technology indicates there are no more barriers to cross



than for the klystron or amplitron. The overall system application will ultimately determine which device is best for SPS. Much more study on solid-state is needed just to bring the level of information up to a par with the klystron/amplitron designs.

### 3.2.3 INTERRUPTED CONTINUOUS-WAVE OPERATION OF MPTS

The primary candidate transmission link designs for SPS have been continuous wave. This section describes a preliminary examination of the possibility of running the system in an interrupted-continuous-wave (ICW) mode.<sup>1</sup> ICW operation will be examined for a system using klystron power converters; however, similar systems could be designed for transistor or amplitron converters.

Assume that solar panels are used and the prime power is dc. The klystrons can then be turned on and off at rates in the order of tens of kilohertz by driving the mod anode with a low power rectangular wave. A larger cathode is needed to supply a higher beam current, because a higher peak power is needed in order to develop the same average power. For example, a peak power of 200 kW is needed to obtain the point design average power per klystron of 50 kW. However, the size of the tube remains about the same because the average power which must be removed from the drift tubes, resonators, and collector electrodes remains the same. A somewhat larger solenoid with greater focus current is needed to control the higher beam current.

The intermittent load on the collector electrodes and body means that larger smoothing capacitors are needed to prevent voltage sag during ON time, if switching regulators are used to produce these voltages. If the collectors are supplied their proper voltages from dedicated portions of the solar panel, a preliminary calculation shows that the panel capacitance is sufficient to supply the required smoothing.

If the prime power is ac and supplied by alternators driven by turbines (as in the case of the Sterling or Rankine cycle systems), the collector voltages can be produced by secondary windings on a transformer; there is one transformer per klystron. The transformer input is a high-voltage ac bus. The transformer has limited volt-second capacity so that it saturates. This produces output waveforms with flat tops which occur when the transformer core is saturated.

The first advantage of the ICW method of operation is elimination of the pilot off-set and the problems of operating the phase-conjugating electronics in the presence of the high transmitted power. The pilot beam is received during the half of the duty cycle when the transmitter is OFF. The phase-locked oscillator generates the conjugate signal during the ON time, but its control signal is applied during the OFF time. Likewise, if the adaptive system using phase shifters is selected, the shifters are set up during the receive time. They retain this setting during the ON time. All this greatly simplifies the retroelectronics.

---

<sup>1</sup>Suggested by R. Dickenson of JPL

The major payoff occurs in the rectenna design. Pulsed operation permits conversion to ac and step-up to the long-distance transmission-line voltage level without use of thyristor inverters or rotating machinery—as shown in Figure 3.2-17.

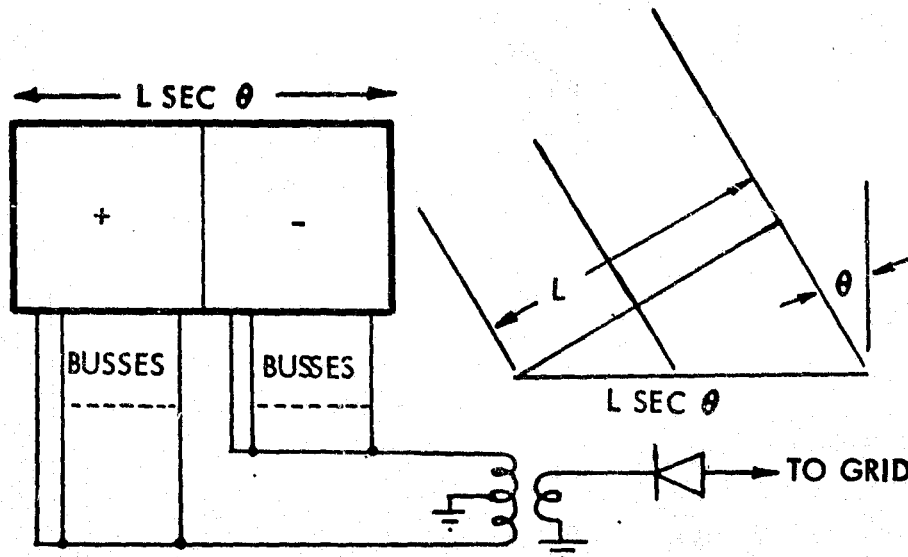


Figure 3.2-17. Rectenna with Direct AC Conversion

A pulse from the satellite falls on the rectenna as shown on the right side of the figure. The wavefront from the satellite takes a time, " $\tau$ ", (where  $\tau = L \tan \theta / 2c$ ) to travel over the first half of the rectenna. The rectenna is shown as having a rectangular form for purposes of establishing the concept. Likewise, it travels over the last half in a time,  $\tau$ .

The received satellite pulse length is  $\bar{\tau}$ . The first half of the rectenna is wired to deliver a positive voltage, and the second half is wired to deliver a negative voltage. The buses from the first half run an extra distance,  $L \tan \theta / 2$ , to a central station compared to the bus run from the last half. The two buses are connected to a transformer primary winding (one at each end of the winding) with a central grounded tap.

The pulse will convolve with square response of each rectenna half to form two sawtooth pulses. The differential delay then converts the pulses into an ac waveform as shown in Figure 3.2-18.

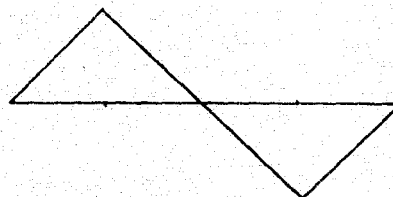


Figure 3.2-18. AC Waveform Generated By Convolution and Delay

The transformer then steps up the voltage to the transmission line voltage where it is rectified for transmission.

In order to eliminate harmonic content, the elliptical rectenna is divided as shown in Figure 3.2-19.

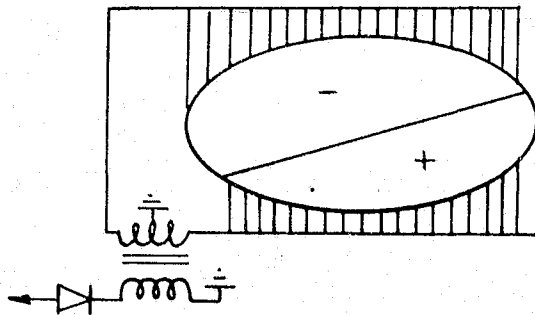


Figure 3.2-19. Phasing on the Elliptical Rectenna

The delay is now very nearly  $L \tan \theta / C$ , instead of  $L \tan \theta / 2C$ . The convolution is a smooth waveform with little harmonic content.

As an example, let the latitude be 34 degrees. Then  $\theta$  is about 40 degrees and  $\tau = 10 \tan 40^\circ / 3 \times 10^5 = 2.8 \times 10^{-5}$  seconds. The power frequency is  $f = 1/4\tau = 8.94$  kHz. The transformer core can be ferrite in order to obtain high efficiency at this frequency.

Since rectifier efficiency is determined by peak power, the efficiency of the Raytheon rectenna design (where there is one diode per dipole) is dramatically raised. The target efficiency of 90% can nearly be reached with currently available diodes without use of subarrays.

Since ionospheric heating is a function of average power, no change in ionospheric effects occurs for the pulsed system, and the average power in the center of the beam is still  $23 \text{ mw/cm}^2$ .

#### 3.2.4 ALTERNATE POWER TRANSMISSION SYSTEMS

Laser transmission of energy has been mentioned as an alternate method of energy transmission. The first problem which occurs is outage due to weather (cloud cover). Because the power link is at nearly optical wavelengths, cloud cover will reduce the efficiency of the laser link.

A second problem is the conversion of the laser beam back to dc electrical energy. There is no equivalent to the diodes which rectify the microwave power to form dc in the IR and visible region. Use of heat engines to make the conversion would result in conversion efficiencies too low to be attractive. MM waves appear to be more attractive than lasers; however, weather penetration will still be poor. In addition MM wave tubes and MM diode rectifiers have low efficiencies. As a result, the overall MM link efficiency may be expected to be very poor compared to the efficiency of a link at 2.45 GHz.



Antenna array alternatives must also be considered. Single large reflectors are unattractive for several reasons. First there are the problems associated with very high power densities which occur at the reflector feed. Also there is no method of compensating for reflector figure errors corresponding to the retrobeam electronics used in the array. As a result mechanical tolerances are very high. At 2.45 GHz, the reflector figure must be held to within about one-half centimeter over the one km diameter structure.

Multiple arrays feeding one rectenna are a possibility if they are operated at different frequencies so that their fields do not beat with each other and form an interferometer problem. However, each array will have to be as large as the single array used in the standard configuration; otherwise, the rectenna will have to be increased in size due to the increase in beamwidth of the arrays over the beamwidth of the single reference array.

Since the arrays cannot be at the same spot in GEO, the rectenna will have to increase in size in the east-west direction to allow for projective effects.

### 3.2.5 CONICAL REFLECTORS IN HEXAGONAL ARRAY

Arrays of parabolic reflector antennas, considered in earlier tradeoff studies were not attractive antenna candidates because of their inability to control grating lobes. An alternate reflector scheme has been proposed where the problem is solved by use of conical reflectors in a hexagonal array. The conical reflector configuration is attractive on a fabrication basis because the cones are easily made out of sheet metal. By attaching heat pipes to the outside of the cones, they can be used as thermal radiators in the same manner as the waveguide or RCR subarrays.

The use of large klystrons ( $\approx 280$  kW AV) will decrease power tube cost because the cost of power tubes goes up approximately as the square root of the power. Since about 25,000 of the large klystrons are needed vs.  $\approx 140,000$  50-kW klystrons the cost savings is about

$$\frac{25,000}{140,000} \times \sqrt{5.6} = 0.42.$$

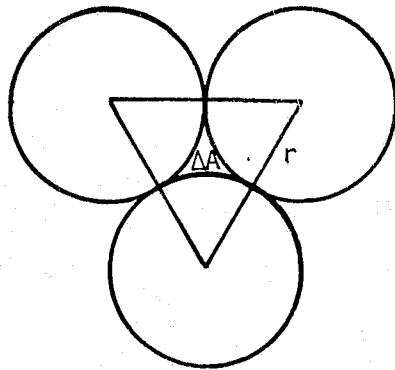
The cost of the conical reflectors could easily be half the cost of either the guide or RCR subarrays.

The major remaining problem is the reduction of beam efficiency due to the fact that the conical reflectors do not completely fill the array aperture as shown in Figure 3.2-20.

About 9% of the aperture is not filled. This will produce a maximum of 9% decrease in beam efficiency from the 88% value (estimated for the guide/RCR arrays) to a value of 79%.

Some of the decrease can be compensated by mounting the klystrons in the interstices with their collectors radiating heat downward in the direction of the microwave radiation. A 3% blockage was accepted in the case of the resonant cavity radiator point design in order to permit the collectors to radiate downward.





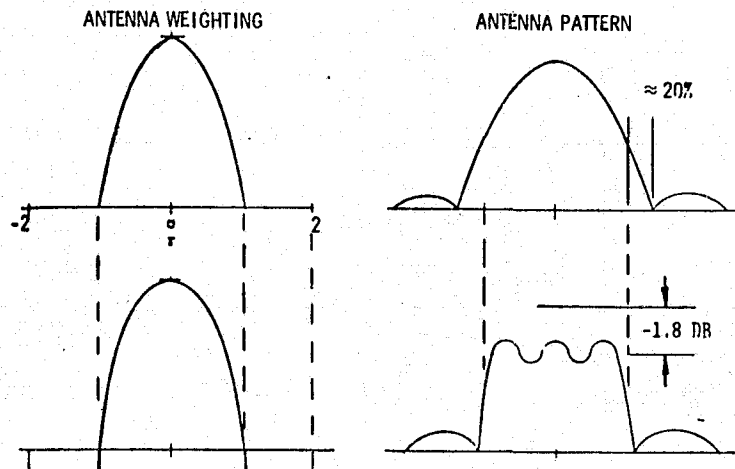
$$\frac{\Delta A}{A_{\Delta}} = \frac{3r^2 \cot 60^\circ - \frac{\pi}{2} r^2}{3r^2 \cot 60^\circ}$$

$$\frac{\Delta A}{A_{\Delta}} = \frac{.161r^2}{1.732r^2} = .093$$

Figure 3.2-20. Conical Reflector Geometry

### 3.2.6 SHAPED BEAM ALTERNATES

There are several alternates to the gaussian beam which can be examined. Rockwell has investigated an alternate aperture excitation function which produces a beam which is much closer to rectangular in shape. The way this is accomplished is shown in Figure 3.2-21.



- SHAPED BEAM ANTENNA IS A STANDARD ANTENNA WITH A RING OF EXCITATION ADDED
- RING WIDTH IS ABOUT THE ORIGINAL ANTENNA RADIUS (RING AREA  $\approx 3 \times$  ANTENNA AREA)
- RING POWER DENSITY IS A FEW PERCENT OF MAXIMUM POWER DENSITY, RING POWER ABOUT 10% OF ANTENNA POWER
- RING IS IN ANTI PHASE WITH ANTENNA
- MAXIMUM POWER DENSITY IS SAME AS STANDARD ANTENNA HALF THE DIAMETER OF SHAPED BEAM ANTENNA

Figure 3.2-21. Gaussian Beam Compared With Shaped Beam

ORIGINAL PAGE IS  
OF POOR QUALITY



The shaped beam antenna weighting is the original tapered weighting with a band of excitation added around the original array edge. The width of the band is about the same as the original array radius. The excitation in the band is a few percent of the peak excitation and is nearly out of phase with the original array.

The beam pattern of the band alone is an interferometer pattern. The central lobe will be in antiphase with the original pattern and depress the gain at beam center.

The purpose of the shaped beam is to lower the peak power density at the ionosphere. If the MPTS is limited to a specified peak beam density and to a peak power density at the array center, the array and rectenna sizes as well as the transmitted and received powers are constrained. Due to the flatter beam, the calculated power received is larger for the shaped beam than the Gaussian beam, 7 GW vs. 5.4 GW for the case calculated in the Rectenna Design section.

Because the shaped beam array has over four times the area, the shaped beam MPTS has a higher cost per kW of power.

One particular item of interest is the design of the array power weighting taking into account the effects of rms phase error in the array in a more optimum manner than is possible when truncated Gaussian weighting is used. The key fact which is ignored in the antenna design theory which we have reviewed up to now is the presence of minimum sidelobe level set by phase errors. When the beam pattern computed from the weighting function has a level well above the minimum sidelobe level (noise level) the total beam pattern is close to the computed pattern. However, when the computed level drops below the noise level, the noise level dominates and sets the actual sidelobe level. This is shown in Figure 3.2-22.

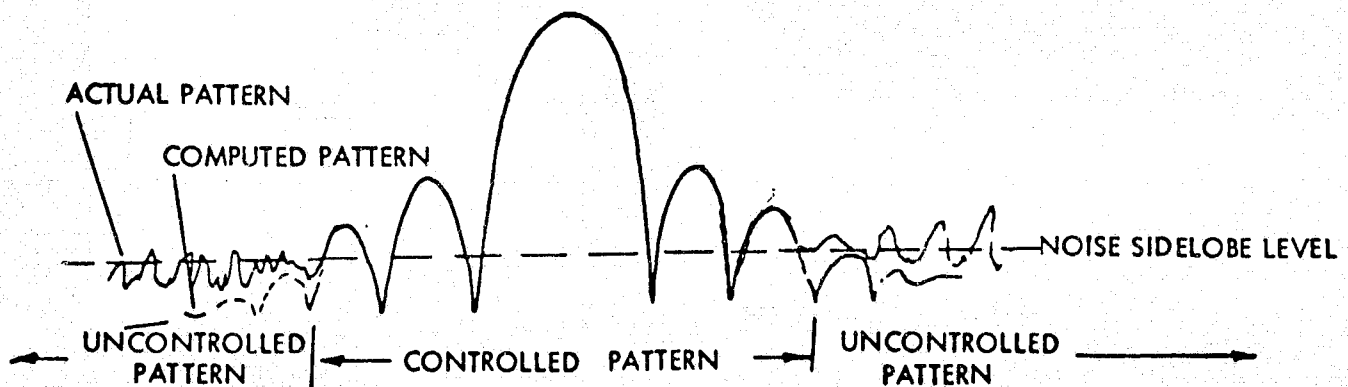


Figure 3.2-22. Influence of Aperture Phase Errors  
On Antenna Pattern



The noise level is the transform of the noise excitation, that is the excitation deviation from theoretical weighting. Ruze\* has shown that, crudely, the noise level is given by

$$L_N = \frac{1}{\eta_A} \left( \frac{A_C}{A_A} \right) \overline{\delta^2}$$

where

$\eta_A$  = aperture efficiency

$\overline{\delta^2}$  = mean sq. phase error in rad<sup>2</sup>

$A_A$  = area of array

$A_C$  = area over which noise excitation is correlated

$L_N$  = ratio of sidelobe noise level power to power at main beam peak,

As an example of the baseline MPTS the dominant correlated area is the subarray, so

$$A_C = 10^2 \text{ m}^2.$$

Also

$$A_Z = \frac{\pi}{4} \times 10^6 \text{ m}^2$$

$$\eta_A = 0.7$$

$$\overline{\delta^2} = 0.031 \text{ rad}^2$$

then  $L_N = -53 \text{ db.}$

Optimum weighting would not attempt to produce sidelobes below the level  $L_N$ . Reduction below the  $L_N$  level requires more taper and increases the beam width. Power density at the array center also goes up. The ideal optimum weighting would produce sidelobes of equal size all at or slightly below the noise side-lobe level.

Tchebycheff weighting does give equal sidelobes. It consists of a continuous tapered distribution plus a pair of point radiators at the aperture edge. This is not a realizable distribution due to the infinite power density in the point radiators.

A practical modification of Tchebycheff weighting is Taylor weighting (see Figure 3.2-23). Taylor weighting is continuous and realizable. It produces  $\bar{n}$  sidelobes which are of approximately equal before declining to very low levels. Aperture efficiency is high compared to that obtained with other weighting functions. There may or may not be peaks in the weighting function at the aperture edges depending on the design level of the  $\bar{n}$  sidelobes.

\*J. Ruze, Antenna Tolerance Theory - A Review, pp 633-640, Proc. IEEE (April 1966)

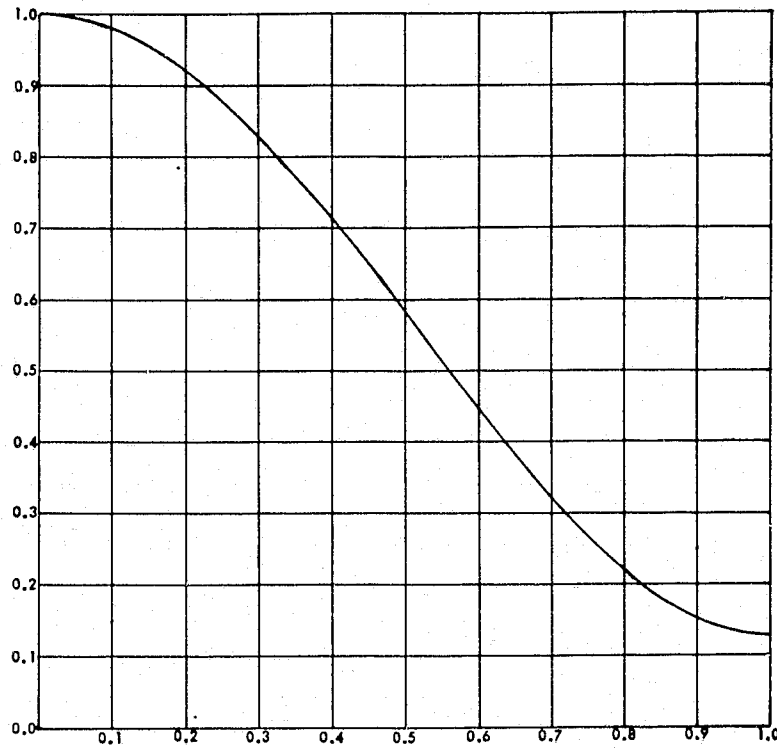


Figure 3.2-23. Taylor Distribution For 40 dB Sidelobe Level

A value of  $\bar{n}$  high enough to produce peaking at the edges is desired. Unfortunately patterns for  $\bar{n}$  values large enough to produce peaking at the edges are not readily available for very low design sidelobe levels. However, the performance can be estimated for a level of -40 dB. This is an appropriate level for an antenna with somewhat higher sidelobes than the numerical example just given. In that case the value of

$$D \sin \theta / \lambda = U$$

at -13 dB off the beam peak, corresponding to the rectenna edge, is about 1.2, then

$$\Delta \theta = 2U\lambda/d = 2.94 \times 10^{-4}$$

and

$$d = h_g \Delta \theta = 10.6 \text{ km.}$$

The beam efficiency is 98.5% vs. 95% for the truncated Gaussian beam. It is believed that  $d$  can be reduced to 10 km by using a higher value of  $\bar{n}$ .

The Taylor distribution appears to be better when compared with the truncated Gaussian weighting. The beam efficiency with Taylor weighting has been raised by 3.5% while the sidelobe level has been decreased by about 15 dB.



Further calculations are needed to define the best Taylor distribution and to calculate its performance. The weighting function and beam pattern for a -40 dB,  $\bar{n}=s$  Taylor case are shown in Figures 3.2-23 and 3.2-24 for illustrative purposes.

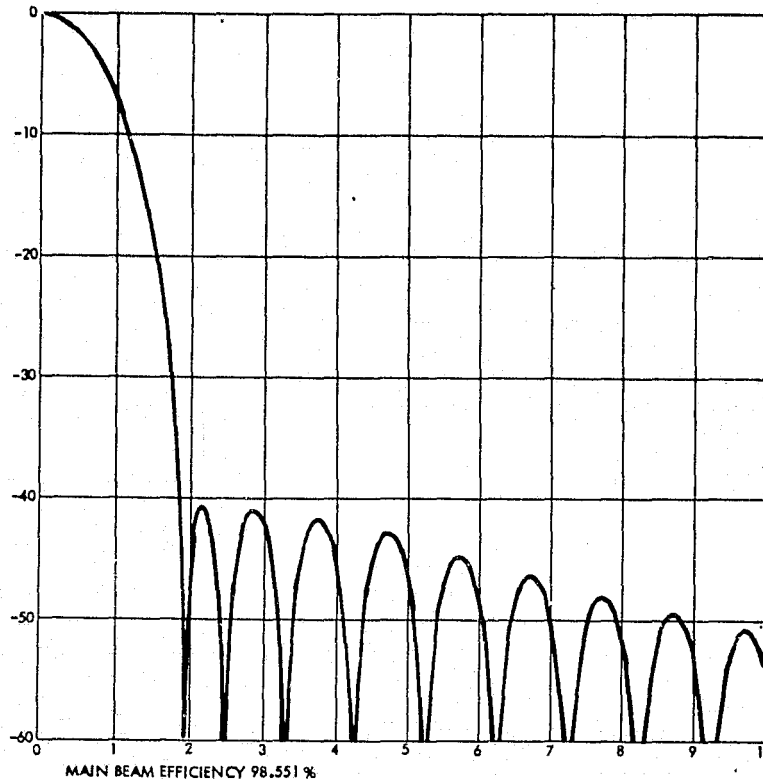


Figure 3.2-24. Beam Pattern From Taylor Weighting Pattern (40 dB)

### 3.2.7 POWER AMPLIFIER CONFIGURATIONS

#### Introduction

Selection of a dc-to-microwave power converter has been one of the more controversial design decisions in selection of a baseline MPTS system. At one time or another, various organizations have proposed the use of amplitrons, crossed-field amplifiers, klystrons and transistors for the application.

This section will review the properties of these converters and make a selection based on the present state of the art. It should be emphasized that the criteria used are the current state of the art. Since the final selection of the best converter will be made a decade or more in the future, improvements in device performance and relative cost may alter the picture in the mean time. Because amplitrons have been examined in great detail many times, the section on these tubes and other crossed-field amplifiers will consist mainly of comment.

Data will be presented concerning the design of a 50 kW, 85% efficiency Varian klystron which will be used in the Rockwell point design. The greatest

detail will be presented concerning the design of power transistors for use as power converters. The use of this device for this application has not been examined in detail in the past.

This effort is divided into two parts. One part is an analytic study of power transistors in Class E amplifier circuits. In addition the efficiency of transistors in Class B/C amplifiers is investigated by Drs. Roulston and Bryant of Waterloo University. Power transistors are not used in the present point design because their theoretical promise has not yet been proved out by experimental work. In addition, means of making such transistors under high volume manufacturing conditions must be worked out.

It is felt that there is a good chance that, if made of GaAs, the transistors can be made by epitaxy on a sapphire substrate in the same manner as the photovoltaic GaAs solar cells. It is also quite possible that the GaAs rectifier diodes can be made this way. In that case, it should be possible to make all three devices in a single high volume production facility. A comparison of the various power converters is shown in Table 3.2-8.

Table 3.2-8. Conversion Device Parametric Trade-Off

	TRANSISTOR	AMPLITRON	KLYSTRON	REGENERATIVE CFA
POWER/RADIATOR (KW)	0.9	5.0	.50	5.0
RADIATOR	DIPOLE	RESONANT CAVITY RADIATORS		
AMPLIFIER GAIN	20 DB (ON CHIP)	7 DB	50 DB	13 DB
AMPL. INPUT PWR (W)	0.6	1000	0.5	250
DRIVER TYPE	TRANSISTOR	TUBE	TRANSISTOR	TRANSISTOR AT .915 TUBE AT 2.45
OPERATING FREQ. (GHz)	2.45	2.45	2.45	.915 OR 2.45
SPECIFIC WT (LB/KW)	?	1.0	1.4	1.0
OPERATING VOLTAGE	35	20 KV	40 KV	20 KV
NO. PRIME PWR VOLTAGES	1	1	7	1
NO. AUX. VOLTAGES	0	2	3	1
EFFICIENCY	80% DESIGN GOAL	68%	85%	80%
ARC SUPPRESSION	NA	CROWBAR	MOD ANODE	CROWBAR
HARMONIC SUPPRESSION (DB)	-50	-20	-40	-20
NOISE (DB/KHz)	-125	.07	125	7
COMMENTS	PRELIMINARY CALCULATION GIVES Si TRANSISTOR EFFICIENCY ≈60%, GaAs ≈77%	MAY NOT START	LARGE NO. OF VOLTAGES REDUCES PRIME PWR DIST. EFF. HIGH-TEMP. COLLECTOR HELPS IN RADIATING HEAT, BUT MAKES TUBE LOCATION MORE DIFFICULT.	HAS HOT CATHODE



### Amplitrons and Crossed Field Amplifiers

The original power conversion tube proposed by Raytheon is the amplitron. The optimum output power level selected was 5 kW. Due to the low gain of the tube (7 dB) the drive level is 1 kW. This power level is too high to be attained by a transistor amplifier, so a tube must drive the amplitron. Raytheon proposed a "Christmas tree light" string of amplitrons, each providing 5 kW for radiation and 1 kW to drive the next tube in the cascade chain. Only one tube in a chain required RF drive from a lower power level source.

There are many drawbacks to this arrangement. First any tube failure in the arrangement disables subsequent tubes in the chain. The cascade connection reduces overall reliability by a factor depending on the total number of tubes in the chain. Due to the exponential rise in the probability of failure as the number of components increases linearly (when the system fails due to any component failure), the reduction in reliability may be large.

Another disadvantage rests in likely need for phase adjustment of the individual amplitron outputs in the chain. Raytheon proposes to use a moveable pole piece in the tube to vary the magnetic field, and thus the operating voltage and phase. However, it will be very difficult to achieve the required level of phase control. A 5° phase correction would require a 10 kV change in operating voltage resulting in a lower power output. In a parallel arrangement, each amplitron would feed only its own portion of the antenna and overall reliability would be much higher. However, now each amplitron must be driven by a preamplifier. Since the preamplifier requires a 100 W drive, it must be preceded by a power transistor amplifier. Alternately, 1 kW klystrons could be used as drivers. In either case, the overall efficiency is no longer the 85% figure obtained in the series arrangement, but about 65%. For now the 1 kW drive power must be produced for each amplitron instead of being passed along the chain as in the series case.

There are serious questions as to whether a high efficiency amplitron will start at such a low drive level as 1 kW. Varian Beverly in a proposal to NASA Lewis Research Center presents calculations to show that it will not start. This same section also argues that the crossed field amplitron will probably not operate even if primed with a thermionic cathode. The Varian viewpoint seems to be substantiated by the difficulties encountered by Raytheon in designing a successful amplitron (or indeed one that will work at all) for this application under NASA-Lewis Contract NAS3-20374.

In view of the above it appears that the 5 kW SPS amplitron is not an attractive candidate device. Much uncertainty remains concerning its performance.

However, the 50 kW SPS klystron design is based on a proven tube, the VKS-2450. A depressed collector assembly must be added and the tube cooling and mechanical structure developed for space use. Depressed, electrostatic, reflex collectors with 57% recovery efficiency have already been operated on a lower power tube.



### Use of Transistors for the SPS Microwave Power Transmission System

Up to the present time only high-efficiency microwave power tubes have been considered for dc to microwave power conversion in the SPS microwave power transmission system. Since efficiencies of over 80% are required at frequencies of a few gigahertz, transistors have not been considered. In the above frequency range transistors have typically attained efficiencies of 50 to 60%.

However, the state-of-the-art in microwave transistor design is advancing rapidly. Therefore, in the time scale of the SPS system design, which extends over decades, it may be that transistors are a valid contender offering advantages in reliability, specific weight or other properties. Since transistors differ greatly in properties from microwave tubes, the design of the power transmission system and the trade-offs must be completely reevaluated. It is to be expected that the resulting system parameters will be quite different.

Transistors have entirely different properties compared with power tubes. In the same frequency region both efficiency and power handling capability are falling rapidly with frequency. In contrast to tubes, lower frequencies do not result in specific weight penalties, since there are no cavity resonators or focussing magnets involved. Motorola has been engaged in the study of transistors to replace magnetrons in microwave ovens. The frequency selected was the power band at 915 MHz, rather than 2.45 GHz.

In exploring the effects on the SPS of selecting the lower frequency of 915 MHz, it is first known that Faraday rotation effects in the ionosphere will be increased. However, the drawback can be avoided by use of circular polarization. It will be found that this is an advantage when using transistors because more than one transistor will be needed to obtain the power required per radiating element. Circular polarization provides a way of combining the outputs of two transistor power amplifiers without suffering loss in a hybrid power combiner.

Going to the lower frequency and keeping the same SPS array size, the beam footprint dimensions at the rectenna increase by the frequency ratio, 2.68. The rectenna area increases by the square of this ratio or 7.17. However, the capture cross section areas of the rectenna increase by 7.17 also. Therefore, the number of rectenna elements remains the same. The amount of real estate required has increased by 7.17. However, land is probably the cheapest ingredient in the system cost budget, especially since desert or waste land will be selected when at all possible. The number of radiators in the SPS array has decreased by a factor of 7.17. This greatly reduces the number of transistor power amplifiers required.

To estimate the number of amplifiers and their design power, assume one amplifier per radiating element. For a radiator spacing of  $0.62 \lambda$ , the area per radiator is

$$AR = (0.62 \times 12.24 \text{ cm})^2 = 57.7 \text{ cm}^2 \text{ at } 2.45 \text{ GHz.}$$





The number of amplifiers is

$$A_A/A_R, \text{ where } A_A = 7.85 \times 10^9 \text{ cm}^2 = \text{area of array,}$$

$$\text{or } n_T = 1.36 \times 10^8 \text{ amplifiers.}$$

At 915 MHz

$$n_T = 1.36 \times 10^8 / 7.17 = 1.9 \times 10^7 \text{ amplifiers.}$$

The peak amplifier power required is 866 W. At present about 100 W per transistor is obtained at 1 GHz or 400 W per dual push-pull amplifier configuration. However, if the present efficiency of 50% is raised to the required 83%, three times more power per transistor will become available at the same junction temperature.

The final major system effect to be considered is power density at the ionosphere. This is reduced by the factor 7.17 from 23 mW/cm<sup>2</sup> to 3.2 mW/cm<sup>2</sup>. This would appear to completely eliminate worries about the effects on communication and navigation caused by ionospheric modification. It appears that only GaAs transistors can be used in the final system because of thermal considerations. Since Si transistor junction temperatures cannot exceed 150°C, Si transistors cannot be used. However, the intrinsic junction temperature for gallium arsenide is about 400°C. Therefore it appears that the GaAs transistor can be used, even if heat is radiated only from one side.

#### Array Organization and Amplifier Configuration

If transistor amplifiers are used, the array configuration will be entirely different than a tube driven array. A basic difference arises because the transistor amplifiers drive individual radiators. In the tube case, the power per tube is much higher than the power per radiometer. Therefore, each tube drives many radiators through a distribution system. The system can be slotted waveguide or the resonant cavity radiator (RCR) proposed by Rockwell.

In the transistor case amplifier drive power must be fed to each amplifier module through a distribution system. Since this system is followed by the power amplifier, it can be a relatively high loss compared to the tube distribution system which follows the power amplifier and must be low loss in order to maintain efficiency. This means that stripline can be used, which is light compared to guide or the RCR. However, the amplifiers must have a reasonably high gain in order to feed a large enough number of amplifiers to form a power module of reasonable size, say 100. If there are 100 amplifiers per module, they need a power gain of about 20 dB. However, at present, power transistors have a gain of only 10 to 11 dB in the L and S band region. Means for increasing the power gain of transistors will be discussed later. However, if conventional transistors are used, two stages will be needed.

The most obvious design is the use of a microwave integrated circuit with separate discrete transistors mounted in the circuit. Considering the enormous number of transistors involved, this design is not attractive. Therefore,



more integrated designs, including several transistors on one chip, will be discussed later.

At 915 MHz a 100 amplifier power module with radiator spacing of  $0.62 \lambda$  will be 2.06 m on a side. Typical feeder runs will be 2.13 m in length (half the width plus half the height). Stripline loss at 1 GHz is about 0.004 dB/cm giving a feed loss of 0.8 dB. A cross section of the power module is illustrated in Figure 3.2-25.

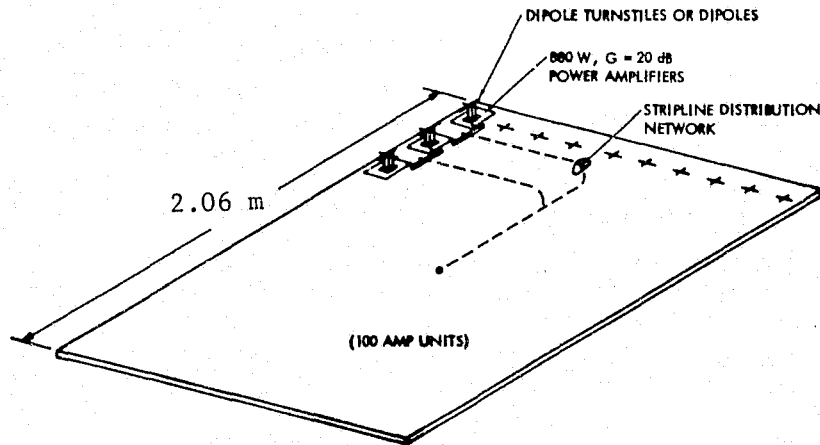


Figure 3.2-25. 87 kW Transistor Amplifier Power Module

The amplifier units are coupled directly to the stripline through slots in the stripline ground plane. In turn, the crossed dipole radiators are coupled directly out of the amplifier modules. The extra dipole shown in the center picks up the pilot signal and radiated signal and feeds them to the phase conjugating electronics.

The transistor chips have their collectors soldered to a bryllia substrate forming the bottom of the module case. Waste heat flows through this substrate and is radiated from the case bottom. The top of the case is a second ceramic substrate. Conductor tabs, which are coupled to the stripline slots in the usual manner shown in the insert, and emitter tuning inductors are lithographically formed on this top substrate and connected by beam leads to the transistor chips. Ground is carried between the upper and lower substrates by means of a metal ring which forms the edge of the case. The collector emitter voltage is fed to track on the lower substrate through a gap in the ground ring.

The outside surface of the lower substrate is covered with a metal ground plane, except at the radiator feed throughs. It shields the transistor amplifier input from the radiated field to prevent feedback and acts as the ground plane for the stripline circuits on the other side of the substrate. Figure 3.2-26 shows the amplifier for one of the polarization channels. It consists of a push-pull common collector stage driving a push-pull common-base output stage. The output circuitry of the final stage is for a class-E power amplifier which will be discussed in a later section. The capacitors  $C_2$ , required for the amplifier configuration, are used as feed through capacitors to the radiator.

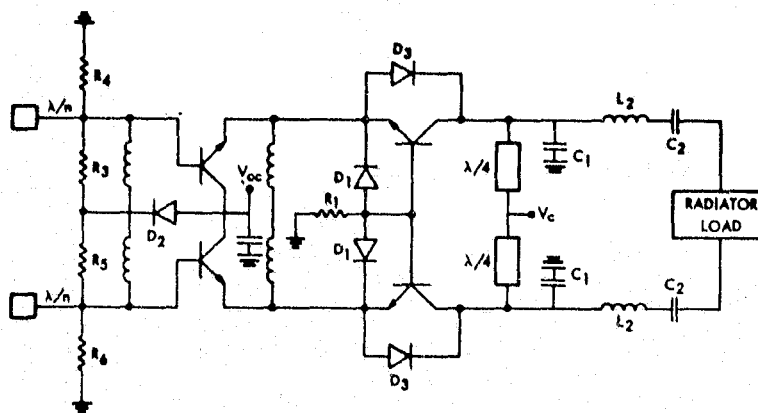


Figure 3.2-26. Transistor Chip Schematic

Ideally, the transistors can all be formed on one chip as shown in Figure 3.2-27. In that case the first stage collector and the second stage collectors must be isolated by means of deep oxide filled grooves etched in the collector side of the chip as shown below.

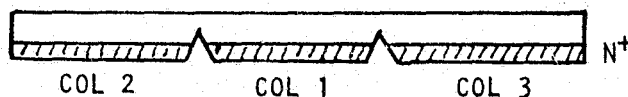


Figure 3.2-27. Chip Collector Configuration

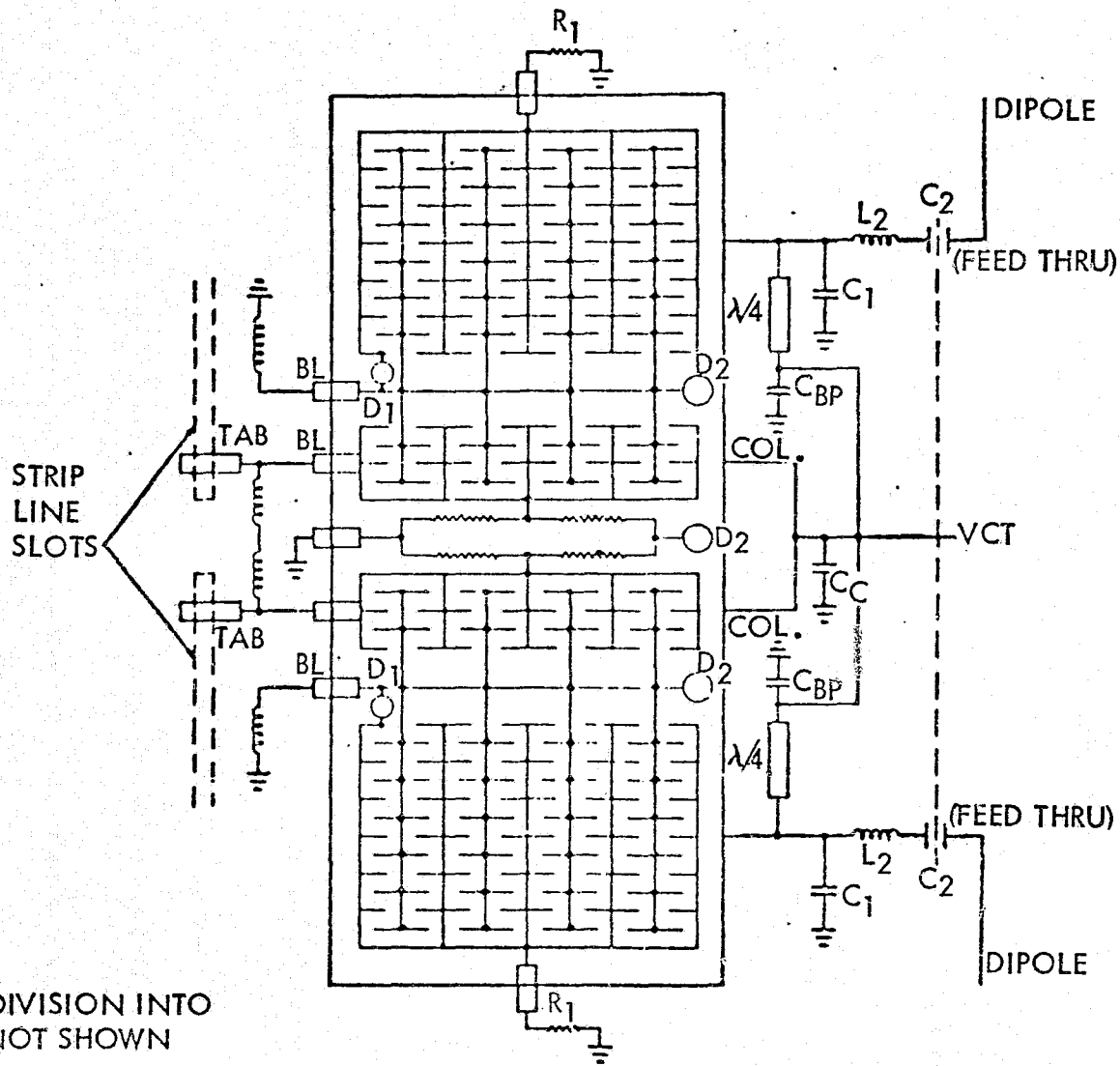
The grooves cut through the gold-silicon alloy used to connect the chip to the MIC and the  $N^+$  region of the chip shown shaded in the figure. Figure 3.2-28 shows the transistor amplifiers and diodes formed on one chip. Alternately, the center transistors can be one die and the two common base transistors on two more dies. All three chips are then soldered to the common substrate and interconnected by beam leads.

Two of these transistor assemblies mounted on common substrates form a radiator module as illustrated in Figure 3.2-29.

### Methods of Obtaining Maximum Power Conversion Efficiency with Power Transistors

Before any detailed consideration of the adjustment of parameters to obtain maximum efficiency we need to determine the basic amplifier configuration most likely to yield high efficiency. Features of the transistor structure which are most important in increasing efficiency and the technology required to control these features should also be identified.

Amplifier efficiency, rather than transistor efficiency, is selected for consideration because only the combination of circuit and transistor can be said to have an efficiency. The circuit is as important as the transistor.



NOTE: DIVISION INTO CELLS NOT SHOWN

Figure 3.2-28. Transistor Chip Layout

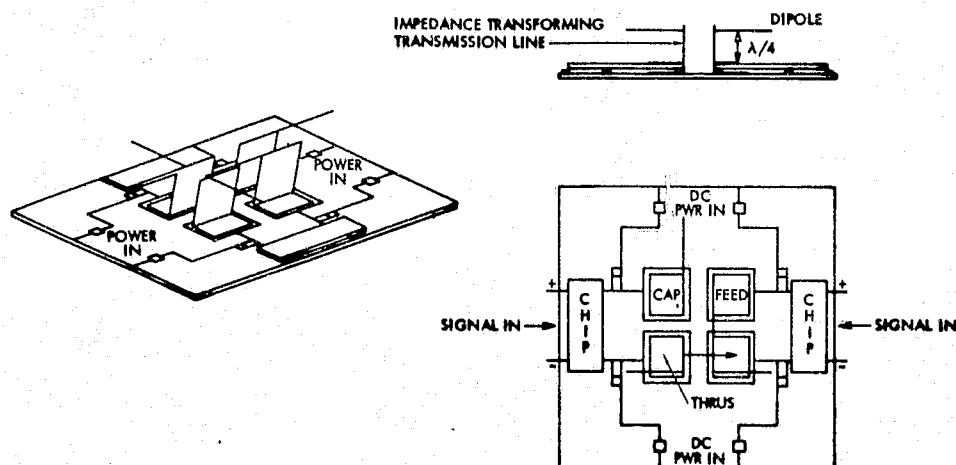


Figure 3.2-29. Transistor MIC Module

A key consideration in the amplifier design is the extremely low load impedances required by conventional class C or B transistor power amplifiers. Usually matching networks are inserted between the amplifier and the final load. This produces losses in the matching circuits and increases complexity. As power increases, more transistor cells are paralleled further lowering impedance and increasing the problem. An obvious step in solving this problem is the use of a push-pull design.<sup>1</sup> This has been common practice in tube amplifier design for many years. Input and output impedances are then four times greater than the impedances obtained when the transistors are operated in parallel. For common base operation the circuit is shown in Figure 3.2-30.

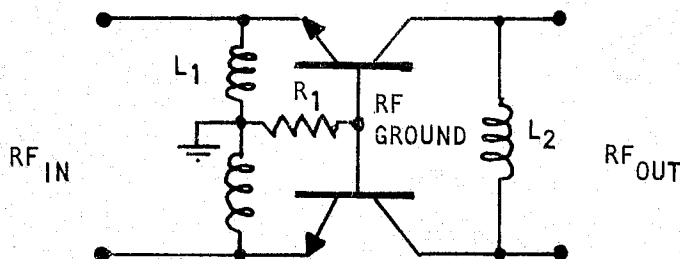


Figure 3.2-30. Common Base Push-Pull Amplifier

Note that bias is established by resistances in the base circuit, rather than in the emitter path. This permits the direct connection of the emitter follower emitter and common base emitter as discussed earlier.

At 1 GHz efficiencies of 50-55% are state-of-the-art values.<sup>2</sup> Ultimate efficiencies of 60-65% are predicted by skilled designers. There is no hope of reaching 80% efficiency with these amplifier types. It might be thought

<sup>1</sup> L. Max, Balanced Transistors: A New Option for RF Design, Microwave pp 42-26, Microwaves (June 1977)

<sup>2</sup> R. Potyku, Personal Communication on the Performance of Motorola Transistor XRF-856 at 915 MHz



that the Class D switching mode power amplifier would offer an escape from the dilemma.<sup>3</sup> However, as Chudobiak notes for frequencies greater than  $0.01 f_T$ , the saturation voltage increases rapidly with frequency. Correspondingly, the efficiency of Class D circuits falls off rapidly above this limit. In fact, about 2 MHz is generally considered to be the practical upper frequency limit for such amplifiers. Neglecting the rise in  $V_{SAT}$  at higher frequencies, three problems become difficult to overcome: (a) generating fast-switching square-waves across the inevitable circuit capacitances, (b) making the transistor switching times sufficiently small compared with the RF period and (c) preventing destructive simultaneous conduction in the two transistors of the push-pull class D circuit.

The only apparent hope for obtaining the efficiencies desired is a modified Class D amplifier called Class E invented by N. Sokal.<sup>4,5</sup> Sokal recognizes that major losses occur in power amplifiers during transition between conducting and non-conducting transistor states when appreciable current and voltage exist simultaneously. Previous approaches to reducing this loss have been only to reduce device switching times. Sokal synthesizes a load network giving a transient response which minimizes switching losses even if the device switching times are appreciable fractions of the ac cycle. It appears that high efficiency can be obtained up to about  $0.5 f_T$ . Sokal has obtained efficiencies of the order 85% up to 100 MHz. He states that there appears to be no reason why this amplifier class cannot be used in the microwave region.

### 3.2.8 BEAM RETRODIRECTION SYSTEM

A review of proposed system design, Table 3.2-9, shows a trade-off of various array phase controls methods which can be used to form the MPTS beam. Beam formation by phase conjugation of a pilot beam originating at the rectenna appears to be the preferred method of controlling the phase of the array. Each subarray of the transmitting antenna array is connected to a circuit which transforms the phase of the received pilot signal at that subarray ( $\omega t - \beta_r$ ), into a conjugated phase ( $\omega t + \beta_r + \theta_r$ ) for retransmission. Here  $r$  is the path delay from the pilot beam antenna to the subarray,  $\omega$  is the operating radian frequency,  $\beta$  is the phase shift constant  $2\pi/\lambda$  &  $\theta_r$  is a constant phase shift resulting from the reference system phase control. It must have the same value for each subarray in the array system.

Since the retransmitted signal from each subarray has a phase which is exactly equal and opposite to the phase shift that results as it propagates back toward the pilot source (rectenna), then all subarray signals will be received at the rectenna with the same phase  $\theta_r$  and the envelope of the spherical wave fronts will be normal to the rectenna.

<sup>3</sup> W. Chudobiak, Frequency and Power Limitations of Class D transistor Amplifiers, pp 25-27, IEEE Trans. Vol SC-4, No. 1 (Feb 1969)

<sup>4</sup> N. Sokal and A. Sokal, Class E - A New Class of High Efficiency Tuned Single-Ended Switching Power Amplifiers, IEEE Trans, Vol SC-10, No. 3 (June 1975)

<sup>5</sup> N. Sokal, Class E RF Power Amplifiers Give High Efficiency and Reliability, with Predictable and Reproducible Performance



Table 3.2-9. Phase Control Trade-Offs

ITEM	PHASE CONTROL	DIRECT	BIT-WIGGLE	ADAPTIVE (JPL)	ADAPTIVE (ELEC)
METHOD	SERVOED PHASE	INVERSE XFORM	SUBARRAY TEST BY 180° $\theta$ SHIFT	CONJUGATE $\theta$	CONJUGATE $\theta$
GROUND COMM.	NO	YES	YES	NO	NO
PILOT BEAM	YES	NO	NO	YES	YES
SPEED	FAST	SLOW	SLOW	FAST	FAST
REF. DIST.	PARALLEL (SERVOED)	NA	NA	SERIAL	PARALLEL (SERVOED)
SUBARRAY STEERING	YES	NO	NO	NO	YES
PWR AMP PHASE CONTROL	YES	NO	NO	NO	YES
PWR AMP $\theta$ NOISE CANCELLATION	NO	NO	NO	NO	YES
GRND STATION EQUIPMENT	PILOT BEAM TRANSMITTER	$\theta$ & AMPLITUDE MEASUREMENT OVER BEAM	ANTENNA AND RECEIVER	PILOT BEAM TRANSMITTER	PILOT BEAM TRANSMITTER

Phase conjugating may be realized in several ways. A well-known technique employs heterodyning and is shown functionally in Figure 3.2-31. Other approaches include servoing phase shifting devices to bring the received signal phase into agreement with a reference phase. Then the transmitted signal is subjected to the same phase shift and phase conjugation results. In practice, the pilot signal must be offset from the transmitted signal in order to prevent the pilot signal receiver from being rendered inoperative by transmitter leakage. This produces a pointing error in the transmitted beam. A received signal at a subarray at a distance L from the antenna reference has a phase offset with respect to the reference signal of

$$\Delta\phi = \frac{2\pi L \sin \theta_r}{\lambda_r}$$

where  $\theta_r$  is the pilot beam angle with respect to boresight.

Phase conjugation will produce the same phase offset (with opposite sign) and hence a transmit angle  $\theta_t$  difference from  $\theta_r$  due to the change in  $\lambda$ . The deviation of the pilot beam from mechanical boresight,  $\theta_r$ , must be very small. For instance, the misalignment of the transmitted beam at the rectenna must be less than 420 meters. This is about 5% of the rectenna diameter. More error can not be tolerated.

In the system proposed in this study a dual pilot beam signal is used with one frequency above  $f_T$  and one below. This permits the generation of a pilot signal exactly at frequency  $f_T$  and eliminates pointing error due to offset between  $f_r$  and  $f_T$ . In systems with offset, it is obvious that the basic reference in Figure 3.2-31 need not be synchronous with the pilot beam. In the system previously proposed by Rockwell, this was the case.

Another source of trouble is the virtual certainty that the high level transmitter signal will leak into all the conjugating circuitry and produce a multitude of spurious signals which produce unforeseen effects. This was one of the major problems encountered in a one megawatt Voice of America transmitter many years ago. The only safe solution is felt to be incorporation of the transmitter signal in the phase conjugating scheme itself.

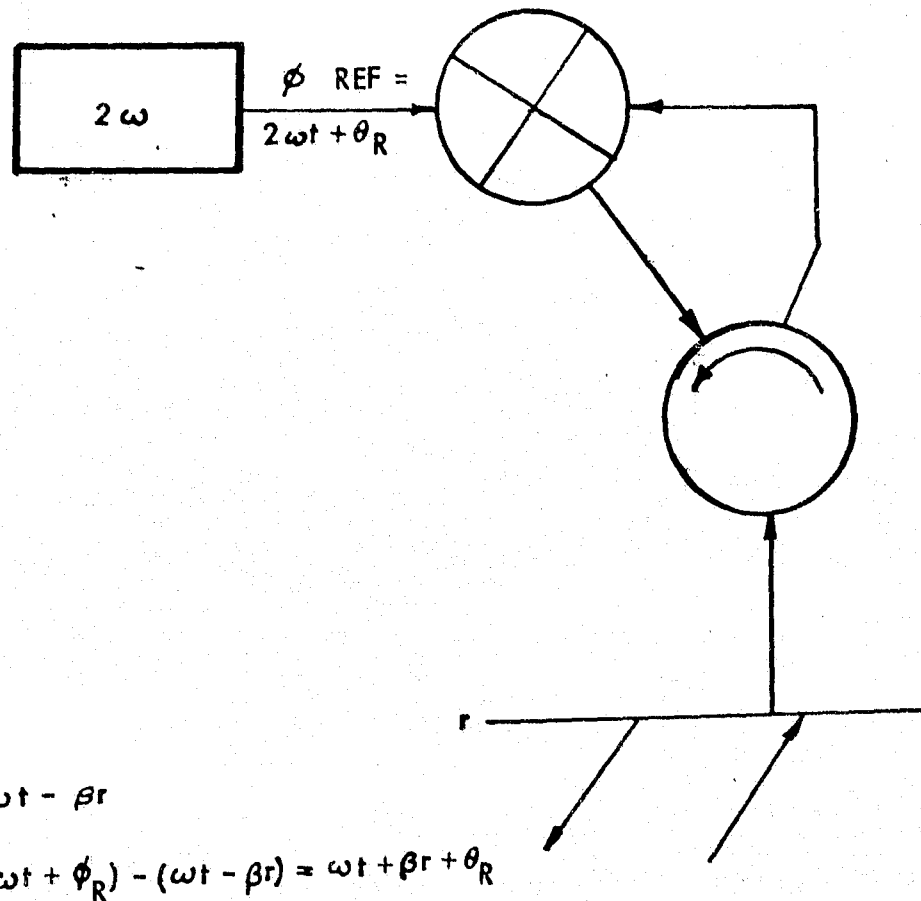


Figure 3.2-31. Simple Heterodyning Phase Conjugating Circuit

This is done by using the transmitter signal as the synchronous reference demodulating the high and low pilot signals. This signal now is used at a level of 10 mW. A leakage level in the order of milliwatts then can be tolerated. Fortunately, the arrangement makes it possible to cancel transmitter noise reducing problems produced by this noise.

In order to reduce the required phase stability of the power amplifiers their outputs are sampled and their input phases servoed to the values determined by the phase-conjugating system. This greatly reduces the regulation requirements imposed on prime dc power, an important point when power conditioning at such high power levels is contemplated. This feature was retained from the earlier Rockwell system. Distribution of the phase reference is similar to that proposed by Seyl and Leopold. Servoes are used to stabilize the phase of the reference signals distributed through feeders to local zones within the array. A less accurate distribution method is then used within the zones. The zone size is selected in order to make this possible. Serial distribution was avoided because build-up in phase error from subarray to subarray may occur.

Figures 3.2-32 and 3.2-33 show the phase conjugating system proposed by JPL, the second figure being a particular embodiment using magnetrons.



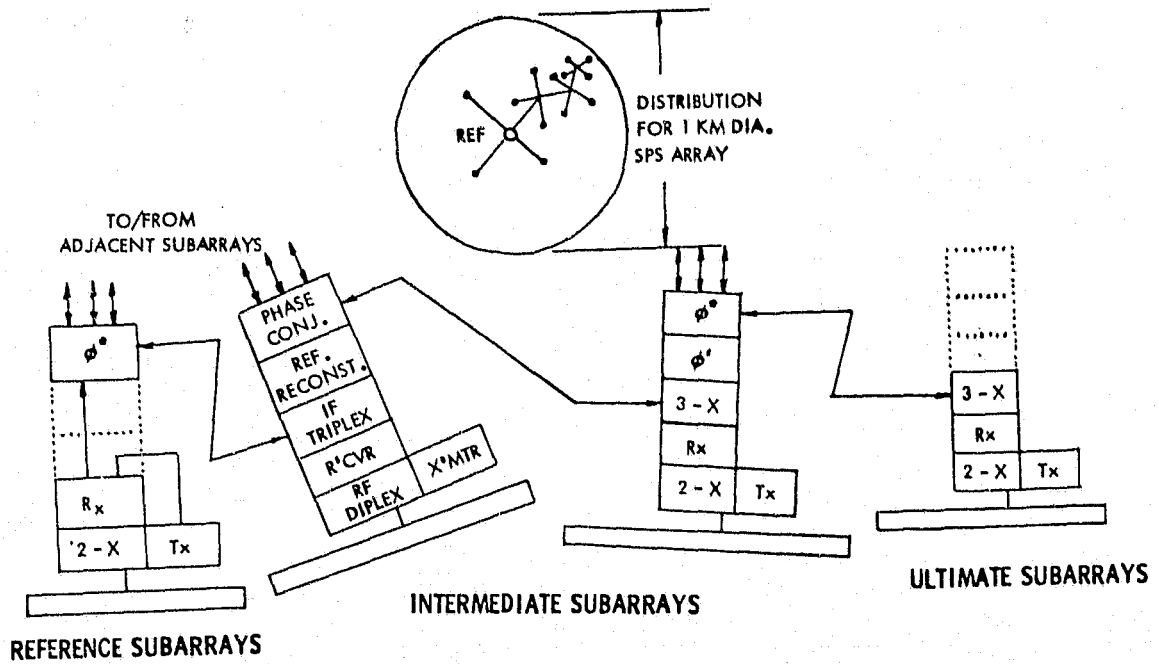


Figure 3.2-32. MPTX Phase Conjugation  
And Reference Distribution

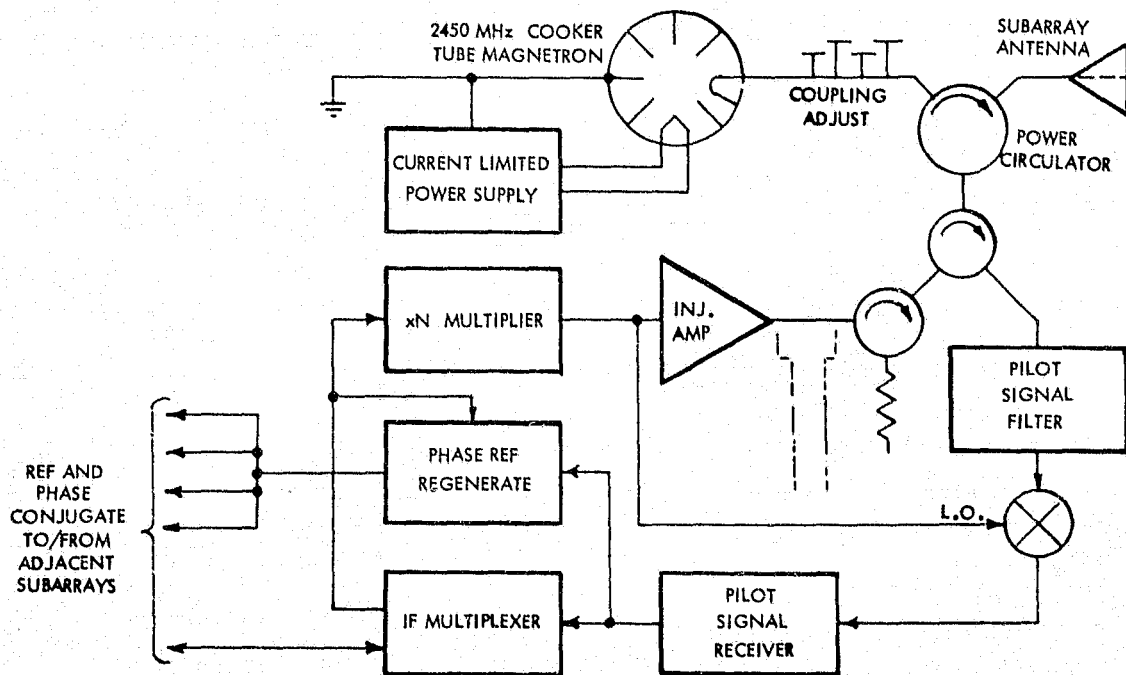


Figure 3.2-33. MPTX Injection Locked  
Magnetron Subarray



Figure 3.2-34 shows the phase-conjugating system proposed by Seyl and Leopold. Finally, Figure 3.2-35 shows the system proposed by Rockwell in an earlier study.

After reviewing these systems, an eclectic system was synthesized which hopefully incorporates the good points of these other systems. It might be mentioned that two features of the earlier Rockwell system which were retained was the use of a non-synchronous local oscillator system and the avoidance of high-order harmonic multipliers.

The use of a non-synchronous local oscillator greatly reduces the complexity of the frequency transformation scheme. Since the intermediate frequency is subtracted and added in the phase conjugating loop, its phase cancels out. Therefore, it need not be synchronous. High order harmonic multiplication was avoided because it is difficult to get high phase stability in such multipliers with change in temperature and with aging. The features of this eclectic system are compared with the other phase conjugating systems in Table 3.2-10.

### 3.2.9 DOE PROGRAM SUPPORT REQUIREMENTS

Table 3.2-11 summarizes the DOE areas of support that are required for the SPS microwave power transmission system. A major requirement that significantly impacts the subsystem design is the permissible microwave power density at the ionosphere. Rectenna size and siting is dependent on the inputs of biological effects of long term low level microwave energy and the permissible power density outside the rectenna site. Standards on RFI will have to be reviewed, updated and assessed for their impact on the design of the SPS. The interface caused by the SPS to terrestrial system will also have to be evaluated and solution obtained.

ORIGINAL PAGE 25  
OF POOR QUALITY

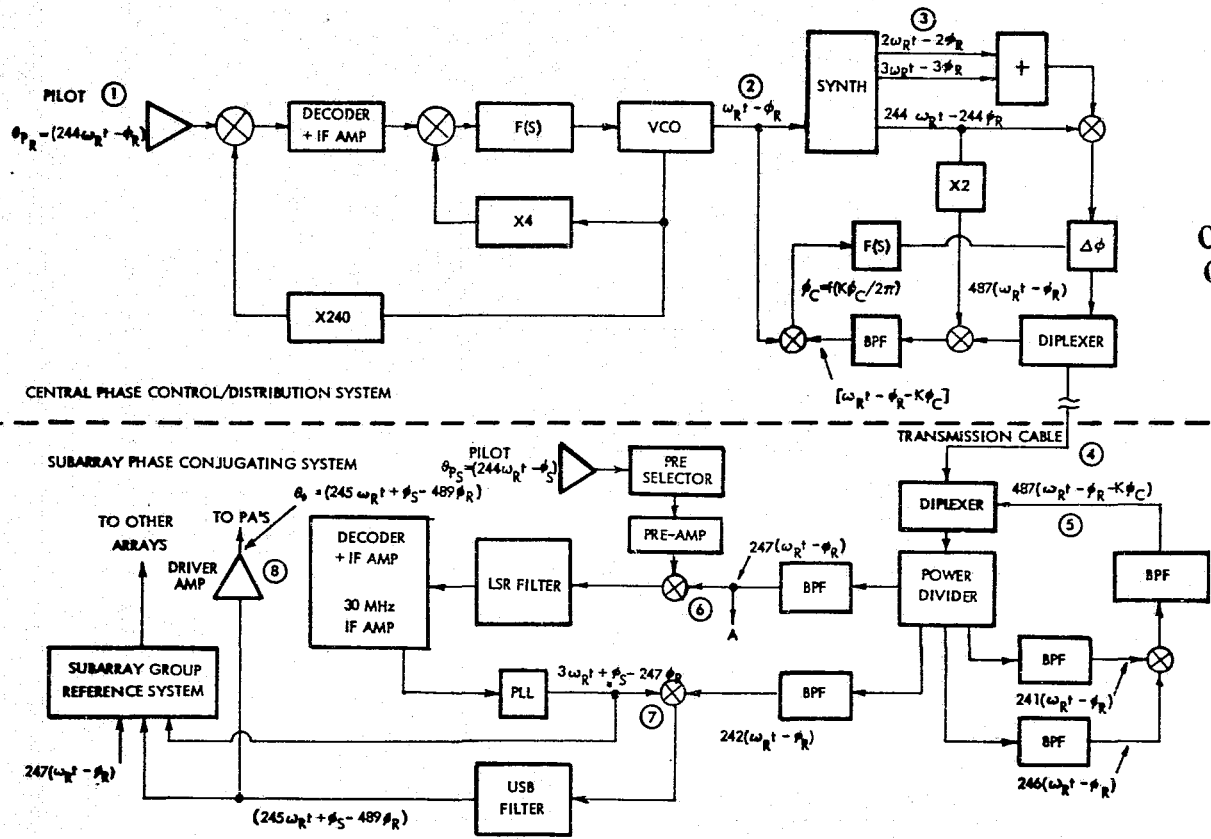


Figure 3.2-34. Phase Control Distribution System

3-136

SD 78-AP-0023-3

ORIGINAL PAGE IS  
OF POOR QUALITY

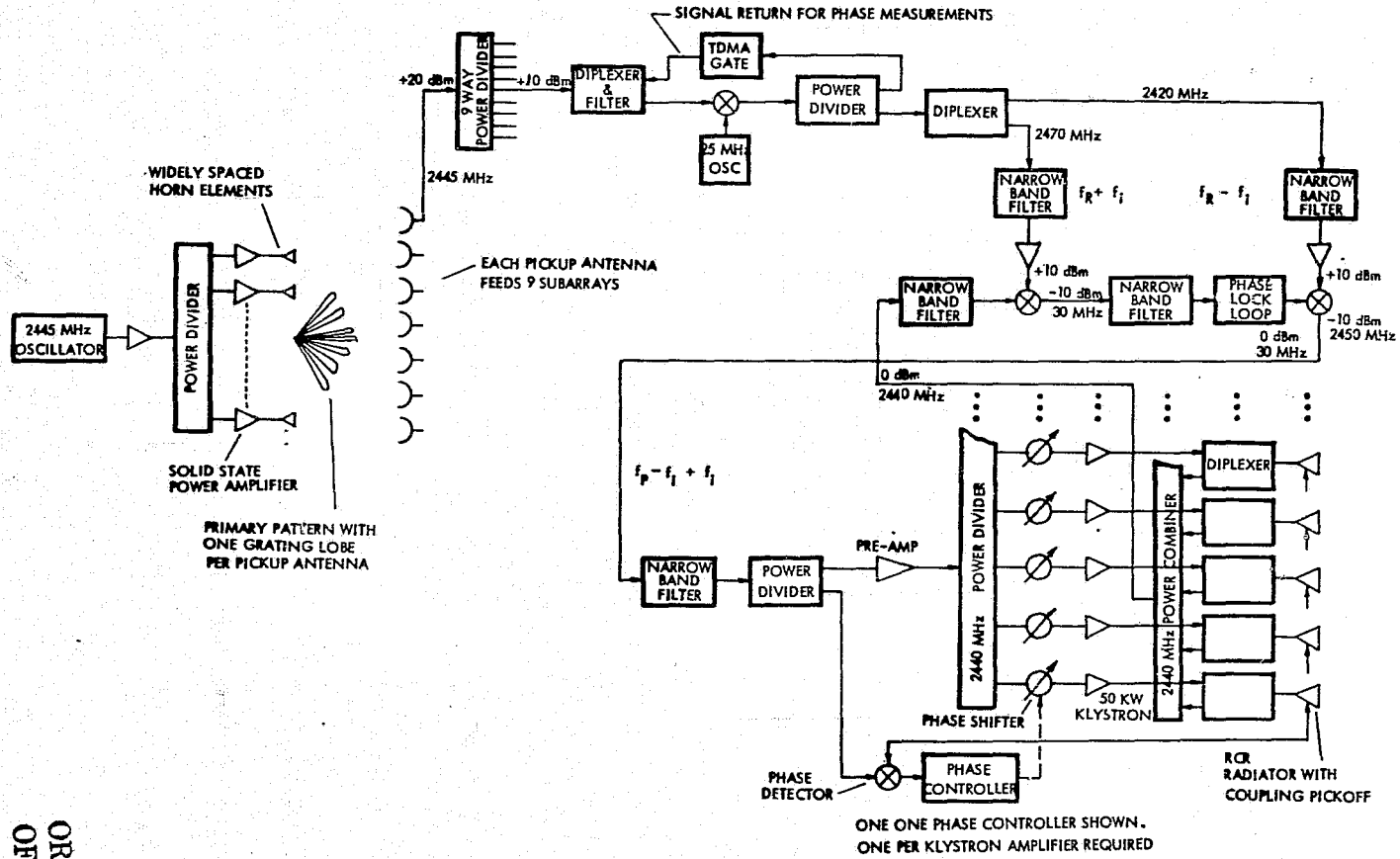


Figure 3.2-35. Antenna Phasing System



Table 3.2-10. Comparison of Four Phase-Conjugating Systems

FEATURE	PILOT OFFSET	REC SIG IN XMITTER NOISE	REF SYNCH WITH PILOT	LO SYNC WITH PILOT	PWR AMP $\beta$ SERVOED	HIGH ORDER MULTIPLIERS	XMITTER SIG PART OF CONJ. SCHEME	SUBARRAY STEERED
Houston	Yes	No	Yes	Yes	No	Yes	No	No
JPL	Yes	No	Yes	Yes	No	Yes	No	No
Previous Rockwell	Yes	Yes	No	No	Yes	No	No	No
Eclectic	No	No	Yes	No	Yes	No <sup>(1)</sup>	Yes	Yes

(1) Quadrupler with error reduced by factor of four by servo loop used

FEATURE	XMITTER NOISE CANCELLATION	REFERENCE DISTRIBUTION	REFERENCE DIST. METHOD	REF $\beta$ CONTROL SERVOS	REFERENCE $\beta$ CONTROL IN ZONES	COMPENSATION FOR IONOSPHERE & FILTER OFFSET ERRORS
Houston	No	Parallel to zones	Coax/Fiber Optic	Yes	Unspecified	No
JPL	No	Serial	Coax	No	NA	No
Previous Rockwell	No	Parallel	Space Fed	Yes <sup>(2)</sup>	NA	No
Eclectic	Yes	Parallel to zones	Coax	Yes	Resonant Feeders	Yes

(2) Time-shared

Table 3.2-11. Data Needed From DOE

PERMISSIBLE POWER DENSITY AT THE IONOSPHERE

BIOLOGICAL EFFECTS OF MICROWAVES AND PERMISSIBLE POWER DENSITY OUTSIDE OF RECTENNA SITE

RFI STANDARDS

### 3.3 POWER DISTRIBUTION AND CONTROL SYSTEM

The major options and trade studies for the power distribution and control subsystem are shown in Figure 3.3-1. An examination of voltage level and power form leads to the conclusion that high-voltage dc is preferred. For an ac system, no real mass advantage can be achieved unless high frequency is utilized (about 40 kHz). However, at these higher frequencies the conductor spacing, skin effects, EMI, capacitive coupling, and plasma losses become critical—which also produces additional losses.

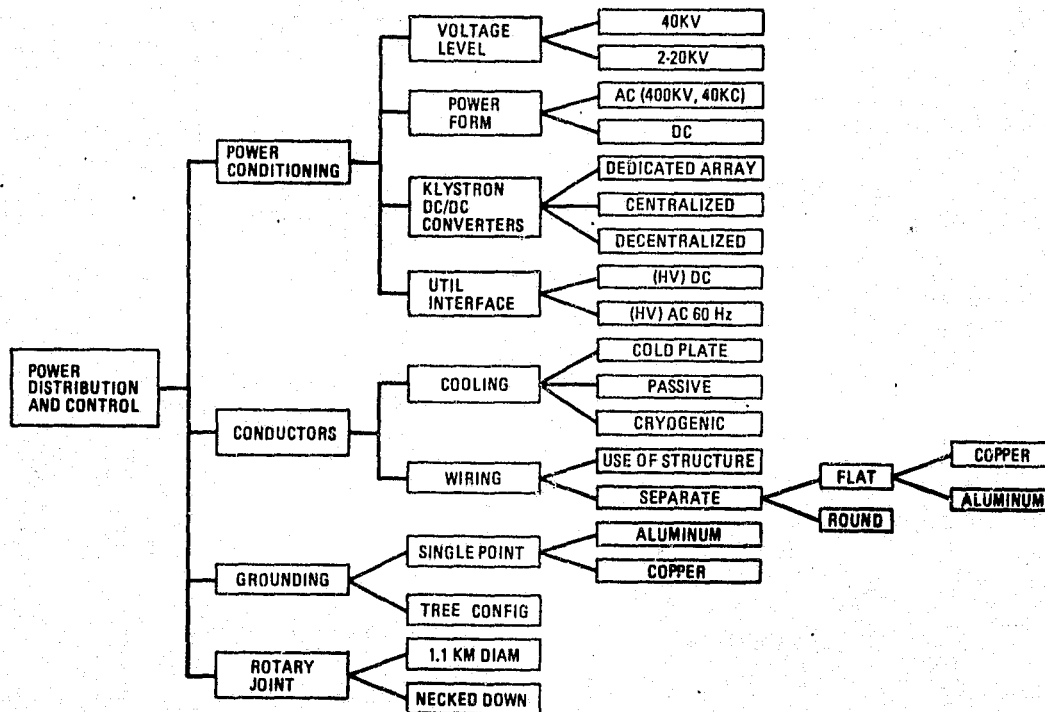


Figure 3.3-1. Power Distribution Control Subsystem Options

Each klystron (microwave power transmission subsystem) on the antenna requires six basic voltages and several secondary voltages. A mass comparison was made to select a dc-to-dc converter approach. Dedicated solar array panels showed the highest mass. A centralized dc-to-dc converter concept was selected with a total of 32 converter units. Further analysis is required to find the optimum number of converters.

Utility interface was taken to be high-voltage dc, since dc transmission is more efficient for delivering power over long distances. The rectenna diodes deliver 40 kV dc which is then converted to 500 kV dc through dc/dc converters, and then interfaced with the utility grid through switch gear. A 60-cycle (ac) interface would require additional power conversion equipment.

Cryogenic cooling of conductors was found to be interesting and potentially could improve system performance by eliminating line losses. The concept suffers



in that the technology development requirements are very severe—particularly when applied to a large planar configuration. Normally, the conductors will be cooled passively by radiation to free space.

Use of the primary structure for current-carrying showed little potential for mass savings, considering the magnitude of complexity introduced. A separate wiring concept was selected using flat aluminum conductors. A single-point ground, located at the center hub of the configuration, and a copper ground bar are favored when compared to multiple-tree configurations. The use of a tree configuration would mean a multiple-level ground which, in turn, would cause possible plasma losses.

Additional study is required to determine an optimum rotary joint configuration. Based on structural consideration, a 1.1-km-diameter rotary joint has been selected for point design. The selected concept has an obvious drawback when considering slip ring redundancy; however, it greatly simplifies structural load paths.

The subsequent trade study discussion will follow the outline shown in Figure 3.3-1: *power conditioning, conductors, grounding, and the rotary joint.*

### 3.3.1 POWER CONDITIONING

The trade studies for power conditioning were extensive because this involves selection of voltage level, power form, power converter approach for providing basic klystron voltages, and the definition of utility interface. These items are major configuration drivers, and results of these trades were utilized in the overall satellite system concepts evaluation.

#### Voltage Level

The major power user in the satellite system is the klystron dc-RF converters. For example, in the photovoltaic approach the solar array output is 9.75 GW, and 8.69 GW of this total is used to power the 135,864 klystrons on the microwave antenna. Each klystron requires 59.2 kW which is distributed between five basic voltages (i.e., 40 kV, 32 kV, 24 kV, 16 kV and 8 kV) plus several minor supporting voltages. Weight and size of the conductors were major considerations in selecting distribution voltage levels.

A comparison of the power distribution and control subsystem (PDS) conductor weights required for CR = 1, CR = 2, and CR = 5 photovoltaic configurations is shown in Figure 3.3-2.

The efficiencies shown are with minimum conductor masses permitted for a given satellite configuration. Corrections have been made for operating temperature. Figure 3.3-2 also shows quantity, length, mass, and current for the various elements representing the PDS conductors. A wide variation of possible temperatures was found between the configurations evaluated. Parametric results of conductor mass, as a function of efficiency for a family of temperatures, are presented in Figures 3.3-3 and 3.3-4. Superimposed on these figures are plots of solar blanket weights as a function of solar output power requirements necessary to provide 5 GW at the utility grid. Summing the two

	ITEM	QUANTITY	LENGTH (M)	MASS (10 <sup>6</sup> KG)	CURRENT AMPS (10 <sup>3</sup> )
<p>2 BAYS FOR 40 KV (20 BAYS) 13 KM 2 KM CR = 1 CONDUCTOR TEMP. = 36C η = 92%</p>	MAIN FEEDER SEC. FEEDER SUMMING TIE BAR TOTAL (20C) ADJ. TEMP.	12 120 4 8	11.7 X 10 <sup>6</sup> 650 1500 500	1.694 .074 .310 .058 2.136 2.264	37.5 3.75 112.5 56.25
<p>(21 BAYS) 12.6 KM 2.05 KM CR = 2 CONDUCTOR TEMP. = 80C η = 90%</p>	MAIN FEEDER SEC. FEEDER SUMMING TIE BAR TOTAL (20°C) ADJ. TEMP.	8 72 4 8	11.4 X 10 <sup>6</sup> 500 2750 500	1.205 .053 .827 .045 2.130 2.643	56.25 6.25 112.5 56.25
<p>(22 BAYS) 15.67 KM 3.35 KM CR = 5 CONDUCTOR TEMP. = 36C η = 88%</p>	MAIN FEEDER SEC. FEEDER SUMMING TIE BAR TOTAL (20°C) ADJ. TEMP.	40 220 8 16	13.2 X 10 <sup>6</sup> 50 3250 500	1.472 .003 .998 .037 2.510 2.698	11.25 1.02 56.25 28.12

Figure 3.3-2. Conductor Weight Comparisons

3-141

SD 78-AP-0023-3



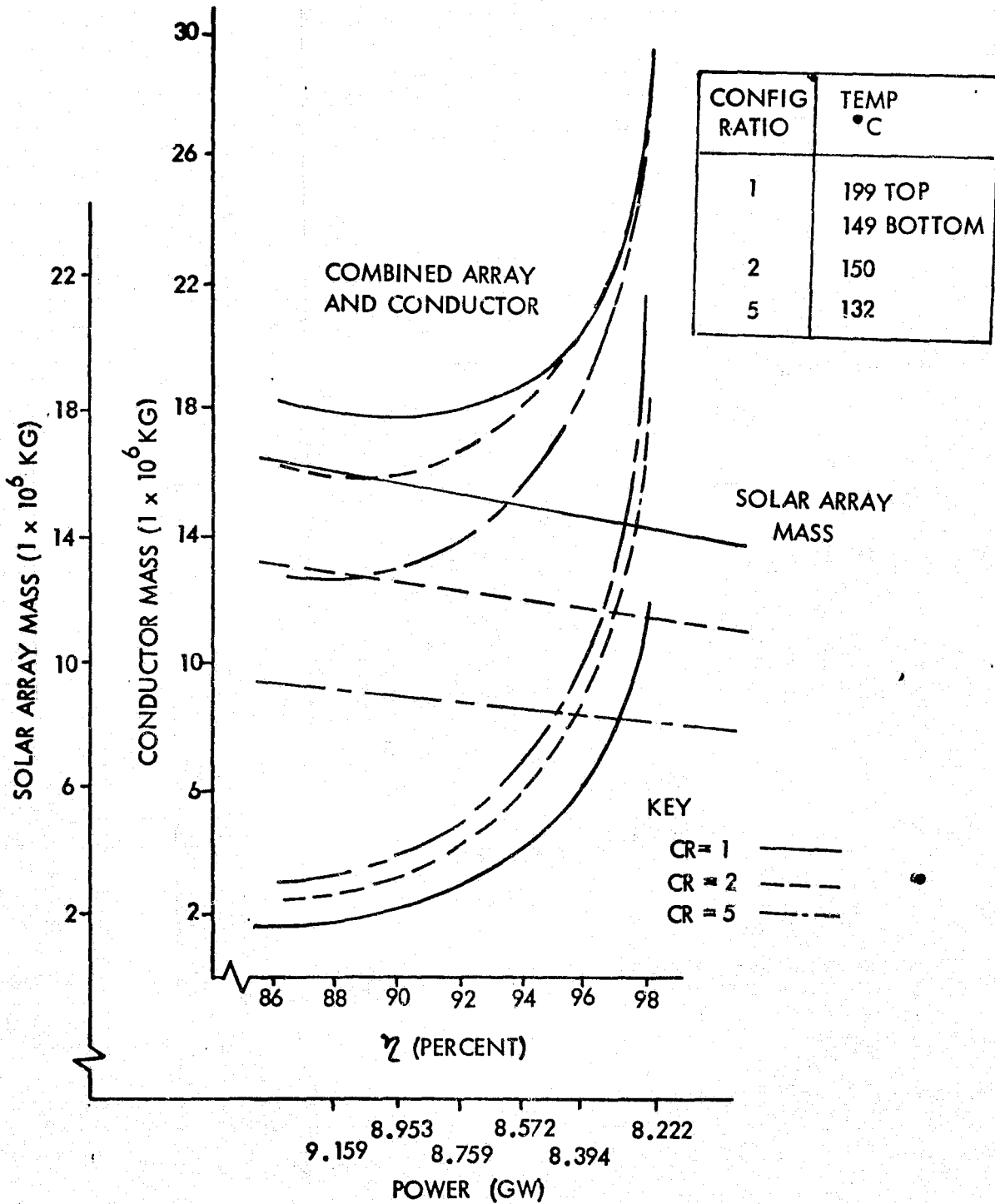


Figure 3.3-3. Solar Photovoltaic Conductor Mass

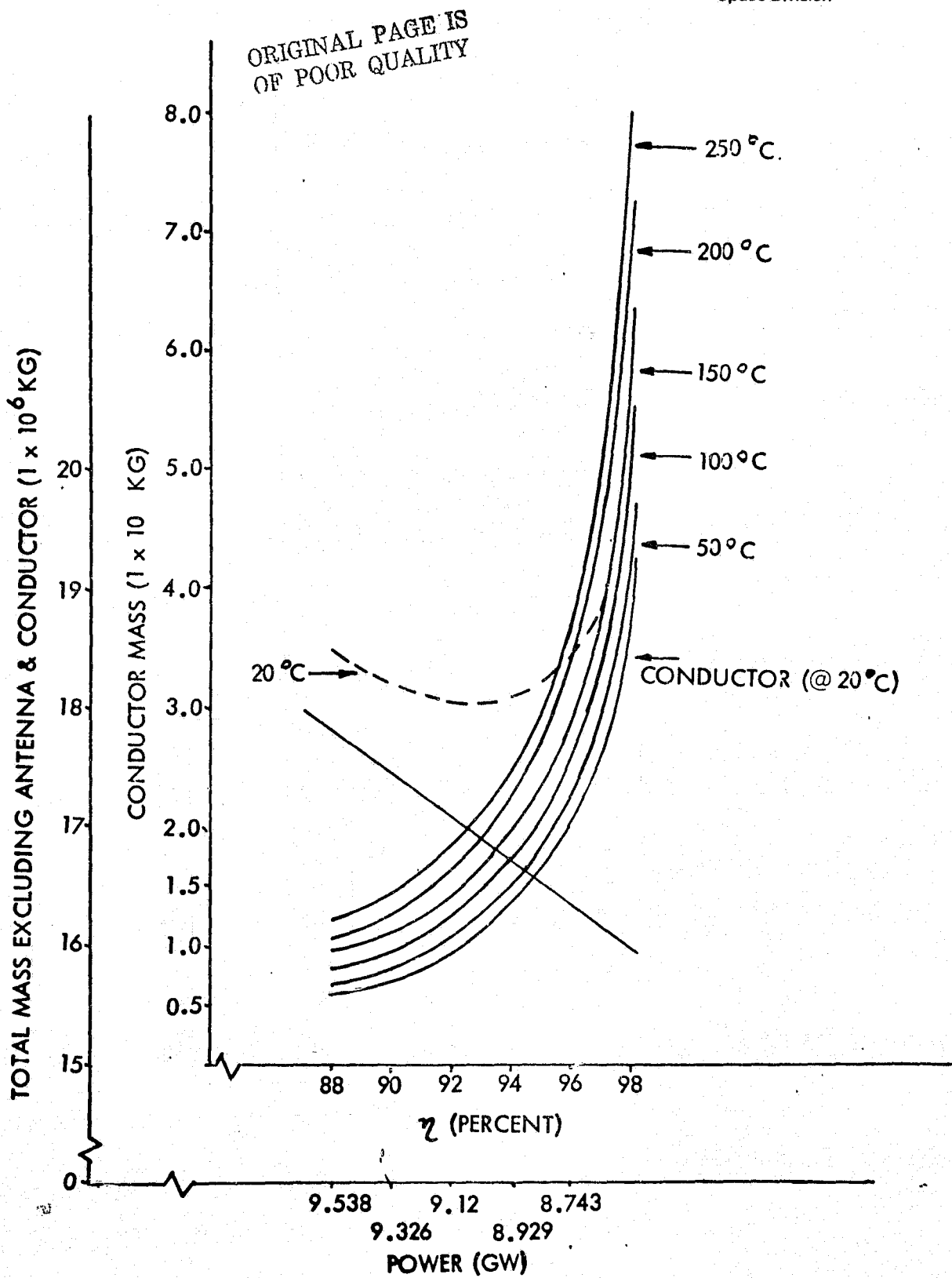


Figure 3.3-4. Solar Thermal (D.C. Configuration)  
Conductor Mass Vs. Efficiency ( $\eta$ )



mass curves, it was found that the optimum mass occurred at different efficiencies (indicating configuration dependence).

Conductor mass was calculated at 50°C, using 1-mm kapton insulation. Flat-aluminum (6101/T6) conductors were selected because they are able to dissipate heat better. Temperatures of conductors were determined by thermal analysis based on conductor location and current being transmitted. Conductor mass was then corrected to reflect the effect of temperature.

The equation used for calculating the conductor size is:

$$A = \frac{\gamma I L}{\Delta V} .$$

The equation used for calculating the conductor mass is:

$$W = \rho A L ;$$

where

- A = Cross-sectional area
- I = Amperes flowing in circuit
- $\gamma$  = Resistivity of wire ( $2.828 \times 10^{-6}$  ohm/cm for Al at 20°C)
- L = Length of conductor
- $\Delta V$  = Voltage drop in conductor
- W = Conductor mass
- $\rho$  = Density of aluminum ( $2.7 \text{ gm/cm}^3, 0.1 \text{ lb/in.}^3$ )

Conductor resistivity as a function of temperature:

$$\gamma = \gamma_0 [1 + 0.0039 \text{ ohm/cm } (T - T_0)] .$$

A block diagram of the power distribution system for the various concepts is presented in Figures 3.3-5, 3.3-6, and 3.3-7. The power distribution consists of the secondary feeders which interconnect the solar array with the regulators, the switch gears, the main feeders, the summing buses, the tie bars, the slip rings, the brushes, and the converters.

The initial CR = 1 photovoltaic system configuration was two troughs, 40 kV, with 20 bays having a wing length of 13 km and a width of 2 km. The mass of the nonrotating PDS system was found to be  $2.264 \times 10^6$  kg with an efficiency of 92 percent. This configuration was then modified to a triangular shape configuration having three troughs and 10 bays per wing. The length of one wing was 8.9 km, with a width of 4.584 km. The nonrotating mass of the PDS system was found to be  $2.798 \times 10^6$  kg with an efficiency of 94 percent.

In the initial trade studies, a 20-kV photovoltaic PDS was approximately 23.4 percent of the total SPS mass, compared to a 40-kV system at 15.0 percent. The higher voltage (40 kV) was the more desirable, based on mass savings.

A comparison of photovoltaic power distribution mass for configurations CR = 1, CR = 2, and CR = 5 is shown in Table 3.3-1; these masses do not include subsystem cabling or antenna distribution because these are assumed equal in all three configurations.



ORIGINAL PAGE IS  
OF POOR QUALITY

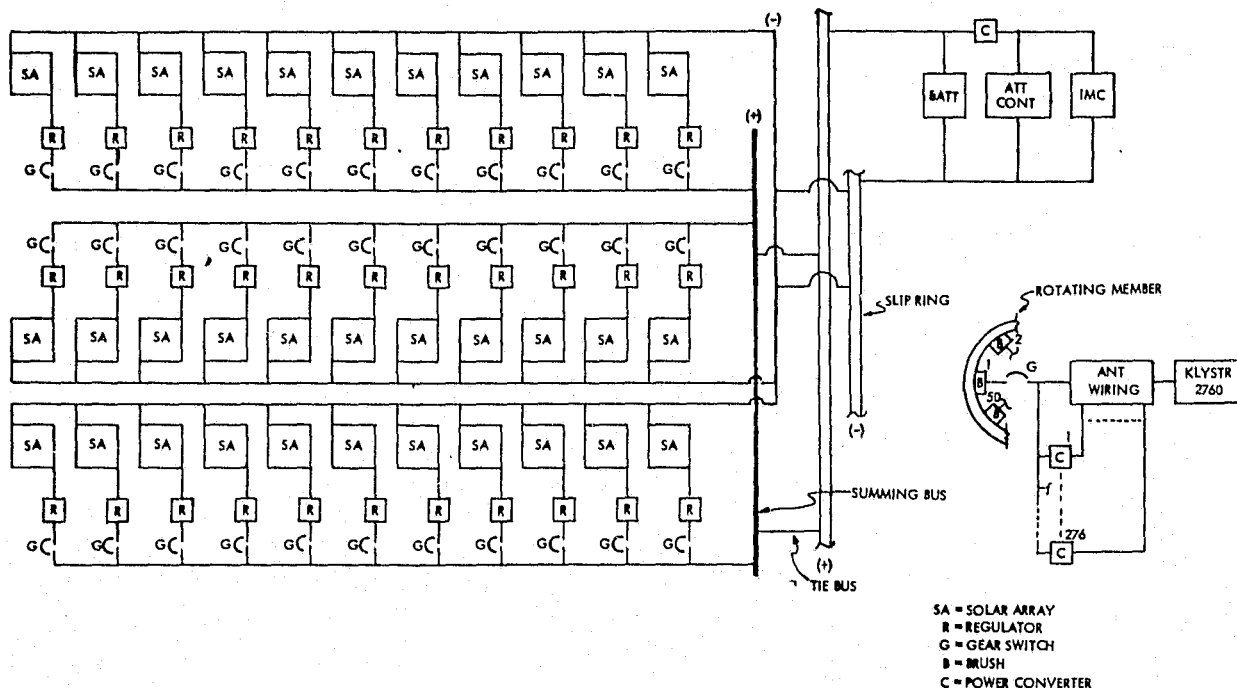


Figure 3.3-5. Power Distribution of Photovoltaic CR-1 Configuration  
(Left Wing Solar Array Shown - Right Wing Symmetrical)

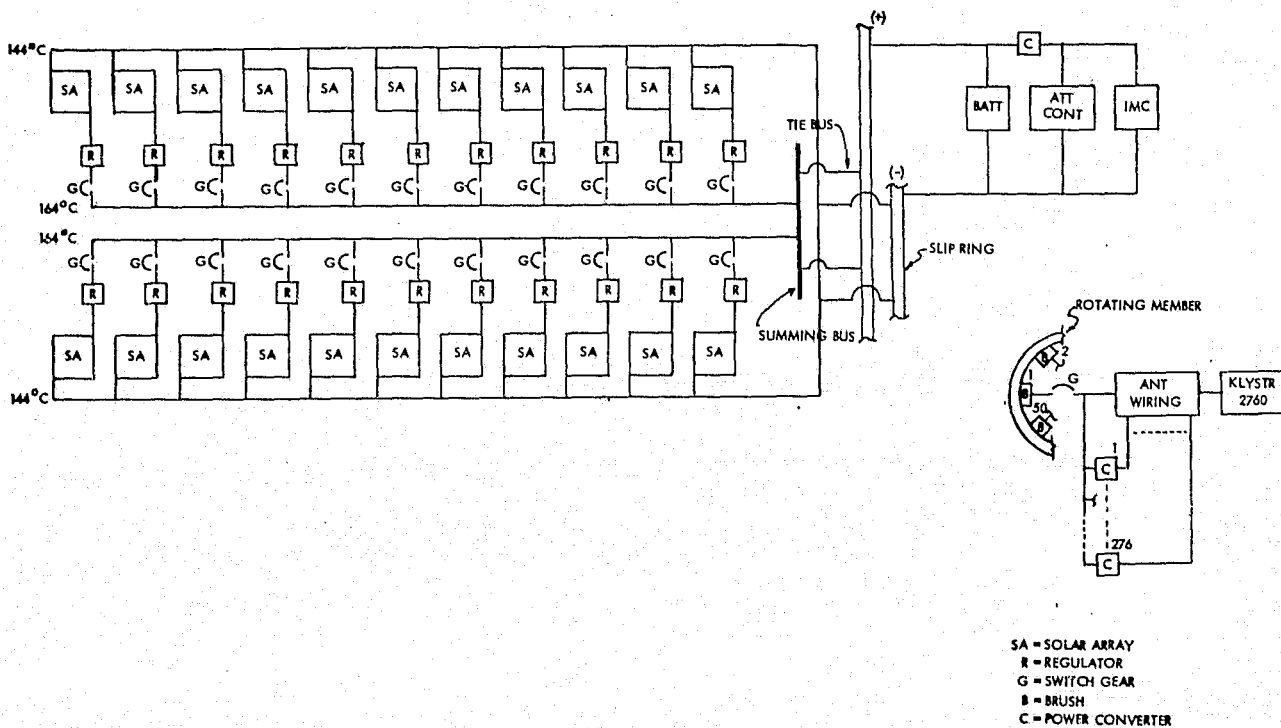


Figure 3.3-6. Power Distribution of Photovoltaic CR-2 Configuration  
(Left Wing Solar Array Shown - Right Wing Symmetrical)

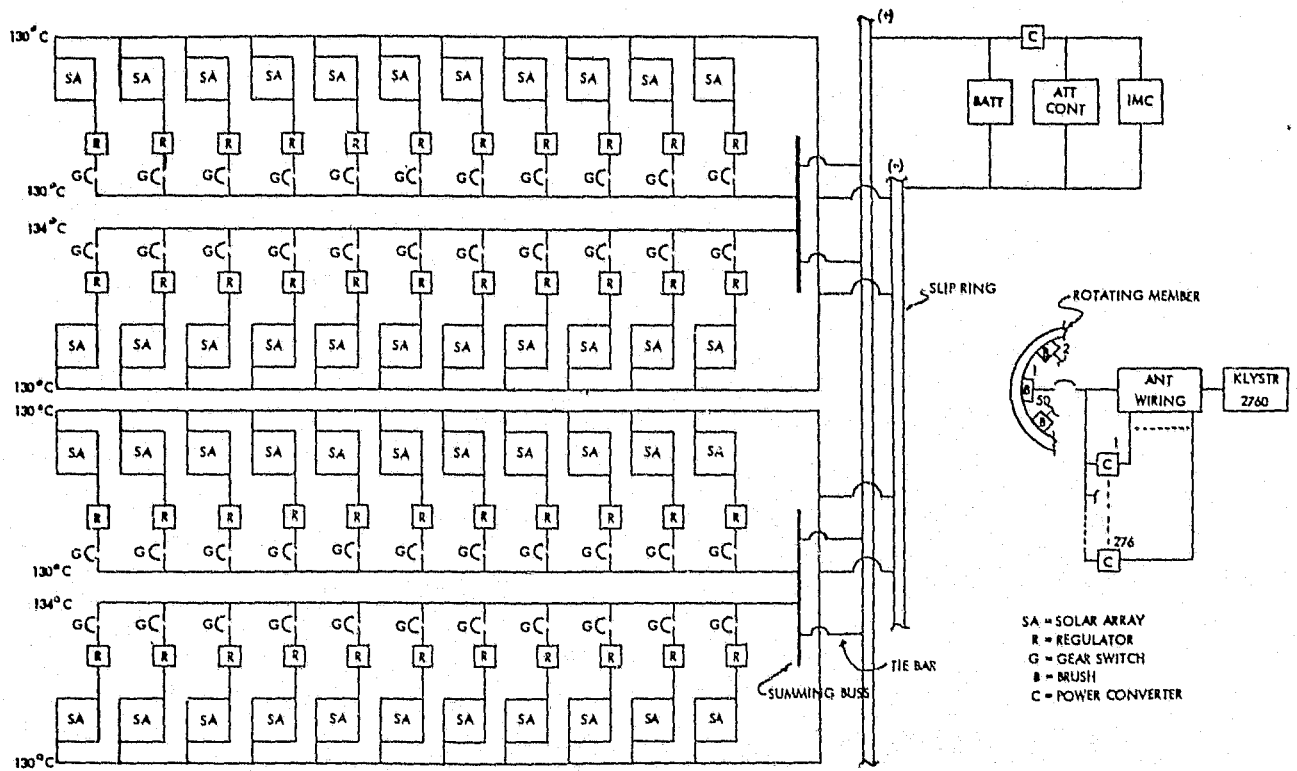


Figure 3.3-7. Power Distribution of Photovoltaic CR-5 Configuration (Left Wing Solar Array)

Table 3.3-1. Power Distribution Mass Comparisons

	CR=1 ( $1 \times 10^6$ KG) $\eta=92\%$ T=36°C	CR=2 ( $1 \times 10^6$ KG) $\eta=90\%$ T=80°C	CR=5 ( $1 \times 10^6$ KG) ACTIVE $\eta=88\%$ T=36°C
CONDUCTOR	2.264	2.643	2.698
INSULATION (IMM KAPTON)	.0446	.028	.0395
ROTARY TRANSF SYST (SLIP-RINGS, BRUSHES, SHOES)	.347	.347	.347
SWITCH GEARS (SOLID STATE)	.0259	.0273	.0283
PWR CONDITIONING (REG & CONVERTERS)	1.027	1.027	1.027
RECTIFIERS	—	—	—
BATTERIES	.006	.006	.006
STRUCTURAL INTG (10% OF WEIGHT)	.371	.408	.415
TOTAL PDS MASS (EXCLUDING ANTENNA WIRING & SUBSYST CABLING)	4.086	4.476	4.560



Power Form

The trade studies associated with the power form consisted in evaluating whether ac or dc PDS would be most suitable for power transmission. The objective of the study was to determine which system approach minimized mass and optimized efficiency. The trade study was performed considering the solar thermal system approach since, in this case, the power source (generators) already had the capability of delivering either ac or dc power. The output of the generators was initially selected to be 40 kV at 400 Hz; this power was then boosted to 400 kV through step-up transformers. The power was then transmitted on the main power buses at this high level and stepped back down to 40 kV on the antenna for supplying power to the klystrons. Various other frequencies (5 kHz, 10 kHz, and 40 kHz) were also evaluated. The results are presented in Table 3.3-2. The studies indicated that the ac system was less desirable than the dc system, since the mass savings achieved by the conductors

Table 3.3-2. Solar-Thermal AC Versus DC Comparison

ITEM	40 KV D.C. CONFIGURATION (10 <sup>6</sup> KG)	40 KV (AC) GENERATOR, 400 KV TRANSMISSION		
		A.C. CONFIGURATION AT 5 KHZ (10 <sup>6</sup> KG)	A.C. CONFIGURATION AT 10 KHZ (10 <sup>6</sup> KG)	A.C. CONFIGURATION AT 40 KHZ (10 <sup>6</sup> KG)
CONDUCTOR ( <sup>38°C</sup> / <sub>88°C</sub> )	1.094	.022	.022	.022
INSULATION (IMM KAPTON)	.007			
ROTARY TRANSFER SYST (SLIP-RINGS, BRUSHES, SHOES)	.347	.347	.347	.347
SWITCH GEAR (SOLID STATE)	.0096	.0096	.0096	.0096
RECTIFIERS	.450	.900	.900	.900
FREQ CONVERTER	-	.250	.250	.250
TRANSFORMERS	-	2.538	.724	.020
POWER CONVERTER	1.027	1.027	1.027	1.027
BATTERIES	.006	.006	.006	.006
STRUCTURAL INTEG.	.249	.510	.328	.258
TOTAL (EXCLUDING ANTENNA & SUBSYSTEM CABLING)	3.189	5.609	3.614	2.839

NOTE. ABOVE 5 KHZ - WIRE SPACING, INSULATION, EMI AND POWER LOSSES DUE TO SKIN EFFECTS BECOME CRITICAL.

were very small in comparison to the mass added by the transformers and rectifiers. In addition, the ac system efficiency was found to be less (74.1%) compared to the dc system (79.6%). The reduction in efficiency resulted in the added elements which were required to configure the overall system (choppers, transformers, rectifiers) for ac transmission. Transformer mass for the various frequencies is shown in Table 3.3-3.

The values in the first column (Table 3.3-3) were extrapolated initially from frequency curves with the assumption that all parameters remain the same within the frequency band selected. The second column on the table shows the results of a computer analysis performed by Westinghouse, wherein the frequency

ORIGINAL PAGE IS  
OF POOR QUALITY



and voltage levels were extended to 64 kHz and 80 kV from that shown previously in SAM-679-4 (see Report LY20686, *Final Report on Satellite Power Systems Study*, December 1977). At frequencies of 40 kHz and above, a mass saving is deemed possible. It should be noted, however, that at these frequencies additional problems may occur. These include EMI filtering (which could increase mass considerably), wire spacing, insulation, and power losses due to skin effects.

Table 3.3-3. Comparison of Transformer Mass Vs. Frequency

Frequency	Transformer Mass (kg)	
	Extrapolated	Liquid Metal Transformer Computer Results
5 kHz	$2.538 \times 10^6$	$1.485 \times 10^6$
10 kHz	$1.27 \times 10^6$	$1.162 \times 10^6$
40 kHz	$0.19613 \times 10^6$	$0.8072 \times 10^6$

Klystron Power Converter

The objective of this trade study was primarily concerned with determining a point design configuration which would result in minimum PDS mass and cost. Three options were evaluated—dedicated array, decentralized array, and centralized array.

Dedicated Array. In the dedicated array study, the objective consisted of determining how various arrays could be dedicated to different voltage levels so that the klystron high-voltage requirements (40 kV, 32 kV, 24 kV, 20 kV, 16 kV, and 8 kV) could be satisfied. For the low-level voltage (20 V) requirements, dc/dc converters would still be utilized. It was thought that the utilization of this technique could minimize or even eliminate the need to develop expensive (and heavy) high-voltage dc/dc converters. Study results showed that this technique did not produce the desired objective since the total mass of the PDS, with a dedicated array concept, was found to be  $7.687 \times 10^6$  kg. This is considerably greater than a decentralized dc/dc converter approach, as indicated in Table 3.3-4. Furthermore, this technique required five additional sets of slip rings on each wing—a total of 12 sets on each satellite.

Decentralized Technique. The objective of this trade study was to have all solar arrays at the same nominal voltage level (40 kV), and then transferring this high voltage through slip rings to the microwave antenna. The voltage at the microwave antenna would then be converted through dc/dc converters (at each klystron) to the desired voltage levels. The total mass of the PDS was found to be  $4.75 \times 10^6$  kg. This method was not favored, even though it showed the lowest overall PDS mass, because of the excessively large number of dc/dc converters (135,864 individual converters) necessary to satisfy klystron voltage requirements. Considerable research and development effort would have to be performed to develop a high-voltage dc/dc converter with the desired mass density of 0.07 kg/kW. It was assumed, however, that such converters could be developed within the 1985 time frame.



Table 3.3-4. Klystron Voltage Converter Concept Comparisons

ITEM	CONCEPT OPTIONS			
	DEDICATED ARRAY 6 VOLTAGES	2 ARRAY VOLTAGES 20 KV, 40 KV	DECENTRALIZED DC/DC EACH KLYSTRON	✓CENTRALIZED DC/DC EACH BRUSH CIRCUIT
MAIN FEEDERS	1.54	0.573	0.382	0.342
SECONDARY FEEDERS	0.077	0.067	0.045	0.045
SUMMING BUS	0.89	0.778	0.519	0.102
TIE BAR	0.262	0.228	0.152	0.162
INSULATION	0.043	0.043	0.043	0.043
SWITCH GEAR	0.244	0.244	0.244	0.244
REG & CONVERTER	0.673	0.673	0.673	0.009
ROTARY JOINT	0.416	0.416	0.208	0.208
AC THRUSTER CABL'G	0.011	0.011	0.0053	0.0053
BATTERY	0.006	0.006	0.006	0.006
SUPPORT STRUCT	0.416	0.303	0.228	0.121
SUB NON-ROTATING	4.578	3.336	2.505	1.327
CABLE FROM ROT. TO ANT.	0.496	0.822	0.548	0.636
ANTENNA TIE BAR	0.696	0.312	0.208	0.696
ANTENNA CABLES	0.11	0.153	0.102	0.132
ANTENNA MODULE CABLE	0.031	0.031	0.031	0.031
SWITCH GEAR	0.930	0.632	0.316	0.931
ROTARY JT	0.417	0.139	0.139	0.139
DC/DC CONV	-	0.383	0.638	0.704
INSULATION	0.2	0.090	0.06	0.20
SUPPORT STRUCT	0.226	0.256	0.204	0.331
SUB ROTATING	3.109	2.817	2.244	3.769
TOTAL PDC	7.687	6.153	4.75	5.096

- ✓ PREFERRED CONCEPT (CENTRALIZED):
- SMALL WEIGHT PENALTY
  - HIGHER OVERALL EFFICIENCY
  - LOWER COST

Centralized Technique. The objective of this technique was to eliminate the need for individual high-voltage dc/dc converters and to obtain the required high-voltage requirements through a centralized method, utilizing series regulators for the small number of precision voltages utilized; dc/dc converters would still be used for the low-voltage (20 V at 0.8 kW) requirements. The total mass of the PDS was found to be  $5.09 \times 10 \text{ kg}^6$ . This technique was selected as being preferred over the other two techniques because considerable cost savings can be achieved by the elimination of the individual high-voltage dc/dc converters. The density of the series regulator was estimated to be approximately  $0.07 \text{ kg/kW}$  at a volume of approximately  $31.17 \text{ m}^3$ . This technique was recommended for the point design concept.

A total of 32-series regulators are specified. The regulators produce the desired voltages and transfer the power to the various buses from which it is distributed to the klystrons. Low-voltage (low-power) requirements at the klystrons are obtained through individual dc/dc converters tapped onto the 8-kV lines.

Utility Interfaces

The objective of this trade study consisted of determining how to process the received energy (rectenna) and transmit it to the utility grid interface. A brief diagram of a typical power receiving station is presented in Figure 3.3-8. The basic blocks of the receiving station consist of the following elements.

- A rectenna farm which receives the microwave energy from the SPS and converts it to dc power. There is a total of 813 rows of rectenna; each row is interconnected in such a manner as to produce a voltage of 40 kV and approximately 205 A (minimum).



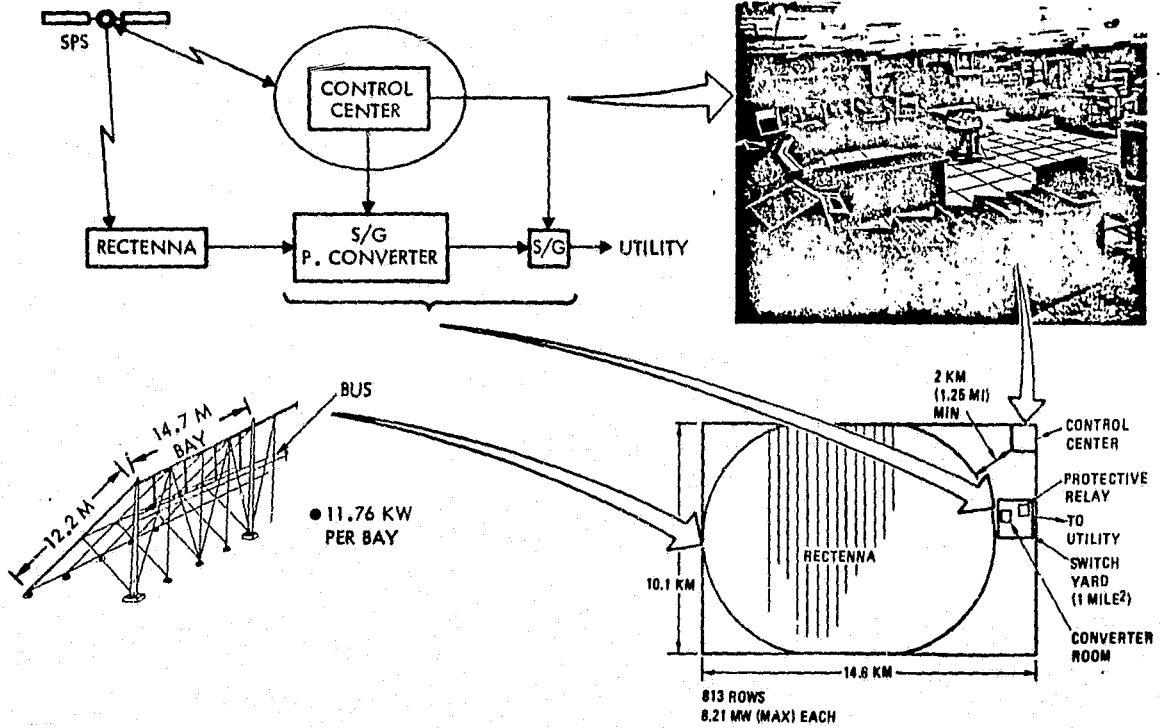


Figure 3.3-8. PDC Ground Facility

- A switchyard which sums all of the rows from the rectenna through switch gears to the main and auxiliary buses. The power is then transferred to the converters in the converter room.
- A converter room which houses the dc/dc converter which boosts the voltage from 40 kV to 500 kV for delivery to the utility grid lines. The high voltage power is transferred to the utility grid lines through isolation switch gears.
- A control center which houses the computer that monitors and controls the rectenna outputs as well as the SPS outputs. In addition, it is interfaced with the utility grid lines to transfer the power where needed.
- A protective relay facility which has a number of real-time units (RTU's) for maintaining and isolating the individual rows to protect the maintenance crew when performing required maintenance.

In this trade study, the interface with the utility grid was assumed to be dc; dc transmission is more efficient for delivering power over long distances. If, however, short distances would be utilized and ac transmission required, under those conditions the dc/dc converters would have to be replaced by dc/ac inverters. The efficiency of the dc/dc converters was estimated to be 98.5% which is easily achieved since weight and size are not drivers in a

ground installation. Aluminum conductors and buses with an efficiency of 91 percent were considered for transmission. The crossed-field interrupter type switch gears were selected for switchyard usage. It is estimated that the efficiency of the switch gears will be 99.9 percent.

### 3.3.2 CONDUCTORS

In the study of space power systems, transmission from the source to the user is a critical part of the overall design in terms of mass, size, cost, and efficiency. Initially, six basic configurations were evaluated with 21 variations; these were later narrowed down to six specific configurations. The PDS was divided into two major areas—nonrotating solar array, and rotating microwave antenna. It was anticipated that there would be a large number of variations on the nonrotating member, holding the antenna section as a common element. Conductor mass was shown in Section 3.3.1, and initial configurations were developed based on minimum PDS mass. It was realized that minimum mass efficiencies were not necessarily minimum cost design. Therefore, after concept evaluations had driven the program to specific point design selections, a parametric cost and mass comparison was made which resulted in the selection of optimum conductor efficiency based on cost. Figure 3.1-31 showed mass and cost of combined subsystems as a function of efficiency. Areas, mass and costs of solar cells, reflectors, array conductors and structure were calculated including launch costs of \$10/kg to \$60/kg to GEO. As the distribution efficiency increases, the solar blanket and reflector size decrease. The structure mass decreases, and the conductor mass increases. The result is that overall system mass increases monotonically as the distribution efficiency increases. The cost curves, however, reach a minimum depending on the launch costs and then increase again with efficiency. The locus line for the minimum cost is shown and, for the SPS photovoltaic point design configuration, the nominal distribution efficiency was selected to be 94 percent for the range of launch costs of \$40 to \$80/kg to GEO.

#### Cooling

The conductors will normally be passively cooled by radiation to free space. A cursory investigation of superconductivity was performed to determine if such a technique would be feasible for SPS conductor mass reduction. The study indicated that such a technique is indeed feasible since a large quantity of heat can be removed by use of vaporized helium (He) moving in a pipe. In general, the conductors would be sized for low efficiency (approximately 80%); then, through the use of superconductivity, the efficiency would be increased to 98 percent (conductors would be submerged in the helium vapor). The mass of the conductor can be reduced by a factor of 9, utilizing this technique (reducing weight as calculated for 98% efficiency versus 80% efficiency). In addition, the 98-percent efficiency permits a reduction in overall solar blanket mass/cost requirements. Also, if superconductivity is lost, then the system momentarily would experience a tolerable 18-percent power loss which is within the generally accepted 20-percent tolerance allowed by the utility industry. However, large superconductivity systems have not been developed at this time; hence, a detailed study of a proposed system for SPS should be conducted to determine the mass penalty of the superconductivity system elements (helium fluid, pumps, radiators, reservoirs, etc.) for determining the net mass savings.



Operations temperature was established for this study by designing to minimum conductor width by operating at the highest allowable temperature. The maximum operating temperature for 6101/T6 aluminum was considered to be 100°C.

Wiring

Early SPS studies found that power conductor mass equaled structural mass and that the mass for each element was near  $10 \times 10^6$  kg for 10 GW photovoltaic satellites. Therefore, most studies combined the two functions and used structure to carry both positive and return power. Resultant mass saving was not as great as might first be expected, however, due to different design requirements of structural members and power conductors. Structural design called for standard uniform 12- to 15-mil thickness beams of high-strength aluminum that could be fabricated in space with one type of beam assembly machine. Power conductors, on the other hand, required tapered members of high conductivity but low-strength aluminum. Tapered conductors were necessary to handle ever increasing current as power was collected over a wide area of solar cells and delivered to slip rings at the base of the solar array wings. It was also concluded that in those satellites employing waffle-type construction, power could not be carried in both X and Y axes due to insulation problems, although the Boeing Company devised a special V-structure for the main frame that avoided this limitation.

The preferred arithmetic favoring the combination of structures and power conductors is shown in Table 3.3-5. Structural mass is  $5 \times 10^6$  kg in either axis, while power conductor mass is  $3 \times 10^6$  kg in the short Y-axis and  $6 \times 10^6$  kg in the

Table 3.3-5. Conducting Structure Comparison for 10-GW SPS

Separate Structure		Integrated Structure
Y-axis structure	$5 \times 10^6$ kg	$5 \times 10^6$ kg
X-axis structure	$5 \times 10^6$ kg	$6 \times 10^6$ kg
X-axis conductor	$6 \times 10^6$ kg	
Y-axis conductor	$3 \times 10^6$ kg	$3 \times 10^6$ kg
Total	$19 \times 10^6$ kg	$14 \times 10^6$ kg

long X-axis for an elliptical planform shape. The ideal integrated approach, shown in the table, reduces mass from 19 to  $14 \times 10^6$  kg by replacing the  $5 \times 10^6$  kg structural X-axis member with a  $6 \times 10^5$  kg power conductor. The full benefit was not realized because electrical grade aluminum lacked sufficient structural strength. The following compromise was necessary:

- Original 1060/H18, 60% conductivity,  $6 \times 10^6$  kg, 13% loss
- Structural 2219/T62, 30% conductivity,  $8 \times 10^6$  kg, 17% loss
- Compromise 2014/T6, 38% conductivity,  $7 \times 10^6$  kg, 15% loss

Therefore, even though mass and power loss were increased to make the conductor suitable for structural purposes, the resultant mass reduction from  $19 \times 10^6$  kg



to  $15 \times 10^6$  kg was justification to adapt a baseline integrated structure/power conductor design for 10-GW satellites.

A brief investigation was made of candidate types of aluminum in search of a combination of high structural strength and high electrical conductivity. Results are shown in Table 3.3-6. The candidate aluminum types were given a "figure of merit" based on the following material properties:

$$\text{Mechanical performance} = \frac{\text{Tensile yield strength}}{\text{Density}}$$

$$\text{Figure of merit} = \frac{\text{Yield strength}}{(\text{Density})^2 \times \text{Resistivity}}$$

Note that structural grade aluminum 2219/T62 and electrical grade aluminum 1060/H18 received a poor figure of merit. The common high-temperature class 2024/T6 rated very high, but 2014/T6 (which had application on the Apollo program) was selected for operation at 100°C.

Table 3.3-6. Candidate Aluminum Alloys for Electrical Conductive Structures

ALUMINUM MATERIAL	DENSITY (gm/cc)	TEMP (°C)	RESISTIVITY @ 20°C	ELECT CONDUCTANCE %Cu "C"		YIELD STRENGTH (KPST)	FIGURE OF MERIT (2)			RELATIVE RATE		
				EQUAL WT	EQUAL VOL		@ 26°	@ 100°	@ 149°	@ 26°	@ 100°	@ 149°
2219-T62 (STRUCTURE REF.)	2.81	26°	5.6	104	31	37	145	133	110	7	6	7
		100°				34						
		149°				28						
1060-H18	2.70	26°	2.828	201	61	16	134	109	84	8	8	8
		100°				13						
		149°				10						
5052-H38	2.68	26°	4.94	116	35	37	180	180	146	6	7	6
		100°				37						
		149°				30						
4032-T6	2.69	26°	4.94	115	35	46	222	212	160	4	5	5
		100°				44						
		149°				33						
2024-T6	2.77	26°	4.55	122	38	50	248	272	163	2	2	4
		100°				55						
		149°				34						
5050-H38	2.69	26°	3.46	165	50	29	200	221	273	5	3	3
		100°				32						
		149°				25						
2014-T6	2.80	26°	4.39	127	40	60	306	286	189	1	1	2
		100°				56						
		149°				37						
2018-T61	2.81	26°	4.32	126	40	46	233	218	203	3	4	1
		100°				43						
		149°				40						

NOTES: (1) TYPICAL ALUMINUM HANDBOOK PROPERTIES GIVEN. TO BE VERIFIED  
(2) ELECTRICAL RESISTIVITY & TEMP. COEFFICIENT UNKNOWN @ ELEVATED TEMPS, ASSUMED "C" REMAINS LINEAR

Potential savings through integrated structure designs were greatly diminished when the SPS size was reduced to 5 GW and transmission voltage was increased to 40 kV. A comparison is shown in Table 3.3-7. Here, the potential ideal mass reduction is minimal ( $4$  to  $3.25 \times 10^6$  kg) but the power loss would be reduced slightly because the X-axis structure ( $1.5 \times 10^6$  kg) is much greater than X-axis requirements for power conduction ( $0.75 \times 10^6$  kg). Power loss was reduced by one percent even with the use of structural grade 2014/T6 aluminum.

C-2



Table 3.3-7. Conducting Structure Comparison for 5-GW SPS

Separate Structure		Integrated Structure
Y-axis structure	$1.5 \times 10^6$ kg	$1.5 \times 10^6$ kg
X-axis structure	$1.5 \times 10^6$ kg	$1.5 \times 10^6$ kg
X-axis conductor	$0.75 \times 10^6$ kg	
Y-axis conductor	$0.25 \times 10^6$ kg	$0.25 \times 10^6$ kg
Total	$4.0 \times 10^6$ kg	$3.25 \times 10^6$ kg

Integrated structure design was not selected for the 5-GW SPS baseline because the potential mass saving was small and did not appear to justify the added complexity of integrating structure and power conductor designs.

### 3.3.3 GROUNDING

A brief evaluation of grounding schemes has been performed and it was found that the preferred concept would be to utilize a single-point grounding scheme. The single ground point would be located at the center of the SPS nonrotating section with the ground bus thermally isolated from the structure. Copper was selected for the ground bus because of the high temperatures. An important factor that needs to be kept in mind is that the electrical system should not be electrically connected to structure on both sides of the slip rings; otherwise, there may be electrical conduction through the rotating support structure in parallel with the slip rings. This is an undesirable situation.

### 3.3.4 ROTARY JOINT

The SPS will require the transfer of gigawatts of power across an interface that must have 360-degree rotation capability. Rotary joint concepts that have been investigated include solid slip rings, rotary transformers, rolling contacts, rollamite systems, and liquid-metal slip rings. All spacecraft flown today have used the brush-type slip ring for a rotary joint requiring 360-degree rotation. Rockwell has conducted design studies of the brush slip ring assembly for a 5-GW SPS system. The slip ring assembly consists of two positive and two negative rings, each rated at 4 GW.

Details of the assembly concept are illustrated in figures 3.3-9, 3.3-10, and 3.3-11.

Analysis of rotary joint efficiency factors and mass for the slip ring design has shown that the drive motor power requirements and mass are negligible, considering both brush friction and solar array inertia (3 hp for a 0.1 friction factor). In addition, slip ring power transfer losses are governed by heat rejection considerations and do not have a significant effect on the SPS efficiency. Total mass of the four ring and brush shoe assemblies (less supporting structure and electrical cabling) is approximately 173,000 kg, which represents about 0.2 percent of the SPS mass.



ORIGINAL PAGE IS  
OF POOR QUALITY

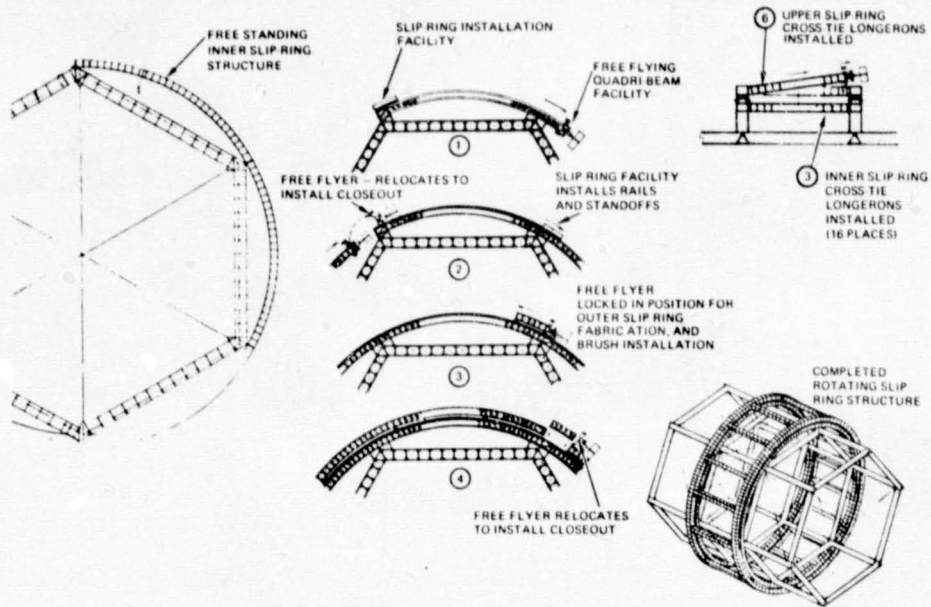


Figure 3.3-9. SPS Rotating Hub Assembly  
Free-Standing Slip Ring Structure

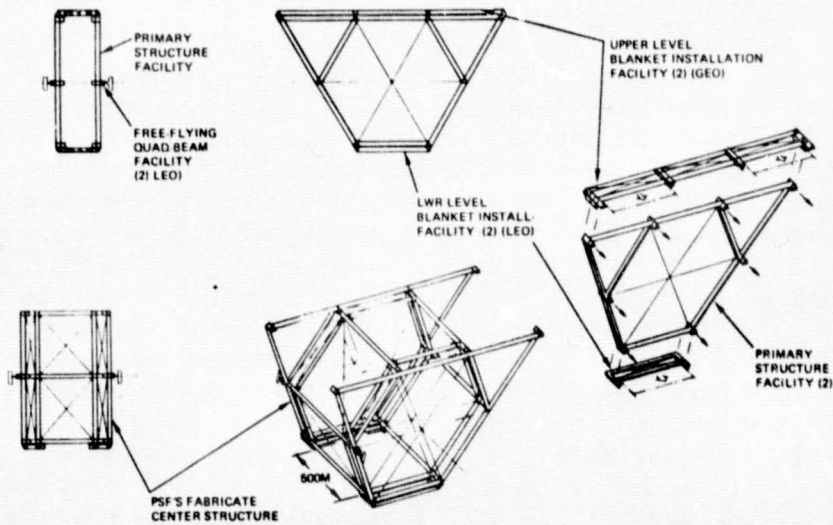


Figure 3.3-10. SPS Rotating Hub Structure  
LEO/GEO Assembly

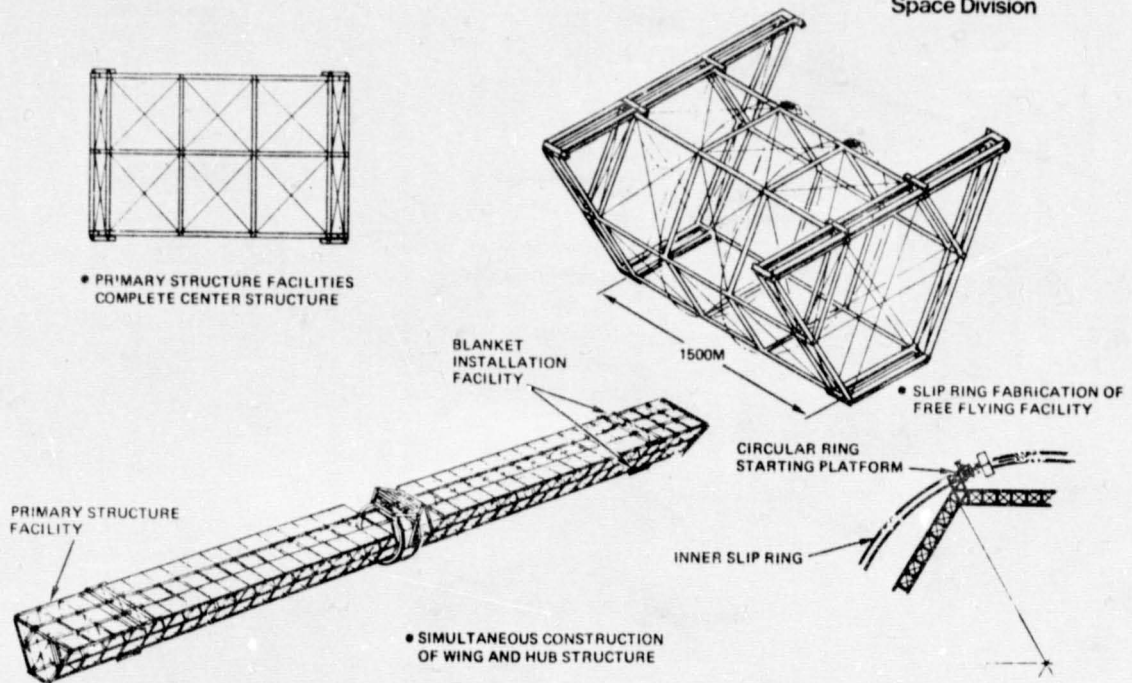


Figure 3.3-11. SPS Rotating Hub Structure Slip Ring Structure Buildup

Liquid-gallium slip rings for geosynchronous orbit applications have been studied under Contracts NAS3-13731, -13730, and -11538 at voltages up to 30,000 V and currents up to 100 A. Test units showed low friction and power losses and no wear debris or contamination was generated in final designs. However, key technology problems for SPS are the small clearances required between the rotating surfaces and the prevention of the loss of the liquid-gallium under all buildup and operating conditions.

#### Alternate Concepts

Earlier SPS studies by MSFC and others recognized that the rotary joints needed for microwave antenna/solar array pointing represent a technology area critical to the feasibility of the SPS. The concepts defined were huge, massive, and complex and intended to show that the rotary joint assemblies were both mechanically and electrically practical for the system. In general, diameter sizes ranged from 100 m to beyond 1.0 km and mass estimates (representing expensive materials) were well above one million kilograms.

#### Design Approach

To assure that rotary joints could be practical as well as feasible for the SPS, various concepts for transferring power across movable joints were re-evaluated and compared for application. Major aspects considered were power loss vs. size and mass, reliable long-life characteristics, design simplicity, cost, technology risk, and the suitability of characteristics affecting attitude control and stabilization. Table 3.3-8 summarizes the results and tradeoffs made. A flexible cable approach appears to be best when limited movement ( $<360^\circ$ ) is suitable. Slip rings with brushes were the best approach for rotational requirements beyond 360 degrees. Rotary transformers incurred the highest size, mass, and power loss penalties and would



Table 3.3-8. Rotary Joint Selection Considerations

Device	Size and Mass	Power Loss	Technology Status	Remarks
Slip ring (dry)	Intermediate	$I^2R$ + torque	State of the art	Baseline selection
Flexible cable	Lowest	Low $I^2R$	State of the art	Baseline selection for non-continuous rotation
Rotary transformer	Highest	Low transformer coupling	Engineering development required	Candidate for ac power generation only
Rolling contact	Intermediate	$I^2R$ + bearing friction	Engineering development required	Possible fatigue problem
Flexible cable w/power clutch	Intermediate	Low $I^2R$ + reset	Concept	Option for flexible cable complex
Liquid-metal slip ring	Intermediate	Low $I^2R$ + low torque	Engineering development required	Complexity—hazards

be a poor choice for a dc photovoltaic system. However, for a high-voltage ac system, the rotary transformer could be a good candidate. The other approaches were considered to be expensive, high technology/operational risk options.

Subsequently, rotary joint requirements and assembly design concepts were studied as part of the system-level studies performed to optimize the performance and economic feasibility of the SPS. For example, various SPS sizes, power levels, configurations, and antenna locations were studied. Compromises among the power conversion, distribution, structure, pointing/attitude control, and propellant subsystems were evaluated and used to enhance the overall system and to develop guidelines for the baseline 5-GW SPS. The rotary joint requirements were reduced substantially during these studies. Electrical, mechanical, and structural aspects were considered simultaneously, to develop a realistic, practical rotary joint approach.

Requirements. The rotary joint evaluation was based on the following requirements and guidelines:

1. Power capability of 4.35 GW from each of two solar array wings.
2. Nominal voltage/insulation rating of 40 kV.
3. Capacity for six isolated circuits per wing (6 positive and 6 negative connections).
4. Minimize power losses consistent with size, mass, cost, and life tradeoffs.
5. Assume that fabrication, complex/precision assembly, and test occur on the ground.
6. Limit unit assembly size/mass to that which can be transported to space by the HLLV.



7. Design for passive cooling if feasible; consider ambient temperature may be 100°C.

Electrical Assemblies. The reduction in power from 10 GW to 5 GW, the increase in voltage from 29 kV to 40 kV, and the smaller physical size decreased the size and enhanced the performance of the rotary assemblies significantly. In addition, based on system trade studies, an X-POP orientation was selected to replace Z-axis sun-oriented approach of the previous baseline. This permitted a simplified rotary joint concept with only two degrees of freedom. One axis with limited freedom can compensate for small pointing/seasonal variations using the flexcable approach. Slip ring-brush assemblies are required for the other axis which must rotate 360 degrees each day.

Preliminary designs of small slip ring-brush assemblies were made and evaluated to assure that adequate space was allowed for conductor connections and to assess the electrical, thermal, and insulation characteristics. The 15-m-diameter slip ring shown in Figure 3.3-12 is considered a practical, typical approach. The ring will rotate within an assembly (not shown for clarity) that will include conductor connections, bearings, and brush holder assemblies. The overall assembly will be less than 17 m in diameter, which is compatible with the HLLV nose cone. Using nominal values for the materials characteristics, performance studies indicated a very high efficiency and the probability that passive cooling would be sufficient. Since power would be received from two wings, and because of the long 1.9-km length required from the central structure, two electrical assemblies of the size shown are required and could be supported within the central structure, near each end.

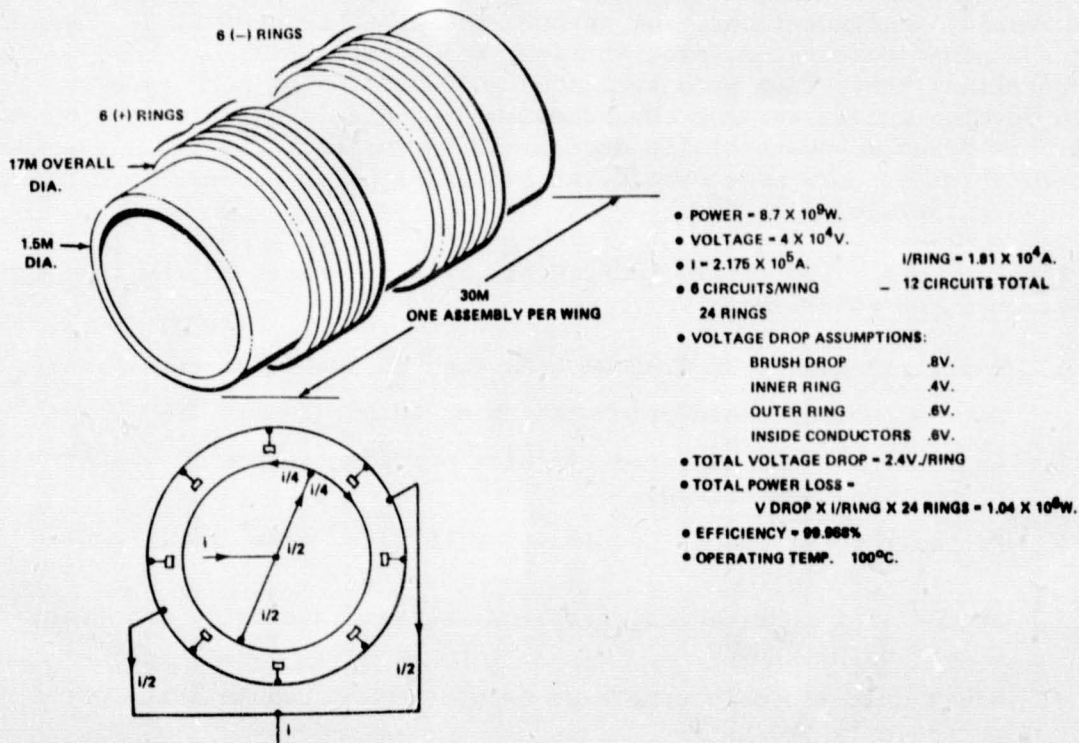


Figure 3.3-12. 15-meter-Diameter Slip Ring

Figure 3.3-13 illustrates a brush assembly design and its relation to the large power connections and to one of the slip rings. To minimize voltage drops and heating, two large-area copper connections, 180 degrees apart, are provided for each inner ring and for each outer ring. Permanent joints would be mechanically supported and silver brazed. The rings are shaped to have large surface area cooling fins which also serve as current conductors. Preliminary analysis indicated that hot-spot temperatures near the brushes and the joints would be less than 10°C above the average ring/assembly temperature.

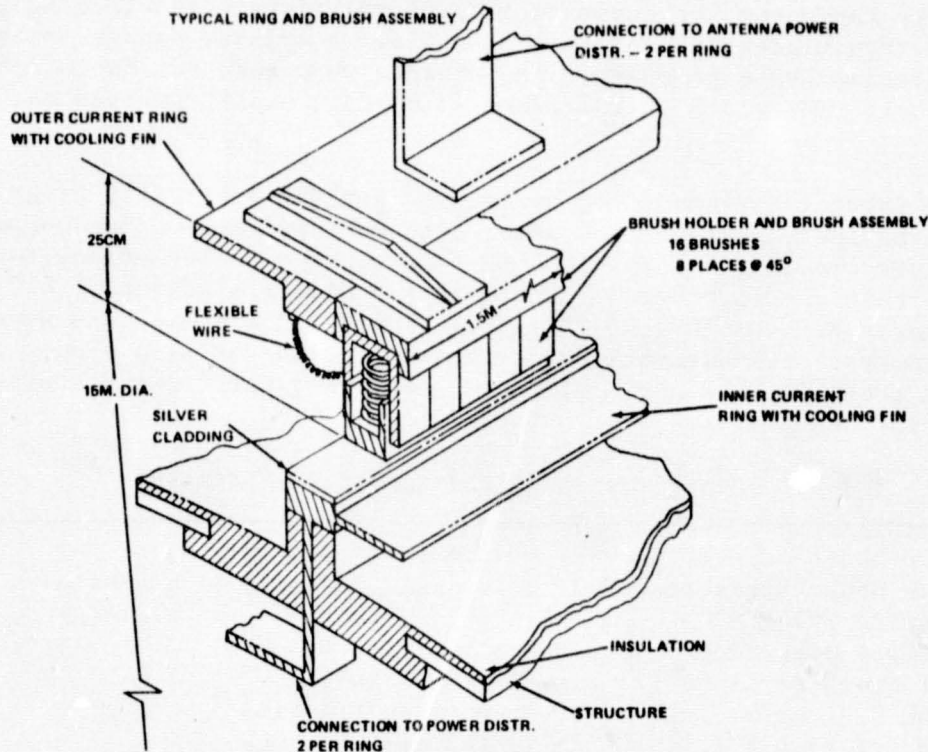


Figure 3.3-13. SPS Slip Ring-Brush Assembly

A brush assembly is 1.5 m long and consists of 16 brushes and 16 brush holders ganged together. The brush assemblies are joined to, and supported by, the outer copper rings. Eight brush assemblies, distributed 45 degrees apart, are required for each of the 12 rings in one rotary assembly. Although investigations showed brush materials usable up to 15-20 A/cm<sup>2</sup>, the design was based on a current density of 7.75 A/cm<sup>2</sup> to avoid hot spots, excessive wear, and power losses. Considering tradeoffs between power loss, wear rates, and frictional torque, a brush pressure of 0.7 kg/cm<sup>2</sup> was used.

A number of materials suitable for space applications of brushes and slip rings were investigated. For example, brass, various copper alloys, silver, and gold plating were evaluated for slip rings. Coin silver (Ag) appears to be the best candidate for slip rings because it is compatible with almost all types of brushes, it can handle current densities more than ten times greater than used in the SPS design, it affords high performance (low voltage drop and high heat dissipation at high currents), and it has very good wear/life



characteristics. Copper, silver, molybdenum-sulfide ( $\text{Mo S}_2$ ), and several alloys of silver were evaluated for brushes.  $\text{Mo S}_2$  alloyed with Mo and tantalum, and Ag alloyed with niobium-selenite ( $\text{Nb Se}_2$ ) offer the best wear rates; Ag alloyed with graphite and  $\text{Mo S}_2$  afforded the highest current density. The characteristics of Ag alloyed with  $\text{Mo S}_2$  or with  $\text{Nb Se}_2$  were about the same and were considered good high-performance, long-life candidates for the SPS design.

The individual brushes shown (Figure 3.3-13) were sized to provide a reasonably large contact surface ( $5.0 \times 3.1$  cm) without sacrificing good control of the brush pressure and contact angle. Beryllium copper springs are used to maintain brush pressure. The brushes were made hollow to conserve mass and cost. The width of the inner slip ring, under the brushes, was 7.0 cm.

Since initial designs using all-silver for the inner slip rings were considered to be too expensive, the inner ring was modified—using copper with a coin-silver cladding as shown on the figure. Wear calculations for the ring speed and brush pressure used indicate that a silver cladding of 0.2 cm thick would be ample for the 30-year SPS life. Table 3.3-9 summarizes some of the design parameters and assumptions for the 15-m-diameter slip ring. It is noted that these factors are similar to those used for present state-of-the-art slip ring designs.

Table 3.3-9. 15-m-Diameter Slip Ring Design Parameters

Assume brush current density = $7.75 \text{ A/cm}^2$ ( $50 \text{ A/in.}^2$ )
Assume brush pressure = $0.7 \text{ kg/cm}^2$ ( $10 \text{ lb/in.}^2$ )
Brush area/ring = $2340 \text{ cm}^2$
Brush pressure/ring = $2340 \times 0.7 = 1.64 \times 10^3 \text{ kg}$
Total brush pressure (24 rings) = $3.93 \times 10^4 \text{ kg}$
Assume 0.3 coefficient of brush on ring friction
Brush friction = $1.18 \times 10^4 \text{ kg}$ (total for 24 rings)
Brush wear rates:
$1.7 \times 10^{-8} \text{ cm/cm}$ (high wear rate) results in 0.87 cm wear/30 years
$7 \times 10^{-10} \text{ cm/cm}$ (low wear rate) results in 0.036 cm wear/30 years
Brush travel for 30 years = $15 \times 10^2 \times 365 \times 30 = 5.16 \times 10^7 \text{ cm}$
Ring wear:
Assume brush width = 6 cm
Length of brush on ring = $2340/6 = 390 \text{ cm}$
Brush travel on ring/30 years = $390 \text{ cm} \times 365 \times 30 = 4.27 \times 10^6 \text{ cm}$
Assume ring wear rate = brush wear rate
Ring wear = $4.27 \times 10^6 \times 1.7 \times 10^{-8} = 0.07 \text{ cm}$
Make ring 0.2-cm-thick silver on copper ring—7.0 cm wide

The mass calculated for major subassemblies and for complete electrical rotary joint assemblies are listed in Table 3.3-10. Included in the masses shown was 1660 kg of silver that would cost \$267,000 at the present value of \$161/kg.



Table 3.3-10. Major Subassembly Mass

Mass	kg
Inner rings	$0.78 \times 10^4$
Outer rings	$0.59 \times 10^4$
Brush assemblies, internal connectors, etc.	$3.60 \times 10^4$
Structure and insulation	$0.98 \times 10^4$
Assembly mass	$5.95 \times 10^4$
Total mass of both assemblies	$11.9 \times 10^4$

Initial torque calculations indicate that a 1/3-hp motor could drive the rotary assemblies against the brush friction. It was estimated that an equivalent power would be needed for the bearing and drive mechanisms. Then, a drive motor of less than 1 hp will be sufficient for the entire rotary joint assembly.

### 3.4 STRUCTURES

Trade studies conducted in the structures area are indicated on Figure 3.4-1, and dealt primarily with: photovoltaic structure configuration performance (both static and dynamic) as influenced by satellite length-to-depth aspect ratio; antenna structure concept selection; structural materials selection; and, finally, the optimum shape and detail configuration of the cap elements that make up the basic beam element produced on orbit by a beam builder. This basic beam element is the heart of all satellite structure configurations studied. The following sections discuss results of these trade studies.

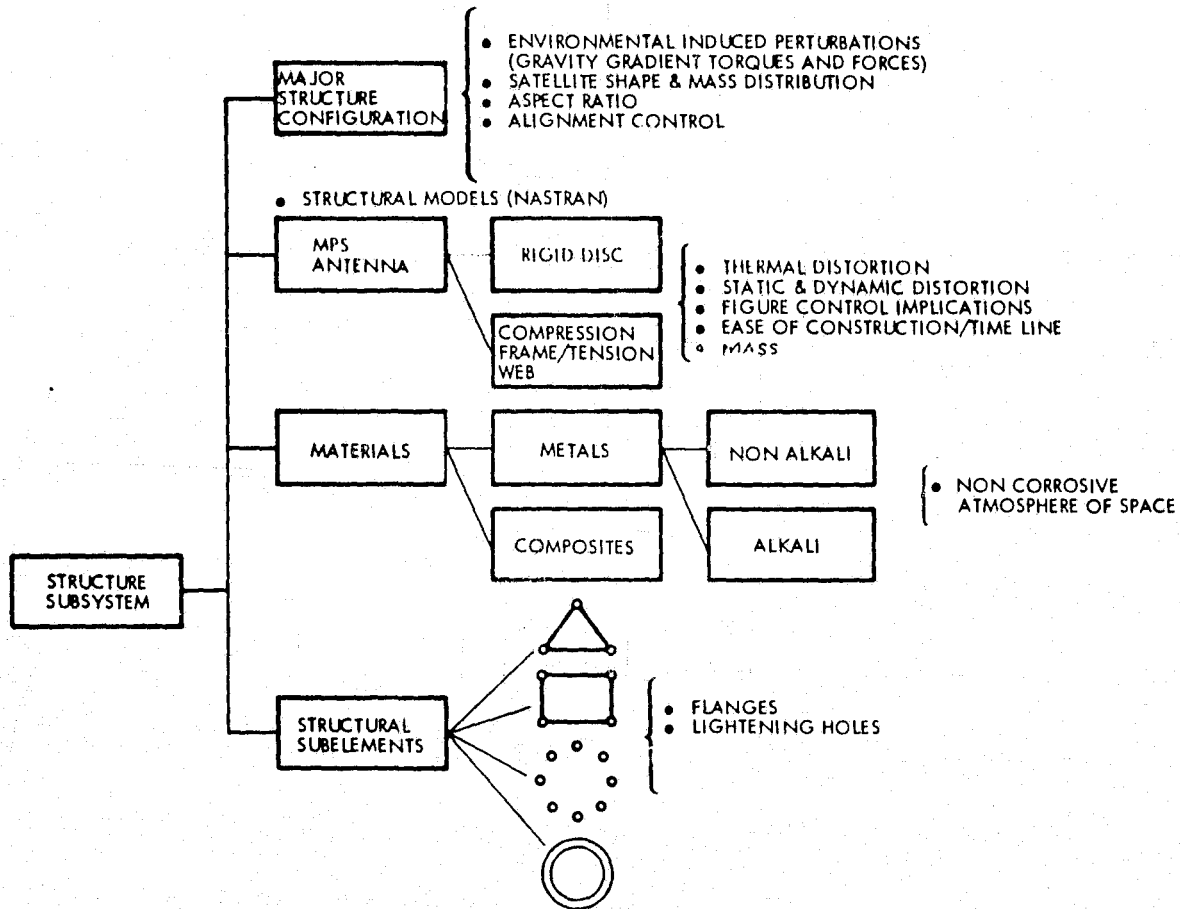


Figure 3.4-1. Structural Subsystem Trades

#### 3.4.1 ASPECT RATIO

The aspect ratio for a satellite structure is defined as the ratio of its largest dimension to its smallest dimension (i.e., length/depth). This aspect ratio influences satellite natural bending frequencies, structural element sizes, and overall satellite distortion due to environmental perturbing and thermal gradients.

Initially, the three photovoltaic satellite configuration concepts, shown in Figure 3.4-2, were used to evaluate the impact of aspect ratio on the

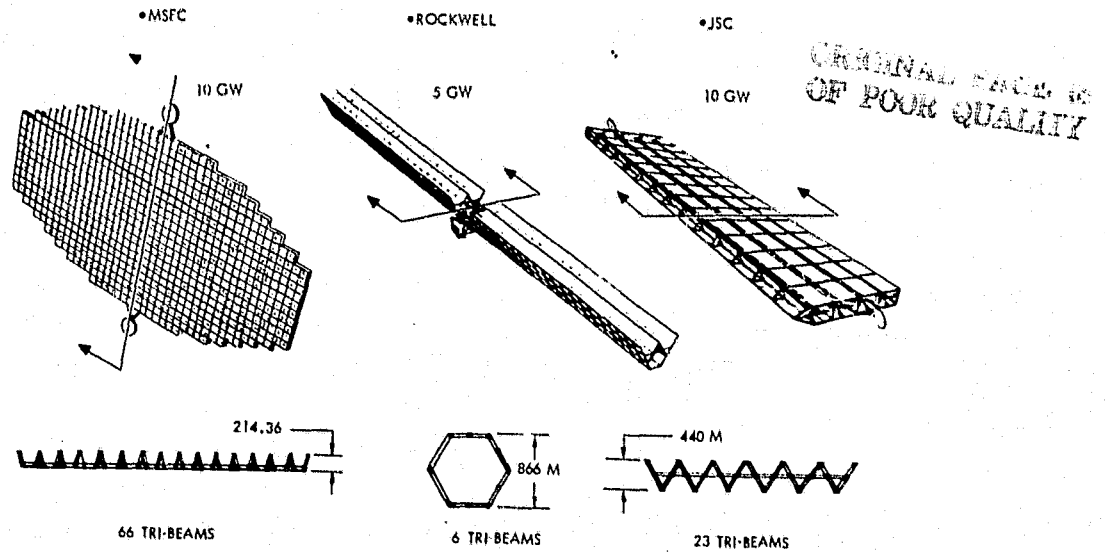
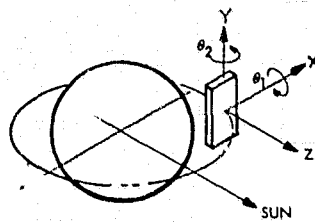


Figure 3.4-2. Configurations Evaluated

magnitude of forces and torques resulting from environmental perturbations and satellite natural bending frequencies. The magnitude of environmental perturbations acting on an SPS is dominated by gravity-gradient torques. These torques are a function of the difference in mass moment of inertia [e.g.,  $I_x = f(I_y - I_z)$ ] which is, in turn, a function of aspect ratio.

Figure 3.4-3 depicts the satellite axis orientation (Y-POP), the gravity-gradient torque ( $T_A$ ) equations used in the analysis and the magnitude of

$\theta_1$ : PITCH  
 $\theta_2$ : ROLL



$$T_x = \frac{3 \rho_0 R_e^2}{2 R^3} (I_y - I_z) \sin 2\theta_1 \cos^2 \theta_2$$

$$T_y = \frac{3 \rho_0 R_e^2}{2 R^3} (I_z - I_x) \sin 2\theta_2 \cos^2 \theta_1$$

$$T_z = \frac{3 \rho_0 R_e^2}{2 R^3} (I_x - I_y) \sin 2\theta_1 \sin^2 \theta_2$$

CONCEPT NO.	ASPECT RATIOS			MASS MOMENT OF INERTIA kg-M <sup>2</sup>			GRAVITY GRADIENT TORQUES: N-M GEO					
							NOMINAL			WORST CASE		
	Y/Z	Y/X	X/Z	I <sub>Y</sub>	I <sub>X</sub>	I <sub>Z</sub>	T <sub>Y</sub>	T <sub>X</sub>	T <sub>Z</sub>	T <sub>Y</sub>	T <sub>X</sub>	T <sub>Z</sub>
1. NASA/MSFC PHOTOVOLTAIC (SUN ORIENTED)	103	2.0	52	5.4 X 10 <sup>14</sup>	4.39 X 10 <sup>15</sup>	4.89 X 10 <sup>15</sup>	4.26 X 10 <sup>6</sup>	25.2 X 10 <sup>6</sup>	12.03 X 10 <sup>6</sup>	4.26 X 10 <sup>6</sup>	3.43 X 10 <sup>7</sup>	3.05 X 10 <sup>7</sup>
2. ROCKWELL PHOTOVOLTAIC (EQUATOR ORIENTED)	19.0	13.0	1.5	5.14 X 10 <sup>12</sup>	8.00 X 10 <sup>14</sup>	8.03 X 10 <sup>14</sup>	2.38 X 10 <sup>4</sup>	≈0	≈0	2.38 X 10 <sup>4</sup>	6.32 X 10 <sup>6</sup>	6.30 X 10 <sup>6</sup>
3. NASA/JSC PHOTOVOLTAIC (MODIFIED) (EQUATOR ORIENTED)	62.5	5.6	12.0	4.47 X 10 <sup>12</sup>	6.2 X 10 <sup>15</sup>	6.29 X 10 <sup>15</sup>	7.13 X 10 <sup>5</sup>	≈0	≈0	7.13 X 10 <sup>5</sup>	4.98 X 10 <sup>7</sup>	4.91 X 10 <sup>7</sup>

Figure 3.4-3. Solar Photovoltaic Aspect Ratio/Gravity-Gradient Torque Comparisons

aspect ratio, mass moment of inertia, and geosynchronous gravity-gradient torque for each of the three configurations used in the trade study. The "nominal" torques are those encountered during normal operation with the Y-axis perpendicular to the orbit plane (POP), and the X- and Z-axis in the orbit plane. The "worst case" torques are produced when the axis in question is at a 45-degree angle with the orbit plane. Results indicate that low aspect ratios (L/D or Y/Z) generate lower nominal and worst-case torques.

If the satellite structure is viewed as a free body, the gravity-gradient torques can be expressed as a triangular force distribution, as illustrated in the upper right-hand corner of Figure 3.4-4. To hold the satellite in the position ( $\theta = 45^\circ$ ) in preparation for returning it to its nominal operating attitude ( $\theta = 0^\circ$ ), a centrally located moment ( $M_R$ ) is assumed to be applied

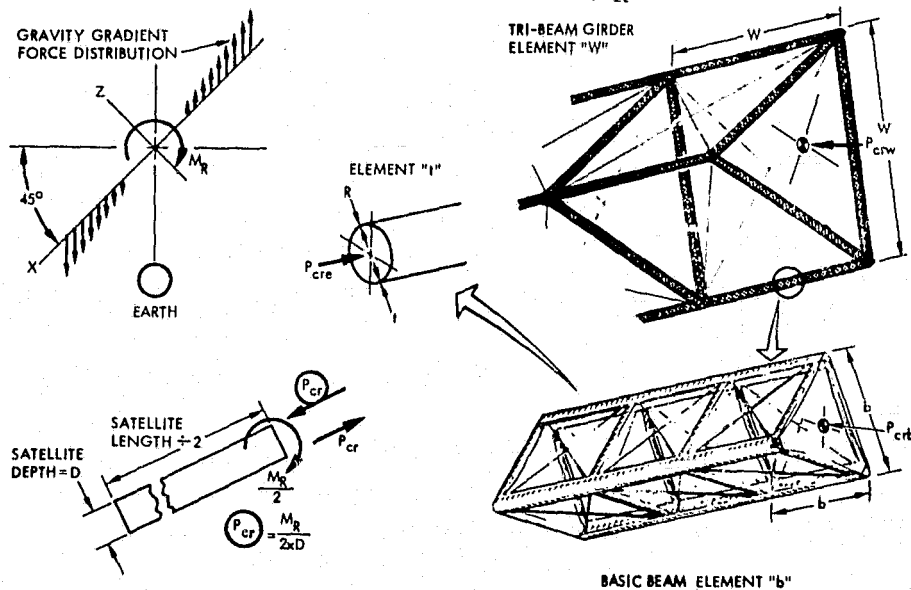


Figure 3.4-4. SPS Aspect Ratio Analysis Load Diagram

with a magnitude  $M_R = 2 T_{\max}$ . This moment source is either a close-coupled thruster system or a momentum wheel device. This gravity-gradient torque/restoring moment system results in a tension/compression force couple ( $P_{cr} \times D$ ) carried by the satellite longitudinal structural beams. These beams or tribeam girders ("W") are common to the three configurations evaluated. They are made from triangular basis beam elements ("b"), fabricated on orbit by a beam-builder or machine. The basic beam elements consist of three cap sections and three transverse struts stabilized by X-tension braces or cables. For purposes of analysis, the caps and struts were assumed to be tubes of radius (R) and wall thickness (t). In an actual application, these caps and struts would be optimized by cross-section shaping and lightening holes to result in a minimum mass per unit length for a given load ( $P_{cr}$ ) consistent with the environmental perturbations. The configuration of a tribeam girder can be defined by the following dimensional parameters:

l = girder length between supports

W = tribeam girder side dimension and bay length dimension



b = basic beam element side and bay length dimension

r = cap radius

t = cap wall thickness

The optimum tribeam girder is one where all critical stress levels are equal to each other and to the applied stress, assuming no factor of safety. These critical stresses can be expressed in terms of the above dimensional parameters as follows:

$$\sigma_{crb} = \frac{\pi^2 Eb^2}{6W^2} = \text{critical buckling stress in basic beam element "b"}$$

$$\sigma_{cre} = \frac{\pi^2 ER^2}{2b^2} = \text{critical buckling stress in cap element "e"}$$

$$\sigma_{cce} = \frac{.24 Et}{R} = \text{crippling allowable for cap element "e"}$$

Using these relationships and the Rockwell structure configuration with a concentration ratio = 2 (Figure 3.4-2) as a discriminator, a dimensional sensitivity analysis was conducted; results are tabulated in Table 3.4-1.  $P_{crw}$  is the critical load on the tribeam girder for the dimensions indicated, and  $MASS_{\ell}$  is the mass of the tribeam girder of length " $\ell$ " in kilograms. From the

Table 3.4-1. Rockwell Sensitivity Analysis

CASE NO.	$P_{crw}$		$P_{crw}/g$		" $\ell$ "	"W"	"b"	"R"	t	$\sigma_{cr}$		$MASS_{600}$
	N	LBS	N	LBS	M	M	M	MM	MM	$\mu Pa$	PSI	KG
1	3,650	820	405	91	600	18.44	0.57	10	.065	107.3	15,556	247
2	15,092	3,393	1,677	377	600	21.05	0.74	15	.127	139.9	20,304	717
3	60,371	13,572	6,708	1,508	600	24.05	0.98	22	.254	184.8	26,800	2,172
4	542,680	122,000	60,048	13,500	600	30.10	1.52	44	.762	286.6	41,601	12,601

relationships of the variables, two may be selected as fixed parameter and the remaining variables solved in terms of the fixed parameters. Case 1 uses the force value of 3650 N for the initial load,  $P_{crw}$  and a tribeam girder length of 600 m as fixed parameters for solving for the other variables—W, b, R, etc. The initial load comes from the previously calculated (Figure 3.4-3) gravity-gradient torques. Cases 2, 3, and 4 use " $\ell$ " and "t" as the fixed parameters for calculating the remaining variables. Table 3.4-2 compares the tribeam girder dimensions for the initial three concepts, with the values of  $P_{crw}$  and " $\ell$ " being dictated by gravity-gradient torques and concept configuration, respectively. The Rockwell concept with the lowest aspect ratio ( $L/D = 19$ ) results in the lightest cap mass ( $M_e = 2\pi Rtp$ ) and, in turn, the lightest weight tribeam girder per unit length ( $M_w = 36 \times 2\pi Rtp$ ).





Table 3.4-2. Sizing Comparison

CONCEPT NO.	M <sub>R</sub> N-Mx10 <sup>6</sup>	P <sub>crw</sub> N	TRI-BEAM GIRDER DIMS.					CRITICAL STRESS - σ <sub>cr</sub>	
			"L"-M	"W"-M	"b"-M	"R"-MM	"t"-MM	# P <sub>σ</sub>	PSI
1. NASA/MSFC	69	7,001	493	16.68	0.80	11	0.086	131	19,000
2. ROCKWELL	12.6	3,650	600	18.44	0.57	10	0.065	98	14,150
3. NASA/JSC	99.6	10,290	508	17.89	0.62	12.5	0.136	107	15,520

The natural frequency of the three initial configurations can be closely approximated if the NASA-MSFC concept is treated as a free-free elliptical flat plate, and the Rockwell and NASA-JSC concepts are treated as free-free beam; then

$$f_n = \frac{6.7}{2\pi a} \sqrt{\frac{\pi EI}{2am(1-\nu^2)}} : \text{elliptical plate}$$

$$f_n = \frac{(4.73)}{2\pi} \sqrt{\frac{EI}{L^3 m}} : \text{beam}$$

where:

a = major axis ÷ 2 (ellipse)

E = modulus of elasticity = 6.895×10<sup>10</sup> Pa for aluminum

I = geometric moment of inertia

m = satellite mass

ν = Poisson's ratio = 0.3 for aluminum

L = length (beam)

Figure 3.4-5 plots the natural frequency of the three configurations as a function of tribeam cross-sectional area. Both the NASA-MSFC and Rockwell configurations have two data points indicated. The lower frequencies are based on the sizing results (Table 3.4-2), and the higher numbers are for structure material thicknesses used in previous feasibility studies which are more consistent with minimum gauge requirements. Also indicated in Figure 3.4-5 are the preliminary requirements for minimum structure natural frequency for both GEO and LEO environments, as dictated by attitude control system (ACS) bandwidth frequencies. During the course of the study, these structure frequency requirements have been reduced significantly based on detailed ACE analysis; however, a structure configuration which results in a relatively high natural frequency is desirable and will minimize the complexity of the ACS.

In summary, the Rockwell concept, which has a low aspect ratio, develops lower axial loads in the tribeam girders due to environmental forces and torques, and yields a relatively high natural frequency. Both of these characteristics are beneficial to the integrity of the SPS structural subsystem.

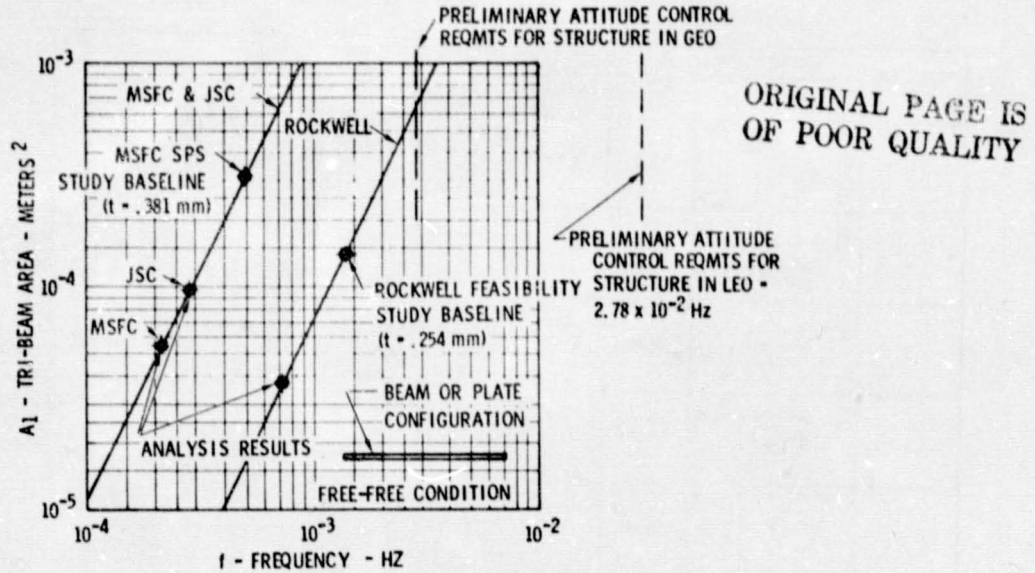


Figure 3.4-5. Satellite Frequency as a Function of Configuration and Tribeam Girder Cross-Sectional Area

Once a low aspect ratio was deemed desirable, a variety of cross-sectional configurations were evaluated, based on the parameters depicted in Figure 3.4-6. All configurations investigated were consistent with projected area requirements dictated by the power conversion subsystem. This evaluation effort is summarized in Figure 3.4-7, and resulted in the selection of the solar array structural cross-sectional configuration for the point design.

MAJOR STRUCTURAL CONFIGURATION CONSIDERATIONS

PARAMETER	AFFECTED BY	GOAL
<ul style="list-style-type: none"> <li>NATURAL FREQUENCY</li> </ul> $f_n = \frac{(4.73)^2}{2\pi} \sqrt{\frac{E(\sum Ad^2)}{L^3 M}}$	<ul style="list-style-type: none"> <li>LENGTH/DEPTH ASPECT RATIO</li> <li>CONTROL SYSTEM BANDWIDTH</li> </ul>	<ul style="list-style-type: none"> <li>LEO &gt; 10 CY/HR</li> <li>GEO &gt; 1 CY/HR</li> </ul>
<ul style="list-style-type: none"> <li>ENVIRONMENTAL FORCES &amp; TORQUES (GRAVITY GRADIENT)</li> </ul>	<ul style="list-style-type: none"> <li>LENGTH/DEPTH ASPECT RATIO</li> <li>ATTITUDE</li> </ul>	<ul style="list-style-type: none"> <li>MINIMUM GAGE MATERIAL</li> </ul>
<ul style="list-style-type: none"> <li>INTERNALLY INDUCED FORCES &amp; TORQUES</li> </ul>	<ul style="list-style-type: none"> <li>BLANKET &amp; REFLECTOR TENSIONING REQMTS</li> <li>OFF CENTER MASS ROTATION (ANTENNA)</li> </ul>	<ul style="list-style-type: none"> <li>MINIMUM GAGE MATERIAL</li> </ul>
<ul style="list-style-type: none"> <li>ACS PROPELLANT CONSUMPTION</li> </ul>	<ul style="list-style-type: none"> <li>2-AXIS MASS IMBALANCE</li> </ul>	<ul style="list-style-type: none"> <li>MATCHED MASS MOMENTS OF INERTIA (<math>I_{XX} = I_{ZZ}</math>)</li> </ul>
<ul style="list-style-type: none"> <li>CONSTRUCTION COMPLEXITY</li> </ul>	<ul style="list-style-type: none"> <li>NO. BEAM ELEMENTS</li> <li>NO. JOINTS</li> </ul>	<ul style="list-style-type: none"> <li>SIMPLICITY</li> </ul>

Figure 3.4-6. Major Structural Configuration Considerations



CONCEPT NO.	CONFIGURATION		CONC RATIO	COMMENTS	DISPOSITION
	X-SECTION	LENGTH KM			
1		13.1	2:1	EXTREMELY LOW NATURAL FREQUENCY (< 1 CY/HR). LACK OF MASS BALANCING ABOUT X AND Z AXIS DICTATES EXCESSIVE PROPELLANT CONSUMPTION	REJECTED
2		26.7	2:1	LONG DEEP STRUCTURE WITH NATURAL FREQUENCY ≈ 4 CY/HR. REQUIRES LESS ACS PROPELLANT THAN CONCEPT NO. 1	ACCEPTABLE FOR CR = 2 AND GEO CONSTRUCTION
3		31.4	1:1	SIMPLEST OF ALL STRUCTURAL CONCEPTS. NATURAL FREQUENCY ≈ 3 CY/HR. GOOD FOR GEO CONSTRUCTION AND OPERATION. SEVERE MASS PENALTY PAID FOR CR = 1	ACCEPTABLE FOR CR = 1 AND GEO CONSTRUCTION
4		31.5	1:1	VARIATION ON CONCEPT NO. 3 FOR LEO CONSTRUCTION. NATURAL FREQUENCY > 6 CY/HR. ASSEMBLY PROCESS COMPLEX	REJECTED IN FAVOR OF CONCEPT NO. 5
5		18.1	2:1	HIGH NATURAL FREQUENCY (> 34 CY/HR). EXCELLENT MASS BALANCING CHARACTERISTICS. GOOD CONCEPT FOR LEO CONSTRUCTION. MAJOR DRAWBACK IS ASSEMBLY COMPLEXITY.	ACCEPTABLE FOR CR = 2 AND LEO CONSTRUCTION
5A		22.3	5:1	VARIATION ON CONCEPT NO. 5 FOR CR = 5. REQUIRES ADDITIONAL SECONDARY STRUCTURE FOR REFLECTOR MOLDFORMING ACCURACY.	ACCEPTABLE W/ MASS PENALTY FOR CR = 5 AND LEO CONSTR.
6		21.3	2:1	RELATIVELY HIGH NATURAL FREQUENCY (> 13 CY/HR). GOOD MASS BALANCING CHARACTERISTICS, COMPATIBLE WITH ON-ORBIT CONSTRUCTION CONCEPTS IN BOTH LEO AND GEO	SELECTED FOR POINT DESIGN ✓

Figure 3.4-7. SPS Solar Array Configuration Evaluation

### 3.4.2 ANTENNA STRUCTURE

The selected microwave antenna structure concept was the tension web/compression frame configuration depicted in Figure 3.4-8. This concept was

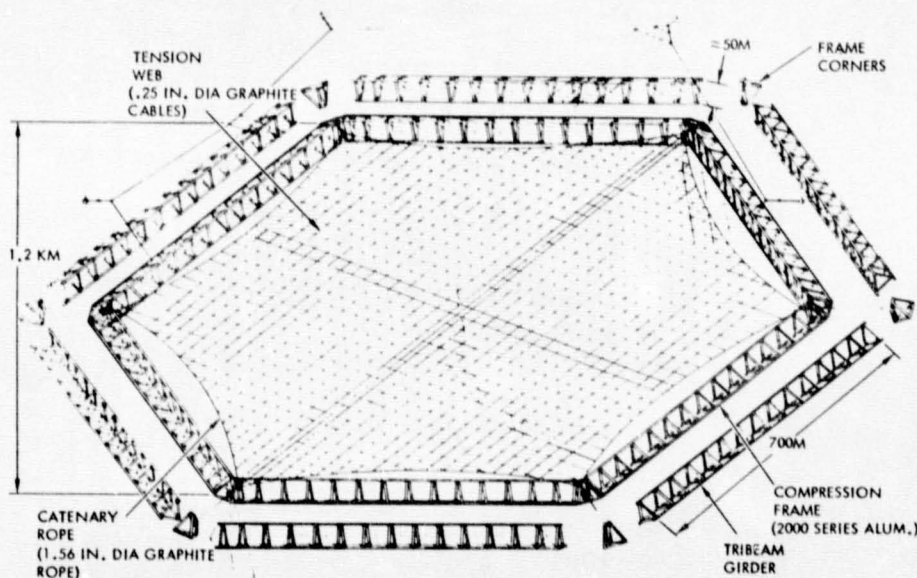
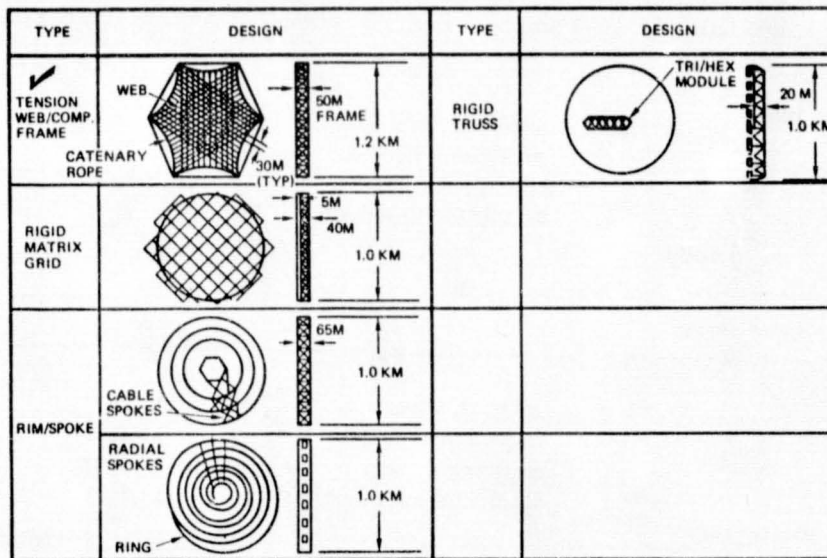


Figure 3.4-8. Microwave Antenna Structure Selected Design Concept



selected based on an evaluation of the concepts depicted on Figure 3.4-9. The discriminators, parameters, and design goals used in the trade study are listed on Table 3.4-3. The surface flatness requirement is dictated by the upper limit of electronic beam steering capability, which is estimated to be  $\pm 0.08^\circ$ . The natural frequency requirement is dictated by the ACS subsystem and the recently estimated requirement for the antenna structure is  $>2$  cycles/hour. Thermal stability is a function of changes in the temperature distribution caused by the 360-degree rotation of the structure with respect to the sun and relates to surface flatness and thermal stresses. The mass discriminator is simply associated with the economic benefits normally derived from lightweight structures. Construction complexity is also an economic consideration and is best measured by the numbers of separate beam elements which must be handled, and the number of structural joints that must be affected, which provides a subjective judgment associated with construction time and complexity.



ORIGINAL PAGE IS  
OF POOR QUALITY

Figure 3.4-9. Antenna Structural Concepts

Table 3.4-3. SPS Microwave Antenna Structure

DISCRIMINATOR	PARAMETER	DESIGN
• SURFACE FLATNESS	- SOLAR PRESSURE - GRAVITY GRADIENT FORCE - MICROWAVE BACK PRESSURE - TEMPERATURE GRADIENTS - CENTRIFUGAL FORCE	$\pm .08^\circ$
• NATURAL FREQUENCY	- DIAMETER/DEPTH - ASPECT RATIO - MATERIAL SELECTION	2 CY/HR (ESTIMATED)
• THERMAL STABILITY	- MATERIAL SELECTION - CONFIGURATION	MINIMIZE IMPACT OF 360° ROTATION
• MASS	- DESIGN CONCEPT - MATERIAL SELECTION	LIGHTWEIGHT
• CONSTRUCTION COMPLEXITY	- N° BEAM ELEMENTS - N° JOINTS	SIMPLICITY



Without conducting a detailed structural and thermal analysis of each of the five concepts depicted (Figure 3.4-9), the selection rationale must be somewhat subjective. All concepts evaluated can be designed to meet the design goals for surface flatness, natural frequency (e.g., the tension web/compression frame concept has the lowest natural frequency, which is estimated to be approximately 6 cycles/hour), and thermal stability. Mass estimates and construction complexity factors clearly favor the tension web/compression frame concept developed by Rockwell in the Satellite Power System (SPS) Feasibility Study (NAS8-32161).

Based on a limit load condition of 128.28 N (see Figure 3.4-10) distributed over the web surface as a pressure force, a sizing analysis was conducted on the configuration shown in Figure 3.4-8. From the sizing analysis, the mass breakdown tabulated in Figure 3.4-11 was generated. The total mass of 73,875 kg is less than half that estimated for the other four concepts evaluated.

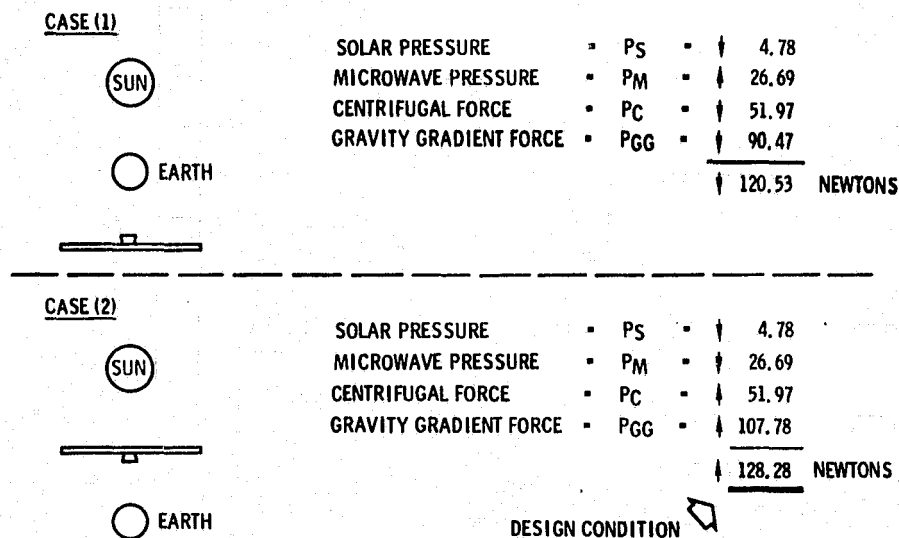


Figure 3.4-10. Microwave Antenna Structure Design Condition

The rigid matrix grid and the rigid truss concepts require the on-orbit fabrication of a multitude of beam elements which must then be joined together to form the finished product. Estimates of the construction time for these two concepts range up to one year—depending on the number of beam machines and EVA personnel dedicated to this activity. The rim/spoke concepts appear to lend themselves to a rapid construction rate. However, they require cable tuning to achieve surface flatness and take an unacceptable amount of time. The compression frame of the selected concept uses the same basic construction techniques as the photovoltaic solar arrays (i.e., tribeam girder fabrication) and does not require additional construction equipment development. The tension webs and catenary cables can be transported to the construction site on spools and laid in place off the antenna construction jig. Based on estimates generated during the end-to-end analysis activity, the Rockwell concept for a tension web/compression frame microwave antenna structure can be constructed in approximately five working days.



NOMENCLATURE	QTY REQD	MASS/UNIT	TOTAL MASS
• COMPRESSION FRAME			(42,678)
- TRIBEAM GIRDERS	6	3,556	21,339
- FRAME CORNERS*	6	3,556	21,339
- STRUCTURE	6		
- ELEVATION JACKS	3		
- IN-PLANE TENSION DEVICES	6		
• CATENARY ROPE	6	1,340	(8,040)
• TENSION WEB	1	3,001	(3,001)
• ATTACHMENTS* (WAVEGUIDE TO WEB)	3,108	1	(3,108)
*ESTIMATED		SUBTOTAL	56,827
		30% GROWTH	+17,048
		TOTAL	<u>73,875</u>
<ul style="list-style-type: none"> <li>• MASS RESULT &lt; 1/2 THAT OF OTHER CONCEPTS</li> <li>• CONSTRUCTION RELATIVELY SIMPLE</li> </ul>			

Figure 3.4-11. Microwave Antenna Mass Summary

In summary, the tension web/compression frame concept was selected because of its superiority in the areas of mass and construction complexity.

### 3.4.3 MATERIALS

Structural aluminum has been selected for all primary SPS structural elements except the antenna tension web and catenary ropes. These two elements will be made from composite systems to take advantage of their high unidirectional properties and relative insensitivity to temperature gradients and temperature changes caused by the operational environment.

Figure 3.4-12 presents the material options available and the key trade parameters which were considered in the trade study. Within the metallic regime, two options are available. Non-alkali materials such as steel, aluminum, titanium, etc., are obvious candidates in that they are well characterized and the trade parameters can be well quantitized. The other metallic option is alkali metals such as sodium, potassium, and lithium. Although they have no application in the oxygen environment here on earth, they potentially have an excellent application as multifunction materials in the operational environment of SPS as both structural materials and electrical conductors. Figure 3.4-13 compares the electrical resistance and material density of alkali materials with electrical conductor materials currently in use on earth. If specific resistance (resistance  $\times$  density) is used as a performance indicator, lithium, sodium, and potassium will all out-perform pure aluminum as electrical conductors for a given mass of material. However, little if any mechanical properties data have been generated for these alkali materials. Hence, they are not considered prime candidates for SPS structure material. Developing material properties for these alkali materials as a backup should certainly receive consideration in future development plans.

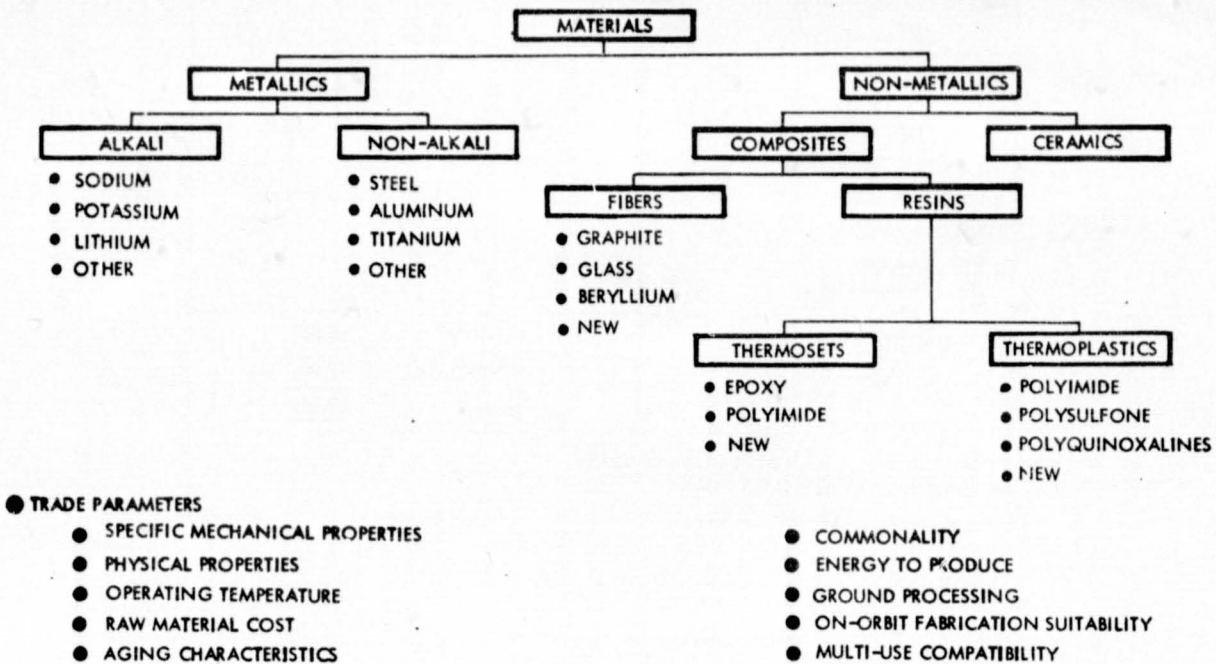


Figure 3.4-12. Large Space Structures Material Considerations

○ CANDIDATE METALS SUITABLE FOR SPACE SERVICE ONLY (ALKALI)

○ SPECIFIC RESISTANCE : MICROHM-CM/ GM AT 250° K.

	RESISTANCE	DENSITY	SPECIFIC RESISTANCE
○ LITHIUM	7.613	.534	4.07
○ SODIUM	3.821	.97	3.71
○ POTASSIUM	5.72	.87	4.98
○ RUBIDIUM	10.01	1.53	15.32
○ CESIUM	16.06	1.873	30.08
○ SILVER	1.34	10.49	14.06
○ COPPER	1.40	8.94	12.52
○ ALUMINUM	2.24	2.7	6.05

○ THE ALKALI METALS : LITHIUM, SODIUM AND POTASSIUM BECOME EXCELLENT CONTENDERS AS CONDUCTORS IN SPACE AT 250°K

○ INFORMATION NEEDED FOR TRADE STUDIES

- MECHANICAL PROPERTIES DATA

Figure 3.4-13. SPS Materials Comparison

At the other end of the materials spectrum are the non-metallics, such as organic composite systems and ceramics. The ceramics appear to have application only in extremely high-temperature environments, as would be encountered in a solar thermal SPS, because of their relatively high cost and fragility. The composite systems, at first glance, appear like the obvious choice for an SPS structure material. Their density is 56% of aluminum, their unidirectional (0°) elastic modules are 3 to 3-1/2 times that of aluminum, and their tensile



strength is over four times that of aluminum. This would indicate a potential for dramatic savings in structural mass. However, for a composite system to have the compressive and torsional stability required by an SPS structural element cap, the fiber orientation is not just unidirectional but also includes  $\pm 45^\circ$  fibers and  $\pm 90^\circ$  fibers. This has the effect of lowering the effective  $0^\circ$  tensile strength and elastic modulus to a point where the structural performance is still superior to aluminum, but the improvement is not as dramatic. It is reasonable to expect a composite system to have a modulus of elasticity of greater than  $10 \times 10^{10}$  pascals, compared to  $6.9 \times 10^{10}$  pascals for aluminum, and an ultimate tensile strength of  $5.5 \times 10^8$  pascals compared to  $4.2 \times 10^8$  pascals for aluminum. However, most of the sizing analyses conducted to date using aluminum allowables indicate that minimum-gauge material is the limiting condition and not material modulus or strength. If this trend is verified by detailed mathematical simulation, then the added strength of composite systems is of little value other than increasing the structural factor of safety.

Considering the other trade parameters of physical properties, operating temperature, and energy-to-produce, composites are a winner over aluminum and all other non-alkali metallics. However, raw material costs, ground processing, on-orbit fabrication suitability, and multi-use commonality parameters favor aluminum. In the final analysis, the aging characteristics parameter is the key to the selection of aluminum for most primary structural elements. Aging characteristics of aluminum over a 30-year life are predictable. No data have been generated to date on the long-term aging characteristics of composite systems. This is particularly true of thermoplastic systems which would appear to lend themselves to rapid on-orbit fabrication because they do not require a cure cycle after forming, and they can be welded or joined together simply by applying heat. Thermoset composite systems, on the other hand, require time-dependent cure cycles for forming and the introduction of a separate adhesive system to effect joining or welding. Aging of composite systems include, but is not limited to, outgassing in the space vacuum and resin strength degradation due to radiation. These effects alone could make composites totally unacceptable for SPS structural applications on a large scale.

In summary, it is less risky from an overall program sense to select aluminum and design a structure that can accommodate its shortcomings, such as a maximum operating temperature of only  $150^\circ\text{C}$  and a relatively high coefficient of thermal expansion ( $23.4 \times 10^{-6} \text{m/m-}^\circ\text{C}$ ), than to select a composite system which may prove unacceptable in the years to come. Developing methods for generating accelerated aging data for composite systems should receive high priority in near-term technology development planning. Finally, it will be much easier to switch from aluminum to composites during the development phase of the SPS than to do the reverse.

#### 3.4.4 TRIBEAM SUBELEMENT STUDY

All of the SPS structural configurations investigated during the course of this study consist of a common structural element termed a *tribeam girder*, as shown in Figure 3.4-14. The tribeam girder is made up of a basic beam element fabricated on orbit by a beam machine. The basic beam element consists of three cap sections, three transverse struts, and X-tension members.



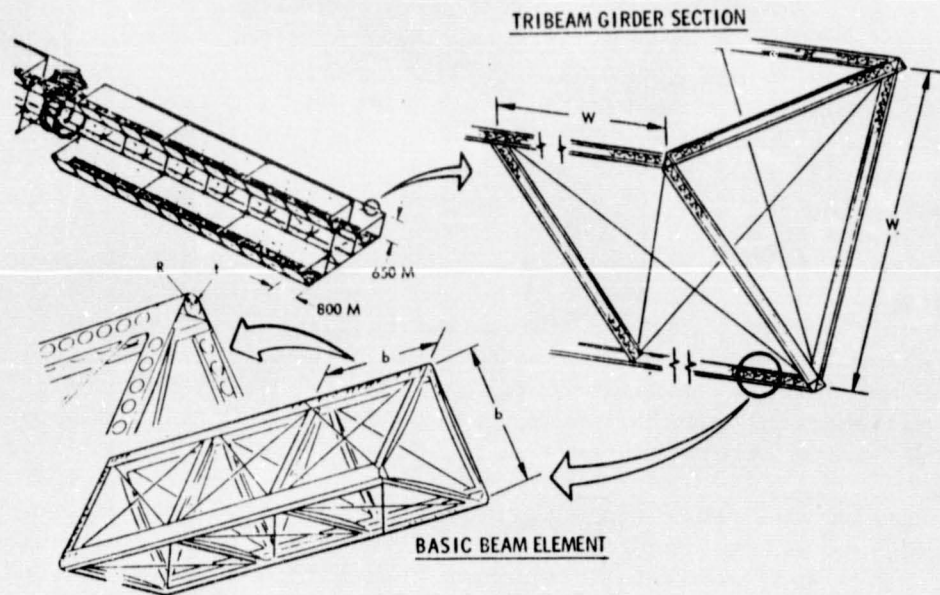
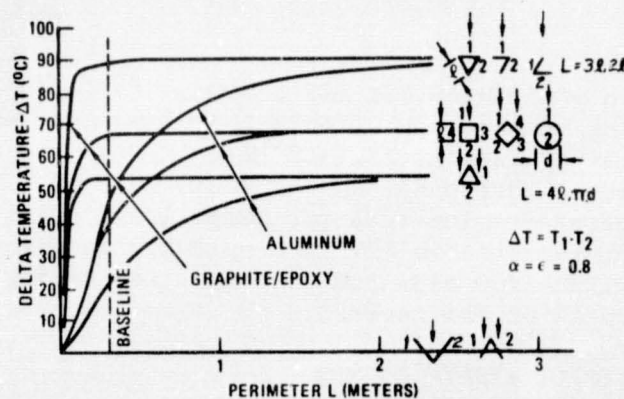


Figure 3.4-14. Photovoltaic Wing Structure Tiering

For purposes of sizing analyses, the caps and struts were considered to be tubes of radius,  $R$ , and wall thickness,  $t$ . In the actual application to SPS, the shape of the caps, in particular, will be dictated by minimum mass and beam machine compatibility considerations. The objective of this study was not to trade one cap shape vs. another but to determine the direction the detail design should take that will result in a minimum mass structural system compatible with on-orbit fabrication.

The first parameter investigated was the effect of shape on temperature gradient across the cap cross-section. Figure 3.4-15 presents results of a thermal analysis, and plots temperature gradient vs. cross-section perimeter



ORIGINAL PAGE IS  
OF POOR QUALITY

Figure 3.4-15. Temperature Gradient as Function of Subelement Shape

for a number of different cap shapes subjected to a heat flux of one sun. The emissivity ( $\epsilon$ ) and absorbtivity ( $\alpha$ ) are assumed equal to 0.8 for all shapes. The open triangular cap with its apex directly toward the sun, or  $180^\circ$  to the sun, experiences little or no temperature gradient as indicated by the shape



located on the ordinate. This is true regardless of the perimeter dimension of the open triangular section. However, in a triangular basic beam element (Figure 3.4-14), for every cap oriented with the apex directly toward or away from the sun, the two other caps are oriented toward the sun, as indicated in the top right corner of Figure 3.4-15, and experience a temperature gradient as high as a closed triangular section with one vertex pointing 180 degrees from the heat source. The conclusion reached is that the temperature gradient problem cannot be significantly minimized by cap shaping when the complete "basic beam element" is considered. The impact of temperature gradients can best be minimized by material selection and the application of thermal coatings to tailor  $\epsilon$  and  $\alpha$  for the environment.

The criterion for cap-shaping is, then, to obtain the highest critical stress for a given mass over a given length—considering beam machine compatibility. The cap sections are critical in general and/or local instability. The optimum cap shape is one that develops the highest column-buckling stress ( $\sigma_{cn}$ ) combined with an equally high local crippling stress ( $\sigma_{cc}$ ). Figure 3.4-16 tabulates properties for three closed tubes with circular, square, and triangular cross-sections. Each section contains the same cross-sectional area and, hence, the same mass for a given length. All results are expressed in terms of equivalent tube diameter. As indicated, the circular tube develops the highest

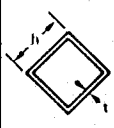

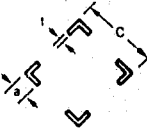
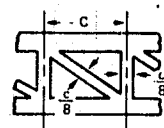
PARAMETER							
		FORMULA	EQUIVALENT CYLINDER	RATIO	FORMULA	EQUIVALENT CYLINDER	RATIO
PERIMETER P (IN)	$\pi D$	$4h$	$\pi D$	1	$3b$	$\pi D$	1
AREA A (IN) <sup>2</sup>	$\pi Dt$	$4ht$	$\pi Dt$	1	$3bt$	$\pi Dt$	1
EQUIVALENT DIMENSION	—	—	$h = \frac{\pi}{4} D$	—	—	$b = \frac{\pi}{3} D$	—
INERTIA I (IN <sup>4</sup> )	$0.393 D^3 t$	$.667 h^3 t$	$.321 D^3 t$	.822	$.250 b^3 t$	$.287 D^3 t$	.731
RADIUS OF GYRATION P (IN)	$0.354 D$	$.408 h$	$.321 D$	.907	$.289 b$	$.302 D$	.854
COL BUCKLING $\sigma_{cn}$ (PSI)	$.125 \frac{\pi^2 E}{(l/D)^2}$	$\frac{\pi^2 E}{[l/(.408 h)]^2}$	$.103 \frac{\pi^2 E}{(l/D)^2}$	.824	$\frac{\pi^2 E}{[l/(.289 b)]^2}$	$.091 \frac{\pi^2 E}{(l/D)^2}$	.730
CRIPPLING $\sigma_{cc}$ (PSI)	$2.76 \times 10^{10} \left(\frac{t}{D}\right)$	$.56 \sigma_{cy} \left[ \frac{12t}{\pi D} \left(\frac{E}{\sigma_{cy}}\right)^{1/2} \right]^{.85}$	$.612 \times 10^{10} \left(\frac{t}{D}\right)^{.85}$	.507	$.56 \sigma_{cy} \left[ \frac{9t}{\pi D} \left(\frac{E}{\sigma_{cy}}\right)^{1/2} \right]^{.85}$	$.479 \times 10^{10} \left(\frac{t}{D}\right)^{.85}$	.399

- 1) CONSTANT AREA, PERIMETER AND THICKNESS
- 2) MODULUS OF ELASTICITY  $E = 6.895 \times 10^4 \text{ MPa}$
- 3) YIELD STRESS  $\sigma_{cy} = 386 \text{ MPa}$
- 4) FOR CRIPPLING COMPARISON  $t/d = .004$

Figure 3.4-16. Allowable Stress Levels as Function of Subelement Shape



column-buckling stress ( $\sigma_{cn}$ ) and crippling stress ( $\sigma_{cc}$ ) and is therefore superior to the square and triangular sections. Figure 3.4-17 operates on the square tube concept and develops higher critical stresses—first, by opening the section and then by introducing cutouts and increasing the envelope size while retaining the same equivalent cross-sectional areas and mass per unit length.

PARAMETER					
EQUIVALENT DIMENSION	$h = \frac{\pi}{4} D$	$b = 1.259D$	$b = 1.312D$	$c = 1.147D$	$c = 1.335D$
FLANGE LENGTH(M)		$a = \frac{b}{4}$	$a = \frac{b}{5}$	$a = \frac{c}{4}$	$a = \frac{c}{5}$
AREA: A(M <sup>2</sup> )	3.142 D <sup>2</sup>	3.142D <sup>2</sup>	3.142D <sup>2</sup>	0.573D <sup>2</sup> : ANGLE 2.29D <sup>2</sup> : X-SECT 3.142D <sup>2</sup> : WEIGHT	0.534D <sup>2</sup> : ANGLE 2.136 D <sup>2</sup> : X-SECT 3.142D <sup>2</sup> : WEIGHT
RADIUS OF GYRATION: e(M)	0.321D	0.102D	0.082D	0.508D: SECTION 0.840: ELEMENT	0.606D: SECTION 1.031: ELEMENT
INERTIA I(M <sup>4</sup> )	0.323D <sup>4</sup>	0.323D <sup>4</sup>	0.322D <sup>4</sup>	0.591D <sup>4</sup> : SECTION 0.0019D <sup>4</sup> : ELEMENT	0.785D <sup>4</sup> : SECTION 0.0016D <sup>4</sup> : ELEMENT
COLUMN BUCKLING $\sigma_{cn}$ (Pa)	$0.103 \frac{\pi^2 E}{(L/D)^2}$	$0.102 \frac{\pi^2 E}{(L/D)^2}$ : COL $0.010 \frac{\pi^2 E}{(L/D)^2}$ : TOR	$0.104 \frac{\pi^2 E}{(L/D)^2}$ : COL $0.014 \frac{\pi^2 E}{(L/D)^2}$ : TOR	$0.259 \frac{\pi^2 E}{(L/D)^2}$ : SECTION $0.206 \frac{\pi^2 E}{(L/D)^2}$ : ELEMENT TOR STAB	$0.366 \frac{\pi^2 E}{(L/D)^2}$ : SECTION $0.226 \frac{\pi^2 E}{(L/D)^2}$ : ELEMENT TOR STAB
CRIPPLING $\sigma_{cc}$ (Pa)	$3.13 \infty \left(\frac{L}{D}\right)^{0.85}$	$2.21 \infty \left(\frac{L}{D}\right)^{0.85}$	$2.21 \infty \left(\frac{L}{D}\right)^{0.85}$	$2.90 \infty \left(\frac{L}{D}\right)^{0.85}$	$3.07 \infty \left(\frac{L}{D}\right)^{0.85}$
% VOID	-	-	-	31.3	41.3

- 1) CONSTANT WEIGHT & THICKNESS
- 2)  $\infty = .56 (\sigma_{cy})^{.575} (E)^{.425}$

Figure 3.4-17. Square Tube Shape Optimization

The data are expressed in terms of the closed tube diameter so that a direct comparison can be made. The results indicate that a square tube with 41.3% cutouts has a column-buckling critical stress

$$\left( \sigma_{cn} = 0.390 \frac{\pi^2 E}{(L/D)^2} \right)$$

as compared with the circular tube

$$\left( \sigma_{cn} = 0.125 \frac{\pi^2 E}{(L/D)^2} \right)$$

or almost a 200% increase in allowable operating stress level. Figure 3.4-18 presents the same type of data for the triangular tube and yields an even greater improvement in column-buckling capability than the square section—i.e.,

$$-0.390 \frac{\pi^2 E}{(L/D)^2} \text{ vs. } 0.366 \frac{\pi^2 E}{(L/D)^2} .$$



ORIGINAL PAGE IS  
OF POOR QUALITY

PARAMETER					
EQUIVALENT DIMENSION	$b = \frac{\pi}{3} D$	$h = 1.25D$	$h = 1.26D$	$c = 1.524D$	$c = 1.76D$
FLANGE LENGTH(M)		$a = \frac{h}{4}$	$a = \frac{h}{4}$	$a = \frac{c}{4}$	$a = \frac{c}{5}$
AREA: A(M <sup>2</sup> )	3.142Dt	3.142Dt	3.142Dt	0.76Dt: ANGLE 2.28Dt: X-SECT 3.142Dt: WEIGHT	0.7Dt: ANGLE 2.14Dt: X-SECT 3.142Dt: WEIGHT
RADIUS OF GYRATION: c(M)	0.302D	0.354D(Y-DIR) 0.088D(X-DIR)	0.376D(Y-DIR) 0.095D(X-DIR)	0.516D: SECTION 0.936t: ELEMENT	0.625D SECTION 1.30t: ELEMENT
INERTIA I(M <sup>4</sup> )	0.287D <sup>3</sup> t	0.397D <sup>3</sup> t(X-X) 0.474D <sup>3</sup> t(Y-Y)	0.444D <sup>3</sup> t(X-X) 0.488D <sup>3</sup> t(Y-Y)	0.607D <sup>3</sup> t: SECTION 0.0023D <sup>3</sup> t: ELEMENT	0.838D <sup>3</sup> t: SECTION 0.0018D <sup>3</sup> t: ELEMENT
COLUMN BUCKLING $\sigma_{cn}$ (Pa)	$0.091 \frac{\pi^2 E}{(t/D)^2}$	0.125 $\frac{\pi^2 E}{(t/D)^2}$ : COL 0.0078 $\frac{\pi^2 E}{(t/D)^2}$ : TOR	0.141 $\frac{\pi^2 E}{(t/D)^2}$ : COL 0.0091 $\frac{\pi^2 E}{(t/D)^2}$ : TOR	0.266 $\frac{\pi^2 E}{(t/D)^2}$ : SECTION 0.445 $\frac{\pi^2 E}{(D/t)^2}$ : ELEMENT TOR STAB	0.390 $\frac{\pi^2 E}{(t/D)^2}$ : SECTION 0.642 $\frac{\pi^2 E}{(D/t)^2}$ : ELEMENT TOR STAB
CRIPPLING $\sigma_{cc}$ (Pa)	$2.64 \infty (\frac{t}{D})^{.85}$	$2.39 \infty (\frac{t}{D})^{.85}$	$2.39 \infty (\frac{t}{D})^{.85}$	$2.45 \infty (\frac{t}{D})^{.85}$	$2.60 \infty (\frac{t}{D})^{.85}$
% VOID	-	-	-	31.3	41.3

1) CONSTANT WEIGHT & THICKNESS  
2)  $\infty = .56 (\nu_{cy})^{.575} (E)^{.425}$

Figure 3.4-18. Allowable Stress Levels as a Function of Size and Shape

However, for the triangular and square sections analyzed, the indicated values of element critical torsional stability stress and critical crippling stress ( $\sigma_{cc}$ ) are significantly lower than the circular tube allowable (i.e., for the triangular section with 41.3% cutouts

$$0.642 \frac{\pi^2 E}{(D/t)^2} = 6.99 \text{ m Pa, and } 2.60 \infty (t/D)^{.85} = 46.6 \text{ m Pa,}$$

while the critical crippling stress for the circular tube is

$$= 2.76 \times 10^{10} t/D = 110.4 \text{ m Pa}.$$

This indicates a need for flanging the cutouts to improve these critical stress levels. This flanging can easily be accomplished by the beam machine during the cap-forming operation.

In summary, pending a detailed design development program aimed specifically at cap design, the results of the above analysis indicate the selection of a cap that is triangular in cross-section. It should incorporate flanged cutouts, sized and placed so that the critical stress levels for the section (and all elements within the section) approach the yield stress of the material and are essentially equal to each other. Figure 3.4-19 depicts a cap design concept that is in line with the results of the above analysis and is



compatible with one of the Rockwell beam builder concepts. The cutouts are circular and are stamped out of the sheet stock during ground preprocessing operations. The sheet stock is rolled on spools and stored in canisters for delivery to the construction site. Three canisters are attached to and fed through a beam builder to form a triangular basis beam element 2 m on a side (Figure 3.4-14). The caps are formed and welded and the cutouts flanged during the on-orbit fabrication process. The cap section shown has not been subjected to the detailed analysis and test activity required to determine the optimum size and shape. It is presented here only as an example of what is envisioned for SPS structure.

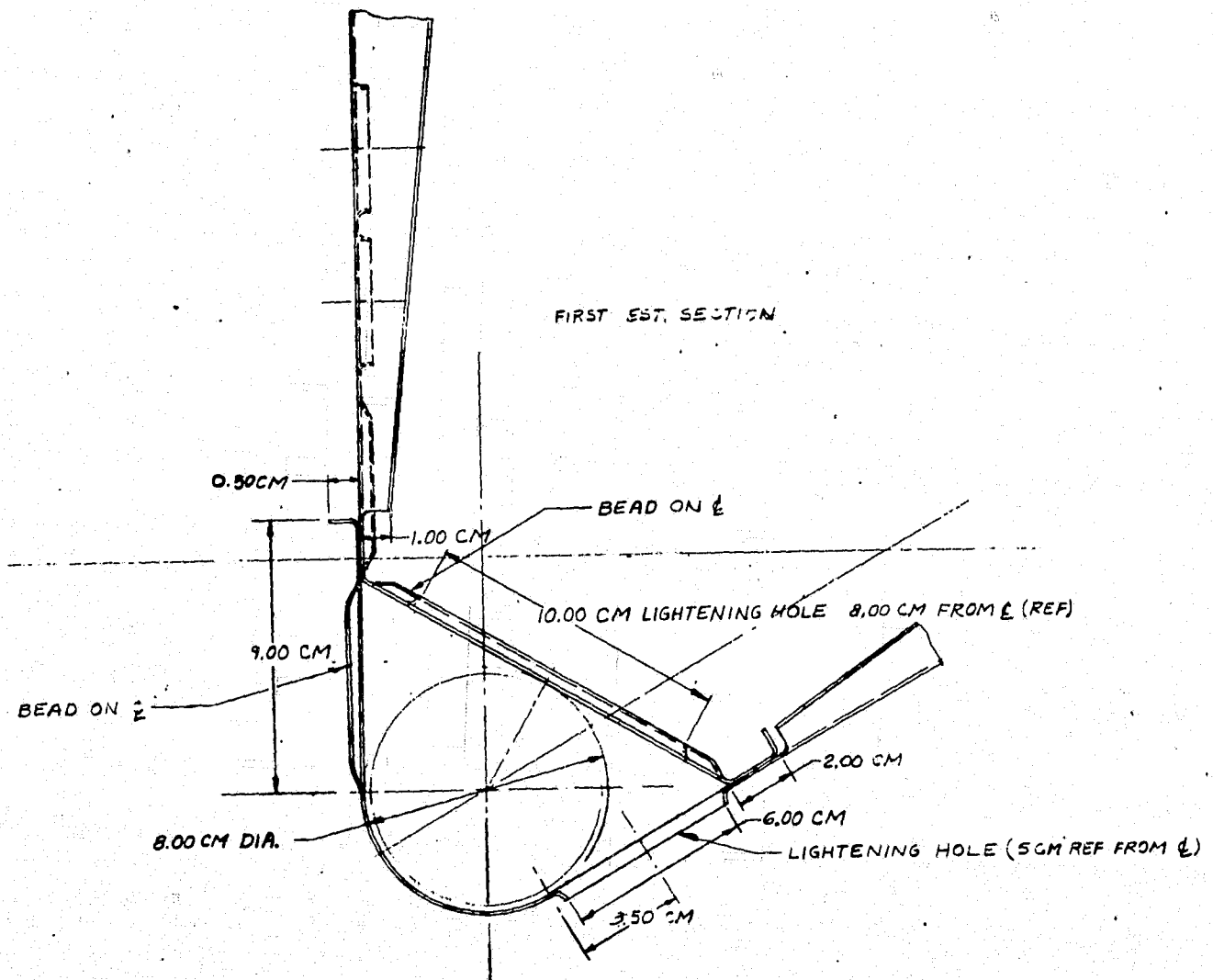


Figure 3.4-19. Basic Beam Element Cap Section

ORIGINAL PAGE IS  
OF POOR QUALITY



### 3.5 ATTITUDE CONTROL & STATIONKEEPING SUBSYSTEM (ACSS) CONCEPT EVOLUTION

The purpose of this section is to summarize the SPS concept evolution trades that impact the attitude control and stationkeeping functions, and to develop the requirements for the point design spacecraft and the ACSS itself. The material reported herein is the joint result of complementary studies performed by NASA/MSFC and Rockwell study teams.

The immense size of the spacecraft relative to contemporary vehicles is found to modify the complexion of the attitude control problem sufficiently so that a reevaluation of many basic stabilization and control approaches is warranted as well as the development of certain new techniques. The factors considered in the trades include:

- Orbit plane selection
- How the control requirements vary with spacecraft dimensions and aspect ratio
- Evaluation of spacecraft configurational alternatives which impact ACSS requirements so as to optimize the overall system
- Consideration of a broad group of control techniques and sub-system alternatives
- An assessment of control system bandwidth requirements and the related structural dynamic frequency requirements
- An evaluation of passive and active figure control concepts for the higher concentration ratio solar collectors
- RCS propulsion type trades and thruster configuration alternatives
- An assessment of the stabilization and control requirements for SPS construction in LEO and low thrust transfer to GEO

Due to the report space limitations the background for developments is either summarized very briefly or reference is given to more complete treatments.

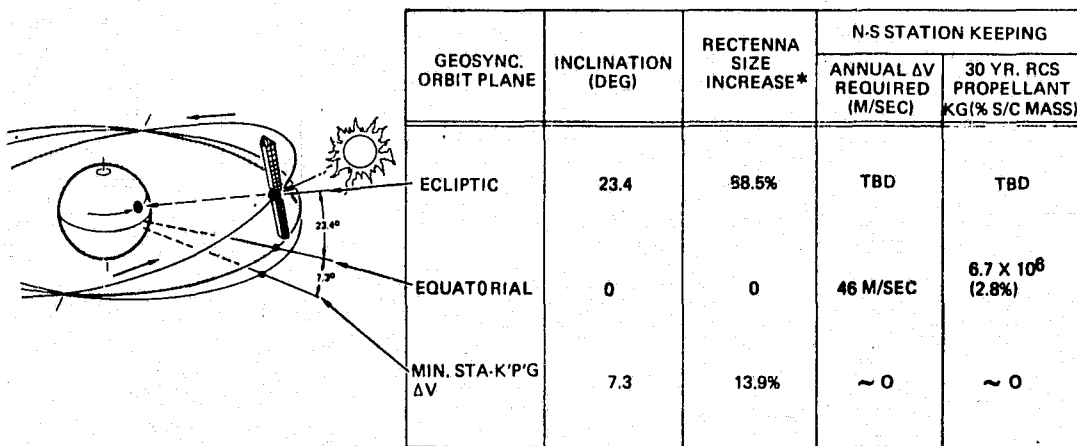
The ACSS requirements are given in Volume II. Some of these requirements are the functional requirements that are used as a starting point for the trades in this section of the report. Other more detailed requirements are based on the results of the analysis presented in this section. The point design which resulted from the trades and requirements analysis of this section is described in Volume IV, SPS Point Design Definition.

#### 3.5.1 ORBIT SELECTION TRADES

The continuous earth visibility and near continuous solar visibility afforded by the geosynchronous orbit makes it highly desirable for SPS and the only remaining issue is the selection of the inclination of the orbit



plane. Three orbits which possess features attractive to SPS are illustrated in Figure 3.5-1. The 7.3° inclined orbit can eliminate the north-south stationkeeping  $\Delta V$  requirement. The ecliptic orbit has the desirable feature that direct solar pointing (no collector pointing losses) can be achieved in a "wings-level" (Y-POP) orientation which minimizes the gravity gradient torques and resulting RCS propellant consumption. However, it suffers from a daily earth eclipse period of 1.23 hours (5.14% of the time). The equatorial orbit is eclipsed less than 0.97% of the year on the average. The equatorial orbit results in a peak collector efficiency loss of 8% when flying in this Y-POP "wings-level" orientation. Other pertinent data are summarized in the figure.



\* FOR 34° LATITUDE (LOS ANGELES)

CONCLUSION: EQUATORIAL ORBIT PREFERRED, DUE TO HIGH \$ COST OF INCREASED RECTENNA SIZE.

Figure 3.5-1. Orbit Selection Trade

The increased rectenna size requirement for various orbit inclinations and rectenna longitudes is found to be the dominant factor in this trade. To illustrate this, the data presented in Figure 3.5-2 have been prepared. The principal parameter of interest is the rectenna length to width parameter (L/W). For the more northern latitudes the L/W may be seen to increase quite rapidly past a latitude of 40°. The rectenna width (W) remains constant for various latitudes. The rectenna cost is expected to be in the same order of magnitude as the spacecraft itself. Hence, it is concluded that rectenna costs will increase substantially for locations at more northern latitudes and for inclined orbits.

For a careful review of the data presented in Figure 3.5-1, it may be deduced that the increased rectenna costs due to the increased rectenna size requirements of the inclined orbits (7.3° and ecliptic orbit) will dominate over all the other factors (propellant supply, eclipse time, and collector losses). The equatorial orbit is selected on this basis.



ORIGINAL PAGE IS  
OF POOR QUALITY

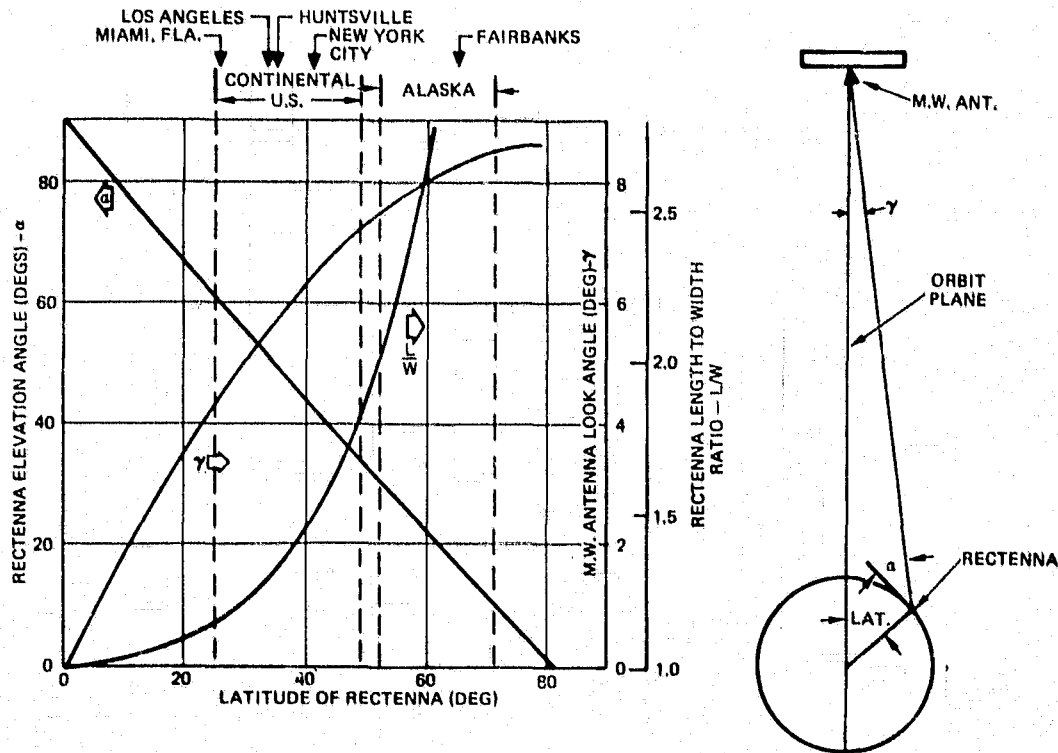


Figure 3.5-2. Rectenna Parameters Vs. Latitude

### 3.5.2 ATTITUDE CONTROL TECHNIQUES TRADES

This section presents the basic attitude control techniques trades including spacecraft configuration alternatives and trade data to support the overall spacecraft configuration design trades. The trade tree presented in Figure 3.5-3 illustrates these trades and the evolution of the point design ACSS. Most of the trades in the upper row are primarily vehicle configuration trades and are motivated by a desire to find configurations which will minimize overall system mass, complexity, cost and the potentially large RCS propellant resupply requirements. These spacecraft configuration trades were clearly the most productive relative to the ACSS system trades and overall system savings. This is due to the dominance of the gravity gradient disturbance torques and the impact of the spacecraft geometry and orientation on these disturbance torques. The selected approaches are underlined and the rejected ones are denoted by an X. The details of these trades are presented in subsequent sections. The trade tree is useful as a road map to track the evolution of the system. The photovoltaic SPS baseline spacecraft that existed at the beginning of the study is generally used as the basis for comparison.

The trades were performed assuming a specific impulse of 5100 sec for an electric thruster RCS. Subsequently a specific impulse of 13,000 sec was found to be feasible and is utilized for the point design. The higher



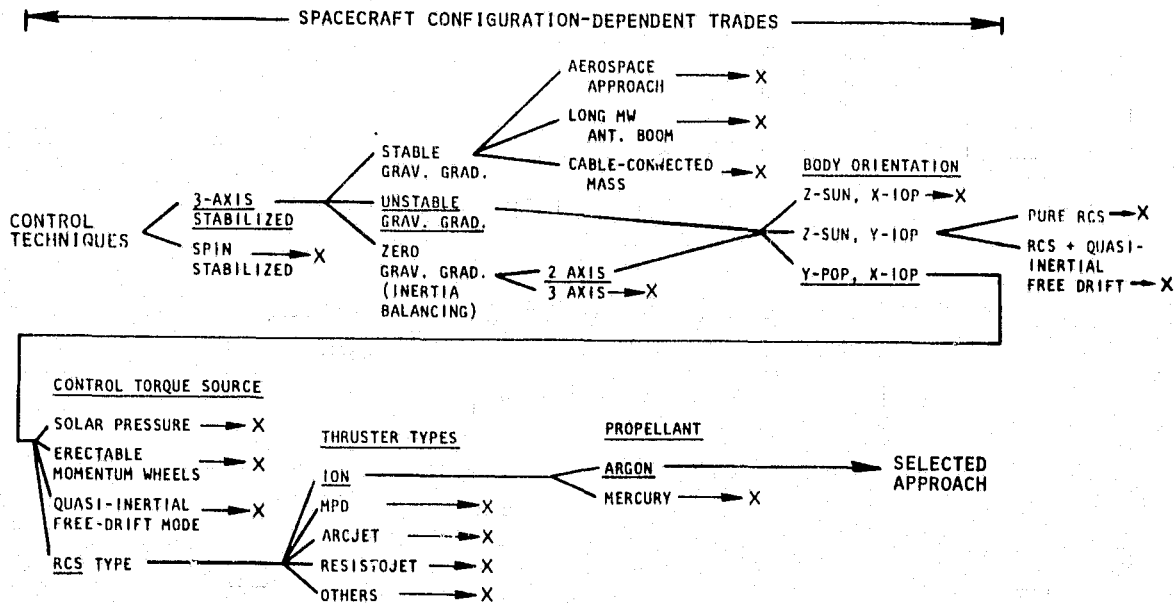


Figure 3.5-3. Attitude Control Techniques Trade Tree


specific impulse makes the selected approach even more attractive than is indicated in the trade study data.

#### Influence of Spacecraft Size on Control Parameters

Initially in the study it was found that the relative magnitudes of some of the SPS parameters of importance to the ACSS designer differed considerably from contemporary spacecraft practice. In order to gain insight into the behavior of these control parameters as a function of spacecraft size, the analysis summarized in Figure 3.5-4 was performed. It is assumed that the spacecraft proportions will remain constant as the size varies, i.e., L/H and L/W are constant. For instance, the SPS mass is dominated by the collector whose mass is proportional to area or dimension squared ( $\sim D^2$ ).

The results help explain why some parameters become much more important to SPS than they are for contemporary small unmanned spacecraft. For instance, the gravity gradient torque increases in proportion to  $(\sim) D^4$  which explains why it dominates over other torques (such as solar pressure) and are extremely large compared to contemporary spacecraft. Similarly, attitude control propellant requirements can become quite large because they are proportional to  $D^3$ . The momentum wheel mass increases rapidly with size ( $\sim D^3$ ) assuming that wheel diameter increases in proportion to spacecraft dimensions. Thus, from the relationships given, it may be deduced that large diameter momentum wheels are necessary if excessively heavy wheels are to be avoided. The first structural bending frequency ( $\sim D^{-2}$ ) gets lower for increasing size and can approach the environmental disturbance frequencies which occur at one and two times orbit frequency. This suggests that there is an upper size limitation for the SPS spacecraft. Fortunately, the data in subsequent sections illustrates that most current SPS designs have not reached this limit, even for operation in LEO.



- S/C MASS (& POWER) -  $M_V \sim L \times W$ ,  $\sim D^2$
  - GRAVITY GRADIENT TORQUE -  $3 \omega_0^2 (I_z - I_x) \sin 2\theta \sim D^4$   
 $\sim M_V r^2 \sim M_V L^2$ 


D - DIMENSION
  - SOLAR PRESSURE TORQUE -  $\sim P_S (1+R) A (CP - CG)$   $\sim D^3$
  - RCS PROPELLANT REQ'S -
    - ATTITUDE CONTROL -  $\sim$  GRAV. GRAD. TORQUE / MOMENT ARM  $\sim D^3$
    - STATIONKEEPING -  $\sim$  S/C MASS  $\sim D^2$
  - MOMENTUM WHEEL MASS -  $M_W$ ,  $\Delta H_{REQ} \sim$  GG TORQUE  $\times t \sim L^4$ ,  
 $\Delta H_{DELIVERED} \sim I_W \Omega \sim M_W D^2 \Omega$ ,  $\Omega \sim \frac{1}{t}$ ,  $\Delta H_{DEL} = \Delta H_{REQ}$   
 $M_W \sim D^3$        $\frac{M_W}{M_V} \sim \frac{D^3}{D^2} \sim D$
  - FIRST BENDING MODE FREQUENCY -  $\omega$ ,  $\sim \sqrt{\frac{EI}{M_T L^3}} \sim D^{-\frac{1}{2}}$
- \* - S/C DIMENSIONS HAVE CONSTANT PROPORTIONS, L/W & L/H ARE CONSTANT

Figure 3.5-4. Influence of S/C Size On Control Parameters\*

### Spacecraft Configuration Trades

Some of the spacecraft configuration options considered are presented in Figures 3.5-5 and 3.5-6. Spin stabilization has the advantage of providing a measure of stability, and the centrifugal acceleration to tension in very light weight structure. It requires considerable additional complexity in the despun drive, antenna articulation and power distribution systems to achieve MW antenna pointing at the earth and is discarded on this basis.

Gravity gradient (GG) stabilization is intrinsically appealing to minimize attitude control RCS propellant requirements. The long MW antenna boom and cable-connected GG stabilization mass concepts can achieve this goal. However, both of these concepts impose substantial hardware mass and complexity penalties relative to the baseline system employing the ion thruster RCS system. The long MW antenna boom concept is rejected on the basis that it imposes a large penalty in additional power conductor and structural mass as well as requiring an additional antenna gimbal so that the boom is not constrained to point at the rectenna. The cable connected GG stabilized concept has the disadvantage of additional mass and complexity beyond the baseline system and is rejected on that basis. It also moves the mass center of the system out of the spacecraft body which produces an RCS propellant penalty (or necessitates RCS propulsion on the stabilization mass) to counter the moments produced by stationkeeping  $\Delta V$  corrections.

The Gravitationally Stabilized Solar Power Spacecraft (GSSPS), a GG stabilized spacecraft concept from the Aerospace Corporation, is included in Figure 3.5-6 because of the recent attention it has seen in several technical society papers and the AIAA journal and magazine. It represents a very

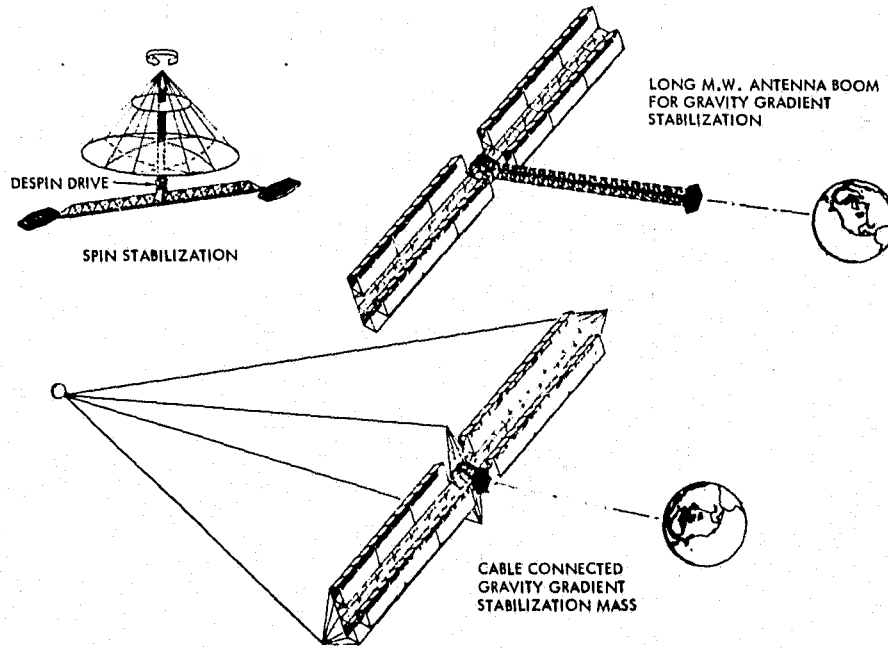
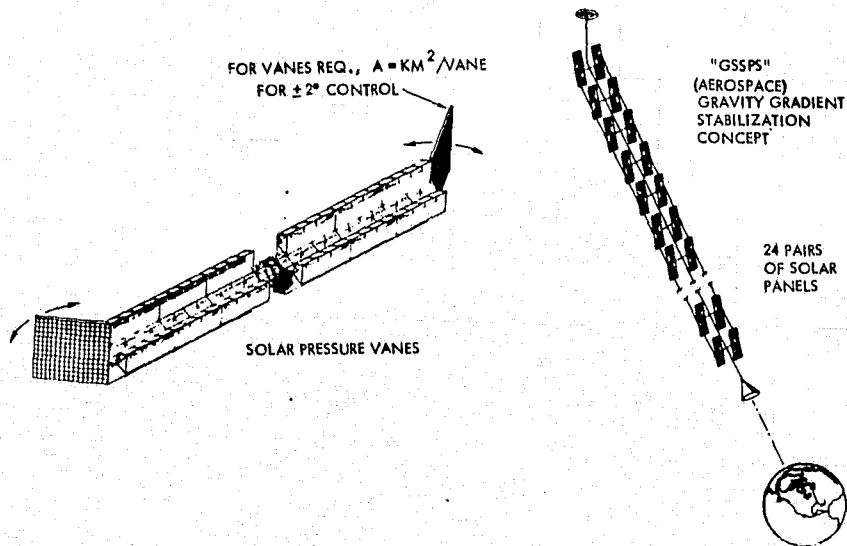


Figure 3.5-5. Some Alternative Configurations Considered



ORIGINAL PAGE IS  
OF POOR QUALITY

Figure 3.5-6. Additional Alternative Configurations Considered



innovative cable-connected approach which employs GG libration control in phase with the orbital position to prevent the shadowing of the lower solar panels by the upper ones. It appears to have the following penalties, any one of which probably qualifies it as inferior to the present point design configuration:

1. The flexibility of the cable connected vehicle necessitates station-keeping thrusters and attitude sensor systems located on virtually all of the solar panel modules (24 modules). The concept designers also suggest the installation of momentum storage equipment on each of the solar panel modules. Thus, each module has the essential equipment and complexity of a free flying spacecraft. The dynamics of the cable connected modules during stationkeeping thrusting constitutes a formidable control problem at best.
2. The concept designers have not investigated the solar panel shadowing problems (libration phasing) at intermediate seasons and it is suspected that shadowing problems may exist during these time periods.
3. The passive libration damper (shown at the top of the vehicle) will be very massive, a feature which has been illustrated in numerous GG libration damper designs from early unmanned spacecraft designs.
4. The phasing of the GG librations with respect to the sun vector requires the libration frequency to be controlled. The natural libration frequency will be significantly less than the desired two cycles per day due to the spacecraft mass distribution and due to the large amplitude libration required for a portion of the year. It is suspected that a significant RCS (or equipment) penalty will be necessary to increase the natural libration frequency to the desired value.
5. The extreme length of the concept ( $> 72$  km) will probably result in substantially greater power losses between the solar arrays and the MW antenna than would be possible with a more compact spacecraft design employing the same power distribution techniques.

The solar pressure torques are large enough to permit spacecraft control using solar pressure vanes (see Figure 3.5-6). A typical system will require four gimbaleed vanes for three axis control. A single vane will require approximately two  $\text{km}^2$  area to counter the gravity gradient torques over a control range of  $\pm 2^\circ$ . The concept is rejected on the basis of its larger mass requirements than for the point design system and its larger potential for structural dynamic interaction.

In addition to the above, spacecraft configurations with equal moments of inertia about all three axes (3-axis inertia balancing) have been explored in an attempt to minimize the gravity gradient torques. The effort proved fruitless and the configurations were so ungainly that they are not illustrated here. The problem is that solar collector designs tend to be flat and the achievement of the desired symmetrical mass distribution results in substantial structural complexity, and structural and power distribution cabling mass

penalties. However, two dimensional mass balancing (zero gravity gradient torque about a single axis) has been found to be quite feasible and will be treated in the next section.

Attitude Control Subsystem Approaches for Photovoltaic Configurations

Figure 3.5-7 conceptually illustrates the control techniques which offer the greatest promise and hence have received more detailed numerical analysis. The concepts have been described more completely in previous study briefings and reports. The erectable momentum wheel parameters shown have been sized

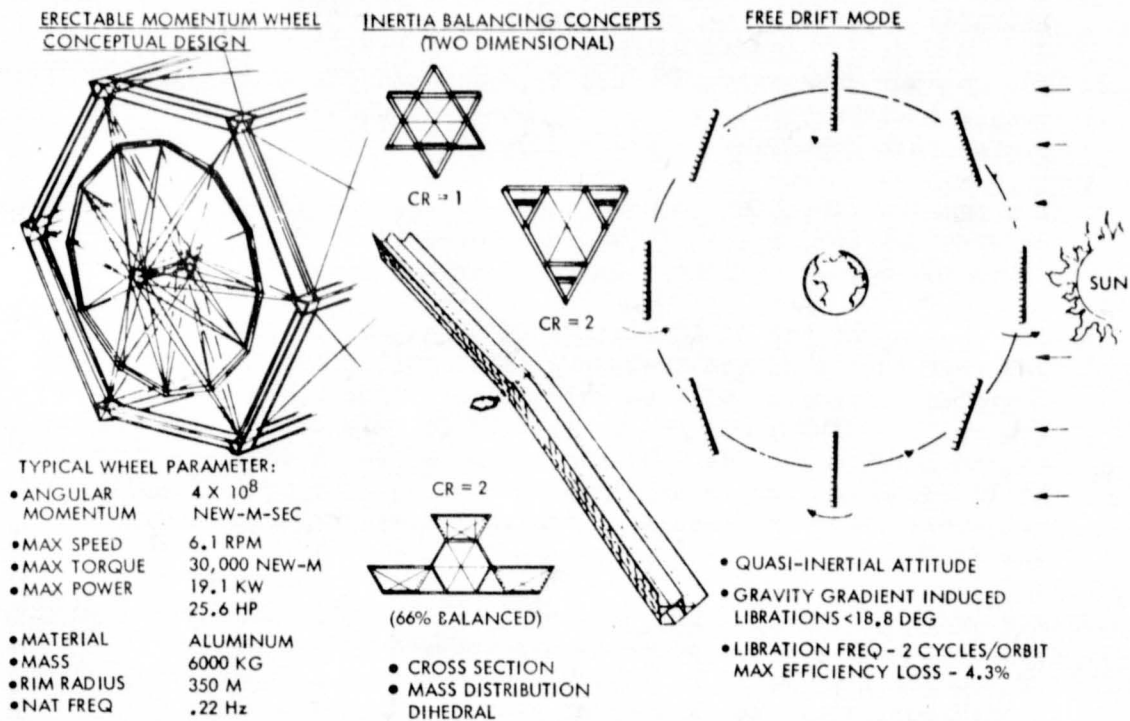


Figure 3.5-7. Attitude Control Subsystem Approaches

to minimize its mass consistent with the size limitations permitted by the spacecraft structure. Parametric sizing data for these wheels is given in Figure 3.5-8. These wheels must be constructed or erected on-orbit due to the payload dimension limitations of the booster vehicle. From this data, the mass saving advantages of large diameter wheels are quite apparent. The use of composite materials results in a wheel mass that is approximately 1/3 the value of an aluminum wheel. However, aluminum is selected for the wheels in order to utilize the same construction machinery (and technology) that is employed to manufacture the SPS satellite structure.

The quasi-inertial free drift mode illustrated in Figure 3.5-7 has been developed to eliminate the RCS propellant consumption due to the cyclic gravity-gradient disturbance torques. This is achieved by permitting the spacecraft to librate in response to the cyclic disturbance torques. The



ORIGINAL PAGE IS  
OF POOR QUALITY

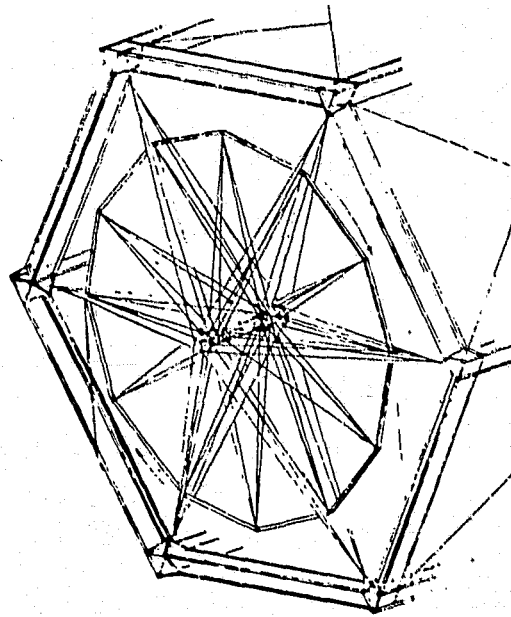
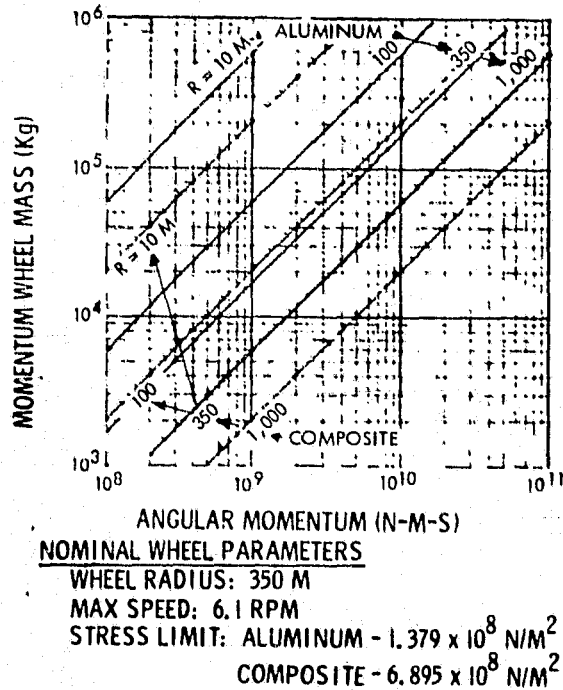


Figure 3.5-8. Momentum Wheel Sizing Data

angular momentum induced in the spacecraft is absorbed as kinetic energy. The maximum gravity-gradient induced libration is  $\pm 18.8$  degrees and occurs at two cycles per orbit. A more comprehensive analytical development and description of this mode is presented in the earlier SPS study.<sup>1</sup>

Several concepts for the achievement of two dimensional inertia balancing are illustrated in Figure 3.5-7. The two dimensional inertia balancing results in approximately zero gravity-gradient torques about the long axis of the spacecraft. The technique thus eliminates the cyclic gravity-gradient torques which the other two techniques described above are designed to accommodate. The balancing techniques illustrated consist of adjusting the mass distribution within the spacecraft cross section (the star or the triangular shape), or by using small amounts of dihedral ( $\sim 5^\circ$ ) to achieve the same effect.

Another factor which impacts the ACSS requirements is the choice of spacecraft reference attitude. Figure 3.5-9 graphically illustrates three potential satellite attitude orientations, and the notation and conventions used in subsequent analysis. For instance, Case B, the Y-POP X-IOP case, is the baseline orientation for the photovoltaic configuration. It means the Y-body axis (long axis of the vehicle) is "perpendicular to the orbit plane" (POP), and the X-body axis (out of the paper) is "in the orbit plane" (IOP). Because the ecliptic plane is  $23.4^\circ$  inclined to the equatorial plane, this orientation does not always point the solar collectors directly at the sun but will always point them within  $23.4^\circ$  of the sun line. The orientation minimizes gravity

<sup>1</sup> "SPS Feasibility Study," Rockwell Report SD 76-SA-0239-2, December 1976

3-188

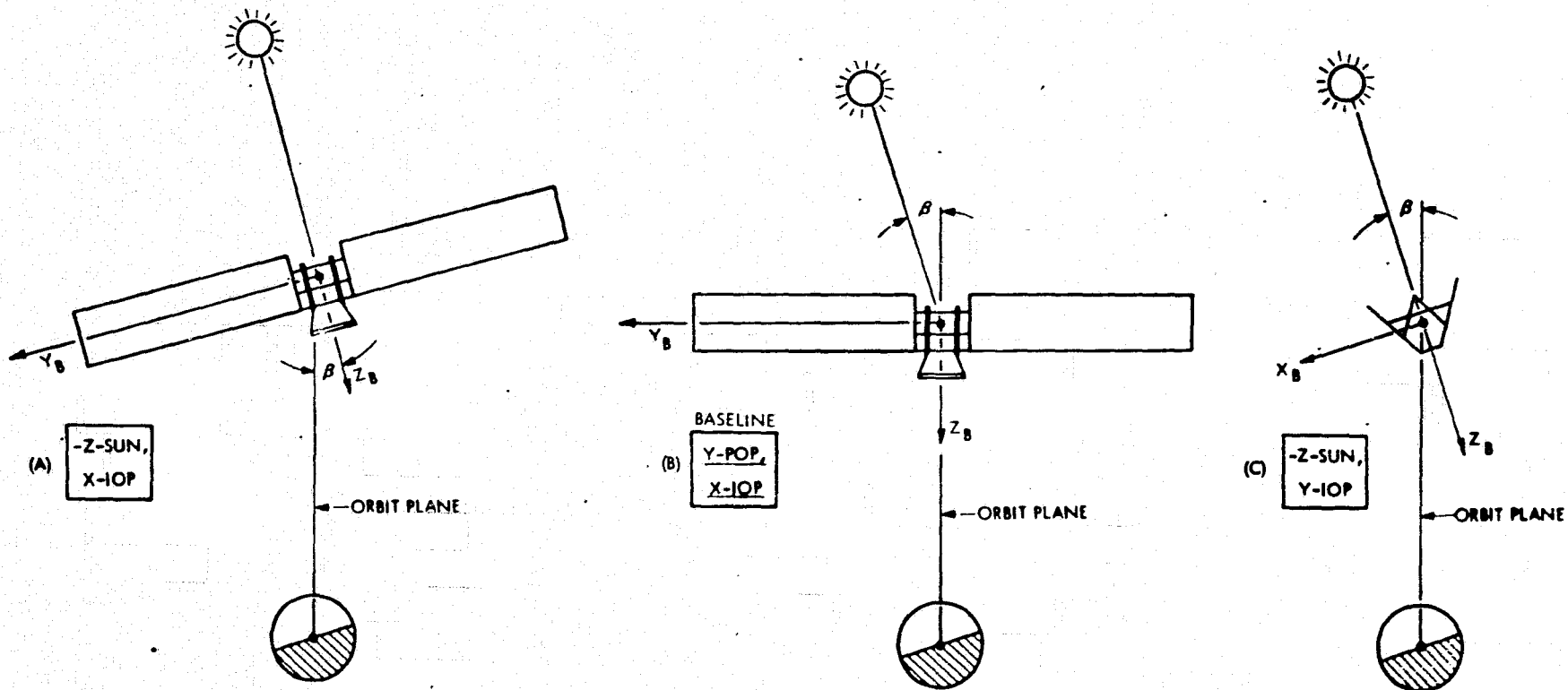


Figure 3.5-9. Attitude Orientation Description

SD 78-AP-0023-3



gradient torques at the expense of solar pointing error. The -Z-sun, X-IOP orientation (Case A) is similar to Case B except the spacecraft is rotated about the X-axis to provide direct solar pointing (-Z-sun). The -Z-sun, Y-IOP case, (Case C) points the solar collector directly at the sun, but places the X-axis (long axis of the vehicle) in the orbit plane. These two orientations (A and C) provide more accurate solar pointing at the expense of larger gravity-gradient torques.

Having developed the necessary background data for the erectable momentum wheels, the quasi-inertial free drift mode, inertia balancing, and the alternative attitude orientations we are prepared to quantitatively evaluate the merits of these techniques. Table 3.5-1 presents the key variables which are of concern in the control technique trades. The mass penalties are the 30-year propellant resupply requirement and the momentum storage equipment. The data was derived using a Rockwell disturbance torque analysis digital program to assess propellant and momentum storage requirements. The collector losses due to pointing error directly impact the solar collector sizing and therefore also impose a mass penalty. The first orientation (Case A) has an excessive propellant penalty and is discarded on that basis. Of the B options, cases B2 and B4 are most attractive. Case B4 results in slightly less total mass required to be placed on-orbit than case B2. However, B2 is expected to result in lower cost than B4 due to the lower cost of RCS propellant than the more complex momentum wheel hardware. On this basis B2 is the preferred approach and will result in a simple mechanization with total mass of only a few percent of the spacecraft mass.

Of the C options, C3 is clearly superior and makes use of the quasi-inertial free-drift mode to minimize the propellant usage due to the large cyclical gravity gradient torques experienced in this orientation. The data makes this option appear very attractive relative to option B2. However, all the C options require two side-mounted microwave antennas in order to simultaneously prevent beam interference with the structure and to obtain solar pressure torque balancing. The spacecraft must therefore be "double-sized" to produce twice the power output. The "double-sizing" is thought to produce additional mass penalties and complexity beyond the single antenna vehicle. The detailed analysis of "double-sized" two antenna vehicles is beyond the scope of the present activity but should be reconsidered in future SPS studies. Based on the above rationale the B2 option is the preferred baseline control technique.

#### Attitude Control Subsystem Approaches for Solar Thermal Configurations

The baseline solar thermal configuration and two alternatives for reducing RCS propellant requirements are illustrated in Figure 3.5-10. The tetrahedral configuration has not been evaluated at this time but is attractive for achieving the stated goal. The gimbaled collector option trades complexities of the gimbaled collectors for RCS propellant savings. A spacecraft with a single collector also offers some attractive features and should be considered in future SPS studies.

Numerical data for several solar thermal spacecraft orientations and control configurations are given in Table 3.5-2. Case 2 on the table achieves a dramatic reduction in RCS propellant consumption relative to the baseline by



Table 3.5-1. Attitude Control System Concept Comparison  
For Photovoltaic Configurations

ATTITUDE	ATTITUDE CONTROL SYSTEM	30-YR RCS PROPELLANT REQMT <sup>1</sup> (% VEH MASS) <sup>6</sup>	MOMENTUM STORAGE SYSTEM MASS - (% VEH MASS) <sup>6</sup>	MAX COLLECTOR LOSS DUE TO POINTING ERROR (%)	COMMENTS
(A) -Z-SUN X-IOP	RCS ONLY	28.6%	0	0	SECULAR DISTURBANCE TORQUES, PROP. REQMTS CANNOT BE REDUCED WITH WHEELS OR FDAMS, NOT VIABLE.
(B) Y-POP X-IOP	1. RCS ONLY (BASELINE)	4.27%	0	8.2% (4.11% ANNUAL AVERAGE)	BASELINE CONFIGURATION
	2. RCS + 2 DIM. BAL <sup>2</sup>	1.60% <sup>3</sup>	0	8.55%	CANTING PAYS OFF, PREFERRED Y-POP OPTION
	3. RCS + FREE DRIFT	1.60% <sup>3</sup>	0	13.4% (CR = 1)	UNACCEPTABLE COLLECTOR LOSS FOR CR > 1
	4. MOMENTUM STORAGE	NEGLIGIBLE <sup>2</sup>	1.5%	8.2%	GOOD ALTERNATIVE IF HIGH I <sub>sp</sub> RCS IS NOT ACHIEVABLE
(C) Z-SUN Y-IOP	1. RCS ONLY	44.1%	-	0	EXCESSIVE RCS PROP. RESUPPLY REQ'D, LARGE CYCLICAL DISTURBANCE TORQUES
	2. RCS + 2 DIM. BAL <sup>2</sup>	33.8%	-	0.38%	EXCESSIVE RCS RESUPPLY REQUIRED
	3. RCS + 2 DIM. BAL <sup>2</sup> + FREE DRIFT	1.52% <sup>3</sup>	-	5.7%	FREE DRIFT REALLY PAYS OFF! PREFERRED Z-SUN OPTION
	4. MOMENTUM STORAGE	NEGLIGIBLE <sup>2</sup>	5.8% <sup>3</sup>	0	ACCEPTABLE ALTERNATIVE
	5. MOMENTUM STORAGE + 2 DIM. BAL <sup>2</sup>	NEGLIGIBLE <sup>2</sup>	5.7% <sup>3</sup>	0.38%	ACCEPTABLE ALTERNATIVE

NOTES

<sup>1</sup>BASED ON ONE-DEG PRINCIPAL AXIS MISALIGNMENT, I<sub>sp</sub> = 5100 SEC

<sup>2</sup>DUMP MOMENTUM WITH GRAVITY GRADIENT TORQUES

<sup>3</sup>THREE MOMENTUM WHEELS

<sup>4</sup>TWO-DIMENSIONAL INERTIA BALANCING

<sup>5</sup>POTENTIAL FOR SIGNIFICANT PROPELLANT REDUCTION WITH SMART CONTROL POLICY

<sup>6</sup>SPACECRAFT MASS = 24.15 × 10<sup>6</sup> kg

3-190

SD 78-AP-0023-3

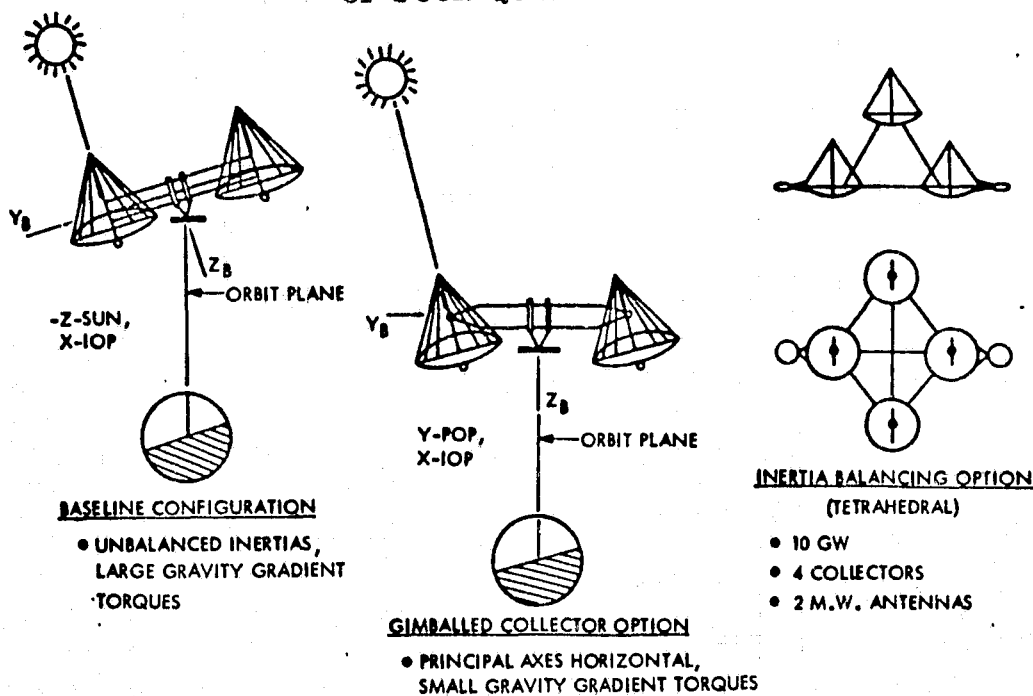


Figure 3.5-10. Solar Thermal Configurations to Minimize ACSS Requirements

Table 3.5-2. Attitude Control Concepts Comparison for Solar Thermal Configurations

ATTITUDE ORIENTATION	CONFIGURATION	30 YR RCS PROPELLANT REQUIREMENT- 10 <sup>6</sup> Kg (% OF VEH. MASS)	MOMENTUM STORAGE MASS 10 <sup>6</sup> Kg (% OF VEH. MASS)	COMMENTS
1) Z-SUN X-IOP	BASELINE, RCS CONTROL	4.0 (17.9%)	-	SECULAR MOMENTUM BUILDUP, MOM. STORAGE NOT APPLICABLE
2) Y-POP, X-IOP	RCS ONLY, GIMBALED COLLECTORS	0.68 (3.0%)	-	APPRECIABLE RCS SAVINGS, COLLECTOR GIMBALING INCREASES COMPLEXITY
3) Y-POP, X-IOP	GIMBALED COLLECTORS + MOMENTUM STORAGE	NEGLECTIBLE	0.068 (0.31%)	APPRECIABLE RCS PROPELLANT SAVINGS FOR SMALL MOM. STORAGE PENALTY



flying with the principal axes of inertia in a horizontal attitude so as to minimize the gravity-gradient torques (illustrated in Figure 3.5-10). Case 3 demonstrates an even greater mass savings through the addition of three momentum wheels. However, the complexity of the momentum wheel approach is unwarranted for the small propellant savings which it achieves and case 2 is preferred on this basis. The case 2 design concept has not been developed and has been selected as the baseline solar thermal spacecraft concept illustrated elsewhere in this report.

### Reaction Control System (RCS) Propulsion Trades

The above control techniques trades resulted in a simple system employing a RCS for attitude control torques and stationkeeping forces. These trades were based on the use of argon ion thrusters with an  $I_{sp} = 5100$  sec. To determine the relative merits of other propulsion types the data in Figure 3.5-11 was prepared.

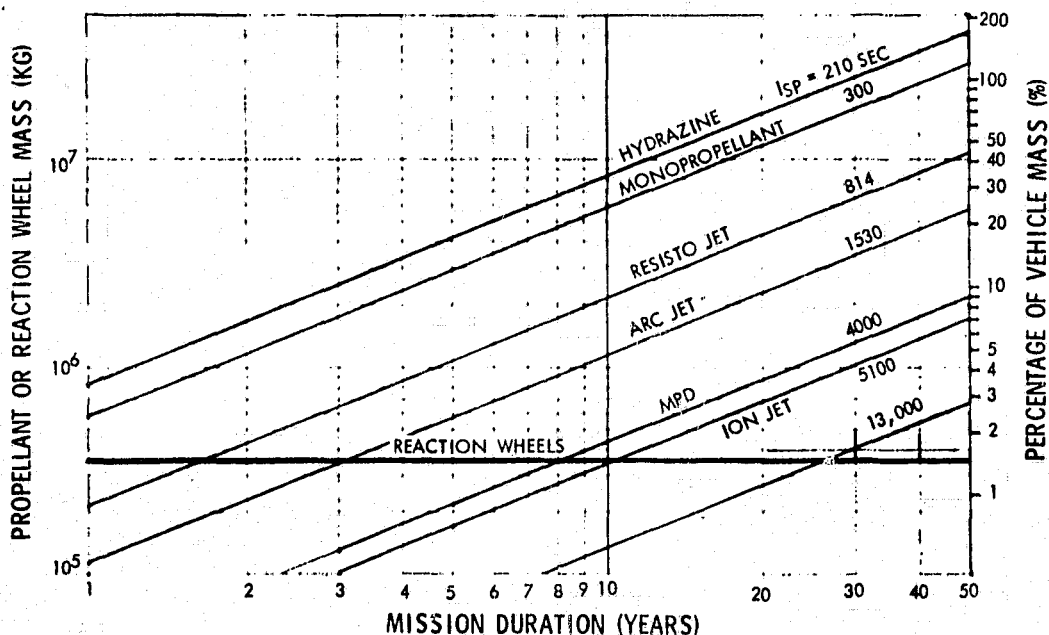


Figure 3.5-11. Attitude Control Propellant & Reaction Wheel Mass Photovoltaic Configuration (Y-POP, X-IOP)

Figure 3.5-11 illustrates that the RCS propellant resupply requirements for SPS are very large (and hence costly) for contemporary RCS with low specific impulse. The development of the high specific impulse electric thruster technology is highly desirable to prevent very large RCS propellant resupply costs. For satellite lifetimes appreciably greater than 30 years the erectable momentum wheels become more attractive even with high  $I_{sp}$  ion thrusters.

The data in Figure 3.5-11 is based on the attitude control requirements for the photovoltaic spacecraft baseline configuration that existed at the beginning of the current study. The addition of the stationkeeping propulsion requirements makes the high performance electric thrusters even more attractive



than is indicated in the figure. Argon is selected over other possible propellants such as mercury on the basis of the technology development status of thrusters using this propellant, the high performance available and relatively low cost. In order to minimize the argon tank mass the storage of the argon propellant in cryogenic form is selected over storage as a gas. This requires a small electrically driven refrigeration system for tankage heat loss makeup. Subsequent to these trades the achievement of a 13,000 sec specific impulse was found to be feasible and this value is employed for the point design. More details of the RCS system are given in the point design ACSS description.

### 3.5.3 STATIONKEEPING ALTERNATIVES AND RCS PROPELLANT REQUIREMENTS

The sources of stationkeeping perturbations, the required  $\Delta V$  correction magnitudes, and the RCS propellant requirements are summarized in Table 3.5-3. The requirement for the correction of the solar/lunar perturbations (north-south) is established as the result of the "Orbit Selection Trades" presented above. This trade selected the equatorial orbit in preference to the 7.1 deg inclined orbit which can reduce this  $\Delta V$  requirement to zero.

Table 3.5-3. Stationkeeping RCS Propellant Requirements

FUNCTION	$\Delta V/YR.$ ( $\sim M/SEC$ )	RCS PROPELLANT REQ'D*	
		(KG/YR)	OVER 30 YR (% S/C MASS)
• EARTH TRIAXIALITY (E-W)	2.1	430	0.05
• SOLAR/LUNAR PERTURBATIONS (N-S)	53.3	11,000	1.25
• SOLAR PRESSURE PERTURBATION (E-W)	344.7	76,500	8.12
• DIURNAL PERTURBATIONS	NOT REQ'D	-	-
• M.W. ANTENNA RADIATION PRESSURE (E-W)	NEGLIGIBLE	-	-
• STATION CHANGE MANEUVERS (E-W) (6 @ 2 DEG./DAY = 34.2 m/sec)	1.1	235	0.03
TOTAL WITH COMPLETE SOLAR PRESSURE CORRECTION***	399.1	87,700	9.4

- \* -  $I_{sp} = 13,000$  sec, PHOTOVOLTAIC CONFIGURATION
- \*\* - ELIMINATED IF  $\pm 3.1^\circ$  LONGITUDE PERTURBATION IS ACCEPTABLE
- \*\*\* - TOTALS ARE NOT ARITHMETIC SUM

The dominant stationkeeping propellant requirement is for the correction of solar pressure induced perturbations. The solar pressure perturbations are cyclical with an annual frequency and an amplitude of  $\pm 3.1$  deg if not corrected. In order to minimize the SPS space requirement in GEO and to prevent interference with the many other satellites using this orbit which do not experience as large a solar pressure acceleration as the SPS, it is assumed that this perturbation must be corrected. A stationkeeping accuracy of 0.1 deg is selected.

Because of the large propellant requirement to correct the solar pressure perturbation, means of reducing or alleviating it should be explored further. The corrective thrusting policy utilized herein places the thrust vector directly toward the sun (except during solar eclipse). A preliminary analysis of an alternate correction policy which corrects the perturbed orbit by



thrusting in the region of its peri- and apo-apse has been conducted. The results indicate a 25% propellant savings utilizing this corrective policy is potentially possible and should be investigated further.

A first order analysis performed in an earlier study<sup>2</sup> has shown that the solar pressure perturbation acting on a closely clustered group of SPS satellites will perturb the orbit of each spacecraft similarly. Therefore, it appears feasible to accept the  $\pm 3.1^\circ$  solar pressure perturbation with SPS spacecraft spacing that is very close. Unfortunately, by the year 2000 the geosynchronous orbit might be expected to be very crowded with spacecraft whose sensitivity to solar perturbations is much smaller (smaller A/M). Hence, the  $\pm 3.1^\circ$  perturbation may still require an excessively large portion of the geosynchronous orbit track. On this basis it is assumed that the solar pressure perturbation must be corrected.

The location of the rectenna sites within the continental U.S. impacts how the SPS spacecraft must be located in the geosynchronous orbit. This is due to a potentially large rectenna size (and cost) penalty if the SPS spacecraft are not located at a longitude within a few degrees of the rectenna longitude. The decision whether or not to correct the solar pressure perturbation should be reevaluated in the future considering the impact of rectenna siting on the SPS GEO space requirements and the space requirement impact on other GEO spacecraft. A requirement for national and international agreements on the utilization of the GEO potentially exists. Fortunately, these space allocation problems can potentially be solved through the use of a smaller number of larger spacecraft.

The earth triaxiality correction given in Table 3.5-3 is quite small and is based on a worst case longitude station.

#### 3.5.4 CONTROL SYSTEM/STRUCTURAL DYNAMIC INTERACTION

Due to the large size and relatively small mass of the SPS structure considerable concern was initially expressed that the structural frequencies would be high enough to permit satisfactory control. As a result, the following analysis was performed to define control system bandwidth and structural frequency requirements. Fortunately, the results indicate that the SPS operational control does not require wide bandwidth relative to some other satellites and satisfactory structural frequencies are easily achievable through the avoidance of structural design concepts that are not excessively thin.

The structural design requirements for SPS's appear to evolve from flight control requirements. A search has been conducted to define the dominant flight control requirement which would size the SPS structure. A preliminary list of requirements was presented at the quarterly briefing and included:

- Thruster forces for attitude control and stationkeeping
- Momentum wheel torques

<sup>2</sup> See section 3.5.2



- Tension in structure due to gravity gradient forces
- Centrifugal acceleration due to tumbling
- First bending mode frequency

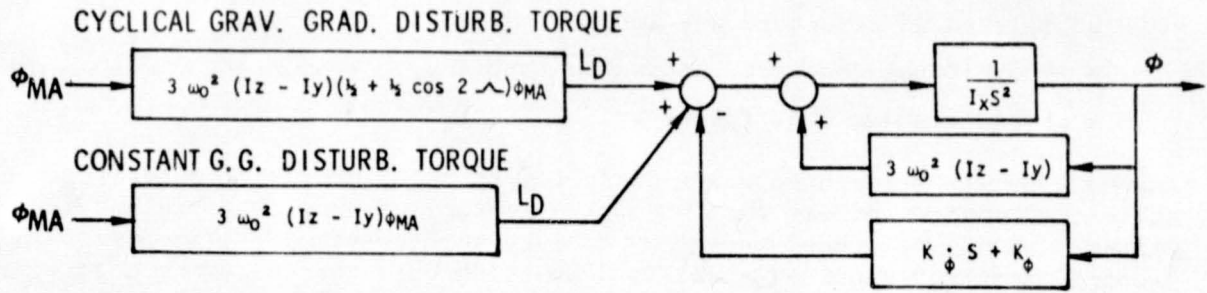
Analysis by the structures staff indicated that the preliminary bending mode frequency requirement was the dominant structural sizing criteria and for this reason it was deemed necessary to make more realistic estimates of the bending frequency requirements. To accomplish this the following control system bandwidth and structural frequency requirements analysis was performed.

#### Control Bandwidth Requirements

Initially it was thought that the fast thermal bending response of the structure would give rise to fairly fast control system response requirements. However, thermal bending is expected to produce symmetrical bending of the structure and hence will not have any appreciable upsetting influence on the control system. The control system must be capable of providing reasonable pointing accuracy in the presence of both constant and cyclical gravity gradient disturbances. Hence, the control system gains must be selected to provide reasonable stiffness in response to these torques. To investigate these requirements a detailed three axis model was developed. An investigation of this model indicated that the dominant requirements would occur about the roll or yaw axis of the spacecraft and it was further shown that the requirements model could be reduced to the simple rigid body single axis model illustrated in Figure 3.5-12. In order that the system would be capable of active modal damping it was assumed that the rigid body control system gains should be selected to produce near critical damping. On this basis the bandwidth data presented in Figure 3.5-13 was developed. The figure presents data for the attitude control bandwidth ( $\omega_n$ ) requirements as a function of pointing error for the cyclical gravity gradient disturbance torque input illustrated. Assuming a principal axis misalignment of  $0.5^\circ$  and a pointing accuracy budget for this error source of  $0.05^\circ$  the control system natural frequency is found to be 5.44 times the orbit frequency. The data in the frequency range shown is essentially identical for both the constant and cyclical gravity gradient torque disturbances. The resulting control system natural frequency requirements for operation in geosynchronous orbit (GEO) or low earth orbit are given in Figure 3.5-13. It may be observed that the LEO frequency requirements are approximately 15 times the GEO frequency requirements. It is noteworthy that the gravity gradient torques in LEO relative to GEO are larger by the square of this number, or 225 times larger.

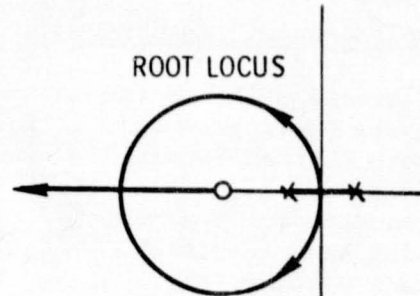
#### Structural Bending Frequency Requirements

Figure 3.5-14 was prepared to gain some perspective into the frequency spectra of the control problem. The control system natural frequency developed in the previous section is only 5.44 times the orbit frequency or 2.72 times the cyclical gravity gradient frequency. Undesirable control system/structural dynamic interaction problems may be presented through the classical frequency separation approach. By making the structural frequencies 5 to 10 times higher than the control natural frequency the interaction problem can be managed and the structural frequency requirements given in the Figure will result



NOMENCLATURE

- $\phi$  - ATTITUDE ERROR
- $\phi_{MA}$  - PRINCIPAL AXIS OF INERTIA MISALIGNMENT
- $L_D$  - DISTURBANCE TORQUE
- $\theta$  - EARTH CENTRAL ANGLE
- $\omega_0$  - ORBIT RATE (FREQUENCY)
- $I_x, I_y, I_z$  - PRIN. AXIS MOM. OF INERTIA



$$\left\{ 1 + \frac{K_\phi / I_x (S + K_\phi / K_\phi)}{S^2 - 3 \omega_0^2 (Iz - Iy) / I_x} \right\} = 0$$

Figure 3.5-12. Simplified Control Bandwidth Analysis Model

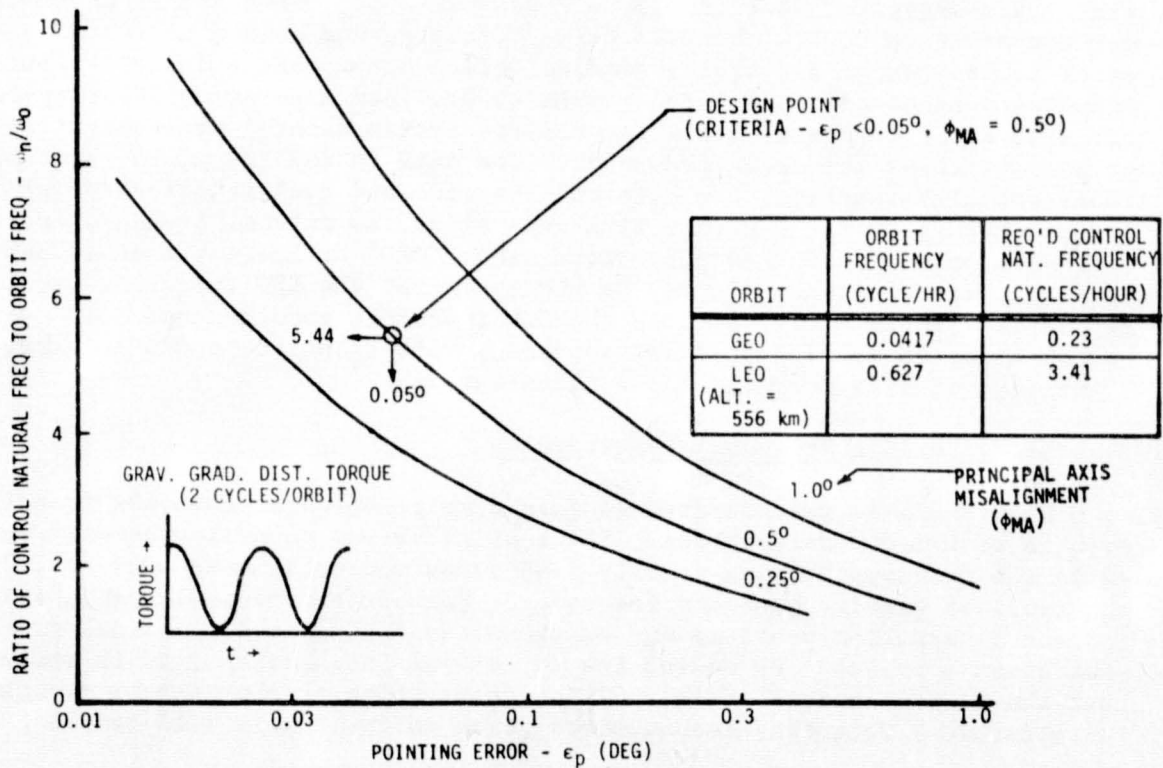


Figure 3.5-13. ACSS Control Bandwidth Requirement



ORIGINAL PAGE IS  
OF POOR QUALITY

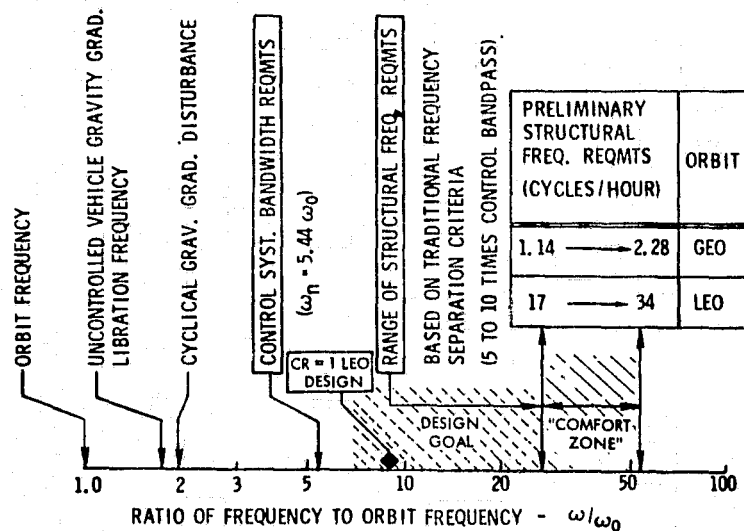


Figure 3.5-14. Preliminary Control and Structural Frequency Requirements

(designated "comfort zone"). Structural analysis of the baseline spacecraft that existed at the study mid-term indicated that its first bending mode frequency was approximately six cycles/hour ( $\omega/\omega_0 = 9.6$ ). This value easily meets the GEO comfort zone requirements but did not meet the "comfort-zone" requirements for LEO. Therefore, it was deemed necessary to investigate the structural frequency requirements in further detail to establish more rigorous bending frequency lower limits and the following analysis was developed.

The problem posed was to stabilize the normal bending modes of the spacecraft (first mode at 6.49 cycles/hour) while maintaining a control bandwidth of 3.4 cycles/hour ( $5.44 \times$  orbit frequency). The techniques investigated to accomplish this task include:

- Classical controller synthesis
- Synthesis using modern control theory and the Luenberger observer approach
- Optimal controller synthesis approach
- Investigation of the merits of distributed attitude sensors and actuators

For the present analysis, the structural model for the photovoltaic vehicle is assumed to be free-free uniform slender beam. Figure 3.5-15 shows the first four mode shapes. The modes were normalized to have a value of unity at  $y = 0$  and the distances along the  $y$ -axis measured from the left are in percent of total length. It may be observed that the attitude sensor, which is initially assumed to be at the center of the beam, will not sense any bending from the first and third modes and hence they are uncoupled from the remaining dynamics.



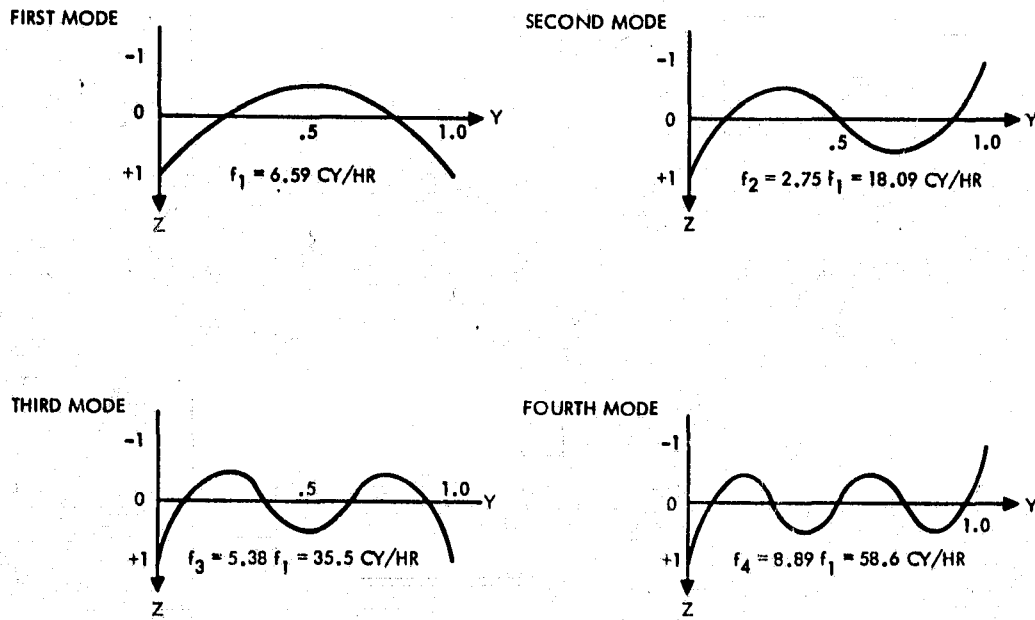


Figure 3.5-15. Bending Modes for Free-Free Beam

Figure 3.5-16 shows the model used in the control system analysis to investigate the interaction of rigid body motion, flexible body motion and the controller. The  $C_i$  represents the coupling between rigid body control and the  $i^{\text{th}}$  mode generalized forcing function. The  $C_{si}$  represents the coupling between the  $i^{\text{th}}$  mode generalized coordinate ( $q_i$ ) and the quantity sensed by the sensor. Linear feedback control was employed in the analysis. Various controller designs were determined using classical techniques, modern and optimal control techniques.

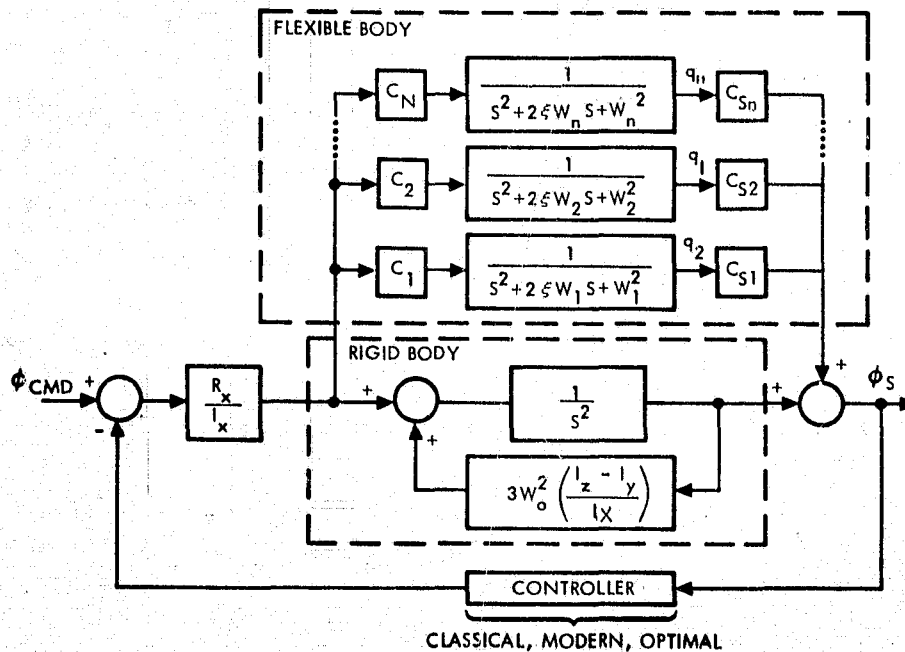


Figure 3.5-16. Model for Control System Analysis

The control problem is to design a control law (compensator) which meets the rigid body control requirements and stabilizes the bending modes. Figure 3.5-17 presents the root locus of controllers synthesized using classical techniques and a modern technique embodying a Luenberger observer. Since the first and third bending modes are uncoupled from the dynamics only the second mode is shown. Although both techniques satisfied the requirements, the investigation showed that the modern control theory approach provides the advantage of a systematic synthesis procedure and better relative stability performance.

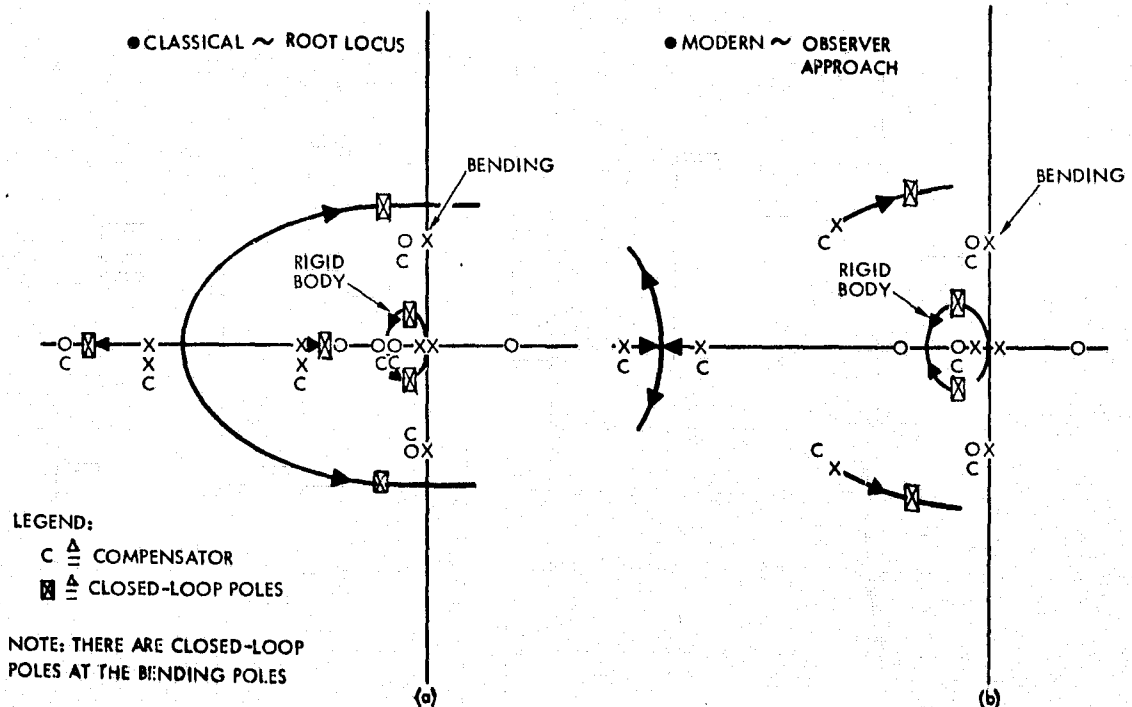


Figure 3.5-17. Control System Dynamics ~ Root Locus

Multiple sensor installation and alternate RCS locations were considered to aid in the stabilization of the bending modes and to reduce the control system sensitivity to the bending modes. Figure 3.5-18 illustrates the approach. A single sensor located in the center of the spacecraft does not sense the first and third bending modes. However, it senses the second mode, and in the above analysis it was found to be highly destabilizing when closing the control loop. A rather sophisticated compensation filter was required to stabilize this mode. The addition of two more sensors (as illustrated in the figure) can be employed and the outputs averaged or weighted to provide an attitude signal. The weighted sensor output still results in zero sensed output for the first and third modes. For the second mode the weighted sensor output now senses a zero or positive mode slope. This is found to permit this mode to be easily stabilized without the necessity for complex filter compensation. It is concluded that a multisensor technique will permit either the decoupling or easy stabilization of the first three bending modes. The higher



- MULTIPLE SENSORS AND ALTERNATE LOCATIONS TO REDUCE SENSITIVITY TO STRUCTURAL BENDING
- ALTERNATE RCS LOCATIONS TO MINIMIZE VIBRATION EXCITATION

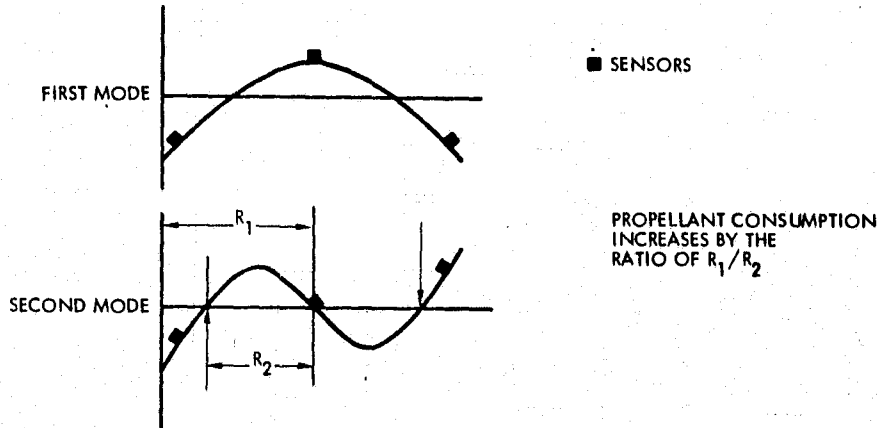


Figure 3.5-18. Multisensor and Actuator Location

order modes are not expected to produce serious coupling problems due to their higher frequency and smaller values for coupling coefficients. Hence, the multi- or distributed sensor approach offers considerable promise of permitting structural frequencies to be even smaller than the 6 cycle/hour value used in the above root locus stability analysis. This can be accomplished without the expense of such exotic techniques as distributed actuators or active structural damping actuators.

Alternate actuator (thruster) locations can be employed to minimize the bending excitation. The application of control torques as torque couples will not excite the odd numbered bending modes (1 and 3). Locating the thrusters at the nodes of the second bending mode (as illustrated in Figure 3.5-18 will result in zero excitation of this mode. However, the reduced moment arms of the RCS thrusters will result in increased propellant consumption for attitude control and the technique is less desirable than the distributed sensor approach on this basis.

Future studies of control system structural dynamic interaction should investigate the interaction of the microwave antenna membrane and support structure as this problem was not addressed in the current study.

### 3.5.5 STABILIZATION & CONTROL SYSTEM CONCEPT EVOLUTION FOR AN SPS SPACECRAFT CONSTRUCTED IN LEO

This section presents results of the stabilization and control system concept evolution for the MSFC photovoltaic spacecraft. This spacecraft is constructed in low earth orbit and transferred to its operational orbit at geosynchronous altitude. The attitude control requirements are found to be considerably more stringent for LEO construction than for GEO due primarily to the large gravity gradient torques and the additional solar occultation



time. As a result the spacecraft and ACSS design requirements are found to differ appreciably from the GEO construction approach. Control techniques are developed for the construction orientation, erection to the operational orientation, low thrust transfer to GEO, and for the operational phases.

### Guidelines and Assumptions

#### Attitude Control and Pointing Accuracies.

- LEO Assembly
  - Orbit Transfer:  $\pm 1$  deg. (3 axes)
  - LEO Operation:  $\pm 1$  deg. (3 axes)
- GEO Assembly
  - Main Body:  $\pm 1$  deg. (3 axes)
  - Microwave Antenna
    - Coarse:  $\pm 2\frac{1}{2}$  arc. min. (2 axes)  
Less than 8 deg. about LOS
    - Fine:  $\pm 3$  arc. sec. with respect to Rectenna Center

Attitude Control Coordinates. Figure 3.5-19 defines the main body and microwave antenna coordinates that are used in the stability and control and pointing definitions and discussions. In the reference position, the antenna coordinates  $X_A$ ,  $Y_A$ , and  $Z_A$  are in alignment with the main body coordinates  $X_B$ ,  $Y_B$ , and  $Z_B$  where:

- The  $Z_B$  axis is normal to the solar array and pointed sunward.
- The  $X_B$  minimum inertia axis is perpendicular to the orbit plane.
- The  $Y_B$  axis in the plane of the solar arrays form a right-hand coordinate frame.

Assumptions. The following assumptions evolved during present and past study efforts and serve to use advantageously the products of projected space programs from the standpoint of both technology and spacecraft. The two most significant items appear to be the Space Construction Base and the electric thrusters. The construction base relieves the SPS subsystems of the tremendous task of providing support functions during assembly. Technology programs on electric thrusters will provide a product that will bring the expendable fuel mass down to a technically feasible value.

- A construction base provides attitude control and stationkeeping during assembly at LEO or GEO.
- Electric thrusters will provide the actuation forces for attitude control and stationkeeping during sunlit portions of an orbit.
- Transfer from LEO to GEO starts immediately after construction in LEO.
- The attitude for orbit transfer will be X-POP, Z-sunward.

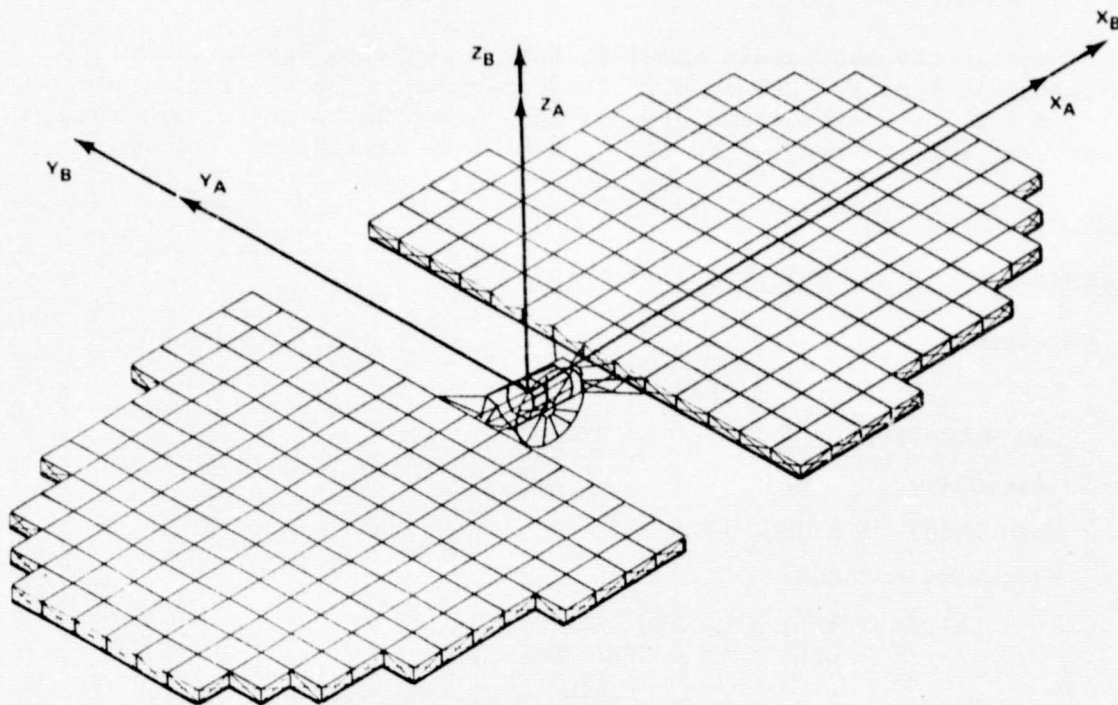


Figure 3.5-19. SPS Control Coordinates

- The GEO operational attitude will be X-POP, Z-sunward.
- After LEO construction an auxiliary propulsion stage will erect the SPS to the transfer attitude.
- Inertia balancing of the Y and Z axis moments of inertia is required for the LEO assembled SPS.
- Orbit transfer thruster modules will be mounted on 2-degrees of freedom gimbal mounts. (360 deg about the X-axis is required.)
- Dedicated fixed electric thrusters will provide 3-axis attitude control.
- An antenna gimbal system will provide antenna coarse pointing.
- Fine pointing and stability of the MW power beam will be provided by a phase control system.

#### Trade Study Approach

Operational Phases. Stabilization and control concepts were determined for the following operational phases:

- LEO Assembly
  - LEO Storage
  - Transfer from LEO to an intermediate orbit
  - Transfer from an intermediate orbit to GEO
  - GEO operation
- GEO Assembly
  - After release by the Construction Base
  - GEO operation



Figure 3.5-20 summarizes the operational phases in the form of a flow diagram and also indicates a number of decision points where control system options must be traded.

Based on the following information that was generated for each operational phase, a recommended concept was selected:

- Thruster systems definitions
- Fuel consumptions
- Special Requirements:
  - Attitude orientations and maneuvers
  - Inertia balancing
  - Energy storage
  - Chemical propulsion
  - Control frequencies

ORIGINAL PAGE IS  
OF POOR QUALITY

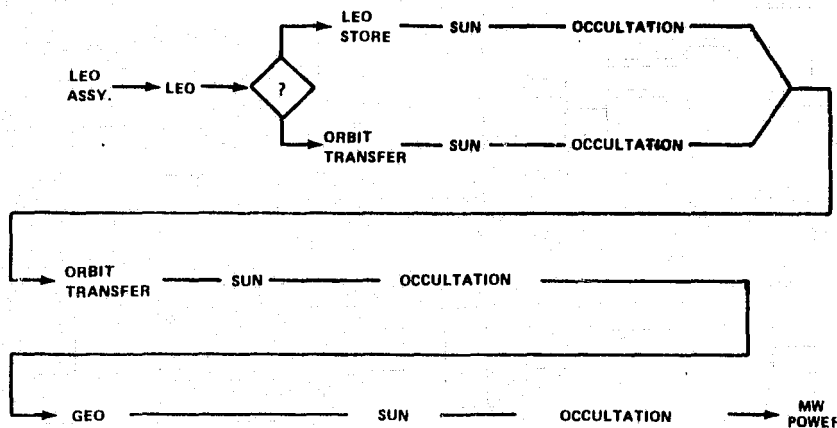


Figure 3.5-20. Stability & Control Flow Diagram

LEO Assembly. Upon completion of assembly in LEO a decision must be made to either store the SPS in LEO or to start immediately the transfer to GEO. The key drivers in making this decision are the large gravity torques present in LEO, and the absence of electric power for electric thruster operation due to the sun occultation periods. Also, the magnitudes of the gravity torques are a direct function of inertia differences. Unless at least 2-axis moment of inertia balancing is accomplished, the number of thrusters and their fuel consumption makes attitude control in LEO unfeasible.

Figure 3.5-21 illustrates the difficulties encountered in a LEO storage mode when using the solar panels to supply power to the attitude control electric thrusters during sunlit portions of the orbit. The storage mode attitude is with the axis of minimum inertia aligned to the local vertical in a gravity gradient stable mode. This storage attitude is necessary to conserve attitude control propellant. For a short period of time each side of high noon the solar panels receive almost no sunlight. If the SPS approaches high noon from orbital position 1, the available sunlight decreases from a maximum to almost zero which could possibly be tolerated. However, immediately past high noon a rapid roll about the local vertical is required to have the active side of the solar panels facing the sun. Likewise, as the SPS



approaches position 1 from the shadow, a rapid roll maneuver must be made to have the solar panel facing the sun. These rapid roll maneuvers are considered to be intolerable and the LEO storage mode should be avoided.

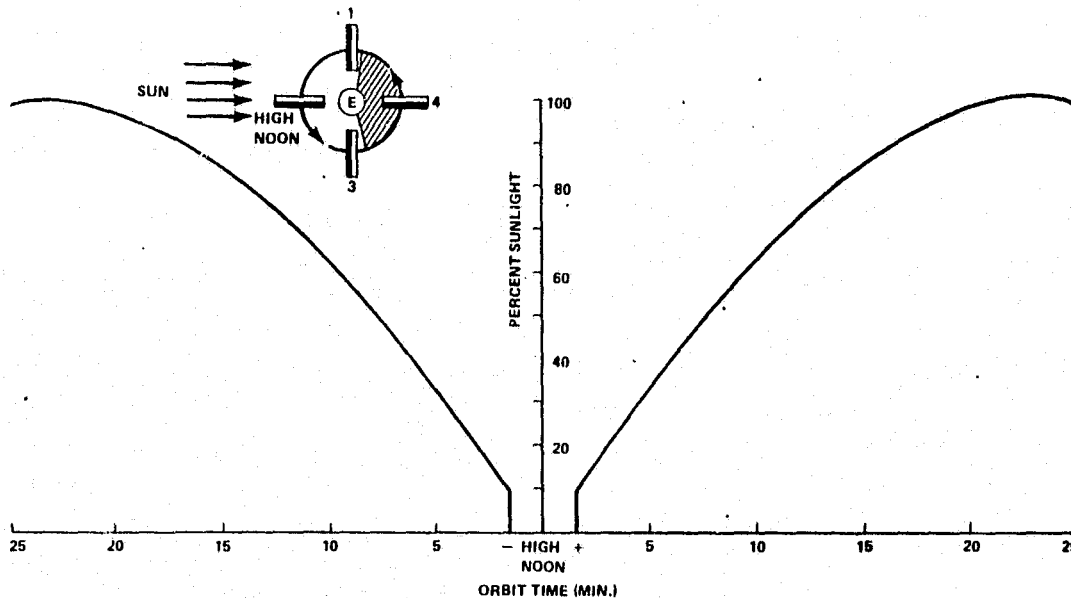


Figure 3.5-21. LEO Sunlight Conditions (Typical)

Orbit Transfer. Maintaining control of the SPS during transfer is a formidable task because:

- The large number of low earth orbits where the gravity effects are large.
- Shadow times necessitate augmenting the electric propulsion system with energy storage or chemical propulsion.
- Two-axis inertia balancing is required.
- Attitude control thrusters separate from the transfer thrusters is desirable.
- Control frequencies are much higher than GEO control frequencies.

Table 3.5-4 provides an estimate of the number of intermediate orbits required to reach GEO, the sun shadow times encountered, and the electric propulsion system fuel usage. The estimate indicates that about 80% of the fuel consumption takes place in reaching an altitude of about 5000 km. Also, the shadow times and the need for chemical propulsion or electric energy storage are greatest up to about 2000 km. Inertia balancing of the Y and Z axes to approximately 0.5% or less appears to be a firm requirement. Without this balance, the cyclical gravity gradient torques about the X-axis are so large that the total number of thrusters required, the total power consumption, and the fuel consumption becomes prohibitively great.



Table 3.5-4. Stability & Control Fuel Consumption  
During LEO to GEO Transfer

ORBIT NUMBER	FINAL ALTITUDE (KM)	PERCENT SUNLIGHT	ELECTRIC THRUSTER FUEL (Kg)
1-78	1145	69	24172
79-146	1887	85	22542
147-208	2761	100	20795
209-262	3824	100	15358
263-308	5065	100	11012
309-350	6690	100	8266
351-384	8513	96	5277
385-408	10342	95	3077
409-428	12408	95	2160
429-446	14942	95.0	1609
447-460	17620	95.0	1049
461-472	20669	96	757
473-482	23955	96	533
483-492	28046	97	443
493-498	31027	98	237
499-504	34042	99	215
505-511	35827	100.0	237
TOTAL FUEL =			<u>117739</u>

The trade studies resulted in the selection of an electric propulsion system for attitude control during sunlit portions of the orbit and a chemical propulsion system for use during the occultation periods. Energy storage to supply the electric thrusters during occultation was not considered acceptable due to the total mass required and the complexity of the power distribution system required. Also, separate electric propulsion thrusters were selected for the attitude control and the orbit transfer functions because of the complexity of a system that uses one system for both functions. In particular, the sensing and control law computations required to determine thruster orientations for a common system requires an in-depth study.

Propulsion System Summary. Table 3.5-5 provides a summary of the propulsion systems for the LEO and GEO assembled spacecraft. The data is based on the inertia balancing in two axes and a 91.3 days trip time for LEO/GEO transfer.

The 3512 thrusters required for control of the LEO assembled SPS largely result from the several days spent in the strong gravity field during orbit transfer. Once GEO has been reached only about 380 thrusters are needed for three axis control. The mass of the LEO assembly is greater than the GEO assembly. This, together with the inertia distribution, led to the larger number of LEO assembly thrusters and the larger associated propulsion system mass.





Table 3.5-5. Propulsion System Summary

- NUMBER OF ATTITUDE CONTROL THRUSTERS
- NUMBER OF ADDITIONAL THRUSTERS FOR STATION KEEPING
- NUMBER OF ORBIT TRANSFER THRUSTERS
  - TOTAL NUMBER OF THRUSTERS
- THRUSTER SYSTEM MASS (K<sub>g</sub>)
  
- PROPELLANT MASS (K<sub>g</sub>/YR)
  - ATTITUDE CONTROL
  - STATION KEEPING (1)
  - ORBIT TRANSFER
  - TOTAL PROPELLANT
- PROPELLANT SYSTEM MASS (K<sub>g</sub>)
  - TOTAL PROPULSION SYSTEM MASS (K<sub>g</sub>)
  
- POWER REQUIREMENTS
  - ORBIT TRANSFER
  - OPERATION

GEO ASSY.		LEO ASSY.	
ELECTRIC	CHEMICAL	ELECTRIC	CHEMICAL
208	22	3512	352
200	0	0	0
0	0	6366	0
408	22	9678	352
18196	242	8.2x10 <sup>6</sup>	3872
7700	38527	0.131x10 <sup>6</sup>	0.428x10 <sup>6</sup>
64500		0.126x10 <sup>6</sup>	0
0	0	4.759x10 <sup>6</sup>	0
72200	38527	5.016x10 <sup>6</sup>	0.428x10 <sup>6</sup>
8022	4281	0.557x10 <sup>6</sup>	47493
262138	43050	13.773x10 <sup>6</sup>	0.479x10 <sup>6</sup>
N/A	N/A	4.31GW	NEGLIGIBLE
90.4 MW	NEGLIGIBLE	58.1MW	NEGLIGIBLE

(1) DURING GEO OPERATION

The 6366 thrusters required for orbit transfer must be traded against a separate orbital transfer vehicle from an overall program standpoint with cost being a big driver. These thrusters are not needed after placement of the SPS into a geosynchronous orbit.

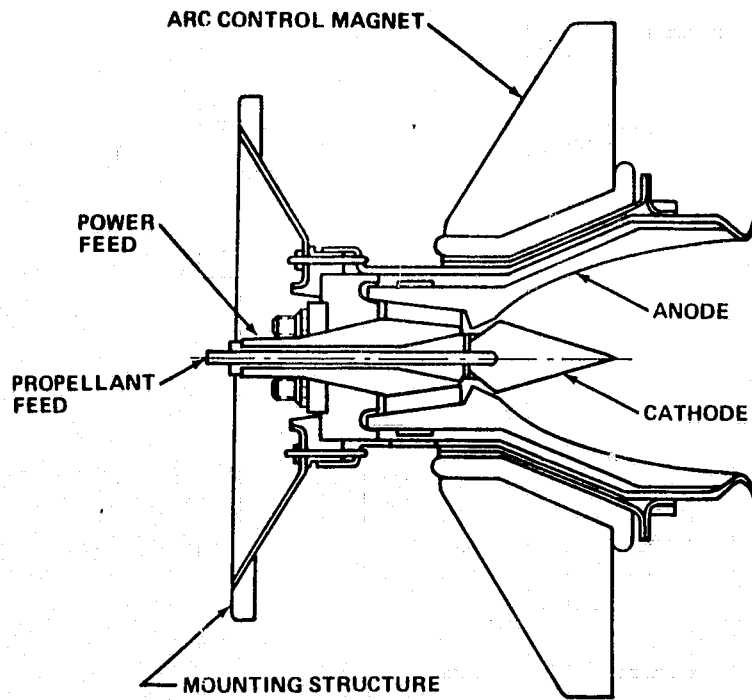
The power required to operate the electric thrusters during orbit transfer is a key driver. The magnitude of the power required approaches the total SPS capability. In addition, special power distribution accommodations must be made to provide the proper voltages, and sectionalization for the various groups of thrusters.

### Attitude Control Propulsion System

Electric Propulsion System. As a result of the electric thruster trades made for the transfer electric propulsion system, the attitude control and stationkeeping thrusters are the MPD electric thruster as shown in Figure 3.5-22, the same thruster as used for transfer. Table 3.5-6 gives the electric propulsion system definition and masses for the LEO assembled SPS, using a 90-day transfer time. The electric propulsion system definition and masses for the GEO assembled SPS is given in Table 3.5-7. The GEO assembled SPS has no requirement for transfer of electric thrusters, therefore, there are none shown in Table 3.5-7. The total electric propulsion system consists of the argon propellant, thruster system, and propellant system. The thruster system includes the thrusters, mounting structure, wiring and cabling, and any power conditioning equipment; while the propellant system includes the tanks, lines, valves, pressurant, and propellant conditioning equipment. The total power required for both the LEO and GEO cases have been based on the maximum number



ORIGINAL PAGE IS  
OF POOR QUALITY



- THRUST: 9.81 N
- WEIGHT: 40.0 kg
- SPECIFIC IMPULSE: 10000 s
- POWER: 587 kW
- EFFICIENCY: 0.82
- PROPELLANT: ARGON
- VOLTAGE: 300 V
- CURRENT: 1958 A
- FLOWRATE:  $10^{-4}$  kg/s
- MAGNET: 40 000 A-TURNS

Figure 3.5-22. Baseline MPD Electric Thruster

Table 3.5-6. LEO Assembled SPS Propulsion System

		<u>ELECTRIC</u>		<u>CHEMICAL</u>
NUMBER OF THRUSTERS FOR ATTITUDE CONTROL PER AXIS	(X)	432	(X)	44
	(Y)	1540	(Y)	154
	(Z)	1540	(Z)	154
	<b>TOTAL</b>	<b>3512</b>		<b>352</b>
NUMBER OF THRUSTERS FOR TRANSFER		6365		.0
TOTAL NUMBER OF THRUSTERS		9877		352
TOTAL THRUSTER SYSTEM MASS		$8.2 \times 10^6$ kg		3872 kg
TOTAL PROPELLANT MASS PER YEAR		ARGON		LOX/LH <sub>2</sub>
1ST YEAR ONLY	TRANSFER	$4.759 \times 10^6$ kg		0
	TRANSFER ATTITUDE CONTRL	$.118 \times 10^6$ kg		388,908 kg
	OPERATIONAL ATTITUDE CONT.	$.013 \times 10^6$ kg		0
	OPERATIONAL STATION KEEPING	$.126 \times 10^6$ kg		38,527 kg
TOTAL PROPELLANT SYSTEM MASS		$.557 \times 10^6$ kg		47,493 kg
TOTAL PROPULSION SYSTEM MASS		$13.773 \times 10^6$ kg		478,800 kg
MAXIMUM NUMBER OF THRUSTERS ACTIVE AT ONE TIME				
TRANSFER		7351		
OPERATIONAL		99		
TOTAL POWER REQUIRED				
TRANSFER		4.31 GW		
OPERATIONAL		58.1 MW		



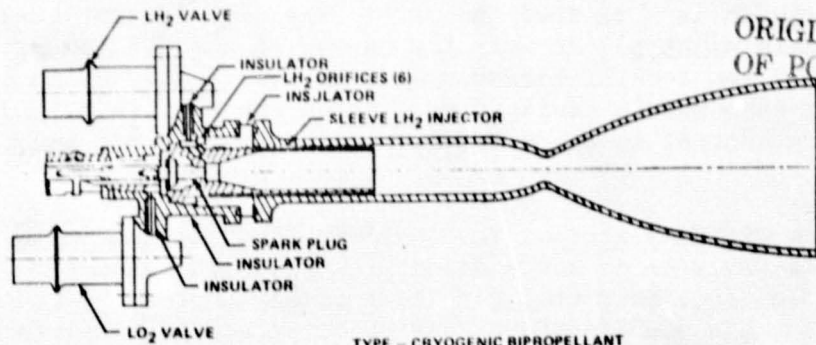
Table 3.5-7. GEO Assembled SPS Propulsion System

		<u>ELECTRIC</u>		<u>CHEMICAL</u>
NUMBER OF THRUSTERS FOR ATTITUDE CONTROL PER AXIS	(X) (Y) (Z)	8 100 100	(X) (Y) (Z)	2 10 10
<b>TOTAL</b>		<b>208</b>		<b>22</b>
ADDITIONAL THRUSTERS FOR STATION KEEPING PER AXIS	(X) (Y) (Z)	0 100 100		0
<b>TOTAL NUMBER OF THRUSTERS</b>		<b>408</b>		<b>22</b>
<b>TOTAL THRUSTER SYSTEM MASS</b>		<b>181,916 kg</b>		<b>242 kg</b>
TOTAL PROPELLANT MASS PER YEAR		ARGON		LOX/LH <sub>2</sub>
ATTITUDE CONTROL		7,700 kg		38,527 kg
STATION KEEPING		64,500 kg		
<b>TOTAL PROPELLANT SYSTEM MASS</b>		<b>8,022 kg</b>		<b>4,281 kg</b>
<b>TOTAL PROPULSION SYSTEM MASS</b>		<b>262,138 kg</b>		<b>43,050 kg</b>
MAXIMUM NUMBER OF THRUSTERS ACTIVE AT ONE TIME		100		--
<b>TOTAL POWER REQUIRED</b>		<b>58.7 MW</b>		--

of thrusters active at one time. For the LEO assembled SPS during transfer, the maximum number of thrusters active at one time is 7351, 6365 for transfer and 986 for attitude control; and during operation at GEO the maximum number of thrusters active at one time is 99, all attitude control thrusters. The GEO assembled SPS has a maximum of 100 thrusters active at one time during the operational mode.

Chemical Propulsion System. Due to occultation periods occurring both during the LEO/GEO transfer and during operations at GEO, both the LEO and GEO assembled SPS require another onboard propulsion system, not dependent upon solar energy, for attitude control during these occultation periods. The baseline thruster is shown in Figure 3.5-23. Cryogenic LOX/LH<sub>2</sub> propellants were chosen because of their high specific impulse in comparison to other chemical propellants. The masses associated with the chemical propulsion system for attitude control during occultation periods, for the LEO assembled and GEO assembled SPS are shown in Tables 3.5-6 and 3.5-7, respectively. The chemical propulsion system consists of the LOX/LH<sub>2</sub> propellants, thruster system, and propellant system. The thruster system consists of the thrusters, mounting structure, and wiring; the propellant system consists of the propellant tankage, feed lines, valves, and the pressurization, propellant conditioning and utilization subsystems.

Thruster Locations. Figure 3.5-24 shows the location of the transfer, attitude control, and stationkeeping thrusters for either the LEO assembled or GEO assembled SPS. The transfer thrusters are located on three, two-axis gimbaled modules, which are on both ends of the SPS and on the microwave antenna at the center of the SPS. One-third of the transfer thrusters are located on each module. The attitude control thruster modules are located



ORIGINAL PAGE IS  
OF POOR QUALITY

TYPE - CRYOGENIC BI-PROPELLANT  
 PROPELLANTS - LOX/LH<sub>2</sub>  
 THRUST - 98N  
 I<sub>sp</sub> - 400 S (AVERAGE)  
 CHAMBER PRESSURE -  $2 \times 10^6$  N/m<sup>2</sup>  
 MIXTURE RATIO - 5.0:1  
 AREA RATIO - 40:1  
 THRUSTER MASS - 2.7 kg

Figure 3.5-23. Baseline LOX/LH<sub>2</sub> Chemical Thruster

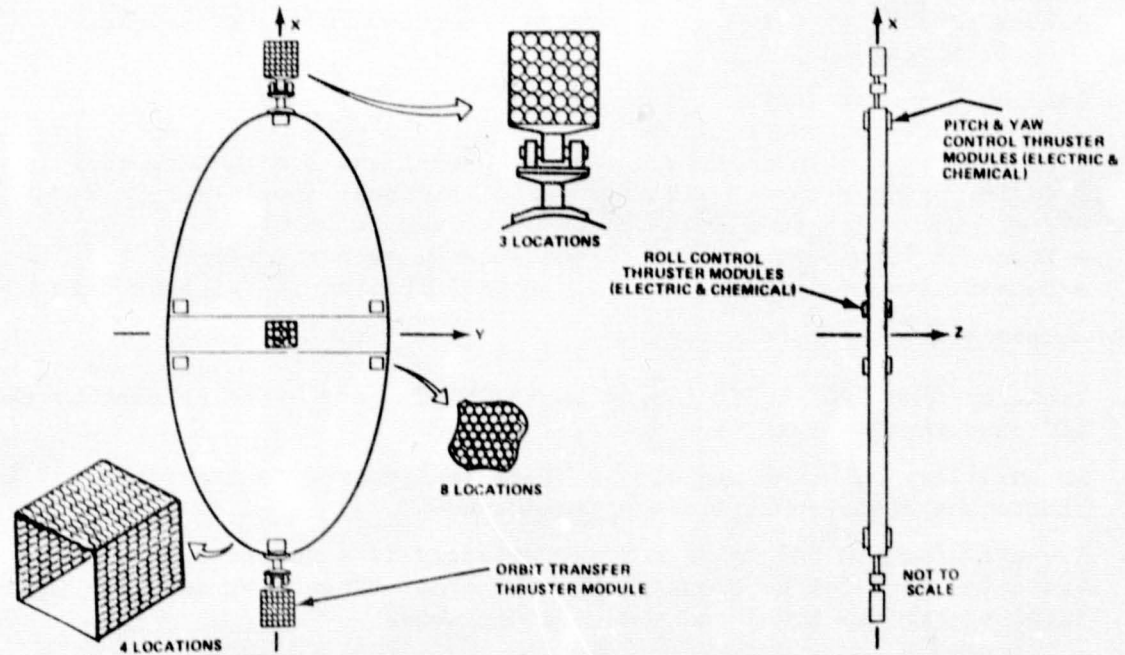


Figure 3.5-24. Electric Thruster Module Locations



at twelve places (six on each side of the SPS). The roll control thruster modules are located in eight places near the center of the SPS (four on each side). The pitch and yaw control thruster modules are located at four places (two on each side); each module having thrusters on the top, left, and right sides. All attitude control thruster modules have both electric and chemical thrusters.

Key Trade Study Discriminators. The following listing summarizes the principal LEO/GEO assembly trade study discriminators with respect to stability and control. The large potential gravity gradient torques of LEO lead to most of the problem areas such as the number of thrusters required to counteract these torques.

- Large gravity gradient torques in LEO
  - Requires inertia balancing
  - Special storage mode required to save fuel
  - Chemical propulsion required during sun occultation
  - A large number of thrusters are required
  - Energy storage must be used as an alternate to chemical propulsion
  - A large number of unnecessary thrusters remain after reaching GEO
  - An auxiliary propulsion stage is required for erection to the transfer attitude
- Higher control frequencies in LEO
  - Impacts structural design
  - Control bandwidths are larger
  - Less separation between the control frequencies and structural bending frequencies
- General discriminators
  - Large thruster power in LEO
  - Problem in combining thrust vector control and attitude control during orbit transfer with the set of thruster modules
  - Requirement for double gimbal thruster module mounts
  - Transfer thrusters mounted on the antenna support frame
  - Sensitivity of attitude control propellant mass to transfer trip time

#### Conclusions and Recommendations

- Transfer from LEO to GEO should begin immediately after release by the LEO construction base.
- An auxiliary external propulsion stage is required to erect the SPS in LEO to the transfer attitude orientation.
- Two-axis inertia balancing for LEO assembly is a requirement to alleviate the need for an unmanageable number of thrusters, and the associated electrical power and fuel consumptions.
- Orbit transfer:
  - X-POP, Z-Sunward is the reference attitude orientation
  - A 2-axis gimbal mount is required for the transfer thrusters. (360 degrees about the X-axis, near  $\pm 90$  degrees tilt.)
  - Thrust impingement due to the large tilt angle is a problem



- Chemical propulsion to provide attitude control during all occultation periods is a requirement.
- Dedicated attitude control thrusters are recommended for all control axes.
- There appears to be no requirement for the orbit transfer thrusters after completion of the LEO to GEO transfer.
- In general, nearly all LEO assembly drivers and problems result from the large gravity gradient torques and the higher control frequencies.

### 3.5.6 SUMMARY OF CONCLUSIONS AND RECOMMENDATIONS

The major conclusions drawn during the ACSS concept evolution analyses and trades are summarized below. Many spacecraft design and operational requirements have evolved from these trades.

1. Geosynchronous equatorial orbit is selected over the ecliptic or  $7.5^\circ$  inclination due primarily to the high cost impact of increased rectenna size for inclined orbits.
2. Rectenna size (cost) increases substantially for northern latitude sites.
3. Gravity gradient torques can produce large RCS propellant resupply requirements.
4. Control techniques investigated can reduce ACSS requirements to a few percent of spacecraft mass (preferred orientations, inertia balancing, free drift modes and momentum storage techniques).
5. The selected system utilizes Y-POP, X-IOP orientation, two dimensional inertia balancing, and ion thruster RCS (erectable momentum wheels and free drift modes not employed).
6. Solar pressure perturbation dominates the stationkeeping requirements, results in a large propellant mass or  $3.1^\circ$  longitude stationkeeping error penalty.
7. Rationale for control system bandpass and structural frequency requirements have been developed and the results indicate:
  - No problems for control in GEO, assembly in LEO imposes substantially more severe requirements and will result in different spacecraft design.
  - New control techniques investigated are attractive for reducing structural frequency requirements.
  - Thrust vector steering for LEO to GEO low thrust transfer is not a dominant structural frequency requirement driver.



8. The ACSS and spacecraft requirements for LEO assembly and low thrust transfer to GEO are considerably more demanding than for a GEO constructed spacecraft.
  - Chemical propulsion is required in addition to the electric propulsion to accommodate the larger gravity gradient torques and solar occultation periods.
  - A gimballed electric thruster configuration is required for the orbit transfer phases.
  - Two dimensional inertia balancing and horizontal principal axis of inertia orientations are highly desirable to prevent excessive control torque and propellant requirements.
  - Thrust vector impingement on the spacecraft is a potential problem for orbit transfers that require significant orbit plane changing and warrants further investigation.

The study results have indicated that the SPS attitude control and station-keeping problems are all tractable and no potential "show-stoppers" exist. Many spacecraft and operational design requirements have evolved from the study as well as ACSS concepts which will minimize the overall system penalties to perform the ACSS functions. The results provide a design base for future SPS studies to build upon. The ACSS point design evolving from these trades is given in Volume IV.

The recommendations for future study activity have already been summarized in preliminary study plans. The study areas of greatest importance with regard to the overall technical feasibility of the SPS are:

1. Stationkeeping and SPS Constellation Definition - The arrangement of SPS satellites in GEO will impose an appreciable volume requirement in an orbit which promises to be quite crowded by the year 2000. The preferred satellite longitude stations are constrained by rectenna locations and rectenna cost penalties for offset microwave beam pointing. Uncorrected solar pressure orbit perturbations also can increase the volume requirements. The correction of this perturbation imposes a large RCS propellant resupply requirement. A more complete evaluation of the factors influencing the SPS constellation requirements is necessary to assess the impact on other GEO users and the necessity for national and international agreements for use of this orbit.
2. Figure Control - Figure control requirements increase very rapidly as a function of collector concentration ratio. Previous preliminary analyses have indicated that passive figure control may be adequate for the lower range of CR's. An analysis is necessary to define the penalties and performance limitations of passive and active techniques to support the selection of the point design CR. This effort will require the joint participation of the design, structures, thermodynamics, and control system analysis staff.



3. Dynamic Analysis - The stable interaction of the flexible SPS structure with the attitude control system, the microwave antenna pointing controls, the figure controls, and the stationkeeping thruster operation, is of vital importance in developing control system, structural, and spacecraft configuration requirements. An investigation emphasizing the control system compatibility with the microwave antenna web flexible modes, and the rotary joint antenna gimbaling, including the slip-ring nonlinear friction is required.
4. Guidance and Control of the EOTV - The attractiveness of the EOTV for cost reduction in the SPS program warrants more detailed definition of the EOTV. As shown above, guidance and control considerations can have an appreciable impact on preferred EOTV design concepts and operations, and should be investigated further.

The DOE data required to support future studies is a definition of the location of representative rectenna sites. As has been discussed in the stationkeeping section above and in the recommendations for future study the location of rectenna sites impacts the preferred GEO longitude stations, the requirement for correcting the solar pressure perturbation and ultimately the SPS space requirement in GEO and its impact on other potential GEO user satellites.





### 3.6 THERMAL CONTROL

The thermal control subsystem mass may be only a small fraction of the total satellite mass (low concentration ratio photovoltaic satellite) or can represent as much as 2/3 of the total system (CR=400 satellite). In any event it strongly influences many of the selection decisions relative to other subsystems and is thus a prominent factor in SPS design regardless of the power conversion technique employed. During the course of this study, a number of trades were conducted to evaluate candidate alternatives and determine preferred options in order to move toward an optimal system design. The initial emphasis of these analyses was to eliminate concepts with high mass penalties. Once these considerations were concluded, the subsequent thrust was directed at minimizing system cost in order to achieve a balanced optimum.

The thermal control subsystem interacts with the satellite elements shown in Figure 3.6-1. The evaluation of thermal storage requirements for eclipse protection was resolved by (1) use of low emissivity coated insulations for solar thermal turbomachinery exteriors to limit cooling cycles, (2) recognition that requirement was more properly power storage with transfer to the power distribution subsystem for determination, and (3) application of heaters using battery power. In certain instances thermal response analysis was a secondary consideration and consequently was introduced subsequent to the trades directly at the point design phase. Even with these modifications the effect of thermal control in the preliminary trades was pronounced as will be shown here. Included in this section are the significant findings of a NASA (MSFC) in-house investigation of thermal response in LEO and GEO during construction and operation.

This section details the results of the following trade studies:

- Concentration Ratio = 400 SPS
- Use of Bandpass Filters
- NaK Heat Pipe vs Condensing Radiators
- Klystron Thermal Control Design
- Thermal Considerations of LEO vs GEO
- Relative Orientation of Electrical Conductors

#### 3.6.1 CONCENTRATION RATIO = 400 SPS

Due to initial uncertainties relative to Ga cost and availability the feasibility of high concentration, GaAlAs, solar photovoltaic systems was investigated. Preliminary cell response data indicates that, at a given temperature, at high concentration ratios ( $\sim 400:1$ ) improved cell conversion efficiency can be achieved. These predictions are derived from inhouse studies.



ORIGINAL PAGE 17  
OF POOR QUALITY

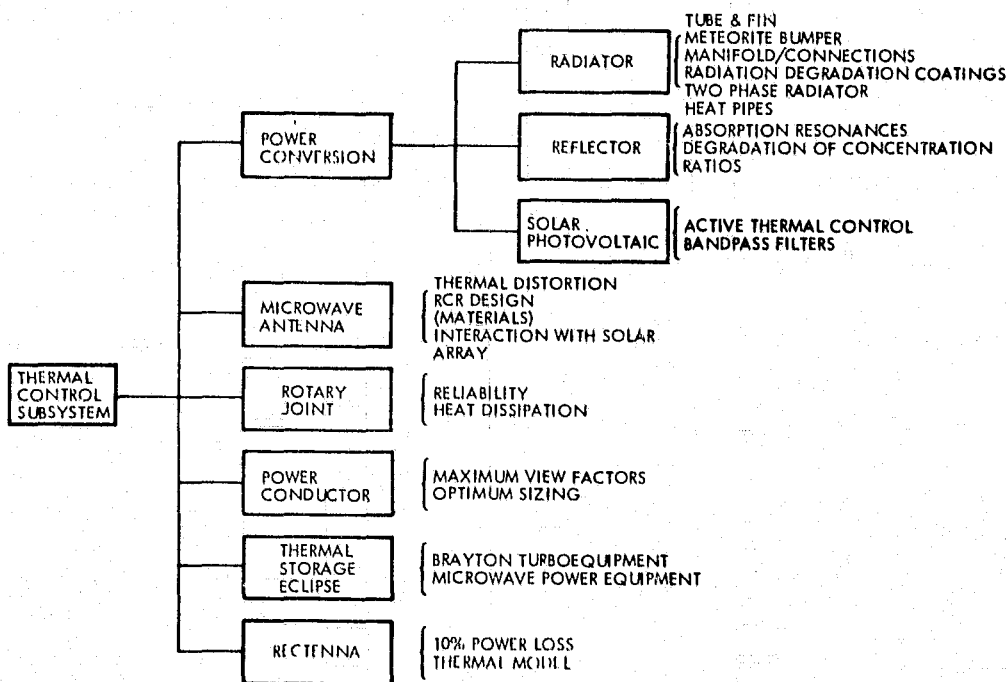


Figure 3.6-1. Thermal Control Subsystem

A detailed model was developed at the Rockwell Science Center for calculating the internal photocurrent collect efficiency of GaAlAs/GaAs heteroface solar cells. The power conversion efficiency of the cell is a product of three factors: short circuit current, open-circuit voltage, and fill factor. The conversion efficiency of GaAlAs solar cells substantially increases at high concentration because of increases in open circuit voltage and fill factor. The open-circuit voltage increases markedly at about  $\sim 10$  suns because virtually all the current is diffusion current as opposed to recombination current at 1 sun. The fill factor increases because under concentration, the device approaches "ideal diode" behavior if the series resistance is controlled to below 0.005 ohm. This increase in efficiency at concentration ratios from 1 to 400 is shown in Figure 3.6-2 for a series resistance of 0.001 ohm. No attempt has been made to project the efficiencies that might be attained at high concentration ratio relative to normal improvements which could be achieved for the cell under a 10 year development as shown in Figure 3.6-2 for CR-1 projected to 1985. The data look attractive for high concentration ratios; even at 300°C, the conversion efficiency that could be reached ( $\sim 13\%$ ) is highly respectable.

From the above considerations it is obvious that high concentration, GaAlAs, photovoltaic concepts would substantially reduce gallium requirements and offer the opportunity of substituting lightweight reflector for relatively heavy solar cell construction.

GaAlAs arrays with a concentration ratio of 400:1 were investigated to determine if the mass reduction/cost saving introduced by substituting lightweight reflector for GaAlAs blanket could compensate for the active fluid/

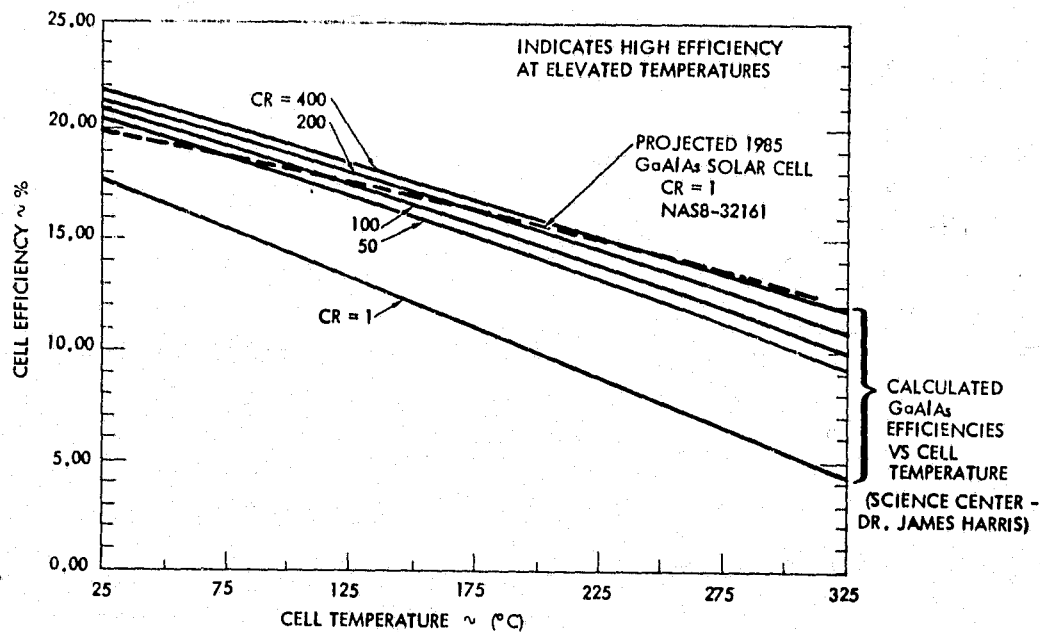


Figure 3.6-2. Comparison of Predicted GaAlAs Cell Efficiencies

radiator loop required to control blanket temperature. The Space Division of Rockwell has built and demonstrated as part of an IR&D program a two mirror 350:1 system. The baseline system was considered to be a feasible extension. Three blanket temperature options were included in the study - 300°C, 200°C, and 100°C. Based on material limitations of the current baseline configuration it is expected that the upper allowable maximum temperature is below 200°C, but no attempt was made to redesign the blanket for this study.

Figure 3.6-3 shows results which demonstrate the large mass penalty incurred by these systems resulting from the low radiator temperatures and the large heat dissipation that is due to the relatively low conversion efficiency of the blanket (compared to competitive dynamic power cycles). The masses shown are optimistic as they include (for the 300°C option) 8-mil aluminum fin thickness and a net radiator mass of 0.01455 kg/m<sup>2</sup> (0.345 lb/ft<sup>2</sup>) which is significantly below the level of existing radiators. The evaluated concept was a balanced moment-of-inertia configuration. Due to the need to provide an active thermal control system to reject the waste heat, these systems are not weight competitive. The radiator concept included tube/fins with heat pipes. The heat pipe systems were ammonia/aluminum, methanol/stainless steel, and water/copper for the 100°C, 200°C, and 300°C cases, respectively. The heat pipes are VCHP's (variable conductance heat pipes) in order to promote start-up after eclipse passage. The heat pipe transfer fluid was water.

The high concentration ratio GaAlAs system was subsequently deleted from the study because of its associated large mass penalty. A secondary reason associated with its rejection was the uncertain cell performance at high temperature for which data substantiating analytical predictions was lacking.



ORIGINAL PAGE IS  
OF POOR QUALITY

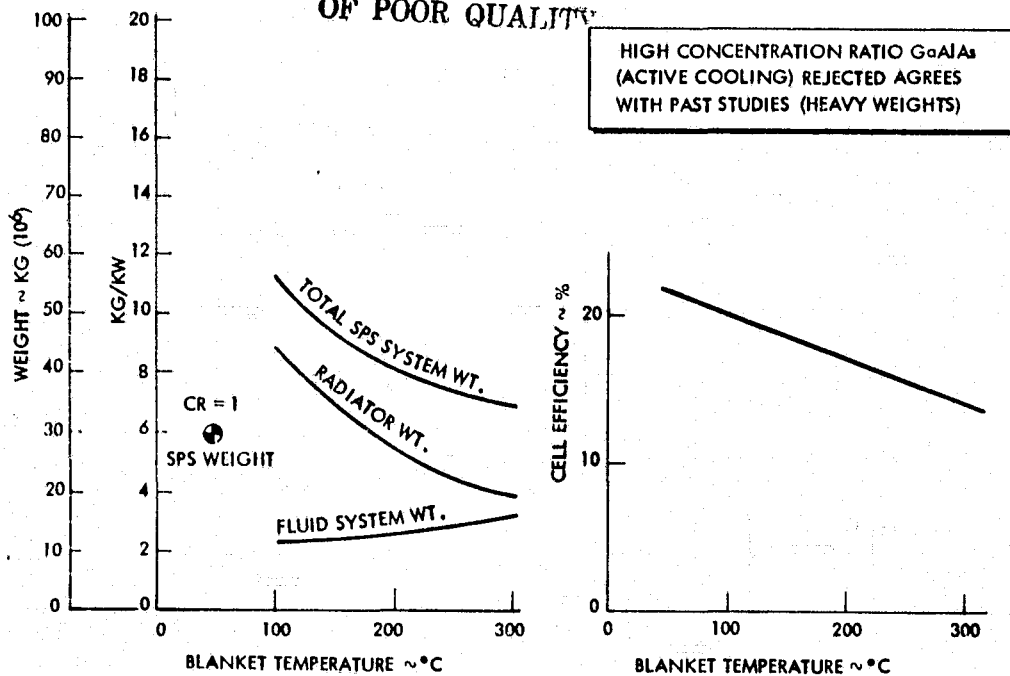


Figure 3.6-3. High Concentration Ratio GaAlAs Mass Comparison CR = 400

### 3.6.2 BANDPASS FILTERS

The advantages of using bandpass filters (more properly, selective spectral mirrors) to permit the operation of GaAlAs arrays at elevated concentration ratios under passive thermal control were shown. Even for a concentration ratio = 1 array, the increase in conversion efficiency resulting from lower temperatures can possibly offset filter cost. Two types of filters were identified: (1) "hot" mirrors which cover the cell and reflect the UV and IR while transmitting the visible, and (2) "cold" mirrors which cover the concentrator and reflect the visible to the cell while transmitting the UV and IR to the mirror substrate. The most experienced industrial organization involved with space application of mirror systems is Optical Coating Laboratory Inc. (OCLI). OCLI have indicated that the relative cost of "hot" mirrors to "cold" mirrors is about 50 to 1. Furthermore the long-term reliability of "hot" mirrors would be questionable due to UV degradation. The optical properties of these mirrors would be altered deleteriously by the UV and the visible energy transmitted to the cell reduced. This problem should not occur as severely with the cold mirrors inasmuch as the UV is transmitted but it may influence selection of the mirror substrate. The cold mirror concept is contrasted with typical constructions in Figure 3.6-4. The hot mirror system may still be useful in designs in which solar heating is not directly incident to the filter, i.e., all energy to the cell is by reflection from the concentrator, if the reflectivity of the concentrator in the UV region is low.

The future realizability of mirror systems appears to be a practical goal. In terms of large-scale productivity, OCLI is currently developing, for commercial usage, instrumentation suitable for application of cold mirrors to

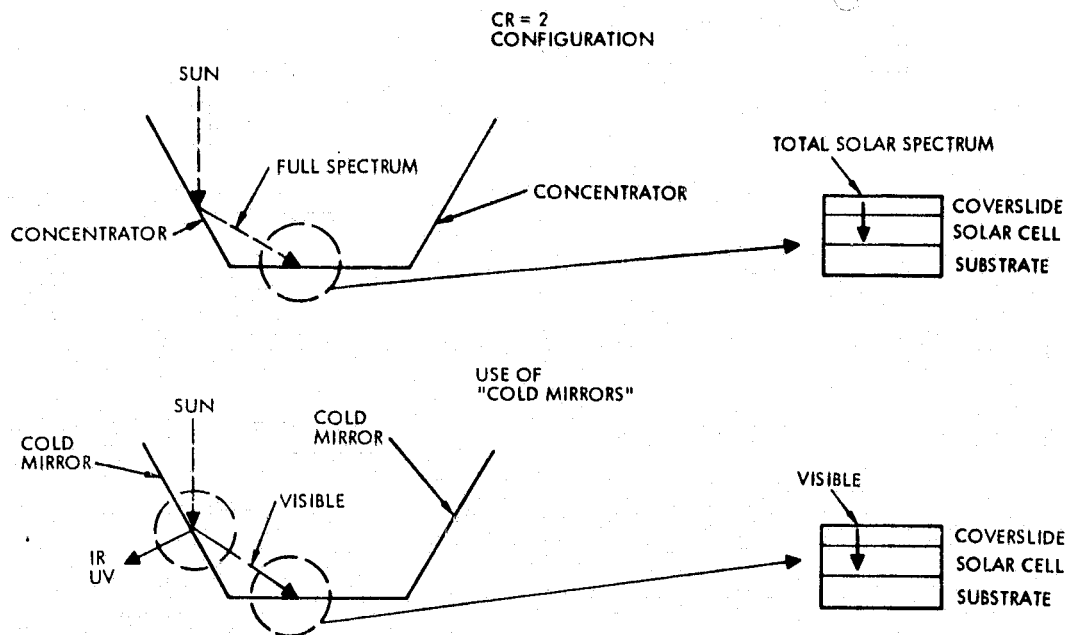


Figure 3.6-4. Spectral Filter Concepts

extended reflector areas. For example, their laboratory evaluation of candidate substrates indicates that Kapton is a more suitable substrate than Mylar. Libbey-Owens-Ford which represents another source of selective filters, have indicated fabrication capabilities relative to the specific wavelengths of GaAlAs.

Following the initial promising capability indications associated with the use of filters, an investigation was conducted to provide definitive performance data for bandpass filter applications relative to the specific configurations under consideration for the CR-1, CR-2, and CR-5 (nominal values) solar photovoltaic systems. Initially, the variation in efficiency and operating temperature was determined for relatively idealized conditions. The results of this computation are shown in Table 3.6-1. The basis of these advantages is the restricted conversion wavelength band (compared to silicon) over which GaAlAs can convert solar energy to electricity. This is approximately 54% of the solar spectrum. The remaining 46% is converted to waste heat.

These predictions did not account for several negative heat rejection factors inherent in the current designs which are configured principally based upon other mass and efficiency considerations. These factors include reduced optical properties, possibility of incident sun on cell rear surface (CR-5), and limited rejection due to an obstructed view of space. Analyses were performed to determine the actual temperature environments of the candidate designs to identify their practical limits. Due to the cost differential of "hot" mirrors versus "cold" mirrors (50 to 1) the study was restricted to "cold" mirror systems (except for CR-1). The use of standing film aluminum reflectors which might be fabricated from excess parts was also evaluated. It was eliminated for two reasons; (1) a processing plant would be required and (2) optical properties of the available aluminum alloy are not equivalent to those of pure aluminum.



Table 3.6-1. Passive Solar Array Performance Summary

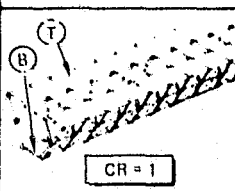
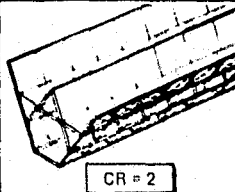
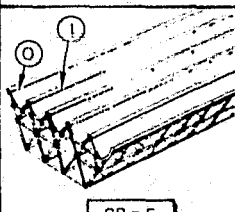
MAXIMUM ALLOWABLE CELL TEMPERATURE  °C	GaAIs				SILICON	
	CONVERSION EFFICIENCY  %	MAXIMUM CONCENTRATION RATIO		CONVERSION EFFICIENCY  %	MAXIMUM CONCENTRATION RATIO	
		FILTERS	NO FILTERS		FILTERS	NO FILTERS
		1985 TIME FRAME			1985 TIME FRAME	
100	18	3-4	< 2	12.8	3-4	< 2
125	17.6	4-5	2.3	11.2	4-5	2.3
150	17	6	3	9.5	6	3
200	16	8-9	4-5	6.1	8-9	4-5
250	14	11	6-7	NA	11	6-7
300	13	16	9	NA	16	9

The results are summarized in Figure 3.6-5. For the CR-1 system the use of "hot" mirrors was considered only because there is some uncertainty with regard to the resistance of Spraylon under prolonged UV exposure at temperatures above 60°C (personnel communication, Dr. McCargo of Lockheed). However, if this should become a real problem it would be more cost effective to utilize an RFP Teflon coverslide. The CR-2 design will also definitely need filters for the current cell stack and, again, may require a Spraylon substitute even if mirrors are used. One possible approach to permit application without mirrors would include a thin outer layer of glass as a coverslide. Temperatures shown for the CR-5 orientation indicate that there may be some questionable performance at these levels. It is tentatively assumed that 150°C is probably a maximum operating level for this blanket. It should be noted that Spraylon degradation due to UV exposure is not a problem because there is no direct UV exposure on the cell and the mirrors will not reflect the UV component of solar radiation. An additional case was considered to determine what the maximum allowable concentration ratio would be for this configuration to limit cell temperature to 150°C (it does not represent a study candidate concept). As shown for case 7 this limit is about CR-3.55 with a corresponding efficiency of 18%.

### 3.6.3 NaK/HEAT PIPE VS. CONDENSING RADIATORS

A number of candidate operational regimes were identified for alternate Brayton, Rankine, and Nuclear concepts involving radiator temperatures varying from 100°C to 1000°C. Because radiator/fluid weights will probably exceed 30% of the total system weights, optimal radiator concepts were defined for specific temperature ranges. Generally, two primary concepts were examined - one involving a condensing fluid loop, and an alternate tube/fin approach using heat pipes. Although the majority of space experience related to active radiator systems has been devoted to tube/fin and heat pipe systems



	RATIO	FILTERS	CONV. EFF.	TEMP °C
 CR = 1	1	NO	19	70 (T) 84 (B)
	1	YES	19.7	5 (T) 16 (B)
 CR = 2	2.44	NO	18	147
	2.36	YES	18.9	67
 CR = 5	6.24	NO	14	277 (O) 292 (I)
	5.86	YES	16	182 (O) 195 (I)
	3.55	YES	18	150

SPRAYLON MAY BE VULNERABLE TO UV ABOVE 60°C. IN ABSENCE OF UV CAN BE USED TO 150C

"COLD" MIRROR DESIGN 50X LESS EXPENSIVE THAN "HOT" MIRROR

NEED FILTERS FOR CR = 5 (PROBABLY FOR CR = 2)

150C MAX TEMP LIMITS CR = 3.55

ABOVE 150C SUBSTITUTE SILICA

Figure 3.6-5. Band Pass Filters

a number of studies were devoted to zero-g applications of space radiators using condensing fluids in the late 1960's. Fluids evaluated included potassium, mercury, Dowtherm A and Refrigerant 12 (R-12). Although testing was restricted to simulated zero-g drop towers and aircraft flying Keplerian trajectories, the limited data available suggest that condensing systems are feasible for space operations. Consequently, in developing radiator concepts both heat pipe and condensing fluid systems were considered although, for purposes of simplicity, condensing liquid metals were not included.

For thermal regimes in which inlet temperatures are low enough to restrict degradation and pressure levels, organics and steam are highly desirable condensing heat transfer fluids and have the potential of providing substantial mass savings. Organics are relatively non-corrosive, easy to handle and tend to be thermally efficient at temperatures up to 400°C. Typically, 400°C represents a maximum allowable temperature for these fluids due to degradation mechanics which occur, yielding various tars and volatile materials which can substantially reduce heat transfer coefficients. Due to the cost of replenishment and separation of tars and volatile products, a design peak temperature of 350°C was fixed for space utilization. Degradation characteristics of organics have been determined for the more widely used heat transfer fluids and are shown in Figure 3.6-6. The most widely used high temperature organic is Dowtherm A which is a diphenyl eutectic having superior degradation characteristics when compared with other candidates. At 350°C, this material would experience an annual degradation rate of about 0.15%. For this rate, it is expected that some makeup fluid will be required approximately every ten years or twice during the SPS lifetime. Although other organics such as toluene may be stable about 400°C, they are in the critical regime and do not make suitable heat transfer fluids.

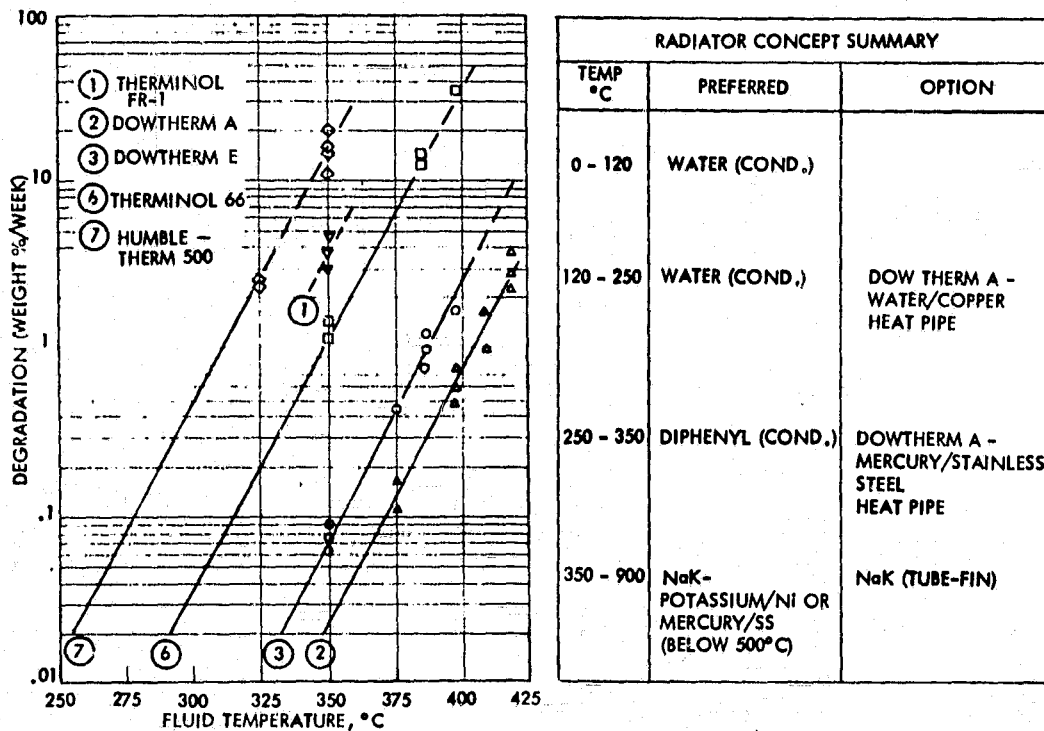


Figure 3.6-6. Organic Fluid Degradation

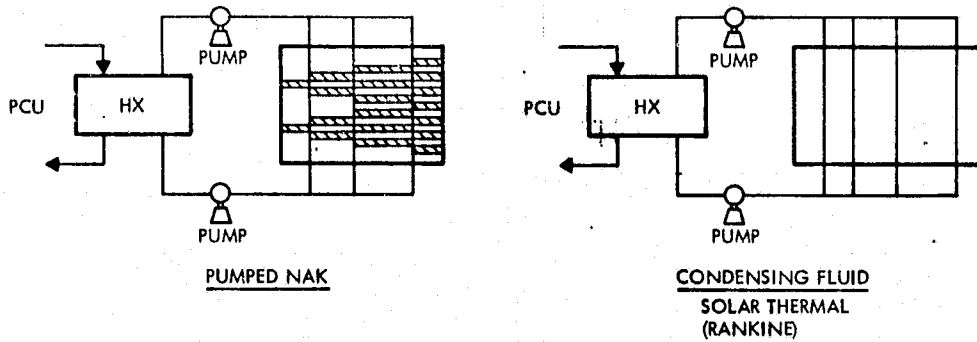
Another advantage of organics at temperatures below 350°C is that they can be used as condensing fluids, thereby reducing mass. Operation in the two-phase regime permits utilization of the fluid latent heat and control of the radiator to higher temperature. Although the eutectic mixture could be used, design simplicity suggests a single component fluid. For instance, at 350°C, diphenyl has a latent heat of about 94 kcal/kg which is considerably higher than the sensible heat than can be obtained in competitive non-condensing approaches. The comparative latent heat of the Dowtherm A mixture is 59 kcal/kg.

At radiator temperatures above 350°C, the high degradation rate of organics required substitution of a NaK fluid loop. Heat pipes are preferred to enhance the overall system effectiveness although if a large gradient is experienced across the radiator different types of heat pipes will be required, which is undesirable. Primary and optional concepts were identified for a range of radiator temperature levels and system weights evaluated for alternate concepts.

A number of candidate operational regimes have been identified for alternate Brayton, Rankine, and nuclear concepts involving radiator temperatures varying from 100°C to 1000°C. These concepts are presented in Figure 3.6-7.

For the Rankine, Brayton, and nuclear cycle systems considered, the radiator designs are presented in Figure 3.6-7. Data for the Brayton solar thermal configuration is based on Boeing results. For the nuclear system the heat transfer fluid selected was NaK.





CONSTRUCTION:	SOLAR THERMAL (BRAYTON)	NUCLEAR	DIPHENYL (TUBE/FIN)
HEAT PIPE	HEAT PIPE/FIN WATER/SS	HEAT PIPE FIN MERCURY/SS	
TEMPERATURE, EFFECTIVE	212°C (355°C IN, 96°C OUT)	385°C (493°C IN, 288°C OUT)	343°C (350°C IN, 337°C OUT)
TOTAL PANEL AREA (2 SIDES)	4.71 KM <sup>2</sup>	1.53 KM <sup>2</sup>	1.66 KM <sup>2</sup>
RADIATOR WT. (WITH PUMPS)	4.33 KG/KW	2.26 KG/KW	2.19 KG/KW

Figure 3.6-7. Radiator Concepts

Further investigation of these radiator systems was conducted to determine the influence of meteoroids on system mass.

Analyses were performed to determine active thermal control system radiator mass penalties resulting from exposure to the space meteoroid environment. The flux model utilized is the NASA space environment guideline contained in NASA SP-8013 with some modification based upon the Rockwell in-house developed directional flux modification. Armor thickness requirements were developed from the spallation threshold equation shown in Table 3.6-2 which was derived from hypervelocity impact data. Where possible, it is desirable to use bumpers rather than armor because the use of a thin outer shield which can break up and slow down the incident particles significantly reduces the total protective mass required. Lifetime survivability can be computed using a Poisson probability distribution if a reliability probability is assigned and the exposed vulnerable tube area is known. It was assumed that the occurrence of a leak can be determined relatively automatically through use of appropriate sensing components but that immediate maintenance is not available. Depending on failure mode, type of failure and time on orbit, scheduled maintenance and/or preventive maintenance will be performed.

Meteoroid penalties were determined for both the Rankine and nuclear cycles. Radiator system weight penalties determined for the nuclear cycle NaK heat pipe radiator configuration are shown in Figure 3.6-8. Optimal (minimum) active fluid loop masses were computed from parametric analytical trades of redundancy versus increased bumper protection; using stainless steel as the heat pipe, header, and bumper material. The results are presented for varying lifetime requirements and indicate that a tube penalty of approximately 55% is required for a 30-year life.



Table 3.6-2. Meteoroid Study Ground Rules

ORIGINAL PAGE IS  
OF POOR QUALITY

- NASA METEOROID ENVIRONMENT SP8013
- RI DIRECTIONAL FLUX MODIFICATION
- PROTECTIVE ARMOR THICKNESS REQUIRED

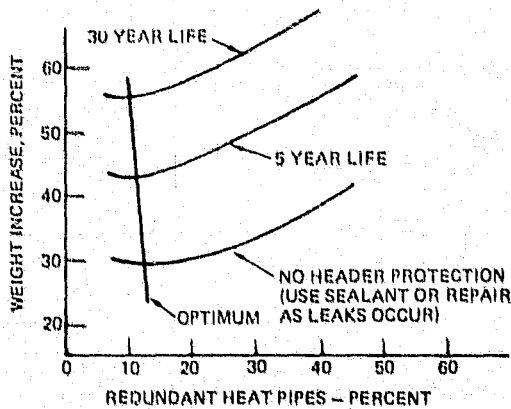
$$F_t = \frac{\rho_p \cdot 133 \cdot V_p^{2/3} \cdot M \cdot 367}{H_t \cdot \rho_t \cdot t^{1/3}}$$

- SURVIVABILITY DETERMINED BY POISSON DISTRIBUTION

- $F_t$  = SPALL FACTOR
- 1.0 FOR TITANIUM & STAINLESS STEEL
- $H_t$  = BRINELL HARDNESS
- $V_p$  = 20 KM/SEC
- $\rho_t$  = SPECIFIC GRAVITY OF TARGET
- $t$  = ARMOR THICKNESS ~ CM

- PROB OF ZERO PERFORATIONS OF A HEADER = 0.96

CONCEPT OPTIONS



- THICKER TUBES
- SINGLE BUMPER SHIELDING
- REDUNDANT CIRCUITS (PANELS)
- REDUNDANT TUBES AND/OR HEAT PIPES
- DESIGN FOR LEAKS & REPLACE FLUIDS
- SELECTIVE RADIATOR ORIENTATION

- FOR NO DEGRADATION 30 YEAR WEIGHT PENALTY ~ 55% ON TUBES\*
- USE COMBINATION OF CONCEPT OPTIONS
- EVALUATE VALVE/TUBES (COMBINATION)

Figure 3.6-8. Meteoroid System Mass Penalty Heat Pipe Radiator

Lifetime mass penalties are shown in Figure 3.6-9 for the condensing Rankine cycle diphenyl radiator as a function of system redundancy. The basic protective header design selected is a double-bumper configuration which substantially reduces protective mass penalties. Although the mass penalties would be more severe than for a comparative heat pipe radiator system, the use of titanium shows a significantly smaller mass than stainless steel and thus the results for the Rankine system cannot be directly compared with the nuclear configuration. Reduction in perforation resistance for titanium is also less than that for stainless steel at elevated temperature, but both materials show a substantial decrease relative to room temperature values.

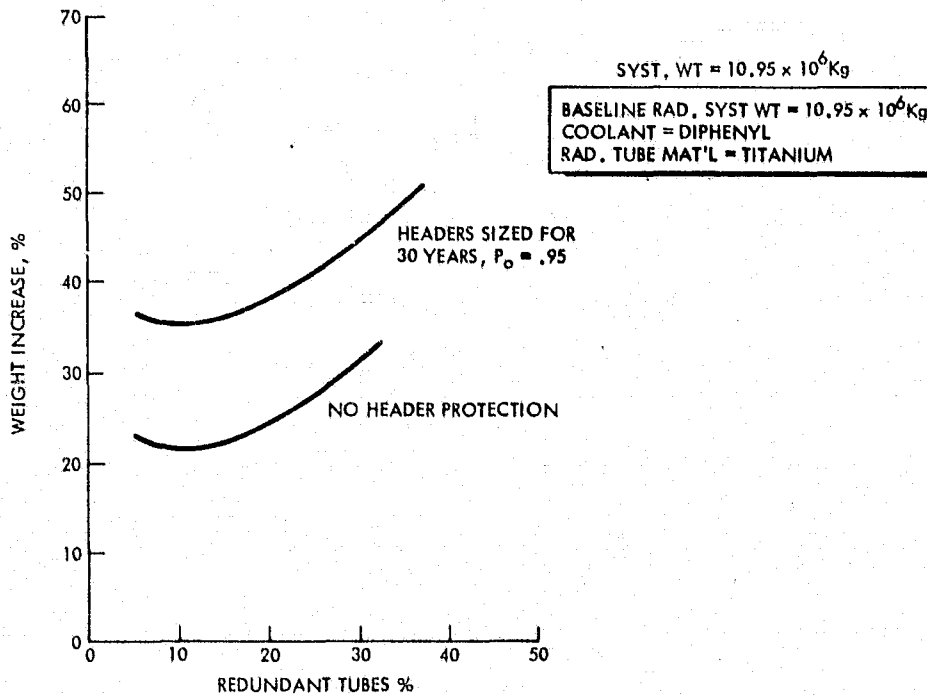


Figure 3.6-9. Effect of Meteoroid Protection on Radiator System Mass-Rankine Cycle SPS

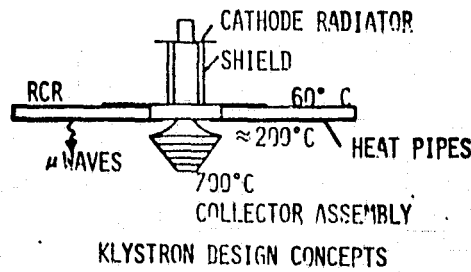
#### 3.6.4 KLYSTRON THERMAL CONTROL DESIGN

An investigation was conducted to evaluate cooling approaches to dissipate the 3.264 kW waste heat dissipated in the driver cavity, the output cavity and the electromagnet areas of the klystron device. One approach considered was to use a NaK loop in which the liquid is circulated by an electromagnetic pump to the body radiator for rejection at about 125°C. This semi-passive system (no moving parts, 30 year life) requires a coolant flow of less than 1 gpm to transport the waste heat load. Due to the low operating efficiency of these pumps, approximately 30 watts electric per pump is required. The alternate design evaluated used a network of heat pipes to transport the heat from the tube to a series of smaller heat pipes which then carried the heat to the radiator. The relative simplicity and substantially lower mass of the second option led to the selection of a heat pipe design. The selected concept is illustrated in Figure 3.6-10.

#### 3.6.5 THERMAL CONSIDERATIONS AT LEO VS. GEO

As part of their in-house evaluation of SPS viability, MSFC conducted an investigation to determine thermal considerations which might influence construction orbit selection. The results of this study, based upon their written inputs, are presented below.

Analyses have been performed to determine the temperature variations and resulting thermal distortions in the rigid members of the MSFC elliptical planform satellite power station (SPS). The SPS was analyzed in low-earth



ORIGINAL PAGE IS  
OF POOR QUALITY

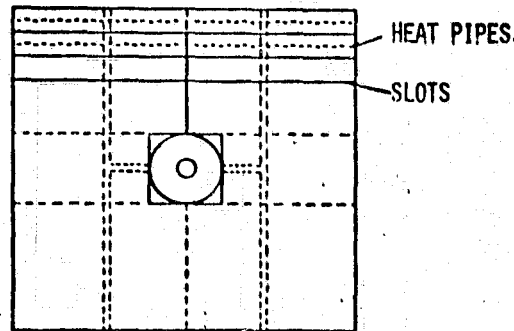


Figure 3.6-10. Heat Radiators on Array Face

orbit (LEO) and geosynchronous orbit (GEO), so that the effects of the different thermal environments on the structure could be compared. The structure was analyzed with and without the solar array in place. The structure, with and without the solar array, is referred to as the operational and construction configuration, respectively. During the SPS construction at LEO, a gravity gradient (GG) attitude with the X and Y axes in the orbit plane was assumed. At GEO, both gravity gradient and X perpendicular to orbit plane, Z solar inertial (X-POP, Z, SI) were assumed. During the operational phase, the X-POP, solar inertial was assumed for both LEO and GEO. A beta angle of zero was used.

The configuration of the 1-m beam, the basic building block of the SPS, is shown in Figure 3.6-11. The material is anodized aluminum with a solar absorptivity of 0.86 and an emissivity of 0.83.

When assembled, most of the 1-m beams (the bulk of the structure) will be parallel to the SPS X and Y axes. Temperatures for these structural members (referred to as X- and Y-axis members) and overall dimensional changes in the X- and Y-directions were determined as a function of orbital position. These are shown for the construction and operational phases in LEO and GEO on Figures 3.6-12 through 19. The maximum and minimum variations are summarized in Table 3.6-3.

In addition to the X-Y (in-plane) dimension changes, the structure will distort, or bend, due to temperature differences between members. These temperature differences are caused primarily by members whether being illuminated by the sun or shaded. During the construction phase, temperature gradients will occur in 1-m beams when one 6.7-centimeter triangular element shades

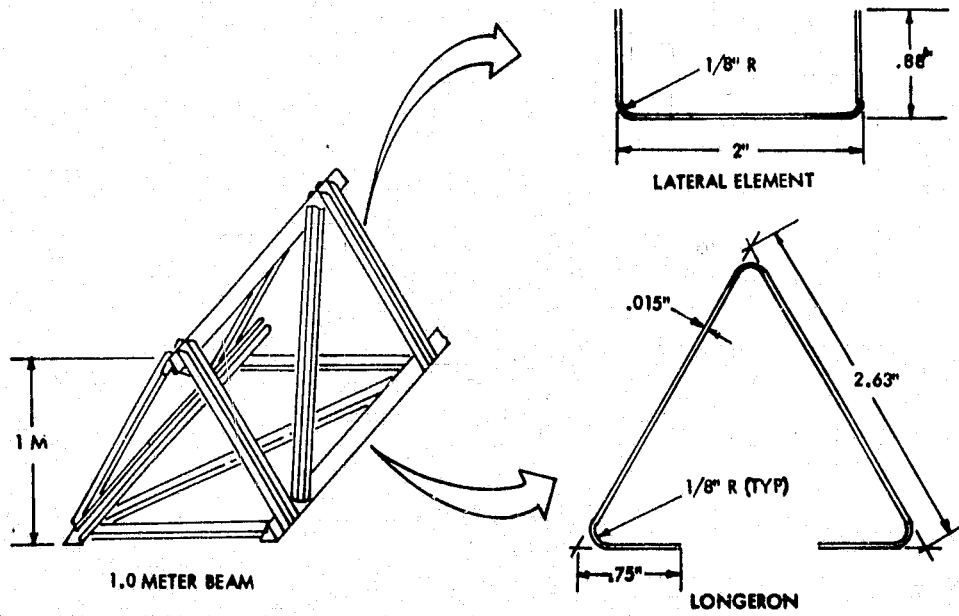


Figure 3.6-11. One Meter Beam Construction

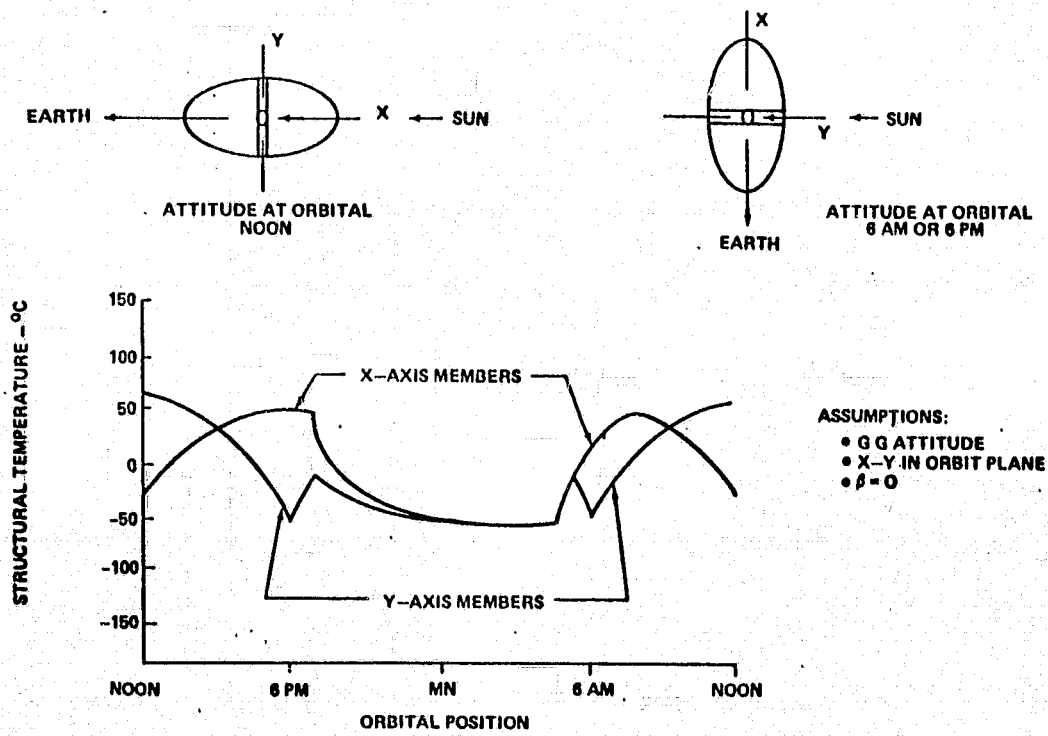


Figure 3.6-12. SPS Structural Temperature, LEO, Construction Phase



ORIGINAL PAGE IS  
OF POOR QUALITY

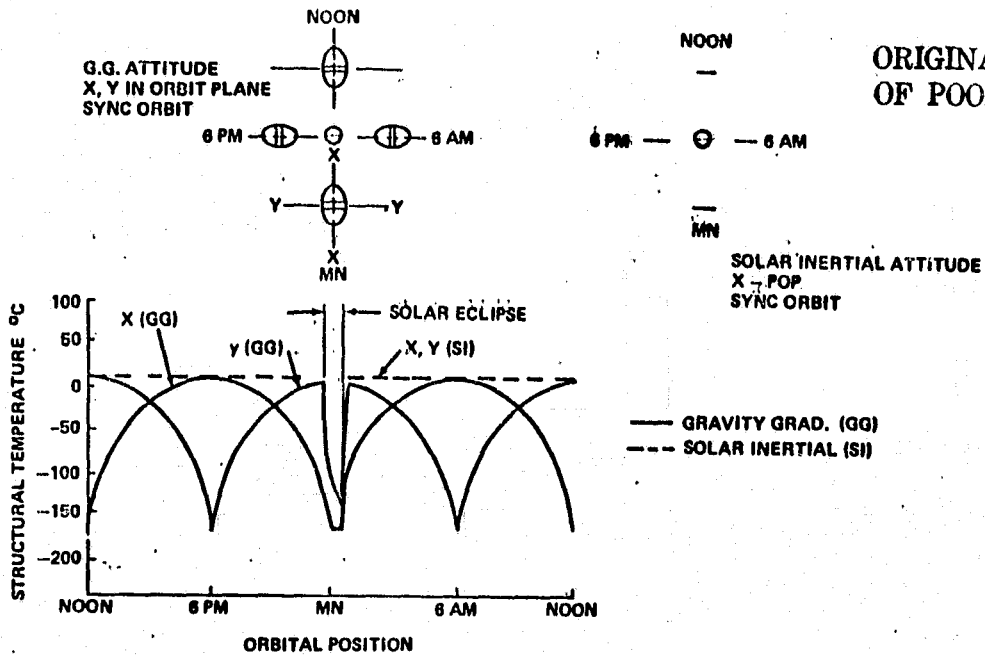


Figure 3.6-13. SPS Structural Temperature  
GEO Construction Phase

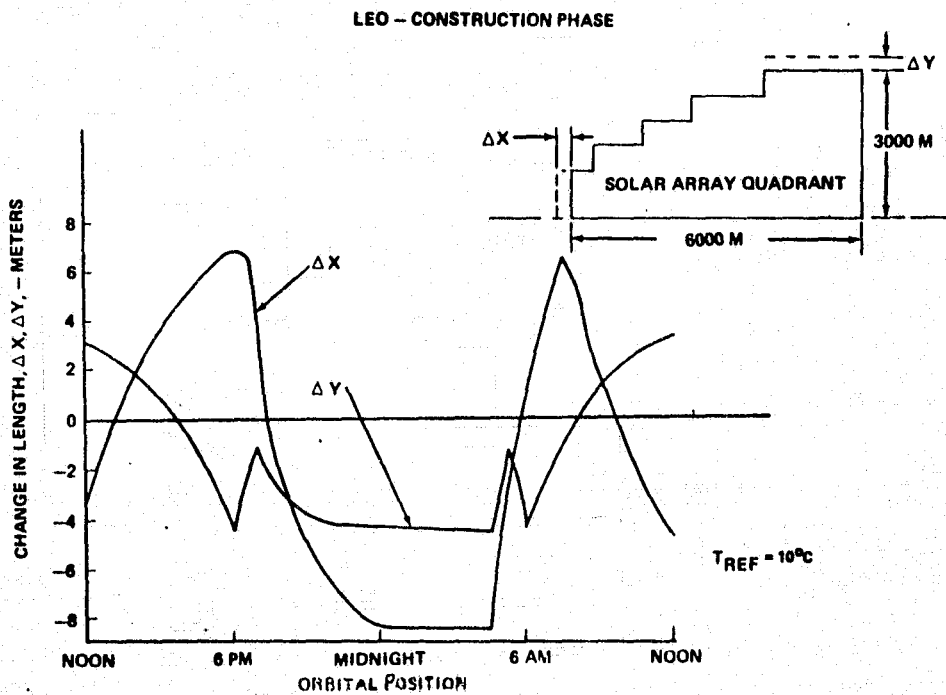


Figure 3.6-14. SPS Thermal Distortion

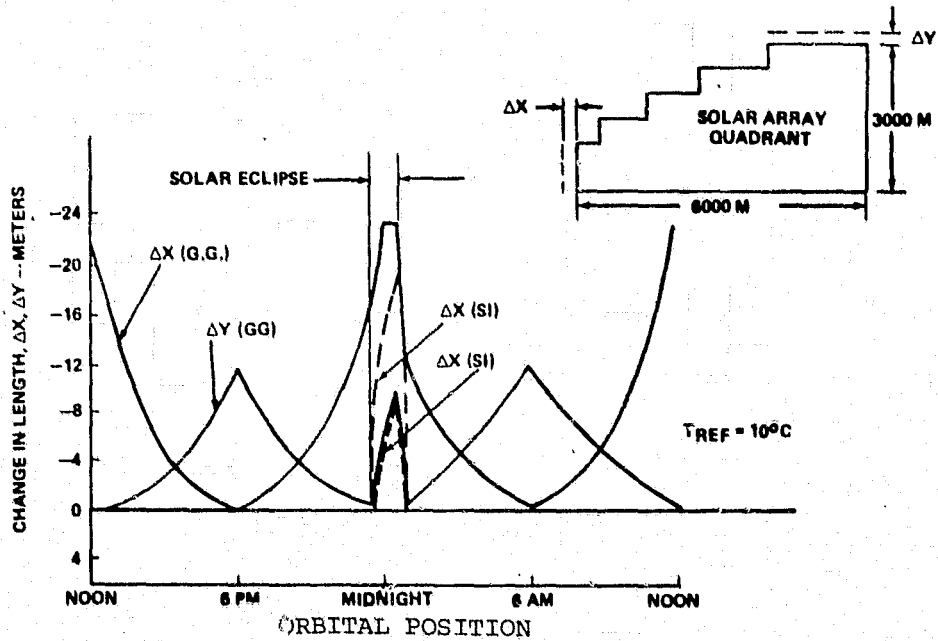


Figure 3.6-15. SPS Thermal Distortion, GEO Construction Phase

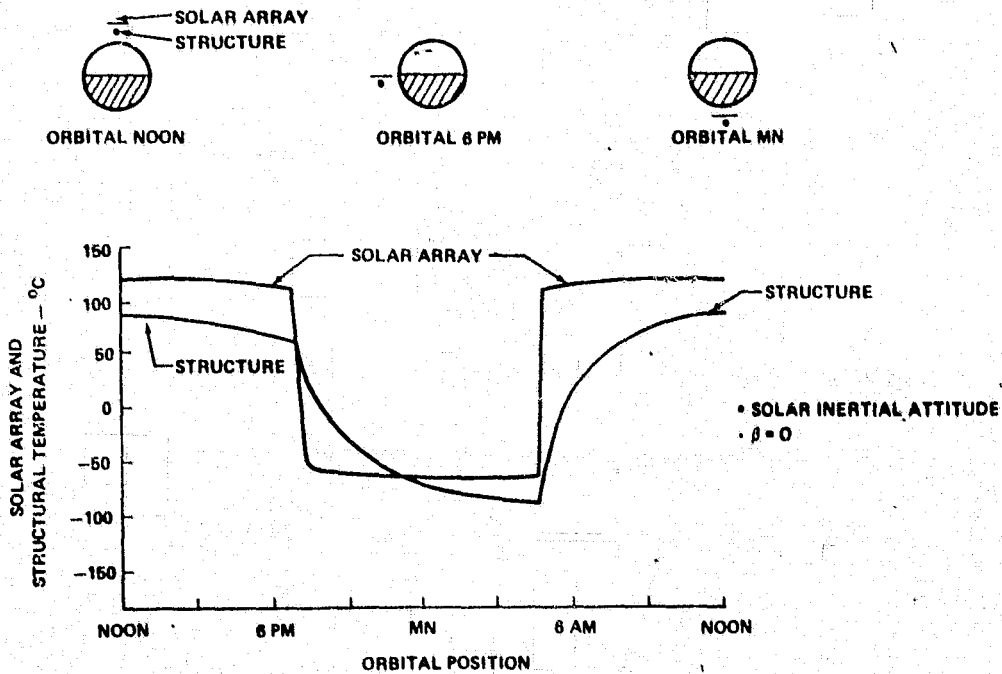


Figure 3.6-16. SPS Structural Temperature LEO - Operational Phase



ORIGINAL PAGE IS  
OF POOR QUALITY

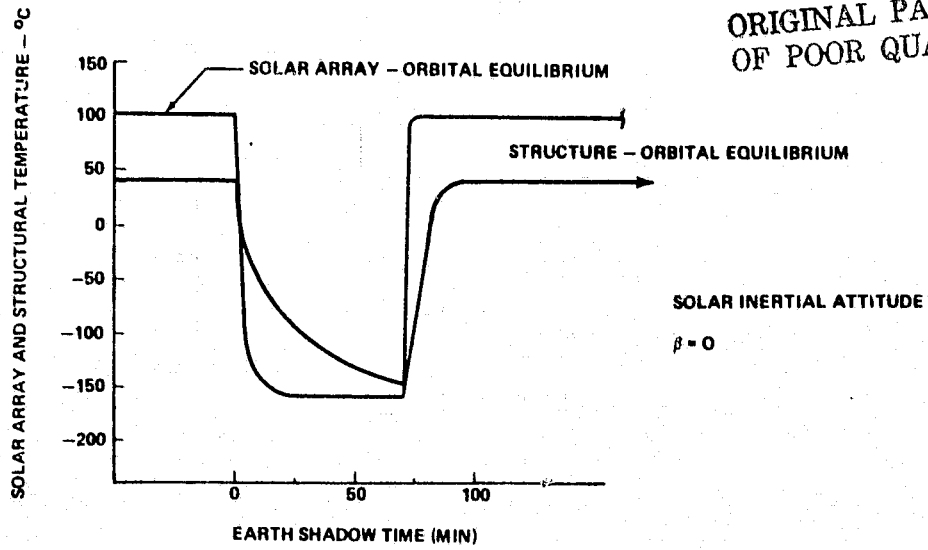


Figure 3.6-17. SPS Structural Temperature  
GEO - Operational Phase

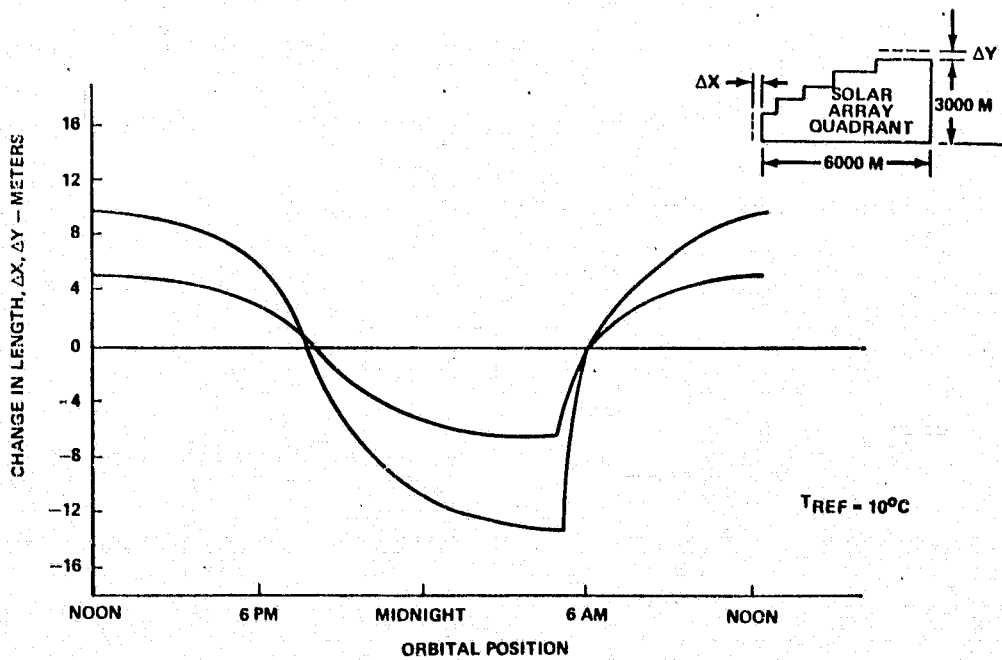


Figure 3.6-18. SPS Thermal Distortion,  
LEO Operational Phase



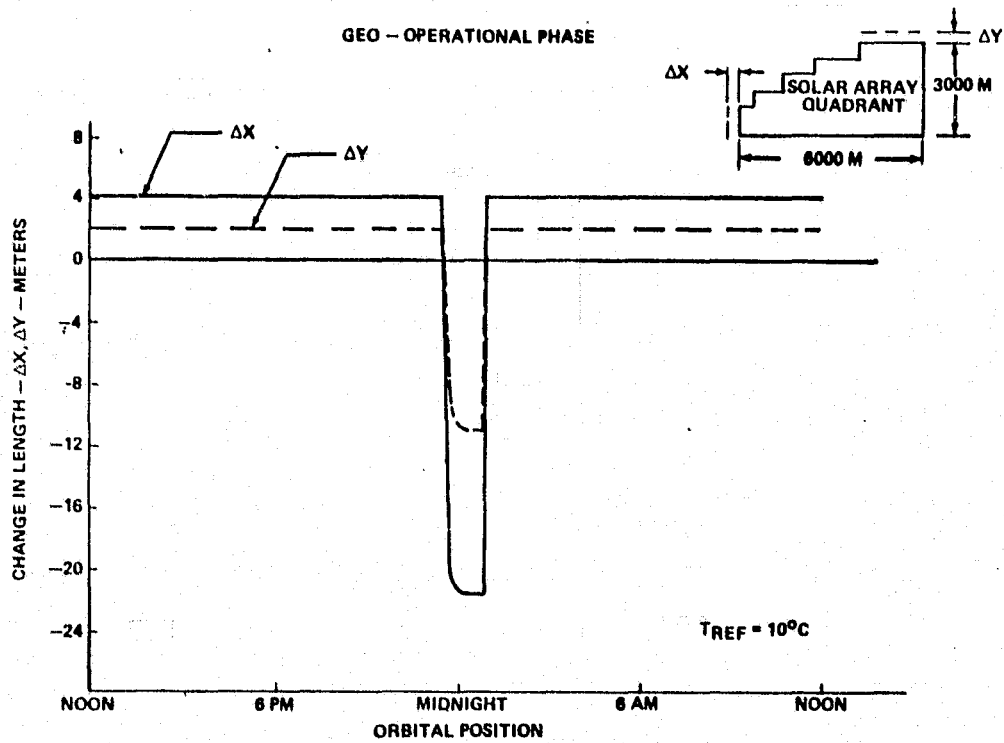


Figure 3.6-19. SPS Thermal Distortion

Table 3.6-3. SPS Maximum Temperature Variations and Corresponding Dimensional Changes (Reference Temperature, 10°C)

Configuration	LEO			GEO (GG)			GEO (SI)		
	T	ΔX	ΔY	T	ΔX	ΔY	T	ΔX	ΔY
Construction Phase	+60	+4	+2	+10	+0	+0	+10	+10	0
	-57	-8	-4	-162	-22	-11	-135	-19.0	-9.0
Operational Phase	+82	9.6	4.8	-	-	-	39	+4.0	+2.0
		-6.5	-13	-	-	-	-145	-21.5	-11.2

T = Temperature, °C  
ΔX, ΔY = Dimensional change, meters

another (as when two elements are in the orbit plane with beta equal to zero). In LEO, the gradient would be 117°C; and in GEO, 172°C. Since each of the three 1-m beams contained in a 20-m-depth girder has the same orientations, each has the same thermal gradient and distortion is limited to 30-m sections between transverse members. The 500-m-long girders are not significantly distorted in bending, but change in length.

During the operational phase, the solar array shades some of the 1-m beams comprising 20-m girders, while others are illuminated by the sun. When sunlight passes through the slot separating adjacent solar array blankets, it will illuminate the beam to which the blankets are attached, and it may or may not illuminate the beams comprising a 20-meter girder on the back side of the structure. The beam that is illuminated will depend on the alignment of the SPS with the sun. Corresponding beam temperatures and temperature gradients are summarized on Figure 3.6-20, for the noon orbital position. Corresponding structural deflections in the 20x500-meter girders and in the 6000-meter half section of the SPS are shown in Figures 3.6-21 and 3.6-22. Since these distortions are dependent upon sun alignment, they can be of an oscillatory nature, coupled to the attitude control system.

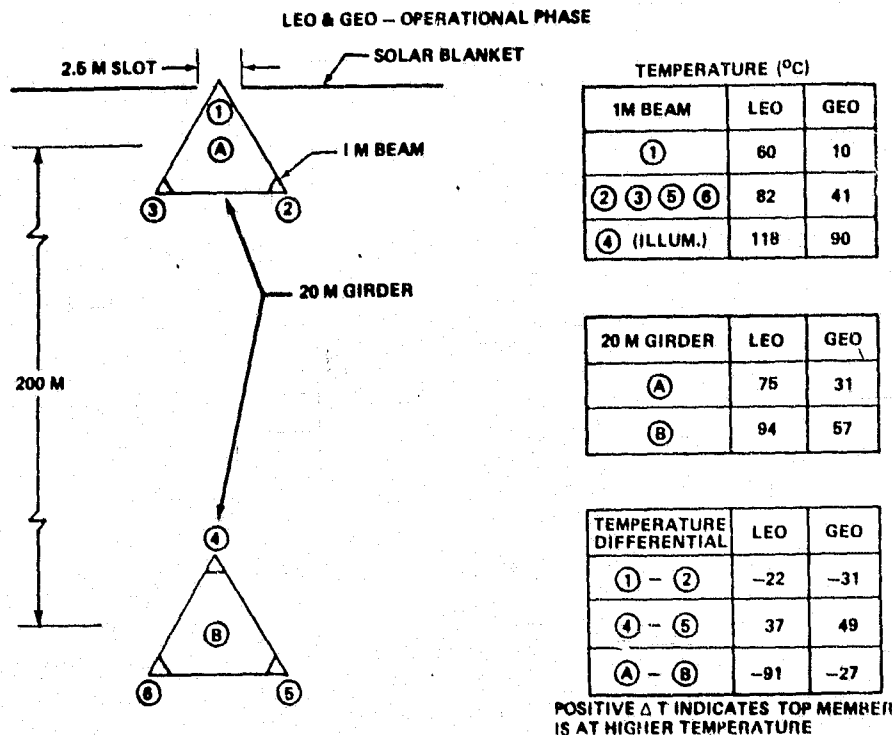


Figure 3.6-20. SPS Structural Temperature Gradients

In summary, some general observations from the thermal/structures trade study are (limited to  $\beta = 0$  consideration):

- Thermal considerations do not preclude assembly of the SPS at either LEO or GEO.
- Construction phase
  - Should the SPS be assembled at GEO, the gravity-gradient attitude should be avoided because of the large continuous changes in structural temperature.
  - Thermal gradients are limited to 1-m beam elements without serious deformation. Overall dimensions change about 0.2%.

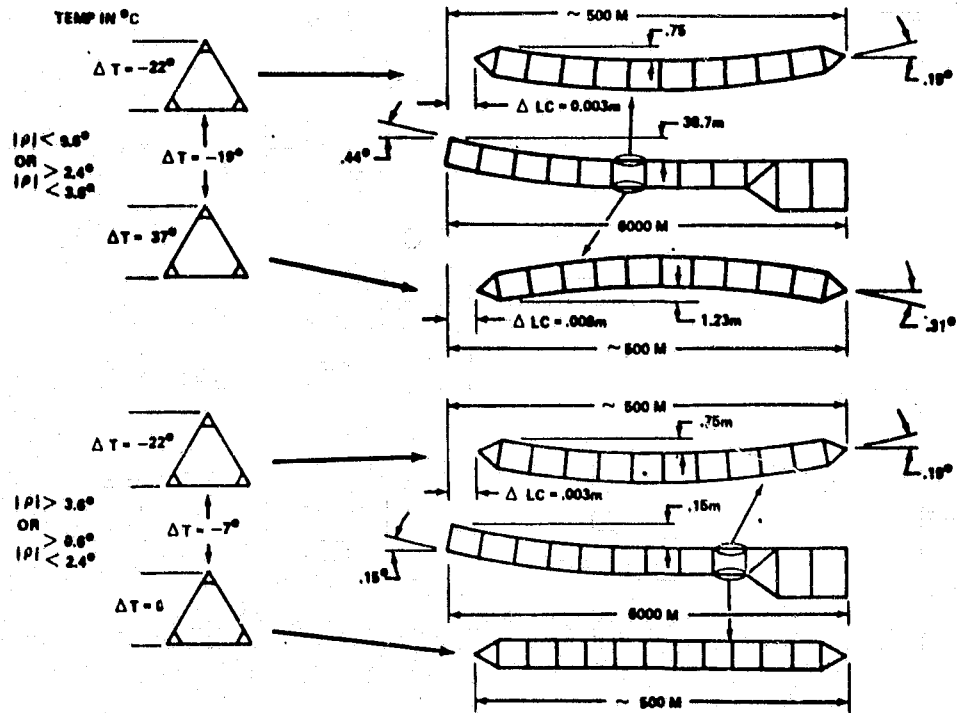


Figure 3.6-21. SPS Structural Distortion Due to Temperature Gradient  
LEO - Operational Phase

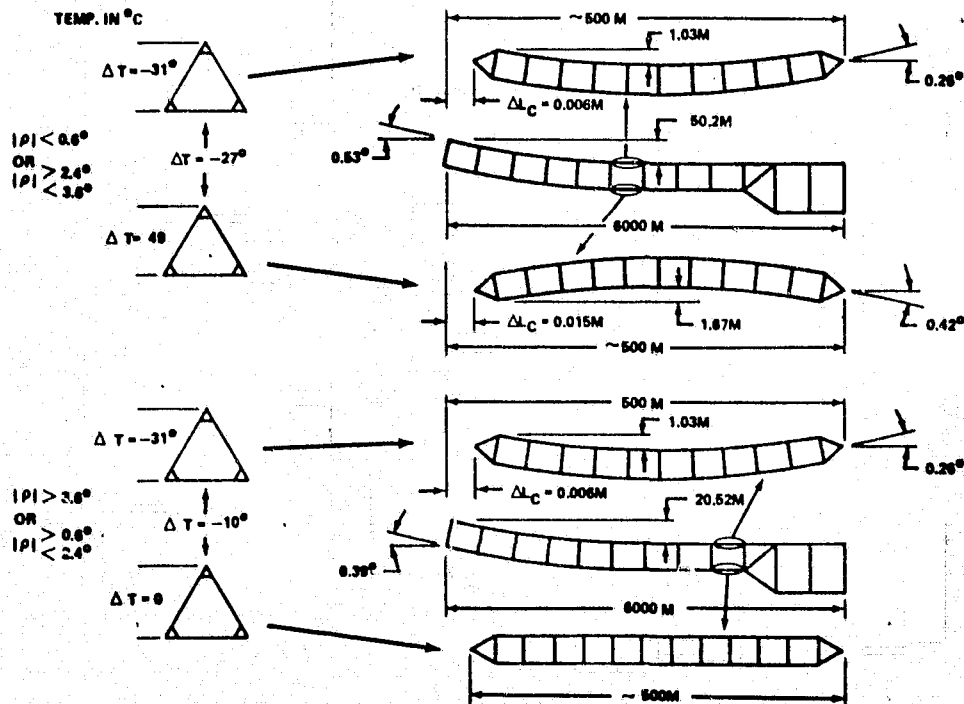


Figure 3.6-22. SPS Structural Distortion Due to Temperature Gradient  
GEO - Operational Phase



- Operational phase

- At LEO, structural temperatures are higher (about 82°C), and dimensions change continuously up to about 0.5%.
- At GEO, temperatures are nearly constant, except when entering the earth's shadow. Then, temperatures drop suddenly, with accompanying dimension changes again of about 0.5%.
- The gap between solar blankets at attachment to the structure causes unacceptable thermal gradients and oscillatory distortion; closure of the gap will eliminate the problem.

### 3.6.6 RELATIVE ORIENTATION OF ELECTRICAL CONDUCTORS

The electrical conductors can represent a significant relative mass of the total satellite system. The required mass of these elements is greatly influenced by their operating temperature. Parametric analyses of conductor thermal response versus (1) location and (2) thickness were performed to determine the extent of weight saving that could be achieved through selective design. The placement of the conductors is important because of the thermal impact of the solar blankets. This becomes particularly vital for high temperature arrays (i.e., high concentration ratio). Reduction of the view of the conductors to the blankets with a corresponding increase in exposure to deep space can greatly reduce the necessary cross section for electrical transmission. Additionally, if the thickness is reduced, the area for reradiation increases and the temperature is also lowered (although this may be offset by a greater cross section). Figure 3.6-23 exhibits some results for the CR-2 configuration with three different placements of the conductors; under the blankets, hung from the sides of the blankets, and hung from the sides of the reflectors. As can be readily observed from the results the most desirable location is reflected by the second option. In Figure 3.6-24, some computations for the CR-1, CR-2, and CR-5 configurations are presented for two different conductor thicknesses, 0.10 and 0.04 cm. Due to practicality, it was decided to restrict the conductor thickness to one millimeter. Results are also presented for different emissivities. These values would be achieved by varying insulator (Kapton) thickness. It was determined that a one mil layer (emissivity = .68) would represent an optimum condition.

### 3.6.7 DOE PROGRAM SUPPORT REQUIREMENTS

DOE program support requirements identified to date are:

1. Subsystem mass/cost data
2. Appropriate level of technical risk
3. Expected ground/flight test demonstration program
4. Thermal atmosphere/ground heating effects
5. Required temperature ranges in human access areas

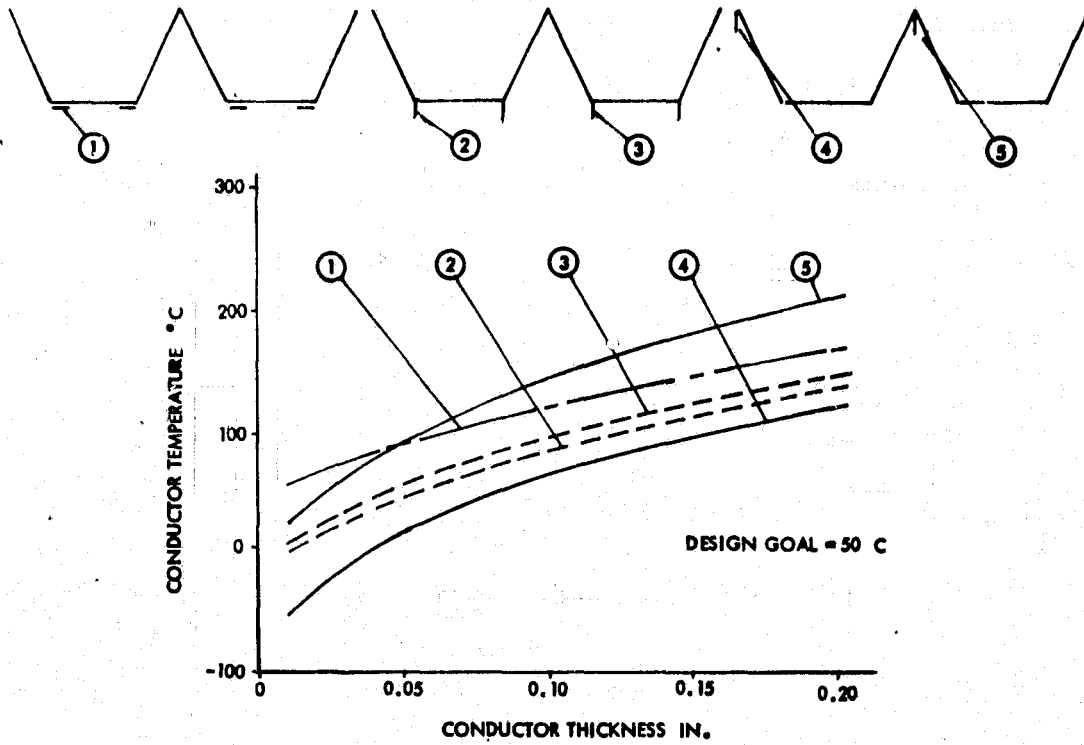


Figure 3.6-23. Electrical Conductor Thermal Response

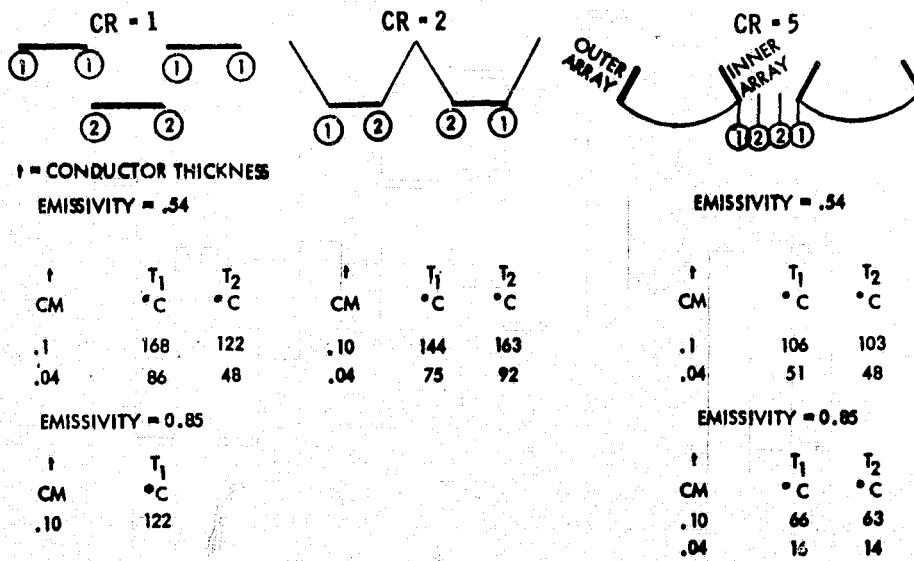


Figure 3.6-24. Electrical Conductor Thermal Analysis

3.7 INFORMATION MANAGEMENT AND CONTROL

Various Information Management and Control Subsystem (IMCS) studies were performed to determine the existence (if any) of any special technological issues that might impact the selection of an SPS satellite. Figure 3.7-1 represents the entire spectrum of trade study areas that will eventually need investigation. Those subject areas that are shaded received only superficial attention and will require study when funds are made available.

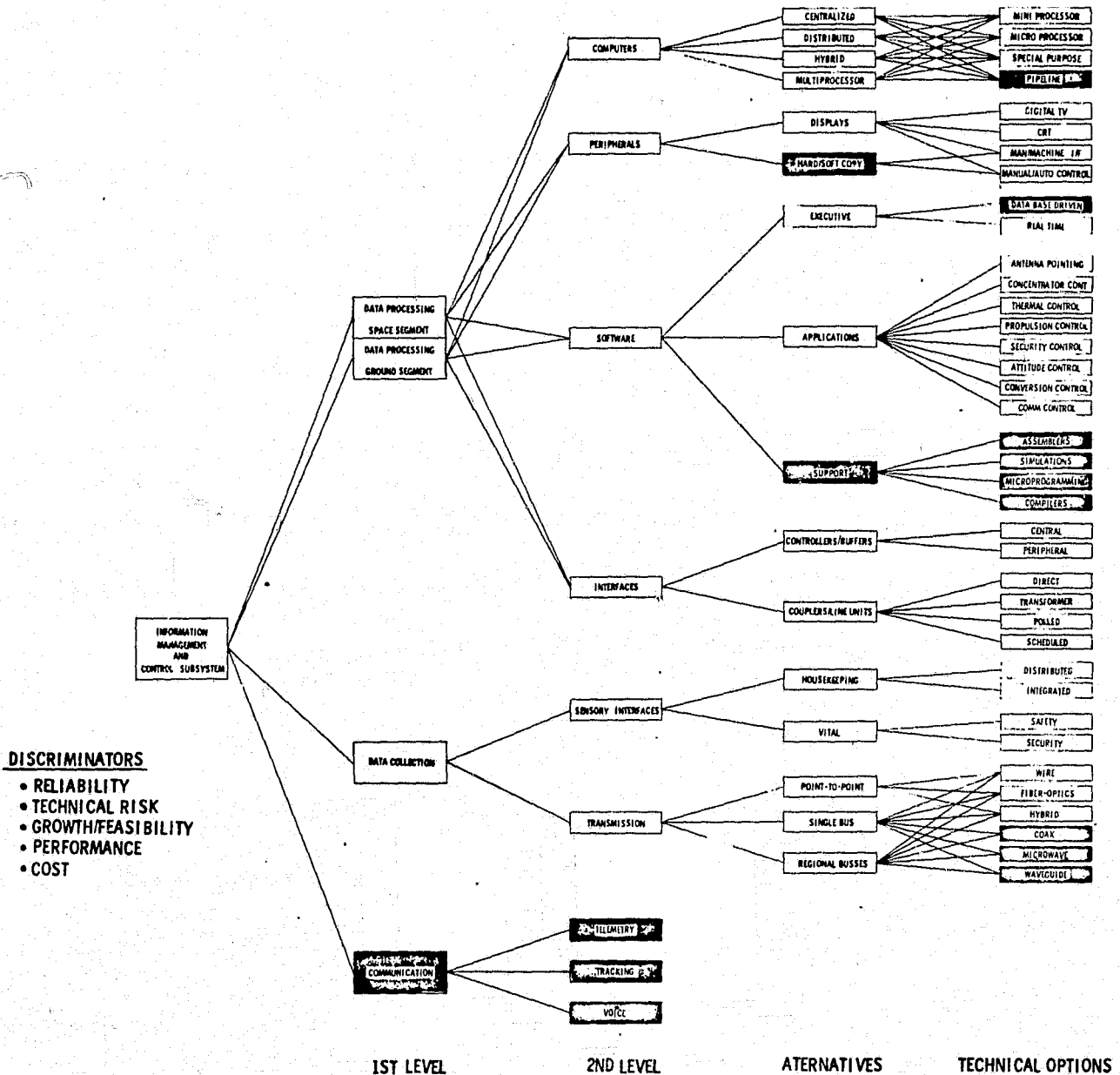


Figure 3.7-1. Trade Tree -  
Information Management and Control Subsystem



Detailed studies were made in two areas—Central vs. Distributed Processing Trades, and Data Bus Trades. A third area—Ground-Based Information Management—was also considered, although in less detail because of requirements uncertainty. The following sections discuss these trades and their results. These trade studies were supported by IBM design and analysis efforts.

### 3.7.1 CENTRAL VS DISTRIBUTED PROCESSING

#### Introduction

The purpose of this analysis was to determine the relative merits of three types of computer systems for the Satellite Power System (SPS):

- Central Computer System
- Distributed System
- Hybrid of the above

The Central Computer System would utilize two individual computers to service the entire Information Management and Control Subsystem (IMCS) for the satellite. One computer would service all subsystems except the Microwave Antenna, which would be serviced by a second relatively large computer; both computers would be located at the same station on the satellite.

The Distributed System is the baseline system concept under consideration for the SPS because considerations of local control for safety and reliability favor this approach. Figure 3.7-2 illustrates the spatial distribution envisioned for the Distributed System assuming a two-trough SPS. Computer centers would be located in or near the center section, stations 6 left and right, stations 16 left and right, and at the ends of each wing of the SPS. The previous Data Bus Trade study utilized IMCS computer system conceptual subparts which were defined by Rockwell to support the Power Distribution, Thermal, Attitude Control, Microwave Antenna and Structural Subsystems. These same distributed computer system architectures were utilized in this study. A hierarchy of remote micro-, mini-, supervisory, and master computers is combined into an integrated processing system. Approximately 3 dozen computers are required for this approach exclusive of micro-processors.

The third approach utilizes a centralized computer system for the SPS subsystems and a distributed architecture for the Microwave Antenna Subsystem. This Hybrid concept was selected because of the large processing loads imposed by the Microwave Antenna as compared to the remaining satellite subsystems. The scope of this analysis is limited to a preliminary set of trade-offs among these three computer system approaches.

#### Analysis Approach

The assumption of a solar photovoltaic satellite and a distributed processing system is basic to this analysis as indicated in Figure 3.7-3. The Central and Hybrid computer system approaches are merely variations about this basic approach.

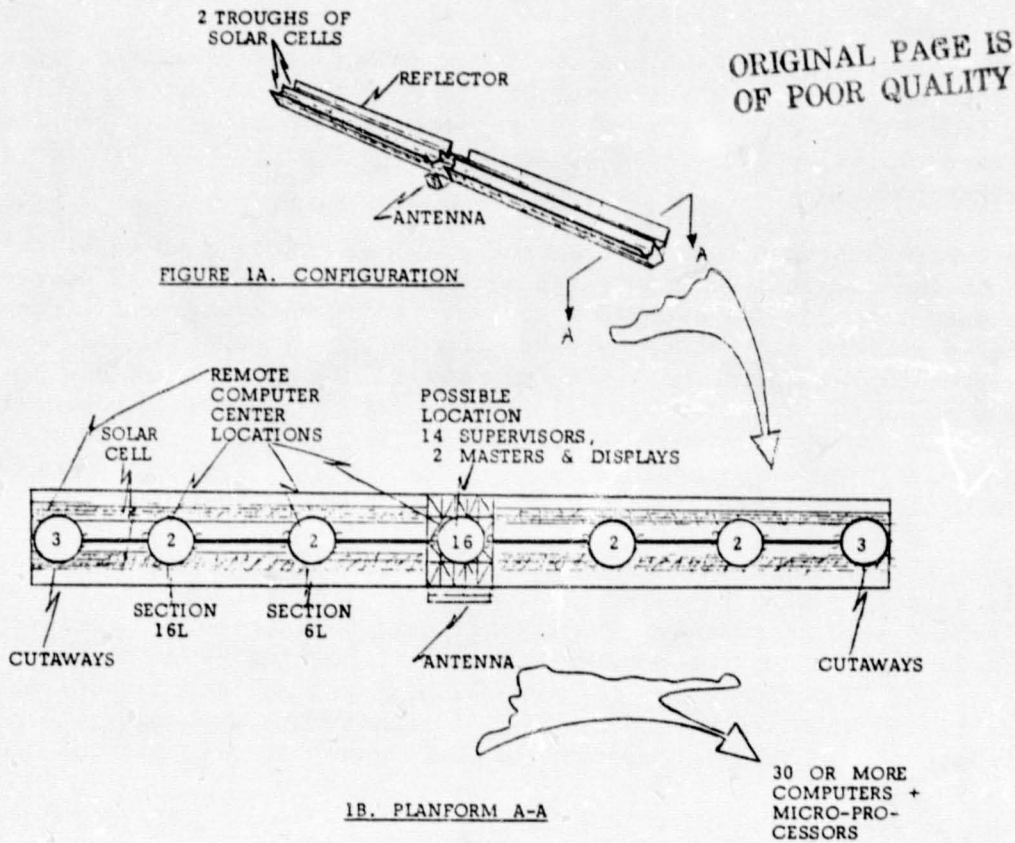


Figure 3.7-2. Distributed Computer Concept

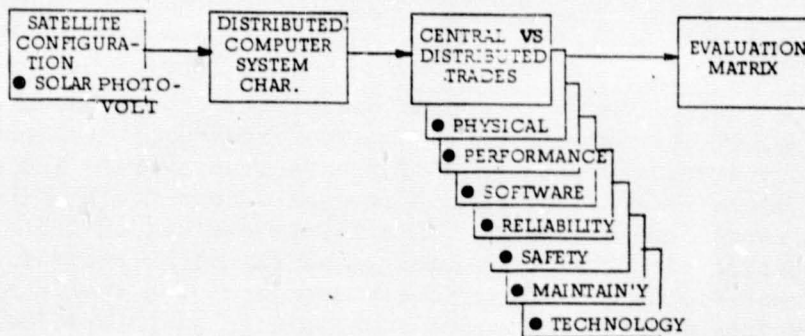


Figure 3.7-3. Analysis Approach

Seven fundamental factors have been identified for trade-offs: physical, performance, software, reliability, safety, maintainability and technology status. Physical characteristics of weight, power and volume must be estimated to rough order of magnitude (ROM) to gain an appreciation for the size and economic impact of the IMCS on the feasibility of the SPS. In all cases, the estimates serve to verify whether the IMCS poses any unique technological problems.





Performance requirements and available technical capabilities must be compared to help confirm any technological impediments to SPS feasibility arising from the IMCS. In this area, requirement estimates are pending and are believed to be accounted for by the assumption of relatively high speed processing needs.

Software complexity and development problems continue to be of major concern in the evolution of any large system today. Centralized systems tend to need more complex executive software and data management functions. Distributed systems may reduce software complexity by partitioning jobs into smaller and simpler operations which may facilitate simplifications in executive and data management functions. In any case, there appears to be a need for design approaches which facilitate software specification, verification, performance monitoring, testing and changes to accommodate evolutions in design maturity.

Reliability, safety and maintainability are all fundamental to any IMCS which is to help result in an SPS system which is justifiably relied upon as a stable source of consumer electrical power. Distributed processing facilitates reliability through redundancy but complicates maintainability because of the large number of components; high reliability fosters safety. A centralized system may reduce reliability and safety although maintainability is probably facilitated through centralization of component location.

The status of computer technology which is needed to implement each of the system architectures impacts any assessment of IMCS key technical issues affecting SPS feasibility. Assuming a 1995 initial operational date, the SPS is probably dependent upon computer technology which is expected to exist by the late 1980's. Today's capabilities must be projected to this time period and assessed against the expected needs of the SPS in the middle-nineties.

Having either quantified by ROMs, or qualitatively estimated these parameters for each of the three concepts, summary trade tables are presented. Using an arbitrary scoring system each of the various factors are subjectively weighted with a score of 1 to 10. The former is a poor score while the latter is best. These scores are summarized in a matrix evaluation table to provide an overall indication of the relative merits of the three processing architectures. Since these scores are subjectively assigned, the reader may wish to assign his own values and judgement; as such this approach applies a convenient method for systematic evaluation. It is believed that any one of the system architectures may be feasible pending more requirements definition and technology verification. The main objective of these trades is the identification of any key technology problems affecting SPS feasibility. The characteristics of the three processing systems seem to verify the existence of at least one feasible approach obviating any key technical impact to SPS.

#### Trade-Off Analysis

Any trade-off analysis for the SPS computer system must pay special attention to the Microwave Antenna Subsystem because of the large number of sensor inputs and control requirements associated with this complex subsystem. The



antenna consists of 7,854 subarrays, each of which is 10x10 meters. These are grouped into 4x4 subarray groups (master arrays). Each subarray utilizes an average of 20 klystrons and 2 dc-to-dc power converters. Each klystron has 12 voltages, 1 temperature, 1 switch position and 4 phase shifter input signals that must be monitored. This results in an estimate of more than 360 sensor inputs per subarray. In addition, the converters require 2 temperature and 2 switch position sensors be monitored resulting in a grand total of more than 364 inputs per subarray. Control outputs required are 22 commands for power on/off and 20 phase shifter signals for beam pointing for a total of 42 commands. Thus, more than 406 inputs and outputs per subarray are required. Since there are 7,854 subarrays, the total antenna requirement is more than 3,188,724 inputs/outputs.

Antenna requirements for sensing and control could be reduced by a factor of 5/6ths if a best case reduced number of klystrons are needed. Conversely, if twice as many klystrons are needed to shape power density, sensing and control requirements could increase proportionally. The klystron density over the face of the antenna may vary up to an order of magnitude from the center to the edge to achieve the required maximum output of about 20 watts per square meter in the center and reduced levels at the edge. This avoids atmospheric interactions and safe human tolerance levels at the antenna's edge.

The processing required for the antenna is a function of: how much direct control of antenna beam pointing is to be directly effected by the computer, how many klystrons are to be controlled by each computer, the degree of control partitioning effected by a central or distributed architecture and how rapidly antenna operational startup is to be implemented following each eclipse. The current antenna design is tending to evolve toward analog inner loops to achieve real time phase control with the computers only providing initiation of coarse pointing and error correction pointing biases. This concept imposes reduced computer requirements. However, in an effort to identify any critical technical issues relative to the IMCS, a worst case is assumed in which startup control must be extremely rapid and real time control demands are made. While data rate requirements and control speed-of-response requirements are forthcoming at a later date, gross estimate of 50 million instructions per second (MIPS) was assumed for each antenna micro-processor which is assumed to service each master array in the given distributed processing system approach. This results in 490 micro-processors being mounted on the antenna. A second tier of supervisory computers, say 5 or 6, would then be connected to the antenna microprocessors to provide overall control. These supervisory computers would then be tied into the top level SPS master computers. This then constitutes the antenna subsystems distributed processing system.

In a similar way, the remainder of the SPS would be serviced by a hierarchy of micro-, mini-, supervisory and master processors to monitor and control the thermal, power, structure and attitude control subsystems. However, speed requirements are considerably reduced. The maximum number of sensor inputs from these subsystems is estimated to result from the thermal subsystem with over 16,000 inputs\*. This compares to millions for the antenna subsystem.

\*Attitude control subsystem speed requirements with 1 sec update cycles may predominate over speed requirements driven by input/output processing.



Further, the Distributed computer system spreads the computational loads so that any given computer can probably be quite low in performance, say < 1.0 to 2.5 MIPS. In this concept, each Submultiplexor (SM) services several dozen sensors and incorporates a small microprocessor for limit checking, local thresholding, alarming, and control. The SM then sends its outputs to a regional Remote Acquisition and Control (RAC) unit which might service 10 to 30 SMs. The RAC may incorporate a microprocessor sized to its computational load. The Distributed system for the non-microwave antenna subsystem requires an estimated 200 RACs and 1500 SMs. In contrast, the microwave antenna is estimated to require 16,000 SMs.

Three computer sizes result with the Distributed system concept: 1) a small microprocessor of less than 1 MIP for the RACs and SMs, 2) a 50 MIPS microprocessor for the antenna, and 3) a medium size general purpose computer of about 25 MIPS for the supervisory functions.

In order to estimate the mass, power, and volume of the various computer system alternatives, current computer technology was considered and estimated projections for the evolution of today's capabilities into the late 1980's. Present space-qualified computers are typified by the Rockwell Autonetics DF224 which performs at 0.6 MIPS within 0.08 m<sup>3</sup>, 45.5 kg, and 100 watts. Follow-on versions of this machine are projected by Rockwell to achieve 2.5 MIPS within 0.008 m<sup>3</sup>, 13.6 kg, and 70 watts by the 1978-80 time period. This is an order of magnitude reduction in volume within about five years and about a one-half order of magnitude increase in performance within the same time period. Mass is reduced by about 2/3 while power is only reduce a third. This appears to reflect the expected advances in large-scale integrated (LSI) circuits which reduce power, mass, and volume for the same performance. The LSI technology will probably reach its photolithography limits of about 2- $\mu$ m line spacing within this time period. Power levels tend to level off because more circuit functions are usually added, such as more memory and speed. Thus, it is expected that if trends such as the introduction of electron beam production technology and magnetic bubble memories continue, the industry by 1990 may achieve in a general-purpose uniprocessor:

- 20 to 25 MIPS within 0.008 m<sup>3</sup>
- 13.6 kg and 100 watts

Other technology projections indicate that special high speed pipeline and array processors will probably achieve the billion instructions per second (BIPS) level during the same time period. With partitioning into multiprocessors, either separate or integrated into the architecture of a single computer, 10 to 50 BIPS will probably be achieved. It should be noted from this last point that even if a "Central" computer system is selected, it will probably be a multi-processing system merely located at a central location, which tends to lead to more favorable consideration of the Distributed system because of its safety and reliability advantages.

These technology projections are summarized in Table 3.7-1, Assumed Equipment Characteristics. The Large Central Computer for the antenna is scaled up from the Distributed system's antenna microprocessors on a speed per unit mass basis. A gross cross-check was made of this mass against some



Table 3.7-1. Assumed Equipment Characteristics

COMPUTERS	MASS (KG)	PWR (KW)	VOL (M <sup>3</sup> )	SPEED (BIPS)
● LARGE CENTRAL COMPUTER FOR ANTENNA	2000	8	1.6	20-25
● SMALL CENTRAL COMPUTER FOR SATELLITE	500	2	0.4	1-5
● GENERAL PURPOSE FOR DISTRIBUTED SYSTEM	14	0.07	0.01	0.025
● ANTENNA MICROPROCESSORS	5	0.02	0.003	0.05
● RAC & SM MICROPROCESSORS	2	0.003	0.003	<0.001
BUS EQUIPMENT				
● RAC W/MICROPROCESSOR	5	0.02	0.005	<0.001
● SM W/MICROPROCESSOR	3	0.01	0.003	<0.001
● RAC ALONE	4	0.017	0.005	0
● SM ALONE	2	0.007	0.003	0

pipeline processing systems currently under production by IBM. These systems involve 1 to 2 tons of equipment including peripherals and can provide 30 MIPS of pipeline processing power from each arithmetic element of which up to 4 in this architecture can be added together for a total of 120 MIPS. Projecting this technology forward 10 to 15 years seems to indicate a reasonable probability of the industry achieving 20 to 25 BIPS within 2000 kg by the 1990 time period. The Small Central Computer is merely scaled down to accommodate the lesser computational loads imposed by the remainder of the SPS systems. The antenna and RAC/SM microprocessors are merely scaled down to the indicated mass, power, volume, and speed characteristics noted in Table 3.7-1.

Two versions of the RAC and SM are shown in Table 3.7-1. The first versions include microprocessors where they are needed for the Distributed or Hybrid processing systems. The second versions are provided for the Central system architecture wherein it is assumed that the Central computers do the entire job and that the data bus capability of up to 500 MHz can accommodate the data transfer requirements.

These equipment characteristics were utilized to estimate the total IMCS computer system mass, powers, and volumes shown in Table 3.7-2. All estimates include a 15% reserve margin and have been rounded up in most cases to reflect the ROM nature of these preliminary estimates. As expected, the Distributed system is the heaviest because of the redundancy in the system in terms of the power supplies, the cases, wiring, etc. The Hybrid utilizes a Distributed approach on the antenna which being the most complex element drives the estimates very close to the Distributed system's characteristics.



Table 3.7-2. Central Versus Distributed Computers

FACTORS	APPROACHES		
	CENTRAL	DISTRIBUTED	HYBRID
PHYSICAL			
● MASS (KG)	35,000	58,000	58,000
● POWER (KW)	130	200	170
● VOLUME (M <sup>3</sup> )	50	50	50
PERFORMANCE (MIPS)			
● GENERAL PURPOSE	BIP RANGE	20-25 MIPS	1-5/20-25 MIPS
● MICRO-PROCESSORS	N/A	0.2 & 50 MIPS	0.2 & 50 MIPS
SOFTWARE COMPLEXITY	HIGH	LOW	MEDIUM
RELIABILITY	LOW	HIGH	MEDIUM
SAFETY	LOW	HIGH	MEDIUM
MAINTAINABILITY	HIGH	MEDIUM	MEDIUM
TECHNOLOGY RISK (1990)	HIGH	LOW	MEDIUM

The Central system saves on mass and power; volumetric savings may not accrue because of access, maintainability, and cooling considerations. Experience with present systems indicates that while volumetric savings accrue with reduced component counts in Centralized systems, heat dissipation requirements increase. Additional volume is required for cooling plenum chambers and cooling support equipment.

Software complexity is expected to be highest for the Central system because of its need for a more complex executive to control interrupts, tasking, and other functions. Data management may also be more complex depending upon random addressable memory capabilities and the amount of data which must be immediately available. Estimates in these areas for requirements are presently pending. If data management problems are avoided in the Distributed system and good partitioning of the various computational functions result, the executive software should be considerably simplified in this case. The Hybrid system obtains both some of the advantages and disadvantages of the two approaches.

Reliability, safety and maintainability may be conveniently grouped together in this trade study. The Distributed system with its high redundancy level offers high reliability with attendant safety advantages in terms of continuity of operation as well as local control. The Distributed system's wide spatial distribution complicates maintainability problems while the Centralized system simplifies access and, hence, maintainability.

The previous technology discussions have implicitly indicated the level of technological risks inherent in each of the approaches. It is believed



that the Central system has the greatest risk since it involves a very large upward scaling of processing power and excessively reduces redundancy levels. The other two approaches provide substantial risk reductions.

These system trades have been translated to relative subjective scores for each factor as shown in Table 3.7-3. A numerical assignment of "10" indicates that the approach for that factor is "best" or has the highest rating. A "1" is a poor rating. This evaluation shows that the Distributed system of computers is most favorable overall. However, the reader must be aware that this is only a very preliminary trade study and requirements data are pending; technology verifications are needed. The main purpose of this analysis was to help verify the belief that there is a feasible, low risk approach available to implement the IMCS in order to avoid any key technology issue impact to SPS. This trade study verifies this from the computer processing system viewpoint.

Table 3.7-3. Evaluation of Central Vs. Distributed Computers

APPROACHES			
FACTORS	CENTRAL	DISTRIBUTED	HYBRID
PHYSICAL			
● MASS	10	3	5
● POWER	10	1	2
● VOLUME	10	10	10
PERFORMANCE (LOW MIPS)	1	10	5
SOFTWARE COMPLEXITY	1	10	5
RELIABILITY	1	10	5
SAFETY	1	10	5
MAINTAINABILITY	10	5	5
TECHNOLOGY STATUS	1	10	5
TOTAL EVALUATION SCORES:	45	69	47
		FAVORABLE OVERALL	

Recommendations and Conclusions

This trade study highlights the importance of the Microwave Antenna Subsystem. It is the driving factor in IMCS design because of the millions of sensors to be serviced and the large number of control requirements. The antenna is also key in achieving safe SPS operations with respect to atmospheric interactions and humanly safe power levels at the edge of the rectenna.



A feasible computer system architecture is available to implement a low risk IMCS system approach. Most likely, the Distributed system approach is best. However, additional study is needed to estimate processing requirements and verify technology available by the late 1980's. The IMCS computing requirements can probably be met by any of the 3 system approaches; but, it is interesting to note that even the Centralized approach still involves considerable multiprocessing which leads to strengthened consideration of the Distributed system.

It is recommended that any further study of this area be broken into three areas in the following order of priority:

- Antenna processing requirements
- Computer technology projections
- Refinement of this preliminary study

### 3.7.2 DATA BUS TRADE

#### Introduction

The purpose of this study was to examine the various types of Information Management and Control System (IMCS) compatible data buses, such as optical or radio frequency, and define their relative advantages for use in the SPS. The scope was limited to the following interconnection schemes:

- |   |   |                         |
|---|---|-------------------------|
| <ul style="list-style-type: none"> <li>• Optical</li> <li>• RF</li> <li>• Dedicated</li> <li>• Coax</li> <li>• Laser</li> </ul> | } | Interconnection Schemes |
|---|---|-------------------------|

Also included in the trade study are considerations of the number and characteristics of any Remote Acquisition and Control (RAC) units and Sub-multiplexors (SM).

Although the factor of computer system architecture has been minimized in this study, the various possibilities include centralized, distributed and hybrid systems. Figure 3.7-4 illustrates the top level computer system organization assumed in this analysis; a hybrid architecture with centralized redundant master computers and displays. The master computers are supported by a number of mini-computers and micro-processors distributed throughout the satellite, assumed to be a 2-trough photovoltaic system as indicated in Figure 3.7-5. Local computer centers are envisioned as shown in Figure 3.7-5 and are to be located at stations about 1/3 and 2/3 along each wing and at the wing end sections. Section 6 left and 6 right (each wing is divided into 600 meter sections and numbered 1 to 21) would house processing centers for thermal and power controls. The wing end sections would house attitude control support centers. Nearly 8,000\* microprocessors would be incorporated into the microwave antenna to control power beam pointing.

\* Reduced to less than 500 subsequent to July 15, 1977.

ORIGINAL PAGE IS  
OF POOR QUALITY

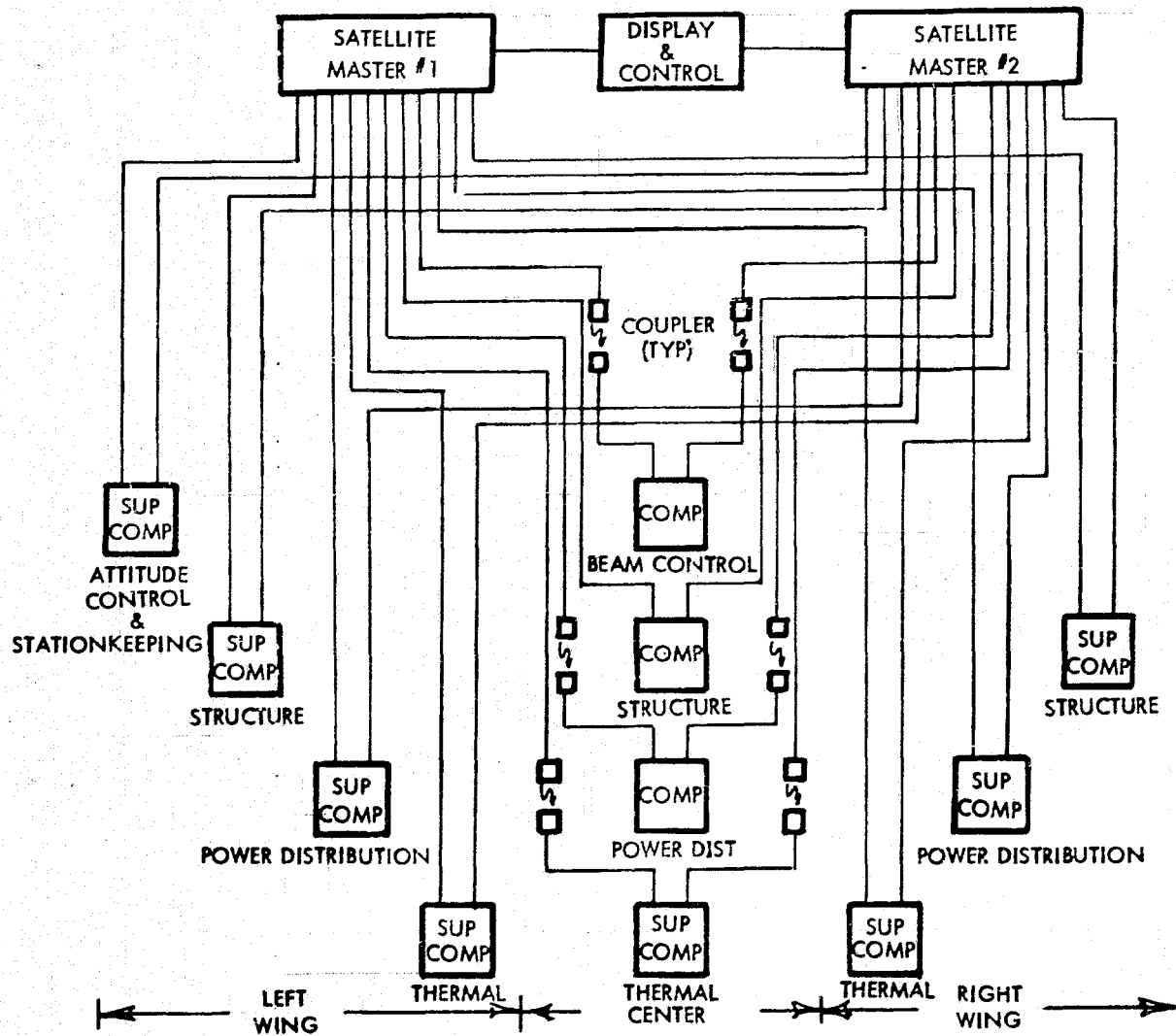
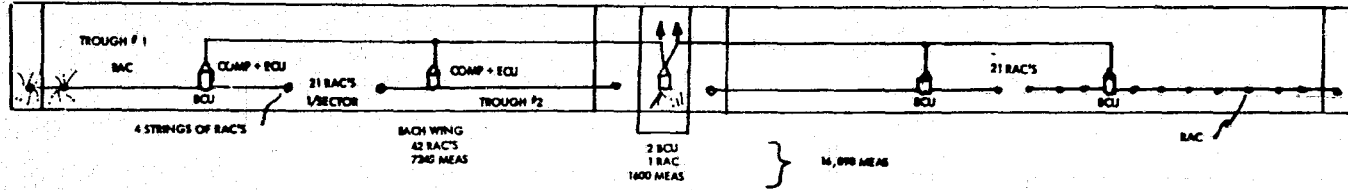


Figure 3.7-4. Data System Computer Net  
(Preliminary)

3-245

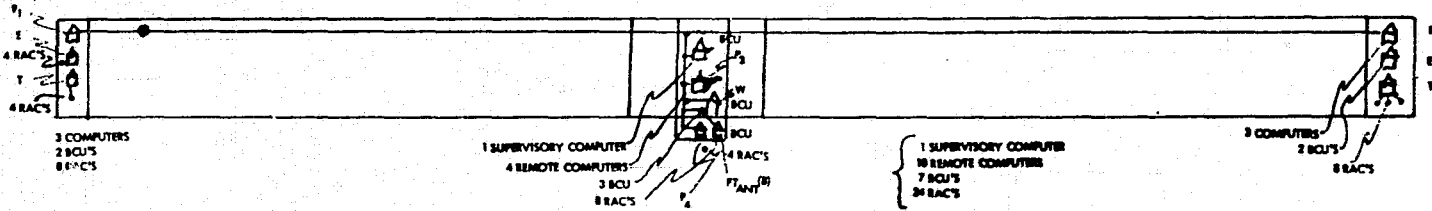
SD 78-AP-0023-3



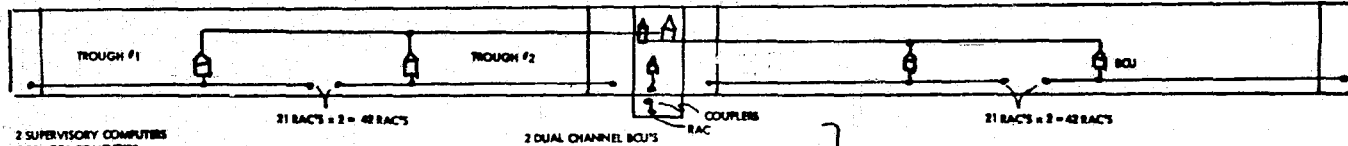


**THERMAL - IMCS**

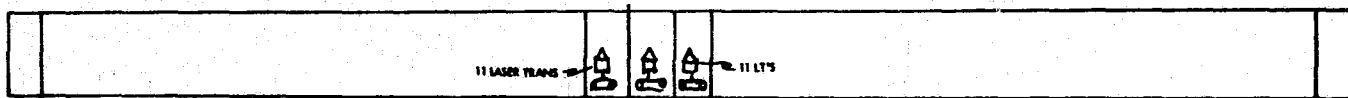
2 SUPERVISORY COMPUTERS  
3 REMOTE COMPUTERS  
3 BCU'S  
42 RAC'S



**ATTITUDE CONTROL - IMCS**



**POWER DISTRIBUTION - IMCS**



**STRUCTURE - IMCS**

ROM WIRE LENGTH: 30 KM

Figure 3.7-5. Spatial Distribution of Computers

3-246

SD 78-AP-0023-3

ORIGINAL PAGE IS  
OF POOR QUALITY

C-4



### Trade and Evaluation Approach

The selected trade-off approach is based upon the assumption of a photovoltaic solar power satellite with a concentration ratio of two. This results in a structural configuration 26.7 km long by 2 km wide and 1 km deep as shown in Figure 3.7-5. A 2-trough solar collection system is incorporated with each of the 2 active collection surfaces 0.5 km wide  $\times$  0.6 km long, and bordered on each side by an inclined reflector 0.5 km wide along the inclined side and 0.6 km long. This configuration and the location of remote computer centers in each wing at sections 6 and 21 establish the assumed top level interconnection patterns as shown in Figure 3.7-4. The remote acquisition and control unit (RAC) pattern of one RAC per section plus the SM pattern shown in Figure 3.7-6 establishes the assumed bottom level bus distributions.

The measurements requirements for thermal, power distribution, antenna, attitude control and structural alignment help determine cabling requirements. The microwave power transmission antenna with its estimated 528 thousand sensors is expected to require the most extensive interconnection cabling. Second is the thermal measurements subsystem with its estimate of over 16 thousand sensors, scattered over the length and width of the satellite.

This trade approach is illustrated in Figure 3.7-7 which shows how configuration assumptions, measurements, RAC distributions, and computer locations influence cabling requirements.

Mass, power and volume are primarily dependent upon bus technology and distributions of RACs and SMs. Each 0.6 km section of the satellite has been allocated a centrally located RAC which is connected to a remote computer. Each wing has 2-troughs so that 42 RAC's are required for each wing of the satellite. The SM distribution is set by sensor distribution and density as well as SM capacity and required wire lengths. The number of sensors depend on the safety and time criticality of the system served by the sensors. The bus technology, such as wire or optics, influence the number and flexibility of the wire "runs". Bus technology which fosters time or frequency multiplexing contributes to reduced wire lengths with attendant savings in volume, weight and power.

Multiplexor approaches become a significant trade as implied above. Where sensor density is concentrated and wire runs are short, dedicated wires might be best for reduced mass and reduced number of SMs to minimize power. Where large structures and wide distributions of sensors are required, time or frequency multiplexed buses promote use of a single cable which is routed to widely scattered sensors. Since the SPS is of the latter type, bus technology approaches which facilitate multiplexing are favored.

Electrical trades relate to cable lengths, which affect signal losses and power requirements, and affect the ability to operate safely in the anticipated noisy environment of SPS. Good isolation of circuits is required to minimize induced surges and electro-optical isolation devices such as LED (Light Emitting Diode) couplers must be considered. Electromagnetic interference (EMI) from the high voltages and current flows of SPS must be eliminated as well as the usual EMI between adjacent bus channels and other RF or electrical devices. Since

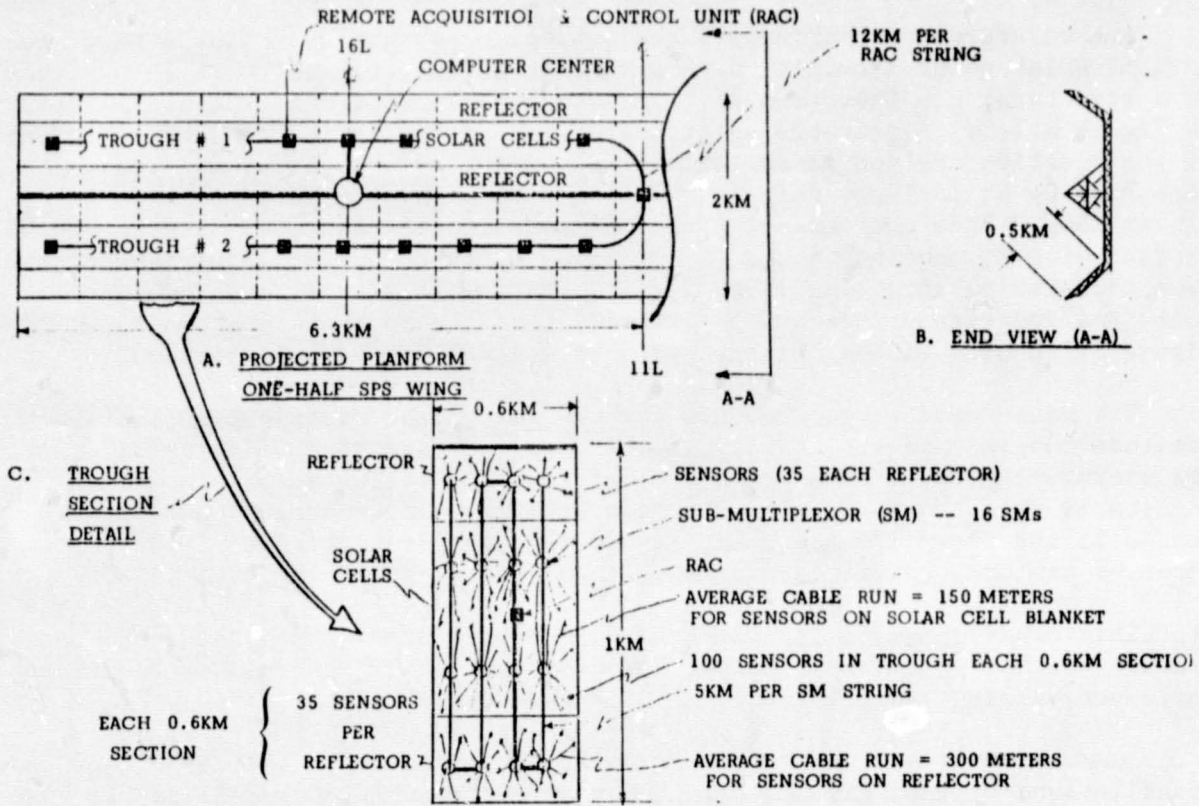


Figure 3.7-6. RAC and SM Interconnections (Thermal)

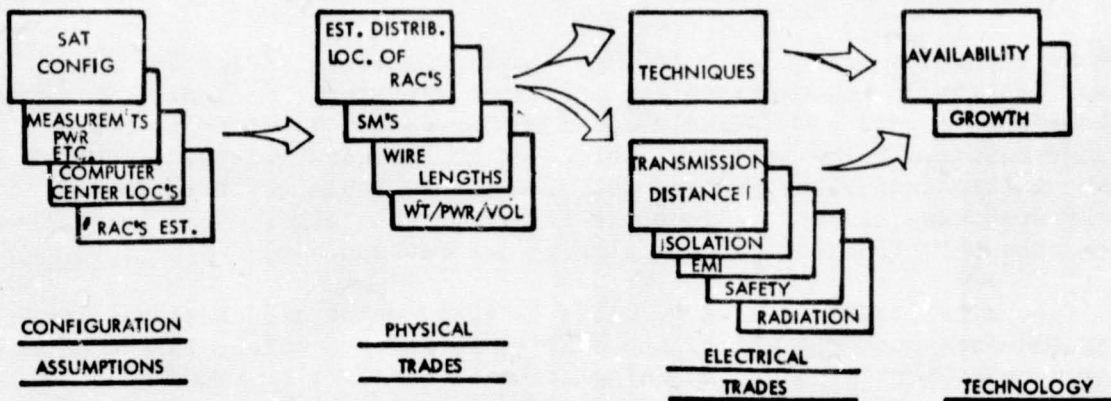


Figure 3.7-7. Trade Approach for Data Bus Study

ORIGINAL PAGE IS  
OF POOR QUALITY



SPS might be assembled in a subsynchronous orbit with high incident Van Allen radiation, resistance to such effects must also be considered in circuit designs. Fail-safe or fail-operational philosophies of design must also be considered in bus placement, technology selected, and RAC or SM approaches. Since the SPS is a manned system as well as an important source of electrical power to the cities served by it, bus electrical design and operating approaches must contribute to manned safety and uninterrupted flow of power.

Finally the technology factors of maturity and flexibility for growth enter into the design equation. Selected bus technology must be acceptably priced and fully mature when design "freeze" occurs which will probably be in the late 1980's, assuming a mid-1990's deployment. Any given bus approach must provide flexibility to accept additional capacity and functions because any deployed SPS will undoubtedly be subjected to major functional additions over its 30 to 40 year lifetime -- the availability of large amounts of power in space and large volumes of open useable structure is bound to attract additional missions.

These trade criteria will be assembled into a Bus Characteristics Trade Table from which a Bus Evaluation Matrix can be developed. This approach is summarized in Figure 3.7-8. The Bus Evaluation Matrix will list the same factors as the Bus Characteristics Trade Table, but the estimated characteristics will be translated into a relative evaluation factor. This is a number from 1 to 10 which is qualitatively assigned based on the judgement of each engineering evaluator. The relative cumulative scores can then be used for prioritization and as an aid to the systematic selection of the best SPS Data Bus approach. The foregoing trade characteristics and evaluation factors are discussed in the next section.

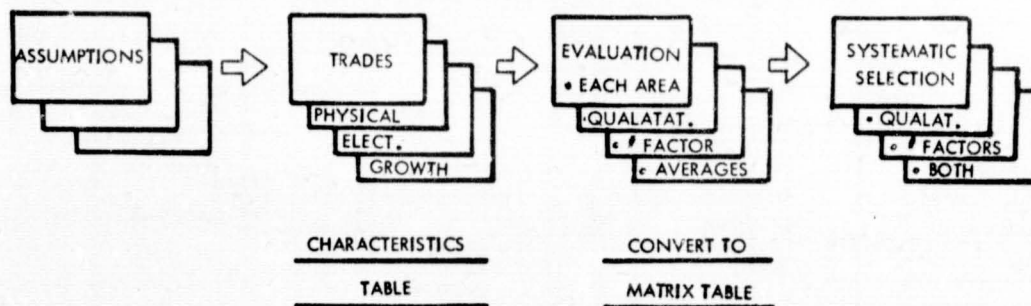


Figure 3.7-8. Evaluation & Selection

General Trades

Optical bus techniques are favored over any of the other 4 approaches when compared on the basis of physical characteristics as shown in Table 3.7-4. Based on available data and data projections, fiber optics are lighter in mass and volume than RF, wire, coax and lasers. Optical methods permit interconnections that are about 85% lighter than 22 gauge twisted pair wire, and even lower in mass than Type 316 coax. Volumetric advantages of optical bus techniques are even more dramatic; 1 to 3 orders of magnitude smaller



than wire or coax, depending on core diameter and sheathing requirements for low loss and strength. While power figures are pending, preliminary indications are that fiber optics would consume less than any of the techniques since line losses will be down to less than 3 to 6 dB per kilometer for graded index fiber. These physical comparisons are based on the following specifications:

- Fiber Optics (1 channel/1 fiber) (Corning Glass)
  - 200 to 1500  $\mu\text{m}$  outside diameter (OD) depending on sheathing thickness, such as ethylene vinyl acetate, and core fiber diameter, which is typically less than 62 to 85  $\mu\text{m}$ .
  - 0.14 kg/km
- Wire (22 gauge twisted shielded pair)
  - 5100  $\mu\text{m}$  OD
  - 12 kg/km
- Coax (type 316)
  - 4800  $\mu\text{m}$  OD
  - 16 kg/km

Table 3.7-4. Data Bus Trade Characteristics

BUSES FACTORS	OPTICAL (FIBER OPTICS)	RF	WIRE (22 GAUGE TWISTED PAIR-SHEILDDED)	COAX (TYPE 316)	LASER
PHYSICAL (13 MILLION METERS)					
● MASS (KG)	1,775	TBD	150,000	200,000	TBD
● VOLUME (M <sup>3</sup> )	0.3 to 30	TBD	265	250	TBD
● POWER (KW)	LOW (TBD)	TBD	HIGH (TBD)	MEDIUM (TBD)	TBD
ELECTRICAL					
● MULTIPLEXOR APPROACH	FM & TDMA	FM & TDMA	TDMA	FM & TDMA	FM & TDM/
● ISOLATION*	HIGH	LOW	LOW	MEDIUM	HIGH
● TRANSMISSION DISTANCE* (MIN/AVG/MAX)	1/120/5000	1/120/5000	1/120/5000	1/120/5000	1/120/5000
● ELECTROMAGNETIC INTERFER*	LOW	HIGH	HIGH	MEDIUM	LOW
● SAFETY	HIGH	MEDIUM	MEDIUM	MEDIUM	LOW
● RADIATION RESISTANCE*	HIGH	LOW	LOW	MEDIUM	HIGH
TECHNOLOGY					
● AVAILABILITY	MEDIUM	HIGH	HIGH	HIGH	LOW
● GROWTH	EXCELLENT	LOW	LOW	MEDIUM	MEDIUM

\* PRIMARY IMPORTANCE

CH



Additional information is needed to verify these comparisons; namely, data on RF and lasers plus the projected size of optical cabling and connectors. The present projections for optical cable appear optimistic and increased cable diameter with resulting mass/volume increases may be needed to accommodate manual handling without breakage.

Additional information is needed on optical connector technology which is rapidly being standardized and improved to facilitate tee, y, x, splice, and tap-off connections. Comprehensive surveys of existing industry projections are needed in the optical bus area. Small diameter low loss fiber optical cable will be required to reduce bending losses and facilitate capability for sharp turns. But large fiber core is needed to allow long cable runs without breakage. Corning's 125  $\mu\text{m}$  Corguide can be pulled through 1 km straight runs without breakage because fiber optic cables are 4 times lighter than coax of the same diameter. Currently, single fiber cables of 1500  $\mu\text{m}$  can withstand tensile loads of 216 kg. These factors must be traded against small diameter for low fiber losses and connector losses. Also connector alignment problems increase with core fiber diameter reductions. Present cables typically bundle 6 core fibers to produce 6-channel cable and facilitate handling. Graded fiber cables presently cost \$1.50 to \$2.50 per meter, but are expected to drop to 25 cents per meter by 1978 and 5¢ per meter in 5 years.

Additional definition is needed in the RF and laser areas to verify bus architecture for these technologies. These methods would probably utilize hybrid approaches and use wire, optical or coax techniques at the submultiplexor level depending on sensor densities and grouping. Longer links could be made major trunk lines for efficient usage of RF and laser channel capacities.

Electrical characteristics are compared in the next group of 6 parameters. Virtually all of the technologies are compatible with both frequency or time division multiple access communications except for dedicated or party-line twisted pair cable subsystems; none therefore offer unique multiplexing advantages.

Isolation characteristics provide a different situation. Optical fiber or laser communications offer potentially excellent inter- and intra-channel isolation as well as superb isolation from the expected noisy electrical or electronic sources of energy aboard the SPS. Coax provides a good to medium capability with good shielding and careful RF and audio frequency selections. RF and wire are believed to be most susceptible to the anticipated noisy electromagnetic environment of SPS. As quantitative data becomes available, these tentative judgements should (and will) be reevaluated.

Transmission distance does not provide a clear trade-off at this time because more definition of the architectural impact of the various technologies is needed. For example, it is conceivable that advanced LSI (Large Scale Integrated) circuits could make RF transmitters sufficiently low cost, while proper frequency and modulation selection within an improved definition of the SPS noise environment could so improve signal-to-noise capabilities that RF would become a favored approach. Many outlying clusters of sensors could be serviced with RF as well as "long haul" intra-satellite links. A similar



situation might result with lasers. With extremely low power and low link losses and error rates, transmission distances of the order of 20 to 30 km might become insignificant. This type of improvement is clearly taking place in the fiber optics area with extremely low line losses being achieved over kilometers without need for repeaters.

Optical fiber optics and lasers offer significant advantages in EMI reduction, which is so important in the anticipated strong electromagnetic fields of the SPS. The other three types of buses are susceptible to this environment in varying degrees and would require trade-offs between use of electro-optic-isolators throughout the subsystem versus voltage or current mode transformer isolation schemes. One area of fiber optics requiring further study is the need for long life light sources; this is presently an emerging technology which is projected to provide suitable products over the next few years.

Safety must be considered as to whether: 1) the bus medium, itself, provides any hazards to man or machines, and 2) the bus technology imposes safety hazards on the SPS systems supported by IMCS. The optical technology offers high safety levels because of its resistance to the anticipated noisy SPS environment and its inherently large channel capacity (500 MHz), among other reasons. This channel capacity can provide highly secure command verification codes and procedures without impacting data timelines. The laser system approach may pose a vision hazard to SPS crew members; hence it is rated low on safety until more data is obtained. The other technologies have reduced ratings because of their EMI and isolation susceptibility.

Radiation resistance is important because of potentially long Van Allen radiation exposures during assembly and transit envisioned for some SPS concepts. Optical technologies may offer significant advantages because of inherent isolation and protection from propagation of unwanted signals due to radiation induced failures of electronic drivers. However, these same isolation schemes can be introduced into all-electronic systems and this "advantage" may not be significant. Also, optical transmitters may still be affected so that receiver decoding or required filters are needed irrespective of whether electronic or optical bus techniques are used.

Technology status is the last trade characteristic of significance considered. All technologies are well established and mature except optical fiber and laser mediums. However, the technology of the middle to late eighties is controlling, not today's technology. Advances in the optical field are occurring so rapidly that it is expected to be fully mature by time of SPS design freeze. So, comparisons should be made using projected technology and more study is needed to clarify this future status.

Growth to accommodate SPS evolution over 30 to 40 years is desirable. The multiplexing and channel capacity of optical buses favor use of this technology. However, this comparison may be irrelevant because of the projected physical size of SPS. Additional functions may be accommodated by merely stringing new buses over the voluminous SPS framework.



These trades are translated into the evaluation matrix of Table 3.7-5. Here each of these characteristic assessments has been subjectively graded on a scale of 1 to 10, "1" being poor, "10" being best, and "5" being average or medium. Where information is to be determined (unavailable at this writing) an arbitrary "5" score was assigned. On this bases, the optical fiber score rated "best". Lasers scored 2nd while RF and coax tied for 3rd. Wire was last.

Table 3.7-5. Data Bus Evaluation Matrix

(KEY: 10 = BEST . 1 = POOR)

BUSES FACTORS	OPTICAL (FIBER OPTICS)	RF	WIRE (22 GAUGE TWISTED PAIR-SHEILDED)	COAX (TYPE 316)	LASER
<b>PHYSICAL</b>					
● MASS	10	5	4	1	5
● VOLUME	10	5	1	1	5
● POWER	10	5	2	5	5
<b>ELECTRICAL</b>					
● MULTIPLEXOR APPROACH	10	10	5	10	10
● ISOLATION*	10	3	3	5	10
● TRANSMISSION DISTANCE*	10	10	10	10	10
● EMI*	10	1	1	5	10
● SAFETY	10	5	5	5	3
● RADIATION RESISTANCE*	10	2	3	5	10
<b>TECHNOLOGY</b>					
● AVAILABILITY	5	10	10	10	3
● GROWTH	10	3	3	5	5
	105	59	47	62	76

\* PRIMARY IMPORTANCE

Conclusions and Recommendations

Based on these analyses, fiber optics has been selected for the SPS Data Bus subsystem because of its low susceptibility to the difficult electromagnetic environment of SPS, low weight, low losses, flexibility to accommodate design changes and projected low cost. Additional study is needed to verify volume, connector, light source and light/electronic interface coupler technologies.

3.7.3 GROUND-BASED INFORMATION MANAGEMENT & CONTROL SUBSYSTEM (IMCS)

Introduction

The purpose of this section is to present a preliminary functional definition of the Ground-Based Information Management & Control Subsystem (IMCS).





Overall IMCS functions are identified with emphasis devoted to those supporting power reception/conversion and distribution. This area was focused on because of the need to verify whether any critical issues affect overall SPS feasibility.

The preliminary level of definition of the ground-based station at this time required the assumption of some rectenna functional and physical characteristics. The need for a unified IMCS design approach, which facilitates economy and systematizes functional definition, resulted in the definition of an overall functional structure which is presented in Figure 3.7-9. The rectenna functional model is presented next along with the theoretical basis for it. Subsequent sections present the overall and more detailed power-related IMCS functions.

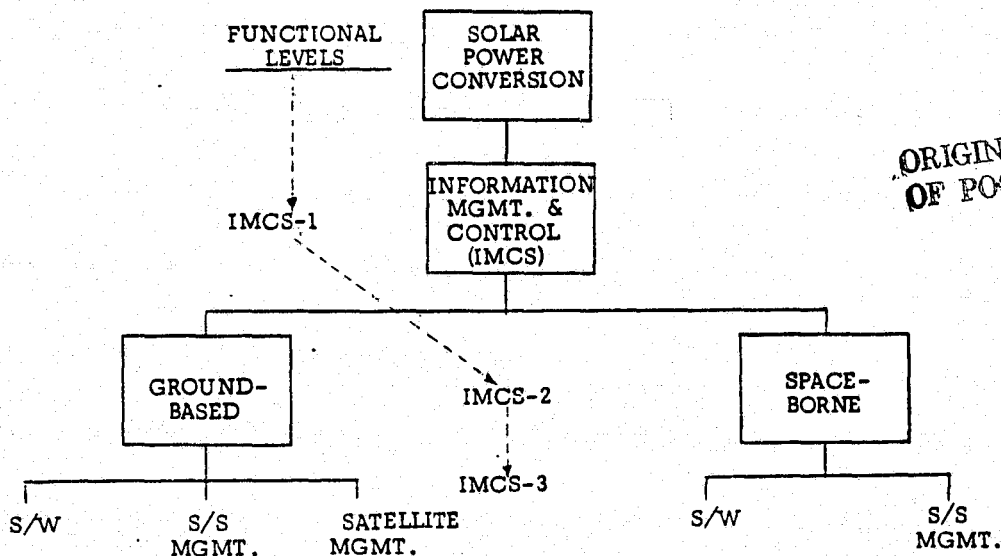


Figure 3.7-9. Definition of Functional Levels

Rectenna System Model

The functional IMCS requirements for a ground based, power converting, receiving station (Rectenna Farm) are in virtually all respects similar to those identified for the Satellite. To illustrate this similarity, a simplified model for the Rectenna/power distribution will be developed in the following paragraphs.

As has been described in other documentation,<sup>1</sup> the Rectenna System performs three basic functions. These are illustrated in Figure 3.7-10. Also shown in Figure 3.7-10 are the system transfer efficiencies for each of the three functions along with the amount of power inputs at each stage required to eventually output 5 GW to the consumer. Figure 3.7-11 illustrates the major control and monitoring interfaces between the power subsystem elements and the IMCS.

<sup>1</sup>PD 77-21 Satellite Power System Concept Definition Study First Quarterly Review, Rockwell International; 23 June 1977; given at NASA/MSFC

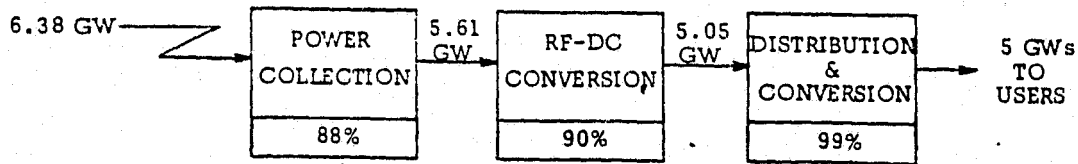
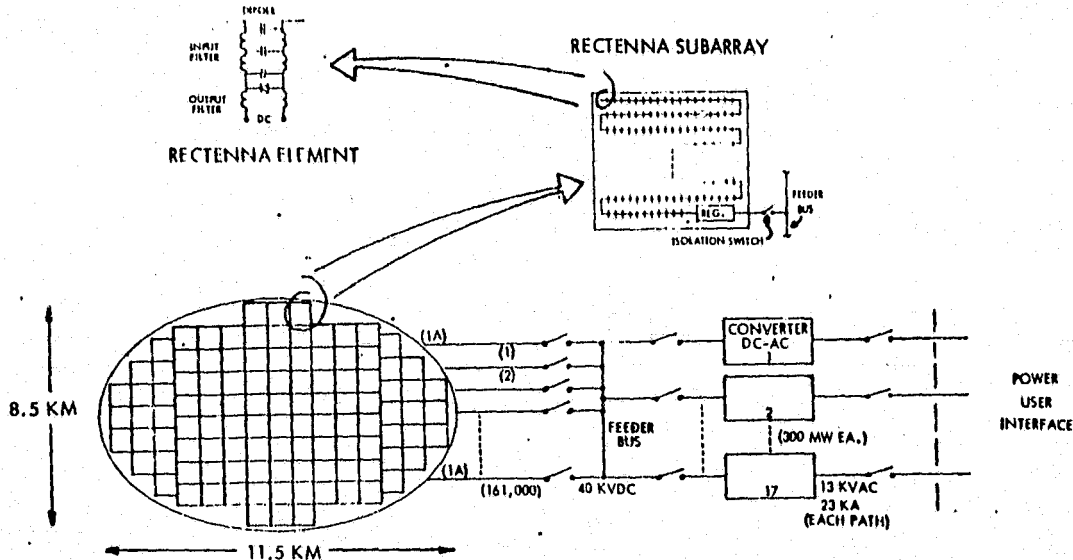


Figure 3.7-10. Basic Energy Flow Diagram



NO. SUBARRAYS	161,000
TOTAL NO. RECTENNA ELEMENTS	4.9 BILLION
RECEIVING RECTENNA AREA	76.7 KM <sup>2</sup>

FIGURE 3 MODEL RECTENNA SYSTEM

Figure 3.7-11. Model Rectenna System

A study of a sample of variable literature on the subject of space located power generation/collection systems has shown that only a limited amount of the analyses have significantly addressed the ground based portions of the system. It is therefore necessary to make certain assumptions in the initial detailing of the Rectenna model. For example, the rectenna elements have been postulated to vary from individually mounted, dedicated dipoles, to multiple elements, (including rectifying diodes), deposited on large blanket material such as teflon or Kapton. Furthermore, power handling capabilities have been described as varying from 400 mW<sup>2</sup> to a maximum of 10 W<sup>3</sup>.

<sup>1</sup> NASA TM X-73344 November 1976, Satellite Power System Engineering and Economic Analysis Summary; NASA/MSFC

<sup>2</sup> Brown, W. C. "The Receiving Antenna and Microwave Power Rectification", The Journal of Microwave Power; Vol. 5, No. 4, December 1970: Pg 279



For the model the manufacturing technique selected is similar to those applicable to the various solarvoltaic techniques considered in the literature, i.e., thick film deposition on Kapton blankets. An individual cell capacity of 1.2 - 1.3 watts, consistant with deposited film technology (2 - 3 mils) was also selected. For simplicity, in subsequent area analysis, this is assumed to be equal to a cell generation with 1.3 volts at 1 Ampere. It was furthermore assumed, arbitrarily, that rectenna farm internal buses would operate at 40 kV dc while the interface to the user system would be at 13 kV ac.

The power reception station will therefore consist of 161,000 rectenna element "strings" (subarrays), each containing approximately 30,000 dipole/rectifier elements connected in series. Each "string" is assumed to be fabricated on Kapton blankets in 50x0.5 meter strips (subarrays). A possible layout of each of the 161,000 subarrays is shown in Figure 3.7-11.

In addition to the conversion/distribution interfaces shown in the simplified model, the farm interfaces will also include thermal monitor (and possibly control), safety monitoring, intrusion detection alarms, communication network(s), ground/ground and ground/satellite communication links, etc.

Overall Ground-Based IMCS Functions

The Ground-Based IMCS is categorized into 3 functional areas as shown in Table 3.7-6; these are divided into software and hardware with the latter related to management of ground-based or spaceborne subsystems.

Table 3.7-6. Overall Functions for SPS Ground System

<u>3RD FNCTL. LEVEL</u>	<u>4TH FNCTL. LEVEL</u>	<u>COMMENTS</u>
SOFTWARE	EXECUTIVE CONTROL DISPLAY MANAGEMENT	INCLUDES DATA BASE MGMT., MICRO-PROGRAMS, INITIAL PRGM. LOAD, ETC.
RECTENNA FARM SUBSYSTEMS MANAGEMENT	MICROWAVE RECEIVING & CONVERSION  POWER DISTRIBUTION  COMMUNICATIONS & TRACKING  SECURITY CONTROL  ENVIRONMENTAL CONTROL  DISPLAY OPERATIONS	ALL SUBSYSTEMS MGMT. FUNCTIONS INCLUDE: CONFIG- URATION CONTROL (WHICH INCLUDES REDUNDANCY & RECOVERY MGMT.)
SATELLITE SUBSYSTEMS MANAGEMENT	GUIDANCE, NAVIGATION & CONTROL  COMMAND & CONTROL	



Management and control of the IMCS software is effected by top level executive software, which includes provisions for task scheduling, data base management, and special areas, such as IPL (Initial Program Load). Provisions may have to be incorporated for display management, depending upon the type and extent of hardware control of the display subsystem.

Application software, computer and communications hardware are included under "Rectenna Farm Subsystems Management." Six major subsystems require IMCS support as shown in the 2nd column. Configuration control is included under each of these 4th level functions. Intra-station data communications are included under "Communications and Tracking," which would also incorporate ground-space communications. The IMCS support to microwave receiving/conversion and power distribution is essential to the SPS power production process; consequently, these functional areas are considered in more detail later.

Ground-based IMCS support to spaceborne subsystems is identified for consideration under any follow-on studies. Long-term tracking and ephemerides updates are traditionally performed by ground-based systems because of the co-location of tracking facilities. Maintenance of required long-term orbits may be more conveniently or efficiently performed by ground-based rather than by spaceborne navigation, guidance and control. Long-term or back-up command scheduling and control of spaceborne power subsystems might also be required at the ground station to minimize satellite crew sizes.

#### Receiver/Conversion and Distribution

The IMCS functions which support Receiver/Conversion and Power Distribution have been analyzed down to example 6th level functions to assure that critical IMCS issues which impact SPS feasibility do not exist. Table 3.7-7 summarizes this functional analysis which did not identify any new management and control requirements which are especially difficult to individually implement. Existing ground-based computerized control systems, such as those presently used by the electrical utilities, are performing these operations today. Perhaps the technical challenge presented by SPS is the large number and concentration of these control devices. For example, several hundred thousand circuit breaker-switches and voltage regulators will be distributed over the 60-70 square miles of the Rectenna Farm. Fourth level power-related functions are split into Receiver/Conversion and Power Distribution. Each will be discussed separately to trace the definition and basis for 5th and 6th level requirements.

Receiver/Conversion includes some 5th level functions which will be identified in a separate logical grouping in any subsequent IMCS studies. Subsystem Monitoring will probably be incorporated in an Instrumentation or Sensor Subsystem function when these needs have been defined across the IMCS support requirements. Monitoring sensors provide the vital inputs from which control responses can be determined. For this reason they are included at this point in the analysis under Receiver/Conversion. Sensors are required for monitoring breaker-switch positions, voltage levels throughout the farm, amperage, temperature and many other parameters. These inputs are used for Configuration Control and Caution & Warning.



Table 3.7-7. Ground-Based IMCS Functions For Power Reception/Conversion and Distribution

<u>4TH LEVEL FNCTNS.</u>	<u>5TH LEVEL FNCTNS.</u>	<u>EXAMPLES OF 6TH LEVEL FNCTNS.</u>
RECEIVER/CONVERSION	SUBSYSTEM MONITORING	BREAKER SWITCHES VOLTAGE AMPERAGE TEMPERATURE
	INTRA-STATION DATA COMMUNICATIONS	POLLING OR FREQUENCY SELECTION COMMAND VERIFICATION (ABOVE DEPENDS ON WHETHER TDMA OR FDMA BUS USED)
	CONFIGURATION CONTROL	STRING CONTROL VOLTAGE REGULATOR MGMT.
	CAUTION & WARNING	OVER VOLTAGE AMPERAGE & TEMPERATURE
	RF INTERFERENCE MANAGEMENT	PILOT BEAM MONITORING PUBLIC COMMUNICATIONS PUBLIC SERVICES
DISTRIBUTION	SAME AS ABOVE 1ST 4 FUNCTIONS	SEE ABOVE-MONITORING INCLUDES PHASE. CONFIGURATION CONTROL INCLUDES BUSES & COMBINATIONS OF CONVERTERS AND BUSES.
	DC-TO-AC CONVERSION	MOTOR-GENERATOR CONTROL OR SOLID STATE CONVERSION CONTROL (DEPENDS ON DESIGN SELECTED)

In an analogous way, Intra-Station Data Communications probably will be eventually grouped for analysis and design purposes under Data Bus functions as part of Tracking and Communications, which includes intra-station and inter-site (space-ground) communications. But early functional requirements definition is needed to identify any critical design issues.

Preliminary analysis has resulted in the selection of an optical or electrical data bus approach. The strong RF and electrical noise environment resulted in the deletion of an RF bus subsystem. The large area to be served suggests the need for a distributed micro-processor system and makes a dedicated wire system impractical. The environmental noise problem results in a fiber optical approach being favored. However, additional follow-on study is required to define whether a time, frequency, or hybrid multiplexed approach is needed. Sixth level functions for a Time Division Multiplexed Approach (TDMA) include polling and command verification. A FDMA would require additional control functions such as frequency (channel) selection.



Configuration Control is the primary Receiver/Conversion subsystem control function. It includes control of the inter-connection of thousands of Rectenna dipole voltage strings which provide the output power. Included in each dipole string are the voltage regulators and breaker-switches. A major functional trade is the degree of distributed versus centralized computer control need. Preliminary study has resulted in the conclusion that the large area and the need for local control for safety purposes dictate the use of a distributed micro-processor system. Just as the string and regulator controls, the various devices making up the distributed processor may be arranged in an ascending hierarchy of control, depending upon failure modes and control scenarios. This results in a hybrid distributed-centralized IMCS, similar to that used on the satellite. This expected commonality of design should result in some economies of design, development and operations. Also included in Configuration Control are such 6th level functions as redundancy management, recovery from outages, and other emergency start-up or shut-down operations.

Caution and Warning will use many of the sensor inputs as used by Configuration Control. Here, the main function is to alert the manned ground-based Operations Center that a potential or actual problem has arisen. Automatic responses may be implemented through Configuration Control or adequate time may be available to allow human intervention.

It is apparent from the above discussion that the IMCS requires a human interface in the form of an Operations Center within which all displays, key-boards, status boards, and other controls and displays are maintained. This central computer center also would (or could) provide the software development and training facilities needed to improve and evolve the SPS.

RF Interference is a potentially significant control consideration. The high electrical field is expected to provide a major source of potential interference with public services and communications in the local area. Such interferences may also impact pilot beam control of the down-line RF power beam. A complete set of monitoring sensors are required and follow-on study is needed to ascertain the extent of this potential problem area and effective means of control.

#### 3.7.4 DOE PROGRAM SUPPORT REQUIREMENTS

No specific program support requirements have been identified at the present time.